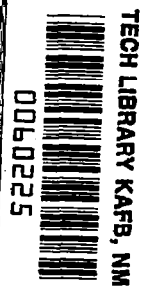


NASA CONTRACTOR REPORT



NASA CR-865

LOAN COPY: RETURN TO
AFWL (WLIL-2)
KIRTLAND AFB, N MEX

ELECTROMAGNETIC GUIDANCE STUDY

by J. H. Lowry

Prepared by
MCDONNELL AIRCRAFT CORPORATION
St. Louis, Mo.
for Electronics Research Center

NATIONAL AERONAUTICS AND SPACE ADMINISTRATION • WASHINGTON, D. C. • SEPTEMBER 1967



ELECTROMAGNETIC GUIDANCE STUDY

By J. H. Lowry

Distribution of this report is provided in the interest of information exchange. Responsibility for the contents resides in the author or organization that prepared it.

Issued by Originator as Report No. E666

Prepared under Contract No. NAS 12-18 by
MCDONNELL AIRCRAFT CORPORATION
St. Louis, Mo.

for Electronics Research Center

NATIONAL AERONAUTICS AND SPACE ADMINISTRATION

TABLE OF CONTENTS

	<u>Page No.</u>
LIST OF FIGURES	v
LIST OF TABLES	xv
LIST OF SYMBOLS	xviii
INTRODUCTION	1
REQUIREMENTS	2
Mission Considerations	2
Docking Guidance Laws	5
Study Constraints	24
RANGE AND RANGE-RATE MEASUREMENT TECHNIQUES	25
CW Radar Systems	25
Pulse Radar Systems	76
Probes as Docking Aids	107
Optical Radar Systems	119
Nuclear Techniques	138
ANGLE MEASUREMENT TECHNIQUES	160
LOS Determination by Amplitude Techniques	160
LOS Determination by Phase Techniques	179
Target Attitude Determination Techniques	195
Target Attitude Rate Determination Techniques	218
INTEGRATED SYSTEMS FOR NONCOOPERATIVE MISSIONS	231
Trade-off of Contending Systems	231
Selection of Most Promising System	243
Preliminary Design of Noncooperative Docking Radar	247
COOPERATIVE INTEGRATED MEASUREMENTS SYSTEMS	270
Description of Systems with Various Degrees of Target Cooperation	270
Integrated Phase System	280
Electronic OMNI System	308
VENDOR SURVEY	331
CONCLUSIONS	334

TABLE OF CONTENTS
(Cont'd) /

	<u>Page No.</u>
RECOMMENDATIONS	336
Analyses of Related Programs	336
Nuclear (Mossbauer) System Program Plan	337
Antenna Probe System Program Plan	338
Analysis of Applicability of Noncoherent Optical Techniques	338
Noncooperative Docking Radar Program Plan	339
Cooperative Docking Radar Program Plan	342
APPENDICES	343
APPENDIX A - Survey of CW Radar Systems	344
APPENDIX B - Phase and Frequency Noise	352
APPENDIX C - Ambiguity Function of Sine-Wave Modulated FM-CW Radar System	354
APPENDIX D - Ionospheric Properties Pertinent to the Propagation Characteristics of Electromagnetic Energy	358
APPENDIX E - Capacity Calculations for Capacity Probe External Circuits	360
APPENDIX F - Target Generated Noise	362
APPENDIX G - The Scalar Near Field for Circular Aperture Antennas	366
APPENDIX H - Thermal Noise Effects on Range Measurement	372
APPENDIX I - Thermal Noise Effects on Range-Rate Measurement	375
APPENDIX J - Multipath Effects on Range-Rate Measurement	377
APPENDIX K - Formation of Swept Null Pattern	381
APPENDIX L - Thermal Noise Effects on Target LOS Determination	385
APPENDIX M - Thermal Noise Effects on Target Yaw and Pitch Determination in the Electronic OMNI System	392
APPENDIX N - Interferometer Angle Noise	395
LIST OF REFERENCES	399

LIST OF FIGURES

	<u>Page No.</u>
1. Comparison of Candidate Docking Mechanisms	3
2. Range Rate Control Laws	6
3. Simplified Control System, Noise Free Case	8
4. Typical Time Plot of Simplified System	10
5. Normalized Phase Plane Plot for Critically Damped Perfect Control System Starting from Rest, Relative to the Target	11
6. Simplified Control System, with Noise	12
7. Sensitivity of Range Rate Error to Measurement Noises, Assuming Perfect Control System with 5Hz Filter	14
8. Coordinate Systems Used by the Simulation	16
9. Range Rate at Impact	19
10. Reaction Jet Location	20
11. Angular Attitude at Impact	21
12. Attitude Angular Rates at Impact	22
13. Lateral and Vertical Offset at Impact	23
14. Lateral and Vertical Translation Rates at Impact	23
15. Heterodyne, Sine-Wave Modulated, FM-CW Radar	27
16. FM-CW Radar Using Modulation Frequency as a Measure of Range	33
17. Frequency Tracking Loop	38
18. Zero Order Bessel Function Squared	41
19. Sine Wave FM-CW Ambiguity Diagram	43
20. Homodyne, Triangular-Wave Modulated FM-CW Radar	44

LIST OF FIGURES

(Cont'd)

	<u>Page No.</u>
21. Transmitted and Received Frequencies Vs. Time	45
22. Mixer Output (Zero Doppler)	45
23. Mixer Output (With Doppler)	46
24. Triangular Wave FM-CW Ambiguity Diagram	48
25. Heterodyne, Sine-Wave Modulated PM-CW Radar	49
26. Heterodyne, Pseudo-Noise, Binary Coded, PM-CW Radar	53
27. Pseudo-Noise PM-CW Ambiguity Diagram	55
28. Heterodyne, Interrupted CW Radar	56
29. ICW Ambiguity Diagram (a) Single Pulse (b) 50% Duty Cycle Repeated Pulses	58
30. Comparison of Range Errors Between FM-CW and ICW Radar System	73
31. Noncoherent Pulse Radar	76
32. Transmitted Signal Autocorrelation Function	78
33. Correlation Coefficients	80
34. Pulse Radar Ambiguity Diagram	81
35. Receiver Noise Effects	81
36. Time Delay Measurement	83
37. Generation of Nanosecond Pulses Using Traveling Wave Tube Amplifier	86
38. Generation of Nanosecond Pulses Using Transistor Switching and Storage Line	87

LIST OF FIGURES
(Cont'd)

	<u>Page No.</u>
39. Generation of Nanosecond Pulses Using an Amplifier Biased Below Cutoff	88
40. Generation of Nanosecond Pulses Using Varactor Diodes	89
41. Generation of Nanosecond Pulses Using Gas TR Tube	90
42. Generation of Nanosecond Pulses Using a Traveling Wave Resonator	90
43. Resonant Ring (Gain Vs. Line Loss)	91
44. In Line SPST Switch	91
45. Generation of Nanosecond Pulses Using Balanced Duplexers	92
46. Cooperative Pulse Radar	94
47. Detection Performance Curves	95
48. Range Accuracy Requirements	96
49. General Ring-Around System	100
50. Transponder System - Single Antenna Operation	102
51. A Docking Transponder	103
52. Magnetic Probe-Equivalent Circuit	107
53. A Monostatic Antenna Impedance Probe	109
54. A Low Directivity Probe	111
55. Multiple Antenna Probes	111
56. Return Signatures	112
57. Rotation Rates from Return Signature	112

LIST OF FIGURES
(Cont'd)

	<u>Page No.</u>
58. Electrostatic Field Representation for Double Electrode System	114
59. External(Probe)Capacities for Double Electrode System	115
60. Capacity Probe Bridge	116
61. RF External Capacity Sensor	117
62. Use of Multiple Capacity Probes in Close Approach	118
63. Spatial Considerations in Photomixing	121
64. ICW Optical Radar-Pulse Ranging and Doppler Range Rate Using Noncoherent Source	127
65. Comparison of Full-Wave Square Law Detector and Linear Detector in Presence of Noise Carrier	129
66. Possible Effects of Path Length Differences in Microwave Modulated Optical Radar	130
67. Comparison of Relative System Weights for Various Optical Radar Systems	134
68. Comparison of Relative System Complexity as a Function of Range Accuracy Capability for Various Optical Radar Systems	135
69. Comparison of Relative System Complexity as a Function of Range Rate Accuracy Capability for Various Optical Radar Systems	136
70. Comparison of Relative Complexity for Combined Range and Range Rate Accuracy Capabilities for Various Optical Radar Systems	137
71. Normalized Nuclear Ranging Accuracy	141
72. Shielding Curve	142
73. Temperature Dependence of Recoilless Emission	146

LIST OF FIGURES
(Cont'd)

	<u>Page No.</u>
74. Mossbauer Resonant Detection Criteria	148
75. Number of Transverse Counts Required as a Function of the Degree of Mossbauer Effect	150
76. Rotating Wheel Velocity Detector	151
77. Range-Rate Detection System Using the Rotating Wheel	152
78. Slanted Belt Velocity Detector	153
79. Counts Required to Hit Absorber for Range-Rate Measurement	156
80. Maximum Operating Range for a Given Source Size	157
81. Increase in Source Size Due to Non-Optimum P_D	158
82. Angle Sensing Accuracies for Various Techniques	161
83. Sum and Difference Amplitude Monopulse	162
84. Null Depth Vs. RF Phase Unbalance	164
85. Decrease in Amplitude Sensitivity Near Boresight	165
86. Boresight Shift Due to Amplitude Unbalance	166
87. Conical Scanning Radar	169
88. Sequential Lobing Radar	170
89. Error Signal Conical Scan	171
90. Error Signal Sequential Lobing	171
91. Characteristic Accuracy Curves	172
92. Biconical Horn	174
93. Biconical Horn Phase Measurement	175
94. Multipath Error	178

LIST OF FIGURES
(Cont'd)

	<u>Page No.</u>
95. Interferometer: Propagation Path Length-Phase Relationship	179
96. Phase Angle Detection	180
97. Sum and Difference Angle Detection	180
98. Phase Measurement of the Modulation Envelope	181
99. Near Range Geometry	183
100. Antenna System for Phase Sensing	186
101. Block Diagram of Basic Monopulse System	186
102. Boresight Shift Resulting from Precomparator Phase Shift for Various Antenna Spacings	189
103. Loss of System Sensitivity Due to Channel Voltage Unbalance	191
104. Loss in Detector Sensitivity Due to Phase Differences from LO to Channel Mixers	193
105. Fixed Coded Reflectors	196
106. Mechanical Attitude Aid	196
107. Timing of Signal Return	197
108. Time Elapsed Between Pulses Vs. Azimuth Angle Off Boresight	198
109. Computation of Reflected Energy Vs. Aspect Angle	199
110. Amplitude Pattern of Reflected Energy	200
111. Module for Decoding the Signal Return-Electromechanical Aid	201
112. Attitude Coding by Orthogonal, Polarized, Moving Reflectors	202
113. An Electromechanical Attitude Aid	203
114. Module for Decoding the Signal Return from Mechanical Aid	204

LIST OF FIGURES
(Cont'd)

	<u>Page No.</u>
115. Target Attitude by Squinted Broad Beam Antennas	206
116. Amplitude Comparison	206
117. Variation of Amplitude Ratios as Functions of the Target Attitude Angles	207
118. Amplitude Ratio as a Measure of Target Attitude	208
119. Superimposed Contour Plots of Four Antennas Squinted 45° with Roll Axis	209
120. Squinted Broad Beam Antenna Crossover Patterns	211
121. Multipath Error Effects	212
122. Null Sweeping Using a Phase Shifter	214
123. Phase Shift - Pattern Null Relationship	215
124. Time Elapsed - Reference Burst to Pattern Null	216
125. Spot Diameter Vs. Range	220
126. Sequential "Painting" Radar	221
127. Imaging System Geometry	226
128. Imaging Lens System	227
129. Range Resolution Cell	228
130. Target Signatures	230
131. Sequential "Painting" Radar	232
132. Imaging Lens System	233
133. Angle Track-Doppler Sample Docking Radar System	234
134. Short Pulse-Doppler Docking Radar System	235
135. Target Size Accuracy	237

LIST OF FIGURES
(Cont'd)

	<u>Page No.</u>
136. LOS Angle Accuracy	238
137. Velocity Components	241
138. Noncooperative Docking Radar	248
139. Antenna Operation Chart	250
140. Beam Selection Switch	253
141. A Switching Element	254
142. A Solid State 70 GHz Transmitter	255
143. Near Range Measurement by Measuring the Phase of the Modulation Fundamental Frequency	256
144. Phase Measurement Time Relationship	257
145. IF Output Envelope	259
146. Degraded Phase Range Relationship	260
147. Video Range Measurement System	261
148. Signal Feedthrough Relationships	262
149. Range Accuracy	264
150. IF Spectrum $R \ll 100$ Feet	265
151. Doppler Measurement Techniques	267
152. Angle Accuracy - Multiple Beam - Angle Track Radar	269
153. Typical Target Attitude Sensing Accuracies	272
154. Typical LOS Performance Characteristics	273
155. Fixed Coded Reflectors	274
156. IPS Docking (and Rendezvous) System	276

LIST OF FIGURES

(Cont'd)

	<u>Page No.</u>
157. EOS Docking and Rendezvous System	277
158. Docking Alignment System - Target Sensing	278
159. Antenna Configuration for Docking Alignment System - Target Sensing	279
160. Range Errors CW, 4 Tone, Radar	282
161. IPS Transponder	283
162. IPS Range, Range Rate and Angle Reference Circuits	285
163. IPS Switching Circuits	287
164. IPS Sample - Hold and Phase Comparison Circuits	288
165. IPS Angle Receiver (B)	289
166. Docked Antenna Configuration	290 & 303
167. EOS-LOS Interferometer System	310
168. Target Craft	311
169. Attitude Angle Receiver	312
170. IPS-EOS Measurement Error Comparisons	313
171. Roll Pair Null Sweep Relationship	323
172. Target Attitude Effects on Relative Roll Measurements	325
173. EOS-LOS Measurement System	328
174. Electromagnetic Measurement System Design Parameters	332
175. Schedule - Nuclear System Program	337
176. Schedule - Antenna Probe System Program	338

LIST OF FIGURES
(Cont'd)

	<u>Page No.</u>
177. Schedule - Noncooperative Docking Radar Program	339
178. Schedule - Cooperative Docking Radar Program	342

LIST OF TABLES

	<u>Page No.</u>
1. Survey of Impact Tolerances	5
2. Nominal Noise Power Spectral Densities	18
3. Sensor Accuracy - Areas of Interest	24
4. Summary of the Characteristics of Sine-Wave Modulated FM-CW Systems	43
5. Summary of CW Radar Characteristics	75
6. R F Switch Comparison	92
7. Ring-Around Performance Characteristics	106
8. Scan Rate Requirements	219
9. Target Tumble - Doppler Relationships	223
10. FM Noise Reduction Factor	225
11. Spot Diameter Vs. Range	234
12. Rotation Axis Accuracy Vs. Spot Range	240
13. System Complexity	243
14. Measurement Technique	244
15. Performance Comparison	245
16. System Complexity	246
17. Switch Terminal Relationships	254
18. Range Measurement - Leading Edge-Trailing Edge Comparison	260
19. Discriminator Vs. Phase Lock Comparison	267
20. Cooperative System Characteristics for Various Degrees of Target Cooperation	271

LIST OF TABLES
(Cont'd)

	<u>Page No.</u>
21. Target - Chasecraft Frequency Relationships	293
22. RFI Considerations	295
23. Summary of Ranging Parameters	299
24. IPS-RMS Angular Errors Near Boresight	309
25. Summary of Yaw and Pitch Angular Errors	322
26. Summary of Roll Measurement Errors in the Electronic OMNI System	327
27. Summary of LOS Angular Errors in the Electronic OMNI System	330

SYMBOLS

B	bandwidth
c	velocity of light
e	voltage
E	energy in received pulse
\vec{E}	electric field
f	fraction of total emissions which are recoilless
f'	fraction of total captures which are recoilless
f	frequency
G	gain
\vec{H}	magnetic field
I	nuclear counts
J	current density
k	Boltzman's constant
L	system losses
n	instantaneous noise voltage
NF	noise figure
N ₀	noise power spectral density
N	noise power spectral density of parameter in watts/Hz
P	power
R	range
S	signal power.
T, t	time

T	temperature
v	velocity
V	voltage
β	phase modulation index
Γ	Mossbauer radiation line width
δ	rms error
ϵ	error, difference
λ	wavelength
σ	radar cross section
σ	standard deviation
τ	time
ϕ	phase angle
$\psi(\tau, \omega)$	ambiguity function
ω	$2\pi f$

A dot over a variable indicates derivative with respect to time; two dots denote a second derivative with respect to time.

IEEE recommendations have been followed in the designation of units throughout this report (reference 1).

INTRODUCTION

The Gemini program has demonstrated that docking can be accomplished by the use of visual observation and manual control, after rendezvous has been completed. However, many future spacecraft require tighter control of terminal conditions in operational situations which preclude direct visual monitoring of the contact area. The Gemini spacecraft and the Agena docking adapter were designed to function properly under a range of terminal conditions which are readily achieved by manual control; whereas spacetugs, for example, will be required to handle fragile structures requiring significantly less velocity at contact. The attainment of more precise control of docking terminal conditions (or of any docking control in unmanned spacecraft) requires a combination of sensors and displays or automatic control. The Electromagnetic Guidance Study, conducted under Contract NAS 12-18 for the NASA Electronics Research Center, had as its main objective the analysis of sensors for this docking application. The docking phase is defined as that portion of a mission between the completion of rendezvous and the engagement of the latching mechanism. The transition from the rendezvous phase to the docking phase is defined, for the purpose of this report, to occur when the chasecraft is within range of the docking sensor and has reduced relative velocity to the point where differential gravity is negligible.

The study was divided into four overlapping phases - analyses of requirements, of measurement concepts, of communication concepts, and of sensor systems.

The definition of sensor requirements and study constraints required analyses of mission requirements, control systems, and operational considerations. The study area receiving major emphasis was Task II, Measurement Concepts, in which capabilities and limitations of known applicable sensors were investigated. The evaluation of the sensors in a communications mode was a secondary objective; results of that effort were merged with the Task II data and presented in two sections of the report: Range and Range Rate Measurement Techniques and Angle Measurement Techniques.

Since the optimum combination of sensors and control logic is obviously a function of the specific mission requirements for a specific spacecraft, and since this study was not constrained to specific missions, the sensor systems described in the sections on integrated systems are only representative of those which might be required. Thus they serve to illustrate the application of the data developed during the study and to indicate fruitful areas of applied research, which are outlined in the Conclusions and Recommendations sections.

REQUIREMENTS

The Electromagnetic Guidance Study conducted under Contract NAS 12-18 had as its objective the analysis of electromagnetic radiators to determine their applicability to docking procedures of space vehicles. Investigations included (a) the resolution and accuracy which can be attained in measuring the relative positions and attitudes of two spacecraft and (b) the possibility of transmitting intelligence via the same electromagnetic radiators. The lack of restrictions as to types of space missions to be studied required that the Contractor establish broad bounds on the study. Missions requiring docking were identified and analyzed to evaluate the effect of their characteristics on sensor requirements. Sensitivity factors were determined by considering typical guidance and control configurations, and analyzing their transfer functions. The analysis showed that sensor performance requirements are very dependent on specific mission constraints, and that sensors having capabilities falling anywhere within broad performance bounds must be considered to be potential candidates for one or more mission applications. This section presents the results of these analyses, indicating the role of mission requirements, structural characteristics, and control system characteristics in establishing docking sensor requirements.

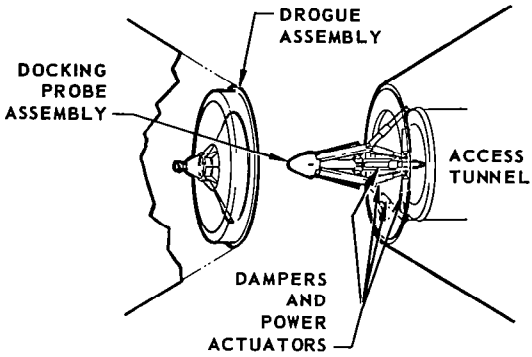
MISSION CONSIDERATIONS

Most major space systems of the future require a docking maneuver during an operational phase. The requirement is obvious for spacecraft performing missions such as lunar or planetary exploration, orbital assembly, logistics supply, satellite inspection, and orbital repair. Other spacecraft also occasionally require docking capability for emergency situations, rescue operations, etc. In selecting operational procedures, displays, and navigational sensors to be employed, certain parameters evolve from mission considerations, as discussed in the following paragraphs. These parameters are categorized by descriptors such as:

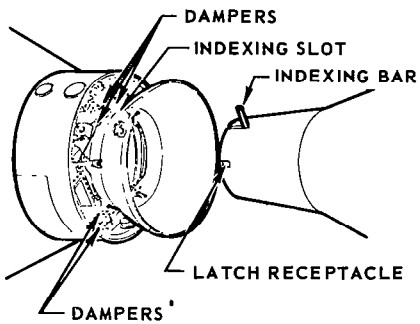
- a. Level of cooperation by the mating spacecraft.
- b. Availability and participation of man in the loop.
- c. Amount of fuel and time available for the docking phase of the mission.
- d. Availability of docking mechanisms (couplers, shock absorbers, etc.)
- e. Availability of electrical power.
- f. Mission duration and reliability requirements.

Orbital assembly operations include many types of rendezvous and docking situations. The optimum distribution of sensors and cooperative devices is a function of the number of parts to be assembled. When two bodies are to be joined in orbit (e.g., a spacecraft with a new booster for a lunar mission), the optimum configuration may include an approximately equal amount of docking equipment in each; whereas when one spacetug must gather and assemble many subassemblies in space, a more sophisticated set of docking sensors can be justified aboard the spacetug to minimize the subsystem requirements aboard the more numerous subassemblies. However, some orbital assembly problems are significantly simplified if the subassemblies have provisions for automatically latching together before the assembly crew arrives; therefore, the orbital assembly mission also has a potential requirement for an unmanned docking capability. In general, it is expected that docking mechanisms will be used (see figure 1), and that the level of cooperation designed into the system will be adequate to avoid the stringent requirements imposed by some of the less cooperative systems. Stabilization and control techniques used may be quite varied; but, in general, docking time will not be overly critical; i.e., docking within a few minutes will usually be satisfactory.

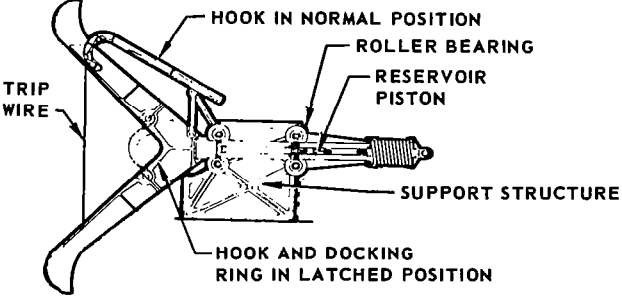
APOLLO PROBE AND DROGUE



GEMINI - AGENA MATING CONES



MCDONNELL RING AND FORK



MENASCO RING AND RADIAL ARMS

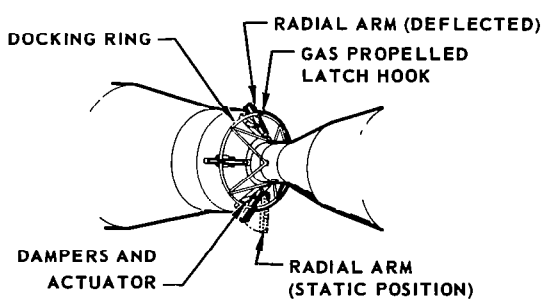


FIGURE 1 - COMPARISON OF CANDIDATE DOCKING MECHANISMS

Logistics supply operations impose few additional requirements on the docking sensor, over those mentioned above. It is reasonable to expect, however, that some situations will be encountered in which provisions for resupply have not been included. These require greater precision in controlling the docking maneuver.

Satellite inspection requirements introduce a further complication to a class of docking requirements - that of docking with an unknown object having unknown motions without exposing a human to danger. This mission requires that an unmanned spacecraft sense the entire set of target parameters (relative attitude, position, velocity, and physical characteristics) without relying on cooperation of the target. Furthermore, to avoid damage to the other spacecraft, control of terminal conditions must be very precise.

Rescue operations can be expected to include nearly all of the docking requirements of the other missions at one time or another, except for the fact that they will be predominantly manned. Docking time will normally be critical, but a few minutes for the final mile might still be acceptable.

The total spectrum of docking situations includes:

- a. Manned and unmanned missions
- b. Various levels of target cooperation
- c. Various levels of attitude control
- d. Various time allowances
- e. Various structural configurations

The variation in structural configuration is particularly significant in that it tends to establish the maximum allowable velocity and misalignment at contact. Velocity and alignment parameters of interest at the time of contact are:

- a. Range Rate - The rate of change of the distance between the spacecraft.
- b. Lateral Displacement - The shortest distance between the center of the chascraft and the extended centerline of the other spacecraft.
- c. Lateral Rate - The rate of change of lateral displacement.
- d. Alignment Angles - The angle between vertical planes passing through the two spacecraft's centerlines and the angle between planes normal to the vertical planes which also pass through the two spacecraft's centerlines.
- e. Angular Rate - The rate of change of the alignment angles.

TABLE 1 - SURVEY OF DOCKING CONDITIONS AT TIME OF CONTACT

PROGRAM	MAXIMUM ALLOWABLE VALUE OF INDICATED PARAMETER AT TIME OF CONTACT				
	RANGE RATE (FPS)	LATERAL DISPLACEMENT (FT.)	LATERAL RATE (FPS)	ALIGNMENT ANGLE (DEGREES)	ANGULAR RATE (DEG/SEC)
GEMINI	1.5	1.5	0.5	10	0.75
MOL	1.5	1.5	0.5	10	0.75
MOD. APOLLO	2.0	1.0	1.0	10	1.00
DOUGLAS MOL	0.5		0.5		0.25
STL DOCKING STUDY	10.0	0.67	0.1	5	
M-2, HL-10	0.2-1.5		0.75	10	1.5
MARTIN SIMULATOR	0.5	0.42	0.1	1	
MRLS	2.0	1.0	1.0	10	1.00
CONCENSUS	0.1-5	0.5-2	0.1-1	5-10	0.25-2

Range rate usually has some nominal negative value at contact to assure closure within an allotted time interval, and a tolerance such that the maximum allowable value will not be exceeded. The other parameters are usually controlled to zero, with plus or minus tolerances. A survey of many current programs, simulation facilities, and earlier studies (see table 1) indicates the wide range in which these maximum allowances tend to fall. For example, some spacecraft need range rate control to within ± 0.1 fps, while others can tolerate ± 5 fps. The sensitivity of sensor requirements to these tolerances is obviously a function of the guidance and control system. Typical guidance and control systems are discussed in the following section to establish levels of sensor performance which might be useful in the various applications.

DOCKING GUIDANCE LAWS

The docking guidance law establishes the nominal relationships between the dynamic parameters (relative attitude, position, and rates of change). The guidance and control system transfer functions determine the actual relationships. The definition of sensor requirements is critically dependent on the selection of docking guidance laws, since they establish the sensitivity of terminal conditions to sensor tolerances.

The guidance law for docking in the Gemini program is determined by the astronaut in conformance with the established operational procedures. The typical phase plane plot (figure 2) shows the final range increment being closed at a fixed relative velocity of approximately 0.5 feet per second. This particular control sequence was selected after considering the ability of man to perform the docking maneuver (reference 1), the ease in providing a docking mechanism capable of withstanding the impact conditions, and various control system characteristics.

Other manned spacecraft will be faced with other constraints, as discussed earlier under mission considerations, and may require additional displays during the docking operation. Television can often be used to advantage when visibility is restricted. Extremely tight tolerances on impact conditions may require precision indication of spatial data and, in some cases, automatic control. The guidance law will be modified to take advantage of these differences, maximizing performance within the constraint of adequate safety margins to provide for measurement and control tolerances.

The degree of target cooperation is an important consideration in establishing the performance of sensors (the use of transponders and data links), but is also significant in establishing the guidance law. The best operational sequence for performing docking is obviously a function of target motion, of the controllability of target attitude from the chasecraft, and of

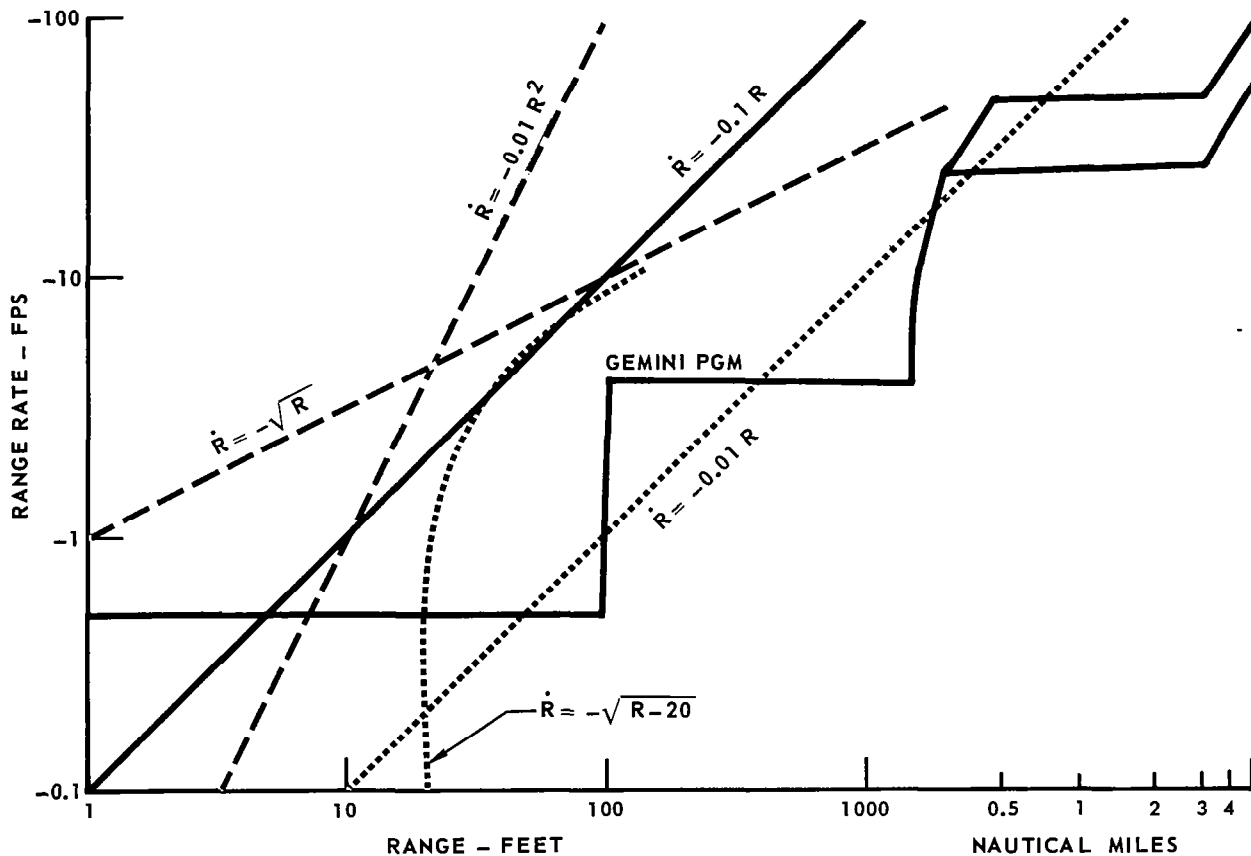


FIGURE 2 - RANGE RATE CONTROLS LAWS

the ability of the target to independently align itself with the docking line-of-sight. Rendezvous to within approximately 100 feet will normally be performed as if the target were a point mass. Docking is simplified for the chasecraft if the target aligns itself to the line-of-sight between the two spacecraft, thus avoiding the requirement for a go-around maneuver and simplifying the guidance law. From a guidance law point of view, an equivalent situation results when the chasecraft commands this type of target attitude control. A different set of guidance laws is required for a go-around maneuver when docking with a stabilized target, and still another for a nonstabilized or spinning target.

The guidance law must obviously be properly mated with the control system. Thruster and torquer parameters (range of variability, if any; start and stop times; predictability; etc.) significantly affect the guidance law tradeoff. On-off control of fixed thrusters tends to yield large variations of impact conditions, but, in some cases, the thrusters can be pulsed to approximate the control capabilities of linear systems having variable thrust.

When docking time is extremely critical, the control law should maintain the maximum closing velocity which can be safely reduced to the desired value at contact. This requires knowledge of the probable errors in the sensors in order to provide adequate but not excessive margins at all times during the maneuver. This approach to docking yields a phase plane plot in which range rate is approximately proportional to the square root of range (see figure 2). Figure 2 also shows the phase plane plots of control laws in which:

- a. The application of constant thrust is timed to stop closure at a range of 20 feet ($\dot{R} = -\sqrt{R-20}$).
- b. Proportional thrust is applied to control range rate to be proportional to range ($\dot{R} = -0.1R$, $\ddot{R} = -0.01R$), resulting in very slow closure as the range approaches zero.
- c. Proportional thrust is applied to control range rate to be proportional to the square of range ($\dot{R} = -0.01R^2$), resulting in extremely slow closure as the range approaches zero.

A range rate bias can be added to the proportional thrust control laws to reduce the time required to close the last few feet, controlling range rate to approach asymptotically the desired impact velocity as the range approaches zero; e.g.,

$$\dot{R} = \dot{R}_{\text{IMPACT}} + KR.$$

Typical Linear Control System

The time plot of range and range rate for the simplified control system shown in figure 3 illustrates factors involved in the selection of reasonable values for a docking system. This control system is representative of those which control range rate to be proportional to range ($\dot{R} = KR$), but is not necessarily optimum for a particular application. The guidance and control law represented in figure 3 is:

$$\ddot{R} + K_2 \dot{R} + K_1 R = 0, \quad (2)$$

where:

R = range, distance between spacecraft,

\dot{R} = rate of change of range,

\ddot{R} = second derivative of range,

K_1, K_2 = system gains, including the mass factor.

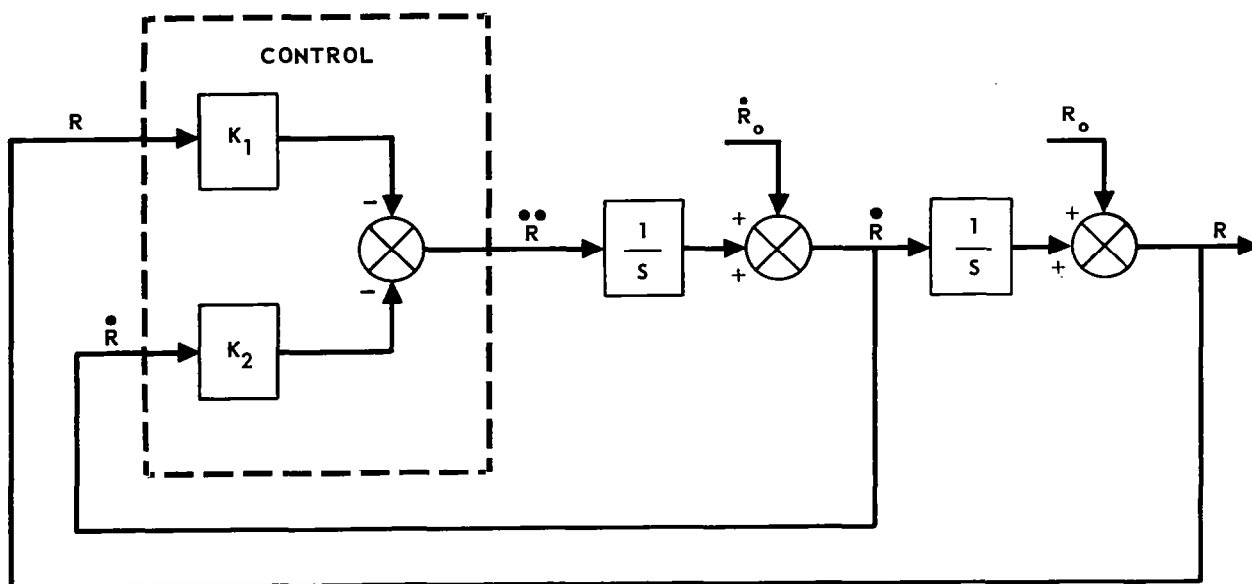


FIGURE 3 – SIMPLIFIED CONTROL SYSTEM, NOISE FREE CASE

Since this control law is initiated at a time which yields a smooth transition from the rendezvous phase, significant transients are not normally encountered. However, to illustrate the transient response of the system, a case in which the system starts from rest at a range of 100 feet is examined. The transfer function with these initial conditions is:

$$R(S) = \frac{R_0 S + K_2 R_0}{S^2 + K_2 S + K_1}, \quad (3)$$

from which it can be shown that the natural frequency is:

$$\omega_n = \sqrt{K_1}, \quad (4)$$

and that the damping ratio is:

$$\zeta = \frac{K_2}{2\sqrt{K_1}}. \quad (5)$$

For the critically damped case ($\zeta = 1$), the transient response is:

$$R(t) = R_0 (1 + \sqrt{K_1} t) e^{-\sqrt{K_1} t}, \quad (6)$$

$$\dot{R}(t) = -R_0 K_1 t e^{-\sqrt{K_1} t}, \quad (7)$$

and from equation 5,

$$K = \frac{\Delta}{K_2} \frac{K_1}{2\sqrt{K_1}} = \frac{1}{2} \sqrt{K_1}. \quad (8)$$

From equations 6 and 7,

$$\frac{\dot{R}(t)}{R(t)} = \frac{K_1 t}{1 + \sqrt{K_1} t} = \frac{4K^2 t}{1 + 2Kt}, \quad (9)$$

$$\frac{\dot{R}(t)}{R(t)} \rightarrow 2K, \text{ when } t \gg \frac{1}{2K}. \quad (10)$$

Figure 4 shows a specific example of this case when $K = 0.1 \text{ sec}^{-1}$, $K_1 = 0.04 \text{ sec}^{-2}$, $K_2 = 0.4 \text{ sec}^{-1}$. Although this represents the noise free case of a perfect control system, it can be seen that the total docking maneuver consumes a time interval of only thirty to fifty seconds, depending on allowable impact velocity, even with these very low gains; and that the bandwidth of the system is quite narrow ($\omega_n = \sqrt{K_1} = 0.2 \text{ sec}^{-1}$). Sensitivity of the system to noise is discussed below. A normalized phase plane plot of this critically damped system with zero initial range rate, figure 5, shows the scaling introduced with changes in K , the ratio of the range and range rate gains.

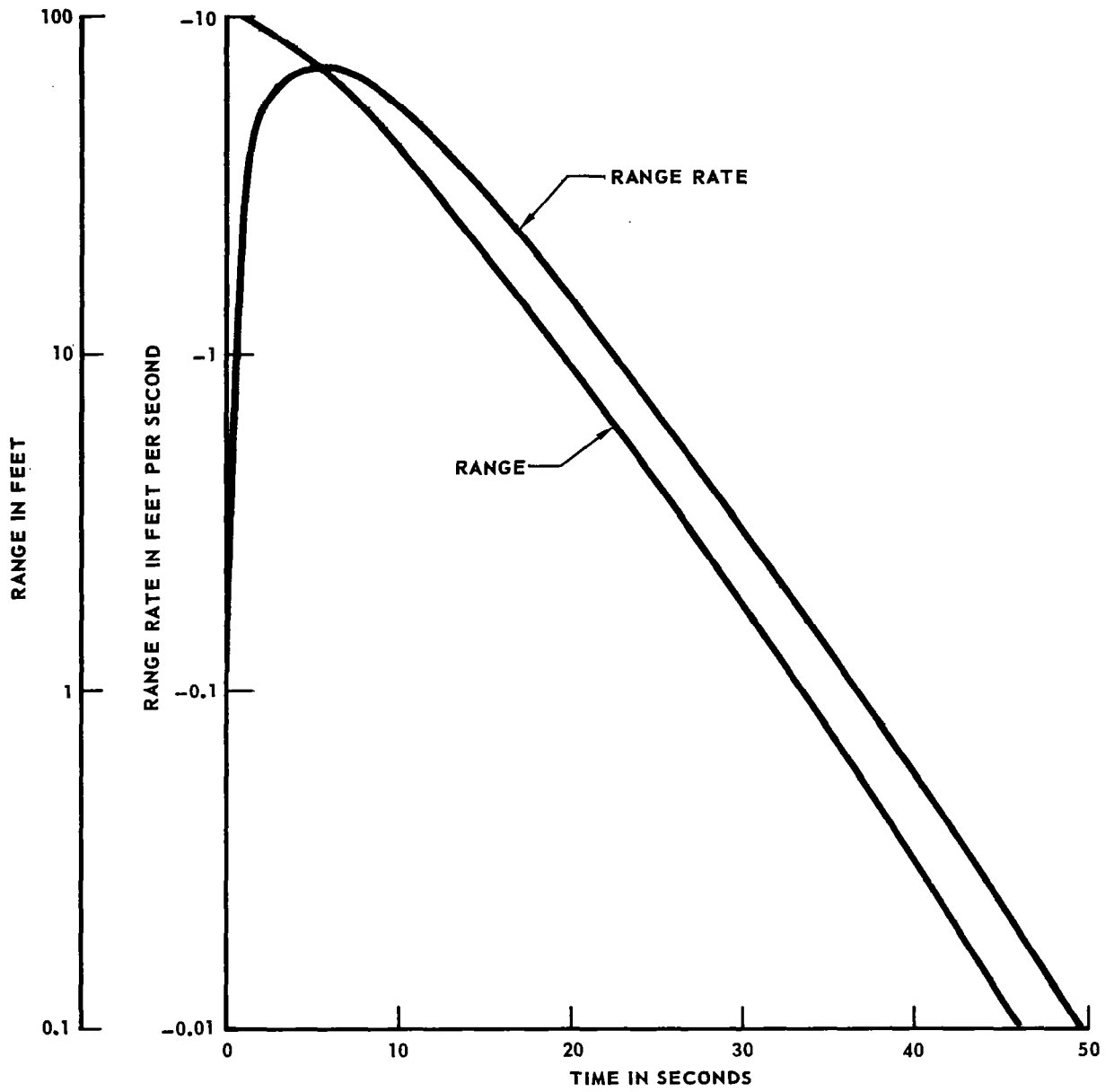


FIGURE 4 – TYPICAL TIME PLOT OF SIMPLIFIED SYSTEM

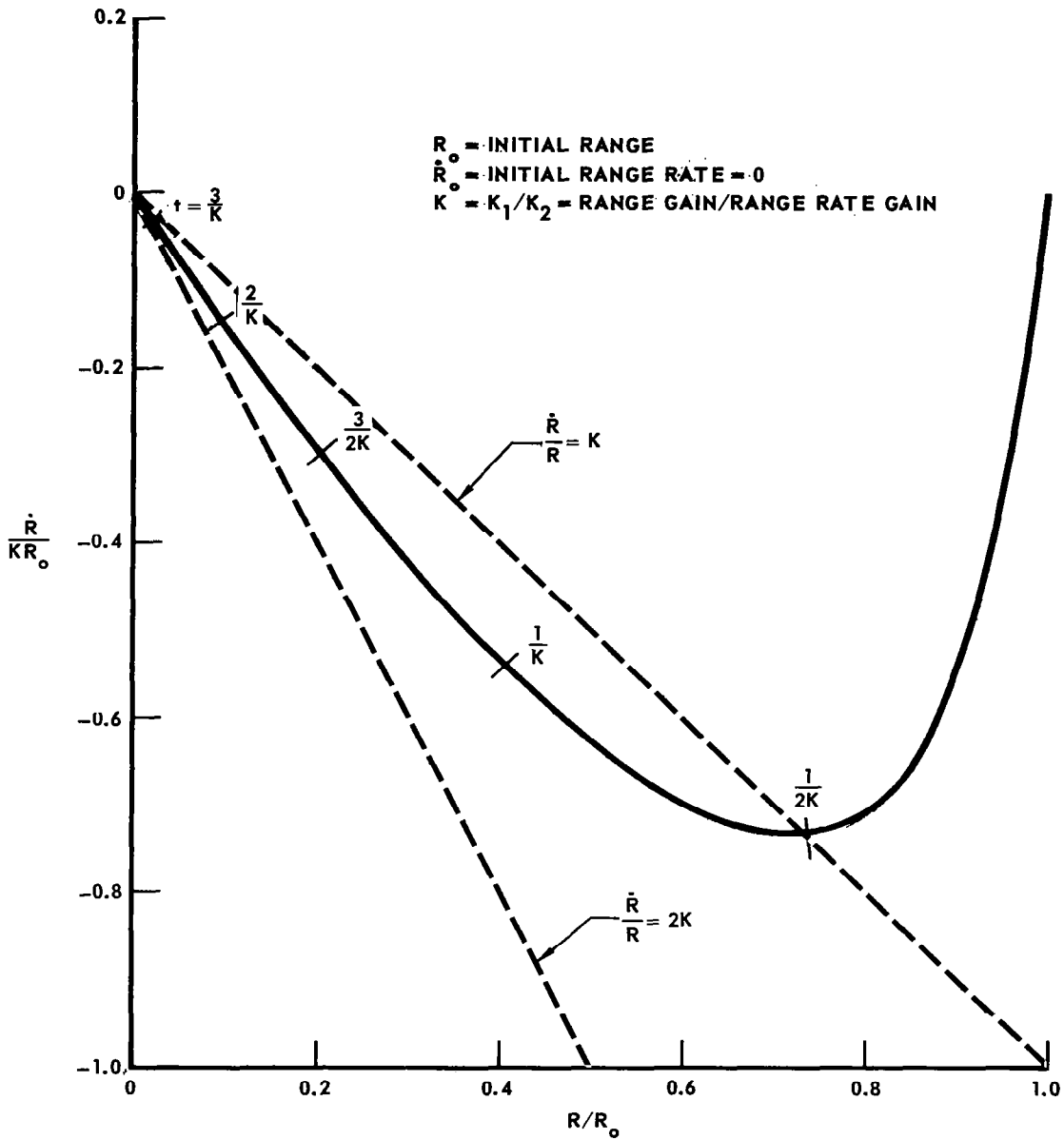


FIGURE 5 – NORMALIZED PHASE PLANE PLOT FOR CRITICALLY DAMPED PERFECT CONTROL SYSTEM STARTING FROM REST, RELATIVE TO THE TARGET

Sensitivity of the Linear System to Noise - Modification of the basic system diagram shown in figure 3, to include noise on the sensors and a filter in the control system leads to the system shown in figure 6, where:

$$\frac{\dot{R}}{N_R}(S) = \frac{-K_1 S}{\tau S^3 + S^2 + K_2 S + K_1}, \quad (11)$$

$$\frac{\dot{R}}{N_{\dot{R}}}(S) = \frac{-K_2 S}{\tau S^3 + S^2 + K_2 S + K_1}, \quad (12)$$

where

τ = time constant of the guidance filter ,

$N_R, N_{\dot{R}}$ = magnitudes of the noise power spectral density, N_0 , in the range and range rate measurements, respectively, assuming $N_0 = N_R, N_{\dot{R}}$ over the positive frequency range of interest.

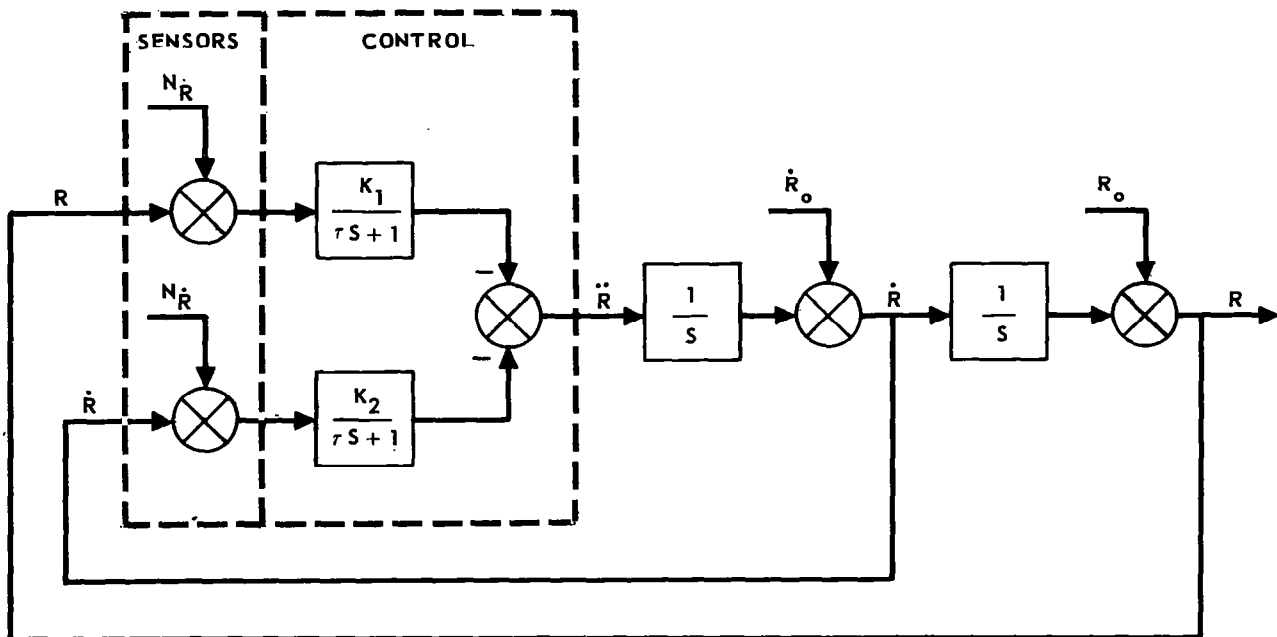


FIGURE 6 - SIMPLIFIED CONTROL SYSTEM, WITH NOISE

The mean square value of the noise output $\frac{\sigma_n^2}{\epsilon_n^2}$ is given by:

$$\frac{\sigma_n^2}{\epsilon_n^2} = \frac{1}{2\pi} \int_0^\infty |G(j\omega)|^2 N_o(j\omega) d\omega, \quad (13)$$

$$= \frac{N_o(s)}{2\pi j} \int_0^{j\infty} G(s) G(-s) ds. \quad (14)$$

Substituting equations 11 and 12 and summing (assuming uncorrelated noise) yields (page 176, reference 2):

$$\frac{\sigma_R^2}{\epsilon_R^2} = \frac{K_1^2 N_R + K_2^2 N_R}{4(K_2 - K_1 \tau)}, \quad (15)$$

where $\frac{\sigma_R^2}{\epsilon_R^2}$ is the mean square value of noise output on the range rate and is equal to the variance, σ_R^2 due to the noise power densities N_R and N_R .

Figure 7 shows the partial derivatives of $\frac{\sigma_R^2}{\epsilon_R^2}$ with respect to N_R and N_R as functions of K_1 and K_2 for $f_c = 5\text{Hz}$. Damping ratios are also shown for reference. It can be seen from equation 15 that τ has little effect on this

noise output unless $K(\frac{\Delta K_1}{K_2})$ is quite large. This was to be expected since the closed loop acts as a narrow band filter:

$$\omega_n = \sqrt{K_1}. \quad (16)$$

Impact Velocity - It should be noted that the mean square value of noise on the range rate, developed above, is added to an exponentially decaying function:

$$\dot{R}(t) = -R_o K_1 t e^{-\sqrt{K_1} t}, \quad (7)$$

and that although the noise is Gaussian, the problem is to find the probability density function of $\dot{R}(t)$ when R first goes to zero. Since there is little probability of R reaching zero until its slope, \dot{R} , has become quite small; the stated problem reduces to the classical zero crossing problem. S. O. Rice (reference 3) has given an analysis of the zero crossing problem for the case of this Gaussian random process. Using his analysis, it can be shown that the probability density function for crossing zero with negative slope is given by:

$$P(0, \dot{R}) = \frac{\dot{R}}{\sigma_{\dot{R}}^2} \exp\left(-\frac{\dot{R}^2}{2\sigma_{\dot{R}}^2}\right) \quad \dot{R} \geq 0, \quad (17)$$

$$= 0 \quad \dot{R} < 0. \quad (18)$$

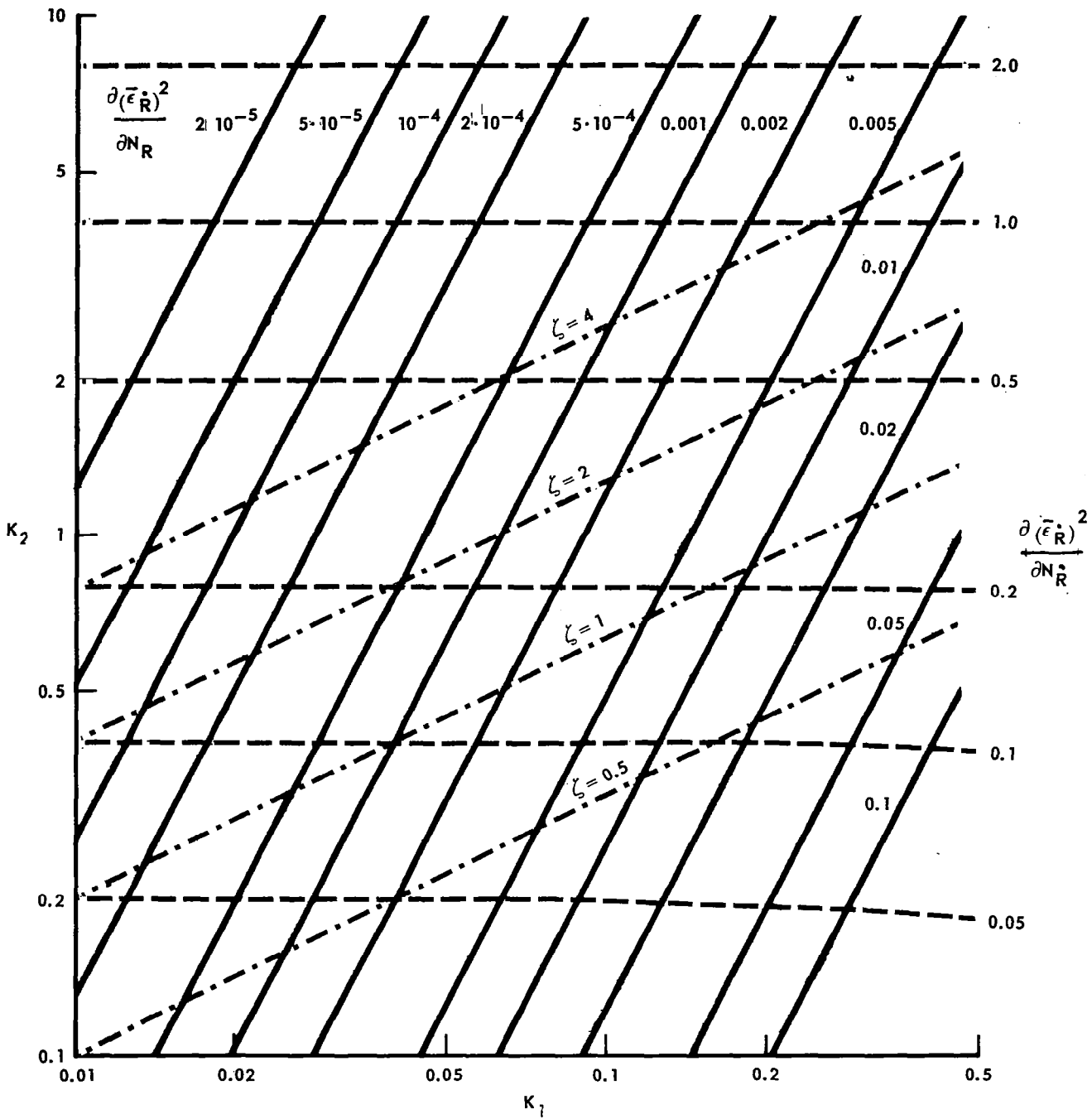


FIGURE 7 – SENSITIVITY OF RANGE RATE ERROR TO MEASUREMENT NOISES, ASSUMING PERFECT CONTROL SYSTEM WITH 5 Hz FILTER

This is the Rayleigh probability density function. The variance of $\dot{R}(\sigma_{\dot{R}}^2)$ is given by the second moment of the noise power spectral density and is equivalent to the values $\frac{2}{\epsilon \dot{R}}$ plotted in figure 7. Although this leads to a slightly higher probable impact velocity (e.g., probability of 0.01 that it will exceed the 3σ value), it is apparent that the wide spectrum, range invariant, noise in the sensors can usually be neglected if the system can be made to approximate this linear control mode. The primary error sources are, therefore, calibration and instrumentation errors which cannot be removed by filtering.

Other state variables can be driven to zero by equivalent guidance and control laws if the ratios of their initial values to final tolerances are equivalent. Otherwise, higher gains can be used to improve their response, or the range rate can be driven to zero with a range offset, be held there until the other state variables are within specified bounds, then be switched back to the impact mode.

Nonlinear Control Systems

The effects of sensor noise on nonlinear control systems are best analyzed by simulation techniques. An analysis of some data derived from a recent analog simulation indicates some of the problems involved in trading off response time, noise filtering, system complexity, and sensor performance against each other.

Analog Simulation - A six degree of freedom analog simulation of the Gemini control system and dynamics was modified to incorporate a guidance and control system which reflects some of the practical problems. The simulation provided for docking a chasecraft (with Gemini attitude and maneuver control characteristics) with an ideally stabilized target. Sensor characteristics and noise and the guidance and control logic were the design variables. The coordinate systems are shown in figure 8. The case investigated was one in which the range, each of the angles shown in figure 8 ($\alpha, \beta, \psi, \theta,$ and ϕ), and their rates of change were sensed in the chasecraft and used to control acceleration in the chasecraft's six degrees of freedom. A linear switching law was selected for the basic guidance, on which variations were made. The control equations were of the form

$$K_1 \dot{R} + K_2 \ddot{R} = E_{\ddot{R}}, \quad (19)$$

where $E_{\ddot{R}}$ represents the \ddot{R} error signal. In accordance with the "on-off" mode

COORDINATES

XYZ – TARGET CENTERED RECTANGULAR COORDINATES

RED – CHASECRAFT CENTERED RECTANGULAR COORDINATES

R LIES ALONG THE LOS

D LIES IN THE Y-LOS PLANE

x,y,z – CHASECRAFT CENTERED RECTANGULAR COORDINATES

x IS THE ROLL AXIS

y IS THE YAW AXIS

z IS THE PITCH AXIS

ψ, θ, ϕ – ORDER OF ROTATION FROM RED COORDINATES

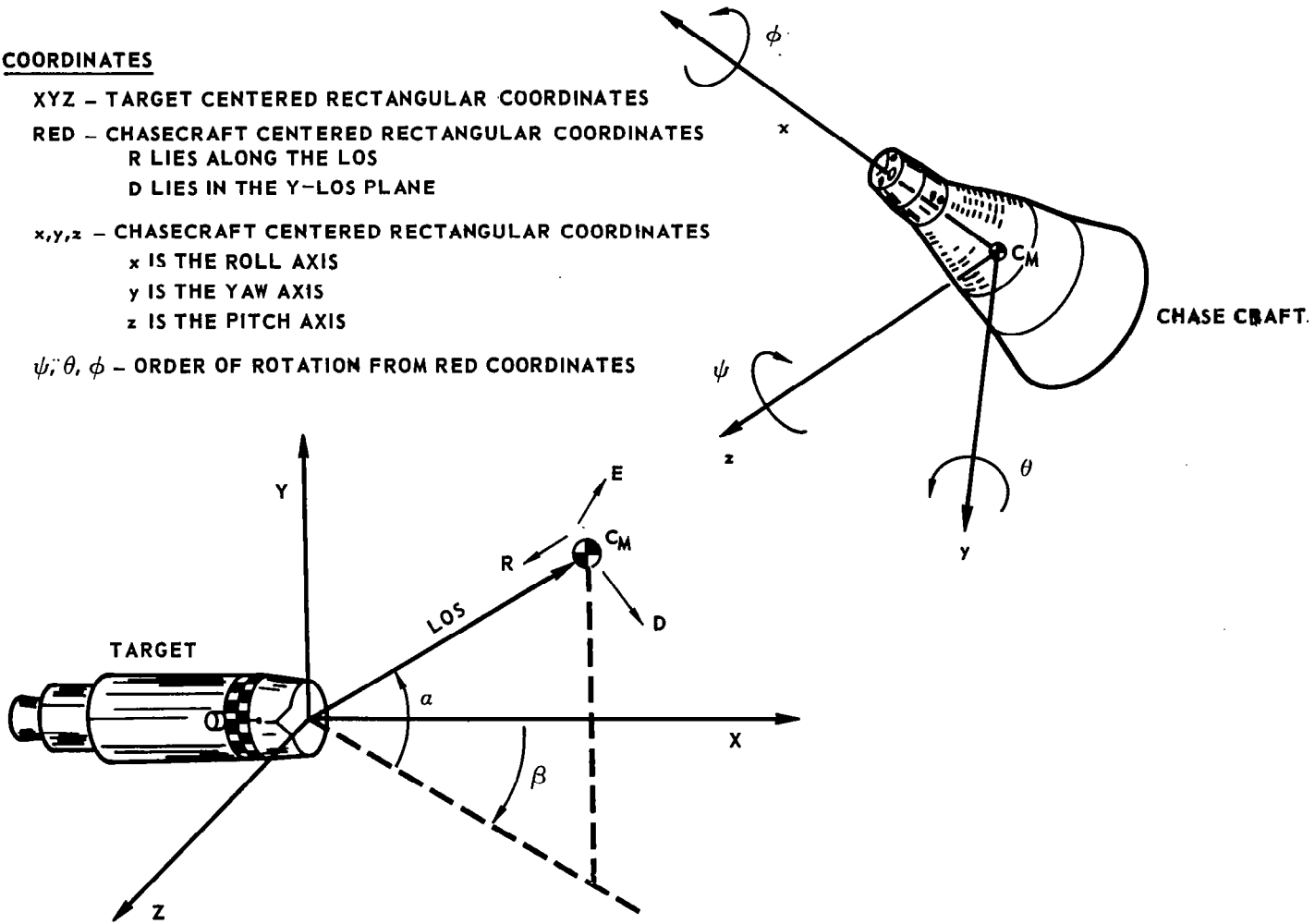


FIGURE 8 – COORDINATE SYSTEMS USED BY THE SIMULATION

of the Gemini control system, the appropriate thruster fires when E_R'' exceeds a specified threshold, known as the dead zone (DZ). Two types of noise, range dependent and range independent, were added to each of the measured variables, which were then passed through a guidance filter. The cutoff frequency of the filter was variable and changed according to the guidance control logic.

The modifications in the guidance laws were based primarily on the trade between filtering the control variable to reduce the noise power and imposing a time lag on the guidance information. To investigate control under very adverse conditions, the following initial conditions were selected for use in the simulation study:

$$\begin{aligned}
 R &= 100 \text{ ft.}, & \dot{R} &= 0 \text{ fps}, \\
 y &= 10 \text{ ft.}, & \dot{y} &= 4 \text{ fps}, \\
 z &= 10 \text{ ft.}, & \dot{z} &= 4 \text{ fps}, \\
 \psi &= 10^\circ, & \dot{\psi} &= 10^\circ/\text{sec}, \\
 \theta &= 10^\circ, & \dot{\theta} &= 10^\circ/\text{sec}, \\
 \phi &= 10^\circ, & \dot{\phi} &= 10^\circ/\text{sec}.
 \end{aligned} \tag{20}$$

Correction of these initial conditions required limiting the initial guidance filtering to approximately 10 Hz, then switching to 5 Hz filtering before glint noise became significant. Three variations on the basic switching laws were investigated:

- a. Home all the way in \ddot{x} , \ddot{y} , \ddot{z} control, using linear switching, changing the guidance filtering from 10Hz to 5Hz at a range of 20 feet, and switching attitude control to a short term inertial reference at a range of 20 feet.
- b. Same as "a" except range is biased to cause predocking at a range of 20 feet, where control loops are allowed a few seconds to settle before closing the remaining distance at a rate of approximately 0.5 feet per second, using

$$E_R \dot{R} = K_2 (\dot{R} + 0.5 \text{ fps}). \tag{21}$$

- c. Same as "b" except all translation thrusters are placed in detent at a given range and attitude control is based on the LOS sensor data all the way (no inertial reference).

Simulation Results - Impact parameters as functions of multiples of a nominal set of noise power spectral densities are shown in figures 9 thru 14. Each datum was computed from nine samples and is shown with its confidence level which was computed from classical sampling equations. The nominal set

of noise power spectral densities, shown in table II, were derived from the assumed variance and bandpass characteristics of a hypothetical set of sensors and assume that the noise is single sided; i.e., considers only positive frequencies.

TABLE 2 - NOMINAL NOISE POWER SPECTRAL DENSITIES

VARIABLE	RANGE SENSITIVE (GLINT)	RANGE INSENSITIVE	UNITS
RANGE	0.16/R	0.016	$\frac{FT^2}{RAD/SEC}$
RANGE RATE	0.16/R	0.004	$\frac{(FT/SEC)^2}{RAD/SEC}$
ANGLES	0.64/R	0.004	$\frac{DEG^2}{RAD/SEC}$
ANGLE RATES	0.64/R	0.004	$\frac{(DEG/SEC)^2}{RAD/SEC}$

Figure 9 represents the mean range rate at impact for the systems studied. Although the performance of these systems could be significantly improved by a more optimum control system, this data illustrates the potential need for very accurate, low noise sensors for some applications. In this case, impact velocities are relatively high for all guidance systems studied. This results from a practical problem - location and orientation of maneuver thrusters. It was found that if the maneuver thrusters were oriented along the y and z body axes of the Gemini spacecraft, the moments produced from thrusting off the center of gravity put an excessive load on the attitude control system. To reduce this load, the thrusters were oriented so that their line of thrust passed close to the vehicle C.G. (See figure 10). This introduced a component of thrust along the + x axis of the body. The α and β channels used in this study limit cycle at short range, hence the translation thrusters continually tend to drive the spacecraft toward the target with increasing velocity while the range/range-rate control channel tries to hold or reduce the impact velocity. This produces a range rate bias, due to system response times, and results in a high impact velocity. Range rate could be controlled to fractions of a foot per second were the translation thrusters oriented along the y and z body axes, or some decoupling thrust programmed into the deceleration thrusters when the translation thrusters are actuated.

The results shown in figures 11 through 14 indicate that there may be promise in using any of a number of homing systems (e.g. Linear switching, Irish Proportional, etc.) to cancel initial condition errors then switch to a short term inertial reference in the R-R channel and the attitude control channels.

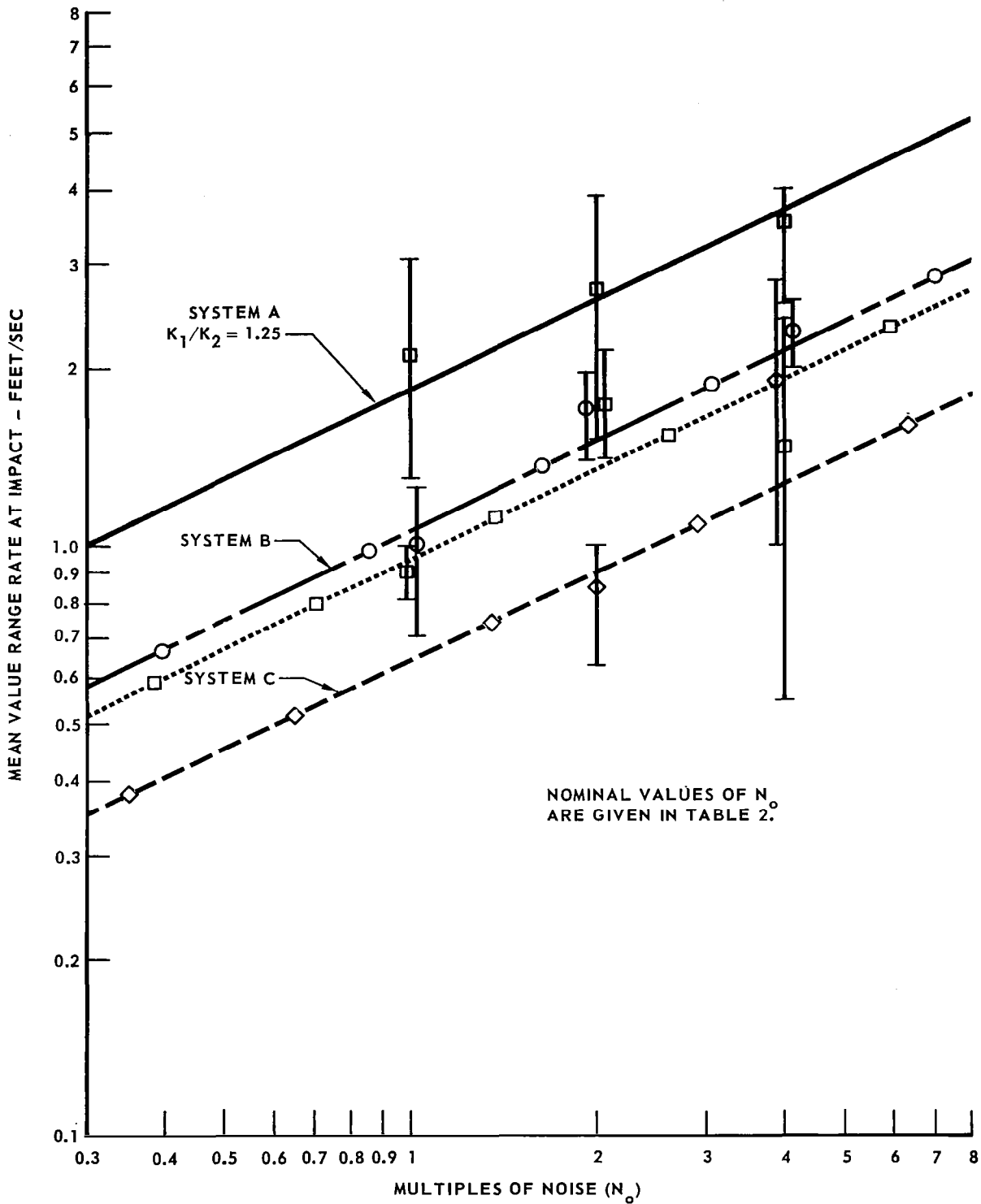


FIGURE 9 - RANGE RATE AT IMPACT

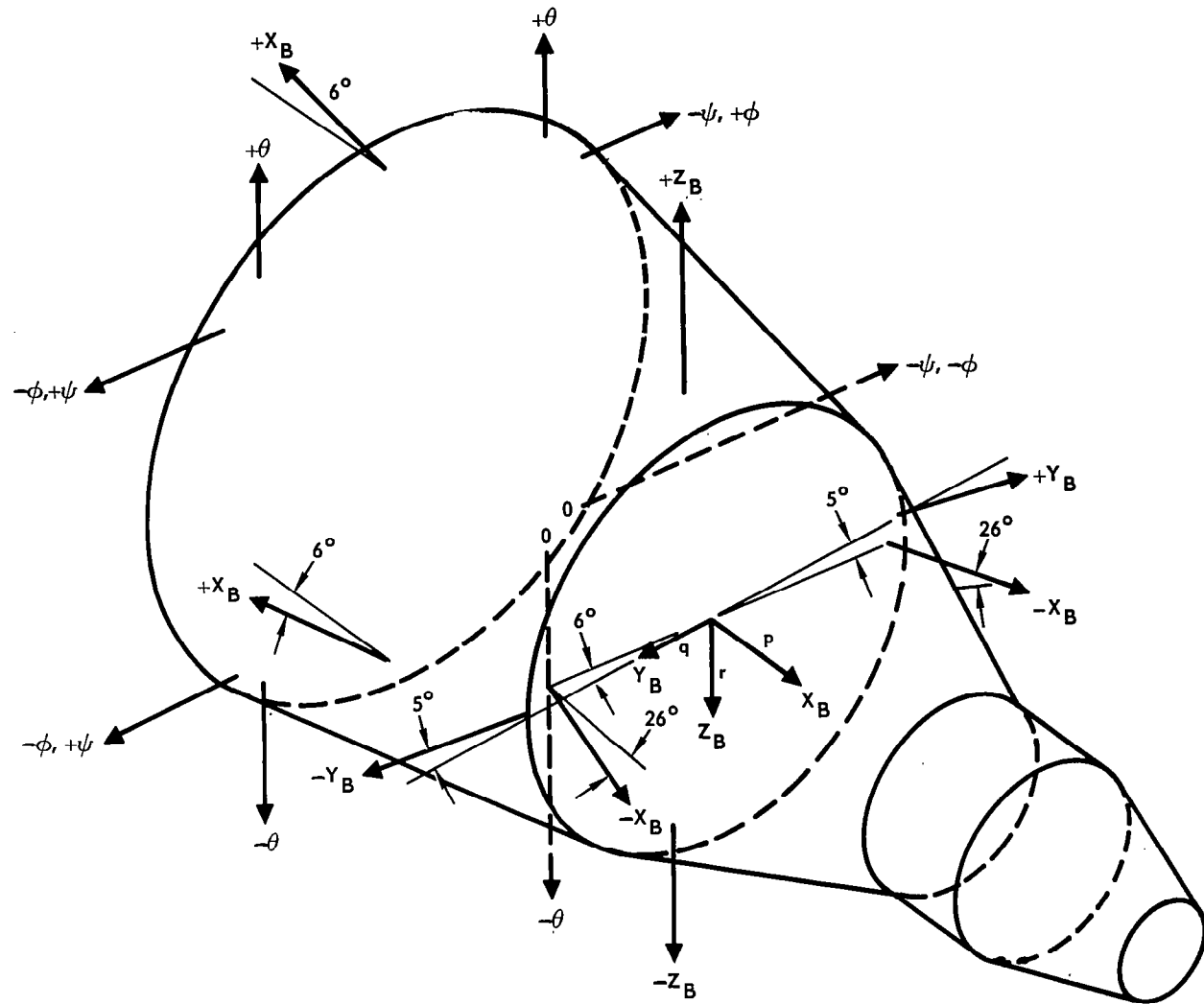


FIGURE 10 - REACTION JET LOCATION

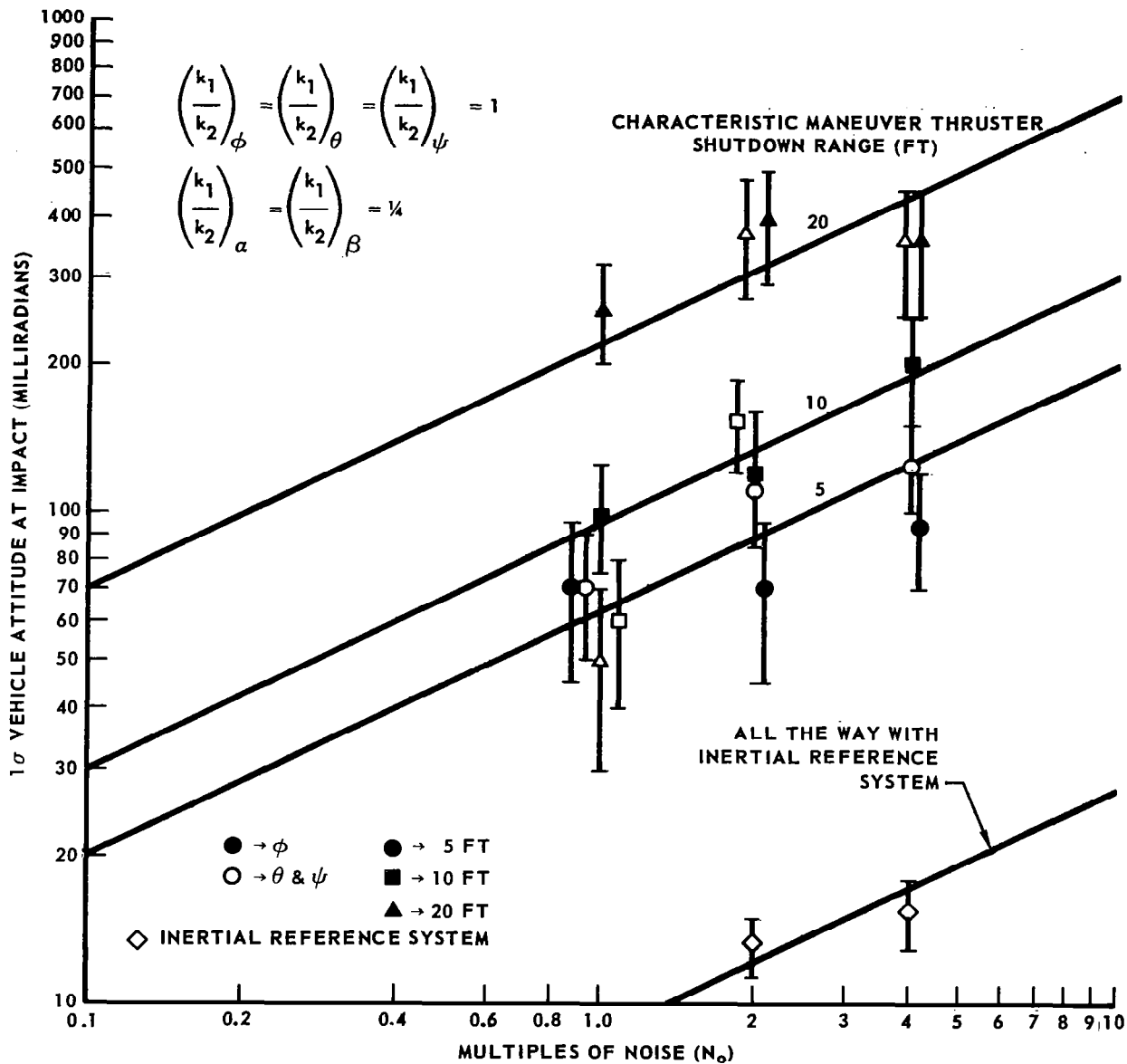


FIGURE 11 – ANGULAR ATTITUDE AT IMPACT

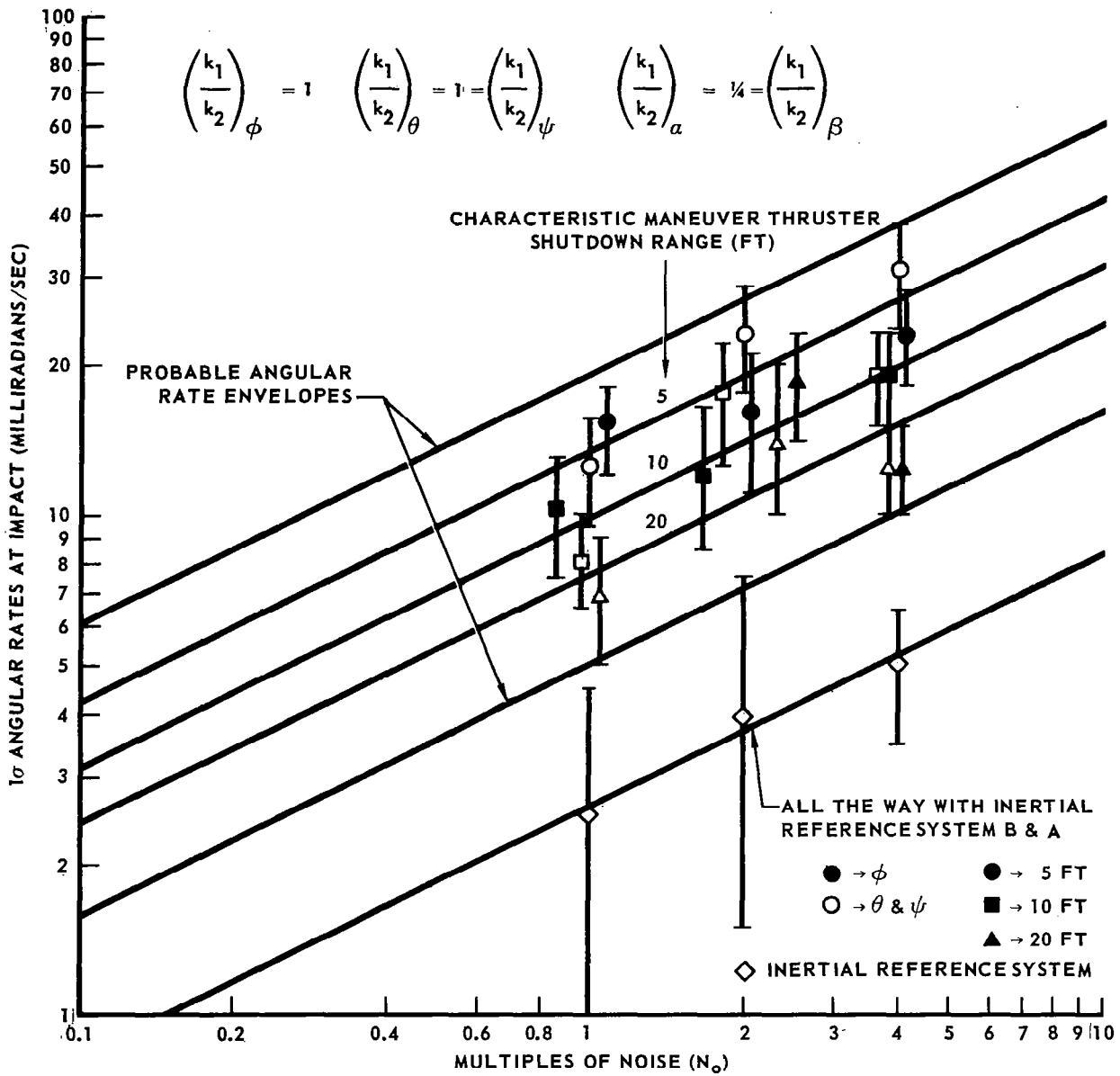


FIGURE 12 – ATTITUDE ANGULAR RATES AT IMPACT

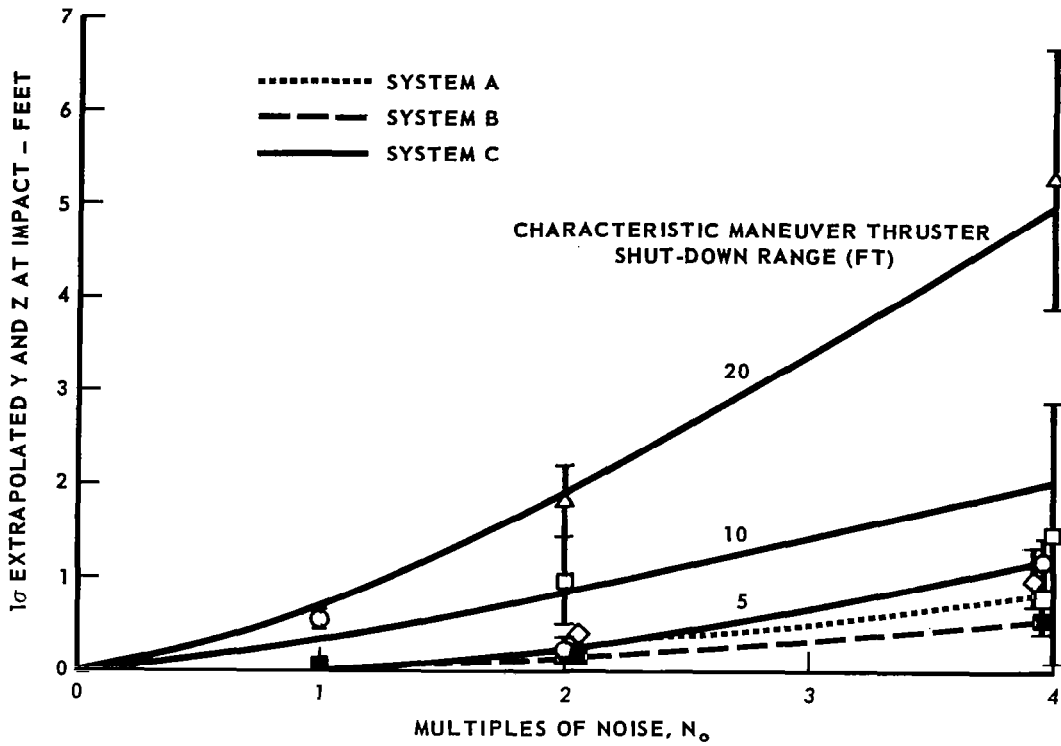


FIGURE 13 - LATERAL AND VERTICAL OFFSET AT IMPACT

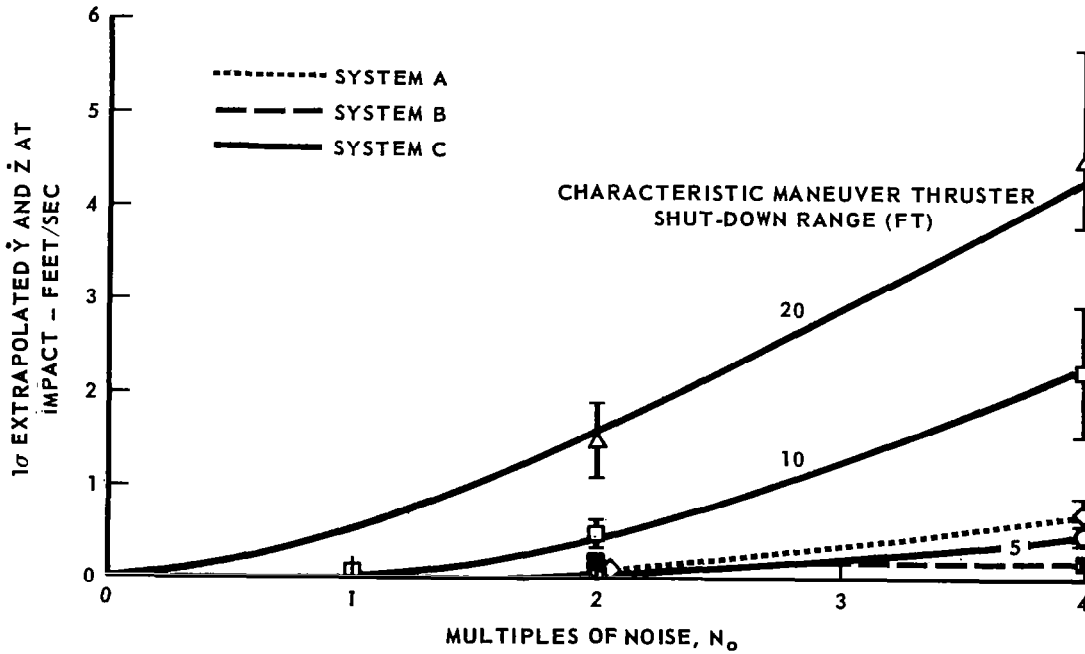


FIGURE 14 - LATERAL AND VERTICAL TRANSLATION RATES AT IMPACT

STUDY CONSTRAINTS

It is clear from the preceding paragraphs that the measurement requirements imposed on docking sensors vary widely as a function of the application. The measurement requirements are determined by (a) allowable terminal conditions, and (b) the sensitivities of these terminal conditions to sensor accuracy. Allowable terminal conditions are very dependent on spacecraft and mission factors, varying from those associated with fragile structures or small latching mechanisms to those associated with heavy structural docking mechanisms which provide for large misalignments. The relationship of achievable terminal conditions to sensor performance has been shown to be dependent on the type of control system, the allowable docking time interval, and the availability of maneuvering fuel. The results of the nonlinear simulation illustrate the need for highly accurate sensors (with low noise spectral densities) for some applications, while the results of the linear analysis indicate that a high noise spectral density does not necessarily disqualify sensors for other applications in which the noise is essentially eliminated by the low pass characteristic of the system transfer function. Since this study was not constrained to specific missions, no significant constraints on sensor performance areas of interest are apparent. An examination of the many potential applications substantiates the early premise that sensors capable of performance anywhere within the broad areas shown in table 3 could be a "best solution" for one of the applications. The remainder of this report therefore considers the characteristics of sensors having limited applicability, as well as those which are suitable for fully automated, precision applications.

TABLE 3 – SENSOR ACCURACY – AREAS OF INTEREST

PARAMETER	ACCURACY REQUIREMENT (1σ)
RANGE (FT.)	0.1–5.0
RANGE RATE (F/S)	0.02–5.0
LOS ANGLE (DEG.)	0.5–10.0
LOS ANGLE RATE (MRAD/S)	0.5–20.0
TARGET ATTITUDE (DEG.)	0.5–10.0

RANGE AND RANGE RATE MEASUREMENT TECHNIQUES

Measurement of range and range rate to the accuracies required during the docking phases of the various missions can be accomplished by many techniques. Radar systems have received wide application for these types of measurements. CW radar systems provide these measurements with low peak powers and have the potential of providing less ambiguity in measuring velocity than pulse radar systems, but suffer from the standpoint of range ambiguities. Pulse radars can provide high resolution nonambiguous range for noncooperative applications. Certain probes offer very high resolution at short ranges. Optical radars show promise of providing these same advantages plus angle resolution, but are in an earlier stage of development. Nuclear techniques, using the Mossbauer effect, can yield range rate accuracies which exceed any known requirements. The capabilities and limitations of these techniques in measuring range and range rate are discussed in the following paragraphs.

CONTINUOUS WAVE (CW) RADAR TECHNIQUES

CW radar systems appear applicable for measuring range and range-rate in both cooperative and noncooperative docking situations. Two types of FM-CW systems are investigated: (1) systems employing sine waves, or tones, to frequency modulate the transmitted carrier, and (2) systems employing the more familiar triangular wave modulation. The two types of phase modulated CW systems considered are those which compare the transmitted and received phases of multiple tones and of a pseudo-noise binary code, respectively. Since an amplitude modulated, interrupted CW (ICW) system with 50% duty cycle has resolution limitations similar to other CW systems, it is also discussed in this section.

For each of these system types, equations for range and range rate errors due to receiver noise are derived; instrumentation errors are discussed; and ambiguity limitations associated with measuring range and range rate are presented. The characteristics of a few CW radars of each type are presented in appendix A. Finally an attempt is made to define the best CW radar techniques for cooperative and noncooperative docking.

Before beginning the discussion of CW radars, it is worth reviewing briefly the classical arguments concerning transmitter to receiver leakage (feed-through) and "step-error".

With cooperative CW radar systems, feedthroughs can be alleviated by utilizing a transponder (beacon) which incorporates a frequency offset. That is, the received signal is translated in frequency by a known amount at the transponder before being transmitted back to the interrogating radar. In this way, the interrogating radar and the transponder are utilizing different frequencies

for transmission and reception, and any transmitted signal that leaks into the receiver is easily eliminated by frequency filtering.

However, transmitter to receiver feedthrough cannot be so easily eliminated in noncooperative systems which rely on the transmitted signals that are reflected directly from the target. Thus, feedthrough and step-error are problems associated with noncooperative applications only.

To set the stage for the discussion that follows, all CW radars can be generally classified into heterodyne or homodyne systems. A heterodyne system utilizes a reference signal for the receiver mixer that is at a different frequency than the received signal, which results in a mixer output at an intermediate frequency (IF). A homodyne system utilizes a receiver reference signal at the same frequency as the received signal. (Usually the reference is a sample of the transmitted signal.) This results in a mixer output signal centered at zero cycles (zero IF).

If the difference frequency (or offset frequency) for the heterodyne system is high enough, it is easy to see that the signal out of the receiver mixer can have frequencies both above and below the offset frequency, depending on whether the received signal frequency was above or below the reference signal frequency. However, with the homodyne system, with zero IF, the frequency of the signal out of the mixer can only be positive with respect to zero. That is, receiver signal frequencies above or below the reference signal frequency must both result in a positive frequency output. This is often called spectrum folding and results in the classical problem of step-error in FM-CW radars which utilize homodyne mixing. The step-error occurs with this type system because of the abrupt phase changes that must take place in the signal out of the mixer when the difference frequency goes from positive to negative. A detailed discussion of step-error is not incorporated here. Step-error is mentioned with regard to triangular wave modulated FM-CW radars in a later section and is well documented in the literature.

The logical alternative to avoid step-error would appear to be to utilize a heterodyne system and avoid the spectrum foldover that causes it. However, before doing this, let us look at the nature of the feedthrough signal for the homodyne system. The homodyne system utilizes a sample of the transmitted signal as the reference for the receiver mixer. Thus, the transmitter to receiver feedthrough signal at zero range has the same frequency as the mixer reference signal throughout the modulation cycle. These two identical signals mixing together result in a mixer output at DC. This feedthrough can be eliminated by adding a simple high pass filter in the receiver, or causing the receiver to have no response to DC.

Now, if a heterodyne system is utilized in order to eliminate spectrum foldover and resultant step-error, feedthrough cannot be so easily controlled. The feedthrough is no longer at DC, but in the center of the IF bandpass. That is, if a sample of the transmitted signal is offset in frequency and used as the reference for the receiver mixer, it will beat with the transmitter leakage to give an output precisely at the offset reference frequency. This is the center frequency of the IF bandpass. Consequently, a very narrow rejection

filter at the IF center frequency is required, which is much more difficult to construct than the high pass filter at DC for the homodyne system. However, synchronous feedthrough nulling techniques have been developed in the past few years for accomplishing this rejection with heterodyne systems. They are well documented in the literature and are mentioned briefly in the paragraph on transmitter-receiver feedthrough considerations.

To simplify discussion of basic CW concepts and their respective error analyses, feedthrough considerations are ignored. Feedthrough is considered primarily in those sections dealing with practical implementation of each technique.

Sine Wave Frequency Modulated Systems

A simple block diagram of an FM-CW system utilizing a sine wave for modulation is shown in figure 15 .

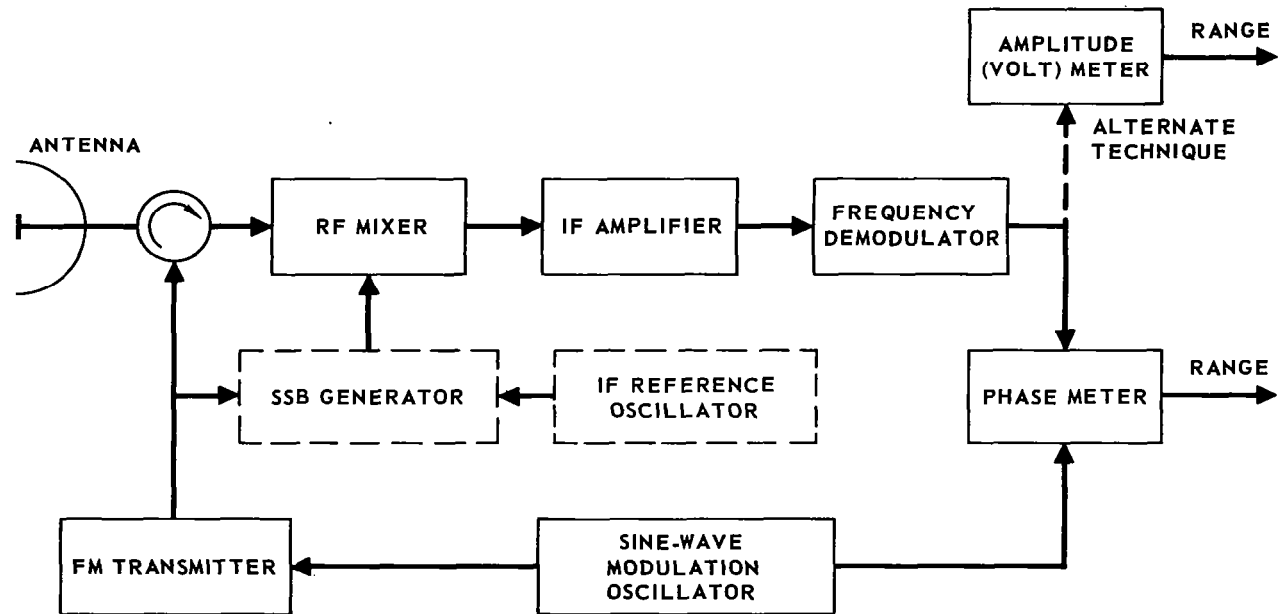


FIGURE 15 – HETERODYNE, SINE-WAVE MODULATED, FM-CW RADAR

The transmitted signal can be represented as:

$$e_t = A \sin[\omega_0 t + \phi(t)],$$

where $\phi(t)$ is the phase modulation of the transmitted signal. The frequency modulation is the derivative of the instantaneous phase modulation (i.e., $\omega(t) = \dot{\phi}(t)$). A portion of the transmitted signal is offset by a frequency ω_{IF} and used as a reference for the receiver mixer. The output of the mixer is the product of the reference offset transmitted signal and the received signal. For a point target at a range $R = \frac{Cr}{2}$, the received signal will be the transmitted signal delayed by time τ , and the mixer output will be $e_o = AA' \sin[(\omega_o + \omega_{IF})t + \phi(t)] \sin[\omega_o(t-\tau) + \phi(t-\tau)]$ which can be shown to be equal to:

$$e_o = \frac{AA'}{2} \cos[\omega_{IF}t - \omega_o\tau + \phi(t-\tau) - \phi(t)] - \frac{AA'}{2} \cos[(2\omega_o + \omega_{IF})t - \omega_o\tau + \phi(t) + \phi(t-\tau)]. \quad (23)$$

The second half of the above expression (at twice the transmitted frequency) is not allowed to pass through the IF amplifier.

Therefore, the signal out of the amplifier can be represented as:

$$e_o' = B \cos[\omega_{IF}t - \omega_o\tau + \phi(t-\tau) - \phi(t)]. \quad (24)$$

Let the coefficient of the frequency modulation of the transmitter be $-K_T$ (the minus sign is typical for a klystron and K_T has units of radians/sec/volt). Since the modulation signal is a sine wave, the frequency of the transmitted carrier due to modulation is:

$$\omega_m(t) = -K_T e_m(t) = -K_T (E_m \sin \omega_m t),$$

and the phase of transmitted carrier is then:

$$\phi(t) = \int \omega_m(t) dt = \frac{K_T E_m}{\omega_m} \cos \omega_m t. \quad (25)$$

Letting $K_T E_m = \Delta\omega$ be the peak frequency deviation of the transmitted carrier, the transmitted phase modulation is:

$$\phi(t) = \frac{\Delta\omega}{\omega_m} \cos \omega_m t = \frac{\Delta F}{f_m} \cos \omega_m t. \quad (26)$$

Therefore, the phase of the signal out of the IF amplifier (due to this modulation) can be represented as:

$$\phi_o'(t) = [\phi(t-\tau) - \phi(t)] = \frac{\Delta F}{f_m} [\cos \omega_m(t-\tau) - \cos \omega_m t], \quad (27)$$

which can be written as:

$$\phi_o'(t) = \left[\frac{2\Delta F}{f_m} \sin \frac{\omega_m \tau}{2} \right] \sin \left[\omega_m \left(t - \frac{\tau}{2} \right) \right]. \quad (28)$$

The signal out of the IF amplifier can now be written as:

$$e_o' = B \cos \left[\omega_{IF} t - \omega_o \tau + \frac{2\Delta F}{f_m} \sin \frac{\omega_m \tau}{2} \sin \left[\omega_m \left(t - \frac{\tau}{2} \right) \right] \right]. \quad (30)$$

The voltage out of the frequency discriminator is proportional to the instantaneous frequency of this signal, i.e., $e_d = K_D \dot{\phi}(t)$. Assuming the discriminator is adjusted for zero output at ω_{IF} :

$$e_d(t) = K_D \frac{d}{dt} \left\{ -\omega_o \tau + \frac{2\Delta F}{f_m} \sin \frac{\omega_m \tau}{2} \sin \left[\omega_m \left(t - \frac{\tau}{2} \right) \right] \right\}, \quad (31)$$

$$= K_D \frac{d\tau}{dt} [-\omega_o + 2\pi \Delta F \sin \omega_m (t - \tau)] \quad (32)$$

$$+ 4\pi \Delta F K_D \sin \frac{\omega_m \tau}{2} \cos \omega_m \left(t - \frac{\tau}{2} \right).$$

Since the time delay $\tau = \frac{2R}{c}$, and $\frac{d\tau}{dt} = \frac{2}{c} \dot{R}$,

$$e_d(t) = - \frac{2K_D \dot{R} \omega_o}{c} + \left[\frac{4\pi K_D \Delta F \dot{R}}{c} \right] \sin \omega_m \left(t - \frac{2R}{c} \right) + \left[4\pi K_D \Delta F \sin \frac{\omega_m R}{c} \right] \cos \omega_m \left(t - \frac{R}{c} \right). \quad (33)$$

Note that there are two sine function terms at the modulation frequency. The amplitude of the first term is proportional to range-rate and the amplitude of the second term is a function of range. It is impossible to separate these terms - which leads to the ambiguity between range and range rate for FM-CW systems (will be discussed later). However, assuming that ω_m is selected so

that $\frac{\omega_m R}{c} < \frac{\pi}{2}$ for the docking maneuver, the relative amplitude of the

two terms is:

$$\frac{\dot{R}}{c} : \sin \frac{\omega_m R}{c} \approx \frac{\dot{R}}{c} : \frac{\omega_m R}{c}. \quad (34)$$

Therefore, if:

$$\dot{R} \ll \omega_m R,$$

the first term due to velocity can be neglected. In the docking maneuver, an attempt is made to keep range rate proportional to range. If the proportionality constant were unity, i.e., $R = \dot{R}$, the closing rate would lead to a most precarious maneuver. However, even in this case a modulation frequency ω_m somewhat greater than unity would allow the above to be satisfied. The modulation frequency will be much greater than unity to satisfy the accuracy requirements as will be seen later.

Therefore, the first term at the modulation frequency due to velocity will be neglected, and the signal out of the frequency demodulator will be considered a sine wave at the modulation frequency:

$$\left[4\pi K_D \Delta F \sin \frac{\omega_m R}{c} \right] \cos \omega_m \left(t - \frac{R}{c} \right), \quad (35)$$

with a fixed DC bias:

$$\frac{-2K_D \omega_o \dot{R}}{c}. \quad (36)$$

Since both the phase and amplitude of the signal out of the demodulator are a function of range, either can be used to measure range. The accuracies associated with these two measurements will be discussed next.

Range Accuracy. - If the peak value of the signal out of the frequency discriminator is used to measure range, from equation 35

$$E_p = 4\pi K_D \Delta F \sin \left(\frac{\omega_m R}{c} \right). \quad (37)$$

It will be assumed that ω_m is selected for the docking mission so that:

$$\frac{\omega_m R}{c} \ll \frac{\pi}{2}, \quad \text{or} \quad f_m \ll \frac{c}{4R}, \quad \text{in which case:} \quad E_p \approx 4\pi K_D \Delta F \frac{\omega_m R}{c}.$$

Solving for range:

$$R = \left(\frac{c}{4\pi K_D \Delta F \omega_m} \right) E_p. \quad (38)$$

Assuming all noise in the measurement is due to receiver noise that enters through the measurement voltage E_p , the variance in the range measurement is:

$$\sigma_R^2 = \left(\frac{c}{4\pi K_D \Delta F \omega_m} \right)^2 \sigma_{E_p}^2. \quad (39)$$

Since the voltage is the output of a frequency discriminator, the variance of the voltage is proportional to the variance of the frequency of the received signal. From equation B11 of appendix B, the frequency variance is:

$$\sigma_\omega^2 = \left(\frac{2\pi}{\sqrt{3}} \right)^2 \left(\frac{N_o}{S} \right) B_o^3. \quad (40)$$

Where S/N_o is the ratio of carrier power to noise power spectral density at the discriminator input, and B_o is the output noise bandwidth of the frequency discriminator. That is:

$$\sigma_R^2 = \left(\frac{c}{4\pi K_D \Delta F \omega_m} \right)^2 \sigma_{E_p}^2 = \left(\frac{c}{4\pi K_D \Delta F \omega_m} \right)^2 (K_D)^2 \sigma_\omega^2. \quad (41)$$

or

$$\sigma_R^2 = \frac{c^2 B_o^3}{12 (2\pi \Delta F f_m)^2 (S/N_o)} \quad (42)$$

The discriminator bandwidth B_o must be made equal to or greater than the modulation frequency f_m in order to pass the modulation. Making $B_o = f_m$;

$$\sigma_R^2 = \frac{c^2 f_m}{12 (2\pi \Delta F)^2 (S/N_o)} \quad (43)$$

This error can be reduced by further filtering of the range signal (the voltage that represents the peak amplitude of the received modulation). If the smoothing bandwidth is B_s , the variance in the final range measurement is:

$$\sigma_R^2 = \frac{c^2 B_s}{12 (2\pi \Delta F)^2 (S/N_o)} \quad (44)$$

If the phase of the signal out of the frequency discriminator is used to measure range, from equation 35 :

$$\theta = \frac{\omega_m R}{c}, \quad (45)$$

or:

$$R = \frac{c}{2\pi f_m} \theta, \quad (46)$$

and the variance of range is:

$$\sigma_R^2 = \left(\frac{c}{2\pi f_m} \right)^2 \sigma_\theta^2, \quad (47)$$

where σ_θ^2 is the variance in the phase of the frequency modulated signal.

To find the variance in the phase of the frequency modulation, the instantaneous frequency of the carrier must first be considered. From appendix B, the output of the discriminator with no frequency modulation has a frequency noise

power spectral density of $\eta_\omega = \frac{d}{df} N_\omega = K_D^2 \left(\frac{\omega^2 N_o}{2S} \right)$. The frequency

modulation signal at the output of the discriminator is represented by equation 35, and can be assumed to add linearly to the frequency noise at the output of the discriminator. Using the same method employed in appendix B, let the discriminator output be represented as the sum of the modulation signal and a noise component:

$$n(t) = A_n \cos \omega t. \quad (48)$$

That is:

$$e_d(t) = A_m \cos(\omega_m t - \theta) + A_n \cos \omega t, \quad (49)$$

where:

$$A_m = 4\pi K_D \Delta F \sin \frac{\omega_m R}{c}. \quad (50)$$

and

$$\frac{A_n^2}{2} = \eta_\omega df = \left(\frac{K_D^2 \omega^2 N_o}{2S} \right) df. \quad (51)$$

By expanding and combining terms, equation 49 becomes:

$$e_d(t) = A_d \cos(\omega_m t - \theta + \theta_m), \quad (52)$$

where:

$$\theta_m = \tan^{-1} \left\{ \frac{A_n \sin[(\omega - \omega_m)t + \theta]}{A_m + A_n \cos[(\omega - \omega_m)t + \theta]} \right\}.$$

θ_m is the phase noise on the modulation signal out of the discriminator which adds to the phase θ to be measured. If one assumes a large signal to noise ratio, i.e., $A_m \gg A_n$, the phase noise of the modulation equation 52 becomes:

$$\theta_m = \frac{A_n}{A_m} \sin[(\omega - \omega_m)t + \theta]. \quad (53)$$

The power in the noise component at frequency $(\omega - \omega_m)$ is:

$$dN_{\theta_m} = \frac{1}{2} \left(\frac{A_n}{A_m} \right)^2 = (\eta_\omega df) \frac{1}{A_m^2}, \quad (54)$$

for

$$\frac{\omega_m R}{c} \ll \frac{\pi}{2}, \quad A_m^2 = \left(\frac{4\pi K_D \Delta F \omega_m R}{c} \right)^2 \quad (55)$$

and

$$dN_{\theta_m} = \left(\frac{K_D^2 \omega^2 N_o}{2S} \right) \left(\frac{c}{4\pi K_D \Delta F \omega_m R} \right)^2 df. \quad (56)$$

The total noise power in a bandpass $\pm B_s$ around f_m is then:

$$N_{\theta_m} = \left(\frac{c}{4\pi \Delta F f_m R} \right)^2 \left(\frac{N_o}{2S} \right) \int_{f_m - B_s}^{f_m + B_s} f^2 df. \quad (57)$$

Which on integrating yields the variance of the phase noise on the frequency modulation signal:

$$\sigma_\theta^2 = \left(\frac{c}{4\pi \Delta F f_m R} \right)^2 \left(\frac{N_o}{S} \right) \left[B_s \left(f_m^2 + \frac{B_s^2}{3} \right) \right]. \quad (58)$$

Since the modulation signal frequency will be much higher than the smoothing bandwidth B_s (i.e., $f_m \gg B_s$), equation 58 can be approximated by:

$$\sigma_\theta^2 = \left(\frac{c}{4\pi \Delta F R} \right)^2 \left(\frac{N_o B_s}{S} \right). \quad (59)$$

Substituting for the variance in range:

$$\sigma_R^2 = \left[\frac{c^2}{(2\pi)^2 2 \Delta F f_m R} \right]^2 \frac{B_s}{(S/N_o)} \quad (60)$$

Thus, the range error increases as range gets smaller, for a fixed signal-to-noise. This is expected since the amplitude of the received frequency modulated sine wave is decreasing with range. It therefore becomes harder to measure its phase in the presence of a fixed amount of noise.

Another technique which has been proposed for measuring range with the frequency modulation system is to vary the frequency of the modulation signal in a tracking loop to keep the modulation signal at the output of the discriminator at peak amplitude. This can be accomplished if $f_m = \frac{c}{4R}$ in equation 35. Then the peak value of the modulation signal is:

$$A_m = 4\pi K_D \Delta F \quad (61)$$

Figure 16 is modified as shown below:

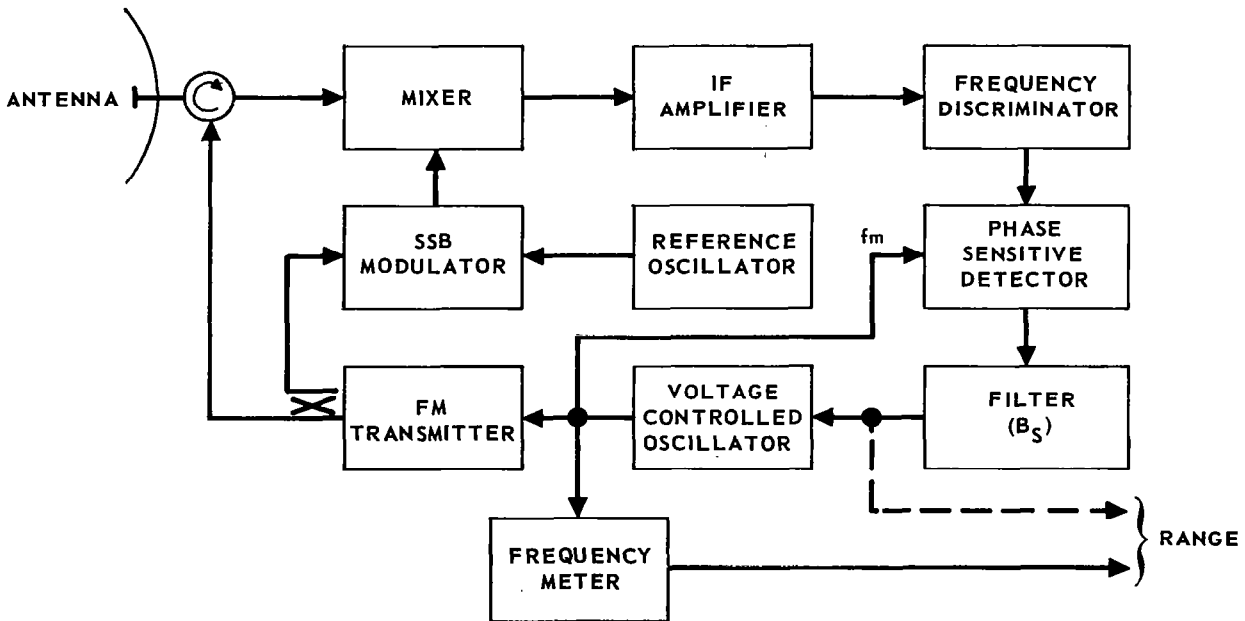


FIGURE 16 – FM-CW RADAR USING MODULATION FREQUENCY AS A MEASURE OF RANGE

Range is measured by measuring the frequency of the modulation signal out of the voltage controlled oscillator with a frequency meter as shown. However,

the input voltage to the VCO will be a linear function of frequency, and thus a function of range, also. Assuming perfect components, the range error is the same if either output frequency or input voltage of the VCO is used to indicate range.

The signal input to the VCO will be a function of the phase difference between the transmitted and received modulation signals. That is, from equation 35:

$$e_o = (\theta_m)_{\text{TRANS}} - (\theta_m)_{\text{REC.}} = \frac{\omega_m R}{c} \quad (62)$$

Therefore:

$$R = \frac{c}{\omega_m} e_o \quad (63)$$

Thus, the variance in range is:

$$\sigma_R^2 = \left(\frac{c}{2\pi f_m} \right)^2 \sigma_{e_o}^2 \quad (64)$$

Now the variance of the error voltage out of the PSD is equal to the variance of the phase noise on the received modulation signal out of the frequency discriminator.

Since $A_m = 4\pi K_D \Delta F$ by adjustment of f_m , the phase noise power on the modulation signal is:

$$N_{\theta_m} = \int_{f_m - B_s}^{f_m + B_s} \frac{\eta_{\omega}}{A_m^2} df = \int_{f_m - B_s}^{f_m + B_s} \left(\frac{K_D^2 \omega^2 N_o}{2S} \right) \left(\frac{1}{4\pi K_D \Delta F} \right)^2 df, \quad (65)$$

Or,

$$N_{\theta_m} = \left(\frac{1}{2\Delta F} \right)^2 \left(\frac{N_o}{2S} \right) \int_{f_m - B_s}^{f_m + B_s} f^2 df. \quad (66)$$

On integrating, the variance of the error signal into the VCO is:

$$\sigma_{e_o}^2 = \left(\frac{1}{2\Delta F} \right)^2 \left(\frac{N_o}{S} \right) \left[B_s \left(f_m^2 + \frac{B_s^2}{3} \right) \right], \quad (67)$$

which for $f_m \gg B_s$ becomes:

$$\sigma_{e_o}^2 = \left(\frac{f_m}{2\Delta F}\right)^2 \left(\frac{B_s}{S/N_o}\right). \quad (68)$$

Substituting equation 68 into 64, the variance in range becomes:

$$\sigma_R^2 = \left(\frac{c}{2\pi f_m}\right)^2 \left(\frac{f_m}{2\Delta F}\right)^2 \frac{B_s}{(S/N_o)}, \quad (69)$$

or,

$$\sigma_R^2 = \frac{c^2 B_s}{4 (2\pi\Delta F)^2 (S/N_o)}. \quad (70)$$

Range-Rate Accuracy. - With each of the preceding techniques used to measure range, there are basically only two techniques available for measuring range-rate. (Differentiation of range is not considered since this can be accomplished in the autopilot of the docking control system.) These consist of (1) measuring the average value of the voltage out of the frequency discriminator, or (2) turning the modulation off and measuring the doppler shift of the received carrier.

When the average voltage out of the discriminator is used as a measure of range-rate, we obtain from equation 35 the DC voltage out of the frequency discriminator:

$$e_{DC} = -\frac{2K_D \omega_o \dot{R}}{c}, \quad (71)$$

or,

$$\dot{R} = -\frac{c}{4\pi K_D f_o} e_{DC}, \quad (72)$$

and since $\lambda = \frac{c}{f_o}$, the variance in range-rate is:

$$\sigma_{\dot{R}}^2 = \frac{\lambda^2}{(4\pi K_D)^2} \sigma_{e_{DC}}^2. \quad (73)$$

The variance of the DC voltage out of the frequency discriminator is equal to the variance of the carrier frequency. Thus, from appendix B:

$$\sigma_{e_{DC}}^2 = \sigma_{\omega}^2 = K_D^2 \frac{(2\pi)^2}{3} \left(\frac{N_0}{S}\right) B_0^3, \quad (B11)$$

where B_0 is the output noise bandwidth of the discriminator. Substituting equation B11 into equation 73 :

$$\sigma_{\dot{R}}^2 = \frac{\lambda^2}{(4\pi K_D)^2} \left(\frac{K_D^2 (2\pi)^2 N_0}{3 S} B_0^3 \right), \quad (74)$$

or,

$$\sigma_{\dot{R}}^2 = \frac{\lambda^2 B_0^3}{12 (S/N_0)}. \quad 75$$

The DC voltage is further smoothed in a filter with noise bandwidth B_s . B_0 is made equal to f_m for the discriminator. Therefore, equation 75 becomes:

$$\sigma_{\dot{R}}^2 = \frac{\lambda^2 f_m^2 B_s}{12 (S/N_0)}. \quad (76)$$

If the modulation is removed and range-rate is determined by measuring the doppler frequency directly, the bandpass of the discriminator B_0 does not have to equal f_m . That is, the bandpass of the discriminator can be reduced to B_s and the smoothing filter eliminated. In this case, equation 76 for the variance in range rate becomes:

$$\sigma_{\dot{R}}^2 = \frac{\lambda^2 B_s^3}{12 (S/N_0)}. \quad (77)$$

Instrumentation Errors in Range Measurement. - Modulation amplitude can be used as a measure of range. From the section on range accuracy, the peak voltage of the received modulation sine wave out of the discriminator was:

$$E_p = 4\pi K_D \Delta F \sin\left(\frac{\omega_m R}{c}\right). \quad (78)$$

Assuming the modulation frequency was chosen so that $f_m \ll \frac{c}{4R}$, then:

$$E_p = 4\pi K_D \Delta F \frac{\omega_m R}{c}. \quad (79)$$

Solving for R, range is:

$$R = \frac{c}{2(2\pi)^2 K_D \Delta F f_m} E_p . \quad (80)$$

Assuming that all of the parameters are subject to change, except for c, the differential change in range can be represented by:

$$dR = \left\{ \frac{\partial R}{\partial K_D} dK_D + \frac{\partial R}{\partial \Delta F} d\Delta F + \frac{\partial R}{\partial f_m} df_m + \frac{\partial R}{\partial E_p} dE_p \right\} . \quad (81)$$

Taking the above partials and dividing by R, the fractional change in range is:

$$\frac{dR}{R} = -\frac{dK_D}{K_D} - \frac{d\Delta F}{\Delta F} - \frac{df_m}{f_m} + \frac{dE_p}{E_p} . \quad (82)$$

Now each of the above errors can be assumed independent from any of the others, so that the rms percentage error in range will be:

$$(\%R)_{RMS} = [(\%K_D)^2 + (\%\Delta F)^2 + (\%f_m)^2 + (\%E_p)^2]^{1/2} . \quad (83)$$

Thus, the percentage error in range is the rms value of the percentage error in maintaining K_D , ΔF , and f_m constant and the percentage error in measuring the peak voltage e_p .

When the phase of the received modulation sine wave out of the discriminator is used to determine range, we have, as in equation 45:

$$\theta = \frac{\omega_m R}{c} , \quad (84)$$

from which range is found to be:

$$R = \frac{c}{2\pi f_m} \theta . \quad (85)$$

Thus, the rms percentage error in measuring range is:

$$(\%R)_{RMS} = [(\%f_m)^2 + (\%\theta)^2]^{1/2} . \quad (86)$$

Comparing equations 83 and 86 it is seen that phase measurement to determine range is affected by fewer system parameters than the amplitude measurement. Only the stability of the modulation frequency and the accuracy of the phase meter are important.

The closed loop technique of varying the modulation frequency to maximize the received modulation signal resulted in the modulation frequency being an indication of range. The block diagram of figure 17 can be reduced to the following simple servo diagram when the loop is in lock.

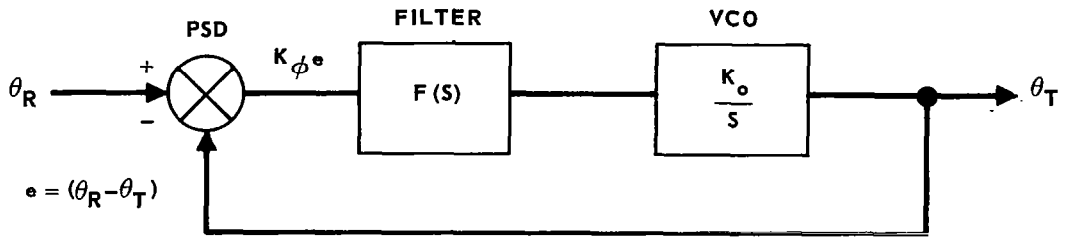


FIGURE 17 - FREQUENCY TRACKING LOOP

θ_R and θ_T are the phase of the received and transmitted modulation signals, respectively.

The error out of the sine wave PSD approaches zero when the phase difference between the transmitted and received modulation is $0, \pm\pi, \pm2\pi, \pm3\pi$, etc. The phase of the transmitted signal is adjusted so that this phase difference is zero. The transmitted modulation was set in the beginning at $E_m \sin \omega_m t$. The received modulation, from equation 35, is $E_R \cos \left(\omega_m t - \frac{\omega_m R}{c} \right)$ the phase difference between the transmitted and received signals is then $\left(\frac{\pi}{2} - \frac{\omega_m R}{c} \right)$ which results in a null of the PSD when $\left(\frac{\pi}{2} - \frac{\omega_m R}{c} \right) = -\pi$ or $\frac{\omega_m R}{c} = \frac{\pi}{2}$. The amplitude of the modulation is then:

$$E_R = 4\pi K_D \Delta F \sin \frac{\omega_m R}{c} = 4\pi K_D \Delta F. \quad (87)$$

However, at steady state, the error in the loop is not zero but equal to $\frac{\omega_m}{K_O}$ (type 0 servo).

$$\text{Thus, } \frac{\omega_m R}{c} = \frac{\pi}{2} + \frac{\omega_m}{K_O}, \quad (88)$$

and range is equal to:

$$R = c \left(\frac{1}{4f_m} + \frac{1}{K_O} \right). \quad (89)$$

If K_O is made much larger than f_m , range is just $R = \frac{c}{4f_m}$. Otherwise, it is a systematic error that can be removed. The differential of range is:

$$dR = \frac{\partial R}{\partial f_m} df_m + \frac{\partial R}{\partial K_O} dK_O = \frac{c}{4f_m^2} df_m - \frac{c}{K_O^2} dK_O. \quad (90)$$

The percentage change in range is:

$$\frac{dR}{R} = -\left(\frac{K_o}{K_o + 4f_m}\right) \frac{df_m}{f_m} - \left(\frac{4f_m}{K_o + 4f_m}\right) \frac{dK_o}{K_o} \quad (91)$$

The rms percentage change in range is then:

$$(\%R)_{\text{RMS}} = \left[\left(\frac{K_o}{K_o + 4f_m}\right)^2 (\%f_m)^2 + \left(\frac{4f_m}{K_o + 4f_m}\right)^2 (\%K_o)^2 \right]^{\frac{1}{2}} \quad (92)$$

Thus, the only two factors affecting range errors are the gain stability of the VCO and the accuracy of the frequency measurement. As can be seen, if the gain of the VCO is made large such that $K_o \gg f_m$ the major part of the range error is due to the frequency measurement inaccuracy, i.e.,

$$(\%R)_{\text{RMS}} \rightarrow (\%f_m) \text{ for } K_o \gg f_m \quad (93)$$

Instrumentation Errors in Range-Rate Measurement. - From equation 35 the DC voltage out of the discriminator is:

$$e_{\text{DC}} = -\frac{2K_D \omega_o \dot{R}}{c} \quad (94)$$

and range-rate is:

$$\dot{R} = \frac{\lambda}{4\pi K_D} e_{\text{DC}} \quad (95)$$

if the DC voltage is used to measure range-rate. Taking partials as before, the rms percentage error in range rate is:

$$(\%\dot{R})_{\text{RMS}} = [(\%K_D)^2 + (\%\lambda)^2 + (\%e_{\text{DC}})^2]^{\frac{1}{2}} \quad (96)$$

Thus, the stability of the transmitter oscillator and the discriminator gain constant, plus the voltage measurement error contribute to the range-rate error.

If the received carrier doppler frequency is measured directly, the doppler frequency is:

$$f_d = \frac{2\dot{R}}{c} f_o = \frac{2\dot{R}}{\lambda} \quad (97)$$

Range rate is then:

$$\dot{R} = \frac{\lambda}{2} f_d \quad (98)$$

The rms percentage error in range-rate is then:

$$(\% \dot{R})_{\text{RMS}} = \frac{1}{[(\% \lambda)^2 + (\% f_d)^2]^{1/2}}. \quad (99)$$

Thus, the effect of the discriminator is removed and the accuracy of a frequency measurement is substituted for the voltage measurement accuracy.

In both cases it was assumed that the modulation was turned off. If the modulation is not turned off, nonlinearities in the gain constants of the transmitter oscillator and frequency discriminator cause distortions of the received modulation sine wave. These distortions cause the average value of the sine wave to be other than zero, thus adding an error to the doppler measurement.

Resolution and Ambiguities of Sine Wave FM-CW Radars. - Ambiguity functions and ambiguity diagrams are a useful tool in analyzing radar waveforms (references 6 and 7). The ambiguity function along the $\omega = 0$ and $\tau = 0$ axis for the sine wave modulated FM-CW radar waveform is developed in appendix C:

$$\psi(\tau, 0) = \left\{ J_0 \left[\frac{2\Delta F}{f_m} \sin \left(\omega_m \frac{\tau}{2} \right) \right] \right\}, \quad (C30)$$

$$\psi(0, \omega) = \frac{\sin \left(\frac{\omega T}{2} \right)}{\left(\frac{\omega T}{2} \right)}, \quad (C31)$$

where T is the total duration of the signal. Woodward (reference 6) considers the square of the ambiguity function as defined by $\psi(\tau, \omega)$ and plots contours of $|\psi(\tau, \omega)|^2$, which in terms of the above is:

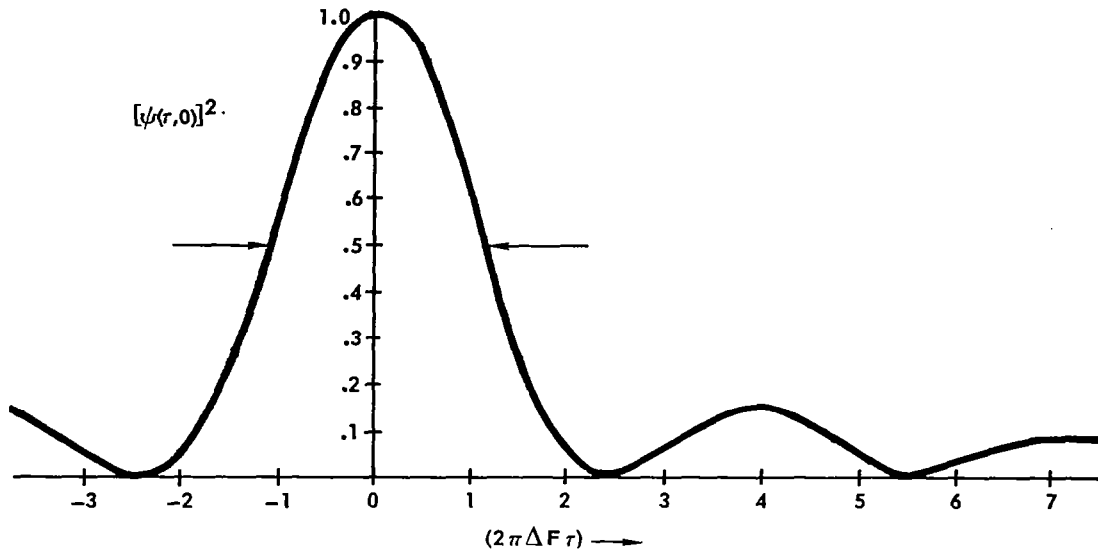
$$|\psi(\tau, 0)|^2 = \left\{ J_0 \left[\frac{2\Delta F}{f_m} \sin \left(\omega_m \frac{\tau}{2} \right) \right] \right\}^2, \quad (100)$$

$$|\psi(0, \omega)|^2 = \left\{ \frac{\sin \left(\frac{\omega T}{2} \right)}{\left(\frac{\omega T}{2} \right)} \right\}^2. \quad (101)$$

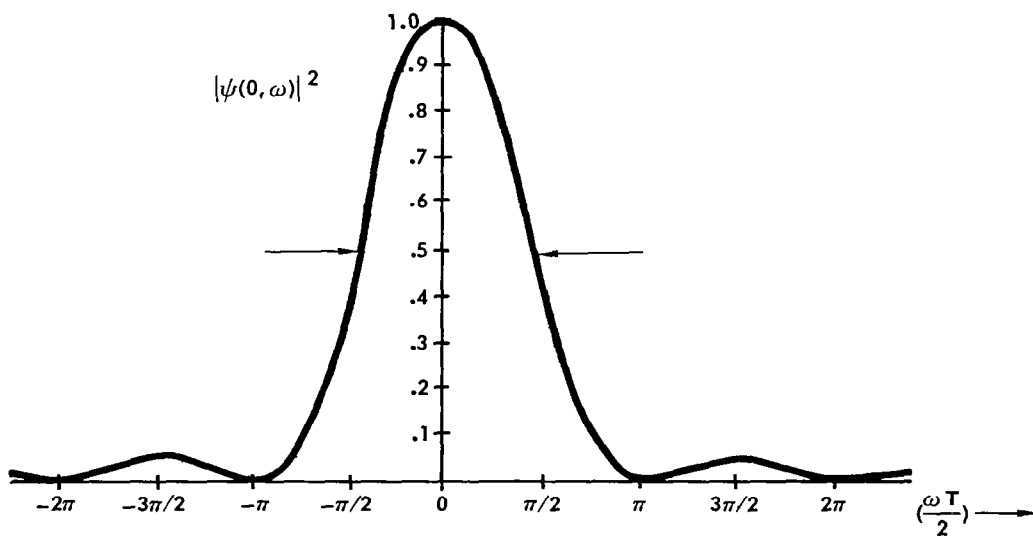
Note that equation 100 is periodic in τ and has a peak value of unity when $\frac{\omega_m \tau}{2} = 0, \pi, 2\pi, \text{etc.}$ or when $\tau = 0, \frac{1}{f_m}, \frac{2}{f_m}, \text{etc.}$. For τ close to zero, $\frac{1}{f_m}, \frac{2}{f_m}, \text{etc.}$ can be approximated by:

$$|\psi(\tau, 0)|^2 = [J_0(2\pi \Delta F \tau)]^2, \quad (102)$$

which is simply the square of the zero order Bessel function which is plotted in figure 18:



(a) AS A FUNCTION OF (t)



(b) AS A FUNCTION OF (ω)

FIGURE 18 – ZERO ORDER BESSEL FUNCTION SQUARED

The function is at half amplitude for $(2\pi \Delta F \tau) \approx 1.1$. If the resolution is defined as the width of the central spike at the half amplitude points:

$$\tau_{\text{RES}} = \frac{2.2}{\pi(2\Delta F)}, \quad (103)$$

where $2\Delta F$ is essentially the bandwidth of the transmitted signal for the FM-CW radar system. Thus the range resolution would be defined as:

$$R_{\text{RES}} = \frac{c \tau_{\text{RES}}}{2} = \frac{1.1 c}{2\pi \Delta F}. \quad (104)$$

The range-rate resolution can be defined from equation 101 which is plotted in figure 18. There is only one central spike.

The above function is at half amplitude when $\frac{\omega T}{2} = 1.4$. Again, if resolution is defined as the width of the central spike at half amplitude,

$$\omega_{\text{RES}} = \frac{5.6}{T}. \quad (105)$$

Now $\omega = 2\pi f$ where f is the doppler frequency associated with the received signal. Since:

$$\omega_d = \frac{4\pi}{\lambda} \dot{R}, \quad (106)$$

the range-rate resolution would be defined as:

$$\dot{R}_{\text{RES}} = \frac{\lambda}{4\pi} \omega_{\text{RES}} = \frac{1.4 \lambda}{\pi T}. \quad (107)$$

This says that range-rate resolution is better for higher operating frequencies and longer observation times.

From the above it appears that there are no ambiguities in range-rate and that the ambiguities in range appear at multiples of $1/f_m$ with fairly well defined lobes.

The complete function $|\psi(\tau, \omega)|^2$ is shown in Reference 8, where it can be seen that the ambiguity function contains bumps and ripples over the entire plane with the energy concentrated according to the contour as shown in figure 19.

An obvious limitation of the waveform is the ambiguity between range and range rate. This was pointed out earlier when it was shown that the received signal out of the discriminator had a frequency modulation term whose amplitude was a function of range rate.

Another more subtle limitation comes from the fact that since the ambiguity function has its energy spread over the entire τ, ω plane, a large target that lies outside the major lobe can result in as much energy as a small target at the peak of the major lobe. This results in an inability of the FM-CW system to resolve the two targets. In general, this is true of all CW radar systems regardless of the modulation function. It essentially means that the FM-CW system is limited to single target situations or cooperative operation.

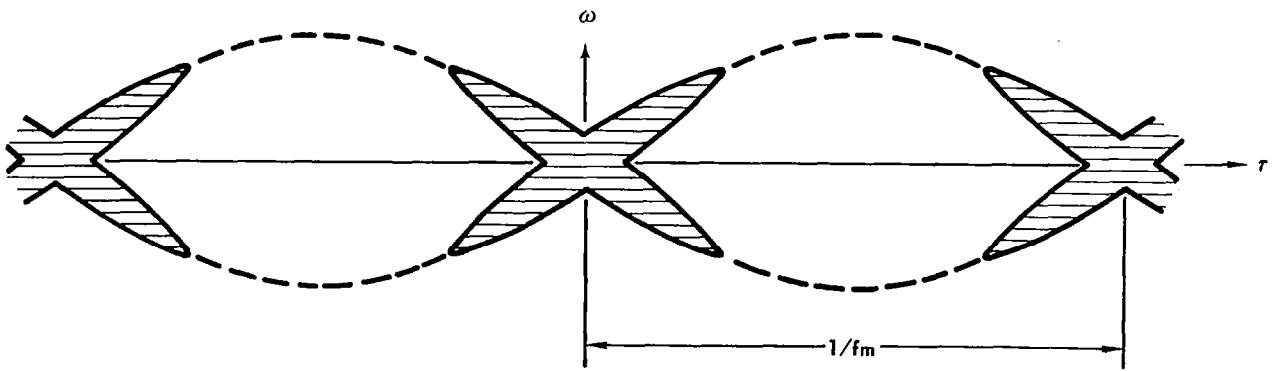


FIGURE 19 - SINE WAVE FM-CW AMBIGUITY DIAGRAM

Summary of the Characteristics of Sine-Wave Modulated FM-CW Systems. - Three basic types of sine-wave modulated FM-CW systems have been discussed. There are others such as the so-called third order Bessel Function extraction system (references 51 and 9). However, these three systems appear most applicable for the docking mission and are summarized in the table below. (Numbers in parenthesis refer to appropriate equations.)

TABLE 4 - SUMMARY OF THE CHARACTERISTICS OF SINE-WAVE MODULATED FM-CW SYSTEMS

	AMPLITUDE MEASUREMENT	PHASE MEASUREMENT	CLOSED-LOOP FREQUENCY MEASUREMENT
RANGE ACCURACY (ALL GET BETTER WITH WIDER FREQUENCY DEVIATIONS AND LARGER (S/NO))	EQ. (44) SMALLEST	EQ. (60) LARGEST - GETS WORSE WITH DECREASING RANGE.	(70) THREE TIMES AS LARGE AS (44)
RANGE INSTRUMENTATION ERROR FACTORS	(83) DISCRIMINATOR GAIN, FREQUENCY DEVIATION, MODULATOR FREQUENCY, AND VOLTAGE MEASUREMENT ACCURACY	(86) MODULATOR FREQUENCY, PHASE MEASURING ACCURACY.	(92) VCO GAIN, AND FREQ. MEASURING ACCURACY.
RANGE-RATE ACCURACY	(77) DIRECT DOPPLER BETTER FOR HIGHER FREQUENCY AND LARGE (S/NO)	(77) SAME	(77) SAME
RANGE-RATE INSTRUMENTATION ERRORS	(99) DIRECT DOPPLER - TRANSMITTER STABILITY, FREQUENCY MEASUREMENT ACCURACY	(99) SAME	(99) SAME
AMBIGUITY LIMITATIONS	(100) & (101) COOPERATIVE OR ISOLATED TARGET.	(100) & (101) SAME	(100) & (101) SAME

The last two systems will not operate down to zero range because: for the second system, the range accuracy deteriorates at zero range; and for the third system, the modulation frequency must be infinite at zero range. The first system works well down to zero range but will not give accurate readings at longer ranges because the percentage range error is affected by so many instrumentation parameters. The second system will not give accurate readings for longer ranges unless multiple modulation frequencies are used, due to inaccuracies associated with phase measurement.

The best system for accurate readings at long ranges plus operation down to zero range would utilize both the first and last techniques. It would utilize a phase lock-loop with modulation frequency varied with range until the range decreases to a specified point. Within this range, the modulation frequency would be held constant and the amplitude of the received deviation measured as the range goes to zero.

This system would interrupt the modulation periodically and measure doppler directly. The same frequency meter used to measure the modulation frequency for range determination could be used to measure doppler for range-rate determination.

Triangular Modulated FM-CW Systems

The triangular wave modulated FM-CW radar is discussed thoroughly in the literature (reference 51, 9, and 10). A simple block diagram for a triangular wave modulated FM-CW radar is shown below.

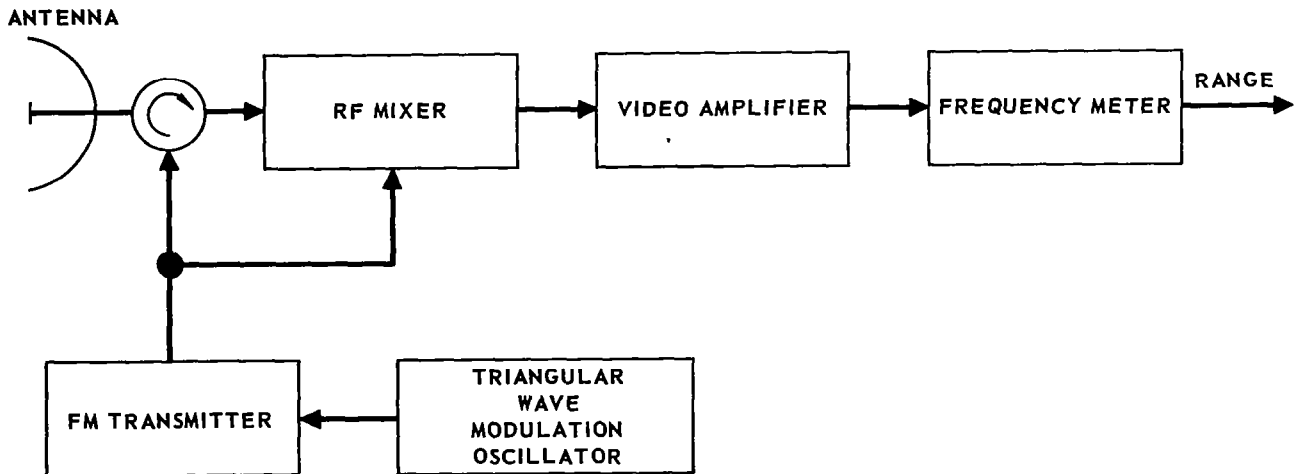


FIGURE 20 – HOMODYNE, TRIANGULAR-WAVE MODULATED FM-CW RADAR

The modulation frequency on transmission and reception is shown in figure 21.

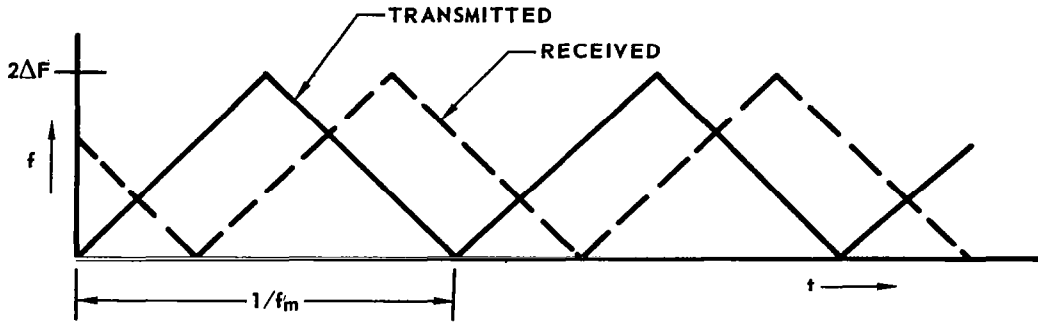


FIGURE 21 – TRANSMITTED AND RECEIVED FREQUENCIES VS. TIME

The difference frequency out of the mixer is equal to:

$$f_d = \frac{8\Delta F f_m R}{c}, \quad (109)$$

and for zero doppler is as shown in figure 22.

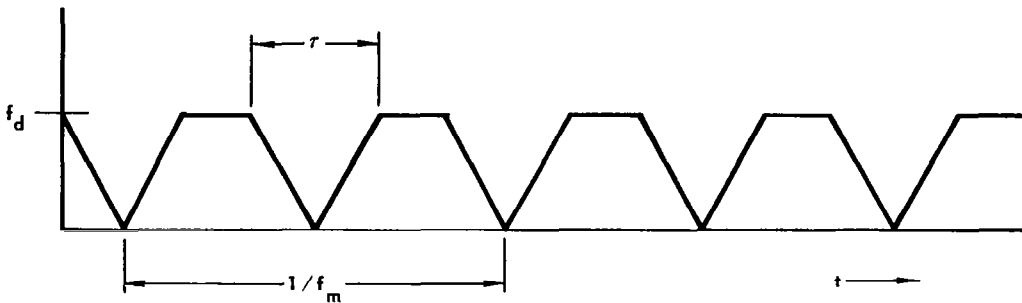


FIGURE 22 – MIXER OUTPUT (ZERO DOPPLER)

Range and Range-Rate Accuracy. - This difference frequency is measured in a frequency meter to determine range. Thus:

$$R = \frac{c f_d}{8\Delta F f_m} = \frac{c}{16\pi\Delta F f_m} \omega_d, \quad (110)$$

and the variance in range is:

$$\sigma_R^2 = \left(\frac{c}{16\pi\Delta F f_m} \right)^2 \sigma_{\omega_d}^2, \quad (111)$$

where $\sigma_{\omega_d}^2$ is the variance in the radian frequency of the received signal. From appendix B, this variance is:

$$\sigma_{\omega}^2 = \frac{(2\pi)^2}{3} \left(\frac{N_0}{S}\right) B_0^3, \quad (B.11)$$

which on substitution into equation 111 results in:

$$\sigma_R^2 = \frac{c^2 B_0^3}{3(8\Delta F f_m)^2 (S/N_0)}, \quad (112)$$

where B_0 is the bandpass of the frequency meter.

Now if there is any relative velocity, the average frequency of the received signal will be shifted up or down and the difference frequency will be as shown in the following figure.

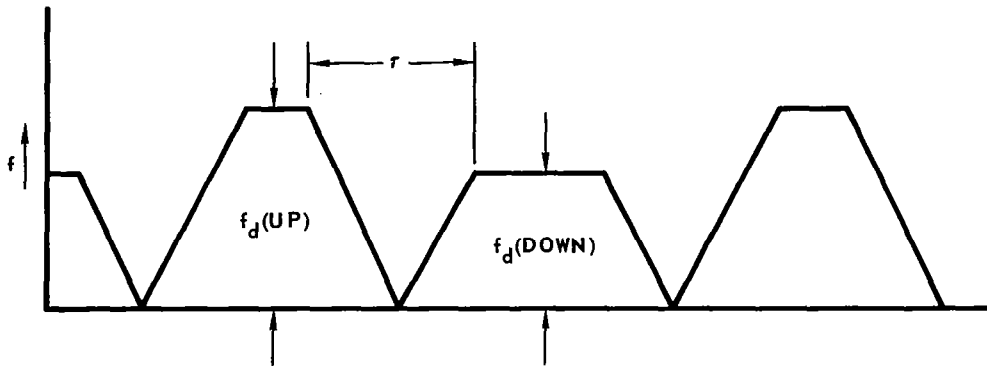


FIGURE 23 - MIXER OUTPUT (WITH DOPPLER)

The average difference frequency will still be the same equation 109. The doppler frequency is:

$$f_d = \frac{f_d(\text{up}) - f_d(\text{down})}{2}. \quad (113)$$

Doppler would be determined by switching two frequency meters alternately on and off in synchronizom with the modulation and measuring the difference between the two as stated by equation 113.

Since the modulation frequency must be passed through the frequency meters in order to measure range rate, B_0 will be approximately equal to f_m and equation 112 becomes:

$$\sigma_R^2 = \frac{c^2 f_m}{3 (8\Delta F)^2 (S/N_0)}. \quad (114)$$

If additional smoothing of the range measurement is employed, equation 114 becomes:

$$\sigma_R^2 = \frac{c^2 B_s}{3 (8\Delta F)^2 (S/N_o)}, \quad (115)$$

where B_s is the noise bandwidth of the smoothing filter. (Note that this is nearly the same as for sine-wave modulation when the rms amplitude of the received modulation is measured.)

In measuring range-rate, the difference between two noise signals is taken (equation 113). The noise between the two intervals of time should be uncorrelated and the variance of each measurement should be the same.

Thus, from equation 113:

$$\sigma_d^2 = (\frac{1}{2})^2 \left[\sigma_{f_d}^2(\text{up}) + \sigma_{f_d}^2(\text{down}) \right], \quad (116)$$

$$= (\frac{1}{2})^2 [2\sigma_{f_d}^2], \quad (117)$$

$$= \frac{\sigma_{f_d}^2}{2}. \quad (118)$$

The variance in range-rate when direct doppler measurements are made is given by equation 75:

$$\sigma_{\dot{R}}^2 = \frac{\lambda^2 B_s^3}{12 (S/N_o)}, \quad (75)$$

Therefore, from equation 118, the range-rate accuracy for the triangular wave modulated FM-CW system is:

$$\sigma_{\dot{R}}^2 = \frac{\lambda^2 B_s^3}{24 (S/N_o)}. \quad (119)$$

Instrumentation Errors. - Instrumentation errors in measuring range are found from equation 110:

$$R = \frac{c}{8\Delta F f_m} f_d. \quad (120)$$

The rms percentage range error is thus:

$$(\%R)_{\text{RMS}} = [(\%\Delta F)^2 + (\%f_m)^2 + (\%f_d)^2]^{1/2}. \quad (121)$$

Instrumentation errors in measuring range are due to instability of the transmitter frequency deviation and the modulation frequency, and the accuracy of the frequency measurement.

Again from equation 99, the rms percentage error in measuring range rate is:

$$(\% \dot{R})_{\text{RMS}} = [(\% \lambda)^2 + (\% f_d)^2]^{1/2}, \quad (122)$$

where $(\% f_d)$ is the rms percentage error of the two frequency meters (from equation 113).

Another error associated with this type system is often called "Step Error". Step error is the result of the discreteness of the cycle count as a measure of range. It can be called quantization error and from reference 51, page 95 is:

$$\delta R = \frac{c}{8\Delta F}. \quad (123)$$

where $2\Delta F$ is the total frequency excursion as shown in figure 21. Step error is generally not serious when the phase of the returned signal is modulated by the randomness of the target (multiple target returns). However, step error can be reduced for single target tracking by jittering the modulation waveform. The amount of step error suppression depends on the choice of the submodulation frequency (and deviation) and then varies with range. For frequency jitter caused by a triangular submodulation waveform, the step error can be reduced to the point where it is always less than 20% of δ_r given by equation 123.

Resolution and Ambiguities of Triangular-Wave FM-CW Radars. - The ambiguity diagram for a single pulse of duration T and a total linear frequency sweep of

Δf has been developed by Woodward (reference 6) and appears regularly in the literature with regard to linear FM pulse compression.

If the triangularly modulated FM-CW signal is considered as a sequence of pulses of duration $\Delta = \frac{1}{2f_m}$ with alternate positive and negative going sweeps, the ambiguity diagram can be drawn as shown in figure 24 (contour of $|\psi(\tau, f)|^2$). The total observation time is τ , and the spectrum is folded on reception due to direct mixing. This is similar to the ambiguity diagram shown in figure 19 for the sine-wave modulated FM-CW system as would be expected.

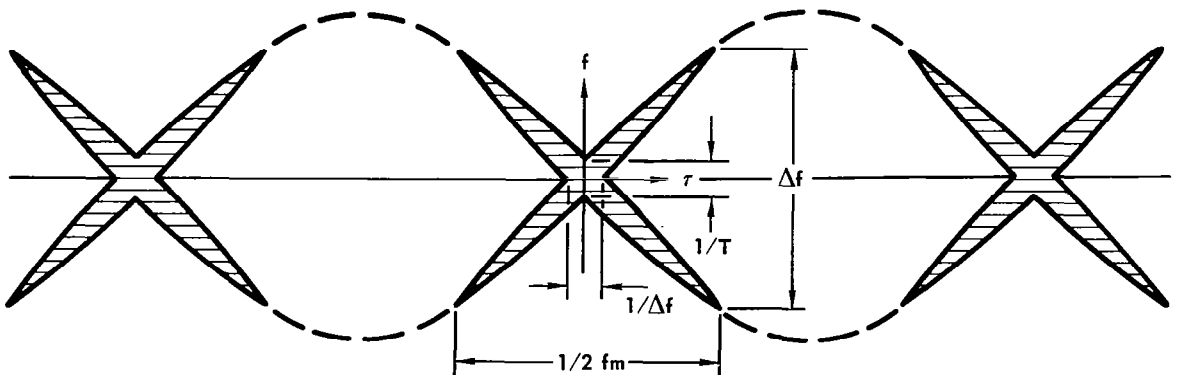


FIGURE 24 - TRIANGULAR WAVE FM-CW AMBIGUITY DIAGRAM

Again, there are no completely clear regions in the r, f plane. This essentially means that the triangle wave FM-CW system is limited to single target situations or cooperative operations.

The range resolution is:

$$R_{RES} = \frac{c}{2} \tau_{RES} = \frac{c}{2} \frac{1}{\Delta F} = \frac{c}{4\Delta F} \tag{124}$$

The range-rate resolution is:

$$\dot{R}_{RES} = \frac{\lambda}{2T} \tag{125}$$

Note that these are nearly the same as equations 104 and 107 for the sine-wave modulated FM-CW system.

Sine-Wave Phase Modulated Systems

A simple block diagram of a phase modulation system (PM-CW) employing a single sine wave for modulation is shown in figure 25. The transmitted signal can be represented as:

$$e_T(t) = A_c \sin(\omega_o t + \Delta\phi \cos \omega_m t), \tag{130}$$

and the received signal after mixing is:

$$e_R(t) = A_c \sin(\omega_{IF} t + \omega_o \tau + \Delta\phi \cos \omega_m (t - \tau)). \tag{131}$$

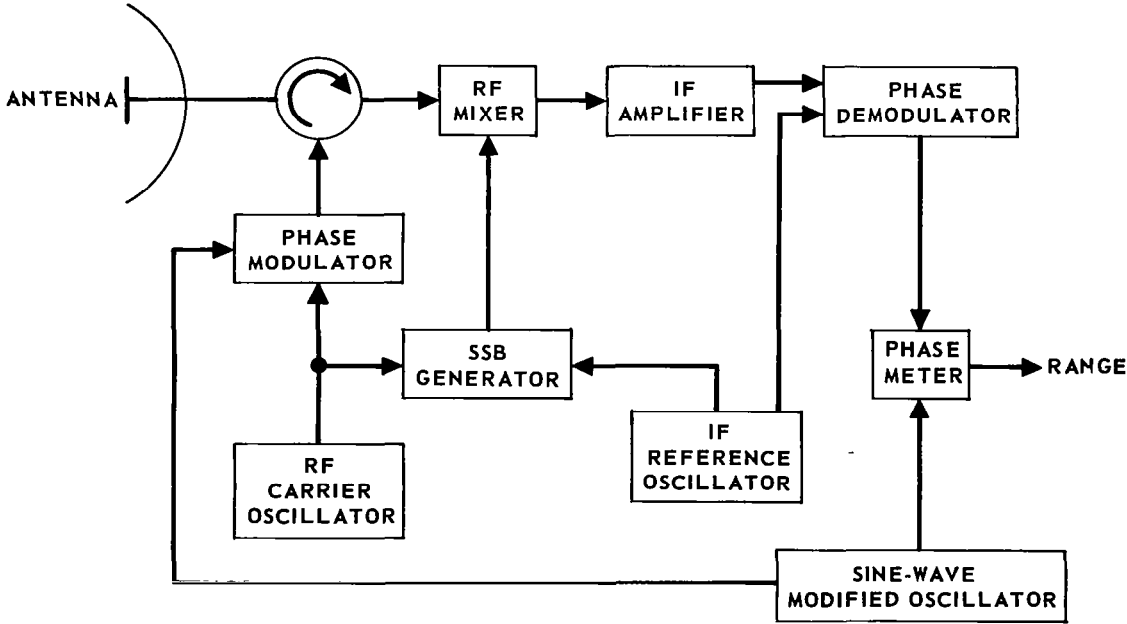


FIGURE 25 – HETERODYNE, SINE-WAVE MODULATED PM-CW RADAR

Range and Range-Rate Accuracy. - Added to the received signal in the IF amplifier is the noise from the receiver input. From appendix B, the power in this phase noise out of the phase detector is:

$$N_{\theta} = \sigma_{\theta}^2 = \frac{N_o B_o}{S}. \quad (B7)$$

The output of the phase detector is the sum of this phase noise $n_{\theta}(t)$ and the received modulation signal $\Delta\phi \cos \omega_m (t - \tau)$. The addition of the modulation signal and the phase noise will cause amplitude and phase modulation of the phase modulation signal.

In the same manner used in appendix B, the phase noise on the phase modulation can be shown to be:

$$\theta_n = \tan^{-1} \frac{A_n \sin [(\omega - \omega_m) t + \omega_m \tau]}{\Delta\phi + A_n \cos [(\omega - \omega_m) t + \omega_m \tau]}, \quad (132)$$

where:
$$\frac{A_n^2}{2} = \eta_{\theta} df = \frac{N_{\theta}}{B_o} df = \frac{N_o}{S} df,$$

is the power of the noise in the incremental bandwidth df . If we assume a large signal to noise, i.e.: $\Delta\phi \gg A_n$

$$\theta_n = \frac{A_n}{\Delta\phi} \sin [(\omega - \omega_m) t + \omega_m \tau]. \quad (133)$$

The power in this noise component at frequency ω_m is:

$$\frac{1}{2} \left(\frac{A_n}{\Delta\phi} \right)^2 = \frac{N_o}{(\Delta\phi)^2 S} df. \quad (134)$$

The total power in this phase noise (i.e. on the phase of the modulation) is:

$$N_{\theta_m} = \sigma_{\theta_n}^2 = \int_{-B_s}^{+B_s} \frac{df}{(\Delta\phi)^2 (S/N_o)} = \frac{2B_s}{(\Delta\phi)^2 (S/N_o)}. \quad (135)$$

Where B_s is the noise bandwidth of the phase meter.

Range is measured by measuring the phase delay of the modulation signal which is:

$$\theta_m = \omega_m \tau = \omega_m \left(\frac{2R}{c} \right). \quad (136)$$

Therefore:

$$R = \frac{c}{4\pi f_m} \theta_m. \quad (137)$$

The variance of the range measurement is:

$$\sigma_R^2 = \left(\frac{c}{4\pi f_m}\right)^2 \sigma_{\theta_m}^2 \quad (138)$$

Which on substitution from equation 135 :

$$\sigma_R^2 = \frac{c^2 B_s}{2 (2\pi f_m \Delta\phi)^2 (S/N_o)} \quad (139)$$

This is the variance of the range measurement at the output of the phase meter.

Now doppler frequency would again be used to determine range-rate. However, with this system the modulation does not have to be turned off if the phase deviation is small. That is, there is enough power in the carrier to allow doppler to be measured while modulating. Equation 75 for the variance of range-rate can be applied where S_c is the power in the received carrier and can be determined from the specified deviation rate, i.e.:

$$\sigma_{\dot{R}}^2 = \frac{\lambda^2 B_s^3}{12 (S_c/N_o)} \quad (140)$$

Instrumentation Errors. - Since range is given by:

$$R = \frac{c}{4\pi f_m} \theta_m \quad (141)$$

The rms percentage error in measuring range is:

$$(\%R)_{RMS} = \left[(\%f_m)^2 + (\%\theta_m)^2 \right]^{\frac{1}{2}} \quad (142)$$

It depends only on the stability of the modulation oscillator and the phase measuring accuracy.

The rms percentage error in measuring range-rate by doppler is again from equation 99:

$$(\%\dot{R})_{RMS} = \left[(\%\lambda)^2 + (\%f_d)^2 \right]^{\frac{1}{2}} \quad (143)$$

It only depends on the stability of the transmitter oscillator and the accuracy of measuring frequency.

Resolution and Ambiguities of Sine-Wave PM-CW Radars. - The ambiguity function derived for the FM-CW waveform applies for PM-CW systems also. Equations 101 and 102 can be written as:

$$|\psi(\tau, \omega)|^2 = \left\{ J_o \left[2\Delta\phi \sin \left(\omega_m \frac{\tau}{2} \right) \right] \right\}^2, \quad (100) \quad |\psi(\alpha, \omega)|^2 = \left\{ \frac{\sin \left(\frac{\omega}{2} T \right)}{\left(\frac{\omega}{2} T \right)} \right\}^2 \quad (101)$$

because $\Delta\phi = \frac{\Delta F}{f_m}$ makes the frequency modulated system a phase modulation system. If the region around the central peak where $\frac{\omega_m \tau}{2}$ is small is considered

$$|\psi(\tau, 0)|^2 = \{J_0[2\pi\Delta\phi f_m \tau]\}^2. \quad (144)$$

The function is at half amplitude when:

$$2\pi\Delta\phi f_m \tau \approx 1.1. \quad (145)$$

If the width of the major lobe at half amplitude is defined as the resolution:

$$\tau_{RES} = \frac{1.1}{\pi\Delta\phi f_m}, \quad (146)$$

and the range resolution is:

$$R_{RES} = \frac{c\tau_{RES}}{2} = \frac{1.1c}{2\pi\Delta\phi f_m}. \quad (147)$$

If the phase deviation is small, it can be seen that the resolution is the reciprocal of the modulation frequency.

Range-rate resolution is the same as for the FM-CW system and given by:

$$\dot{R}_{RES} = \frac{1.4\lambda}{\pi T}. \quad (107)$$

Again it depends on the radar observation time.

In general, the same comments apply to the PM-CW system as applied to the FM-CW system with regard to resolution. The system is limited to cooperative or isolated target operation.

Pseudo-Noise (PN), Binary Coded-Phase Modulated Systems

A simple noncooperative PN/PM-CW system is described in reference 12. The block diagram of a modified version of this system is shown in figure 26. The original system was modified by offsetting the reference signal to the receiver mixer so as not to fold the received spectrum.

In general, PN-coded phase modulation has been used as a technique for cooperative tracking of deep-space vehicles by the Deep Space Instrumentation Facility (DSIF) of Jet Propulsion Labs (JPL) (See Research Summary Reports and Program Summaries published by JPL). It has also been employed as a method for pulse compression (reference 13, 14, and 15). In general, its complexity would not be justified for the short range requirements encountered in the docking maneuver.

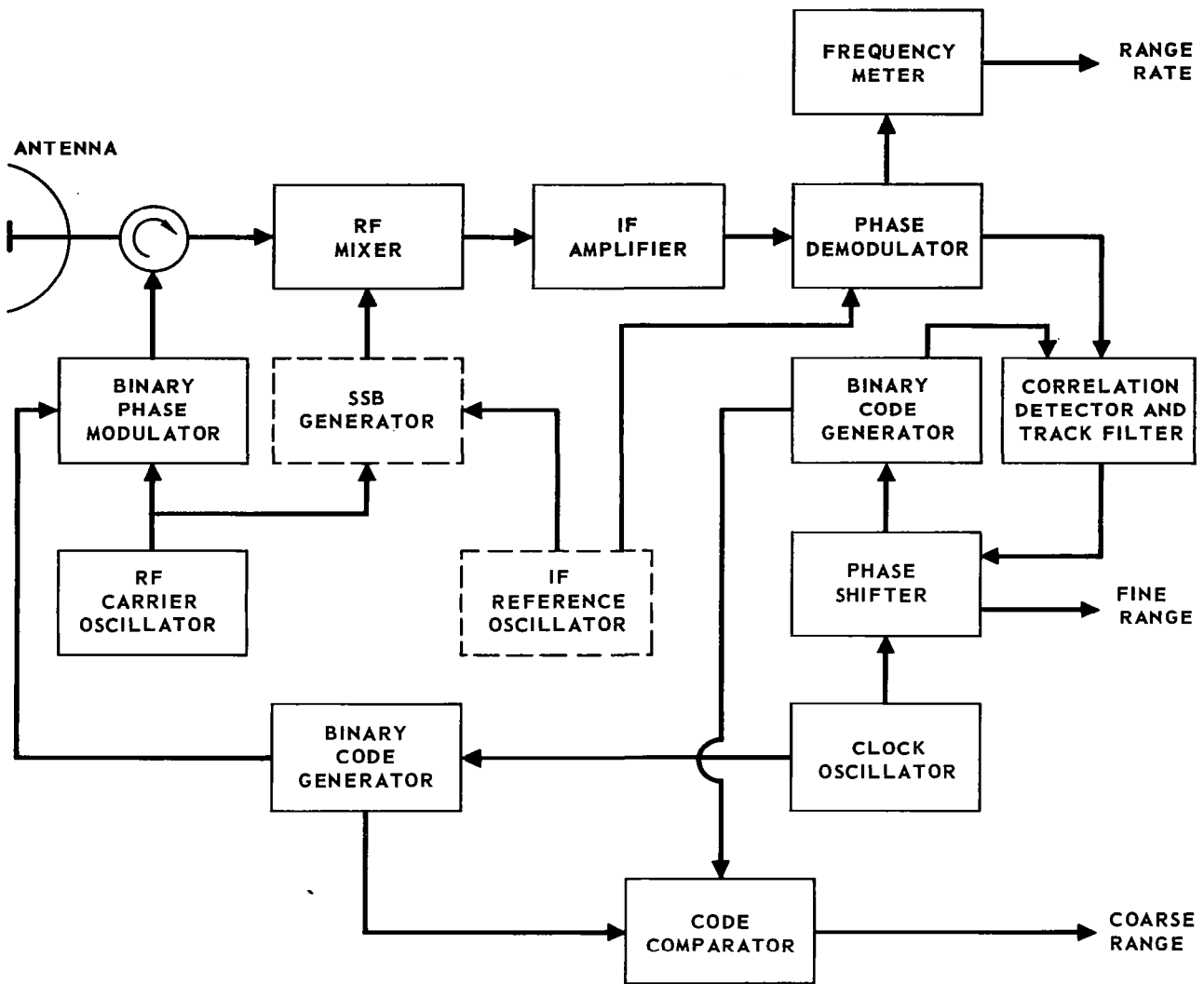


FIGURE 26 - HETERODYNE, PSEUDO-NOISE, BINARY CODED, PM-CW RADAR

In Figure 26, range is measured by the phase shift required to cause the transmitted and received codes to coincide. Direct doppler measurement is made of the signal out of the phase demodulator to determine range-rate.

Range and Range-Rate Accuracy. - The frequency of the clock signal used to generate the binary code will be the ultimate limitation on range measuring accuracy. The length of the code determines the maximum unambiguous range. The process of shifting the phase of the reference clock, and measuring the amount of phase shift employed, results in the same errors as measuring the phase of the received clock signal directly. Thus the variance of the range signal is given by the expression derived for the tone modulated FM-CW system; i.e. from equation 139:

$$\sigma_R^2 = \frac{c^2 B_s}{2 (\pi f_c \Delta\phi)^2 (S/N_o)}, \quad (148)$$

where $\Delta\phi = \frac{\pi}{2}$ radians, f_c is the clock frequency ($f_c = 2 \text{ fm}$), and B_s is the bandpass of the range tracking loop, (see reference 14).

The variance in range rate is the same as developed for direct doppler measurement with the FM-CW system (75), $\sigma_{\dot{R}}^2 = \frac{\lambda^2 B_s^3}{12 (S/N_o)}$. In this expression S is the total received signal power because on range correlation the signal at the output of the phase demodulator is a CW signal at the doppler frequency which contains all of the received signal power.

Instrumentation Errors. - Since the range tracking loop is usually a Type I servo, there is no residual range tracking error when the relative velocity is zero. The instrumentation error in measuring range is due to the stability of the clock generator and the phase measuring (shifting) accuracy of the phase shifter for the clock signal. Thus, the percentage range error is:

$$(\%R)_{\text{RMS}} = \left[(\%f_c)^2 + (\%\phi_m)^2 \right]^2. \quad (149)$$

The instrumentation errors in measuring doppler to determine velocity are again:

$$(\%\dot{R})_{\text{RMS}} = \left[(\%\lambda)^2 + (\%f_d)^2 \right]^{\frac{1}{2}}. \quad (150)$$

Resolution and Ambiguities of PN, Binary Coded FM-CW Radars. - Ambiguity diagrams for the PN coded pulsed waveform are given in references 6 , 13 , and 12 . The ambiguity diagram for the PN/PM-CW system would look similar for codes of the length shown. However, to get good accuracy, the bit rate must be high, in which case the code must consist of a large number of bits with a CW system in order to resolve the range ambiguities. An ambiguity diagram would look as shown in figure 27 , where the complete area between the spikes in the τ, ω plane contains some energy.

There are no ambiguities in ω . However, ambiguities occur in range at n/f_c where n is the number of bits that make up the code. The range resolution is determined by the RF bandwidth of the signal which is equal to the clock frequency. Velocity resolution is again determined by the observation time.

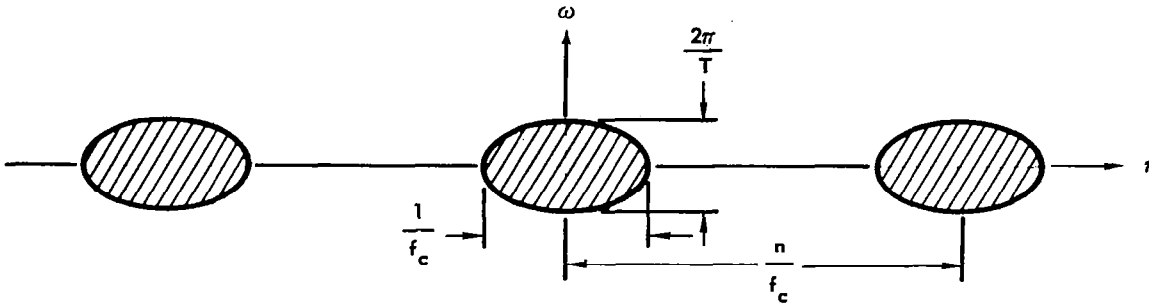


FIGURE 27 – PSUEDO NOISE PM-CW AMBIGUITY DIAGRAM

From the above, range resolution is:

$$R_{RES} = \frac{c \tau_{RES}}{2} = \frac{c}{2f_c}, \quad (151)$$

and range-rate resolution is:

$$\dot{R}_{RES} = \frac{\lambda}{4\pi} \omega_{RES} = \frac{\lambda}{2T}. \quad (152)$$

Since the energy is distributed over the entire τ, ω plane, this system is limited to cooperative or isolated target operation, also.

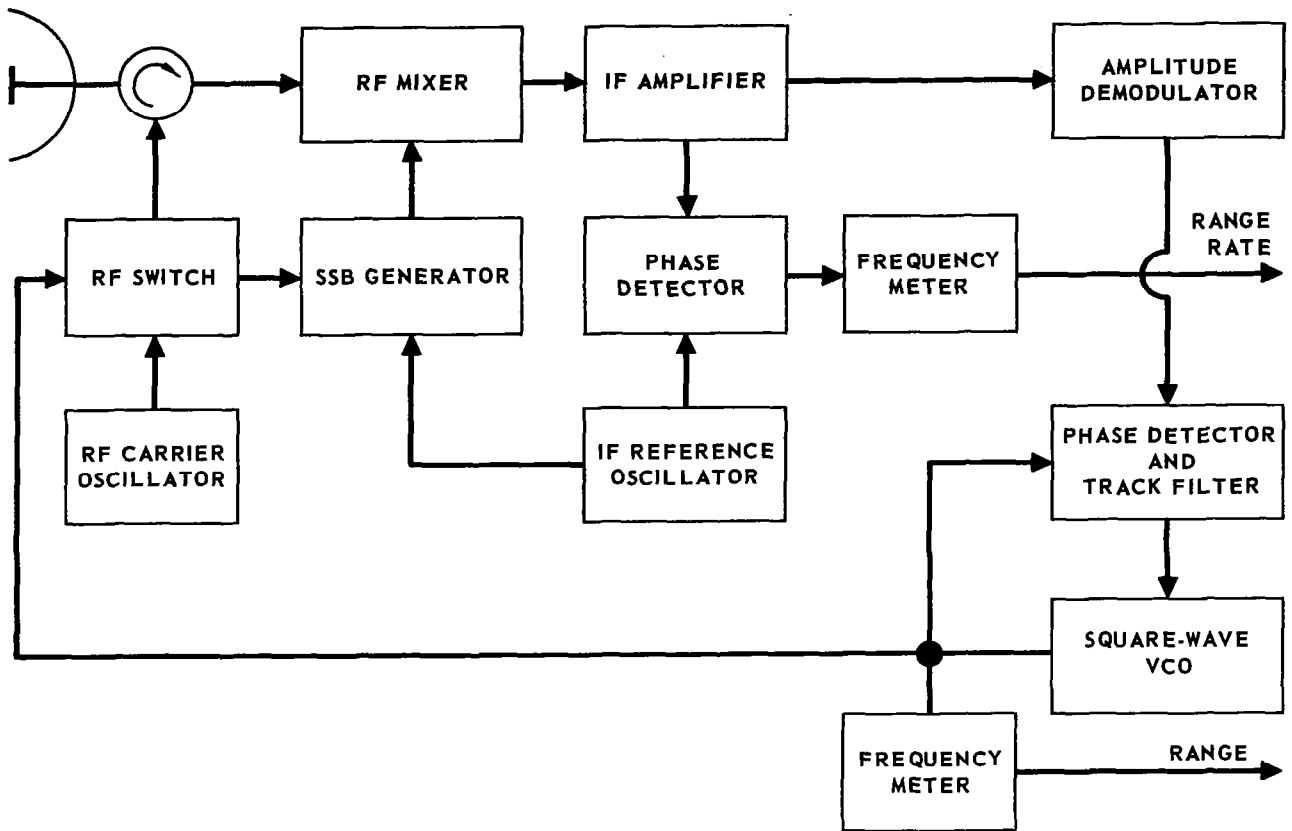
Amplitude Modulated CW Radar Systems

The only amplitude modulated CW system that will be considered is the interrupted CW (ICW) system with 50% duty cycle. This can be thought of as a long pulse system. However, with 50% duty cycle it has resolution limitations similar to the other CW systems so it is considered here.

A simple block diagram of an ICW system is shown in figure 28 . Range is measured by comparing the phase of the transmitted and received square wave modulation. Range-rate is measured by direct doppler processing.

Range and Range-Rate Accuracy. - Range is determined by the time between the transmitted and received modulation:

$$R = \frac{c\tau}{2}. \quad (153)$$



SINGLE FREQUENCY

FIGURE 28 – HETERODYNE, INTERRUPTED CW RADAR

From reference 51, page 468, the variance in the time delay measurement for leading edge tracking is the same as for optimum processing. This variance is:

$$\sigma_r^2 = \frac{T}{4B_{IF} (E/N_o)} \quad (154)$$

Now E is the energy in the received pulse. So $E = S_p T$, where T is the pulse width and S_p is the peak pulse power. For 50% duty cycle $S_p = 2S$ where S is the average signal power. Also, the pulse width is half the interpulse period, i.e., $T = \frac{1}{2f_m}$. Thus, the variance in range from equations 153 and 154:

$$\sigma_R^2 = \left(\frac{c}{2}\right)^2 \sigma_r^2 = \left(\frac{c}{2}\right)^2 \frac{T}{4B_{IF} (E/N_o)}, \quad (155)$$

which on substitution for Γ and T is:

$$\sigma_R^2 = \frac{c^2}{32 B_{IF} (S/N_O)} \quad (156)$$

Now the IF bandwidth need be only twice the highest modulation frequency, i.e.,

$$B_{IF} = 2 f_m, \text{ so then: } \sigma_R^2 = \frac{c^2}{64 f_m (S/N_O)} \quad (157)$$

If the range signal is then further smoothed in a filter with a noise bandwidth B_S , the range variance becomes:

$$\sigma_R^2 = \frac{c^2 B_S}{(8 f_m)^2 (S/N_O)} \quad (158)$$

Again doppler is used to measure velocity and equation 75 can be used:

$$\sigma_{\dot{R}}^2 = \frac{\lambda^2 B_S}{12 (S_O/N_O)} \quad (159)$$

Where S_O is the signal power in the received carrier. For 50% ICW, half of the received power should be in the carrier. Thus:

$$\sigma_{\dot{R}}^2 = \frac{\lambda^2 B_S}{6 (S/N_O)} \quad (160)$$

where S is the total received signal power.

Instrumentation Errors. - The accuracy of the ICW system is entirely dependent on measuring the time delay between transmitted and received signals. If a phase detector is used to measure this time delay, the instrumentation errors are the same as for the phase modulated system. Thus the rms percentage range error is:

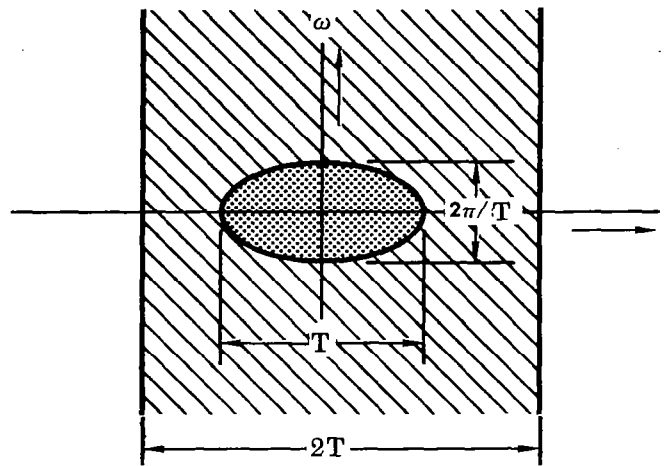
$$(\%R)_{RMS} = [(\%f_m)^2 + (\%\theta_m)^2]^{1/2} \quad (142)$$

Also the rms percentage error in measuring range rate is:

$$(\%\dot{R})_{RMS} = [(\%\lambda)^2 + (\%f_d)^2]^{1/2}, \quad (99)$$

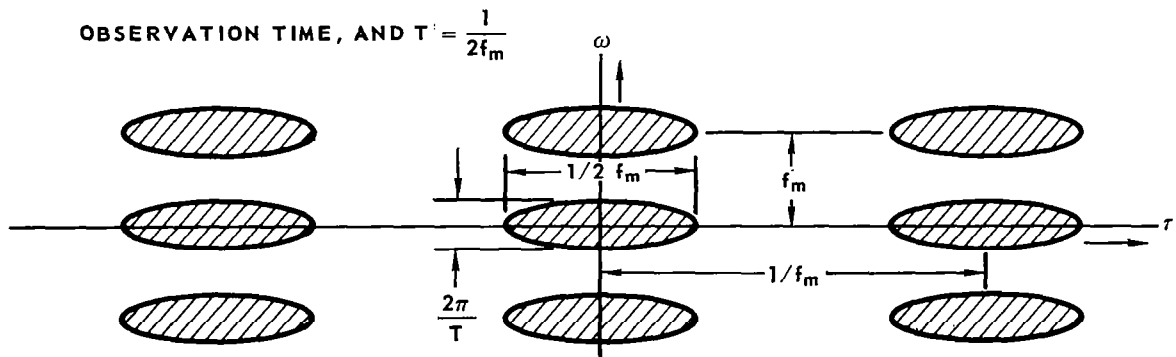
because direct doppler is used.

Resolution and Ambiguities of ICW Radars. - The ambiguity diagram for the ICW system can be derived from the ambiguity diagram for a single pulse given in references 6 and 7. This is for a pulse of duration T .



(a) SINGLE PULSE

For 50% duty cycle ICW, the ambiguity diagram is as shown below where T is the total observation time, and $T = \frac{1}{2f_m}$.



(b) 50% DUTY CYCLE - REPEATED PULSES

FIGURE 29 - ICW AMBIGUITY DIAGRAM

Again the ambiguity diagram contains energy throughout the entire (r, ω) plane which limits operation to cooperative or isolated target operation.

With this system range and range-rate ambiguities occur at multiples of $1/\text{fm}$ and fm respectively.

Range and range-rate resolution can be determined from the diagram of figure 29b:

$$R_{\text{RES}} = \frac{cT_{\text{res}}}{2} = \frac{c}{4f_m}, \quad (161)$$

and:

$$\dot{R}_{\text{RES}} = \frac{\lambda \omega_{\text{res}}}{4\pi} = \frac{\lambda}{2T}. \quad (162)$$

Cooperative Operation

Any of the cw radar systems previously described may be used with a transponder. The transponder will allow (1) decreased transmitter power for the docking radar, (2) a frequency offset between the transmitted and received signal in the docking radar to eliminate transmitter to receiver feedthrough problems, and (3) better target definition by the choice and location of transponder antennas.

Transmitter Power. - For cooperative operation, the received average signal power to noise density is given by the beacon equation (reference 51).

$$(S/N_o) = \frac{P_t G_t G_r \lambda^2}{(4\pi R)^2 FkTL}, \quad (163)$$

where:

- P_t = average transmitted power
- G_t = transmitter antenna gain
- G_r = receiver antenna gain
- λ = operating wavelength
- R = distance between radar and transponder
- F = receiver noise figure
- k = Boltzmann's constant (1.38×10^{-23} Joules/ $^{\circ}\text{K}$)
- T = Standard noise temperature (290°K)
- L = system losses

The same equation is used for determining power required when either the docking radar or the transponder is the transmitter.

Equation 163 can be substituted into the equations for the variances of range and range-rate that were derived in the preceding sections. For a given set of system parameters, this will allow the errors to be determined as a function of range, or the required transmitter power to be determined for a specified maximum range and error.

Transponder Consideration. - As mentioned in the previous paragraph, a frequency offset can be employed in the transponder to alleviate problems associated with transmitter-to-receiver feedthrough in both the docking radar and the transponder. The transponder receives the signal from the docking radar, shifts the frequency by a known amount and retransmits the signal back to the docking radar. The frequency offset must be known precisely if accurate doppler frequency measurements are to be made with the docking radar.

The accurate offset frequency can be obtained by (1) dividing and multiplying the carrier frequency of the signal received from the radar, (2) multiplying a sub-carrier frequency that has been added to the signal from the docking radar specifically for this purpose, or (3) using a precision reference oscillator in the transponder. The last technique will probably be inadequate due to the low doppler frequencies encountered in docking and corresponding stability required of the reference oscillator. The offset frequency must be greater than the bandwidth of the signal if the transmitted and received signals are to be separated by frequency filtering.

The transponder antenna must appear as a point source of transmitted energy for accurate angle tracking by the docking radar. The docking geometry and joining structure for the two vehicles must be such that the docking radar enjoys an unobstructed view of the transponder antenna. There must be no chance of multipath to cause range or angle boresight shifts.

Angle Tracking Techniques. - The cw radar systems are compatible with any of the standard radar techniques for accomplishing angle tracking such as conical scan, phase monopulse, amplitude monopulse, interferometry, electronic lobing, etc. These schemes for generating angle error signals are discussed in the section on angle measuring techniques. All arguments for each technique apply to cw radars as well as pulsed systems.

Noncooperative Operation

The cw radar systems can be used for noncooperative operation (skin tracking) if proper attention is given to reducing the transmitter-to-receiver feedthrough.

Transmitter Power. - When operating with a target vehicle that does not employ a transponder, the received average signal power to noise power density is given by the familiar radar equation (reference 51):

$$(S/N_0) = \frac{P_t G^2 \lambda^2 \sigma}{(4\pi)^3 R^4 F k T L}, \quad (164)$$

where:

- P_t = docking radar average transmitted power
- G = docking radar antenna gain (assumed the same for transmission and reception)
- λ = operating wavelength
- σ = target vehicle radar cross section
- R = distance between docking radar and the reflecting target
- F = receiver noise figure
- k = Boltzmann's constant
- T = standard noise temperature
- L = total system losses

This equation assumes that the target dimensions do not extend through the entire antenna beam. For extended target operation, the radar cross section is:

$$\sigma = \frac{4\pi\mu R^2}{G}, \quad (165)$$

where μ is the average relative reflectivity of the extended target. Substituting equation 165 into equation 164 the average received signal power to noise power density is:

$$(S/N_o) = \frac{P_t G \lambda^2}{(4\pi R)^2 FkTL\mu}. \quad (166)$$

This equation would apply when the antenna beamwidth is narrow and is illuminating a relatively small spot on the target vehicle.

Again equations 164 and 165 can be used with the equations for range and range-rate errors as discussed in the previous section for cooperative operation.

Transmitter - Receiver Feedthrough Considerations. - Maximum range is limited by the transmitted signal that is fed directly into the radar receiver. This feedthrough appears as a target at zero range.

For the FM-CW systems where the transmitted signal is used as the receiver reference, the spectrum of the feedthrough signal is very narrow in the system IF, and is centered at zero doppler frequency. A narrow filter centered at this frequency will reduce the feedthrough but will also reduce the minimum range to which the system can operate.

For the PM-CW systems where the unmodulated transmitter carrier is used as the receiver reference, the feedthrough will occupy the same bandwidth as the desired signal in the receiver IF. If a phase lock receiver was used, the feedthrough would have the same wide bandwidth but the desired signal would occupy a narrow frequency band in the IF when the system is in lock. Thus, the feedthrough power could be reduced by a narrowband filter around the desired signal after phase-lock is obtained.

In the ICW system, feedthrough can be disregarded if the modulation frequency is made to vary with range by a range tracking loop such that the system is alternately receiving when not transmitting and vice-versa.

If the total isolation between transmitter and receiver is I, the ratio of received signal power to feedthrough power is from equation 164:

$$\left(\frac{S}{P_{FT}}\right) = \frac{I G^2 \lambda^2 \sigma}{(4\pi)^3 R^4 L} \quad (167)$$

Approximately 10 db feedthrough reduction can be accomplished by feeding a controlled feedthrough signal through a tailored delay line and subtracting it directly from the received signal. Also, if separate antennas are used, approximately 60 db of isolation can be obtained. The maximum range for unity signal to feedthrough ratio is from equation 167:

$$R_{MAX} = \left[\frac{I G^2 \lambda^2 \sigma}{(4\pi)^3 L} \right]^{1/4} \quad (168)$$

Substituting typical parameters in the above equation, i.e.:

$$\begin{aligned} I &= 10^7 \text{ (10 db for direct cancellation and 60 db for} \\ &\quad \text{separate transmit and receive antennas)} \\ G &= 10^3 \text{ (30 db - 16" dia. antenna at X-band)} \\ \lambda &= 0.1 \text{ ft (X-band)} \\ \sigma &= 10 \text{ ft}^2 \text{ (1 sq. meter)} \\ L &= 2 \text{ (3 db losses)} \end{aligned}$$

$$R_{MAX} = \left[\frac{10^7 \times 10^6 \times 10^{-2} \times 10^1}{1.95 \times 10^3 \times 2} \right]^{1/4} = 127 \text{ feet.} \quad (169)$$

If an additional 40 db of feedthrough filtering were employed, the maximum range would be 1,270 feet. With 80 db of feedthrough filtering, the maximum range would be 12,700 feet.

To reduce the minimum range limitation caused by frequency filtering, the filters could be switched out after the docking vehicle got within 127 feet of the target in the above illustration.

If a single antenna with a circulator-duplexer is used, the maximum isolation that can be obtained is approximately 25 db. Thus, the maximum range with no filtering would be reduced to approximately 10 feet. The extra isolation could be obtained with additional filtering. All filtering could be switched out at 10 feet to allow operation to zero range.

Techniques for feedthrough filtering with an FM-CW system have been described in the literature (references 16, 17, and 18).

Angle-Tracking Techniques. - When the target occupies a small portion of the antenna beam, conventional angle tracking techniques can be employed. However, as the target gets larger than the cross section of the antenna beam, some other technique must be employed for pointing the antenna. With a manned

docking vehicle and a noncooperative target, the antenna could be slaved to an optical sight that is positioned by the pilot. The pilot would sight to that point on the target to which he wishes to measure range and range rate.

Docking Applications of CW Radar Techniques

The previous theoretical discussions for the different CW radar types do not provide adequate basis for choosing the best CW system for docking. Each system type must be further considered in view of the docking requirements, using the previous theoretical developments to help specify certain parameter values. Only after looking at the required values for certain parameters, seeing the ramifications of using some of these values, and further considering the total instrumentation required for each type system, can the best CW radar systems be evaluated for docking. Even this does not provide a clear case as to which is the best system, until specific integrated approaches are defined.

Therefore, an examination of each of the CW radar techniques will be made in this section, in light of the docking problem, in order that their cooperative and noncooperative docking capabilities and limitations can be defined.

Sine-Wave Modulated, FM-CW Radars. - It was stated earlier that the best system of this type (1) utilizes a range tracking loop and measures the modulation frequency to determine range for long ranges, and (2) uses a fixed modulation frequency and measures the amplitude of the received modulation to determine range for short ranges. This two-mode system results in the best range accuracy at all ranges for a given received signal to noise density ratio.

An alternate system for obtaining the required range accuracy at all ranges would measure the phase of the received modulation sine-wave to determine range. However, it would use more than one modulation frequency. Multiple modulation frequencies are required because as range decreases with a fixed modulation frequency, the variance in range increases per equation 60. Modulation frequencies greater than the maximum unambiguous frequency will result in a smaller variance. Thus, the high modulation frequencies would be used to obtain the desired accuracy and the low modulation frequencies would allow the ambiguities to be resolved.

Also, from equation 86, the percentage range instrumentation error is approximately equal to the percentage error in measuring phase over the unambiguous range interval of the modulation frequency (assuming f_m can be controlled very accurately). Therefore, if higher modulation frequencies can be used, the unambiguous interval is smaller, resulting in a smaller absolute error in range for a given phase measurement accuracy.

A well known limitation of wide-band FM communication systems is the threshold of the frequency discriminator. This limitation must be considered for the FM-CW radar system, also. In general, conventional frequency discriminators (Foster-Seeley type) have a threshold that is defined in the bandwidth of the IF amplifier preceding the discriminator. It varies with the deviation of the received signal, but for wide band systems it is approximately 13 db. That is:

$$(S/N)_{TH} = (S/N_o)_{TH} \frac{1}{B_{IF}} > 20, \quad (170)$$

and since B_{IF} must be approximately twice the frequency deviation of the received signal (i.e., $B_{IF} = 2\Delta f$), the threshold signal to noise density is:

$$(S/N_o)_{TH} \approx 40\Delta f. \quad (171)$$

Conventional second order phase-lock discriminators have a signal to noise density threshold that is described by:

$$(S/N_o)_{TH} \approx 2.68 \omega_n, \quad (172)$$

where ω_n is the natural resonant frequency of the phase-lock loop. ω_n is usually fixed at:

$$\omega_n = \sqrt{113\Delta f f_m}, \quad (173)$$

to make the loop phase error equal to 0.36 radians at threshold. Substituting equation 173 into equation 172:

$$(S/N_o)_{TH} \approx 28\sqrt{\Delta f f_m}. \quad (174)$$

A Phase-lock discriminator employing tuned circuits in the feedback path has been used (reference 16) that results in a threshold of:

$$(S/N_o)_{TH} \approx 20 f_m. \quad (175)$$

Ideally, the frequency discriminator should have a threshold that is not a function of the frequency deviation, or the modulation frequency. If a threshold must exist, it should only be a function of the smoothing bandwidth of the radar which is dictated by the target dynamics. However, to date, no such discriminator has been developed.

The threshold limitation of the wide band FM-CW system dictates some of the system parameters for operation out to 10,000 feet. For cooperative operation, equation 163 gives the received signal to noise density. Using equation 163 with $R = 10,000$ feet, $P_t = 0.1$ watts, $\sigma = 0.1$ ft. (X-band), $G_t = 0$ db (omni antenna on target vehicle), $G_R = 30$ db (16" parabolic antenna on docking vehicle), $F = 12$ db, and $L = 3$ db; the received signal to noise density is $(S/N_o) = 98$ db (6.3×10^9). This would allow the use of a conventional frequency discriminator, because of equation 171 the signal to noise threshold would only be 96 db (4×10^9) if a 100 MHz frequency deviation were used. Since the received signal to noise is above threshold, any of the techniques for determining range could be used for cooperative operation.

For noncooperative operation, equation 16⁴ dictates the received signal to noise density. Using equation 16⁴ with $R = 10,000$ feet, $\sigma = 10 \text{ ft}^2$ (1 sq. meter), and the other parameters just listed; the received signal to noise density is $(S/N_0) = 34 \text{ db}$ (2.5×10^3). Using the best discriminator whose threshold is given by equation 17⁵ the modulation frequency is limited to 125 Hz. Now, the modulation frequency required, using the frequency tracking scheme, is $f_m = c/4R = 2.5 \times 10^4 \text{ Hz}$ at 10,000 ft. range. Thus, at a range of 10,000 ft., the technique of range tracking with the modulation frequency is eliminated unless the transmitter power is increased to an impractical value.

However, the phase measuring technique can be used with a modulation frequency less than 125 Hz. If the maximum noncooperative range were decreased to 1,000 feet, the received signal to noise density would be increased to 74 db, and either scheme could be used with a conventional phase-lock discriminator.

With the phase measuring scheme, the variance in range (given by equation 60) varies at $1/R^2$. However, for noncooperative operation, the received signal to noise density varies as $1/R^4$. Thus, the standard deviation of range is proportional to range, or the system operates with a constant percentage error. If a percentage error of 0.1 percent were acceptable, the absolute error would be 10 feet at a range of 10,000 feet. The required frequency deviation could be found from equation 60. Solving equation 60 for Δf when $f_m = 125 \text{ Hz}$, $R = 10,000$ feet, $\sigma_R = 10$ feet, $B_s = 10 \text{ Hz}$, and $(S/N_0) = 2.5 \times 10^3$; $\Delta f = 63 \text{ MHz}$. The maximum deviation of the received signal would be one megahertz. From the standpoint of measurement errors, a phase measuring accuracy of 0.1% is obtainable at a frequency of 125 Hz.

In summary, it appears that the frequency measuring technique (in a modulation frequency tracking loop) would provide the best absolute accuracy for cooperative operation from 10,000 to zero feet and noncooperative operation from 1,000 to zero feet. However, this scheme could not be used for noncooperative operation from 10,000 feet because of the demodulator threshold. The phase measuring technique can be used and should be capable of providing a fixed percentage range accuracy of approximately 0.1 percent over the range from 10,000 to zero feet. A phase-lock demodulator with a tuned circuit in the feedback path is required to provide an acceptable signal to noise threshold.

For noncooperative operation, active feedthrough cancellation (or filtering) must be employed for operation down to 100 feet with dual antennas (or 10 feet with a single antenna). The cancellation must be switched out at these ranges so that operation to zero range can be accomplished. Approximately 80 db active feedthrough cancellation is required with dual antennas and 120 db with a single antenna.

The modulation frequency must be turned off periodically to measure doppler directly to determine range rate. For noncooperative operation at ranges where feedthrough filtering is employed, the feedthrough filter will cancel the unmodulated received signal if the doppler frequency is near zero. Thus, velocity measurement through zero is not possible.

The frequency deviation would be approximately ± 60 MHz. The modulation frequency would be approximately 120 Hz. The range error would be approximately 0.1% for all ranges. Range rate errors (equation 75) due to receiver noise at 10,000 feet ($S/N_0 = 34$ db) would be approximately 0.02 ft/sec (at X-band). Instrumentation errors in measuring range rate will be negligible due to the accuracy associated with measuring frequency.

Triangular - Wave Modulated, FM-CW Radars. - Triangular wave, FM-CW systems with zero IF were limited for many years because of the poor noise figure obtainable with mixer diodes (1/f noise). With new "back-diodes" and "hot-carrier diodes", (references 28 and 29) the knee where 1/f noise starts to predominate is for an IF of approximately one kilohertz rather than one megahertz for conventional diodes. A 30 db improvement in noise-figure is obtainable at frequencies below one kilohertz. Typical noise figures (reference 30) are 10 db at 10 kHz and above, 20 db at 1 kHz, and 30 db at 100 Hz. This advancement in receiver mixers places this type system in a competitive position for the docking sensor. Some of the practical considerations associated with using this radar are discussed in the following paragraphs.

For the triangular-wave modulated FM-CW radar, the signal out of the amplifier must be switched between two frequency meters in synchronism with the modulation frequency in order to measure doppler, as was mentioned before. If a wide-band amplifier is used just after the mixer, and this amplifier is followed directly by the doppler switch and frequency meters, the frequency meters will exhibit a threshold similar to conventional frequency discriminators. The threshold will be determined by the bandwidth of the wide-band amplifier and described by equation 170, where B_{IF} is the bandwidth of the zero IF amplifier. The bandwidth of this amplifier is proportional to the difference between maximum and minimum range. That is, from equation 109:

$$B_{IF} = (f_{dmax} - f_{dmin}) = \frac{8\Delta F f_m}{c} (R_{max} - R_{min}) \cdot \quad (176)$$

Due to the 1/f noise just discussed, the minimum frequency should be greater than 100 Hz. The maximum frequency will be near a megahertz. Thus:

$$B_{IF} \approx \frac{8\Delta F f_m}{c} R_{max} \cdot \quad (177)$$

To minimize the threshold and reduce the required power, phase-lock tracking filters should be used after the doppler switch before each frequency meter. The signals out of the doppler switch are at frequencies f_d (up) and f_d (down) (from equation 113) which are amplitude modulated by a square wave at the modulation frequency f_m . The phase-lock loops must have some gain at the modulation frequency, f_m , to insure that they lock on the center spectral line of these signals and not on one of the side-bands. The threshold of these tracking filters (and the resultant threshold of the frequency meters that follow are established by the natural resonant frequency of the phase-lock loops (equation 192). Assuming $\omega_n = 2\pi f_m$, the threshold is:

$$(S/N_o)_{TH} = 2.68 (2 \pi f_m) = 16.8 f_m \quad (178)$$

If the (S/N_o) at maximum range is equal to the threshold $(S/N_o)_{th}$, the variance of the range measurement is (from equation 114 and 178):

$$\sigma_R^2 = \frac{c^2 f_m}{3(8\Delta F)^2 (S/N_o)_{TH}} = \frac{c^2}{3 \times 16.8 (8\Delta F)^2} \quad (179)$$

which can be solved for the required frequency deviation, given the required variance at maximum range. Letting the variance be one foot, the required frequency deviation is 18 megahertz.

Using the parameters of the previous section, a transmitter power of 0.1 watt will produce a signal to noise density of 34 db (i.e., $S/N_o = 2.5 \times 10^3$) at 10,000 feet during noncooperative operation. If this is to be the threshold, from 178 the modulation frequency must be less than 150 Hz.

The difference frequency (from 109) at a range of two feet would be 43 Hz with $\Delta F = 18$ MHz and $f_m = 150$ Hz. To keep the difference greater than 100 Hz (because of the $1/f$ noise and resultant lower cutoff frequency of the zero IF amplifier), the frequency deviation should be increased to approximately 50 megahertz to measure range in to two feet. ($f_{d_{min}} = 120$ Hz).

However, with a 100 Hz lower cutoff frequency and 150 Hz modulation frequency, the difference frequency must be at least 250 Hz for measuring doppler (in order that the center spectral line of the spectrum can be tracked). Thus, the minimum range for measuring velocity would be four feet with $F = 50$ MHz and $f_m = 150$ Hz.

The accuracy of the system will be limited by the instrumentation errors when the above frequency deviation and modulation frequency are used. From equation 121, the principle source of error will be the accuracy of maintaining the deviation ratio. This can be held to within 0.1 to 1.0 percent, depending on the circuit complexity that can be tolerated.

A sub-modulation signal must be used to reduce the step error in this application. The step error from equation 122 is 2.5 feet. The sub-modulation will reduce step error to where it is never greater than 0.5 feet.

In summary, the triangular FM-CW system will be capable of cooperative, or noncooperative, operation to ranges of 10,000 feet with a transmitter power of 100 milliwatts if the newest low-noise diodes are used for the mixer. The frequency deviation should be approximately 50 megahertz, and the modulation frequency 150 Hz. The minimum range for measuring range with this deviation would be 2 feet. The range for measuring velocity would be 4 feet. Velocity can be measured through zero for ranges greater than 4 feet. The accuracy of measuring velocity will be approximately 0.014 ft/sec (at X-band).

The complexity of the system has been increased over that for standard FM-CW altimeters. Frequency tracking circuits are employed; plus the doppler switch, the extra frequency meter, and the logic circuit for taking the sum and difference frequencies to get range and range-rate, respectively. A sub-modulation frequency oscillator must be added to reduce step error, and extra control circuitry is necessary to stabilize the frequency deviation to reduce the range measurement error. However, no active feedthrough cancellation is necessary.

Sine-Wave Modulated FM-CW Radars. - This system would be the simplest of the CW radar systems to instrument. However, it would only be useful for cooperative operation.

For noncooperative operation, some active feedthrough cancellation (or filtering) is necessary. To accomplish this feedthrough filtering, the transmitted signal is mixed with the received signal to cause the feedthrough to occupy a narrow bandwidth at the center of the IF bandpass. For dopplers near zero, the feedthrough filter will cancel out the carrier on the desired signal so that doppler cannot be measured directly but must be derived by locking a phase-lock loop to the modulation side-bands. This means that the bandwidth of the phase-lock loop (or natural resonant frequency) must be greater than the modulation frequency.

Using the same parameters as in the previous calculation for received signal to noise density, $(S/N_0) = 34$ db for noncooperative operation at 10,000 ft. However, the threshold of the best phase-lock demodulator is described by equation 175 which says that the highest modulation frequency is 125 Hz for a threshold of 34 db.

Substituting this modulation frequency and signal to noise in equation 139, the variance of the range measurement will be:

$$\sigma_R^2 = \frac{c^2 B_s}{2(2\pi f_m \Delta\phi)^2 (S/N_0)} = \frac{(9.83 \times 10^2)^2 \times 1}{2(2\pi \times 125 \times 1)^2 \times 2.5 \times 10^2} = 3.2 \times 10^{10}, \quad (180)$$

or

$$\sigma_R = 1.8 \times 10^5 \text{ ft.} \quad (181)$$

for a smoothing bandwidth of one Hz, and phase deviation of one radian. A modulation frequency of 220 kilohertz is necessary to get 100 foot accuracy with $B_s = 1$, $\Delta\phi = 1$, and $(S/N_0) = 34$ DB.

In summary, for noncooperative operation to 10,000 feet, the signal to noise threshold of the demodulator must be equal to (or less than) the received signal to noise. Since the received signal to noise is so small, the bandwidth of the demodulator must be small. This narrow bandwidth requires a small modulation frequency, which limits the range accuracy that can be obtained.

The sine-wave modulated, FM-CW system can be considered as an extension of the sine-wave modulated, PM system. The phase-modulated system becomes a frequency-modulated system by increasing the deviation ratio of the transmitted signal. The range accuracy cannot be achieved with a phase-modulated system with small phase deviation. However, by increasing the deviation and changing the system to a wide-band FM system, the accuracy can be obtained. This all results because of the threshold of the demodulator which is proportional to the modulation frequency instead of the allowable smoothing bandwidth.

As was stated before, this system would be very easy to instrument for cooperative operation. Doppler can be measured continuously with no switching required. The required range accuracy can be obtained by using two modulation frequencies. The coherent offset could be derived in the transponder from one of the ranging sub-carriers.

PN, Binary Code Modulated PM-CW Radars. - The coded PM-CW system could be used for cooperative operation with a frequency offset supplied by the transponders. However, this system offers no advantages over the two-tone PM-CW system for cooperative operation, and the extra complexity of the coded system would make it a poor choice.

For noncooperative operation the system does have some advantages. The block diagram of figure 26 must be modified for noncooperative operation at ranges where the feedthrough is larger than the received signal. For feedthrough filtering, the spectrum of the feedthrough signal must be compressed. This can be accomplished by offsetting in frequency a sample of the transmitted signal and using it as the reference for the receiver mixer. The compressed feedthrough spectrum can be attenuated by a narrow band filter that is synchronous with the offset frequency (reference 16).

Using the transmitted signal as the receiver reference causes the code of the desired signal to be changed to a new code. However, the new code has the same pseudo-random characteristics as the original code and has the effect of being shifted to a new time delay (reference 12). It still has the same power spectral density as the original code and is affected very slightly by the removal of the small amount of power in the center of the spectrum by the feedthrough filter. The new code does not possess a continuous delay with range, however. After the feedthrough has been cancelled in the IF, the original code can be regained by again modulating the received signal with the transmitted code. This modulation flips the phase of the received signal back to where it was before being mixed with the transmitted signal.

The correlation with the delayed transmitted code can now be accomplished to determine range. In the simple system of figure 16, the doppler is offset by the IF reference frequency. The doppler can be recovered in magnitude and "sense" by in phase, and quadrature mixing with the offset reference signal. The two quadrature doppler outputs are then compared in a phase sensitive detector to get the doppler "sense" signal which can be used as the error signal for the range tracking loop.

From a previous section, the feedthrough cancellor can be switched out at 100 feet with dual antennas and 10 feet with a single antenna. In order to have adequate resolution so as not to cancel the desired target at these ranges, the bit rates must be 5 megahertz and 50 megahertz respectively (from equation 151). This system requires less feedthrough cancellation than the FM-CW system because range search can start at maximum range and correlation with the received signal accomplished when the feedthrough is approximately 20 db larger than this signal (with a 100 bit word).

With the signal to noise density of 34 db, the variance in range would be less than one foot with a 5 megahertz bit rate, and 10 Hz smoothing bandwidth (equation 148). The instrumentation error in measuring range would be due to the accuracy of measuring the phase of the code fundamental. With a phase measuring accuracy of between 0.1 and 1 percent, the error would be between 0.2 2 feet with the 5 megahertz bit rate. The variance in range rate should again be 0.02 ft/sec by direct doppler measurement.

With a 5 megahertz clock frequency, each bit corresponds to 100 feet of range. For the code to be unambiguous at 10,000 feet, it must contain 100 bits. An eight element shift register can generate a code of 128 bits in length.

In summary, the system can measure doppler directly with no switching required, the instrumentation errors are small, and the errors due to receiver noise at maximum range are small. However, for noncooperative operation, active feedthrough filtering is necessary; and for both cooperative and noncooperative operation, it requires a range tracking loop.

ICW Radars. - The ICW system with the modulation frequency adjusted so that the transmitter is not transmitting while the signal is being received from the target allows noncooperative operation with no feedthrough filters. A range tracking loop is established to lock the period of the modulation to twice the time delay associated with the range interval, i.e., $T = 1/f_m = 2 \left(\frac{R}{c} \right)$, so that $f_m = \frac{4R}{T}$. At the maximum range of 10,000 feet, the minimum modulation frequency will be 25 kHz.

From equation 158, with the received signal to noise density of 34 db (for noncooperative operation at 10,000 feet) and smoothing bandwidth of 10 Hz, the variance in range will be 317 feet. This is a percentage error of approximately 3%. However, as range decreases, the error decreases rapidly because f_m and S/N_0 both increase. For example, a factor of two decrease in range results in a factor of 8 decrease in the variance, or a factor of 4 decrease in percentage error. That is, at 5,000 feet the percentage error is reduced to 0.8%. The frequency of the modulation would be measured to determine range.

Obviously, the modulation frequency cannot be decreased indefinitely as range approaches zero. An acceptable technique is to allow the modulation frequency to vary with range until range decreases to approximately 100 feet ($f_m = 2.5\text{MHz}$). The modulation frequency is then held at this value, and the phase of the fundamental of the amplitude modulated signal out of the receiver is compared to the phase of the transmitted modulation to determine range. The phase difference will vary from 180° to 90° as the range varies from 100 to zero

feet. If this phase difference can be measured with an accuracy of 0.1 to 1.0 percent over a 180° interval, the error in range will be between 0.2 and 2 feet from 100 feet into zero.

Range rate can be measured continuously with no switching. From equation 148, the range rate accuracy will be .028 ft/sec at 10,000 ft during non-cooperative operation.

Frequency shift keying for the transmitter provides a technique for switching the transmitted signal on and off while simultaneously providing an offset signal to the receiver mixer (reference 23).

Limiting could be employed in the receiver since phase of the received amplitude modulated signal is measured to determine range. This limiting and phase measuring technique will reduce the effect of the finite switching time of the transmitter so that the minimum range will be a foot or less.

Best CW Radar for Cooperative Docking. - After analyzing each of the CW radar systems, it appears that the following system represents the best CW choice for most cooperative docking missions. For both manned and unmanned cooperative operation (employing a transponder), 0.1 watt transmitter power and a 16 inch aperture will provide a received signal to noise density adequate to:

- a. Overcome threshold problems in all systems and allow conventional discriminators to be used with FM systems.
- b. Provide range and range-rate accuracies that are dictated by instrumentation.

Of the various CW radars, the Sine-Wave modulated PM-CW radar is the best system because of the following:

- a. It is easiest to instrument for a given range accuracy. Two tones (50 kHz and 9MHz) will resolve range ambiguities at 10,000 feet and provide 0.3 feet error at all ranges with a phase measuring accuracy of only 2 degrees.
- b. Range-rate is measured continuously by direct doppler processing of the received carrier. No switching is required. Range-rate accuracy is limited by doppler frequency measurement errors.
- c. The transponder is simple to instrument. The coherent offset can be derived by either (1) proper multiplication of the received carrier before re-transmissions, or (2) multiplying the frequency of a ranging subcarrier.
- d. The radar and transponder are the easiest to modify to add communication channels. Subcarrier oscillators can be added to either equipment (with the associated modulators and demodulators for communication) with minimum effects on the radar.

- e. The FM-CW system is adaptable to all angle tracking techniques, including phase interferometry.

Best CW Radar for Noncooperative Docking. - For manned, noncooperative operation, the radar could angle track the target vehicle until range decreased to the point where the angular cross section of the vehicle is greater than the antenna beamwidth. From these short ranges on in, the radar beam could be pointed manually by the astronaut with an optical aid. In this "searchlight" mode, range and range-rate would be measured to the point on the target vehicle that is illuminated by the antenna beam. Only angular resolution would be required, allowing the CW radar to be used. (Range resolution characteristics of CW radar will not allow "leading edge tracking" of a target extended in range.)

Among the CW radars considered for noncooperative operation, only two do not require active feedthrough rejection. These are:

- a. Homodyne, triangular-wave, FM-CW
- b. Interrupted CW

Both of these systems have similar complexity in that they require about the same number and type of circuits. Both have similar range-rate measurement errors. (Error due to receiver noise at 10,000 feet is approximately 0.02 ft/sec.) Range errors due to receiver noise in both systems are well below instrumentation errors at all ranges less than 10,000 feet. Plots of range error versus range for both systems are shown in figure 30.

The range error for the FM-CW is dictated by the accuracy with which the frequency deviation can be controlled for long ranges and step error at short ranges. The range error in the ICW system is dictated by the bias errors in the tracking loop while tracking with the modulation frequency, and the accuracy at which phase can be measured at short ranges where the modulation frequency is held constant. The curves of figure 30 merely indicate that the instrumentation errors can be made smaller with the ICW system.

In summary, the ICW radar is considered the best system for manned, noncooperative docking because:

- a. It requires no active feedthrough rejection.
- b. It has smaller instrumentation errors in measuring range than the homodyne FM-CW radar which also requires no active feedthrough rejection.

If one sensor is required for both cooperative and noncooperative operation, the ICW radar could be used for both. However, it is believed that the sine-wave modulated PM-CW system is much better for the cooperative mode because:

- a. The transponder would be much simpler than for the ICW system.

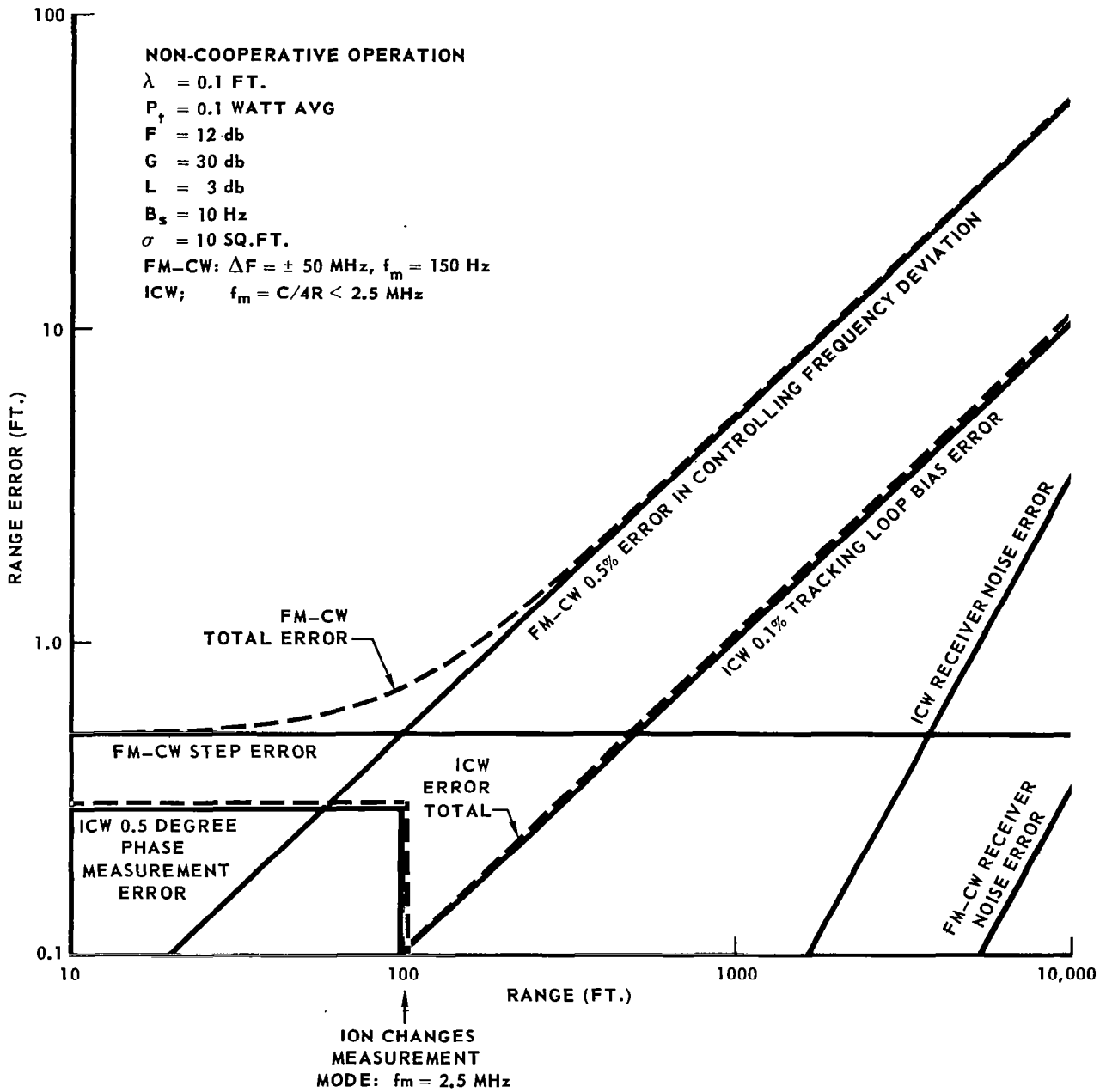


FIGURE 30 – COMPARISON OF RANGE ERRORS BETWEEN FM-CW AND ICW RADAR SYSTEMS

- b. The FM-CW scheme is more adaptable to adding communication channels.
- c. The FM-CW system will have smaller instrumentation errors at the longer ranges (as stated before, approximately 0.3 feet fixed error at all ranges can be obtained with a modulation frequency of 9 MHz and a phase measuring error of 2 degrees).

For unmanned, noncooperative operation, the range-rate resolution characteristics of a CW radar may be of value in determining target vehicle spin orientation and spin rate. However, to determine size and shape of the target vehicle, extremely fine range, or angle resolution is necessary. Due to the range resolution characteristics of a CW radar and the difficulty associated with providing a range display, a pulse system would be required to get a range "paint" of the target. However, a CW radar could be used with a narrow beam scanning antenna to get an angular "paint" of the target. A one degree beam-width would provide one foot angular resolution at 57 feet. Either the FM-CW or the ICW system (discussed in the preceding paragraphs for noncooperative operation) could be used for this angle paint. However, the ICW looks best for unmanned, noncooperative operation because of the ability of the system to separate the center line of the received signal for target spin analysis.

A summary of CW radar characteristics is presented in table 5.

**TABLE 5
SUMMARY OF CW RADAR CHARACTERISTICS**

SYSTEM TYPE	COOPERATIVE OPERATION (FREQUENCY OFFSET PROVIDED IN THE TRANSPONDER)		NONCOOPERATIVE OPERATION		
	RANGE MEASUREMENT	RANGE-RATE MEASUREMENT	RANGE MEASUREMENT	RANGE-RATE MEASUREMENT	FEEDTHROUGH
SINE-WAVE MODULATED FM-CW	FOR LONG RANGES: RANGE TRACKING LOOP; MODULATION FREQUENCY ADJUSTED WITH RANGE TO PEAK RECEIVED DEVIATION; MEASURE MODULATION FREQUENCY TO DETERMINE RANGE. FOR SHORT RANGES: SINGLE MODULATION FREQUENCY AND DEVIATION OF RECEIVER SIGNAL MEASURED TO DETERMINE RANGE.	INTERRUPT MODULATION AND MEASURE DOPPLER.	USE SINGLE MODULATION FREQUENCY ($f_m = 120$ Hz AND $\Delta f = 240$ MHz); AND MEASURE PHASE OF RECEIVER MODULATION TO DETERMINE RANGE. HAVE CONSTANT PERCENTAGE ERROR DUE TO RECEIVER NOISE OF APPROXIMATELY 0.1 PERCENT. INSTRUMENTATION ERROR OF 0.1 TO 1 PERCENT. NEED PHASE-LOCK DEMODULATOR WITH TUNED CIRCUIT AT MODULATION FREQUENCY IN FEEDBACK PATH).	INTERRUPT MODULATION AND MEASURE DOPPLER. VARIANCE IN RANGE-RATE AT MAXIMUM RANGE APPROXIMATELY 0.02 FT/SECOND. CANNOT MEASURE THROUGH ZERO DOPPLER BECAUSE OF FEEDTHROUGH FILTER.	ACTIVE FEEDTHROUGH REJECTION: 80 DB WITH TWO ANTENNA 120 DB WITH SINGLE ANTENNA. MOST TURN OFF FEEDTHROUGH REJECTION AT 100 FEET WITH TWO ANTENNAS AND 10 FEET WITH SINGLE ANTENNA TO ALLOW RANGE TO BE MEASURED TO ZERO.
TRIANGULAR WAVE MODULATED FM-CW	MEASURE DIFFERENCE BETWEEN TRANSMITTED AND RECEIVED FREQUENCY TO DETERMINE RANGE.	SWITCH BETWEEN TWO FREQUENCY METERS IN SYNCHRONIZATION WITH MODULATION AND TAKE DIFFERENCE BETWEEN THE TWO FREQUENCY MEASUREMENTS TO DETERMINE RANGE-RATE.	SAME AS FOR COOPERATIVE OPERATION. NEED TRACKING FILTERS BECAUSE OF SMALL (5 M) IN IF BANDWIDTH (MODULATION FREQUENCY = 150 Hz, $\Delta f = 50$ MHz); MINIMUM RANGE = 2 FT; MEASURED ACCURACY LIMITED BY STABILITY OF Δf TO APPROXIMATELY 0.1 PERCENT; USE SUB-MODULATION TO REDUCE STEP ERROR TO LESS THAN 0.5 FT.	SAME AS FOR COOPERATIVE OPERATION. NEED TWO TRACKING FILTERS - ONE FOR EACH FREQUENCY METER BECAUSE OF SMALL 5'N IN REQUIRED IF BANDWIDTH. MINIMUM RANGE FOR MEASURED VELOCITY IS 4 FT. VARIANCE IN RANGE-RATE AT MAXIMUM RANGE APPROXIMATELY 0.014 FT/SECOND.	NO ACTIVE CANCELLATION REQUIRED.
SINE-WAVE MODULATED PM-CW	USE TWO MODULATION FREQUENCIES AND MEASURE PHASE TO DETERMINE RANGE. ONE MODULATION FREQUENCY TO OBTAIN REQUIRED ACCURACY, AND THE OTHER TO RESOLVE AMBIGUITIES.	MEASURE DOPPLER BY PHASE-LOCKING TO RECEIVED CARRIER. NO SWITCHING NECESSARY.	CANNOT BE USED FOR NONCOOPERATIVE OPERATION. (WOULD NEED FEEDTHROUGH FILTERING AND BANDWIDTH OF RECEIVED SIGNAL IS 50 HAZARD THAT IT WOULD BE REJECTED ALSO.)		
PM-CODED MODULATED PM-CW	WOULD USE A BINARY CODED SIGNAL GENERATED BY SHIFT REGISTERS TO PHASE MODULATE THE CARRIER 180 DEGREES. RANGE DETERMINED BY DELAYING THE TRANSMITTED CODE AND CORRELATING WITH THE RECEIVED SIGNAL. THE AMOUNT OF DELAY IS A DIRECT INDICATION OF RANGE. REQUIRES A RANGE TRACKING LOOP.	CORRELATED SIGNAL AT OUTPUT OF RECEIVER IS AT THE DOPPLER FREQUENCY. MEASURE DOPPLER DIRECTLY TO DETERMINE RANGE. NO SWITCHING NECESSARY.	SAME AS FOR COOPERATIVE OPERATION. THE PHASE DELAY OF THE CLOCK SIGNAL PROVIDES A FINE RANGE MEASUREMENT WITH SINGLE ANTENNA. CLOCK FREQUENCY OF 50 MHz IS REQUIRED; WITH DUAL ANTENNAS COULD USE A 5 MHz CLOCK, AND 8 ELEMENT SHIFT REGISTERS TO GENERATE 128 BIT WORDS. RANGE ERROR LESS THAN 1 FT. DUE TO RECEIVED NOISE AND -0.2 TO 2 FT. DUE TO PHASE MEASUREMENT ERRORS.	SAME AS FOR COOPERATIVE OPERATION. VARIANCE IN RANGE-RATE AT MAXIMUM RANGE IS APPROXIMATELY 0.02 FT/SECOND.	ACTIVE FEEDTHROUGH REJECTION: 80 DB WITH TWO ANTENNA 100 DB WITH SINGLE ANTENNA. MUST SWITCH OUT FEEDTHROUGH FILTERS AT SHORT RANGES TO MEASURE RANGE TO ZERO FEET.
INTERRUPTED AM-CW	RANGE TRACKING LOOP; VARY MODULATION FREQUENCY TO LOCK PERIOD OF MODULATION TO TWICE THE RADAR TIME DELAY. MEASURE FREQUENCY TO DETERMINE RANGE. AT SHORT RANGES, FIX MODULATION FREQUENCY AND MEASURE PHASE OF THE MODULATION FUNDAMENTAL OUT OF THE RECEIVER TO DETERMINE RANGE.	MEASURE DOPPLER OF RECEIVED CARRIER TO DETERMINE RANGE-RATE. NO SWITCHING NECESSARY.	SAME AS FOR COOPERATIVE OPERATION. MODULATION FREQUENCIES VARY FROM 25 kHz AT 10,000 FT. TO 2.5 MHz AT 100 FT; AND FIXED AT 2.5 MHz FROM 100 FT. TO ZERO ERROR DUE TO RECEIVED NOISE 3% AT 10,000 FT AND DECREASES WITH RANGE (0.8% AT 5000 FT, ETC). MEASUREMENT ERROR 0.2 TO 2 FT FROM 100 TO ZERO FEET. NEGLIGIBLE FROM 10,000 TO 100 FT.	SAME AS FOR COOPERATIVE OPERATION. ACCURACY OF 0.028 FT/SEC AT 10,000 FT DUE TO RECEIVED NOISE.	NO FEEDTHROUGH REJECTION NECESSARY. RECEIVING WHEN TRANSMITTER IS SHUT OFF AND VICE VERSA.

ALL OF THE ABOVE BASED ON THE FOLLOWING PARAMETERS:

$$P_t = 0.1 \text{ WATTS}$$

$$F = 12 \text{ DB}$$

$$R_{\text{MAX}} = 10,000 \text{ FT.}$$

$$L = 3 \text{ DB}$$

$$\lambda = 0.1 \text{ FT (X-BAND)}$$

$$a = 10 \text{ SQ.FT. (FOR NONCOOPERATIVE)}$$

$$G_R = 30 \text{ DB (16 INCH PARABOLA ON DOCKING VEHICLE)}$$

$$G_t = 0 \text{ DB (OMNI ANTENNA ON TARGET VEHICLE FOR COOPERATIVE OPERATION)}$$

$$B_s = 10 \text{ Hz (FOR RANGE AND RANGE-RATE MEASUREMENT)}$$

$$(S \text{ No}) = 98 \text{ DB FOR COOPERATIVE OPERATION}$$

$$(S \text{ No}) = 34 \text{ DB FOR NON-COOPERATIVE OPERATION}$$

PULSE RADAR SYSTEMS

The radar that received the most intensive early development was the noncoherent pulse radar. This radar system is a basic one where target range information is obtained by measuring the time delay between the transmission of a short burst of RF energy and the reception of the echo from the target. A simple block diagram is shown in figure 31.

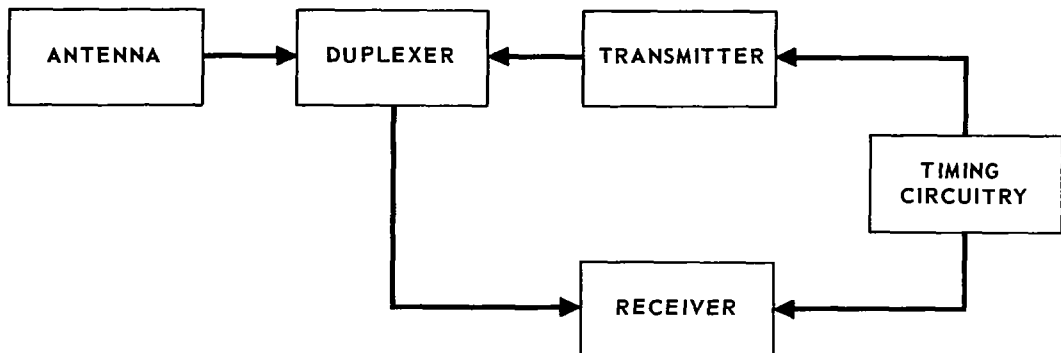


FIGURE 31 – NON COHERENT PULSE RADAR

General System Operation

The transmitter generates a pulsed RF signal $s(t)$ where:

$$s(t) = \begin{cases} Ae^{j\omega_0 t}, & 0 < t < T; \\ 0, & \text{otherwise}; \end{cases} \quad (182)$$

$A = \text{Constant}$
 $T = \text{Pulse Width}$

This signal is transmitted, reflected from the target, and received after a time delay τ . This time delay is a measurement of range (R).

$R = \frac{c\tau}{2}$ where c is velocity of electromagnetic wave propagation. The reflected signal, y , is greatly reduced and noise is also added to the receiver.

$$y = s(t - \tau) + \text{Noise}. \quad (183)$$

This signal can then be processed in a matched filter receiver for maximum signal to noise ratio.

Matched Filters Receiver. - The matched filter idea is credited to D.O. North of R.C.A., 1943. A matched filter receiver is defined as one whose transfer function is the complex conjugate of the Fourier transform of the input signal or:

$$H(\omega) = S^{*}(\omega), \quad (184)$$

where:

$$S(\omega) = \int_{-\infty}^{\infty} s(t) e^{-j\omega t} dt, \quad (185)$$

The output of the matched filter is given by:

$$E_o(\omega) = Y(\omega) H(\omega), \quad (186)$$

$$e_o(t) = y(t) * h(t), \quad (187)$$

$$e_o(\tau) = \int_{-\infty}^{\infty} y(t) h(\tau - t) dt, \quad (188)$$

$$e_o(\tau) = \int_{-\infty}^{\infty} [s(t) + n(t)] h(\tau - t) dt, \quad (189)$$

$$e_o(\tau) = \int_{-\infty}^{\infty} s(t) h(\tau - t) dt + \int_{-\infty}^{\infty} n(t) h(\tau - t) dt. \quad (190)$$

The first integral is the convolution of the transmitted signal with the system function and the second integral is the convolution of noise with the system function. The convolution of noise with the system function causes noise ambiguities and false alarms, if the noise is large enough. This can be alleviated by raising the receiver threshold. Since adequate measurement accuracies will require a large signal to noise ratio, this portion of the received signal will be negligible in determining the resolution capability of the radar. Therefore, the output of the receiver for large signal to noise ratio signals will be:

$$e_o(\tau) = \int_{-\infty}^{\infty} s(t) h(\tau - t) dt, \quad (191)$$

$$= \int_{-\infty}^{\infty} s(t) s(t - \tau) dt, \quad (192)$$

which is the autocorrelation function of the transmitted signal, $c(\tau)$.

Range Resolution. - The resolution capability of the radar waveform is of interest when the target is of an extended nature. For maximum range resolution, the transmitted waveform should be as different from its time shifted self as possible. A measure of the resolution capabilities of the transmitted waveform is taken as the mean departure or integrated square error.

$$\epsilon^2 = \int_{-\infty}^{\infty} |s(t) - s(t - \tau)|^2 dt, \quad (193)$$

$$\epsilon^2 = \int_{-\infty}^{\infty} |s(t)|^2 dt + \int_{-\infty}^{\infty} |s(t - \tau)|^2 dt - 2 R_e \int_{-\infty}^{\infty} s(t) s(t - \tau) dt. \quad (194)$$

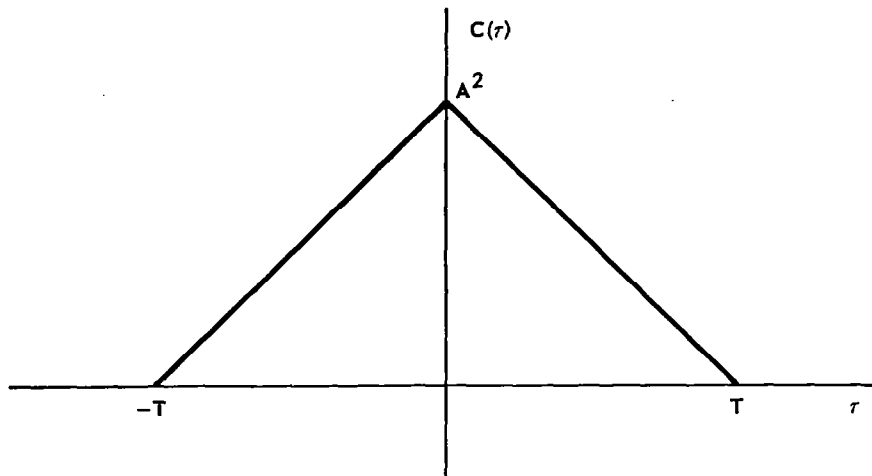


FIGURE 32 – TRANSMITTED SIGNAL AUTOCORRELATION FUNCTION

The first two integrals are proportional to the energy of the signal and the last term is an oscillatory function of τ . Since no use can be made of the fine structure due to ω_0 , only the magnitude is of interest. This term then becomes:

$$|2 \operatorname{Re} \int_{-\infty}^{\infty} s(t) s^*(t-\tau) dt| = \int_0^T A(t) A(t-\tau) dt, \quad (195)$$

which is $c(\tau)$, the autocorrelation function of the envelope of the transmitted signal. This has previously been shown to be the output of a matched filter receiver.

Because comparison of uncorrelated signals should be made on power rather than voltage basis, we are interested only in the squared magnitude of or $|c(\tau)|^2$.

A similar analysis can be made in the frequency domain, arriving at the complex frequency correlation function:

$$k(v) = \int U(f) U^*(f-v) df, \quad (196)$$

$k(v)$ = complex frequency correlation coefficient,

$U(f)$ = spectrum of the transmitted signal.

For the frequency matched filter:

$$H(f) = U^*(f). \quad (197)$$

Then the output is the convolution of:

$$e(f) = U(f) * U^*(f), \quad (198)$$

$$= \int_{-\infty}^{\infty} u(t) u(-t) e^{j2\pi vt} dt, \quad (199)$$

$$= \int_{-T}^T A e^{j2\pi ft} A e^{-j2\pi ft} e^{j2\pi ut} dt, \quad (200)$$

$$= A^2 \frac{\sin 2\pi f T}{2\pi f T}, \quad (201)$$

the familiar $\frac{\sin X}{X}$ spectrum (figure 33).

The combined correlation function:

$$|\psi(\tau, \omega)|^2 = |c(\tau)k(\omega)|^2, \quad (202)$$

is a three dimensional plot.

$$\psi(\tau, \omega) = \int_{-\infty}^{\infty} u(t) u^*(t - \tau) e^{j\omega t} dt. \quad (203)$$

$$\text{For } \omega = 0: \quad \psi(\tau, \omega) = \int_{-\infty}^{\infty} U(f) U^*(f - \nu) e^{j2\pi ft} dt, \quad (204)$$

$$\psi(\tau, 0) = \int_{-\infty}^{\infty} u(t) u^*(t - \tau) dt, \quad (205)$$

$$\psi(\tau, 0) = c(\tau). \quad (206)$$

$$\text{For } \tau = 0: \quad \psi(0, \omega) = \int_{-\infty}^{\infty} u(\nu) u^*(\nu - \omega) d\nu, \quad (207)$$

$$\psi(0, \omega) = k(\omega). \quad (208)$$

Figure 34 divides the τ, ω plane into three regions:

- a. REGION I. - If two targets differ in τ or ω such that the τ, ω difference falls in this region, they cannot be resolved except with the aid of unrealistic a priori knowledge as to target sizes.
- b. REGION II. - If two targets have a τ, ω difference which falls in this region, and if they are known to be of equal amplitude, they may be readily resolved. Generally, substantial probability of resolution exists even for those targets known to be only approximately equal in size. An investigation of the relative amplitude is necessary to determine the target resolvability as a function of τ, ω displacement.
- c. REGION III. - Resolution is possible for all signals different in τ, ω such that the difference falls in this region.

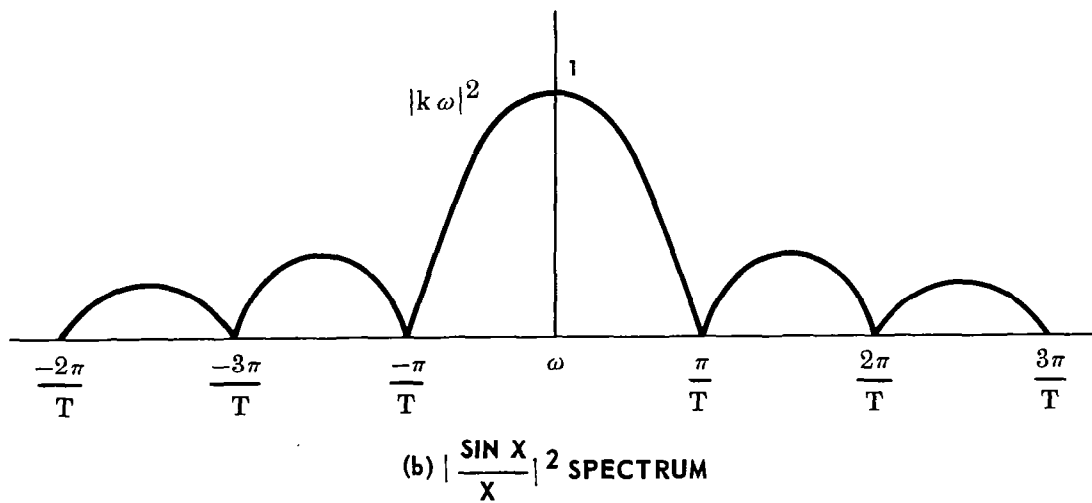
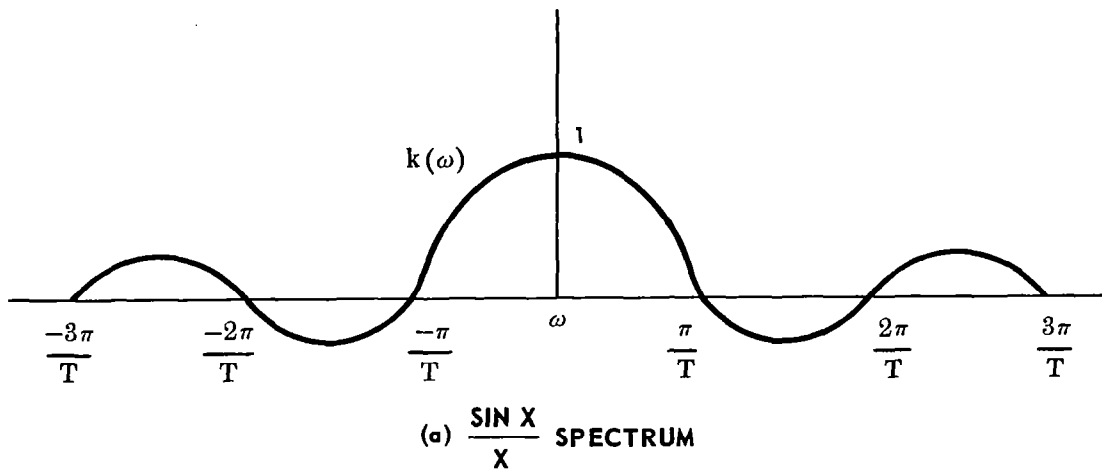


FIGURE 33 – CORRELATION COEFFICIENTS

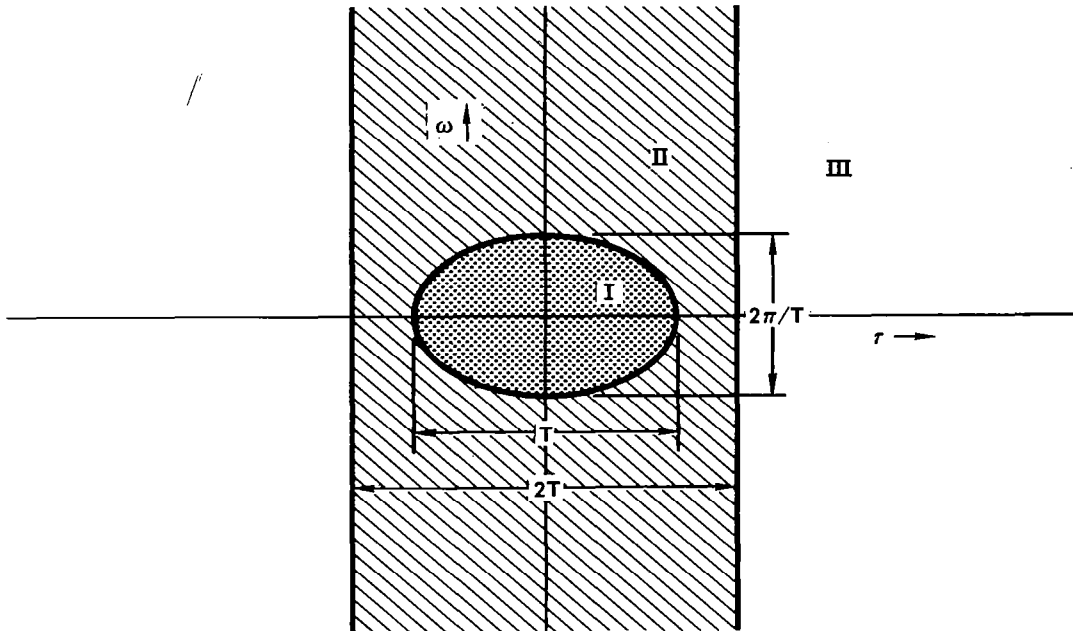


FIGURE 34 – PULSE RADAR AMBIGUITY DIAGRAM

Range Measurement Errors by Channel Noise. - The effect of channel noise is to distort the shape of the received pulse and to cause the time at which the received pulse exceeds a preset threshold to be incorrect. This can be explained with the aid of the figure 35 .

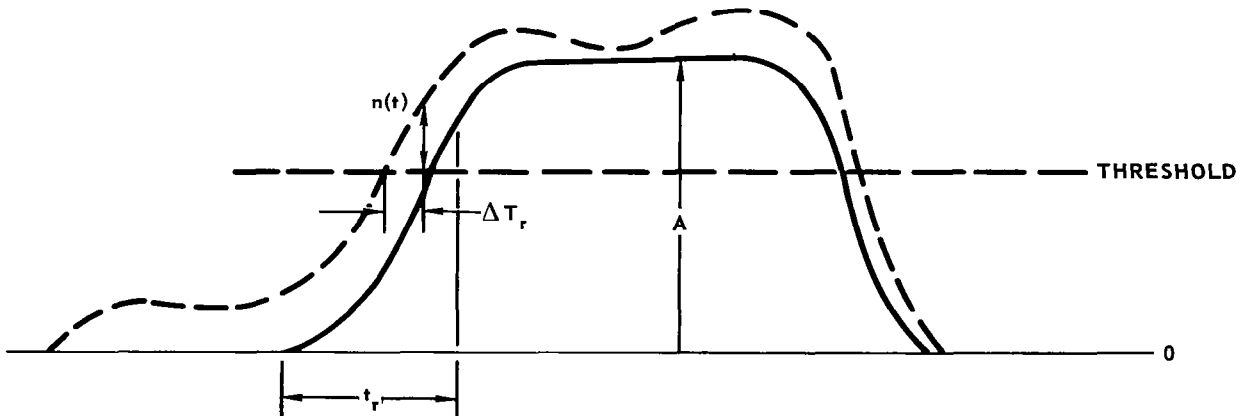


FIGURE 35 – RECEIVER NOISE EFFECTS

The rise time, t_r , of the pulse will be determined by the bandwidth of the I.F. amplifier. This will also limit the frequency of the noise to approximately $\frac{1}{t_r}$. Therefore, for large signal to noise ratio signals, the slope of the pulse with noise will be essentially the same as the slope of the pulse without noise. The effect of noise will be to shift the threshold crossing back and forth in time.

$$\text{Slope Signal} = \frac{A}{t_r}, \quad (209)$$

$$\text{Slope Signal} + \text{Noise} = \frac{n(t)}{\Delta T_r}. \quad (210)$$

Equating the two slopes:

$$\Delta T_r = \frac{t_r}{\left(\frac{A}{n(t)}\right)}, \quad (211)$$

$$\left[\left(\frac{A}{n} \right)^2 \right]^{\frac{1}{2}} = \delta T_r = \frac{t_r}{\left(\frac{A^2}{n} \right)^{\frac{1}{2}}} = \frac{t_r}{\left(2 \frac{S}{N} \right)^{\frac{1}{2}}}, \quad (212)$$

$$\delta T_r = \frac{t_r}{\left(2 \frac{S}{N} \right)^{\frac{1}{2}}}, \quad (213)$$

where:

$\frac{A^2}{n}$ is the video signal to noise ratio (power)

$\frac{S}{N}$ = IF signal to noise ratio (power)

For large signal to noise ratios and linear detection:

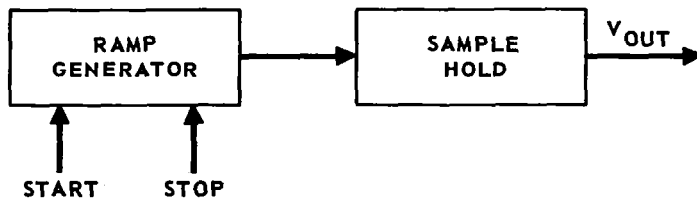
$$\frac{A}{n} = 2 \frac{S}{N} \quad (214)$$

In cases where the receiver is matched to the transmitted waveform, the rise-time will be equal to the pulse width. The same expression will apply with T , the pulse width, replacing t_r , the rise time. This expression is converted to range error δ_R by:

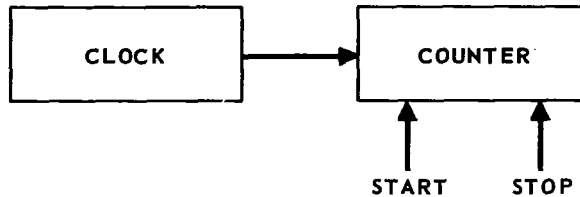
$$\delta R = \delta T_r \frac{c}{2}, \quad (215)$$

$$\delta R = \frac{c}{2} \frac{t_r}{\left(2 \frac{S}{N} \right)^{\frac{1}{2}}}. \quad (216)$$

Analog and Digital Measurement Errors. - The time delay corresponding to the range measurement can be converted to a voltage in either an analog or digital manner. The transmitted pulse can be used to start a ramp generator and the received pulse used to stop the ramp, or a counter can be started and stopped with the transmitted and received pulses. (See Figure 36.)



(a) RAMP GENERATOR (ANALOG OUTPUT)



(b) COUNTER (DIGITAL OUTPUT)

FIGURE 36 - TIME DELAY MEASUREMENT

For the ramp generator measurement:

$$r = K a (t_2 - t_1), \quad (217)$$

where:

- r = Range in Feet,
- K = Scale factor feet/volt,
- a = Slope of ramp generator volt/sec,
- t₁ = Start Time,
- t₂ = Stop Time,

$$\Delta r = \frac{\partial r}{\partial a} \Delta a + \frac{\partial r}{\partial t_1} \Delta t_1 + \frac{\partial r}{\partial t_2} \Delta t_2. \quad (218)$$

If a, t₁, t₂ are statistically independent:

$$\sigma_r^2 = K^2 [(t_2 - t_1)^2 \sigma_a^2 + a^2 (\sigma_{t_2}^2 + \sigma_{t_1}^2)], \quad (219)$$

$$\sigma_r^2 = r^2 \sigma_a^2 + K^2 a^2 (\sigma_{t_2}^2 + \sigma_{t_1}^2). \quad (220)$$

The σ_a error is an error in the slope, or the setting of the slope of the ramp generator, and results in a fixed or slowly varying range dependent error.

The σ_{t_1} , σ_{t_2} errors are most likely due to threshold jitters that are random in nature. If measurements are taken at intervals spaced sufficiently far apart in time so that succeeding samples are independent, errors due to time jitter can be reduced by averaging;

$$\sigma_r^2 = r^2 \sigma_a^2 + \frac{K^2 a^2}{n} (\sigma_{t_2}^2 + \sigma_{t_1}^2) . \quad (221)$$

The improvement in accuracy by averaging will be limited by the permissible lag in the data, the number of samples that can be averaged before the range changes significantly, and bias errors.

Range can be measured by using the transmitted pulse and the received pulse to start and stop a counter driven by an accurate clock. In this case:

$$\begin{aligned} r &= \frac{c}{2} \times \frac{1}{f} \times (\text{No. of Counts}), \\ c &= \text{speed of light}, \\ \frac{1}{f} &= \text{period of each count.} \end{aligned} \quad (222)$$

Errors will result in this type of measurement system due to quantization and errors in the counter frequency.

The state of the art in digital logic is currently in the neighborhood of 100 MHz clock rates. This results in an error, due to the 1 count uncertainty associated with the counter, of 10 ns or 5 feet. If the prf of the radar is varied in a random manner (varies with respect to the range clock in such a manner that they are not in step), this error can be reduced by averaging successive readings. The RMS value of this error will be reduced by $\frac{1}{\sqrt{N}}$.

$$\sigma_{r(\text{AVG})} = \frac{\sigma_{r(\text{SAMPLE})}}{\sqrt{N}} . \quad (223)$$

Since the frequency directly determines the number of counts, any error in frequency will show up as a range error.

$$dr = -\frac{c}{2} \frac{1}{f_c^2} \times (\text{No. of counts}) df_c . \quad (224)$$

Range Rate Measurements. - With a noncoherent pulse radar, range rate will not be measured directly but will be obtained by differentiating range. This will be done in the autopilot control loop. If a coherent pulse radar is used, velocity can be measured by measuring the doppler frequency of the received signals. The relationship between doppler and velocity is:

$$f_d = \frac{2v}{c} f_o . \quad (225)$$

Noise in the system will show up as a variation in frequency.

The improvement in range rate measurement of coherent radar over non-coherent radar has been calculated (reference 31) for two types of target motion:

- a. A series of alternate and equal positive steps of velocity occurring at random with a Poisson distribution of spacings.

b. A random step of acceleration.

These calculations were based upon optimum linear filter theory with a minimum mean square error criteria. The improvement ratio depends considerably on the type of target motion.

Short Pulse Radar. - Range resolution and RMS range error have been shown to be functions of the transmitted bandwidth. The reciprocal relationship between pulse width and bandwidth shows that one method of obtaining a wide bandwidth is to use a simple pulse radar with a very short pulse. At the range of interest, 10,000 feet, the power requirement may not be too great.

Transmitter Power Requirements.

$$S_{\text{rec}} = \frac{P_t G_t^2 \sigma \lambda^2}{[4\pi R^2]^2 4\pi} \quad (226)$$

For unity S/N ratio:

$$\frac{S_{\text{rec}}}{k\text{TBNF}} = 1 = \frac{P_t G_t^2 \sigma \lambda^2}{(4\pi)^3 R^4 k\text{TBNF}}, \quad (227)$$

$$P_t = \frac{(4\pi)^3 R^4 k\text{TBNF}}{G_t^2 \sigma \lambda^2}, \quad (228)$$

with:

$$\begin{aligned} R &= 10,000 \text{ ft}, \\ B &= 500 \text{ MHz}, \\ G_r &= 31 \text{ db } (1\frac{1}{2}' \text{ at } 10\text{gc}), \\ \lambda &= 3 \text{ cm}, \\ \text{NF} &= 10 \text{ db}, \\ \sigma &= 1 \text{ m}^2, \end{aligned} \quad (229)$$

then: $P_t = 6 \text{ kw.}$

This power yields a range resolution of one foot. At a range of 1,000 feet, the transmitted power need only be .6 watt.

When following the docking control law of:

$$\dot{X} = .01X. \quad (230)$$

the maximum velocity is 100 fps. The range is therefore changing slow enough so that pulse integration is possible. With a maximum range of 10,000 feet, the maximum allowed prf for unambiguous range measurement is:

$$\text{prf} = \frac{1}{2T} = \frac{1}{\frac{4R}{c}}, \quad (231)$$

$$\text{prf} = \frac{3 \times 10^8}{4(3080)}, \quad (232)$$

$$= 24.5 \text{ kHz}. \quad (233)$$

and in one integration time interval, .01 sec, 245 pulses are available for integration. If this integration can be implemented, an additional improvement in signal to noise ratio will result. The improvement will depend upon the type of integration that can be instrumented.

Nanosecond Pulse Generation Techniques. - Nanosecond pulse generation and detection hardware techniques require nonconventional pulse radar circuitry. Techniques that can be considered for nanosecond pulse generation are:

1. The regenerative pulse generator
2. Impulsing TWT amplifier
3. Direct carrier pulse generation with semiconductors
4. Microwave switching circuits

The regenerative pulse generator has been rejected as being too complex and requiring an excessive amount of equipment.

The impulse response of a TWT method of generating nanosecond pulses has been used extensively because of its simplicity. A block diagram of this system is shown in Figure 37.



FIGURE 37 - GENERATION OF NANOSECOND PULSES USING TRAVELING WAVE TUBE AMPLIFIER

The impulse generator forms a short video pulse. The spectrum of this pulse has significant energy in the passband of the TWT amplifier. This energy is amplified and the output is a short R.F. pulse. The exact analysis of this type of pulse generator depends upon the exact waveform of the pulse and the transfer characteristic of the TWT. These factors are not usually known.

A maximum gain of 40-60 db is readily attained by a low power traveling wave tube over the frequency ranges from L thru K_u band. A practical value of gain is limited to this region by the best achievable transmission line match (which is required for stability). Miniaturization of TWT's has progressed to the point where size is no longer dependent only on operating frequency. An operating frequency can be chosen anywhere from C through X band with little effect on the size, weight or power requirement for the TWT. Below C band, the size of the TWT starts increasing. At high frequencies, K_u and mm frequencies, TWT's are not as available, and those that are available have lower gains, are heavier, and require higher voltages.

Therefore, this technique is applicable in the C through X band region. At millimeter waves, this approach does not appear promising because of the fall off of spectral energy contained in the spectrum of the video pulse and the lower gain, greater weight, and larger size of the mm wave TWT amplifiers.

Some of the methods that have been used to generate baseband nanosecond pulses are:

1. Mechanical switched line type modulator,
2. Avalanche transistor switched line type modulator,
3. Biased class C amplifier,
4. Pulse shaping.

Methods 1 and 2 are the same except for the switching mechanism. Figure 38 is a block diagram of a line type modulator.

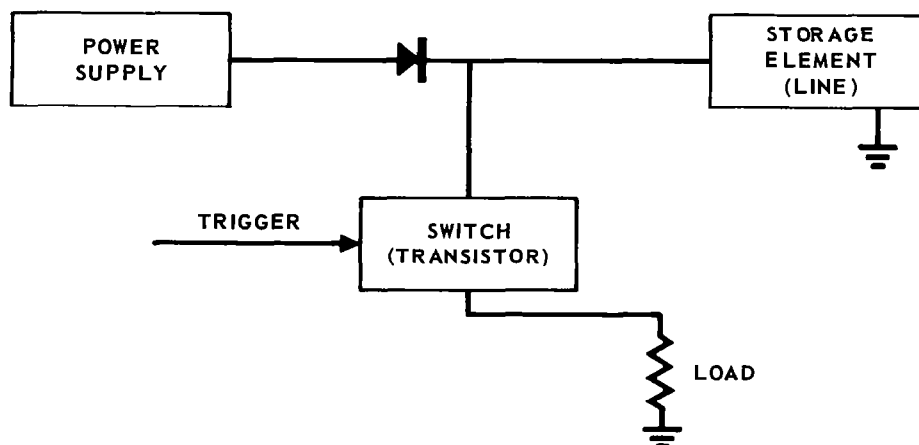


FIGURE 38 – GENERATION OF NANOSECOND PULSES USING TRANSISTOR SWITCHING AND STORAGE LINE

This circuit has been extensively used in radar. Its theory of operation is well established and the results are repeated here.

1. T_p , the pulse width, is determined by length of line used for storage.
2. T_r , the rise time, is determined by the switching time. In avalanche transistors this can be very short.
3. E_p , the peak voltage, is limited by the breakdown voltage of the transistor.

4. The repetition period is limited by the charging time of the storage element.

The same circuit can be used with a mechanical switch replacing the transistor. The advantage of the mechanical switch is the high voltage capability of the switch. Rise and fall times can be very short (< 1 ns), but the repetition rate is limited (typically 400 Hz or less). Therefore, the mechanical switch can be eliminated at repetition frequencies of interest to this study.

Another method of obtaining short pulses (figure 39) is to drive an amplifier biased below cut off. This requires broadband output circuitry. A one

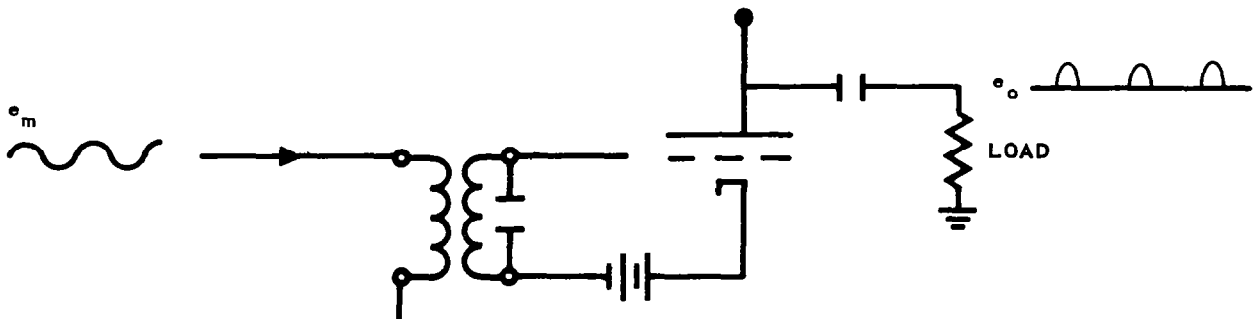


FIGURE 39 - GENERATION OF NANOSECOND PULSES USING AN AMPLIFIER BIASED BELOW CUTOFF

nanosecond pulse requires a minimum of 1 GHz bandwidth. Either the drive frequency or the drive voltage is required to be high to produce a short pulse output, since conduction occurs on the peak of each cycle. The prf is also determined by the drive frequency. This method of generating nanosecond pulses is not attractive because of circuit inefficiency and the lack of flexibility in setting pulse width.

Pulse shaping varactor diodes have been developed that have characteristics suitable for use in pulse shaping circuits. These varactor diodes are called "snap-off" diodes or step recovery diodes. Any pn junction will conduct heavily in the reverse direction for a short length of time immediately following forward conduction. This is because of the presence of stored minority carriers which were injected and stored during the forward conduction. Step recovery diodes are designed to enhance this storage and to achieve a sharp transition from this reverse storage conduction to cutoff. This transition can switch tens of volts and hundreds of milliamps in less than a nanosecond. This can be used to sharpen rise and fall times of ordinary pulses. The circuit shown in Figure 40 can be used for this pulse generation.

At point (1), D_1 will normally be conducting and the voltage at this point will be the voltage drop of the diode. A step voltage will be applied, and with $e_p > R_1 i_f$, D_1 will be back biased; however, current will continue to flow in the forward direction until all the minority carriers have been used and the

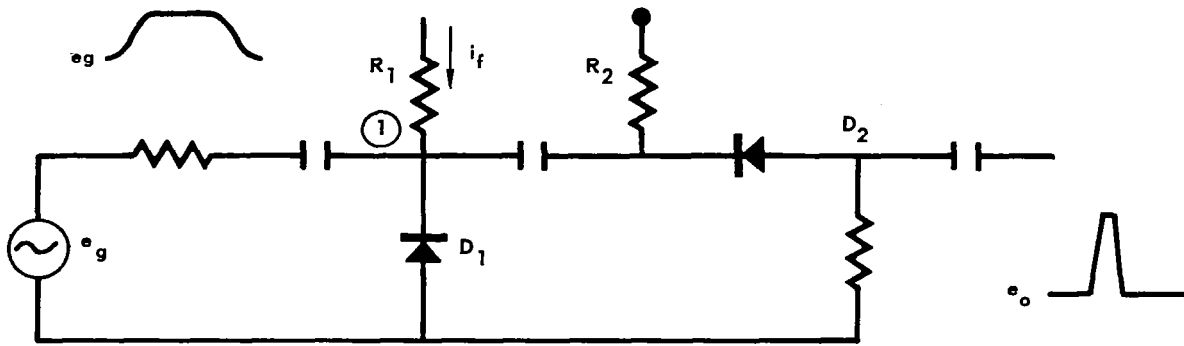


FIGURE 40 - GENERATION OF NANOSECOND PULSES USING VARACTOR DIODES

sharp transitron occurs. This produces the sharp leading edge. D_2 is initially in the forward conduction state. The applied pulse back biases D_2 but due to the storage of minority carriers the diode conducts and presents a low impedance to the pulse. This conduction continues until these carriers are depleted and the rapid transitron occurs providing the short fall time of the pulse. With present diodes it is possible to produce pulses less than 1 ns in width of 8-10 volts across a 50 Ω impedance.

Nanosecond pulses can be formed by logical switching functions in transmission line circuits. Some switch devices and the circuitry that can be used are discussed below:

1. TR Tube Leakage - A TR tube is normally used in pulse radar to protect the receiver during the time the transmitter is pulsed on. The TR tube is a gas-filled device that is placed in the transmission line to the receiver. When high power reaches the TR tube, the tube ionizes, the line is mismatched, and most of the high power is reflected. However, a finite time is required for the TR tube to ionize and the first part of the RF pulse passes the TR tube. This ionization delay (being in the order of a few nanoseconds) has been used to produce nanosecond pulses. The advantage of this technique is the simplicity with which existing radars can be converted to short pulse operation. This could be useful in a multi-mode radar when the pulsewidth is switched at short ranges. The performance will be determined by the TR tube. Peak power will be determined by:
 - a. The circuit insertion loss,
 - b. The rise time of the RF pulse,
 - c. The bandwidth of the TR cavity and RF circuitry.

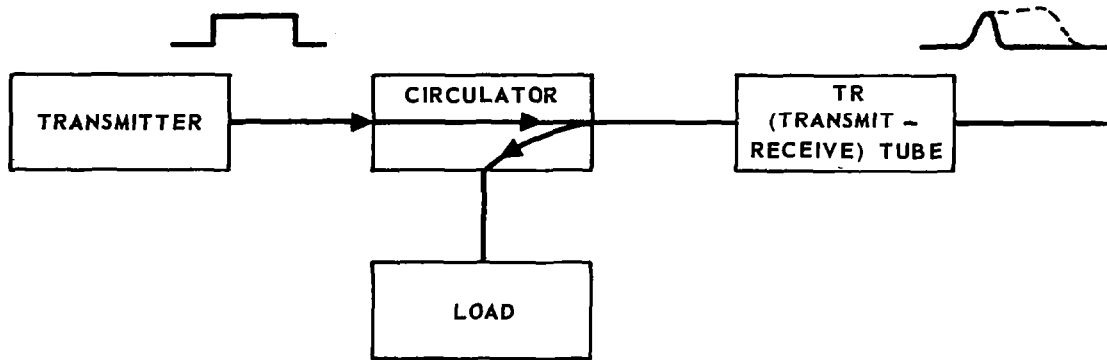


FIGURE 41 - GENERATION OF NANOSECOND PULSES USING GAS TR TUBE

It appears that the rise time of the RF pulse will be the limiting factor. If the rise time of the RF pulse is greater than the ionization time of the gas fill, the peak RF power output will be determined by the breakdown characteristics of the gas. The pulse width is determined by the gas breakdown and the rise time of the pulse.

Schwarzkopf (reference 33) has suggested the use of a traveling wave resonator as a short pulse generator (figure 41).

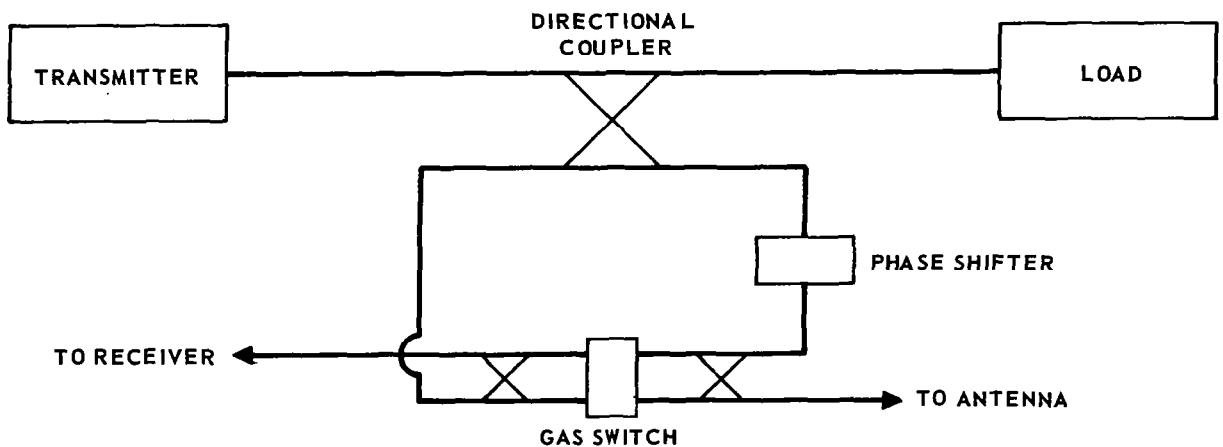


FIGURE 42 - GENERATION OF NANOSECOND PULSES USING A TRAVELING WAVE RESONATOR

The traveling wave resonator has primarily been used as a method of obtaining high power for component testing; however, with the addition of switching circuitry it can be used as a short pulse generator. Circuit operation is explained with the aid of Figure 43. Energy is coupled from the main line, travels around the ring of $n\lambda$ length, and returns to the coupler in phase. This process continues and after a number of pulses the ring is charged to its maximum value. The line is then switched and the energy stored in the resonant ring will be directed to the antenna port. The pulse width is determined by the time required to discharge the resonant ring:

$$T_P = \frac{l}{v_g},$$

where l = length of ring, (234)
 v_g = velocity of energy propagation on the line.

The peak power gain depends upon the coupling coefficient and the path loss.

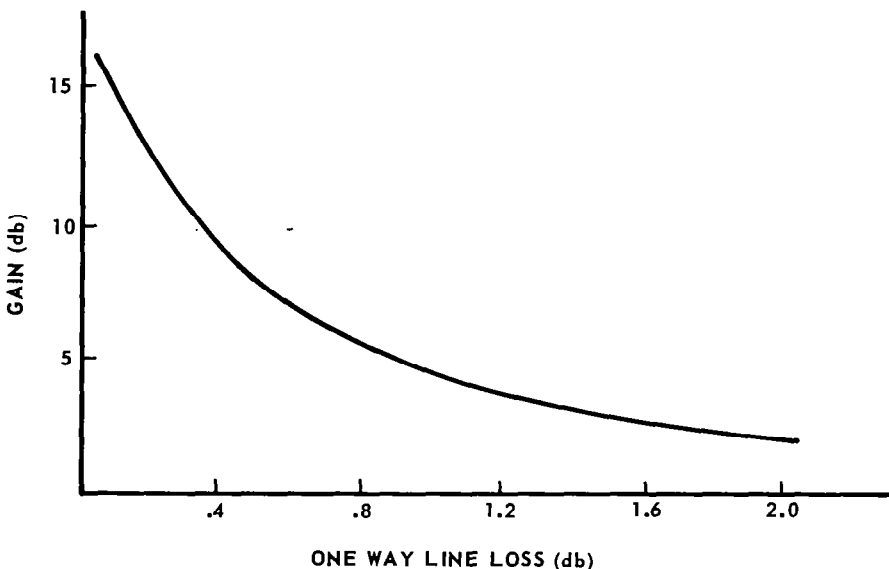


FIGURE 43 - RESONANT RING (GAIN VS. LINE LOSS)

As can be seen from the above graph, gain decreases rapidly with waveguide loss. This technique does not appear promising above X or Ku band because of component and waveguide losses.

The simplest circuit that can be devised to produce short pulses is the in-line SPST switch shown in Figure 44.



FIGURE 44 - IN LINE SPST SWITCH

Microwave switches are usually one of the three types shown in Table 6 .

TABLE 6 - R.F. SWITCH COMPARISON

	SPEED	POWER	MAXIMUM FREQUENCY
GAS TUBE SWITCH	1 NS	MÉGAWATTS	MILLIMETER
DIODE SWITCH	1 NS	WATTS	MILLIMETER
FERRITE SWITCH	100'S NS	KILLOWATTS	MILLIMETER

A natural division occurs. The gas switch is used when switching is at high power. The diode switch is used for low power.

The bandwidth required for 1 ns RF pulses is 1 GHz. This bandwidth is readily achievable over most of the frequency range from X-band up through mm waves.

The gas tube switch can handle very high power (1 MW at X band) in relatively short switching times (few nanoseconds); however, because of its long recovery time, a single gas switch cannot be used to produce a short pulse. This is not a major problem.

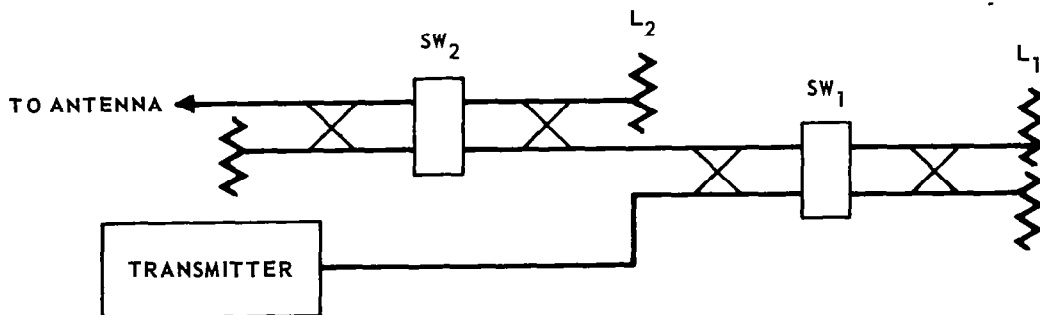


FIGURE 45 - GENERATION OF NANOSECOND PULSES USING BALANCED DUPLEXERS

One circuit that can be used is shown in Figure 45. This circuit consists of two balanced duplexers in series with the switches, which are triggered gas discharge devices. The transmitter will produce a pulse substantially longer than the pulse width to be transmitted. Before SW₁ is fired, the transmitted pulse is coupled to L₁ and dissipated. At t₁, SW₁ fires and the transmitted pulse is switched through the second switch assembly to the antenna. SW₂ is fired at t₂ and the pulse is then switched to L₂. The transmitted pulse width will then be determined by the time difference t₁ - t₂. Rise times and fall times will be determined by the switch speed. Other circuit configurations can be arrived at for this type of circuit.

The advantages of this system are:

1. High power capability,
2. Flexible pulse widths,
3. Variable pulse width capability,
4. High Frequency capability (through mm waves).

The disadvantages of this system are:

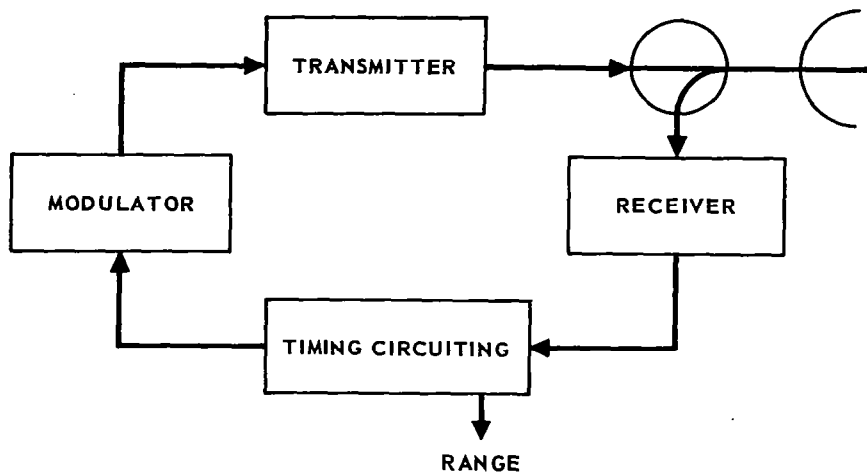
1. Wasteful of RF power,
2. Minimum pulse width limited to a few nanoseconds because of the switching time of gas switches.

Cooperative Pulse Radar

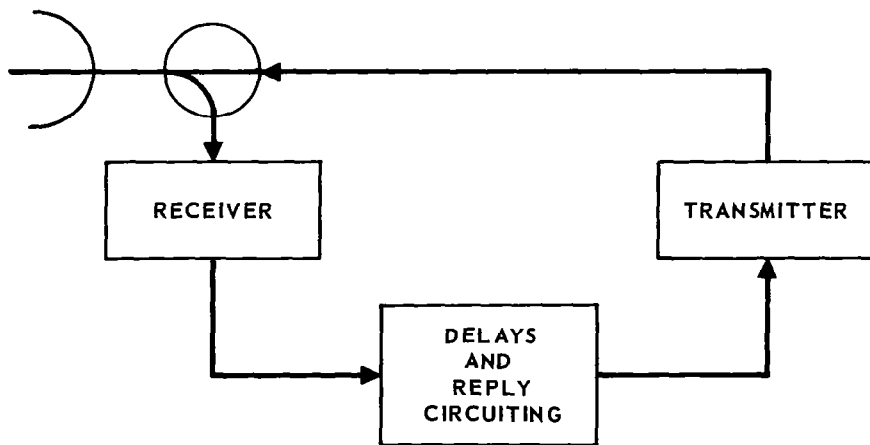
In the cooperative pulse radar system, a transmitter and receiver are located on both the docking vehicle and target vehicle. Figure 46 shows the usual distribution of equipment in the cooperative system. The main advantages of this system are the reduced power requirements and the minimum range performance. It is conventional for the radar on the docking vehicle to be called the interrogator and the radar on the target vehicle to be called the transponder. The transmitter frequencies on the interrogator and the transponder can differ by the IF frequency. This is advantageous since the transmitter source can be used as the local oscillator source also. Range will be measured by measuring the time delay between transmission of a pulse from the interrogator and the reception of a reply from the transponder.

$$R = \frac{c}{2} (T_{\text{delay}} - T_{\text{fixed}}). \quad (235)$$

To insure operation to zero range, T_{fixed}, the time delay in the transponder must be greater than the interrogator transmitter pulse and recovery time.



(A) DOCKING VEHICLE



(B) TARGET VEHICLE

FIGURE 46 – COOPERATIVE PULSE RADAR

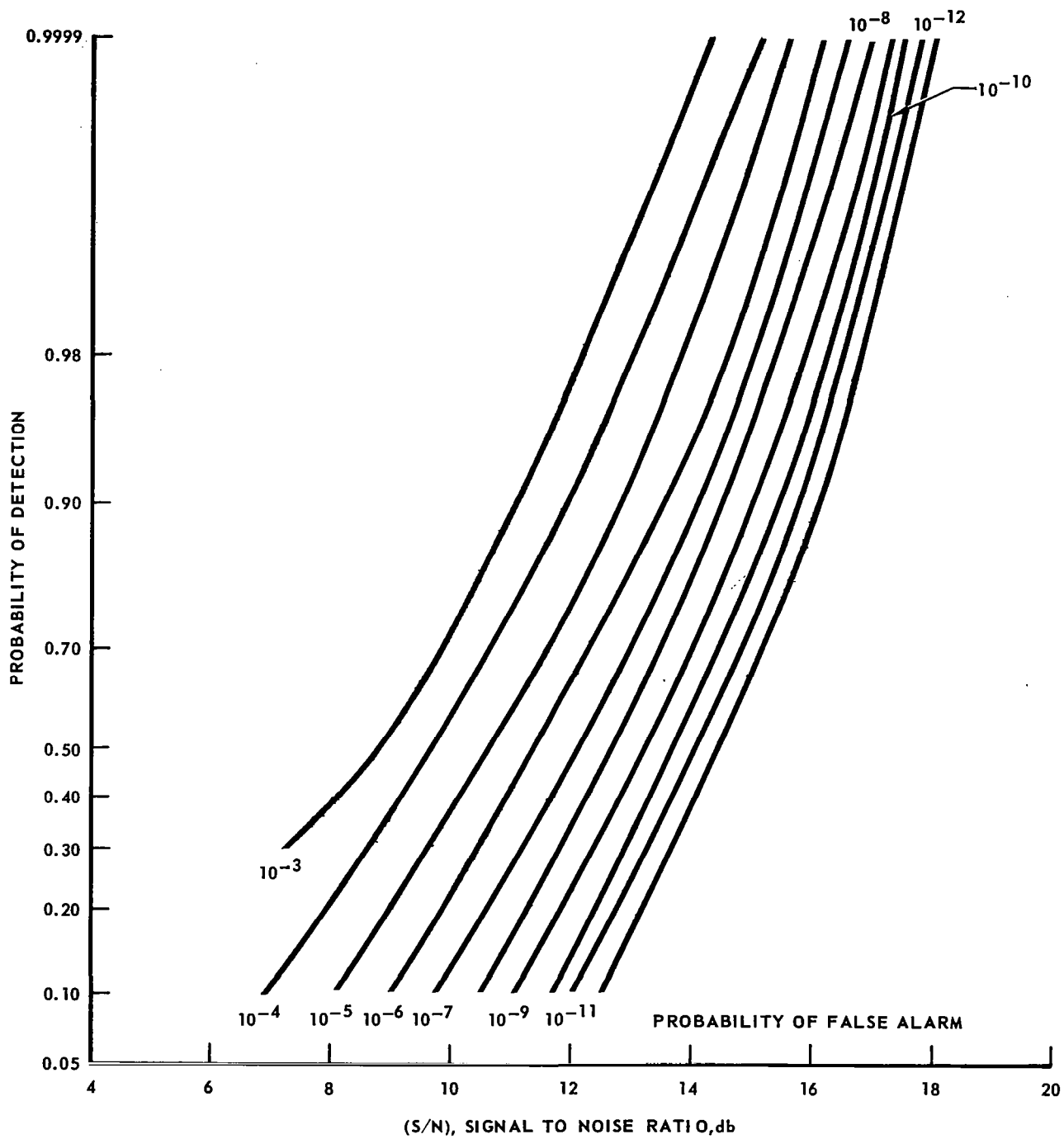


FIGURE 47 – DETECTION PERFORMANCE CURVES

The power requirement for this system is much less than for the non-cooperative system because of the one-way path loss instead of two-way path loss. Since a reply from the transponder on each interrogation is required, the received S/N ratio on each pulse must be sufficiently high to allow a proper threshold setting to obtain a high probability of detection and low false alarm rate. Figure 47 is a plot relating S/N ratio to probability of detection and false alarm rate. A 15 db signal to noise ratio will give a probability of detection and a false alarm rate adequate for most envisioned missions.

To eliminate loss of signal due to target attitude variations, one antenna should be circularly polarized and the other antenna linearly polarized. This results in only a 3 db power loss, which is much less than can be expected for attitude misalignment.

In a previous section, the range accuracy requirements for most missions were determined. Figure 48A is a plot of the range of these requirements.

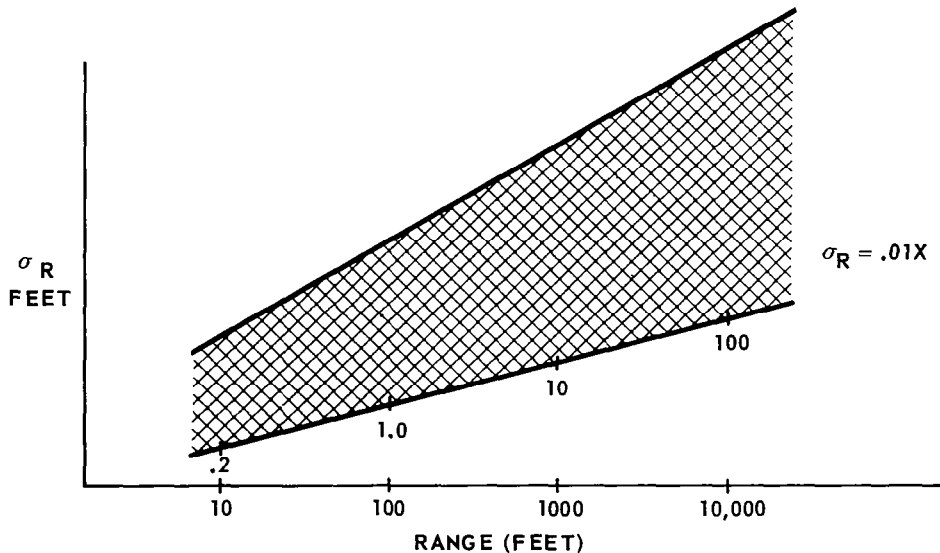
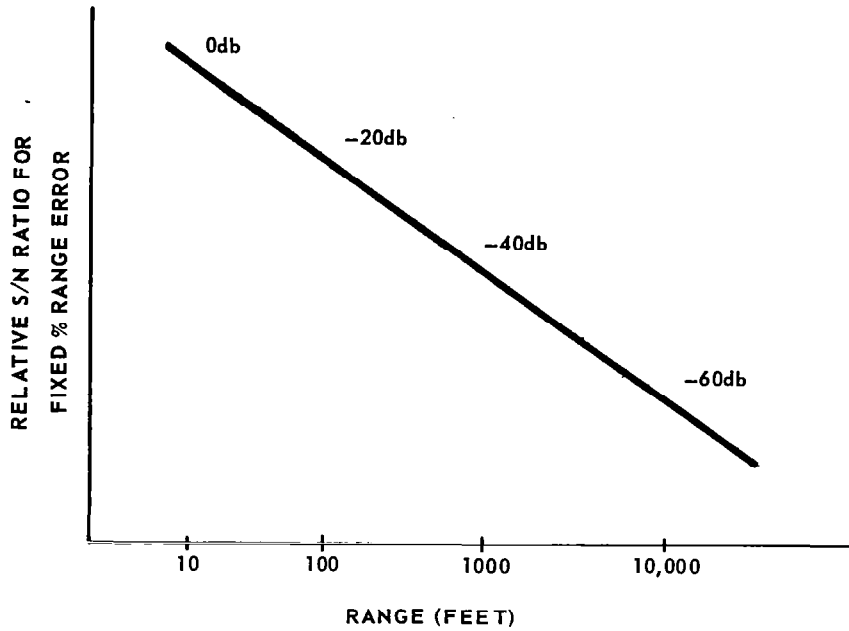
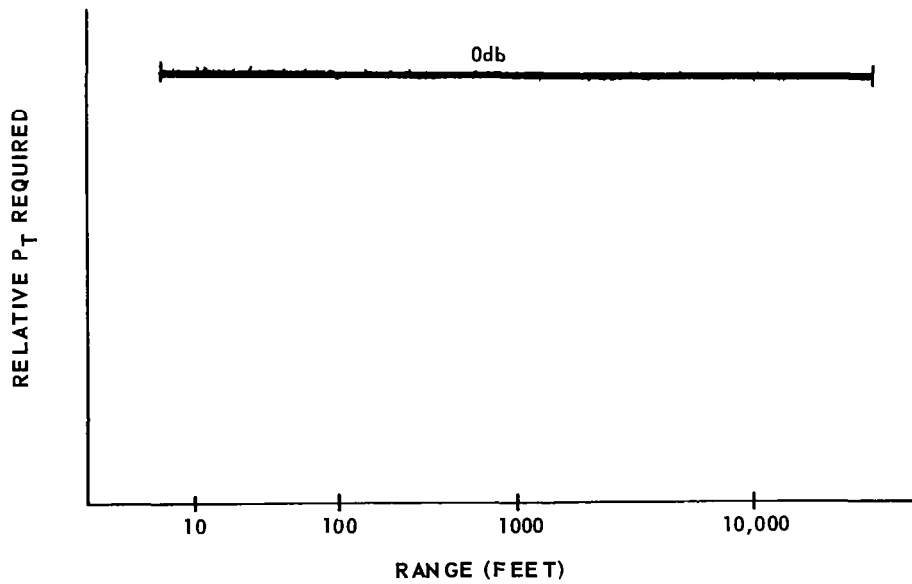


FIGURE 48A - RANGE ACCURACY PROFILES

If the range accuracy requirement is a constant percentage of the range, the change in accuracy requirement will track the change in S/N ratio due to space loss. See Figure 48B and 48C .



(B) S/N VS RANGE



(C) POWER REQUIREMENTS vs RANGE

FIGURE 48 - RANGE ACCURACY REQUIREMENTS

A representative power calculation will be made. This calculation can be then used as a baseline system for scaling purposes. Let $\sigma_r = .01R$ and perform the calculations at 100'.

$$\sigma_r = 1 \text{ ft. ,}$$

$$\delta_T = 2 \text{ ns ,}$$

from $\delta_T = \frac{T}{\sqrt{\frac{2S}{N}}}$ developed in a previous section, and assuming a

1 μ s pulse width and 1 MHz bandwidth receiver:

$$2 \times 10^{-9} = \frac{10^{-6}}{\sqrt{2} \frac{S}{N}} ,$$

$$\frac{S}{N} = \left(\frac{10^{-6}}{8 \times 10^{-9}} \right)^2 ,$$

$$\frac{S}{N} = 2 \times 10^6 = 51 \text{ db .}$$

(236)

(237)

The required signal to noise ratio at 100 ' will be 63 db. At 10,000 ft. the required signal to noise ratio will be 23 db. This is more than adequate to insure proper transponder operation.

$$P_{\text{req}} = \frac{R^2 (4\pi)^2 kTB NF \left(\frac{S}{N}\right) L}{G_t G_r \lambda^2} ,$$

(238)

$$R = 100' = 30.4 \text{ meter} = 14.8 \text{ db ,}$$

$$kT = -204 \text{ db ,}$$

$$B = 60 \text{ db ,}$$

$$NF = 10 \text{ db (x-band) ,}$$

$$\frac{S}{N} = 51 \text{ db ,}$$

$$L = 6 \text{ db (3 db polarization loss + 3 db system loss) ,}$$

$$G_T = 30 \text{ db ,}$$

$$G_R = 0 \text{ db ,}$$

$$\lambda = 15.7 \text{ db ,}$$

$$4\pi = 11.2 \text{ db ,}$$

$$P_{\text{req}} = -23.6 \text{ dbw .}$$

(239)

Therefore, transmitter power required for an x-band system with a 30 db antenna would be ≈ 5 mw.

The previous calculation assumed a 30 db antenna at 10 GHz. This corresponds to a 15" diameter parabolic reflector. If it is assumed that the reflector size is limited to this value, it can be seen that the power requirement will not be a sensitive function of frequency. Since G_T is proportional to $1/\lambda^2$ the numerator of the power requirement equation will not vary with frequency. There will be a slight decrease in power requirements because of the noise figure improvement with decrease in frequency, as found in the numerator of the power requirement equation.

If omnidirectional antenna coverage ($G_T = G_R = 0$ db) is required on both the docking vehicle and the target vehicle for rendezvous acquisition, the frequency of operation should be chosen as low as possible to minimize the transmitted power requirement.

The instrumentation range errors that will be encountered in this system can be divided into bias error and random errors. The bias errors will be caused by drifts in time delays through IF amplifiers and delay lines, and shifts in threshold levels. Typical delay accuracies in practical equipment are ten to twenty nanoseconds. This corresponds to 5' to 10' accuracy. Random errors due to threshold jitter can be held to the low nanosecond region by careful circuit design. Since this jitter will be independent from sample to sample, the range error caused by this error can be reduced by successive averaging.

Ring-Around

The ring-around system, which has been used extensively as a miss distance indicator, has some potential as a range measurement technique for docking. The basic system employs two transponders one of which acts as a free-running beacon until the second transponder comes into range and replies. The reply reverts the first to the transponder mode, and the two transponders then each receive the others transmitted pulse, delay it for a calibrated time interval, and retransmit it, as shown in figure 49. Range information is contained in the equation for the ringing frequency, f_0 .

$$f_0 = \frac{1}{t_e + t_{sp}} \quad (240)$$

where: t_e is the equipment time delay ,
 t_{sp} is the space time delay, $\frac{2R}{c}$.

The accuracy of the range measurement can therefore only be as accurate as the knowledge of the combined equipment delay, which must be some reasonable interval (e.g., 20 μ sec) in order to keep the ringing or oscillating frequency to a realistic value as range goes to zero.

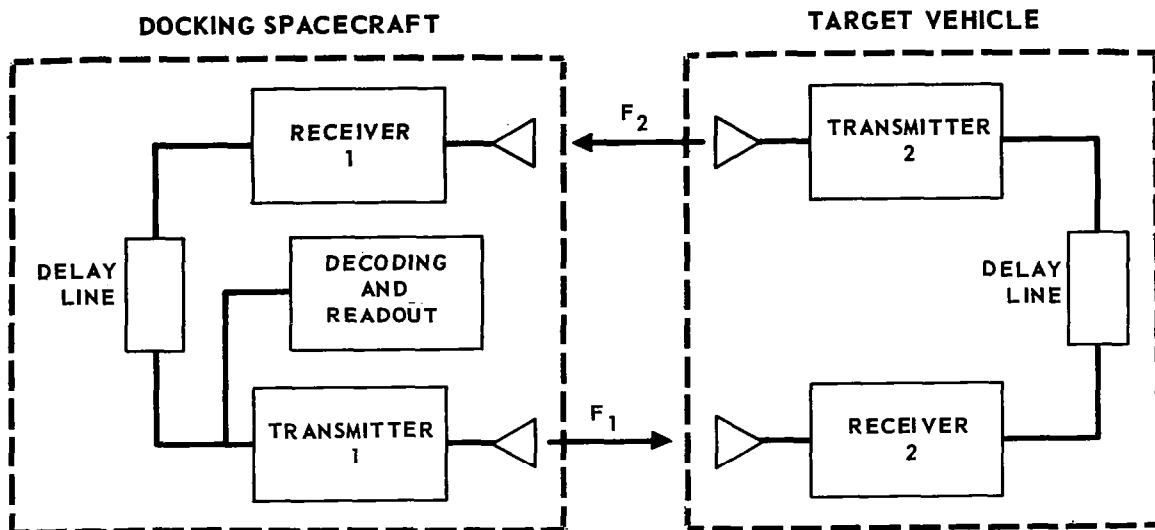


FIGURE 49 - GENERAL RING-AROUND SYSTEM

The total delay through each transponder is measured and controlled to some predetermined value (10 u sec., in the example cited) by adjusting the variable delay line. For close ranges where range accuracy becomes more stringent, direct video detection off the receiver and transmitter rf lines is used to measure transponder delay.

Range is determined from the pulse train, not directly by a measurement of frequency, but rather by a measurement of time between pulses. The effects of system fluctuations are minimized by measuring the interval occupied by a specified number of consecutive pulses. One microsecond pulses with approximately 50 nanosecond rise time are utilized to provide for leading edge detection.

Noise Induced Measurement Errors. - The time error in determining when the leading edge of a pulse corrupted with noise is received is a function of the S/N ratio and the pulse rise time, i.e..

$$\delta_T = \frac{\tau}{(2 S/N)^{1/2}}, \quad (241)$$

where: δ_T is the time error of the measurement,
 τ is the pulse rise time,
 S/N is the signal to noise ratio.

The time measurement error translates to an error in the range measurement by :

$$\delta_R = c \delta_T, \quad (242)$$

where c is the velocity of light.

To minimize the time and range measurement errors then, the received pulse S/N ratio should be maximized. For the cooperative case this is related to transmitter power by:

$$(S/N) = \frac{P_t G_t G_r \lambda^2}{(4\pi R)^2 F k T_0 B}, \quad (243)$$

where P_t = transmitter power average,
 G_t = transmitter antenna gain,
 G_r = receiver antenna gain,
 λ = operating wavelength,
 L = system losses,
 R = range,
 F = receiver noise figure,
 k = Boltzmann's constant,
 T_0 = standard noise temperature 290°K,
 B = bandwidth.

System Diagrams. - Figures 50 and 51 are block diagrams for the target vehicle and chase vehicle (S/C) ring-around transponders in the UHF frequency band. Single antenna operation is shown with filter action producing the needed isolation between the 400 MHz and 500 MHz carrier frequencies. The receivers of both systems are of the heterodyne type with a 100 MHz IF. The IF amplifiers have a 20 MHz bandwidth and provide approximately 70 db of gain.

After being detected and conditioned, a received pulse is delayed by the variable delay by the amount needed to bring the total transponder delay to 10 μ sec. The pulse then triggers the modulator and transmitter to produce the output pulse which is transmitted back to the other vehicle. The technique shown for measuring time delay is discussed in the next section.

In the S/C transponder (Figure 51), the output of the video detector and amplifier is fed into the decoding equipment for extraction of the range information. As noted earlier, the range information is contained in the time interval between pulses, and an appropriate averaging technique is used to suppress system fluctuations and noise induced errors.

Delay Stabilization. - In general, delay stabilization is achieved by measuring the time interval between a received pulse and a transmitted pulse. Should the measured delay differ from 10 μ sec, corrections are made in the delay of the variable delay line. With both the target and S/C transponders so equipped, the total equipment delay is held to 20 μ sec.

The time delay measurement circuits of Figures 50 and 51 smooth over a number of pulses to increase accuracy and range. In either vehicle's transponder, a received pulse registers in the frequency divider which, in turn,

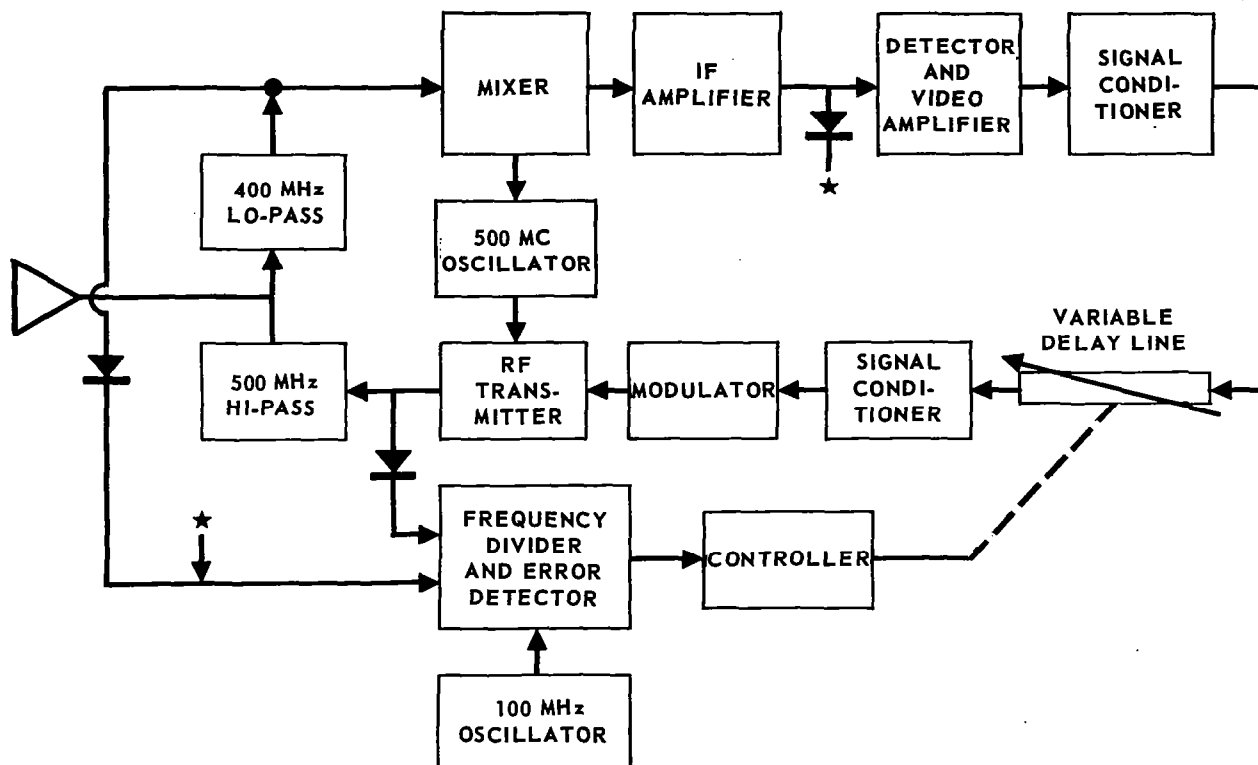


FIGURE 50 - TRANSPONDER SYSTEM - SINGLE ANTENNA OPERATION

starts the 100 MHz clock. The following transmitted pulse registers in the divider and stops the clock. The next received pulse initiates the same sequence, which is repeated until the frequency divider has counted to some specified number, A. The error detector then supplies the error signal, e, to the controller, where "e" is of the form:

$$e = A t_{\text{measured}} - A \times 10 \mu \text{ sec.} \quad (244)$$

The controller utilizes this signal to make corrections in the variable delay line to adjust the total delay of the transponder to 10 μ sec.

At close ranges where direct video detection is possible, received and transmitted pulses are detected directly from the rf lines as shown. At ranges exceeding the video detection range, the received pulse is detected by a diode at the output of the IF amplifier and fed into the frequency divider as before. A bias is applied to the error detector circuitry to compensate for the average delay in the front end of the receiver, reducing the total error in the range measurement to 5 feet or less.

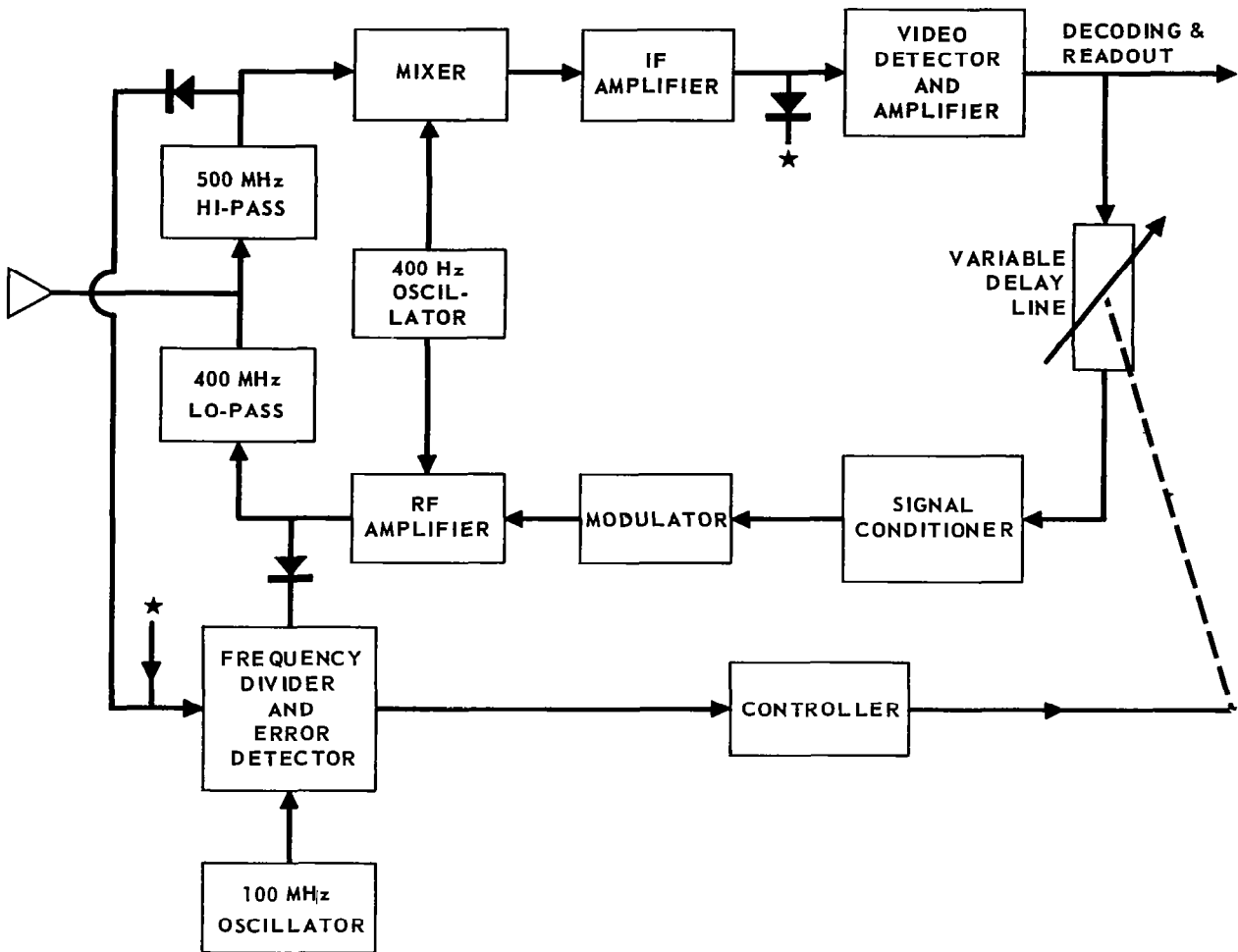


FIGURE 51 – A DOCKING TRANSPONDER

System Operation at UHF. - The path losses at 400 MHz and 500 MHz for 2 statute miles are 95 db and 96.5 db respectively. Assuming 0 db gain antennas and 7.5 db noise figure, the S/N ratio at 2 miles for 50 mw output is:

$$S/N_{400 \text{ MHz}} = -13 \text{ dbw} - 95 \text{ db} - 7.5 \text{ db} + 204 \text{ dbw} - 73 \text{ db} , \quad (245)$$

$$S/N_{400 \text{ MHz}} = 15.5 \text{ db} , \quad (246)$$

$$S/N_{500 \text{ MHz}} = S/N_{400 \text{ mc}} - 1.5 \text{ db} = 14 \text{ db} . \quad (247)$$

From equation 241 the time error, δ_t , in leading edge detecting the 500 MHz signal is:

$$\delta_T = \frac{50 \times 10^{-9}}{(2 \text{antilog } 1.4)^{1/2}} = 7.07 \times 10^{-9} \text{ sec.} \quad (248)$$

and from Equation , the range measurement error is:

$$\delta_R = c\delta_T = 7 \text{ feet} \quad (249)$$

At a range of 100 feet, the S/N ratio is 55 db. The error in the range measurement due to noise then becomes 0.054 feet.

From the standpoint of extracting the range information from the receiver when within 100 feet of the target, accuracies of 1 ft. and less are possible with only 50 mw of transmitter power. However, because of the inability to keep the delay stabilized to the same degree of accuracy, the accuracy of the range measurement is a function of delay stability. Maximum delay stability will occur when video detection directly off the rf lines is possible. The threshold for detectors at UHF is approximately -40 dbm. The additional margin required for a stability accuracy equivalent to a range accuracy of 1 ft. is, from Equations 241 and 242:

$$S/N = \frac{1}{2} \left[\left(\frac{r}{\delta_R} \right)^2 (9.84)^2 \times 10^{16} \right] \quad (250)$$

$$S/N = 605 = 27.8 \text{ db} \quad (251)$$

With 50 mw of transmitted power, this corresponds to a range of about 4.5 ft. If a number of pulses are averaged so that the allowable deviation per pulse is greater, this accuracy (1 ft.) can be achieved at a range of about 40 feet.

System Operation at 10 GHz. - The basic characteristics, such as transmitted power, pulse width, pulse rise time, and system delay, remain the same for a ring-around system operating at 10 GHz as for the UHF system.

The path loss for 2 miles at 10 GHz is 112.5 db. This is an increase of almost 30 db over the UHF case, and requires approximately 9 watts of transmitted power for the same S/N ratio (14 db). Hence, to be competitive from the transmitted power standpoint, the gain of the antennas must be increased. For a 14 db S/N ratio at two miles with 50 mw of transmitter power, and a receiver noise figure of 10 db, the antenna gains must be:

$$G_t + G_r = 122.5 + 10 - 204 + 73 + 14 + 13 = 28.5 \quad (252)$$

$$\text{or } G_t = G_r = 14.3 \text{ db} \quad (253)$$

A horn with an aperture of approximately 3 inches will give sufficient gain but the 3 db points in its pattern limit spacial coverage to approximately 35 degrees.

The minimum power level for video detection at x-band is about -53 dbm. As previously established, the S/N ratio above threshold for 1 ft. accuracy is 27.8 db. Then the power level required is -53 dbm + 27.8 db or -25.2 dbm. With 17 dbm transmitted power and 28.5 db antenna gain, this corresponds to a path loss of 70.7 db. The range for video detection is then:

$$R = \frac{r}{4\pi} \text{antilog} \frac{70.7}{20} , \quad (254)$$

$$R = 27.2 \text{ ft.} . \quad (255)$$

By smoothing over 128 pulses, the deviation of any one pulse can be:

$$\sigma = \sqrt{128} \times 1 , \quad (256)$$

$$\sigma = 11.31 \text{ ft.} . \quad (257)$$

The required S/N ratio above threshold is then only:

$$S/N = \left[\frac{1}{2} \frac{(5 \times 10^{-8}) (9.84 \times 10^8)^2}{11.31} \right] \quad (258)$$

$$S/N = 9.42 \text{ db.} . \quad (259)$$

The range for video detection is thus extended to 220 ft.

System Operation at 70 GHz. - The path loss for 2 miles at 70 GHz is 139.5 db. The antenna gains required for 50 mw transmitter power and received S/N ratio of 14 db are:

$$G_t + G_r = 139.5 + 20 - 204 + 73 + 14 + 13 = 55.5 \text{ db} , \quad (260)$$

$$\text{or: } G_t = G_r = 28 \text{ db.} . \quad (261)$$

A 28 db parabolic dish has a 3 db beamwidth of approximately seven degrees.

The threshold for video detection is approximately -45 dbm. If smoothing over 128 pulses is used, the required S/N ratio for 1 ft accuracy is 9.42 db. The signal level required for 1 ft accuracy is then -35.58 dbm. With 17 dbm transmitter power and 56 db antenna gain, this corresponds to a path loss of 108.58 db and a video detection range of 300 ft.

Conclusions. - The system of ring-around provides an accurate measure of range to zero feet. Factors producing inaccuracies are time errors in leading edge detection, instrumentation errors in deducing the range from the detected pulse train, and inability to keep the system time delay at its predetermined value. As range closes, the leading edge detection errors essentially disappear with the rising S/N ratio. Similarly, when the S/N ratio is sufficiently high to allow video detection, the errors due to the delay stabilization can be held to less than 1 ft. The instrumentation errors can be made small compared to those due to delay stabilization.

An advantage exists in the ring-around system in that the range information is contained throughout the entire loop. This allows each of the two vehicles to monitor range during the docking maneuver. A failure in readout equipment in one vehicle, then, does not necessarily abort the docking maneuver.

The antenna system plays an important role in the ring-around system. For acquisition purposes at the beginning of the docking maneuver, it is desirable to have omnidirectional radiators. As has been seen and is noted again in table 7, a trade-off between spacial coverage and transmitter power is necessary at the higher operating frequencies. In conjunction with the radiation patterns of the antenna system, it is necessary that one system be linearly polarized and the other circularly polarized, since aspect of approach at the beginning of the mission is unknown.

Requirements for equal performance of the ring-around system at UHF, 10 GHz, and 70 GHz are summarized in table 7.

TABLE 7 - RING AROUND PERFORMANCE CHARACTERISTICS

SYSTEM	TRANSMITTER POWER	SPACIAL COVERAGE (DEGREES)	RANGE FOR VIDEO DET. (FEET) (1 FT ACCURACY)
UHF	50 mW	360 (ONE PLANE)	≈ 40
X-BAND	50 mW 9 WATTS	35 360 (ONE PLANE)	220
70 GHz	50 mW 20 KW	7 360 (ONE PLANE)	300

* ACCURACY FOR RANGES CLOSING TO VIDEO DETECTION FOR ALL SYSTEMS < 5 FT. TERMINAL ACCURACY OF SYSTEMS < 1 FOOT.

PROBES AS DOCKING AIDS

The electromagnetic probes considered here may be divided into three classifications: electrostatic, magnetic, and electromagnetic (or antenna) probes. The electrostatic or "capacity" probes operate on the principle that the electrostatic field lines of flux, emanating from a capacity probe, theoretically extend to infinity. The intensity of the field varies inversely with the distance from the probe by the familiar point charge equation:

$$|\bar{E}| = \frac{\int_V \rho_V dV}{4 A \epsilon_0 R} \quad (262)$$

The field of the capacity probe is therefore an inverse function of range. As a target vehicle enters the measurable field of the probe, some flux lines terminate on the target vehicle and the target vehicle becomes a part of the external capacitance associated with the probe. Obviously, the size of the vehicle also enters into the capacity contribution. This is a major problem in the use of the capacity probe and will be shown to be a problem in the use of the magnetic and electromagnetic probes as well.

The magnetic probe operates on the principle that the magnetic lines of flux emanating from a current loop (or loops) extend theoretically to infinity. The magnetic field intensity is given by:

$$|\bar{H}| = \frac{\oint_S J \cdot \bar{n} da}{2\pi R} \quad (263)$$

This field also varies inversely with (R). The lines of flux couple with a target vehicle, as it approaches, causing current to flow on the target vehicle. If the target vehicle is considered as a closed loop, the impedance (Z_{21}) reflected back into the primary circuit (probe circuit) is illustrated in figure 52

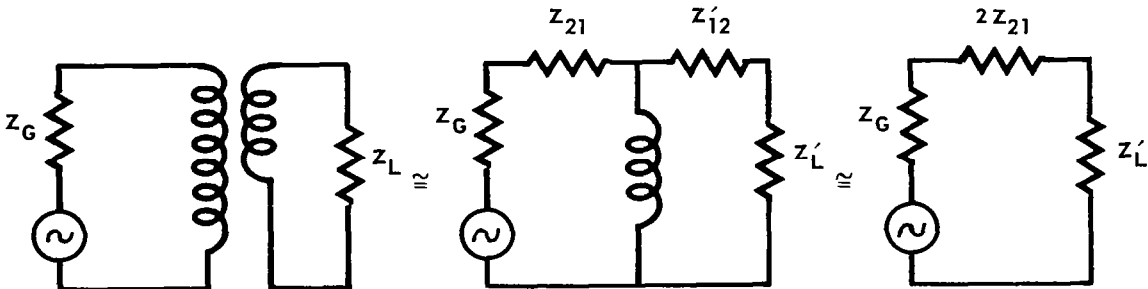


FIGURE 52 - MAGNETIC PROBE - EQUIVALENT CIRCUIT

Variations in Z_{21} supply the information to be measured. It is apparent that Z_{21} is a function of target size, geometry and material.

Antennas differ as to the amount of energy that is intentionally radiated by the probe to a much greater extent than do the other two cases. This radiated energy is reflected by a target vehicle back into the primary probe circuit and modifies the input impedance to the probe in a somewhat similar manner. Since both the (E) field and the (H) field vary inversely with (R), the power density in the radiated field varies inversely with (R^2) . The return energy modifies the antenna impedance and the return signal level is found from the familiar radar equation:

$$\frac{P_r}{P_t} = \frac{K G_t^2 \lambda^2}{(4\pi)^2 R^4} (\sigma) . \quad (264)$$

As shown here, the return is inversely proportional to range to the fourth power; however, the gain squared in the numerator tends to offset this, and sensitivity at 100 feet is not a problem, even with low power output levels. As the target closes on the antenna probe, its impedance continues to be modified, even after entry into the very near field. The near fields of an antenna are complex, and reactive or pulsating components become large. For example, the expressions for the fields associated with a current element, as given in reference 34 are:

$$E_\theta = \frac{I dl \sin \theta}{4\pi \epsilon} \left(\frac{-\omega \sin \omega t'}{r v^2} + \frac{\cos \omega t'}{r^2 v} + \frac{\sin \omega t'}{\omega r^3} \right), \quad (265)$$

$$E_r = \frac{2 I dl \cos \theta}{4\pi \epsilon} \left(\frac{\cos \omega t'}{r^2 v} + \frac{\sin \omega t'}{r^3 \omega} \right), \quad (266)$$

$$H_\phi = \left(\frac{I dl \sin \theta}{4\pi} \frac{-\omega \sin \omega t'}{r v} + \frac{\cos \omega t'}{r^2} \right). \quad (267)$$

These expressions show that in general, the field is a composite of the electrostatic ($1/r^3$ term), the magnetic ($1/r^2$ term), and the radiation ($1/r$ term) fields. When the target is very near, the antenna coupling with the higher order fields produces drastic changes in probe impedance. The range of impedance variation is therefore of many orders of magnitude, going from a slight change in radiation resistance to a completely reactive impedance.

Antenna Probes

The movement of a vehicle in proximity to an antenna results in changes in the input impedance of the antenna, which can be extracted to provide information about the target vehicle. Antennas which are highly directional are useful for better long range (100 feet) sensitivity, but antennas having low directive give better "close-in" resolution.

Highly Directional Antenna Probes. - An antenna with a directivity of 10 db or more, such as a "horn" antenna, can be arranged as shown in figure 53.

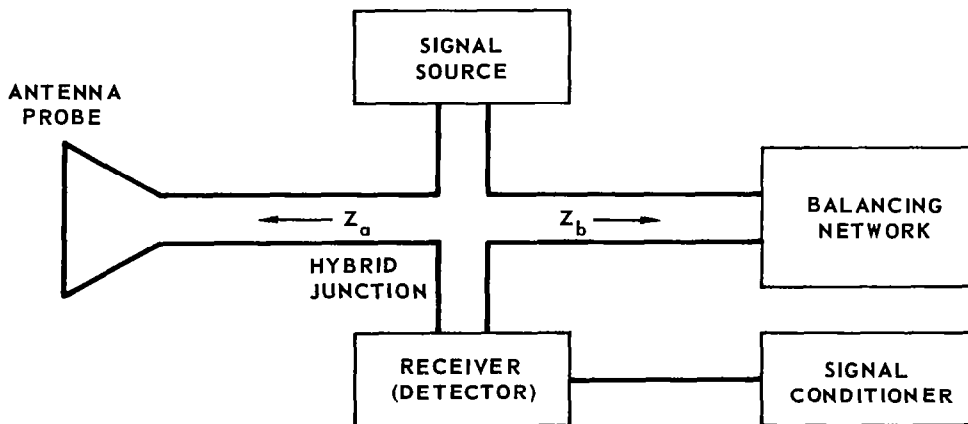


FIGURE 53 - A MONOSTATIC ANTENNA IMPEDANCE PROBE

The sensitivity of an arrangement such as this can be rather remarkable. A 20 db horn, a 100 mW signal source, a detector with 10 u volt sensitivity for 20 db signal to noise ratio, and a precision balancing network should be capable of detecting a vehicle of 0.01 meters cross section at 100 feet. Since the target vehicle will probably have a cross section at least two orders of magnitude larger than this, detection of its presence and its movements at 100 feet should be little problem. The signal source for this arrangement must be very stable since the impedance Z_a is a complex function of frequency. To some extent Z_b can be arranged to vary in the same manner as Z_a to reduce the frequency drift problem, but it is probably not realistic to expect this to solve the entire problem. To investigate the magnitude of the frequency drift problem, consider a case in which the frequency drifts to $f_0 + 50 \times 10^{-6} f_0$ and the impedance (Z_a) follows in direct proportion and changes to (Z_a) + $50 \times 10^{-6} (Z_a)$. Let (Z_a) be simply 52Ω resistive. When Z_b does not change and the signal source is 100 mW, the voltage produced at the receiver is:

$$V_r = \sqrt{P (\Delta R)} , \quad (268)$$

$$V_r = \sqrt{(100 \times 10^{-3}) (50 \times 10^{-6})} , \quad (269)$$

$$V_r = 2.23 \mu . \quad (270)$$

It is evident that a frequency drift of 50 parts per million is therefore several orders of magnitude too high. If it is desired to keep the short term frequency drift error below 10 uV at the receiver, frequency stability of approximately one part per 100 million is required. However, this can be obtained by state-of-the-art techniques. The design of the receiver is also important since it is required to have a dynamic range of from ten microvolts to one volt without saturating. The one volt requirement occurs when the target vehicle is so close to the antenna that its impedance becomes completely reactive. This large dynamic range implies the use of a logarithmic amplifier to convert the range of the signal output to that which is more suitable for display or further processing. Since the system must be calibrated to provide the required measurements, near field antenna effects have little significance in system design considerations.

This type probe suffers from at least one of the same handicaps as the capacity and magnetic probes, i.e. measurements are functions of target vehicle size, geometry, and material. Additional problems with the directional probe are its narrow field of view and its near field defocusing, which must be calibrated out of the system. The single directional antenna probe would therefore not appear to be capable of providing the essential information required for docking. However, multiple antenna probes offer some promise, as discussed later.

Antenna Probes with Low Directivity. - Antennas with less than 10 db directivity have the advantage of a wider field of view, but their application for range measurement will probably be limited to 50 feet or less. This may not be a real disadvantage since other limitations restrict the usefulness of higher gain antenna probes to approximately 100 feet. The antenna probe may

be arranged as shown in figure 54.

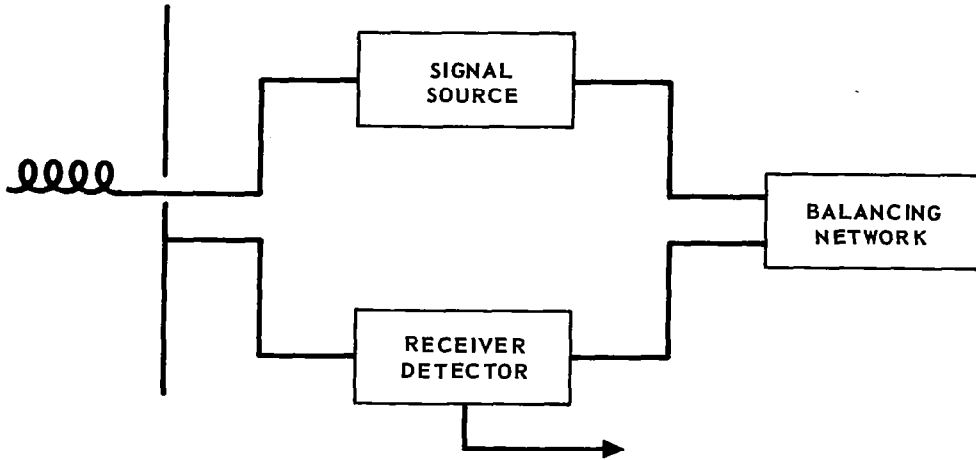


FIGURE 54 - A LOW DIRECTIVITY PROBE

The lower gain probe does not necessarily imply lower frequency. It is desirable to keep the frequency high enough to provide for operation in the ionosphere with only minor degradation. The limitations of the low directivity probe are the same as for the high directivity probe with the substitution of the range limitation for the narrow field of view.

Multiple Antenna Probes. - Multiple probes arranged as two mutually perpendicular pairs (or in other arrangements) offer some interesting possibilities for the production of the raw data from which target angular rotation, range, range rate, bearing angle, and possibly target rotational axes orientation can be determined. Consider the configuration shown in figure 55.

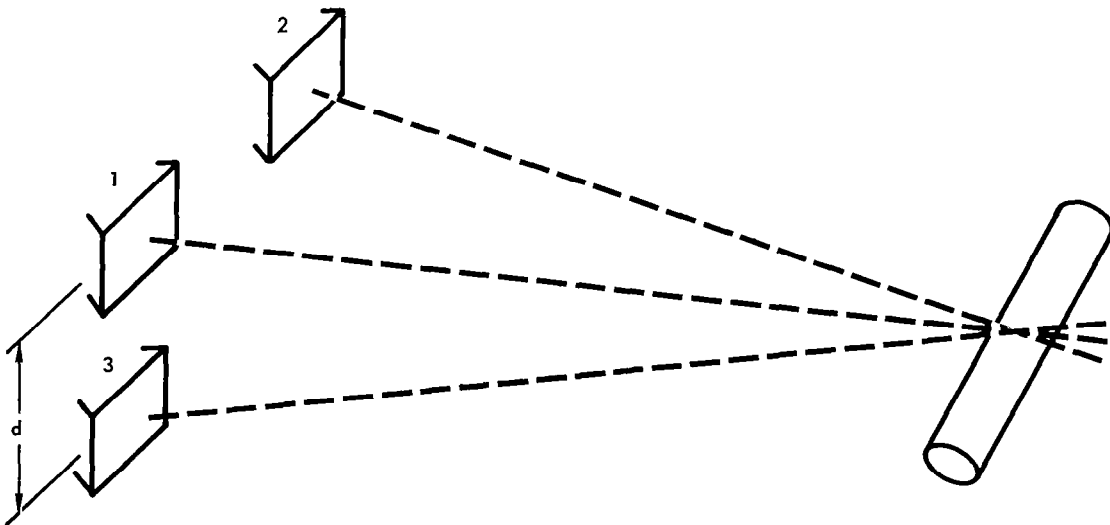


FIGURE 55 - MULTIPLE ANTENNA PROBES

The outputs of each antenna will be similar as functions of time. However, the peak return (for the general case) will occur at a slightly different time. The output of three channels may appear as shown in figure 56.

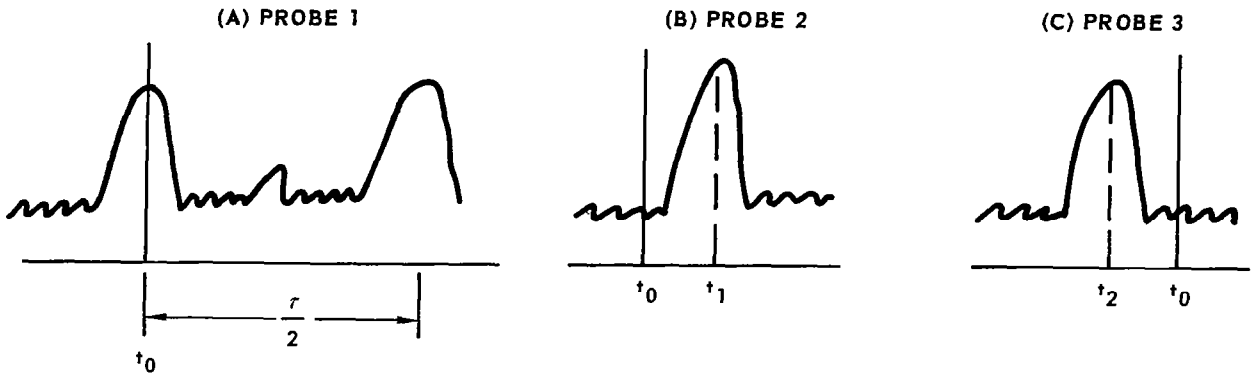


FIGURE 56 - RETURN SIGNATURES

This difference in time is a function of angular rotation, bearing angle, and the antenna spacing (d). Angular rotation can be obtained, since peak return to peak return is $\frac{T}{2}$. The bearing angle can be obtained by maximizing the return of the fixed antennas. Since (d) is known, the range can be measured as shown in figure 57.

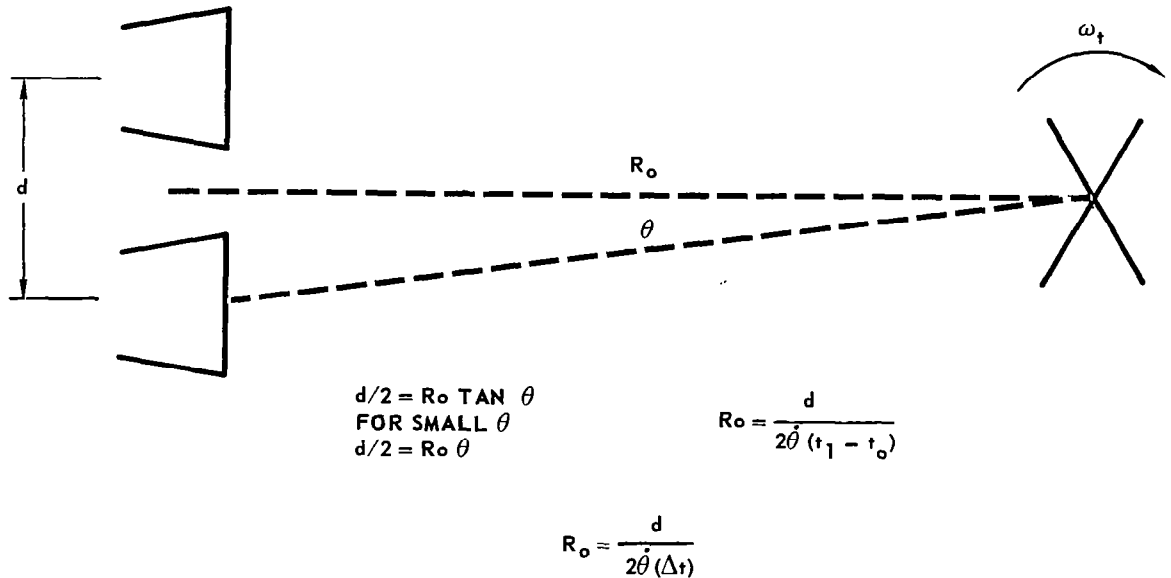


FIGURE 57 - ROTATION RATES FROM RETURN SIGNATURE

For arbitrary rotation of the target vehicle, the magnitude of the peak response will not be exactly the same for each channel. The response at one aspect angle, however, will probably be much stronger than at any other in each of the antennas. Range error due to surface response ambiguities are therefore unlikely. Extraction of these parameters requires a memory unit and data processing.

Measurement of range, range rate, bearing angle, and tumble rate has been discussed. Target vehicle size, geometry, and tumble axis are other desired parameters. The magnitude of the response is a measurement of the vehicle size if range and vehicle geometry are known. The magnitude of the response, however, is an absolute quantity. System calibration is therefore required before significance can be given to the absolute readings. The shape of the signal return versus time for each probe provides the data to deduce the geometrical shape of the object in one plane of observation. The slightly modified returns from the other three channels help to gain a three-dimensional "look" at the object. Ideally, the rotational axis could also be determined by observing the data from each channel from several spacecraft positions.

Limiting Factors. - Little or no useful data can be obtained directly from antenna probe measurements. The amount of data processing required appears to be a serious disadvantage. The accuracy of the final parameters is, in some cases, a function of absolute channel gain, requiring a high degree of gain stability. Frequency stability directly affects channel sensitivity, as previously discussed. Data obtained in the near field of the antennas is altered since the channel return is affected by the amplitude and phase illumination of the target vehicle.

Capacity Probes as Docking Sensors

Capacity probes show promise as aids in the final stages of docking. Many other types of sensors lose their usefulness in this stage because of near field effects, short pulse width requirements, large object angle subtended, and so on. These probes can be mounted on extendable-retractable booms, or fixed permanently on the docking vehicle.

As the vehicles come into close proximity, comparable to their own physical sizes, measurement of range becomes relatively independent of vehicle geometry. Accurate range, range rate, and relative attitude measurements in this region should be obtainable. At distances of 100 feet or more, the sensitivity of the capacity measurements are not sufficient to provide useful information. At ranges which are less than 100 feet but still greater than the diameter of the target, range measurements are confused by the size of the target vehicle. At vehicle separations which are such that the capacity probe has a reasonably well formed image within the target vehicle, accurate measurements of range are possible. Range and range rate measurements from one meter to zero separation can be made with reasonable accuracy in many

missions to assure soft capture. Multiple probes can also be used to provide close approach relative attitude information, as discussed herein.

Two capacity probe concepts are discussed. The first approach utilizes a system of double electrodes and a capacity bridge similar to the "Direct Capacitance Altimeter" (reference 35). The second approach uses single ended capacity probes. Two techniques for the measurement of the probe capacitance variations are discussed.

Double Electrode Capacitance Measurement Description. - Electrodes may be located on the docking face of the vehicle as shown in figure 58 . Lines of flux, also shown on figure 58 , are provided to indicate the approximate field distribution. In figure 59 , the field lines are replaced with the various capacities present in the system. It is the variable capacity associated with C_{pt} (probe to target capacity) that is to be measured for range determination.

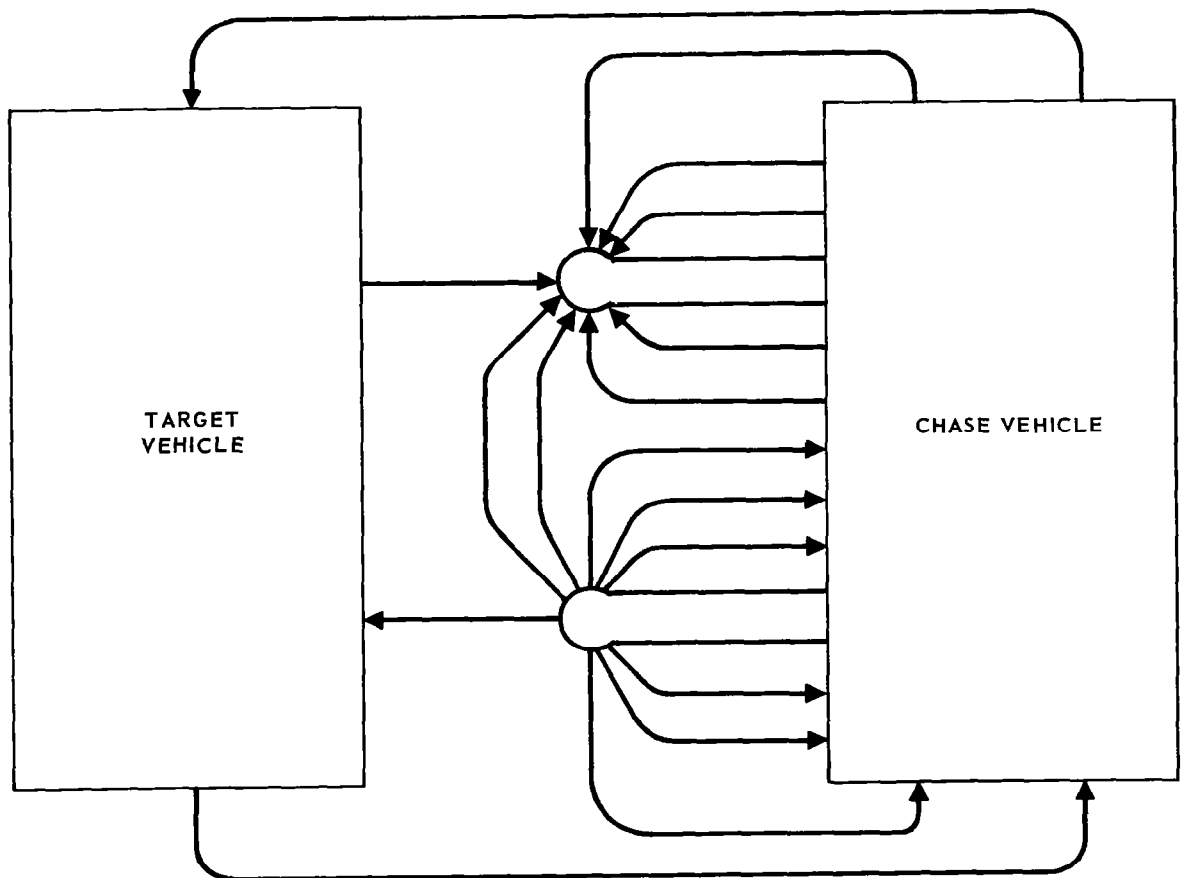


FIGURE 58 - ELECTROSTATIC FIELD REPRESENTATION FOR DOUBLE ELECTRODE SYSTEM

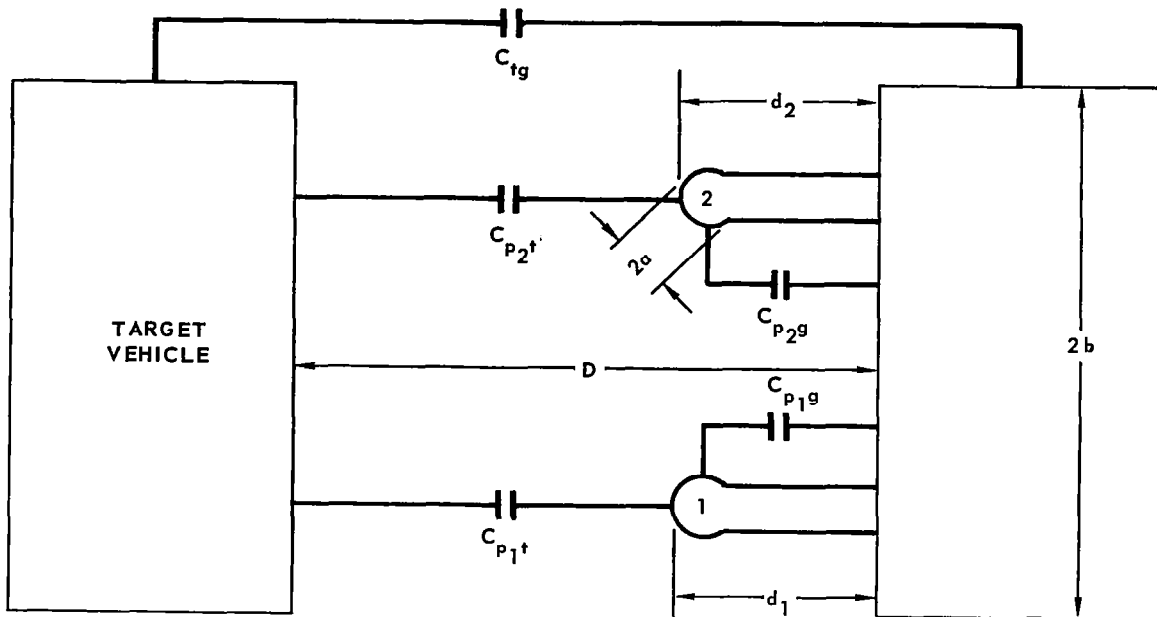


FIGURE 59 - EXTERNAL (PROBE) CAPACITIES FOR DOUBLE ELECTRODE SYSTEM

The capacities in figure 59 are computed in appendix E. In order to measure the variable capacity, the fixed capacity of the system, which is much larger except at very close ranges, must be balanced out by use of a bridge circuit. A bridge circuit, shown in figure 60, has been used with the "Direct-Capacitance Altimeter" (reference 35) and is capable of the measurement of 1 af. When the probes are required to measure range from only 0 to 10 meters, the capacity variation is much greater than this. At 10 meters, the capacity variation may reasonably be 100 af, which should be easily measured by this method.

Relative Attitude Information. - A tumbling target presents periodic fluctuations in capacitance. The period of this fluctuation is a measure of relative tumble rate and the amplitude fluctuation is a measure of the geometry of the target in one plane of observation. A single system has limited usefulness, however, since relative attitude changes in only one plane can be determined. Multiple capacity probes, however, have promise for the provision of precision range and relative movement information at very close range for missions that require soft docking or very close approach.

Limiting Factors. - The presence of free electrons and ions in the ionosphere present severe limitations in the use of this technique at certain distances from the earth. Ionospheric characteristics have the effect of a

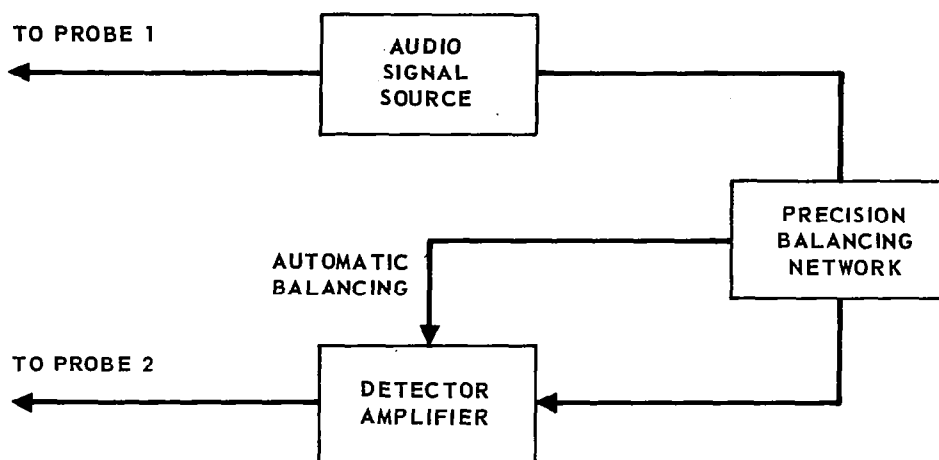


FIGURE 60 - CAPACITY PROBE BRIDGE

low reactance short on all capacitors in the external circuitry of figure 59 . The appropriate low reactance depends on the geometry of the probes, vehicles, and vehicle separation, on the number of free electrons in the rendezvous region and the frequency used with the bridge. At 5kHz, this problem occurs throughout much of the ionosphere.

Other limiting factors are as previously mentioned; i.e., variation in target vehicle geometry and material, and the capability for the measurement of small capacity variations. Maintaining the impedance balance in the bridge circuit during measurement is also a problem when very small capacity variations are to be measured. When the device is not in use, however, it can be made self-balancing so that a zero balance can be maintained until ready for use.

Single Electrode Capacitance Measurement Description. - A single electrode can be arranged to measure range as illustrated in figure 61. Probe-to-target capacity variations can be measured with a bridge very similar to the one used with the double ended probe method mentioned previously. Another technique for the measurement of small capacity variations is to arrange the probe capacity as a part of the frequency determining resonant circuit of an RF oscillator as shown in figure 61.

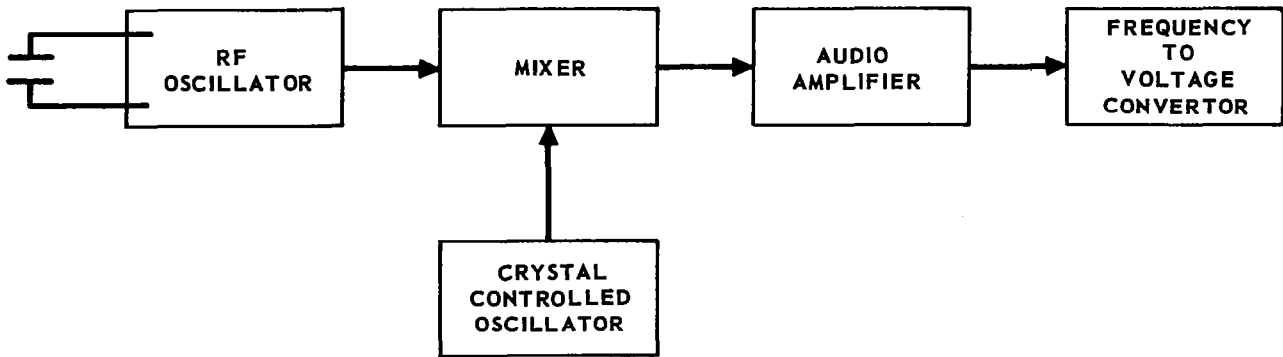


FIGURE 61 - RF EXTERNAL CAPACITY SENSOR

With the target vehicle at infinity (greater than 200 feet), the circuit is arranged to produce an RF output at, for example, 10 MHz. As the target vehicle approaches, the probe capacity is increased and the frequency of the resonant circuit (and oscillator output) is lowered slightly. This change in frequency is detected by mixing the oscillator output with the output of a crystal controlled local oscillator with a fixed 10 MHz output. The audio difference signal is a measure of the probe capacity variation. This signal is amplified and processed as required.

The circuitry required for the ultimate production of an audio difference signal could, no doubt, be made quite compact and light in weight. In fact, it might be desirable to place this portion of the circuitry in the probe or probe support structure (if temperature variation is not a severe limitation).

Extraction of Other Information. - Time differentiation of range data can, of course, be processed to extract closure rate. One probe will also provide limited target tumble information in terms of the periodic variation of probe capacitance with the target movement, unless the target is symmetrical in the observation plane. Multiple probes, however, would appear to be very desirable for the measurement of relative attitude of the vehicles and attitude change rates. For example, attitude differences as shown in figure 62 are readily observable by appropriately arranging the outputs from probes 1 and 2. Additional probes (3 and 4) in a line perpendicular to probes 1 and 2, provide relative attitude in a normal plane. Relative angular tumble rates are also available when multiple probes are used.

Limiting Factors. - The limiting factors are generally the same as in the previous section. If the heterodyne detection method is used, the frequency stability of the probe oscillator becomes a significant factor because frequency drift causes a direct range measurement error. Ionospheric EM wave attenuation characteristics are important also, but as discussed in

appendix D, RF frequencies above 30 MHz are affected little during normal ionospheric conditions.

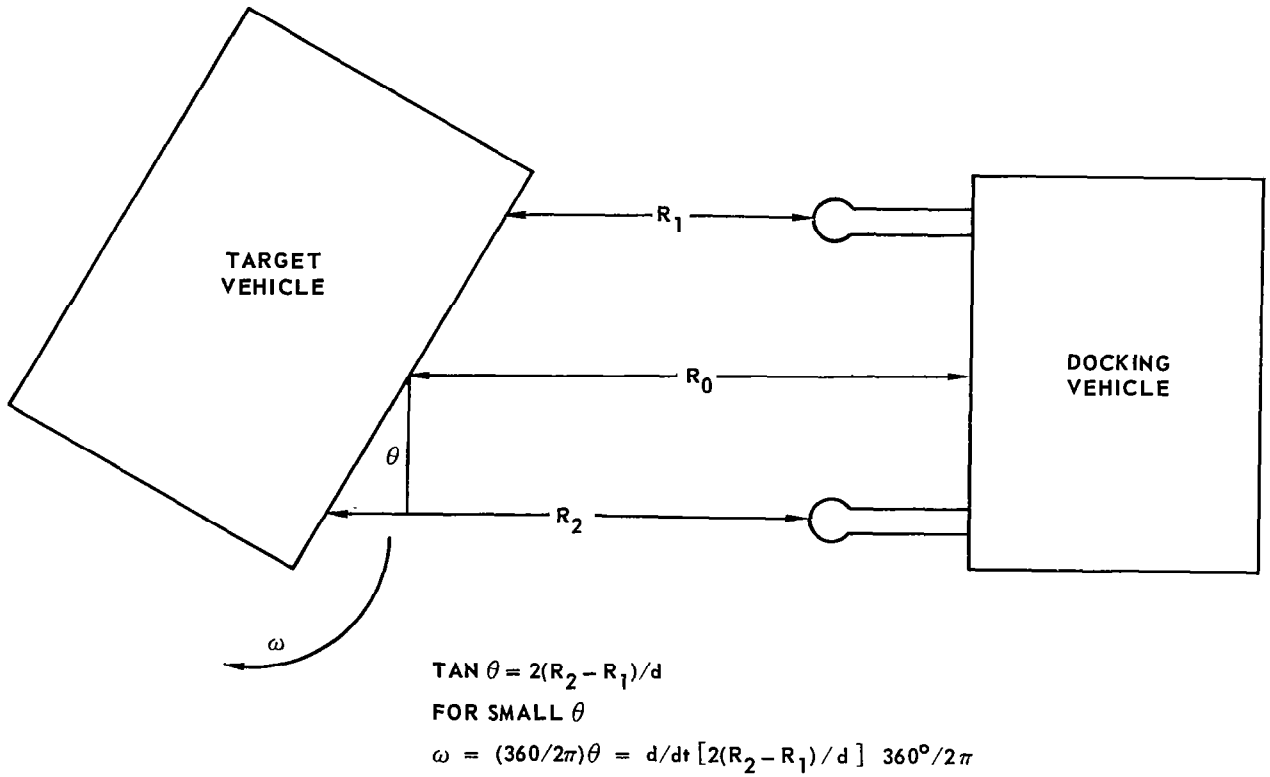


FIGURE 62 - USE OF MULTIPLE CAPACITY PROBES IN CLOSE APPROACH

OPTICAL RADAR SYSTEMS FOR DOCKING

Laser or other optical systems deserve serious consideration as alternates to other electromagnetic systems for acquisition, rendezvous, and docking. Some of the possible benefits from an optical system are: (1) reduced antenna sizes, (2) less weight, volume, and power, (3) simplicity for equivalent accuracy, and (4) greater possible accuracies.

Optical systems can be divided into two types, active and passive. The passive system types can be useful in spacecraft alignment for docking but possess no range or range rate capability. Use of an active element such as a laser source provides the possibility of attaining highly accurate range and range rate data. Separate examination of optical systems for the tasks of alignment and ranging is indicated, although an active optical system can include alignment capability.

In general, accurate alignment can be attained with optical systems because of the small wavelength (and consequently small size sources) and narrow beamwidth. The alignment system may be improved and/or simplified by the use of an active optical system incorporated primarily for range and range rate purposes.

In order to provide range and range rate with the type of accuracies required, an active source is required on at least one vehicle. The following sections discuss various active optical systems from the viewpoint of one active source. The systems discussed fall into two general categories, (a) coherent carrier, and (b) noncoherent carrier systems. Coherent carrier systems make use of the laser coherent aspects, both spatial and temporal. Noncoherent systems do not require lasing action in the optical source. The additional complexities of coherent carrier systems, compared to noncoherent carrier systems, will be evident in the following discussions. The accuracies, however, of coherent systems can be significantly better than noncoherent systems. Both coherent and noncoherent systems possess characteristics which may be advantageous for docking applications. These characteristics are compared with those of lower frequency systems and advantages and disadvantages noted.

Coherent Carrier Optical System

Systems using lasers for obtaining range and range rate information in docking applications can take the form of radar systems previously described at lower frequencies. The use of the laser enables one to achieve a very high antenna gain and, because of its high frequency and the greater resultant doppler shift, much greater range rate resolution. The technical difficulties associated with coherent carrier systems appear to preclude the achievement of the potentially higher resolutions in the near future. The coherent systems,

their potential, and their problems are discussed below.

Lasers which make use of their spatial and temporal properties utilize a photomixing (or heterodyne) receiver which is able to discriminate against external noise sources. The major external noise source is the sun. The narrow spectral passband of a photomixing receiver effectively reduces the contribution from the sun's broadband spectrum to a negligible proportion. The photomixing process also provides conversion gain which minimizes the internal noise contributions. Ideally, then, in systems where signal fluctuations are not the limiting factor, the coherent system can improve the signal to noise ratio by the square root of the ratio of the optical filter bandwidth of the non-coherent detection system to the IF bandwidth of the coherent detection system (reference 41). The optical filter bandwidth of the non-coherent system can be as narrow as 5 Angstroms (150 GHz), within present technology, but a wider bandwidth is required when using a non-coherent emitter, to avoid re-jection of the signal energy. For example, a non-coherent Gallium Arsenide system requires a bandwidth of approximately 500 Angstroms (15 THz). The IF bandwidth required in the coherent system is established by the range of doppler shifts associated with the radial velocities of interest, unless an electronically tunable laser local oscillator is used to track the doppler shift changes thereby keeping the difference frequency constant. The doppler shift is given by:

$$f_d = \frac{c + v}{c - v} f_o , \quad (271)$$

$$\approx \frac{2v}{c} f_o , \quad (272)$$

where: f_d is the doppler shift frequency,
 v is the radial velocity,
 c is the velocity of light,
 f_o is the carrier frequency.

For a typical wavelength (1 micrometer), $f_o = 300$ THz, and the doppler frequency is approximately 2 MHz per m/s. Thus, very small changes in velocity can theoretically be measured, but a bandwidth of approximately 150 MHz is required to maintain the doppler shift frequency within the IF for radial velocities of interest. However, this bandwidth yields a 50 dB improvement over the Gallium Arsenide system cited above, and a 30 dB improvement over the 5 Angstrom system. An additional improvement of approximately 50 dB could be obtained if an electronically tunable laser were available.

As indicated above, range rate can be determined with great precision by the coherent system. ICW techniques can be used for measuring range. Coherent ranging techniques, such as those used in FM-CW radars, are presently beyond the state-of-the-art and will likely remain so in the near future.

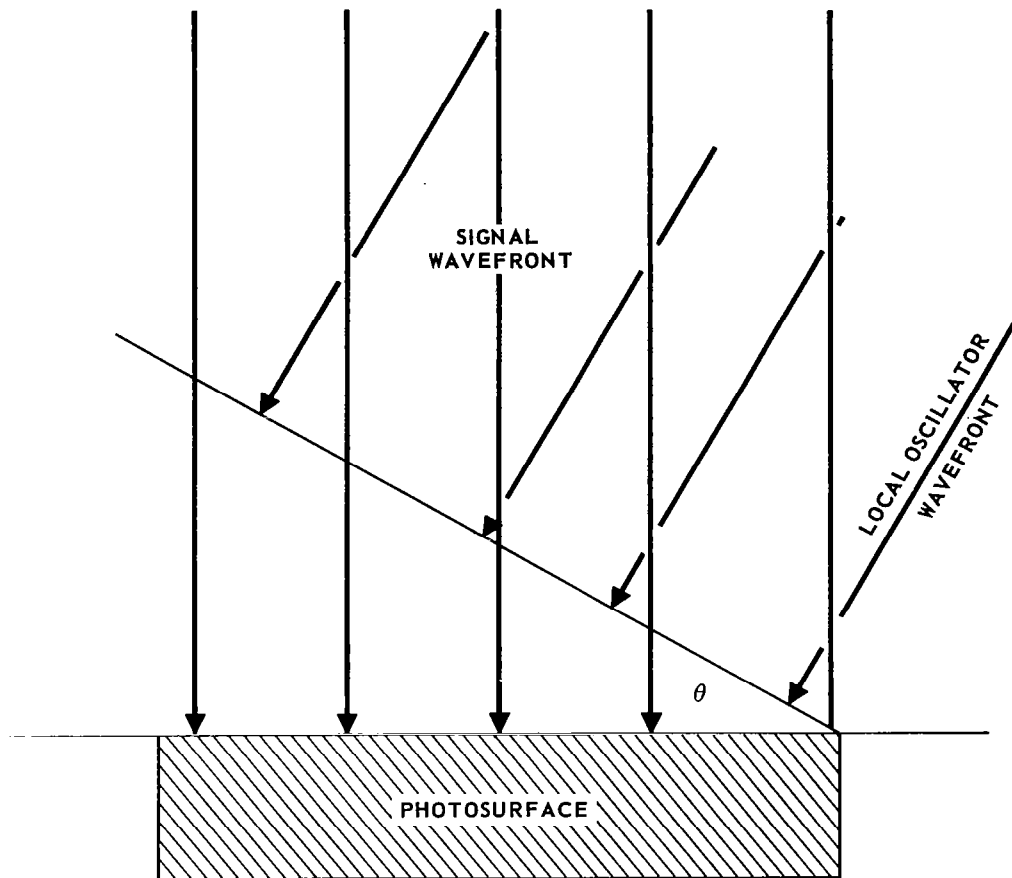


FIGURE 63 – SPATIAL CONSIDERATIONS IN PHOTOMIXING

In order to perform photomixing adequately, spatial and temporal requirements exist that are difficult to fulfill in an operational system. The temporal requirements are related to the spectral purity of laser source and local oscillator. (In some system concepts, the laser transmitter and local oscillator may be the same component, with a frequency off-set provided.) Unless the laser is very narrowband, mixing will occur with different spectral components of the local oscillator signal and/or the received signal spectrum to produce interference and noise products within the IF bandwidth. The spatial requirements for photomixing are related to the alignment of the return signal and local oscillator waves (See figure 63). Analysis of this application (reference 36) has shown that the resultant difference frequency current is of the form:

$$i = a \cos \omega_{IF} t \frac{\sin \frac{\beta l}{2}}{\frac{\beta l}{2}} . \quad (273)$$

where : $\beta = \frac{\omega_r}{v_x} = \frac{2\pi \sin \theta}{\lambda_r}$, v_x = wavefront velocity in the x-direction across the photosurface .
 l = length of photosurface ,
 θ = misalignment angle ,
 λ = local oscillator wavelength ,

Physically, when the local oscillator wavefront is tilted with respect to the photo surface, the phase differs over each part of the photosurface, which is many optical wavelengths long. The beating effect, from which the difference frequency arises, is thus reduced. As noted by equation 273, when the quantity $\sin(\beta l/2)$ becomes less than unity, the amplitude of the difference frequency begins to decrease. Although only one dimension has been discussed, the same effect applies to both. For example, the two plane waves must be aligned to within approximately 10^{-4} radians with 1 cm^2 photocathodes. Any effects which distort the signal wavefront (such as atmospheric effects, rough targets) make photomixing much more difficult, since critical wave components are out of phase at the surface.

The spatial coherence problem is not as serious in the docking application as in many other applications due to the lack of atmosphere and the short ranges of interest. The spectral purity requirement of the laser, however, restricts the choice of laser to He-Ne at the present time. This in turn places restrictions on the minimum weight, size and power requirements. The He-Ne laser is highly inefficient. Typical 0.5 to 1 milliwatt He-Ne lasers require 20 to 100 watts of DC power, are approximately 1 foot long, and weigh 13 to 25 pounds. In addition, the stability requirements place a burden on the mechanical considerations. Sufficient rigidity must be provided to keep vibration effects out of the system.

Laser Interferometric Possibilities.- Developments in laser interferometry have indicated that a return beam from a He-Ne laser, if allowed to reenter the laser, will mix with the original laser frequency. If the optical path length is changing, a modulation will result due to the doppler shift of the return beam. The modulation can be detected by a photomultiplier at the other end of the laser. Interferometric measurements have been made with this technique with the beam reflected from a mirrored surface as far away as 60 feet. It is conceivable that this technique may be used in low velocity short range doppler such as occurs in the docking situation. This technique eliminates the alignment requirements of photomixing and considerably simplifies the optics and the receiving system in range rate measurements. Ranges up to several hundred feet may be possible with present milliwatt He-Ne sources, if corner reflectors are utilized on the target vehicle. The frequency response of this system is limited to approximately 100 kHz by the interactions within the laser (reference 37). This corresponds to a maximum range rate of .05 meters/second. The frequency response utilizing the other He-Ne wavelength (3.4 micrometers) appears to be at least 1 MHz which corresponds to 0.5 meter/second range rate. Thus, extremely fine range rate resolution is possible for very low velocities and short ranges.

Range information can be obtained by phase comparison of video modulation of the laser, as described below in the noncoherent system section.

Because of the present lack of experimental verification of this technique for radar purposes and the lack of quantitative data regarding signal to noise ratio as a function of range, this technique is not included in later system comparisons.

Noncoherent Carrier Systems

A large class of electro-optical systems exists which can advantageously use the available bandwidth, small antennas, and high directivity of optical systems without the constraints imposed by the coherence aspects of lasers. These systems require neither a coherent laser nor coherent detection at the laser frequency. This aspect makes them of more immediate practical concern since (a) the coherence of most laser types is not sufficient to be of use, (b) quasi-monochromatic light emitting sources are available which are not coherent, (c) coherent optical detection is extremely difficult to achieve outside the laboratory and has a number of operational restrictions, and (d) at docking ranges, the noise discrimination of coherent systems is not a necessity.

In this class of noncoherent radar optical systems, the optical frequency is used simply as a carrier of electromagnetic energy for RF and microwave systems. Theoretically, all RF systems that have been discussed can modulate an optical carrier, and, after reflection from the target and demodulation, process the RF signal as before. The RF radar systems function as they did before, except that in place of an RF transmitter and associated transmitting and receiving antennas, the RF source modulates a noncoherent optical source. An optical detector demodulates the optical signal and sends the information to the RF receiver.

A number of advantages result from the use of this class of system for docking purposes:

- a. Large antennas are not required, since optical lens and/or reflectors can be physically small and give large antenna gain (i.e., narrow beamwidth).
- b. The RF frequency in the radar system is selected without regard of directivity, since this is being attained by the optical carrier, which sometimes results in a more compact, lighter weight, and less power consuming design.
- c. The problem of isolation between transmitter and receiver in RF systems is eliminated by the use of the optical carrier.

There are two major disadvantages:

- a. An optical source, the power supply for it, and associated optics must be added.

- b. Receiving optics, a photodetector, and its power supply must be provided.

These disadvantages are not serious at the relatively short ranges typical of docking missions since noncoherent semiconductor sources are available. At long ranges, obtaining sufficient source power for CW or quasi-CW systems becomes a more serious problem, requiring the use of more complex optical sources such as the YAG laser or the noble gas types. These currently require much larger power supplies, as well as cooling systems, and significantly increases the size and weight. However, there is evidence that solid state lasers, such as YAG, and forthcoming pump sources may achieve 9% efficiency, in which case much longer ranges may be achieved without cooling and with reasonable power supply requirements.

At present, the use of a noncoherent semiconductor diode emitter in a noncooperative system is limited to ranges of a few miles, assuming reasonable beamwidth, bandwidth and background levels. In a passive cooperative system, where a corner reflector array is employed, the range may be extended to approximately 10 nautical miles, provided acquisition has been achieved. The acquisition requirements of wider transmitter and receiver beamwidths reduce the range capability for acquisition to less than a mile, unless an active cooperative source is utilized. The use of an active cooperative semiconductor source extends the acquisition range to approximately 10 nautical miles, when both the field of view and the source beamwidth are 10 degrees.

Pulse System.- The simple pulse laser ranging system has been developed to a greater extent than any other laser technique. Range is obtained, as in radar, by measuring the time between the pulse transmission and the echo return from the target. At close ranges, this technique suffers from minimum range problems quite analogous to those of pulse radars. Laser pulse ranging systems have been shown to have accuracies of a few feet or more and to be useful for ranges exceeding 10 feet. Experimental systems have achieved accuracies of a few inches. Use of the currently low-powered semiconductor types, such as GaAs, restrict the range, whereas the use of the heavier, more complex and higher power pulse types such as ruby, argon, and YAG achieve much longer ranges. For the ranges involved in docking, GaAs is sufficient in pulse power output.

Range rate can be derived from pulse systems by differentiating range. The repetition rate of GaAs can be made sufficiently high to insure essentially a continuous flow of range rate information. However, as in conventional pulse radar, the range rate accuracy depends on target induced noise on the range signal, and on the pulse recurrence frequency.

Pulse ranging accuracies of 3 to 6 inches have been indicated for the docking application. Achievement of these accuracies may be obtained by:

- a. Smoothing over 5 to 20 pulses at 1 kHz to 10 kHz repetition rates.
- b. Use of retro-reflectors to aid in eliminating the extended target problem of multiple return pulses.

c. Normalization of the detected pulse amplitude before further processing.

Range rate accuracy is approximately 1 fps, when measured in 1/2 to 1 second intervals. These figures can reasonably be expected to be the maximum accuracies attainable in active optical pulse ranging systems in the near future. Single pulse operation results in a lower accuracy.

CW Systems.- A noncoherent CW system combines a coherent RF or microwave CW system with a noncoherent optical source as a carrier. Two specific system types are discussed below.

One CW system makes use of the noncoherent optical diodes and works on the doppler shift of microwave modulation of the light source (reference 38). In this system, spectral purity and stability of the source are not required, nor is a laser local oscillator required. The detected doppler shift of the transmitted spectrum provides the microwave modulation which, upon mixing (at microwaves) with the original microwave modulation frequency, results in a difference output which is proportional to range rate. Range is obtained as in microwave FM-CW radars.

Present limitations on FM-CW systems are primarily associated with the modulator. Although considerable research on microwave modulation of light has taken place, no satisfactory wideband modulator has been developed. The present state-of-the-art can be expressed by giving the specifications on the best available microwave modulator for potential aerospace use. With a modulation percentage of 15%, an S-Band unit (3 GHz) will have a 3 MHz bandwidth with an average power input of 1 watt. Increasing the bandwidth will increase the required microwave drive power considerably. Internal CW microwave modulation of low power semiconductor sources at low modulation percentage and narrow bandwidth has also been accomplished with milliwatts of microwave drive power. Successful development of wide-band microwave modulation of the optical carrier is required to make ranging by wide-band frequency excursion feasible.

Microwave demodulation is less of a problem. Experimental photomultipliers have been built with response out to 4.5 GHz. One specific type performs optical detection, microwave mixing, and amplifying all in one device, thereby making it well suited for microwave modulated optical systems (reference 39). Other microwave response photodetectors are commercially available (traveling wave phototubes, semiconductors, photodiodes), but are not as sensitive to low level signals as photomultipliers.

Another ranging system, known as the phase difference system, exploits the fact that the phase of the modulation signal at the transmitter differs from that of the reflected wave. The phase shift is directly proportional to time, and hence, to range. For example, a 5 MHz signal impressed on a carrier changes 360° in phase (one cycle) in 200 nanoseconds, equivalent to about 100 feet of range. Thus, when the reflected energy from a target at 25 feet arrives at the receiver, the transmitter modulation frequency has

changed phase 90° . Detection of this phase shift by any of the standard phase measurement techniques provides a ready analog of target range.

The advantage of phase difference systems is that highly accurate ranges are possible with narrow receiver bandwidths and at very short ranges without the difficulties of pulse overlap and determination of leading edges. Four inch accuracies have been achieved in the laboratory. The phase shift resolution of the system determines the ultimate accuracy of the phase difference technique. A range resolution of $1/3$ foot is equivalent to phase shift resolution of approximately 1° at a modulation frequency of 5 MHz. Inaccuracies are introduced into the phase difference method by extended targets due to multiple path lengths from target to source since the return from each path length will have a slightly different phase at the modulation frequency.

Although the phase difference method is suitable for unambiguous short range measurements, an additional technique must be incorporated to provide unambiguous long range information. Range ambiguity occurs every 100 feet in a 5 MHz phase difference system. A second modulation frequency or pulse ranging may be utilized to resolve these ambiguities.

The modulation and demodulation component problems are less severe in the phase shift system because of the lower modulation frequency. However, there are other problems, such as the sensitivity of the phase detector output to a large change in received power. Received power may vary over 40 db as range varies from a few hundred feet to zero. This change in power to the phase detector can be controlled by changing voltage on the photomultiplier dynodes as a function of range, but this introduces transit time errors. Limiting before the phase detector has helped the system performance to some extent.

ICW Systems.- Combination noncoherent systems, utilizing pulsed operation in conjunction with coherent modulation, have some practical advantages for optical systems. In the previously described systems, there arose a wideband modulator component problem for the FM system and an ambiguity problem for the phase difference system. Further, range is limited by CW capabilities of optical sources. A system which avoids these problems is one using pulse operation for ranging and microwave modulation for accurate range rate information. (see figure 64). Since the range rate information is supplied by the doppler shift of the microwave frequency, the pulse rate considerations need not take into account the problems of range differentiation.

Special Characteristics of Noncoherent Optical Systems.- The use of RF and microwave systems on the noncoherent carrier is in general straight forward. However, there are a few special considerations which must be taken into account.

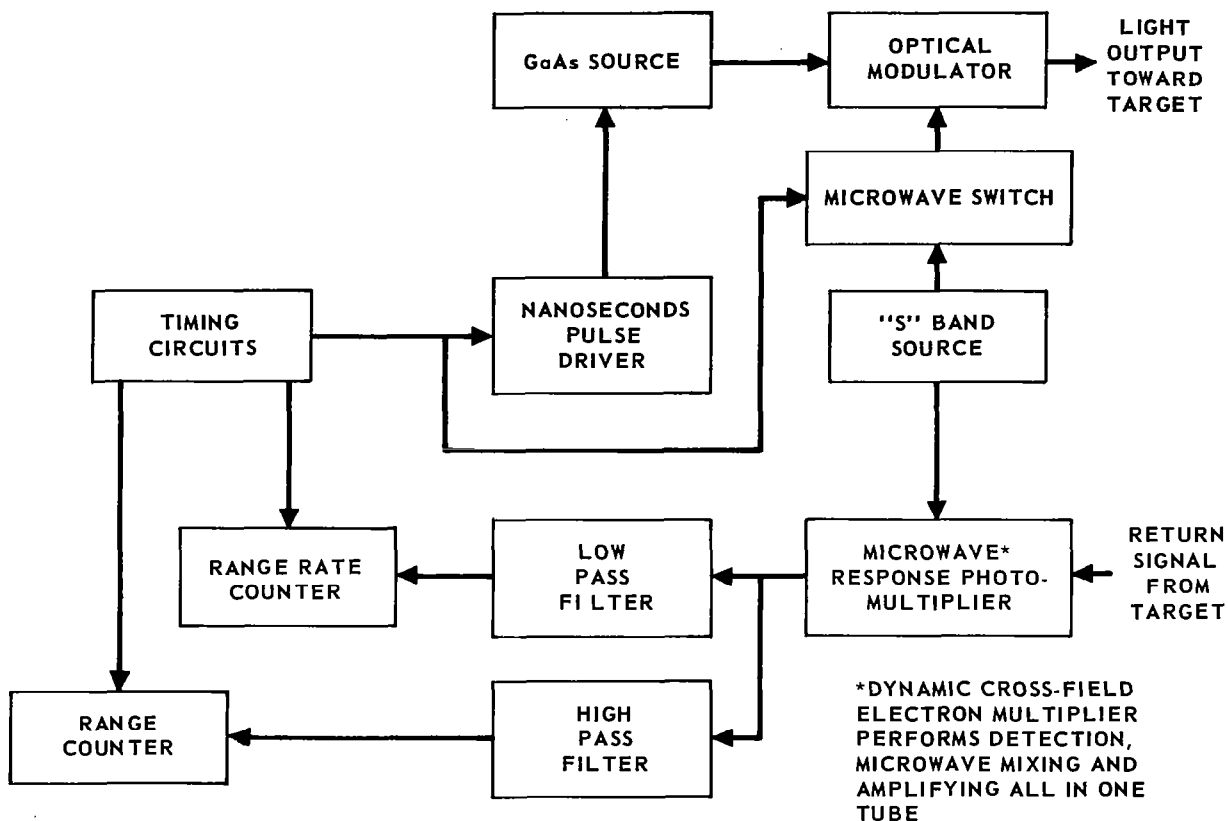


FIGURE 64 – ICW OPTICAL RADAR-PULSE RANGING AND DOPPLER RANGE RATE USING NON-COHERENT SOURCE

The noise considerations at optical frequencies are different from those at RF and have been emphasized in the literature (references 40 and 41). However, the use of noncoherent carrier and square law direct photodetection, as in a photomultiplier, leads to special noise considerations. Modulation of a noncoherent carrier can be treated as a modulation of a noise carrier. Upon detection, the noise carrier components combine with the modulation signal to produce noise components. The resultant signal-to-noise ratio can be determined from the relationship of carrier bandwidths to modulation frequency. There are two distinct cases: one in which the carrier bandwidth B_0 is greater than the modulation frequencies (the baseband condition), the other in which a microwave subcarrier frequency is utilized which is larger than the carrier bandwidth.

The detailed results for a linear detector have been determined (reference 42). The performance of a square law detector has been determined for the baseband case (reference 43). (See figure 65 .) The microwave subcarrier case of square law detection should yield results comparable to those of the linear detector case.

When considering the noncoherent GaAs semiconductor, any microwave modulation can be considered to be still in the baseband region, since the spectral width of GaAs is several hundred Angstroms. As noted from the curves, it is advantageous to operate with the noise carrier bandwidth much greater than the information bandwidth. This result can be seen by considering on-off modulation of the noise carrier. If the pulses are long compared to the envelope fluctuations of the carrier, the post-detection bandwidth can better discriminate against the fluctuations. From the curves, considering semiconductor noncoherent sources, very little signal-to-noise reduction occurs because the signal bandwidth/carrier bandwidth ratio is much less than 0.01.

Another characteristic of noncoherent optical systems is that the path length difference to the receiver between parts of the target that intercept the beam must be of the order of or less than the highest modulation wavelength if degradation of the detected modulation signal is to be avoided. The energy reflected will be at slightly different times. The energy reflected from different parts of the target will have slightly different phases of the modulation frequency. Because of the small optical wavelength and noncoherent source, the target can be considered to consist of many essentially independent point sources, each one optically uncorrelated with any other. At the detector, these will be seen, not as a function of the instantaneous field intensities, but as a function of the instantaneous power from each source. The result (shown in figure 66) is a decrease in the detected modulation frequency amplitude relative to the total detected power. No significant reduction occurs until the path length difference becomes approximately equal to the modulation frequency wavelength, as most of the received energy path length differences will still be considerably less than the maximum path length difference of the received energy.

COMPARISON OF FULL-WAVE SQUARE LAW
DETECTOR AND LINEAR DETECTOR
IN PRESENCE OF NOISE CARRIER

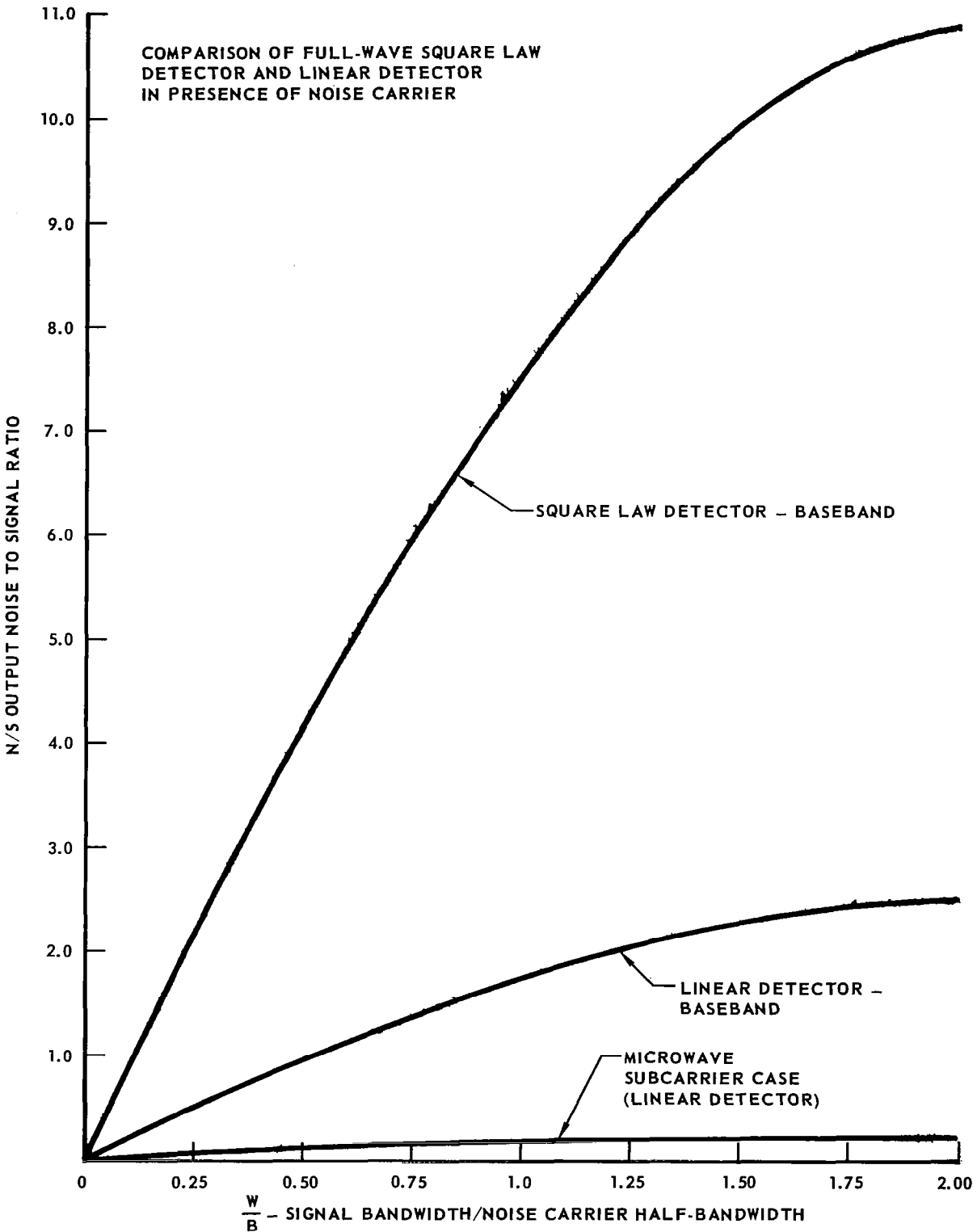
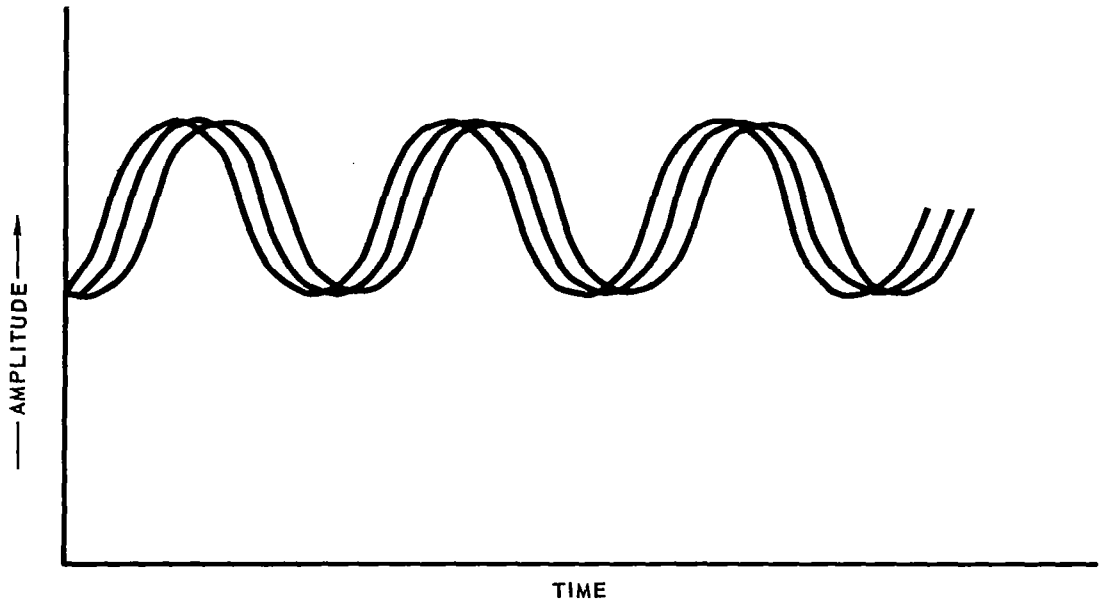
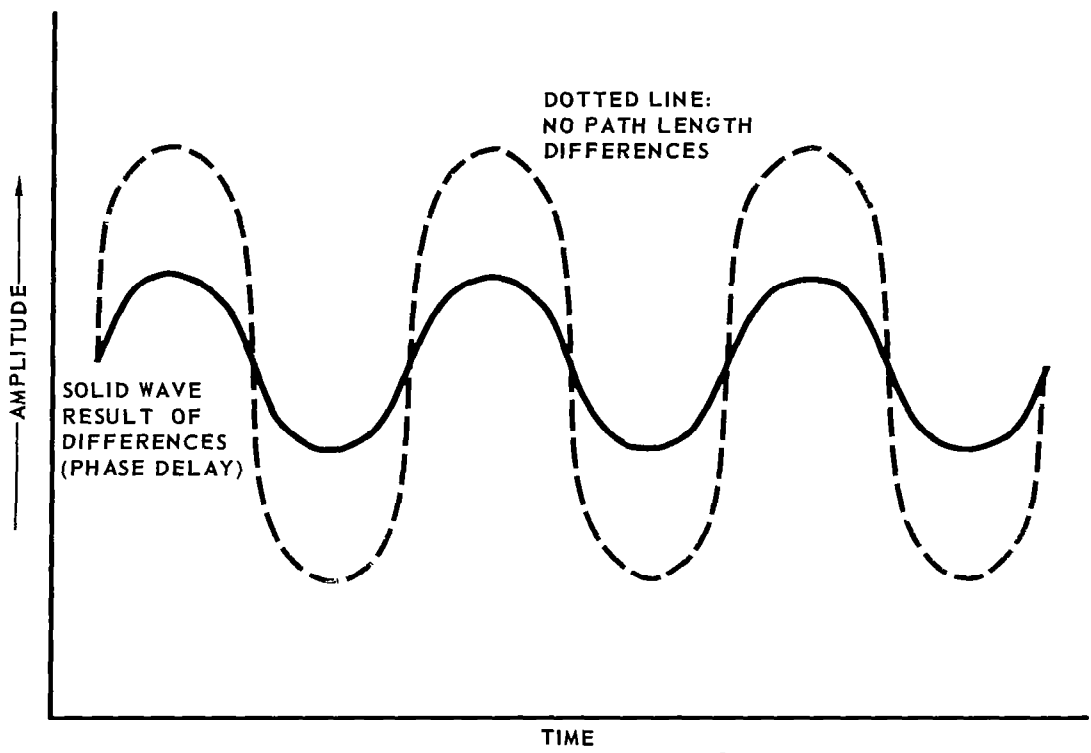


FIGURE 65 - COMPARISON OF FULL-WAVE SQUARE LOW DETECTOR AND LINEAR DETECTOR IN PRESENCE OF NOISE CARRIER



(a) PHASE DELAY FROM DIFFERENT PARTS OF TARGET



(b) RESULTANT OUTPUT

FIGURE 66 – POSSIBLE EFFECTS OF PATH LENGTH DIFFERENCES IN MICROWAVE MODULATED OPTICAL RADAR

The path length difference can become significant if the target is approached at small angles to the target surface. By keeping the beamwidth narrow, the path length difference effect can be substantially controlled. However, this may pose tracking problems at long ranges. In ICW systems discussed previously, where microwave modulation for accurate range rate is used only at short ranges, this problem is less serious. A 1 milliradian beam at 100 meters covers approximately a .1 meter length which is approximately the S-band wavelength. The path length difference will be smaller than .1 meter. Tumbling of the target vehicle may be indicated by sudden decreases in the signal level as the intercept angle becomes very oblique.

Specific comparison with RF systems for weight, size, and power requirements would require a detailed theoretical and experimental design study of the optical system, taking into account expected improvements in the state-of-the-art as well as present achievements. A preliminary design utilizing the ICW concept of pulsed and S-band microwave modulation results in a system having the following characteristics:

Modulation.- Interrupted CW; pulse mode for range and range rate down to 300 feet; interrupted 3 GHz subcarrier doppler used for range rate down to zero range; pulse ranging during interruptions.

Transmitter.- Gallium Arsenide light emitter - noncoherent CW operation at 40 milliwatts; with modulation frequency tracking loop in receiver, only 4 milliwatts. Pulse output is 2 watts.

Receiver.- Direct photodetection with subcarrier mixing in CW mode.

Passive cooperative range.- By means of a 1 foot² corner reflector array - 0 to 15 nautical miles; accuracy - 3 inches.

Noncooperative range.- 0 to 4000 feet, accuracy 3 to 6 inches.

Range-Rate Accuracy.- To 100 meters by range differentiation, ± 1 fps; from 100 meters to zero, $\pm .25$ fps with continuous flow of information to derive real time acceleration.

Antenna.- Two 4 inch diameter optical lenses or reflectors.

Weight.- Approximately 12 pounds.

Size.- Approximately 700 cubic inches.

Power Requirements.- Approximately 15 watts.

The system specifications are based on present developmental and experimental components. Substantial improvements in modulation efficiency, light source conversion efficiencies, and quantum efficiencies of photomultipliers would improve the over-all system. On the other hand, although the components included have been built as separate items, some developmental improvements or modifications have been assumed. One example is that a commercially available X-band microwave modulator weighs 1-1/8 pounds, has 8% modulation index, and has an average power input of 1 watt. An S-band model with 15% modulation weighs 7-1/2 pounds. Interpolation to an improved S-band model with 10% modulation index, weight of 2 pounds, and 1/2 watt average power input has been made. The present S-band model has a bandwidth of 3 MHz, whereas in this application a much smaller bandwidth can be utilized.

Because of the rapid development of electro-optical components, assumptions about significant expected improvements may be considerably in error in either direction. Significant improvements can occur in optical sources, modulators, and detectors. Presently, Gallium Arsenide can lase in the pulse mode at room temperature. Substantial improvement in signal-to-noise ratio can occur because of better background discrimination due to narrower spectral width of the source in the lasing mode (although it may still be treated as a noncoherent carrier). Improvement of laser capability for docking applications at room temperature can take the following paths:

- a. A semiconductor CW lasing capability to give better signal-to-noise ratio, easier collimation of beam.
- b. A solid state laser capability such as YAG, 1 watt CW, with 9% efficiency may require no external cooling system and greatly extend CW and ICW systems range.

Modulator improvements may take many forms since many different techniques are being researched at present. One method of putting a cooled GaAs laser in the RF cavity has achieved 25% modulation at X-band, with but 50 milliwatts of drive power (reference 44). A great deal of the modulation work involves development of better electro-optic crystals. Significant detector improvements can occur by achievement of better quantum efficiency in the near IR for photomultipliers, or by development of semiconductor detectors (which do have high quantum efficiencies) which can compete in sensitivity with photomultipliers.

An improvement in one area can mean significant over-all system improvements. As an example, with a highly efficient 1 watt CW source, the modulation percentage requirements are less, which decreases the power requirements of the microwave modulator.

The interrupted phase difference system can be smaller and lighter at present than the microwave modulation ICW system because it requires neither an optical microwave modulator, demodulator, nor the microwave drive source. The CW power requirements are reduced due to the higher modulation index. The system can operate in the pulse mode for range and range rate until

100 meters is reached. At this point, phase differences of the 5 MHz sub-carrier can be used with brief interruptions for coarse ranging to avoid ambiguities. The major disadvantage of this technique is that range and range rate measurements are not independent, resulting in a restriction on real time measurement of range rate and changes in range rate. The weight can be reduced to perhaps six pounds and the size to 400 cubic inches.

The relative complexities and weights of optical radar systems for docking are indicated in figures 67 through 76. These figures are based on the present capabilities of lasers and optical components and thus are subject to sudden change. Development, for example, of a highly coherent, efficient, spatially pure laser that is small in size would reduce the complexity of a pulse doppler system (G) considerably. An easily tunable coherent laser would enable the complexity of (A) to be substantially reduced. A significant improvement in modulators would reduce the weight of (F) to approach that of (E). This last consideration may be emphasized, since the complexity of (F) is least when considering the docking requirements. Its excess weight over that of (E) and (B) is due mainly to the optical modulator weight and the weight of the required drive source.

Conclusion

In the docking operation, lightweight noncoherent optical systems can be successfully utilized in a noncooperative mode. For ranges much greater than a few thousand feet, either some cooperative mode, through use of a corner reflector array or more complex active optical system of much greater size and weight, is required. The choice of modulation to apply to the noncoherent carrier is primarily governed by the analysis of the various methods at RF, although there are a few important special considerations when using the noncoherent system.

Comparison of optical systems is subject to error because of the rapid change in the state-of-the-art of electro-optical components. Reasonable extrapolation of present state-of-the-art indicates two forms of ICW noncoherent carrier systems to be most suitable until smaller, more efficient coherent sources of high spectral purity are available.

Advantages and disadvantages with respect to RF systems are noted. Comparison with RF systems is subject to the uncertainties of comparing proven operational techniques with unproven concepts utilizing unproven components.

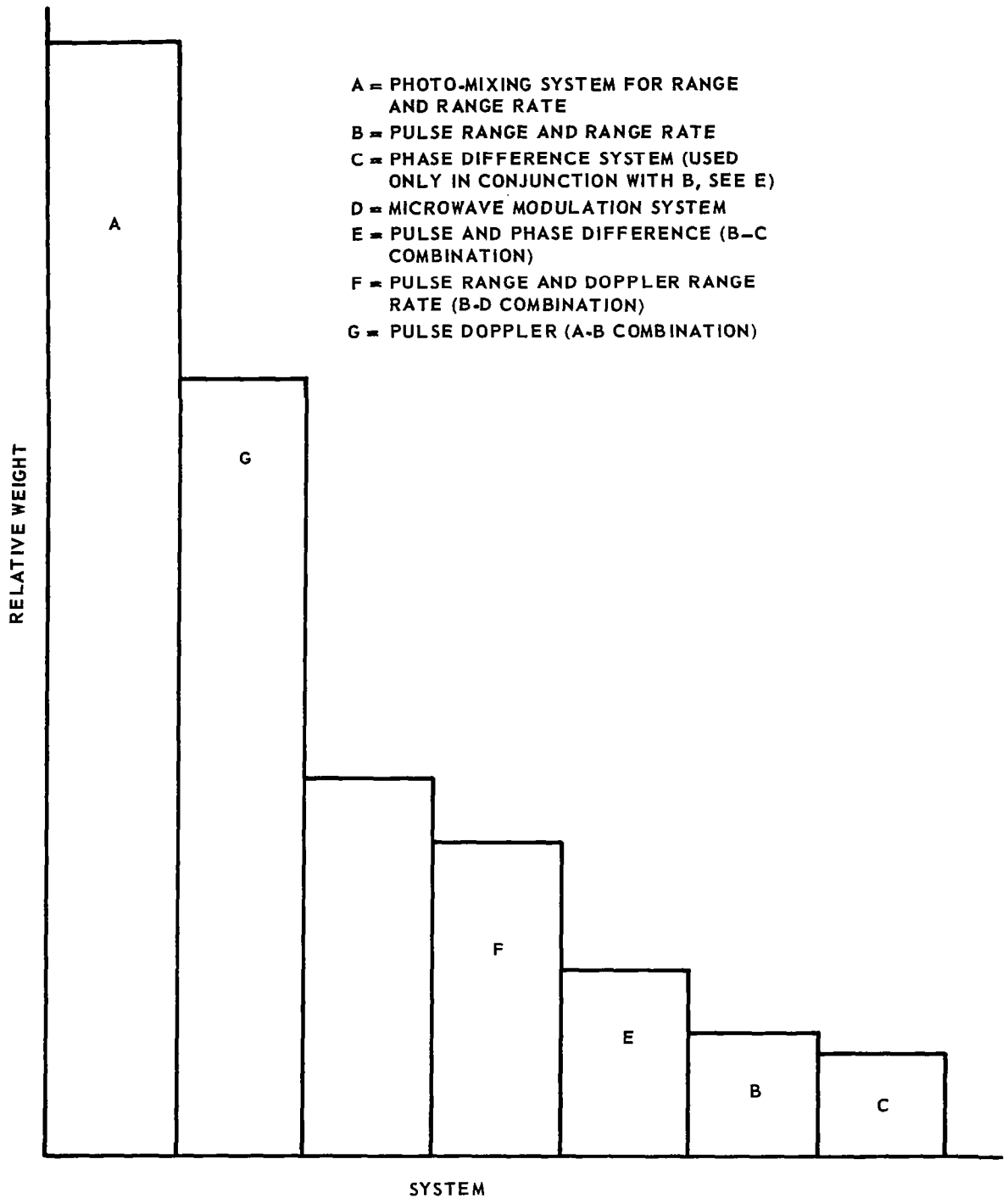


FIGURE 67 – COMPARISON OF RELATIVE SYSTEM WEIGHTS FOR VARIOUS OPTICAL RADAR SYSTEMS

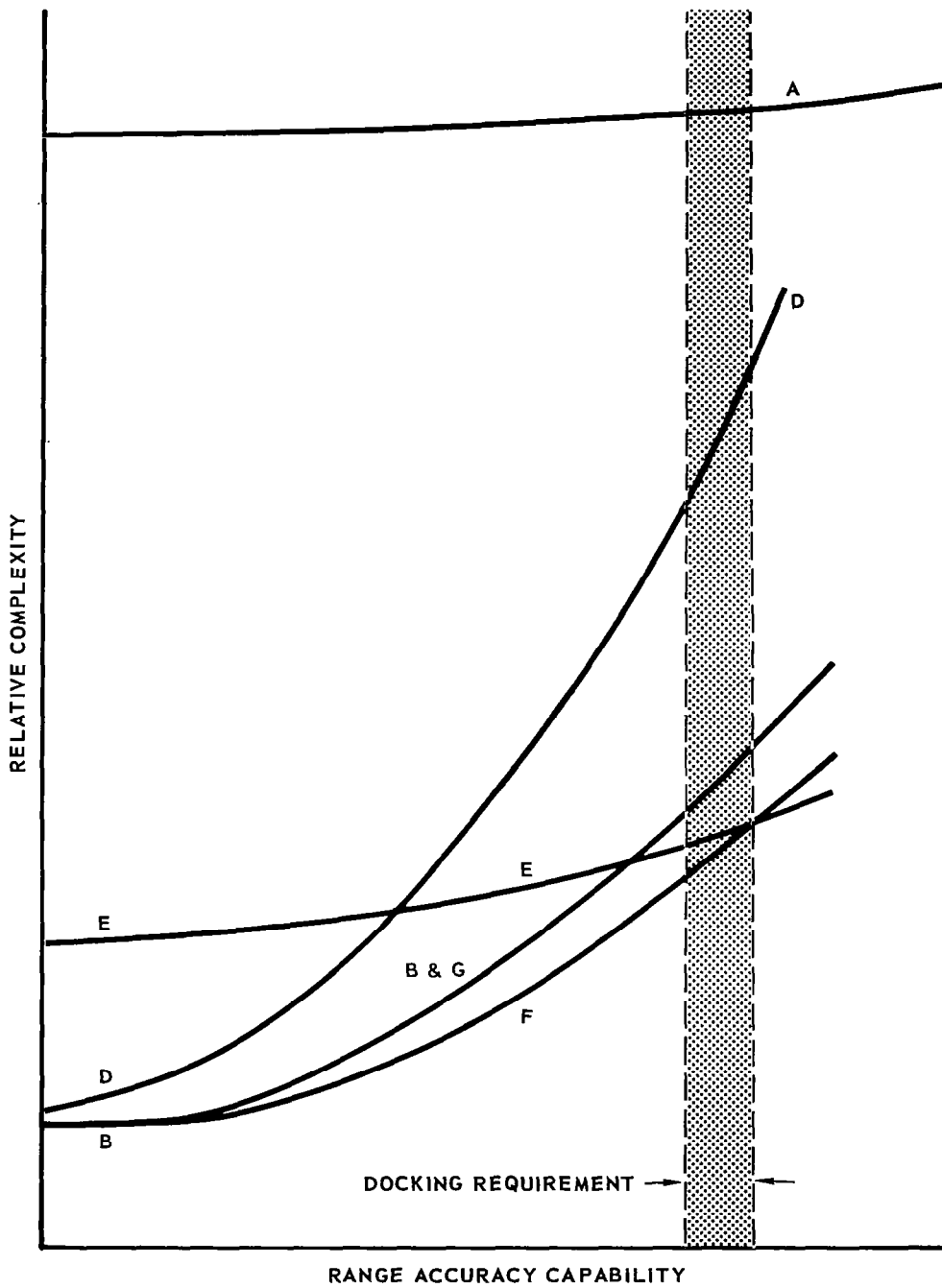


FIGURE 68 – COMPARISON OF RELATIVE SYSTEM COMPLEXITY AS A FUNCTION OF RANGE ACCURACY CAPABILITY FOR VARIOUS OPTICAL RADAR SYSTEMS

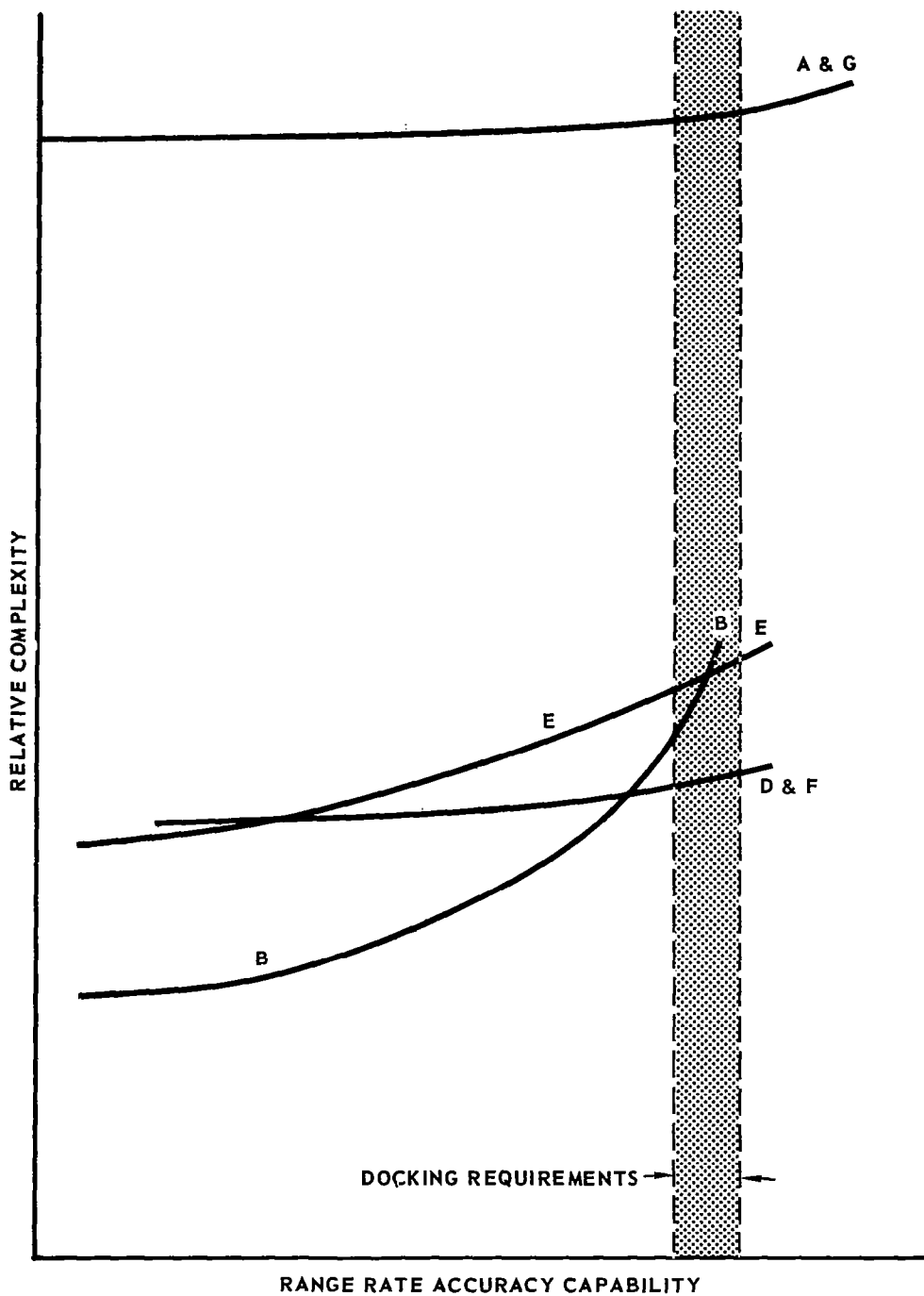
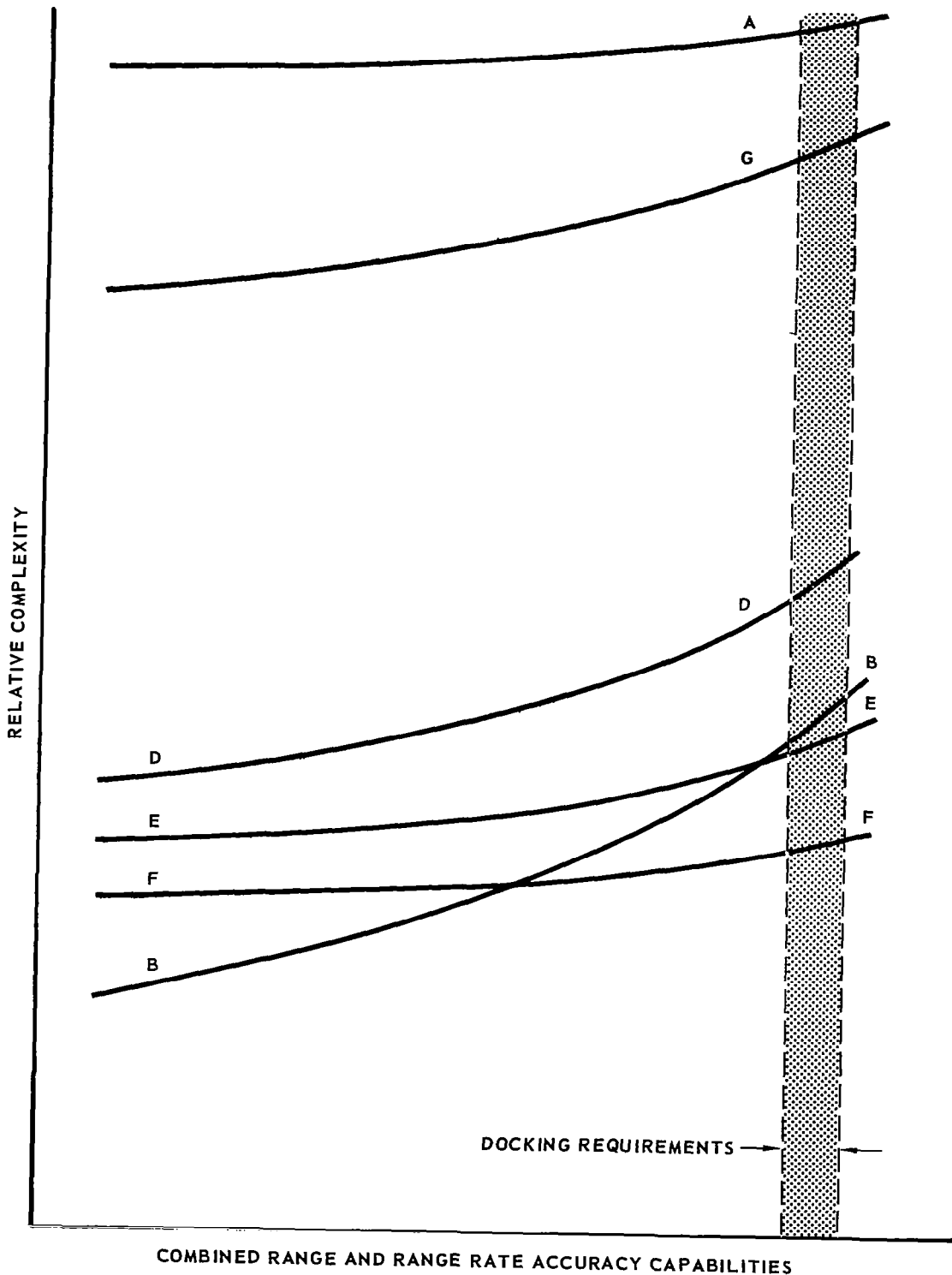


FIGURE 69 – COMPARISON OF RELATIVE SYSTEM COMPLEXITY AS A FUNCTION OF RANGE RATE ACCURACY CAPABILITY FOR VARIOUS OPTICAL RADAR SYSTEMS



COMBINED RANGE AND RANGE RATE ACCURACY CAPABILITIES

FIGURE 70 – COMPARISON OF RELATIVE COMPLEXITY FOR COMBINED RANGE AND RANGE RATE ACCURACY CAPABILITY FOR VARIOUS OPTICAL RADAR SYSTEMS.

NUCLEAR TECHNIQUES

Employing nuclear techniques for measuring range and range rate between two spacecraft immediately implies that the mission is classed cooperative. The degree of cooperation is nominal, however, in that it is required only that one of the docking participants have a radioactive source, and the other participant have the proper means of measuring the radiation, coupled with a knowledge of the source characteristics.

A direct measurement of range can be accomplished by employing one or more strategically placed radiation detectors to ascertain the amount of radiation being intercepted at that particular range. The velocity function will then be the time derivative of the measured range function.

A direct measurement of range rate is provided by proper utilization of the Mossbauer effect.

Nuclear Techniques for Range Measurements

When an isotropically emanating radioactive source is separated from a detector by a range, R , the radioactivity received by the detector is:

$$I_A = \frac{A I_e e^{-\mu R}}{4\pi R^2}, \quad (274)$$

where I_A is the average counts/sec noted by the detector

I_e is the average counts/sec emitted by the source

μ is the absorption coefficient for the medium

A is the surface area of the detector

If the medium is free space and the detector efficiency is η , the average number of detected counts at range, R is:

$$I_A = \frac{\eta A I_e}{4\pi R^2}, \quad (275)$$

where μ for free space is zero.

Equation 275 is the basis from which the range measurement by the use of nuclear techniques is performed.

Statistics of Radioactive Decay. - The phenomenon of radioactive decay follows the binomial distribution law (reference 45). Then the probability, $P(m)$, of observing exactly m disintegrations in time Δt is:

$$P(m) = \frac{N_0!}{(N_0 - m)! m!} p^m (1-p)^{N_0-m}, \quad (276)$$

where p is the probability an atom will disintegrate in time, Δt ,

N_0 is the total number of original atoms.

If N_0 is large and the observation time, Δt , is very small compared to the source material half-life, the binomial distribution law can be approximated by the Poisson distribution. Equation 276 then becomes:

$$P(m) = \frac{M^m e^{-M}}{m!}, \quad (277)$$

where p of Equation $\ll 1$.

M is the expected average number of atoms disintegrating in time, Δt .

For large M , the Poisson distribution is symmetrical for values of m not far from the mean value M , and the Gaussian distribution may be used, i.e.:

$$P(m) = \frac{1}{\sqrt{2\pi M}} e^{-\frac{(m-M)^2}{2M}}. \quad (278)$$

Since the docking application will require sources large in M to measure range out to several hundred feet, the approximation of equation 278 will suffice.

If M is the average expected disintegrations in time, Δt , the average disintegration rate will be:

$$I_A = \frac{M}{\Delta t}. \quad (279)$$

From equation 278 it is seen that the standard deviation in m total number of counts is:

$$\sigma_m = \sqrt{M}. \quad (280)$$

Similarly, the standard deviation in the count rate will be:

$$\sigma_{I_A} = \sqrt{\frac{I_A}{\Delta t}}. \quad (281)$$

Accuracy of the Range Measurement. - From equation 275:

$$R^2 = \frac{K}{I_A} \quad \text{where } K = \frac{\eta A I_e}{4\pi}. \quad (282)$$

And the incremental change in R for a like change in I_A is:

$$dR = \frac{-K}{2RI_A^2} dI_A. \quad (283)$$

Therefore the standard deviation of the range is approximately:

$$\sigma_R = \frac{K}{2RI_A^2} \sigma_{I_A} \cdot \quad (284)$$

Using equations 281 and 282 , equation 284 becomes:

$$\sigma_R = \frac{\sqrt{K}}{2I_A^{3/2}} \times \sqrt{\frac{I_A}{\Delta t}} , \quad (285)$$

$$\sigma_R = \frac{\sqrt{K}}{2I_A \sqrt{\Delta t}} \cdot \quad (286)$$

By equation 275 it is noted that:

$$I_A = \frac{\eta AI_e}{4\pi R^2} = \frac{K}{R^2} \cdot \quad (287)$$

Substituting this value into equation 287 yields:

$$\sigma_R = \frac{R^2}{2\sqrt{K\Delta t}} \cdot \quad (288)$$

Dividing through by R^2 yields the function:

$$\frac{\sigma_R}{R^2} = \frac{1}{2\sqrt{K\Delta t}} \cdot \quad (289)$$

With a detector face area and efficiency of $2.5 \times 10^{-3} \text{ ft}^2$ and 50% respectively, K becomes approximately 10^{-4} and equation 289 is:

$$\frac{\sigma_R}{R^2} = \frac{50}{\sqrt{I_e \Delta t}} , \quad (290)$$

where, as defined previously, I_e is the average counts/sec actually leaving the source.

Equation 290 is plotted in figure 71 and shows the standard deviation of the range measurement as a function of source emission rate and sample time.

Source Size Requirements for A Specified Source. - In general, any number of the radioactive materials known could be used as the source in the range measurement. However, if an additional independent range-rate measurement is to be made from the Mossbauer effect of the next section, a logical source selection would be one which is compatible with both the ranging technique and the range-rate technique. As is shown in the next section, a good source for the range-rate measurement is Sn^{119} . The following is an example of the size requirements placed on Sn^{119} by the range measurement technique for specified accuracy and sample time.

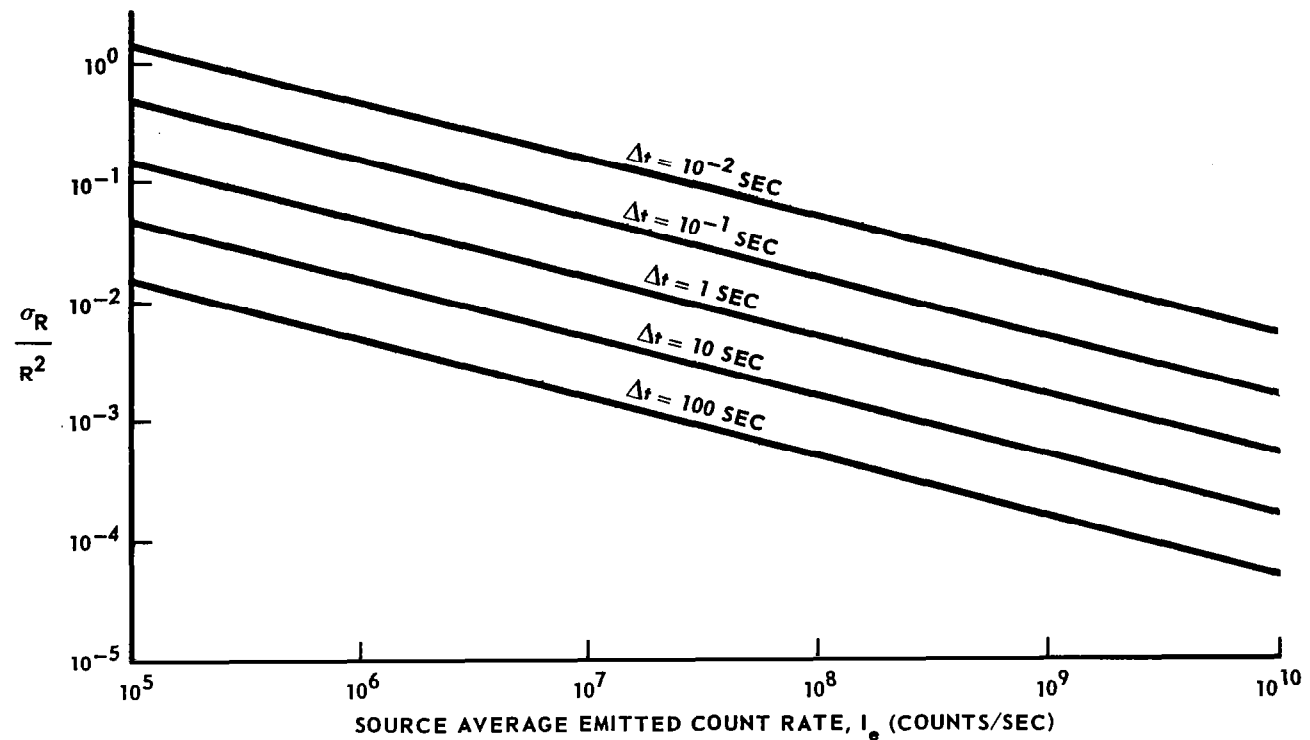


FIGURE 71 - NORMALIZED NUCLEAR RANGING ACCURACY

From equation 290, a range standard deviation of 1 ft at 100 ft with a sample time of 10^{-1} sec requires the average emitted source count rate to be:

$$\frac{1}{10^4} = \frac{50}{\sqrt{I_e \times 10^{-1}}}, \quad (291)$$

$$I_e = 2.5 \times 10^{12}. \quad (292)$$

As is shown in equation 323 of the next section, the relationship between source size, I_0 , in curies and I_e for Sn^{119} is:

$$I_0 = \frac{I_e}{8.44 \times 10^8}, \quad (293)$$

so that the required curie size for the source is:

$$I_0 = \frac{2.5 \times 10^{12}}{8.44 \times 10^8} = 2960 \text{ curies}. \quad (294)$$

Shielding. - Figure 72 shows that a 1000 curie source of Sn^{119} can be shielded to a safe handling level by using only 0.2 cm of steel. Then, for the low energy emission sources such as Sn^{119} , shielding presents no problem.

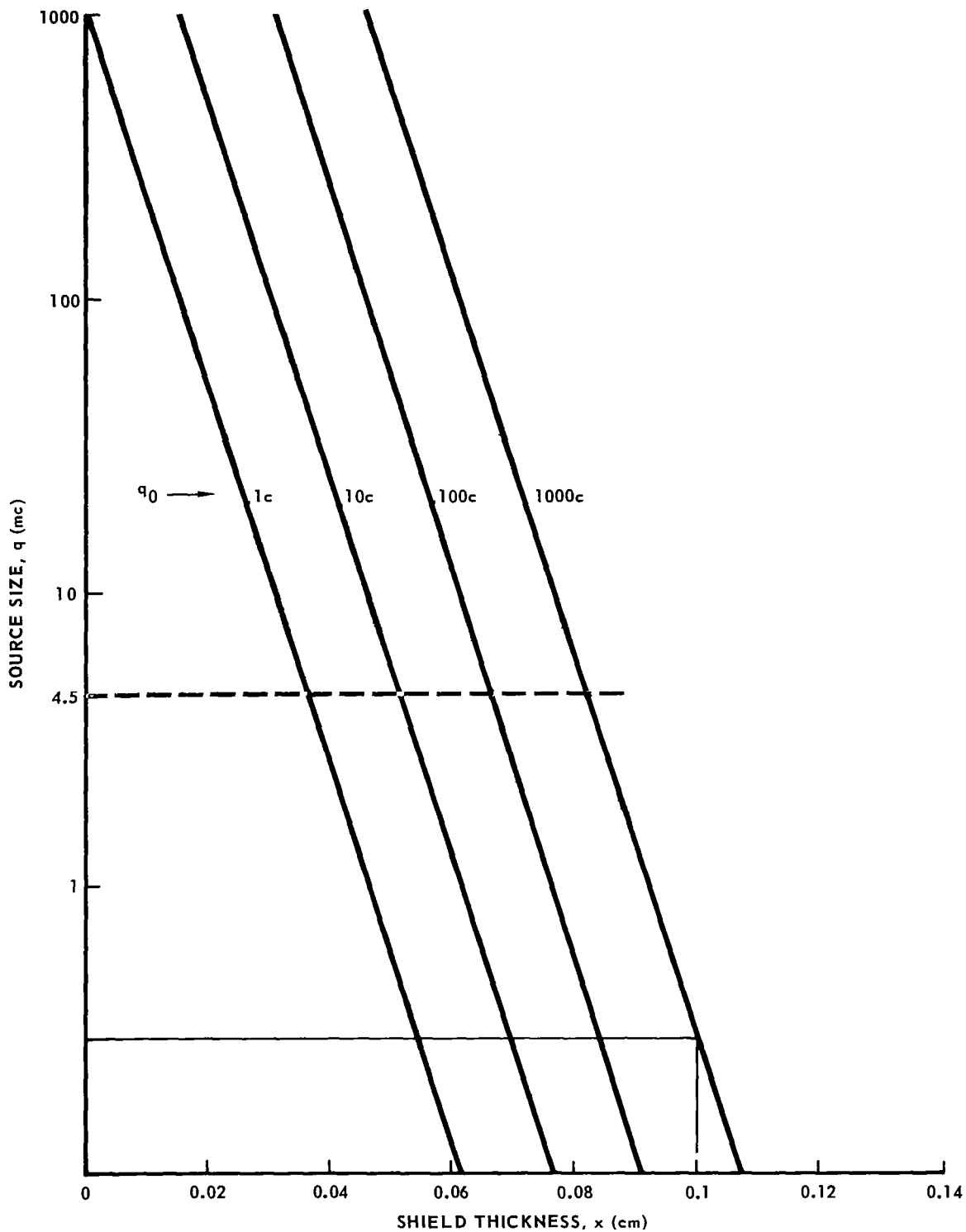


FIGURE 72 - SHIELDING CURVE

However, the man in the chasecraft is exposed to the radioactive source during the range measurements. A method for his protection must be provided.

Conclusion. - The entire idea of the nuclear measurement of range is based on the premise that the source characteristics can be accurately estimated at the time of the docking maneuver. The characteristics include the average count rate being emitted by the source at the time of the docking maneuver and the degree to which the source radiation is emanated isotropically.

The first of these characteristics is predictable to a high degree of accuracy from the half-life equation of the source. The second of these two characteristics is important in that, if the radiation emanated into free space is collimated to any degree, the collimation will change the radiation intensity range dependence of equation 275. Slight collimation would then have to be accounted for in deducing the range from the average count rate detected. For low energy level emissions, such as from Sn^{119} , the isotropic property is easily obtained.

A constant to be subtracted out during the ranging maneuver is the radiation background count. A calibration sequence is required at the beginning of the ranging measurements to establish the average background count. Wide variations from this average occurring during a range measurement time, Δt , will of course degrade the measurement accuracy. This ranging technique will, therefore, perform more satisfactorily in a quiet region of space.

Utilizing The Mossbauer Effect as a Range-Rate Sensor

Introduction. - Excited nuclei of certain radioactive isotopes emit gamma rays of extremely narrow frequency linewidths when decaying from their high energy levels to the ground state. If the nuclear emissions are recoilless (Mossbauer) and are allowed to fall on unexcited atoms in a sample of like material, the gamma radiation will be blocked from passing through. This blockage is due to the nuclei of the "absorber" capturing the incoming gamma ray energy by rising to an excited state. The absorber nuclei have a very short lifetime in this new state before decaying to the stable ground level by re-emitting the energy in a direction transverse to that of the original. The blockage of the direct radiation is not complete, but the decrease is detectable and indicates a resonant condition existing between the source and absorber. If a differential velocity exists between the source and absorber, the resonant condition is broken or degraded by doppler shift. This loss of resonance is characterized by an increase in direct radiation counts and a decrease in transverse radiation counts.

Because the resonant condition between source and absorber is inherently sensitive to a relative velocity between the two, the possibility of using the scheme as a velocity sensor is obvious. The following delves into the parameters, problems and systems associated with using the Mossbauer effect as a range-rate sensor for the docking maneuver.

The ratio of center frequency to bandwidth for Mossbauer gamma ray emissions yields effective Q's ranging from 10^{10} to 10^{15} . At the frequencies of the emissions, this yields radiation spectral linewidths, in terms of doppler shift, of 0.05 ft/sec and less. In general the docking maneuver will not require the detection of such small velocities, and, as a result, the ability to track the degree of resonance will not be necessary.

If the relative velocity between the two craft can be compensated for at the absorber so that only the presence or absence of resonance is detected, then the velocity can be predicted to within one resonant linewidth with correct threshold adjustment. This yields accuracies of 0.05 ft/sec or better and reduces problems in the detecting and sampling system when velocities vary significantly. Should the requirement for measuring slow velocities be imposed, a two mode system is recommended.

Source Considerations for Pure Range-Rate Measurements. - From the standpoint of pure velocity sensing utilizing the Mossbauer effect, the ideal source is one which decays through the process of emitting only gamma rays at the resonant energy level. Most practical Mossbauer sources, however, emit both non-resonant gamma rays and other radiation (some due to secondary emission of the shielding) that will degrade the S/N ratio when used in a system. The two materials (Sm^{151} and Sn^{119}) used here to evaluate the potential of a Mossbauer system demonstrate extremely good radiation purity as is shown later.

For space docking missions, the half-life requirements on the source can easily vary from several days to several years depending on the goal that the docking maneuver will achieve. For the orbital assembly mission, the half-life requirement might be only a few days. But for the case of communications satellite repair, it would be comparable to the intended life span of the satellite--perhaps 5 years. The requirement on half-life helps determine the material selected as the source, and indirectly determines the efficiency of operation, complexity of equipment and, to some extent, the method of detection.

At present time, the best detector is the scintillation counter. Its levels of operation are from 20 kev to 100 kev, with efficiency approaching 100% at 100 kev. Then, the source resonant energy level should be in the interval compatible with the counter operating efficiency.

The problem of shielding must be considered in source selection. The higher the energy level and the more complex the decay scheme of the source, the greater the amount of shielding that is required. In space applications the weight problem is crucial. Shield weight, therefore, plays an important role in source determination.

Development of the Radiation-Range Equation. - For a source size I_0 , in curies, the number of disintegrations/sec is:

$$E = 3.7 \times 10^{10} I_0. \quad (295)$$

If the decay scheme of the source material is such that only a percentage of the disintegrations are decays from the Mossbauer energy level, then the

maximum number of Mossbauer disintegrations/sec is given by:

$$E_m = 3.7m \times 10^{10} I_0 \quad \text{where } m \text{ is in } \% \times 10^{-2} \quad (296)$$

The quantity, E_m , is not the number of gamma rays emitted at the Mossbauer resonant energy level, however, for all of the nuclear emissions are not recoilless. The major parameter governing the number of recoilless emissions is temperature, as is displayed in figure 73. As temperature is lowered, the atoms are effectively locked tighter in the lattice and the percent of recoilless decays is increased. Figure 73 shows this source property for several isotopes and indicates the importance of this property in source selection (ref 45). For instance, the parent nuclei (Ta^{182}) of W^{182} displays virtually zero recoilless emissions at room temperature and only about 25% of the total are Mossbauer at absolute zero. As a source, then, Ta^{182} is not promising.

The number of recoilless decays occurring per second in the source is then:

$$E_o = fE_m, \quad (297)$$

from equation 296, where f is the temperature parameter in $\% \times 10^{-2}$.

Thus:

$$E_o = 3.7mf \times 10^{10} I_0; \quad m < 1; f < 1. \quad (298)$$

The final number of Mossbauer gamma rays/sec emitted from a source is decreased further from the value of equation 298 by an internal loss factor. This factor exists because the energy emitted by the nucleus can be captured by any of its orbiting electrons. Thus, the available Mossbauer radiation from a source is:

$$E_a = \frac{3.7mf \times 10^{10} I_0}{1 + a}. \quad (299)$$

Since the operating medium will be free space, the decrease in radiation with range will be a function of $1/R^2$ only. The radiation-range equation for a 1 ft² area at range R is:

$$E_{ar} = \frac{3.7mf \times 10^{10} I_0}{(1 + a) 4\pi R^2}. \quad (300)$$

Absorber Considerations. - The absorber must also be optimized to yield the best performance on resonance. The quantity of interest in the absorber is its effective thickness, T ,

$$T = f' n a \sigma_o t, \quad (301)$$

where:

- f' = the fraction of recoilless captures of the total captures,
- n = the number of atoms/cc,
- a = the fractional abundance of resonantly absorbing atoms/cc,
- σ_o = the absorption cross-section at resonance,
- t = thickness of absorber.

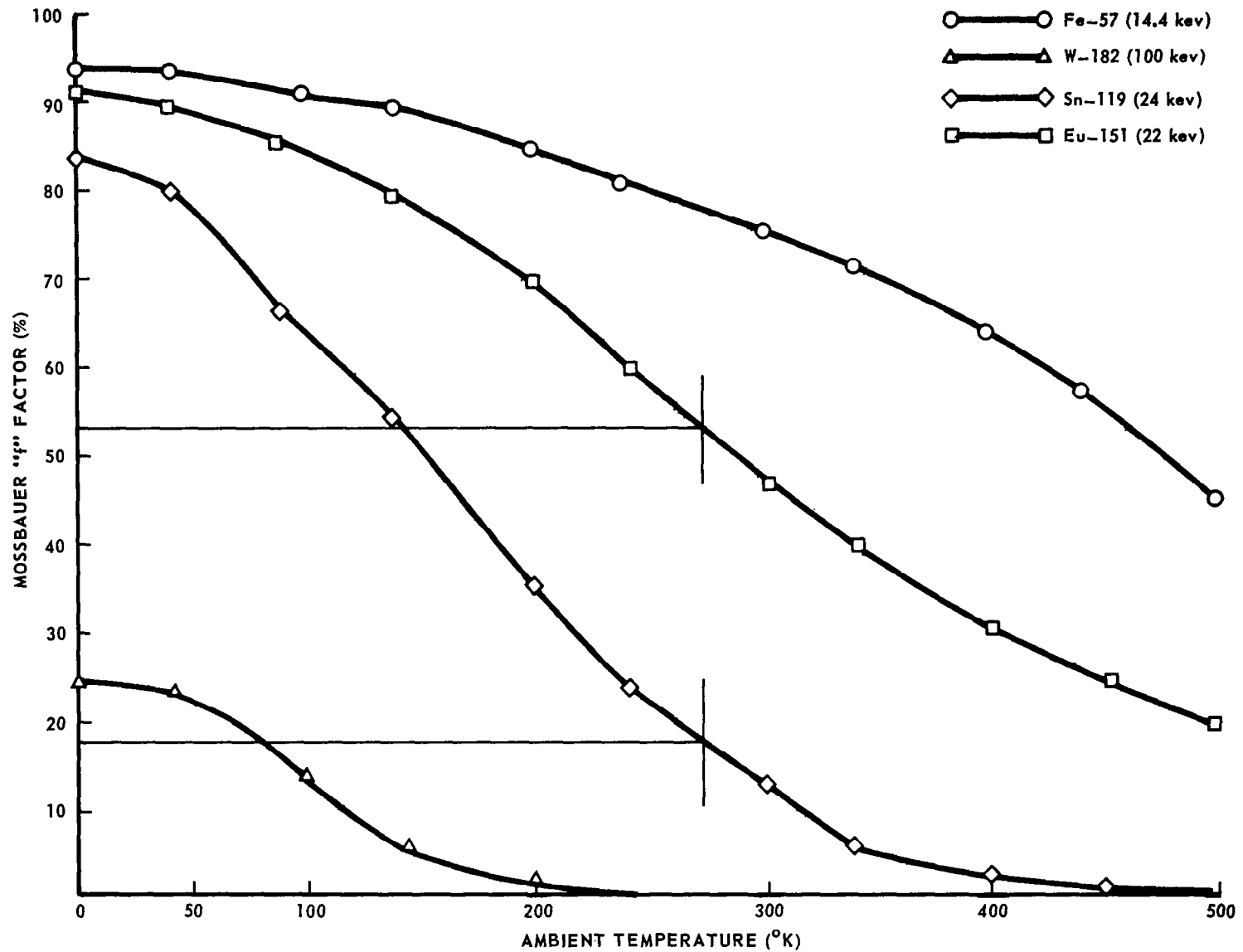


FIGURE 73 - TEMPERATURE DEPENDENCE OF RECOILLESS EMISSION

The effective thickness, T , which is the fraction of the direct radiation absorbed without recoil on resonance, is adjusted to lie in the interval of 0.1 to 0.8, i.e., on resonance from 10% to 80% of the direct radiation will be absorbed.

As was stated earlier, radiation absorbed by nuclei on resonance is re-emitted in the transverse direction. However, because of the absorber internal losses only $1/(1 + a)$ of the re-emissions ever leave the absorber material. This is still an increase, however, in transverse counts over that during the off-resonance condition.

Mossbauer Resonance Detection. - The detection scheme will consist of two counters positioned about the absorber such that one counter registers the direct radiation and the second the transverse scattering and re-radiation. Resonance will exist when the ratio of the direct to transverse counts is less than an established threshold; i.e.:

$$\frac{I_D}{I_T} < X_T \quad \text{where } X_T \text{ is the threshold value.} \quad (302)$$

The threshold value, X_T , should be chosen such that there is small probability of giving a false resonant indication when in an off-resonant condition and a high probability of detecting the resonant condition when it exists. Since the number of disintegrations from the source in time Δt is a probability function, a given number of counts must be detected before the ratio of direct to transverse counts can be determined within the set probability for resonant or non-resonant detection. Since it is known that the direct count rate will be much higher than the transverse, the standard deviation of I_D/I_T will depend primarily on the standard deviation of the transverse intensity count, or:

$$\sigma \left(\frac{I_D}{I_T} \right) = \sigma_{I_T} = \frac{1}{\sqrt{n_T}} \quad , \quad (303)$$

where n_T is the number of transverse counts.

If the threshold value is chosen to be 3 standard deviations below the mean off-resonance ratio value, and if the resonant ratio is required to drop two standard deviations below the threshold value (reference figure 74), then from equation 303:

$$\text{Mossbauer effect} = 5 \sigma \left(\frac{I_D}{I_T} \right) = \frac{5}{\sqrt{n_T}} \quad . \quad (304)$$

The Mossbauer effect is defined as:

$$\frac{\left(\frac{I_D}{I_T} \right)_{OR} - \left(\frac{I_D}{I_T} \right)_R}{\left(\frac{I_D}{I_T} \right)_{OR}} \quad . \quad (305)$$

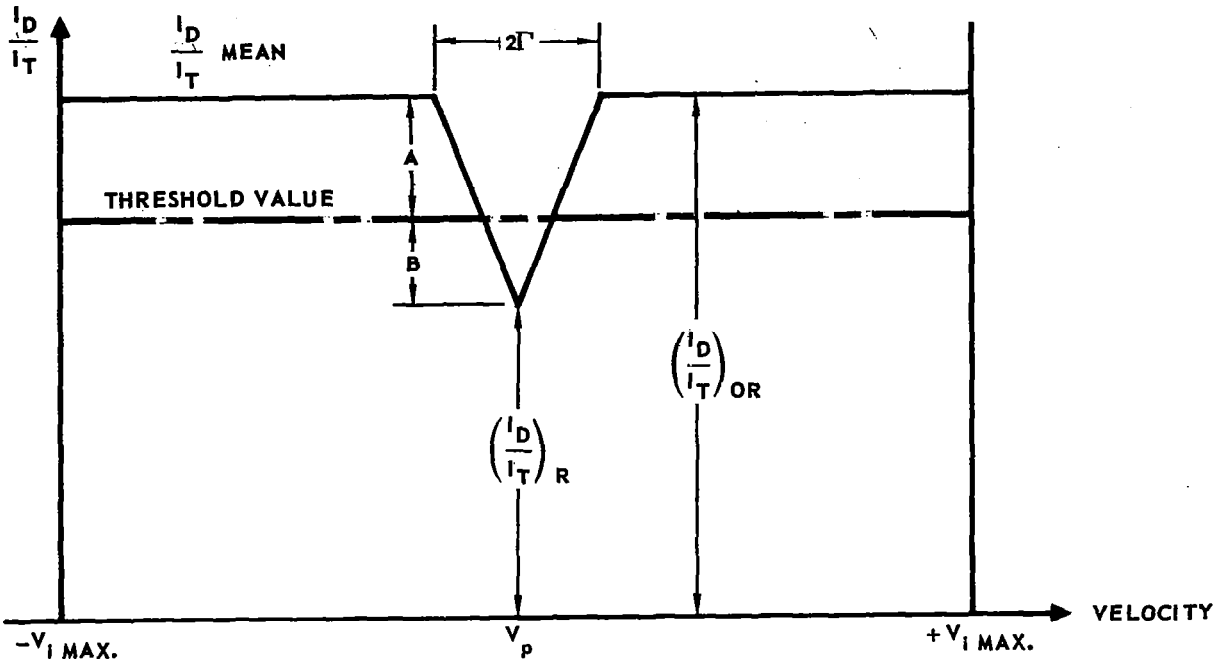


FIGURE 74 - MOSSBAUER RESONANT DETECTION CRITERIA

If:

$$P_D = \frac{(I_D)_R}{(I_D)_{OR}} \text{ and } P_T = \frac{(I_T)_R}{(I_T)_{OR}} , \quad (306)$$

the Mossbauer effect becomes $\frac{P_T - P_D}{P_T}$ and equation 305 is:

$$\frac{P_T - P_D}{P_T} = \frac{5}{\sqrt{n_T}} . \quad (307)$$

Solving for n_T :

$$n_T = \frac{25}{\left(\frac{P_T - P_D}{P_T}\right)^2} . \quad (308)$$

Equation 308 represents the number of transverse counts required to make a velocity sample with the probability of a false resonance indication of 0.01% and the probability of not detecting a resonance indication of 0.04%.

Equation 308, then, shows the importance of the degree of the Mossbauer effect in detecting the resonant condition. If the absorber blockage of direct radiation on resonance lies in the interval of from 10% to 80%, then:

$$.1 \leq P_D \leq .8 .$$

Figure 75 shows the dependence of the required number of transverse counts on both the degree of direct Mossbauer effect, P_D , and the degree of the transverse Mossbauer effect, P_T . The family of curves is for $1.1 \leq P_T \leq 1.5$.

The Rotating Wheel Detection System. - The rotating wheel of figure 76 possesses the geometry to compensate for the differential velocity, for each point on the periphery of the wheel possesses a different magnitude of velocity component parallel to the incoming radiation (the incoming radiation is assumed to travel in parallel paths). However, if a detector is to be placed inside the wheel to detect the portion of the periphery that is in resonance, the linewidth of the circumference of the wheel in resonance must be sufficiently large to allow a practical detector to work. Consider the example where the maximum differential velocity to be measured is 5 ft/sec. Let the radius of the wheel be 1.5 ft and the angular velocity be 10 rad/sec. Then the velocity components parallel to the incoming radiation are:

$$v = r \omega \sin \theta \quad , \quad (309)$$

where θ is the angle as defined in figure 75 .

If the width of the detector is to cover the part of the periphery of the wheel which possesses the resonant velocity within $1/2$ linewidth, Γ , the allowable change in θ is:

$$1/2 \Gamma = r \omega \cos \theta \Delta \theta \quad . \quad (310)$$

The angle, θ , at which a 5 ft/sec velocity component exists is from equation 309:

$$\theta = \sin^{-1} \frac{5}{1.5 \times 10} = 19.5^\circ \quad . \quad (311)$$

And if Γ is 0.05 ft/sec, the allowable change in θ is:

$$\Delta \theta = \pm \frac{2.5 \times 10^{-2}}{15 \times .333} = \pm 0.5 \times 10^{-2} \text{ rad} \quad , \quad (312)$$

$$|\Delta \theta| = 2 \Delta \theta = 1 \times 10^{-2} \text{ rad} \quad . \quad (313)$$

The projected length, L , that represents the detector width is then:

$$L = \frac{K |\Delta \theta|}{\cos \theta} = \frac{(1.5) (1 \times 10^{-2})}{0.943} \quad , \quad (314)$$

$$L = 1.59 \times 10^{-1} \text{ ft} = 0.486 \text{ cm} \quad . \quad (315)$$

Since the resonant linewidth will increase with decreasing angle, θ , the L of 0.486 cm represents the lower limit on width of detector.

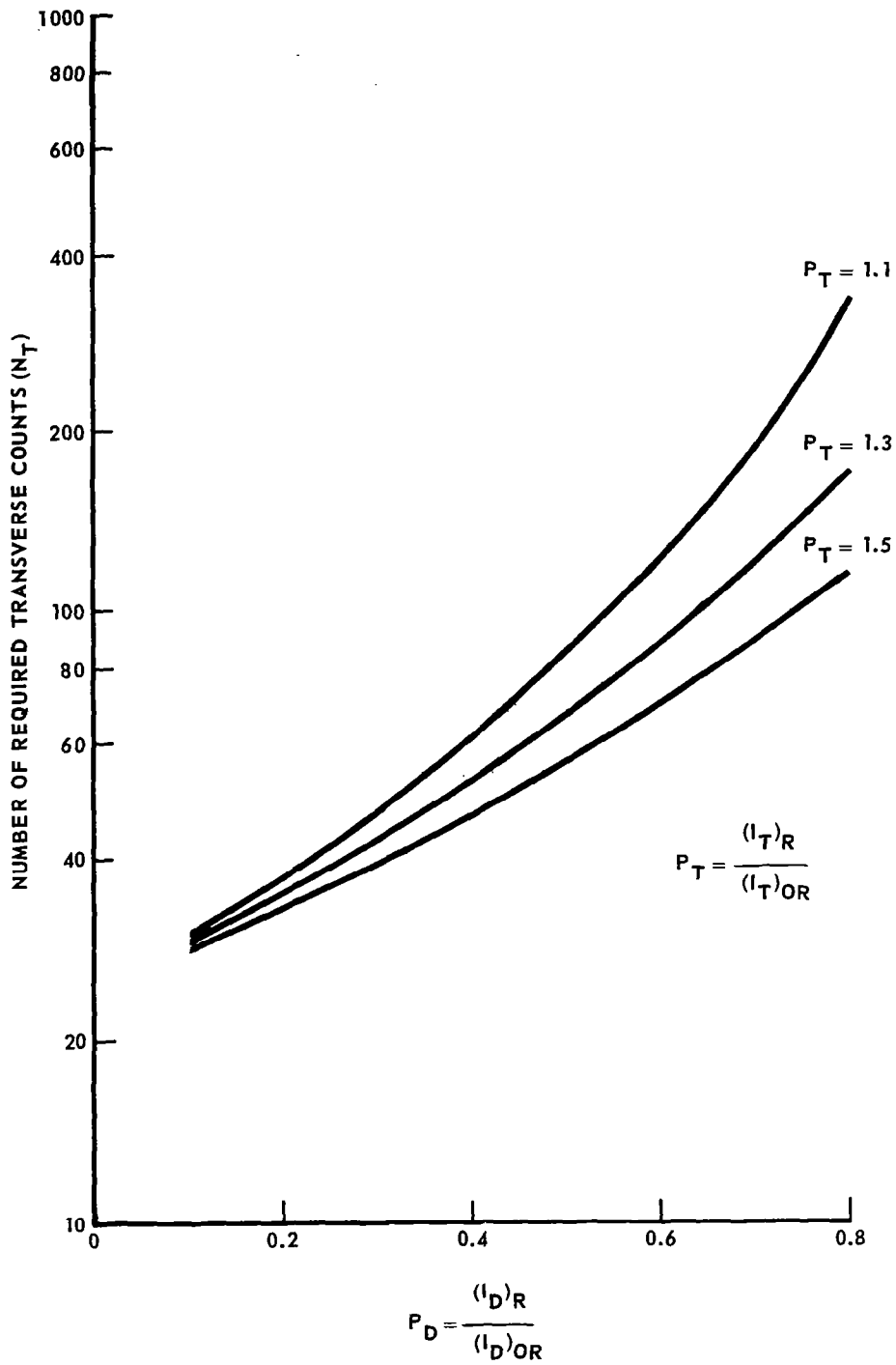


FIGURE 75 – NUMBER OF TRANSVERSE COUNTS REQUIRED AS A FUNCTION OF THE DEGREE OF MOSSBAUER EFFECT

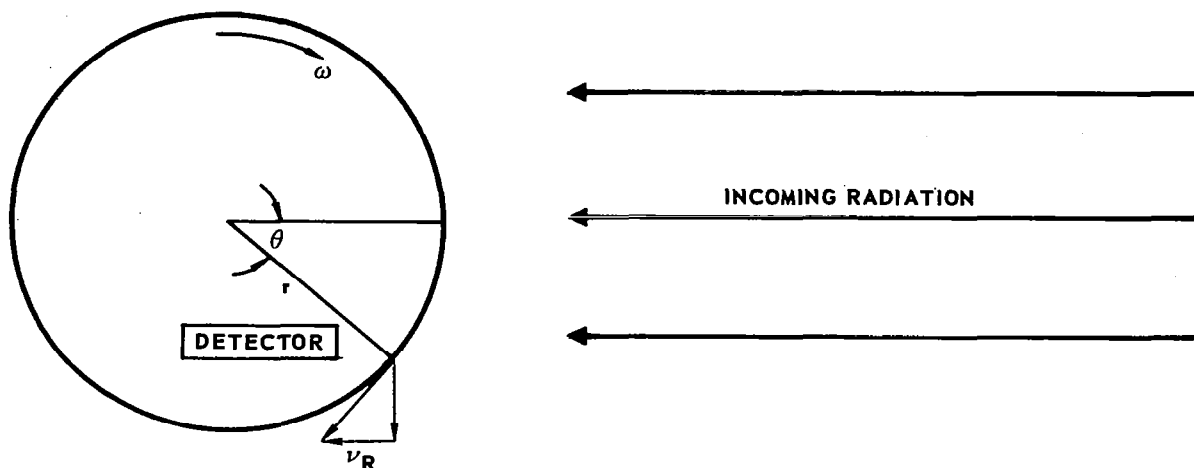


FIGURE 76 - ROTATING WHEEL VELOCITY DETECTOR

The general system utilizing the rotating wheel is shown in figure 77. Since the time required to take a velocity sample is dependent on the transverse count rate, the transverse counter monitor will issue the command ratio signal when the required number, n_T , of transverse counts has been reached. The output of the Ratio and Resonance Logics circuits will be the range-rate information. The Logics circuits will also supply this information to the drive system. It is visualized that when deceleration is experienced due to the chase vehicle's thrusters, the computer on board will supply the predicted ΔV to the velocity compensation drive system. The drive system will act accordingly and the search for the true ΔV will begin and continue until lock-on. Initially, the velocity compensation drive signal will use the velocity indication of the range-rate system to lock on to resonance.

The major disadvantage of this system is the time required to search and lock-on to a new velocity. If the initial velocity and the ΔV occurring later are known to the accuracy of ± 0.1 ft/sec, then a possible four samples would be required to establish resonance. Added to this would be the time required to move the detectors to the next velocity possibility. A search mode would have to be developed to use this method. One solution would be to use three (6 counting the transverse detectors) detectors; one positioned at the expected velocity, one below and the third above. This would shorten the acquisition period to an acceptable value. The system would now track the resonant velocity by keeping the middle detector locked on to resonance. Small velocity increments could be tracked by checking the shift of resonance from detector to detector. The system as shown would be complicated both in the fact that three channels are now required and in the fact that since the periphery resonant

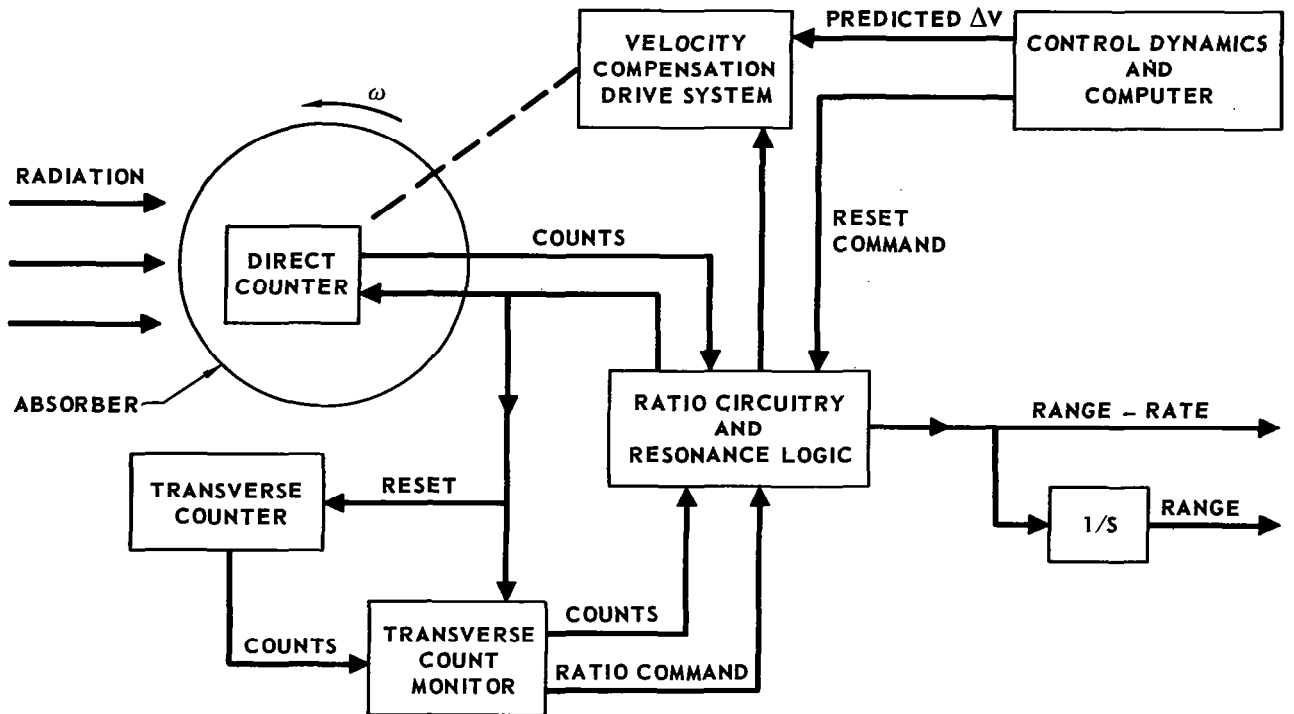


FIGURE 77 – RANGE-RATE DETECTION SYSTEM USING THE ROTATING WHEEL

linewidth changes on the wheel with velocity, the positioning and centering of the detectors will be a function of velocity.

Other Velocity Compensating Schemes. - Another method of compensating for existing differential velocities between chase and target vehicles is to move or vibrate the absorber in a zero net displacement in front of the detector. However, because of the small look-time per cycle for a suspected resonant velocity, the source size would have to be much greater than that for the resonant wheel at the same range and for the same frequency of range-rate read-outs.

A system, perhaps more in contention with the rotary wheel than that just mentioned, is the slanted belt drive system shown in figure 78 . Instead of moving the detectors, the belt speed is accurately controlled with a dither modulation speed on the base speed. Again three channels are used with time sharing of the dither cycle for each detector, i.e. for above, and on, and below the suspected resonant velocity. Since the dither velocity interval is small and the detector face area can be easily increased, this system is competitive with the rotary wheel scheme. The choice narrows down to the selection between variable and accurate speed control and variable and accurate detector placement.

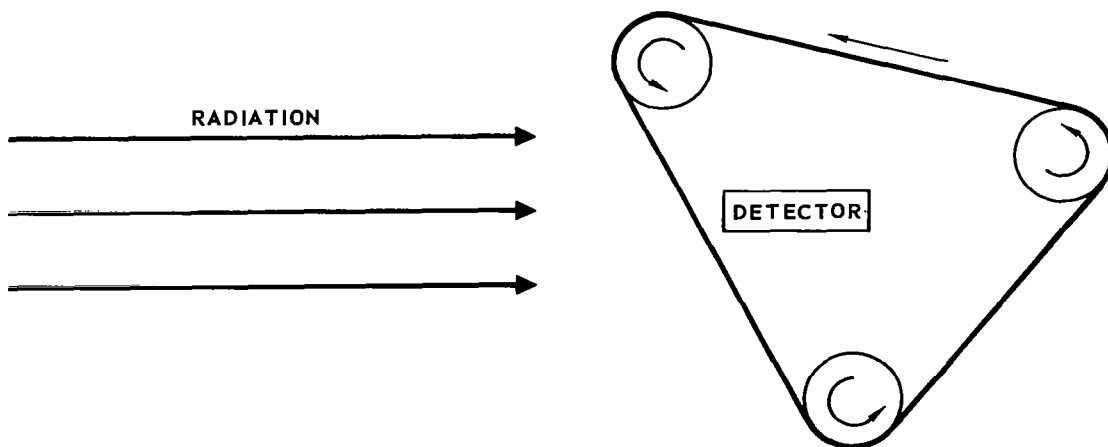


FIGURE 78 - SLANTED BELT VELOCITY DETECTOR

Source Size Estimates. - The basis for making source size estimates have been laid in the foregoing pages. As was noted, the parameters involved in the estimates are quite numerous and no one can be singled out as the limiter. All must be considered for the system to operate.

For the estimates herewith, assume that the maximum operating range is R ft. The frequency of the readouts of range-rate will be solely a function of the count rate at the transverse counter, but let it be stipulated that at the maximum range of R ft, the transverse detector will receive enough counts in the on-resonant condition to yield a range-rate indication every 0.5 sec. The degree of the Mossbauer effect will be taken as before, i.e. $0.1 \leq P_p \leq 0.8$; $1.1 \leq P_T \leq 1.5$. S_m^{151} and an isomer of S_n^{119} will be considered as sources. Both exhibit good purity in their decay schemes, i.e. 98.4% of S_m^{151} is possible Mossbauer radiation and 100% of S_n^{119} is possible Mossbauer radiation. The internal loss factor, a , is 30 and 7.3 for S_m^{151} and S_n^{119} respectively, so that the maximum percentage of Mossbauer radiation that can leave the sources are:

$$\% S_m^{151} = \frac{98.4}{1 + 30} = 3.17\% \quad , \quad (316)$$

$$\% S_n^{119} = \frac{100}{1 + 7.3} = 12\% \quad . \quad (317)$$

The temperature will be taken as 0°C so that the "f" factors from figure 73 are:

$$f = 0.53 S_m^{151} \quad , \quad (318)$$

$$f = 0.19 S_n^{119} \quad . \quad (319)$$

Then from equation 299 the available Mossbauer radiation from these sources is:

$$E_a = (3.7 \times 10^{10} I_o) (3.17 \times 10^{-2}) (5.3 \times 10^{-1}) \quad , \quad (320)$$

$$E_a = 6.21 \times 10^8 I_o \text{ for } S_m^{151} \quad , \quad (321)$$

$$E_a = (3.7 \times 10^{10} I_o) (1.2 \times 10^{-1}) (1.9 \times 10^{-1}) \quad , \quad (322)$$

$$E_a = 8.44 \times 10^8 I_o \text{ for } S_n^{119} \quad . \quad (323)$$

And the radiation-range equation (equation 300) for each is:

$$E_{ar} = \frac{4.95 \times 10^7 I_o}{R^2} \text{ for } S_m^{151} \quad , \quad (324)$$

$$E_{ar} = \frac{6.71 \times 10^7 I_o}{R^2} \text{ for } S_n^{119} \quad . \quad (325)$$

The energy level of emissions of these two sources is approximately 23 kev. Because of this, detector efficiency will be taken as 50%. The transverse detector will be assumed to cover 30% of the total transverse spacial coverage.

Since P_D of the direct radiation is absorbed, and $\frac{1}{1+a}$ is re-emitted, and the transverse counter covers on 30% of the total area with only 50% efficiency, the number of counts, I_a , required to strike the absorber are:

$$\frac{P_D I_a}{1+a} \times 0.3 \times 0.5 = n_T \quad , \quad (326)$$

$$I_a = \frac{(1+a) n_T}{0.15 P_D} \quad . \quad (327)$$

With the aid of figure 75, equation 327 is plotted in figure 79 for S_m^{151} and S_n^{119} over the range defined for P_D and P_T . Figure 79 demonstrates that for a given value of transverse Mossbauer effect there is an optimum value of P_D , the direct Mossbauer effect, that yields the lowest possible number of counts required at the absorber. At this optimum value, the transverse count, n_T , required by the probability law does not have its lowest value for the particular P_T in question.

At the maximum range, R_{max} , a range-rate readout is required every 0.5 sec. and the number of counts hitting the absorber will be twice that per second given in figure 79. The source size required to produce this count rate is given by equations 324 and 325 with modification to adjust the fact that the absorber dimensions are less than 1 ft² (see equation 274). The rotating wheel method had a resonant linewidth of about 1/5 inch. If it is 6 inches wide, its surface area will be 0.83×10^{-2} ft². With this modification, equations 324 and 325 become:

$$E_{ar} = \frac{4.13 \times 10^5 I_o}{R^2} \text{ for } S_m^{151} \quad , \quad (328)$$

$$E_{ar} = \frac{5.59 \times 10^5 I_o}{R^2} \text{ for } S_n^{119} \quad , \quad (329)$$

where E_{ar} = number of counts/sec at the absorber
 I_o = source size in curies.

Equations 328 and 329 are plotted in figure 80 for the optimum values of P_D demonstrated in figure 79. The curves show that S_n^{119} is the better of the two choices. The degree of the transverse Mossbauer effect is also seen, but its significance isn't pronounced as long as it stays in the range demonstrated here. For example, a P_T of 1.005 is expected to greatly increase the source size for the same range interval and 0.5 second range-rate read out requirement.

Figure 81 shows the increase in source size required if the value of P_D is not the optimum shown in figure 80. The curves are for a constant P_T of 1.1. As is shown, the difference in source required for $P_D = 0.1$ and $P_D = 0.7$ is not drastic. A greater difference would be seen were P_T to be 1.3 or 1.5, as can be inferred from figure .

Shield Requirements. - The shield requirements for both sources considered are quite small. This is due to the fact that the sources have low energy

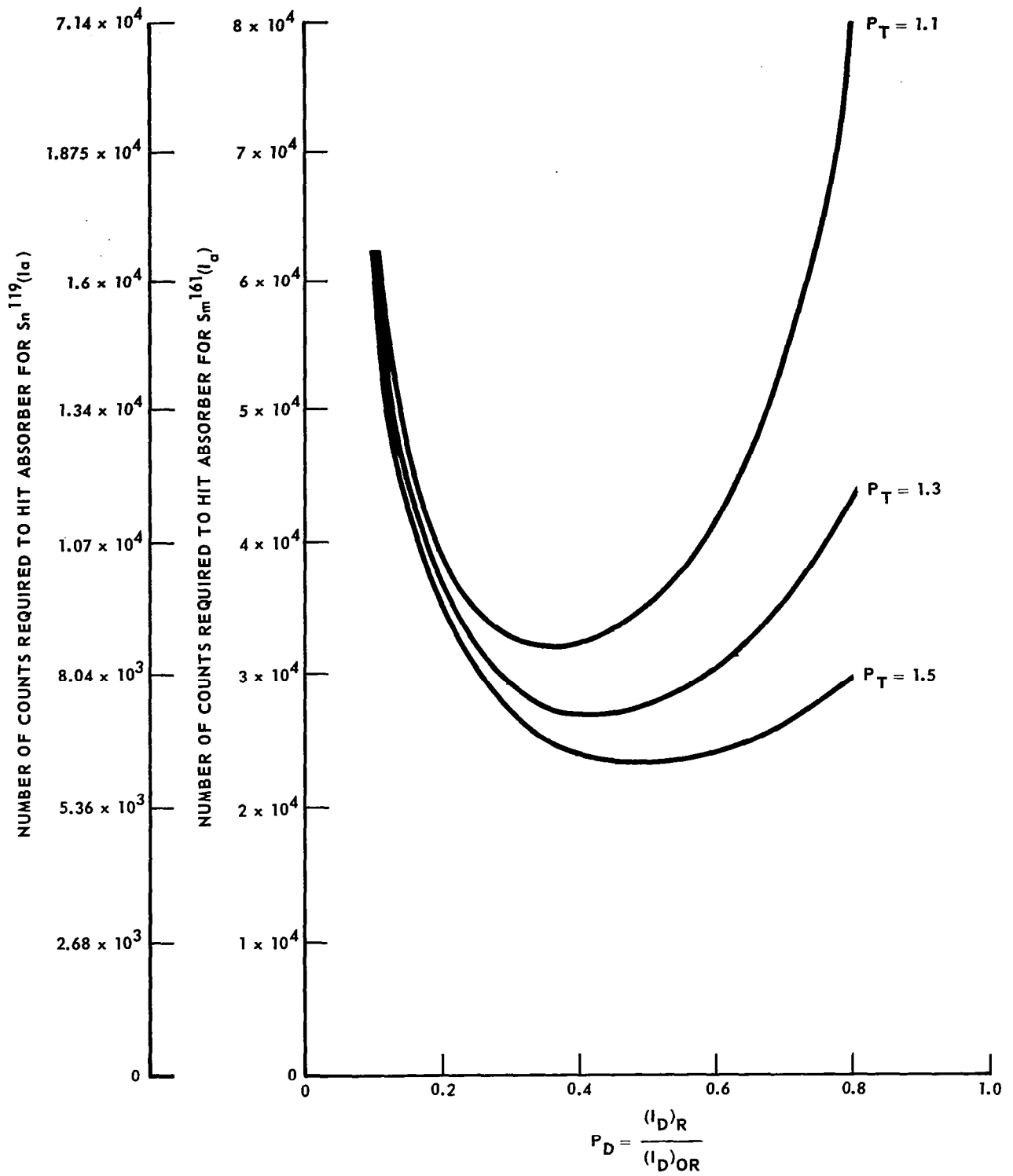


FIGURE 79 - COUNTS REQUIRED TO HIT ABSORBER FOR RANGE RATE MEASUREMENT

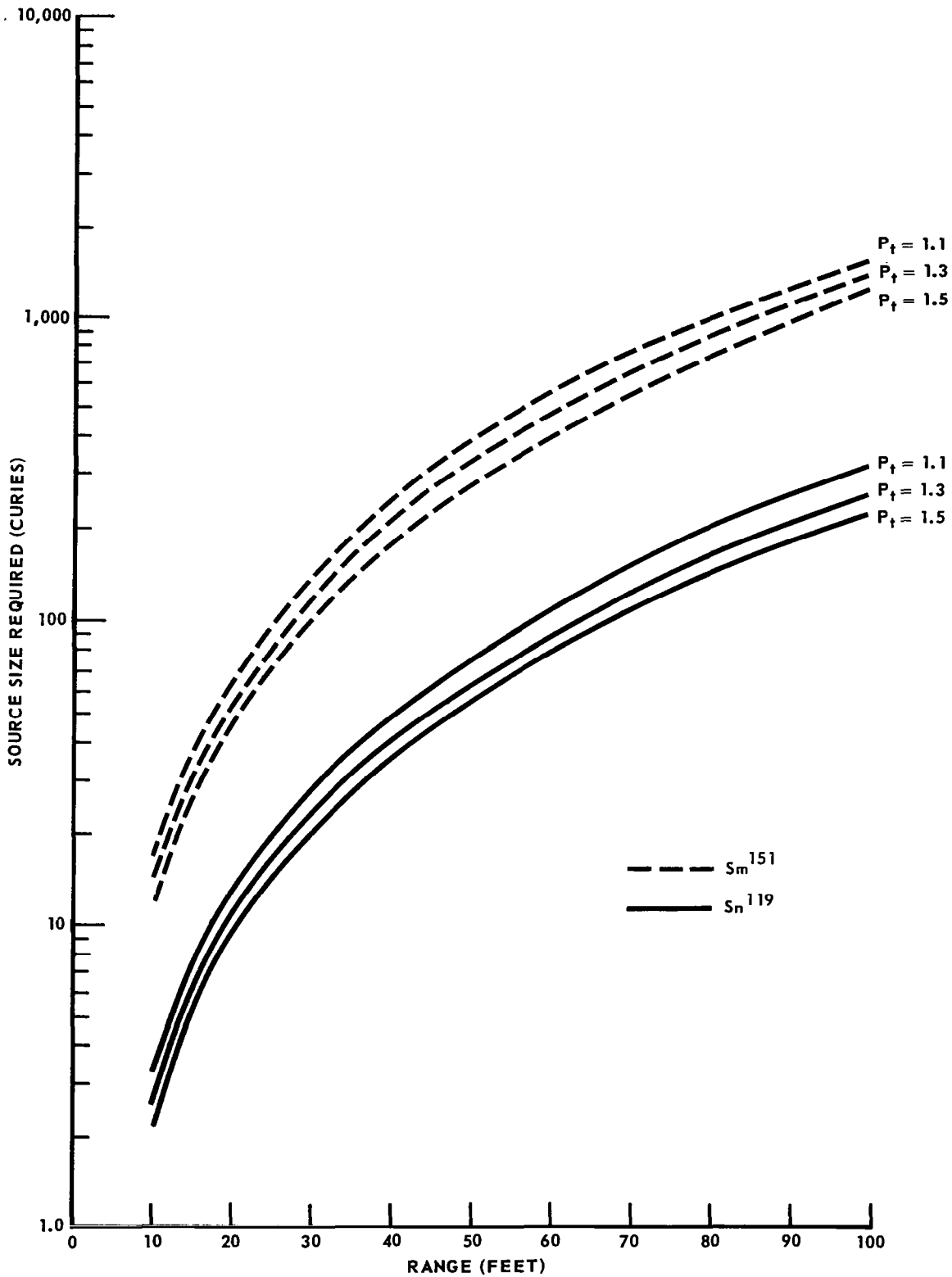


FIGURE 80 – MAXIMUM OPERATING RANGE FOR A GIVEN SOURCE SIZE

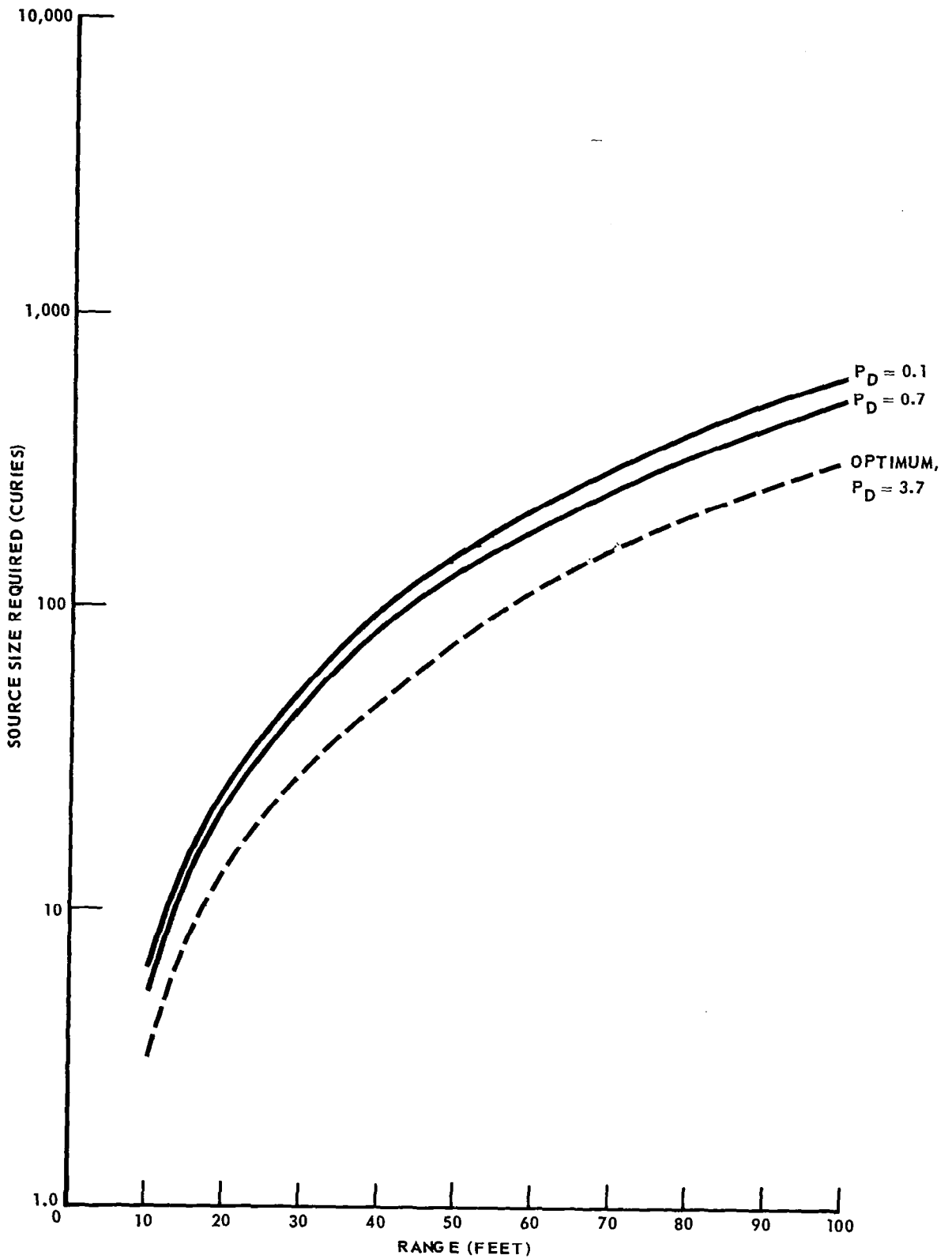


FIGURE 81 - INCREASE IN SOURCE SIZE DUE TO NON-OPTIMUM P_D

levels (22-24 kev) and emit almost 100% gamma rays. Figure 72 shows shielding curves that are applicable for both. The curves indicate that a 1000 curie source can be shielded by 0.1 cm shield of stainless steel and appear as a source of approximately 0.4 mc. This indicates that a 300 curie source is almost completely masked with the same shield. Hence shielding presents no problem in this case. For indeed, the structure designed to hold the source will require greater thickness than the shield requirements.

Problem Areas Requiring Development.-Resonant absorption is well known and has been demonstrated in the laboratory. It is presently being applied by different researchers throughout the world to prove or disprove, through experiments some aspects of Einstein's relativity theory. The only factor that needs investigation in this area is the order of resonant shift due to a difference in temperature between source and absorber. If temperature differences have to be held to 1°C or less, as seems to be the indication, this would greatly complicate the range-rate system.

The range-rate application of the resonant condition requires much development. To date, no system is known that has tracked the resonant dip by direct to transverse count ratioing. In fact, not much has been done to establish in the laboratory the true magnitude of the transverse count that can be expected. Should experimentation prove this to be a problem, the transverse system can be altered to detect conversion electrons. These are loosely bound electrons in the absorber that are freed upon collision with the impinging gamma rays. The

percentage of conversion electrons is $\frac{a}{1+a}$ if the binding energy is exceeded.

Transverse effect, along with optimum angular placement, is thus one of the most important first developments that should be undertaken.

Methods of absorber velocity compensation should be investigated and the more promising ones demonstrated. For the particular application to spacecraft docking, system speed of response to changes in velocity should be one of the major areas of concentration. Elimination of the need of ΔV information from the chase vehicle's computer would relieve some restrictions on the docking mission by allowing both vehicles maneuverability.

And finally, the configuration for the source and absorber must be designed to protect any men that might be in the loop. As range closes the radiation intensity will increase and unnecessary exposure to the astronauts must be avoided.

Conclusion.-A general system for range-rate measurement using the Mossbauer effect has been presented. Sources that are applicable to the docking mission are presently in existence and their required size in the range interval needed has been demonstrated to be moderate. A more definitive and detailed system is not possible at this time without some laboratory investigation and development.

ANGLE MEASUREMENT TECHNIQUES

The selection of angle measurement techniques for use in a particular spacecraft requires knowledge of the capabilities and limitations of many sensors. As discussed in an earlier section, measurements of three types of angles are required:

- (a) The line of sight (LOS) angles from the chasecraft to the target,
- (b) The target orientation angles with respect to the LOS,
- (c) The relative roll angle.

Measurement of target orientation angles can be made in the target spacecraft, using the same techniques used by the chasecraft to measure LOS angles, and relayed to the chasecraft via data link. Two alternate cooperative approaches are presented in which all of the data is derived directly in the chasecraft. Noncooperative measurements are further complicated by the lack of target attitude definition. Although analysis of each of the many variations of these techniques is beyond the scope of this study, those which appear to have most promise for docking application are investigated. Figure 82 shows the approximate accuracies which can be achieved by each of these techniques.

LOS DETERMINATION BY AMPLITUDE TECHNIQUES

Determination of LOS by comparing the amplitude of the signal in two squinted beams is a classical approach. The sum-difference monopulse radar yields very accurate tracking data and has several advantages over other approaches. Sequential lobing and conical scan techniques are competitive for most applications but are subject to errors due to the amplitude noise and scintillation. The biconical horn antenna, which is potentially applicable to the docking problem, is also discussed in this section.

Sum-Difference Amplitude Monopulse

The sum-difference amplitude monopulse utilizes two squinted antenna beams to detect the angle of arrival of the return signal from a target. A block diagram of the amplitude monopulse system for angle detection in one plane (i.e. azimuth or elevation) is shown in figure 83.

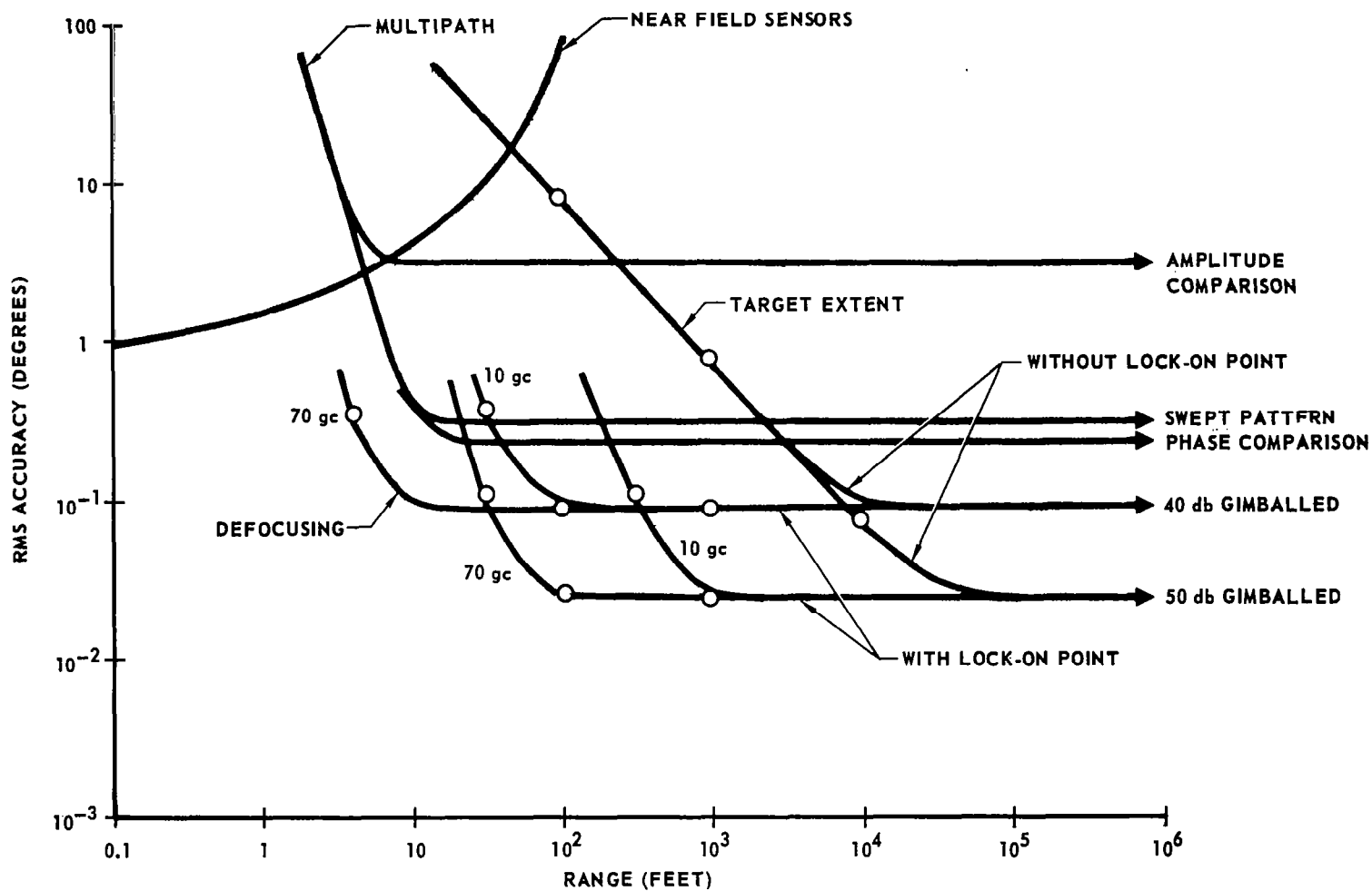


FIGURE 82 - ANGLE SENSING ACCURACIES FOR VARIOUS TECHNIQUES

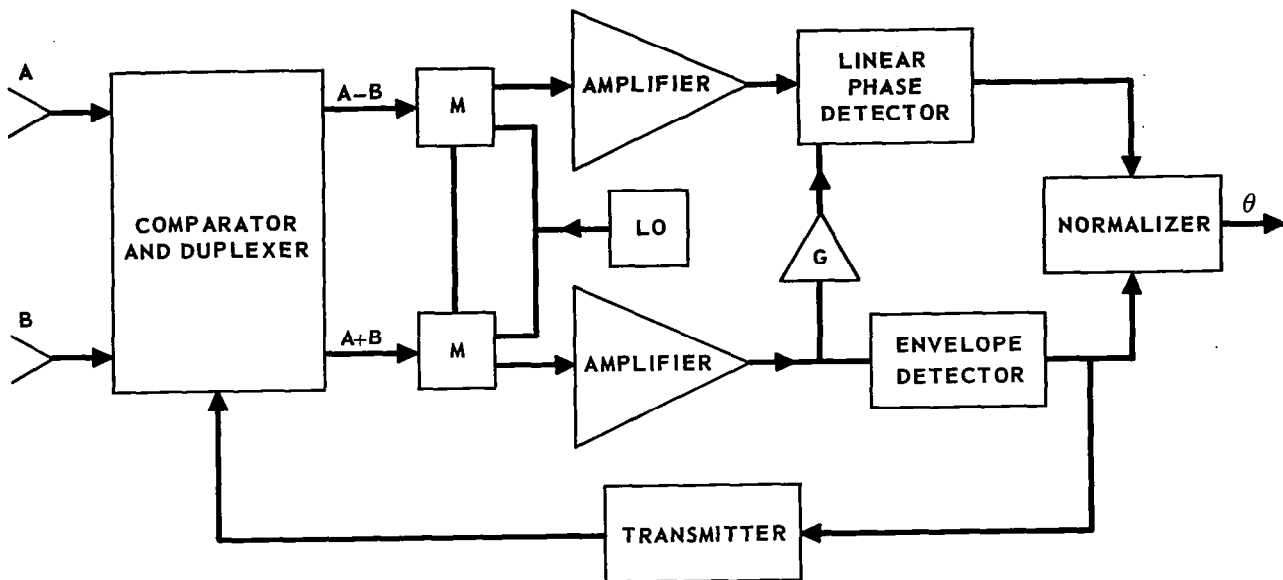


FIGURE 83 – SUM AND DIFFERENCE AMPLITUDE MONOPULSE

The comparator takes the received signals from antennas A & B and forms the sum and difference of these signals. The two channels are then mixed and amplified. The difference channel has a phase of 0 or π , with respect to the sum channel, dependent on the relative magnitudes of the signals received by antennas A & B. To insure linear operation in the phase detector (reference 47):

$$G(A + B) \gg |A - B|. \quad (330)$$

The output of the linear phase detector is then the envelope of the IF but with sense, i.e.

$$A - B = \pm |A - B|. \quad (331)$$

The sum channel is also envelope detected and the two channels fed into a normalizer which forms the ratio containing the angle information:

$$f(\theta) = \frac{\pm |A - B|}{A + B}. \quad (332)$$

In most cases, the antenna system consists of dual horns, or a dish with dual feeds, offset to produce patterns that are symmetrical and squinted off boresight by some angle θ_s . Optimizing the cross-over of the two patterns on

boresight for linear angle output information yields the cross-over to be the 3 db points in the antenna patterns.

For the noncooperative case, a transmitter feeds the separate antennas in phase producing a sum pattern for illuminating the target.

RF Phase - An rf-phase unbalance in the comparator or prior to the comparator results in a degradation of system sensitivity. The system sum-difference output ratio signal for an angle of arrival θ_1 with an rf-phase unbalance, α , is given by:

$$|e_d|_{\theta = \theta_1} = A \left[\frac{(P[u_1] \cos \alpha - P[-u_1])^2 + (P[u_1] \sin \alpha)^2}{(P[u_1] \cos \alpha + P[-u_1])^2 + (P[u_1] \sin \alpha)^2} \right]^{1/2}, \quad (333)$$

where $P[\pm u_1]$ are the antenna difference patterns, and:

$$u_1 = \frac{\pi d}{\lambda} \sin \theta_1. \quad (334)$$

On boresight where $P[+0] = P[-0]$ this becomes:

$$|e_d|_{\theta = 0} = \sqrt{\frac{1 - \cos \alpha}{1 + \cos \alpha}}. \quad (335)$$

Cohen and Steinmetz (reference 46) express the effect of rf-phase shift by the change of null depth on boresight. Null depth is defined as the ratio of the difference channel signal to the maximum level in the difference pattern. figure 84 shows null depth as a function of rf-phase shift for antenna patterns arising from a cosine aperture distribution.

RF phase shifts also produce second order effects in the phase detector. With no phase unbalance, the phase detector output is either 0° ($A > B$) or 180° ($A < B$) with rapid phase shift (theoretically of infinite slope) on boresight. With a phase unbalance, however, the output of the phase detector can assume any value between 0° and 180° , though phase reversal (90°) always occurs on boresight. The shape of this curve is demonstrated in figure 85

for $\frac{d}{\lambda} = 5$, $\theta_s = 0.2$ radians and $\alpha = 5^\circ$. This decrease in detector

sensitivity about boresight can be minimized by making $\frac{2\theta_s}{\theta_{BW}}$ as large as possible without destroying the sum pattern.

RF Attenuation Unbalance: More attenuation in one rf channel than in the other results in a shift in boresight. The degree of boresight shift is dependent on the radiation pattern of the antenna, as demonstrated in figure 86.

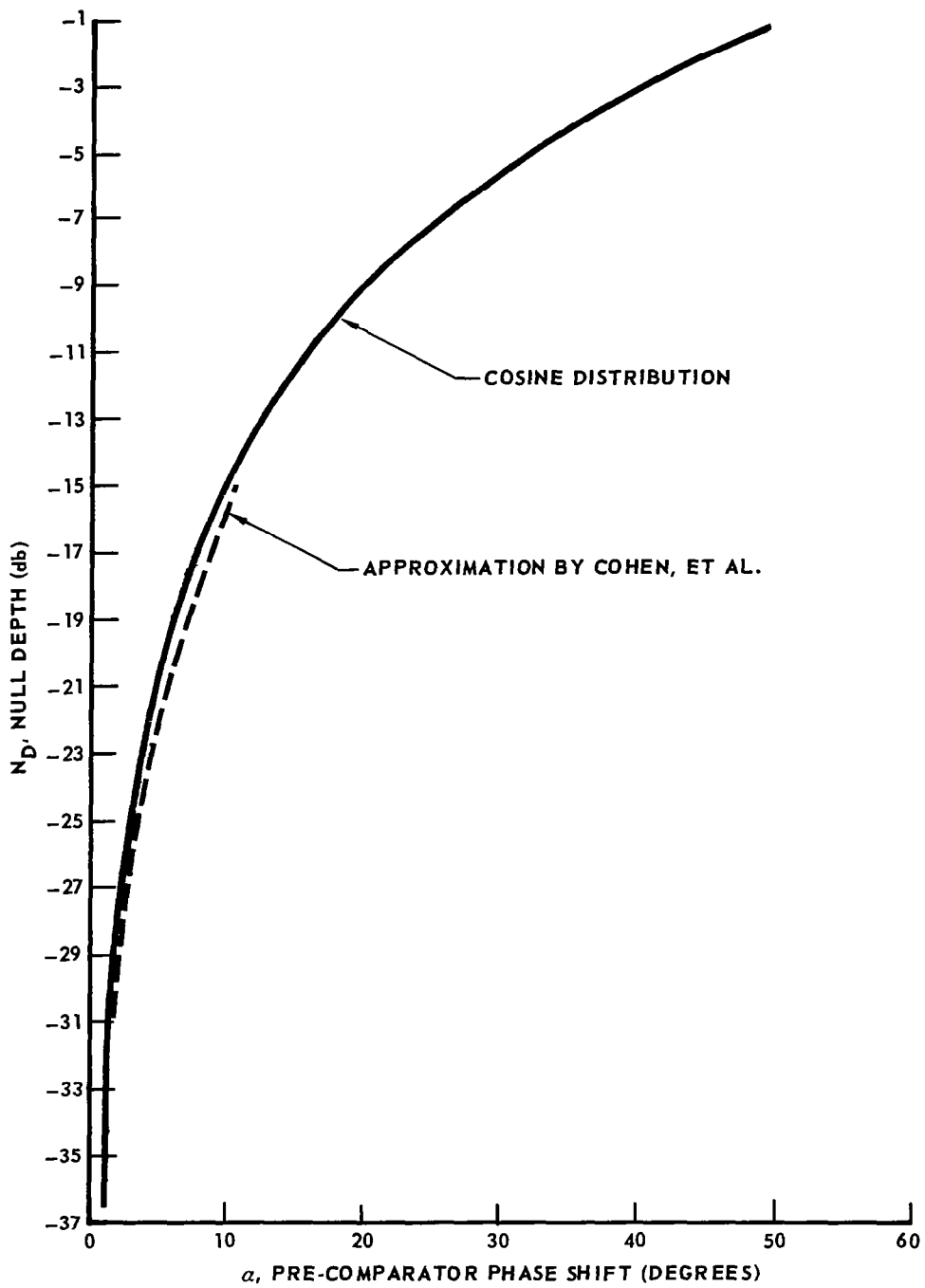


FIGURE 84 – NULL DEPTH vs RF PHASE UNBALANCE

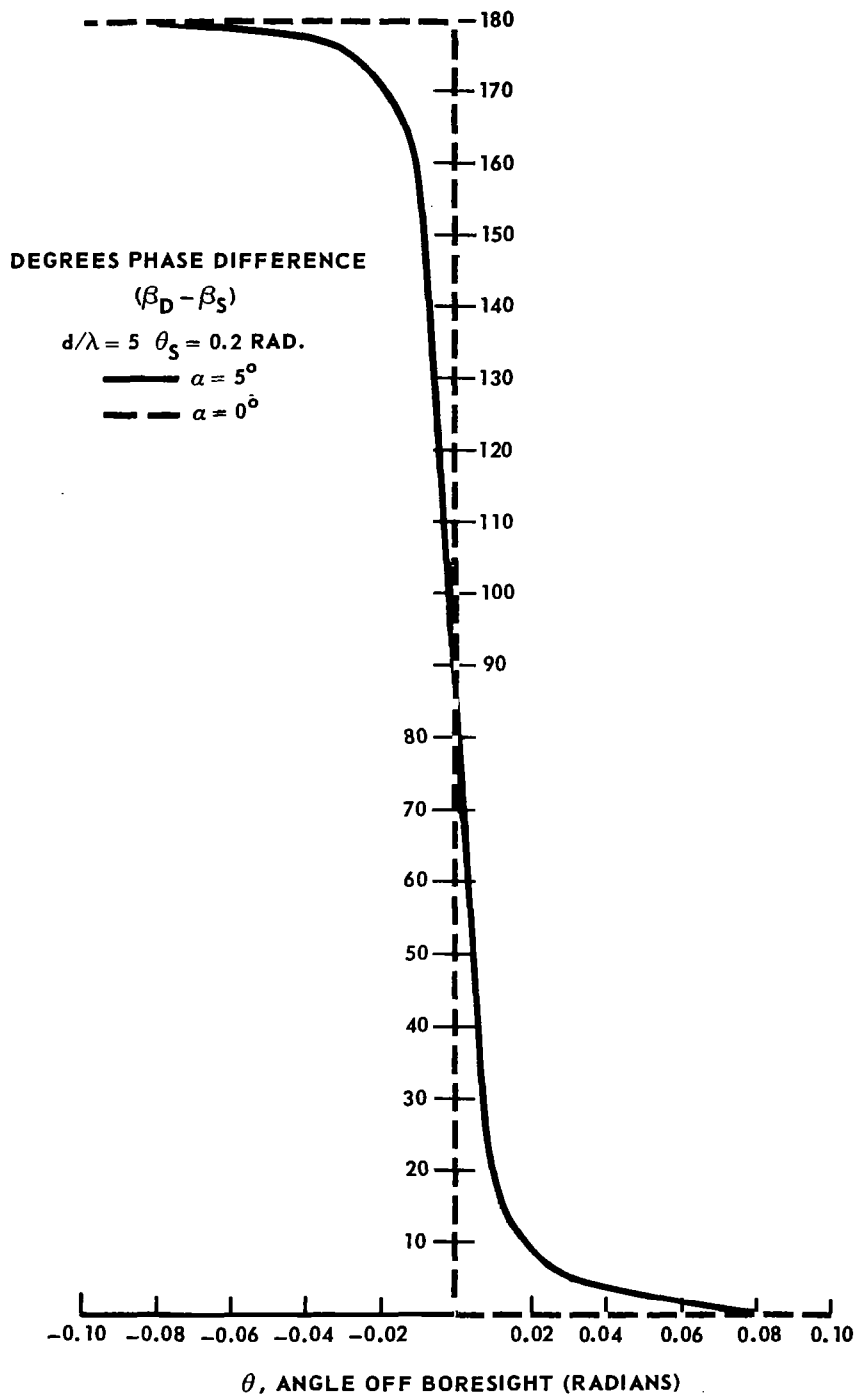


FIGURE 85 – DECREASE IN AMPLITUDE SENSITIVITY NEAR BORESIGHT

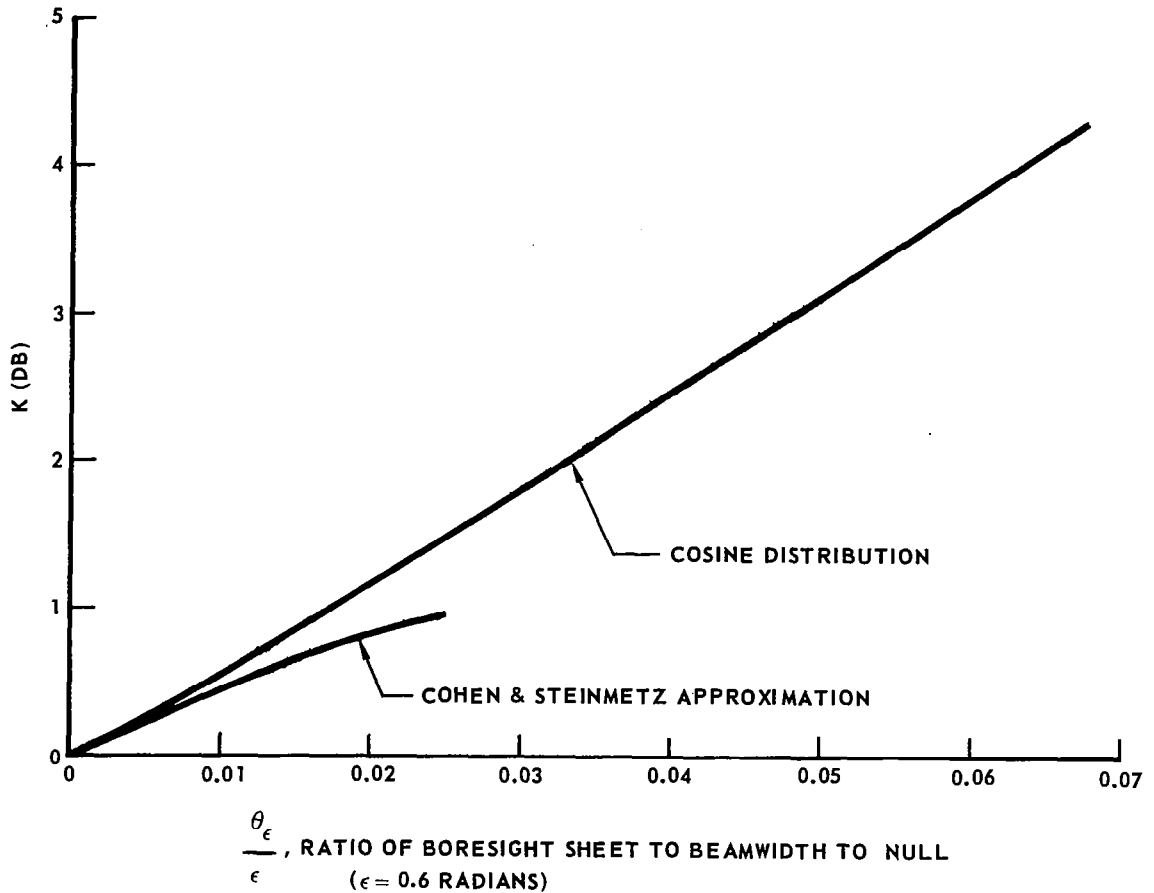


FIGURE 86 – BORESIGHT SHIFT DUE TO AMPLITUDE UNBALANCE

IF Phase Unbalance: In the case of rf phase unbalances, the phase reversal point always occurs on boresight, even though its slope is finite. When the combination of rf and if phase differences are presented to the detector, however, the effect is a shift in boresight indication.

System Accuracy in the Presence of White Gaussian Noise: Sharensen (reference 47) has developed equations for the mean and standard deviation of the measured angle for the monopulse system when both channels are corrupted by white gaussian noise. If the S/N ratio is 12 db or greater, the mean angle measurement, $\bar{\theta}$, is equal to the true angle θ . And the standard deviation of the angle measurement is given by:

$$\sigma_\theta = \frac{1}{c (\sin)^2(u)} [1 - 2pc\theta + c^2\theta^2]^{1/2}, \quad (336)$$

where:

c = slope of the system output function ,

$s(u)$ = sun pattern = $P(u) + P(-u)$,

ρ = correlation of noise between channels, $0 \leq \rho \leq 1$.

The equation shows that the standard deviation increases for angles off boresight and decreases with larger S/N ratios and correlation of noise between channels.

For a system with a 3 db cross-over, the standard deviation on boresight is theoretically:

$$\sigma_{\theta} \Big|_{\theta=0} = \frac{0.5\beta}{(S/N)} \quad \beta = \text{half-power beamwidth} \quad (337)$$

Barton finds experimentally that the standard deviation is: (reference 49)

$$\sigma_{\theta} \Big|_{\theta=0} = \frac{0.707\beta}{S/N} \quad (338)$$

Accuracy of a Precision Monopulse Instrumentation Radar: Dunn and Howard (reference 48) have presented figures of precision for a monopulse system using a 1.25° beamwidth antenna system. Overall absolute rms tracking accuracies of 0.1 mil (0.0057 deg.) in angle are obtained. The angular difference in positions of a target can be measured to less than 0.01 mil for the radar in question. These figures include all system biases and rms errors.

Applicability to Noncooperative Docking Missions: Monopulse radar basically tracks signals received from a point source using the squinted receiver antenna patterns to establish angle of arrival. When range closes and target size begins to increase, the signals received in the antennas involve the integral of the target radar cross section times the receiver antenna pattern over the angle subtended by the target. The output ratio of the monopulse system is then some average (primarily dependent on the kernel of the integrals) of the sum and difference of these integrals and is not in general the correct representation of the target centroid. The system performance becomes even less reliable when considerations are extended to include target surface irregularities, antenna pattern perturbations, extension of target in sidelobe areas, etc. When target angle subtended becomes equal to or greater than the dual beamwidths, the monopulse system, of course, is useless.

It is obvious, then, that the amplitude monopulse system is not a sufficient system in itself to perform the angle measurements down to actual docking in the noncooperative case, unless provisions controlling squint angle are included.

Applicability to Cooperative Docking Missions (Near Field Considerations): In cooperative docking, the monopulse radar can track a beacon or transponder, acting as a point source on the target vehicle. The problem of target size is thus eliminated and the radar-transponder is capable of working down to actual docking, excluding near field effects.

Beam broadening appears to be the most crucial near field effect that can hamper the amplitude monopulse. The degree of beam broadening is a function of the antenna systems used and of the final range between transponder and radar antennas at docking. It is easily conceivable that beams of a monopulse system, with a 3 db-crossover in the far field, could broaden until no null existed in the patterns prior to obtaining the final docking range. For this reason, considerable care must be exercised in choosing antenna gains, cross-over, and placement of the antenna systems on the vehicles.

For the antenna arrangements in which the final docking range is well within the near-field region, another precaution must be taken. As the main beam broadens in the near-field, it loses its monotonic character and becomes wavy with pronounced peaks and nulls. These could produce ambiguous readings about boresight, even though the cross-over of the beams is still present. Gerlock has developed a practical method of plotting the Fresnel region for antennas of rectangular and circular apertures, which is useful when designing the antenna system to alleviate the near field problems associated with using amplitude monopulse. (reference 50).

Sequential Lobing and Conical Scan

Sequential lobing and conical scan angle tracking circuits are considered together, because of the similarity of the two systems. (See figures 87 and 88) Both are sampled data systems; they differ primarily in the number of sample positions available. The error signals, shown in figures 89 and 90 , are essentially the same for both cases, after low pass filtering. Disturbance frequencies greater than the bandpass of the error filter are not passed.

Accuracy - Sources of error for conical scanning and sequential lobing radar may be divided into the following categories.

1. Receiver noise,
2. Servo noise,
3. Amplitude fluctuation,
4. Angle fluctuation.

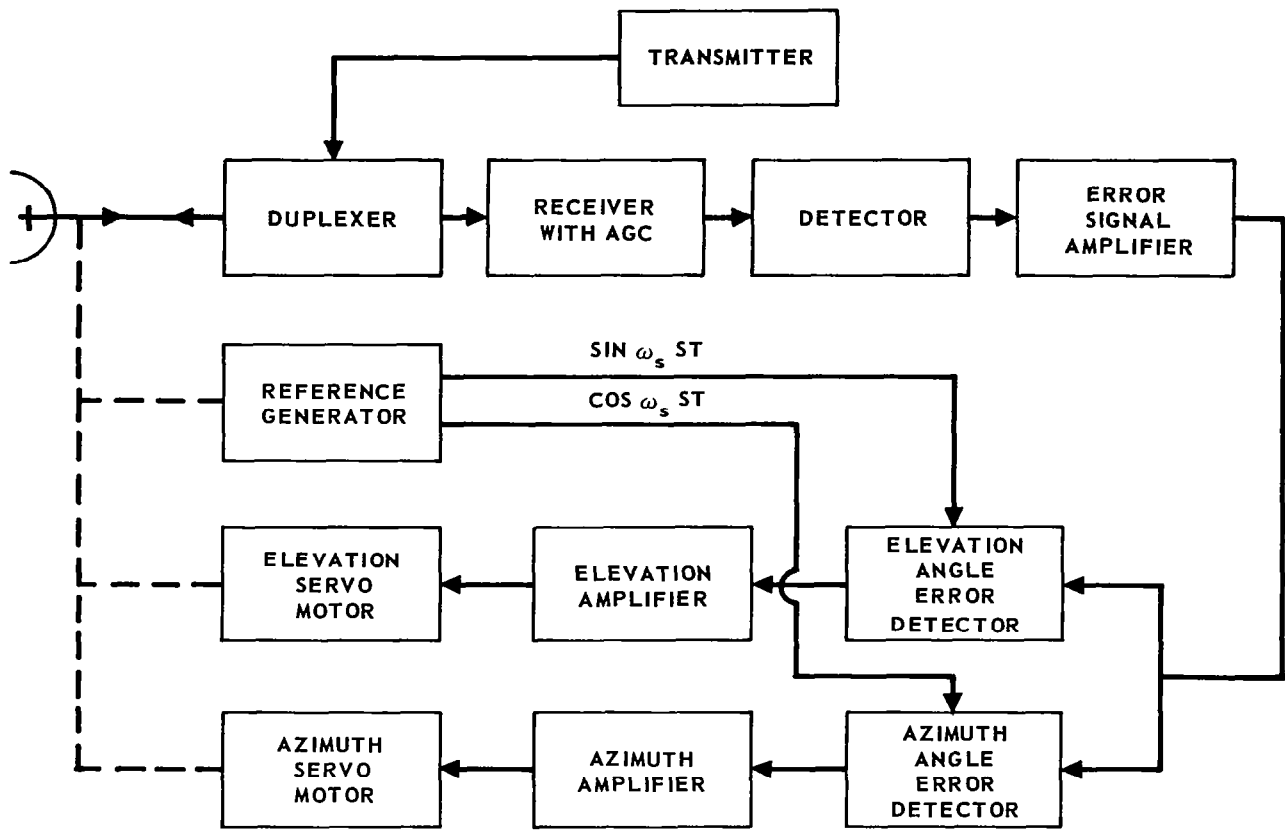


FIGURE 87 – CONICAL SCANNING RADAR

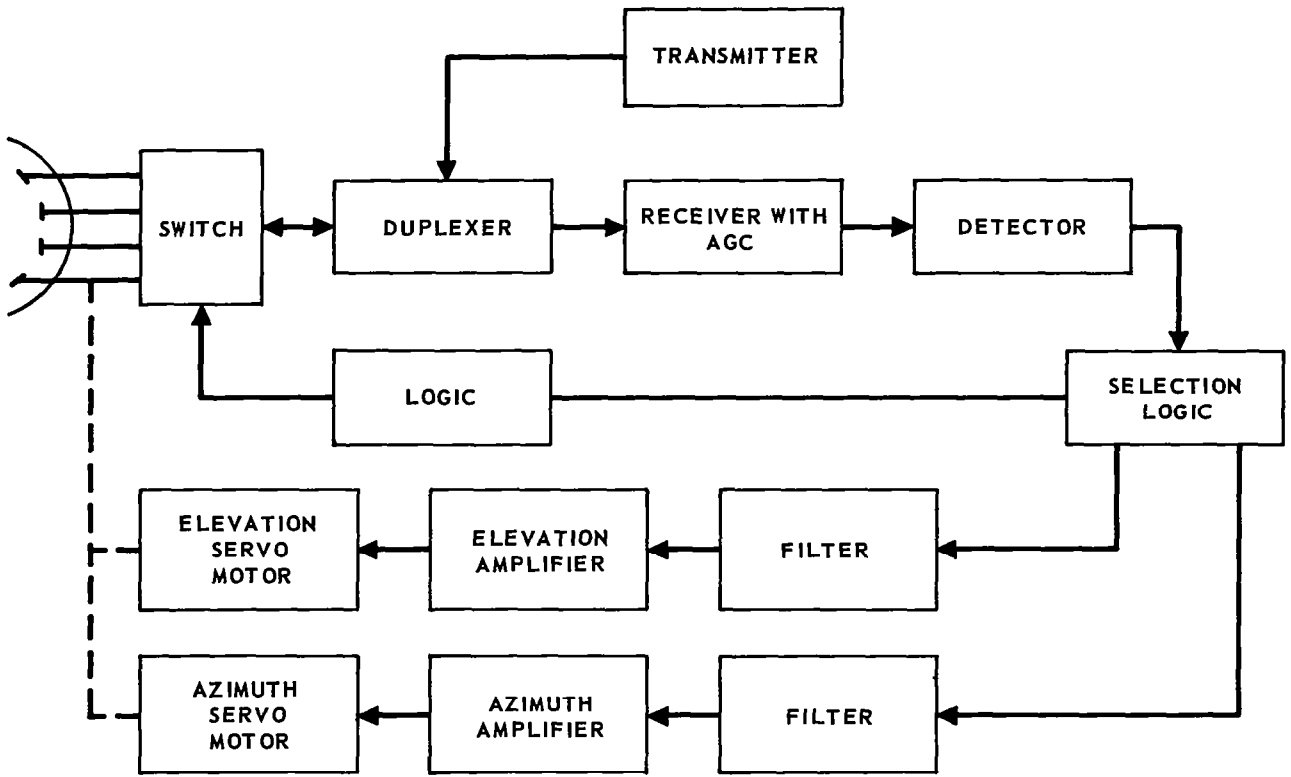


FIGURE 88 – SEQUENTIAL LOBING RADAR

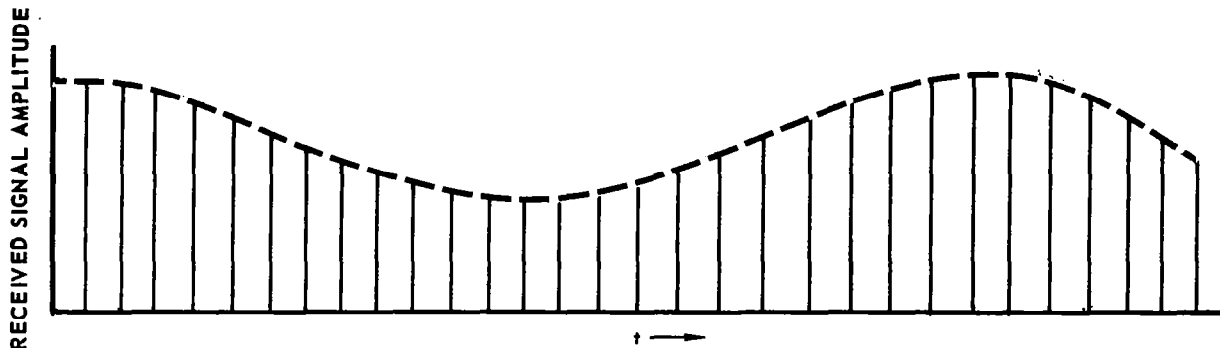


FIGURE 89 – ERROR SIGNAL CONICAL SCAN

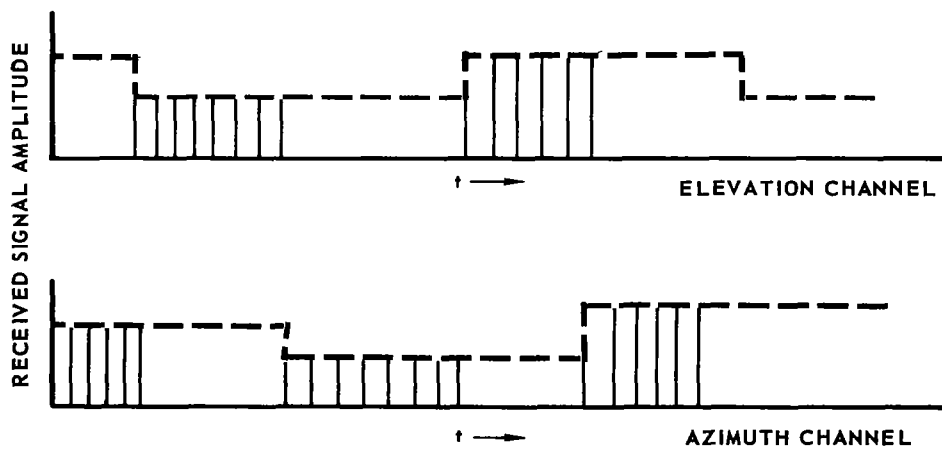


FIGURE 90 – ERROR SIGNAL SEQUENTIAL LOBING

The accuracy of the angle measurement has been shown to be inversely proportional to the signal to noise ratio. (reference 53):

$$\delta\theta = \frac{K\theta_B}{\left(\frac{S}{N}\right)^{1/2}}, \quad (339)$$

where: K = depends on aperture distribution,

θ_B = half power beamwidth.

Since the signal to noise ratio is proportional to $1/R^4$, the angular error due to receiver noise is proportional to the square of the target distance. The servo noise is due to backlash, mechanical tolerances in the gears, etc, and is independent of range. Since there is motion between the docking vehicle and the target vehicle, the amplitude of the returned echo fluctuates because of the change of target cross section with aspect angle. When the fluctuations occur at a rate comparable to the conical scan or lobing frequency, an angle error results. This error cannot be eliminated by AGC action, nor by filtering, and it is independent of range. Angle fluctuation is usually the factor which most degrades the accuracy of the angle measurement at the ranges of interest. Angle fluctuations arise due to vector addition of the reflected energy from many points on the surface of the target vehicle. This addition can cause a tilt in the phase front of the reflected energy and the resulting error in the measured bearing angle. The usual plot of accuracy (figure 91) shows the ranges at which these contributors are significant. In the docking radar situation, noise is not expected to be a problem. Amplitude fluctuation effects can be eliminated, or greatly reduced, by choosing a scanning frequency much higher than the expected amplitude noise. Angle fluctuations (glint) cannot be separated in such a manner, because the noise appears as a modulation of the conical scan frequency and the modulation sidebands are quite close to the scan frequency. (appendix F)

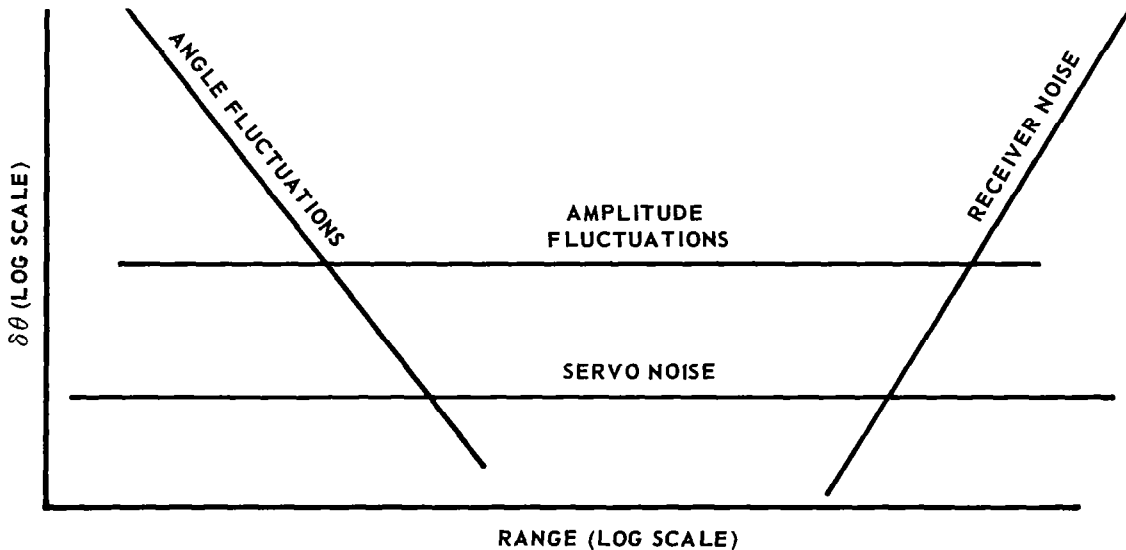


FIGURE 91 - CHARACTERISTIC ACCURACY CURVES

The Biconical Horn

The Biconical Horn antenna, simultaneously excited by two orthogonal modes, can be used as a direction sensing antenna system. By adjusting the amplitude and phase of the excitation fields, the two independent radiation patterns can be combined to produce a single radiation pattern with direction measuring capability. Figure 92a is a cross section view of the biconical horn antenna with a coaxial feed line capable of supporting the TEM and the TE_{11} modes. When the feed is excited with a TE_{11} mode in the coaxial feed, the relationship shown in figure 92b exists, resulting in the radiation pattern shown in figure 92c. Orthogonal excitation with variable amplitude but in time phase will result in a TE_{11} mode with the E field orientation dependent upon the ratio of the amplitude of the orthogonal excitation fields; i.e., in TE_{11} mode excitation (reference 52):

$$E_r = A \sin \theta, \quad (340)$$

$$E_r' = B \cos \theta, \quad (341)$$

adding:

$$E_{r_{total}} = A \sin \theta + B \cos \theta, \quad (342)$$

$$= \sqrt{A^2 + B^2} \sin \left(\theta + \tan^{-1} \frac{B}{A} \right). \quad (343)$$

This results in a variable direction of maximum radiation. The same antenna with this feed can be used in the receiving mode to determine the direction of arrival.

Four probes, located as shown in figure 92d, receive signals:

$$e_1 = A + B \cos \theta, \quad (344)$$

$$e_2 = A + B \sin \theta, \quad (345)$$

$$e_3 = A - B \cos \theta, \quad (346)$$

$$e_4 = A - B \sin \theta. \quad (347)$$

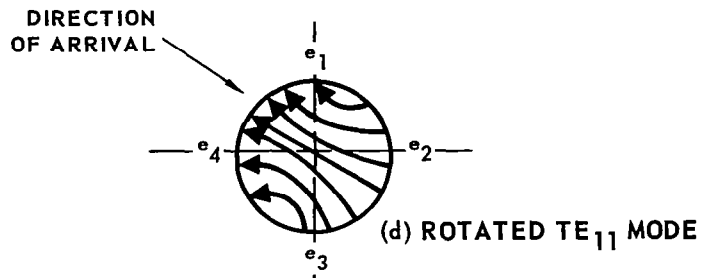
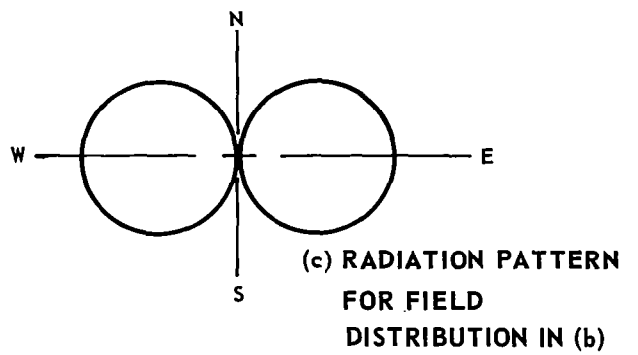
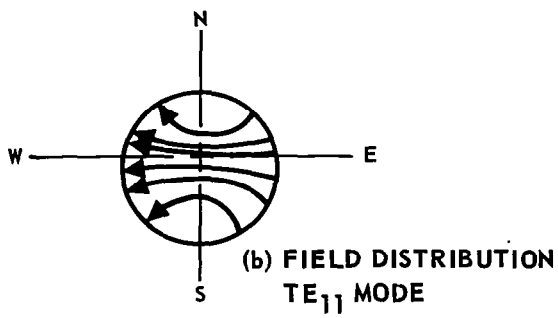
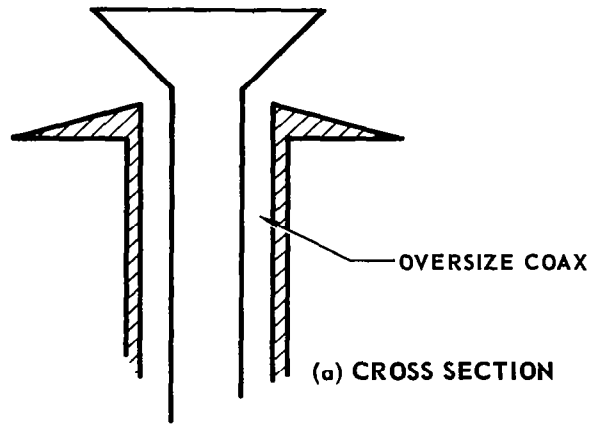


FIGURE 92 – BICONICAL HORN

Differencing e_1, e_3 and e_2, e_4 results in:

$$e_1 - e_3 = 2B \cos \theta, \quad (348)$$

$$e_2 - e_4 = 2B \sin \theta, \quad (349)$$

which would result from the TE_{11} modes only.

Adding the four signals, we obtain:

$$e_1 + e_2 + e_3 + e_4 = 4A, \quad (350)$$

which would result from the TEM mode only.

The direction of arrival information is contained in the amplitude variation. This information can be better processed in the form of a phase angle. Re-introducing the carrier frequency and adding a 90° phase shift to the TE_{11} modes, we obtain:

$$(e_1 - e_3) + (e_2 - e_4) e^{j\frac{\pi}{2}} = \quad (351)$$

$$2B \cos \theta \cos \omega t + 2B \sin \theta \sin \omega t = \quad (352)$$

$$4B \cos (\omega t + \theta). \quad (353)$$

which is the spiral phase TE_{10} mode. Reintroducing the carrier frequency to the TEM mode yields $4A \cos \omega t$. The direction of arrival information is contained in the **phase** difference between the TEM mode signal and the spiral phase TE_{10} signal. Figure 93 is a block diagram of the phase measuring system to measure the direction of arrival angle.

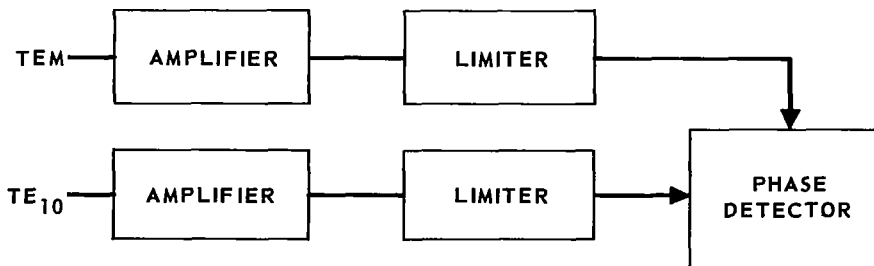


FIGURE 93 - BICONICAL HORN PHASE MEASUREMENT

Noise Induced Errors - The error in angle measurement produced by channel noise can be analyzed by summing the variances of the phase angles of the TEM mode signal and spiral phase TE₁₀ mode signal to obtain the overall phase angle measurement variance.

From appendix B , the angle variance of the phase angle of a noisy signal when passed through a low pass filter is:

$$N_{\theta} = \frac{N_o B_o}{s} = \sigma_{\theta}^2, \quad (B7)$$

where: N_o = noise power density,
 B_o = smoothing bandwidth,
 s = signal power.

Then, when measuring the phase difference between these two signals:

$$\theta_{\text{measured}} = \theta_{\text{TEM}} - \theta_{\text{TE}_{10}}, \quad (354)$$

$$\sigma_m^2 = \sigma_{\text{TEM}}^2 + \sigma_{\text{TE}_{10}}^2, \quad (355)$$

$$\sigma_m = \sqrt{2 \frac{N_o B_o}{s}},$$

$$\sigma_m = \sqrt{2} \sqrt{\frac{1}{S/N}} \text{ radians.} \quad (356)$$

Instrumentation - This antenna is subject to the usual instrumentation errors of phase measuring systems. The following is a list of sources of these errors and their magnitude:

Amplifier phase tracking	2°
Phase matching of combining circuitry	7°
Amplitude balance of hybrid	2°
Mismatch errors (VSWR)	2°
Mechanical asymmetry	negligible
Differential phase shift as a function of frequency	negligible

Environmental Errors. - (reference 53) - Since the biconical horn antenna has 360 degree azimuthal coverage, multipath signals caused by reflections from the spacecraft cause an error in the indicated angle of arrival. The resulting expressions for the TEM and TE₁₀ field distributions are:

$$\text{TEM} = A \cos \omega_0 t + A' \cos (\omega_0 t + \delta), \quad (357)$$

$$\text{TE}_{10} = B \cos (\omega_0 t + \theta_1) + B' \cos (\omega_0 t + \delta + \theta_2), \quad (358)$$

δ is the r.f. phase of the interfering signal,

A' and B' are the amplitudes of the interfering signals.

This situation has been analyzed in an earlier section, where an expression for angular error is given as follows:

$$\frac{\Delta\theta}{\theta_D} = \frac{a^2 + 2a \cos \delta}{1 + a^2 + 2a \cos \delta}, \quad (359)$$

where: $\Delta\theta$ = error,

θ_D = difference of bearing angles,

a = relative voltage amplitude $\left(\frac{\text{undesired signal}}{\text{desired signal}}\right)$.

Figure 94 shows the increase in the error with increases in angular separation of direction of arrival of interfering signals (e.g., when the reflection arrives from the opposite direction and 180° out of RF phase, a reflection 14 db down will produce an error of 45°). Great care must be taken in mounting this antenna so that spacecraft structural reflections will not occur. This is especially critical because of the low gain and broad pattern of this antenna.

Target Induced Errors. - (reference 54) - If this antenna is used in the noncooperative mode and the extent of the target is such that it subtends a large angle, the measured angular direction can be anywhere within or even outside the target due to glint. However, if the antenna is used in the cooperative mode, the situation will essentially be that of a point source and these problems can be eliminated.

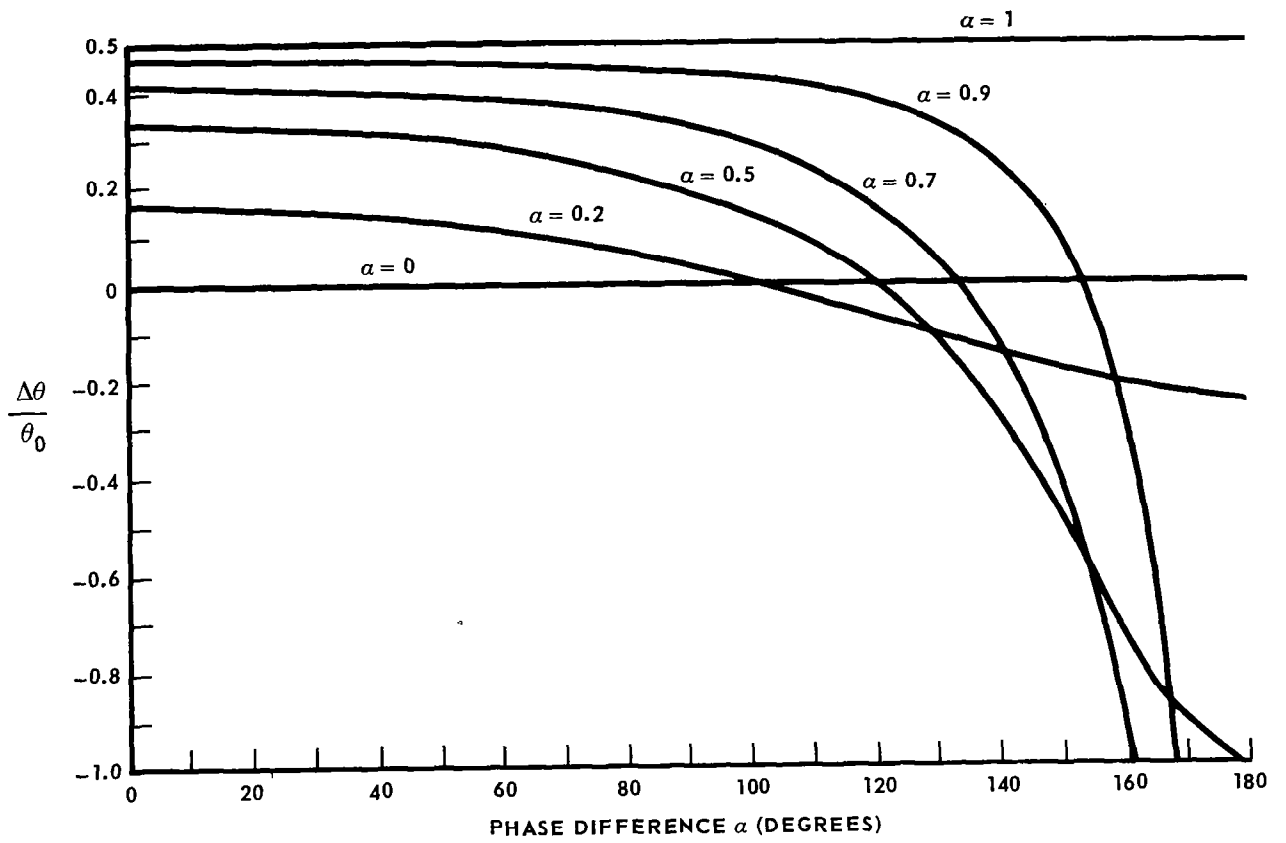


FIGURE 94 - MULTIPATH ERROR

LOS MEASUREMENT BY PHASE SENSING TECHNIQUES

Current angle measurement techniques are limited either to pure amplitude sensing or pure phase sensing. For the case of pure amplitude sensing discussed in the previous section, the angle information is contained strictly in the amplitude patterns of the antenna. Generally, the phase patterns are made nearly identical by minimizing the distance between effective phase centers. For the case of pure phase sensing, the angle of arrival information is contained strictly in the phase patterns of the antenna and the amplitude patterns must be identical (i.e., no beam squinting). Phase sensing techniques have been called phase monopulse, interferometers and phase comparators. As will be shown below, a given phase sensing system may be further classified according to the type of angle detection employed.

The phase sensing measurement technique employs two antennas separated by a distance, d , as shown in figure 95 .

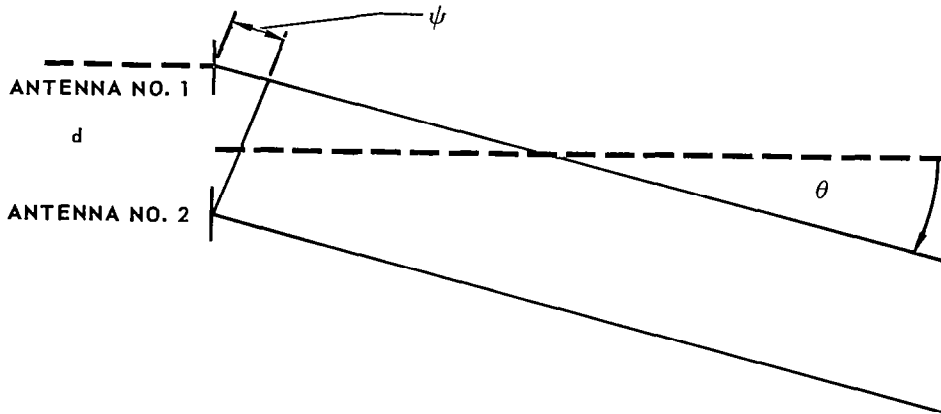


FIGURE 95 - INTERFEROMETER: PROPAGATION PATH LENGTH - PHASE RELATIONSHIP

Formation of Electrical Phase Shift

For a target at an angle, θ , relative to the antenna system boresight the electrical phase difference between the signals received at the two antennas is:

$$\phi = \frac{2\pi d}{\lambda} \sin \theta \quad , \quad (360)$$

where λ is the wavelength. It is this electrical phase difference, ϕ , which is used to indicate the target angular coordinate.

For the case of direct phase sensing, two methods may be used to obtain the angular error information. Consequently, two forms of angle detector implementation are possible. In the sense of reference 55 these two methods correspond to either the multiplicative or additive sensing function, which require either phase angle detection or sum-difference angle detection respectively. Representative models of the two techniques are shown in figures 96

and 97 , where any heterodyning has been omitted for simplicity. The indicated operations may be performed at any convenient frequency.

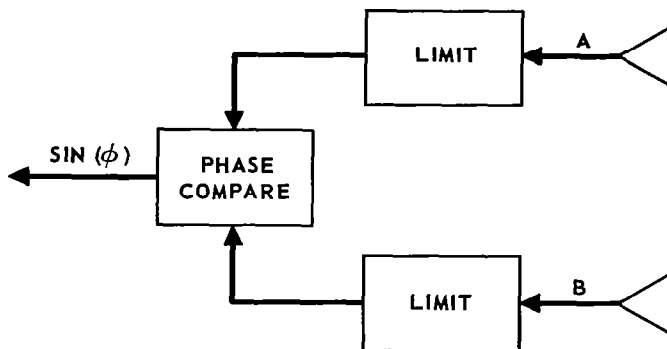


FIGURE 96 - PHASE ANGLE DETECTION

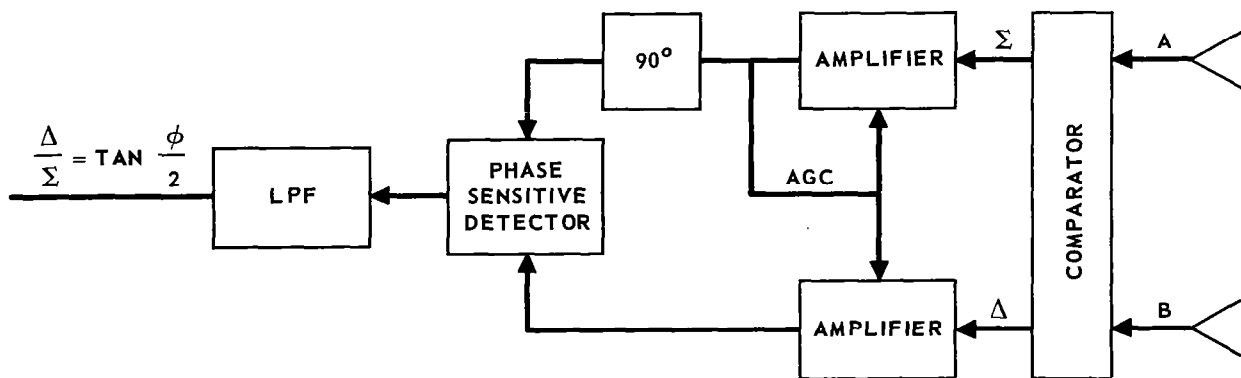


FIGURE 97 - SUM AND DIFFERENCE ANGLE DETECTION

For the case of phase angle detection, the angular error signal is $\sin(\phi)$ where we have assumed a sinusoidal phase comparator.

For the case of the sum and difference system, the magnitudes of the sum and difference comparator outputs are proportional to $\cos \phi/2$ and $\sin \phi/2$ respectively, such that, with proper AGC, the output of the low pass filter following the phase sensitive detector is proportional to $\tan \phi/2$.

It is noted that for either angle detection method, a space angle ambiguity exists when $d > 2\lambda$. Spacings greater than 2λ are commonly used, but in this case, either the angular coverage must be restricted, or the ambiguity resolved.

Sometimes, it is desirable to establish an angular error indication on the basis of a modulating frequency rather than the direct carrier frequency. In this case, the above techniques are employed after appropriate demodulation. This technique can be used to resolve ambiguities in a measurement at the carrier frequency, since the effective wavelength is that of the modulating frequency. A representative method is shown in figure 98 for amplitude modulation.

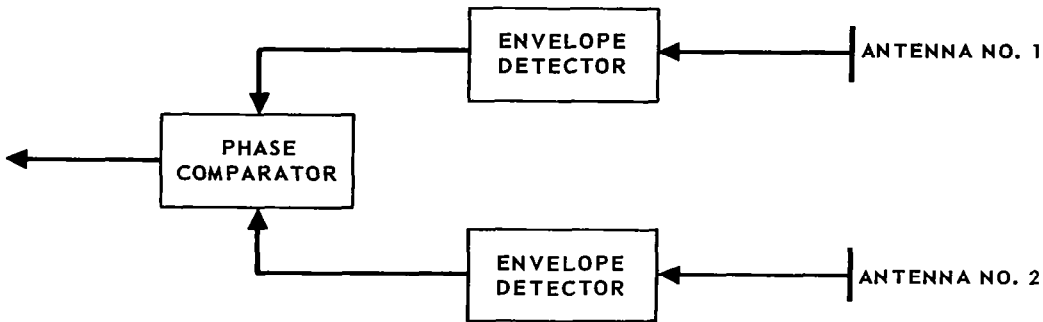


FIGURE 98 - PHASE MEASUREMENT OF THE MODULATION ENVELOPE

The space angle, θ , is defined as the angle between the direction of propagation and a plane which is perpendicular to a line which connects the center of the two antennas. In order to completely define a "line-of-sight", another measurement must be made with an additional antenna pair (usually placed at right angles to the first). The two resulting angles are commonly called "azimuth" and "elevation" angles.

Phase Sensing Errors

There are many factors that can contribute to the accuracy of the phase sensing technique for direction measurement. Some of these are:

1. Mechanical boresight
2. Servodynamics
3. Read out (Digital versus Analog)
4. System receiver noise
5. Unequal channel amplitude
6. Unequal phase tracking
7. Radome (if required)
8. RFI
9. Thermal effects
10. R.F. switching
11. Switch isolation
12. Polarization effects
13. Mutual coupling effects
14. Multipath effects and pattern perturbation
15. Physical radiating element construction and placement
16. Near range geometry errors

Many of these error contributors can be made small. The major contributors generally are: (a) system noise, (b) servo errors, (c) readout errors, (d) near range geometry errors, (e) radiation pattern distortion, (perturbations), (f) polarization effects, and (g) phase tracking.

System Noise.-A phase sensing system which uses null tracking, by the production of an error signal which servo drives the RF system to a null, is only as good as the null which is available. From reference 55 the best obtainable angle accuracy can be expressed by:

$$\Delta\theta = \frac{1}{\pi} \left(\frac{\lambda}{d}\right) \frac{\sqrt{PN/PS}}{\sqrt{2TB}} \text{ for pulsed systems,} \quad (361)$$

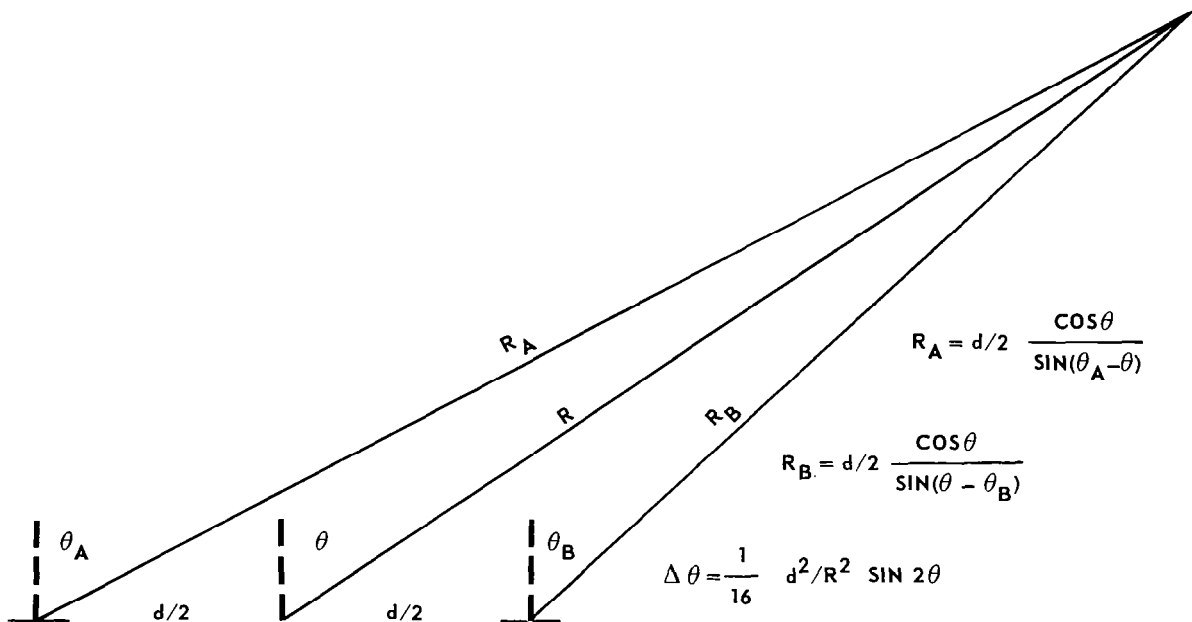
$$\Delta\theta = \frac{1}{\pi} \left(\frac{\lambda}{d}\right) \frac{1}{\sqrt{2(S/N)}} \text{ for CW systems,} \quad (362)$$

where P_N is the noise power
 P_S is the peak pulse power
 T is the pulse width
 B is the RF bandwidth
 S/N is the signal to noise ratio.

For a system having a 1λ baseline, an accuracy of 3 milliradians requires a S/N ratio of 38.4 db. Although resolution is improved for a system having a baseline greater than 1λ , ambiguity resolution is sometimes a problem.

Servo System and Readout Errors.-The mechanical errors associated with tracking and readout are usually significant when precise angle measurements are desired. In the Gemini Rendezvous Radar the 3σ error for these considerations is about 1.5 mechanical milliradians.

Near Range Geometry Errors.-When the direction angles are determined at close range, the signal can no longer be considered to be parallel rays from the source to the interferometer. The geometry of the problem becomes that shown in figure 99.



WHERE: d IS THE BASELINE
 R IS THE RANGE TO THE CENTER OF d
 θ IS THE LOS ANGLE

FIGURE 99 - NEAR RANGE GEOMETRY

Additional error must be added if the source cannot be considered as a point.

Radiation Pattern Perturbations.-Multipath interference and other radiation pattern distortions have a significant effect on the phase system null displacement. From reference 56 it can be shown that:

$$\Delta\theta = \left(\frac{\lambda}{\pi d}\right) \frac{E_i}{E_d}, \text{ where:} \quad (363)$$

$\Delta\theta$ = error angle,

E_i = the field intensity of an indirect or multipath component,

E_d = the field intensity of the direct signal,

d = the interferometer baseline.

When E_i is 20 db above E_d , and $d = 1 \lambda$:

$$\Delta\theta = \frac{1}{10\pi} = 0.0319 = 31.9 \text{ mr of } 1.8^\circ. \quad (364)$$

This system is so sensitive to this kind of interference that reflections from the ionosphere, the earth, appendages, and other space objects must be considered.

Polarization Effects.-If circular polarization is used for both the receiving antenna elements and the source, large errors can be introduced due to axial ratio mismatch. The error is also a function of LOS angles. This error is given by:

$$\tan \sigma = \frac{k + \tan \theta_e}{1 - k \tan \theta_e} \quad (365)$$

where:

$$k = \frac{(k_2 k_3 - k_2 k_6) + (k_1 k_6 + k_2 k_4 - k_2 k_7 - k_3 k_5) \tan \beta + (k_1 k_7 - k_4 k_3) \tan^2 \beta + (k_1 k_2 + k_2 k_5 - k_3 k_7 - k_4 k_6) \tan \theta \tan \beta + (-k_1 k_5 - k_4 k_7) \tan \theta \tan^2 \theta + (-k_2^2 - k_3 k_6) \tan \theta_e}{(k_3 k_5 + k_2 k_7) + (k_2 k_3 + k_4 k_5 - k_1 k_7 - k_2 k_6) \tan \beta + (k_1 k_6 + k_2 k_4) \tan^2 \beta + (k_1 k_5 + k_4 k_7 - k_2^2 - k_3 k_6) \tan \theta \tan \beta + (k_1 k_2 - k_4 k_6) \tan \theta \tan^2 \beta + (k_3 k_7 - k_2 k_5) \tan \theta_e}$$

and:

$$\begin{aligned}
 k_1 &= \epsilon_R \cos \theta_m + \epsilon_S \cos \delta, & k_5 &= \epsilon_A \cos \theta_m + \epsilon_S \cos \delta, \\
 k_2 &= \epsilon_T \sin \theta_m \sin \delta, & k_6 &= \cos \theta_m + \epsilon_A \epsilon_S \cos \delta, \\
 k_3 &= \cos \theta_m + \epsilon_R \epsilon_S \cos \delta, & k_7 &= \epsilon_A \epsilon_S \sin \theta_m \sin \delta, \\
 k_4 &= \epsilon_R \epsilon_S \sin \theta \sin \delta, & \theta_e &= \frac{4\pi d}{\lambda} \sin \theta_m,
 \end{aligned}$$

and β is the tilt angle of the source ellipse,
 θ_m is the mechanical azimuth angle,
 θ_e is the electrical phase shift caused by Θ_m ,
 δ is the elevation LOS angle.

ϵ_R , ϵ_A & ϵ_S are the axial ratios of reference antenna, azimuth antenna, and source, respectively.

σ is the error angle.

This error contribution can easily be several degrees, if great care is not taken to match the axial ratios of the elements. A typical error for a 1 db axial ratio mismatch, and a source with a 6 db axial ratio, on boresight, is about 5 milliradians, and is magnified for off boresight angles.

Mutual Coupling. - This becomes a serious consideration whenever an element of the antenna is required to move with respect to the other or with respect to its surroundings. The magnitude of this error for an "L" interferometer is given by:

$$\psi_R = \frac{A}{B} \quad (366)$$

$$\begin{aligned}
 A &= -(\epsilon_R + \epsilon_S) \sin \beta + A [-(\epsilon_A + \epsilon_R) \sin \beta_A^1 \cos \delta_A + (1 + \epsilon_A \epsilon_R) \cos \beta_A^1 \sin \delta_A] \\
 &\quad + E [-(\epsilon_E + \epsilon_R) \sin \beta_E \cos \delta_E + (1 + \epsilon_E \epsilon_R) \cos \beta_E \sin \delta_E], \\
 B &= (1 + \epsilon_R \epsilon_S) \cos \beta + A [(1 + \epsilon_R \epsilon_A) \cos \beta_A^1 \cos \delta_A + (\epsilon_A + \epsilon_R) \sin \beta_A^1 \sin \delta_A] \\
 &\quad + E [(1 + \epsilon_E \epsilon_R) \cos \beta_E \cos \delta_E + (\epsilon_E + \epsilon_R) \sin \beta_E \sin \delta_E],
 \end{aligned}$$

where A is the coupling factor between antennas A and R', E is the coupling factor between antennas E and R', β , β_A and β_E are the angular distances to the major axis of the antennas ellipse, measured counterclockwise from \bar{a}_x axis.

For a coupling of 30 db, the error in angle can exceed 1 degree in the worst case.

Thermal and Other Effects. - Thermal errors caused by unequal expansion or contraction of the RF feed lines can become very significant in high microwave frequency systems. This can be partially offset by control of temperature, choice of materials, and compensation networks, but only at the cost of added complexity and reduced reliability. At 70 GHz an RF interferometer system is exceptionally sensitive to slight twisting, bending or flexing of even very rigidly constructed feed systems.

Sum and Difference Angle Detection

In the sum and difference system, the comparator accepts the received signals from both antennas (figure100) and has a two channel output: one, the difference of the two signals and the second, the sum of the two signals. Such a system is discussed in reference 44. A basic block diagram for the sum and difference system is shown in figure101. Assume a signal arrives at the angle, θ , shown in figure100. The rf signals induced in the antennas are:

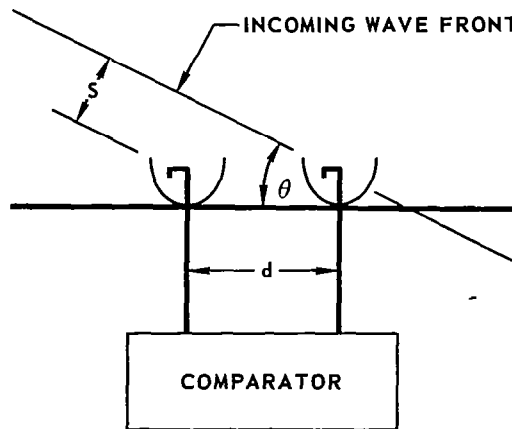


FIGURE 100 - FIGURE 1 ANTENNA SYSTEM FOR PHASE SENSING

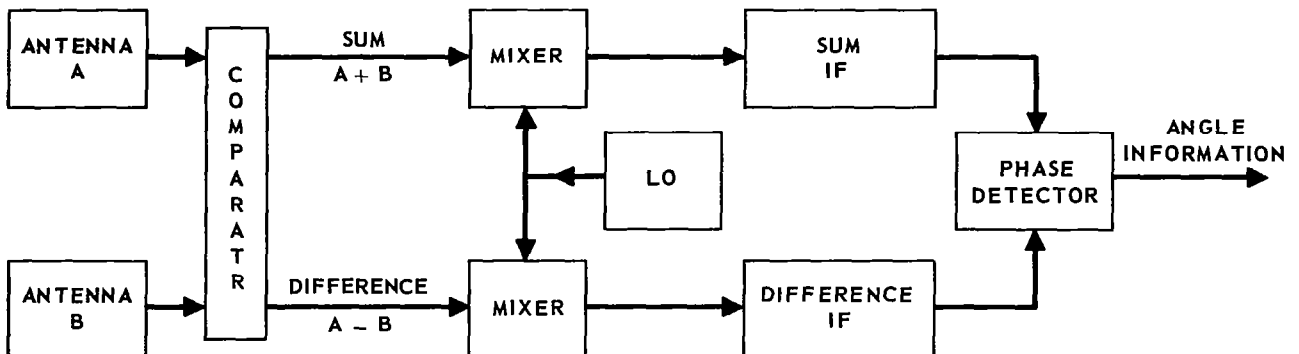


FIGURE 101 - BLOCK DIAGRAM OF BASIC MONOPULSE SYSTEM

$$A = K_1 \sin(\omega_0 t + \phi) , \quad (367)$$

$$B = K_1 \sin \omega_0 t , \quad (368)$$

where k_1 is the amplitude and ω_0 the carrier frequency. The sum and difference channel signals are then:

$$S = 2K_1 \cos \frac{1}{2} \phi \tan^{-1} \left(\frac{\sin \phi}{\cos \phi + 1} \right) , \quad (369)$$

$$D = 2K_1 \sin \frac{1}{2} \phi \tan^{-1} \left(\frac{\sin \phi}{\cos \phi - 1} \right) . \quad (370)$$

The phase angles in equations 369 and 370 can be simplified to be:

$$\alpha_S = \tan^{-1} \left(\frac{\sin \phi}{\cos \phi + 1} \right) = \left(\frac{\phi}{2} \right) , \quad -180^\circ < \phi < 180^\circ ; \quad (371)$$

$$\alpha_D = \tan^{-1} \left(\frac{\sin \phi}{\cos \phi - 1} \right) , \quad (372)$$

$$= \frac{\pi}{2} + \frac{\phi}{2} , \quad 0^\circ < \phi < 180^\circ ; \quad (373)$$

$$= \frac{3\pi}{2} + \frac{\phi}{2} , \quad 0^\circ > \phi > -180^\circ ; \quad (374)$$

Equations 369 through 374 show that a null in the amplitude of the difference channel exists at $\phi = 0^\circ$ and that the sum channel has a maximum at that point. As ϕ passes through zero in the positive direction, an instantaneous phase reversal from $\frac{3\pi}{2}$ to $\frac{\pi}{2}$ occurs at $\phi = 0^\circ$. These properties then define the boresight of the phase nonopulse system.

The equations also show that if ϕ is allowed to exceed $\pm 180^\circ$, the angle functions begin repeating and nulls off boresight are generated. This then puts a limit on equation 360; i.e.,

$$\phi = \left(\frac{-2\pi d \sin \theta}{\lambda} \right) < \pm 180^\circ . \quad (375)$$

Effects of Pre-Comparator Phase Shifts.-When channel B experiences a phase delay, γ , over that in channel A prior to the comparator, the magnitudes of the sum and difference channels of equations 369 and 370 become:

$$S_1 = 2K_1 \cos^{1/2} (\gamma + \phi) , \quad (376)$$

$$D_1 = 2K_1 \sin^{1/2} (\gamma + \phi) . \quad (377)$$

Equations 376 and 377 show that an amplitude null does not exist until ϕ equals $-\gamma$. The phase functions of equations 371 and 372 become:

$${}^a S_1 = \frac{1}{2}(\phi - \gamma) , \quad -180^\circ < (\phi + \gamma) < +180^\circ ; \quad (378)$$

$$\begin{aligned} {}^a D_1 &= \left(\frac{\pi}{2} \right)^{-1/2} (\gamma - \phi) , \quad 0^\circ < (\gamma + \phi) < 180^\circ ; \\ &= \left(\frac{3\pi}{2} \right)^{-1/2} (\gamma - \phi) , \quad -180^\circ < (\gamma + \phi) < 0^\circ ; \end{aligned} \quad (379)$$

$$\begin{aligned} {}^a S_1 - {}^a D_1 &= \left(\frac{-\pi}{2} \right) , \quad 0^\circ < (\gamma + \phi) < 180^\circ ; \\ &= \left(\frac{-3\pi}{2} \right) , \quad -180^\circ < (\gamma + \phi) < 0^\circ ; \end{aligned} \quad (380)$$

Equation 379 indicates that the phase reversal from $\frac{-\pi}{2}$ to $\frac{-3\pi}{2}$ occurs when $(\gamma + \phi)$ equals zero, or when ϕ equals $-\gamma$. Thus by equations 378 and 379, the effect of an rf phase γ is to cause a pointing error by shifting the boresight of the system. Figure 102 shows the dependence of the null shift due to precomparator phase unbalance on the $\frac{d}{\lambda}$ ratio.

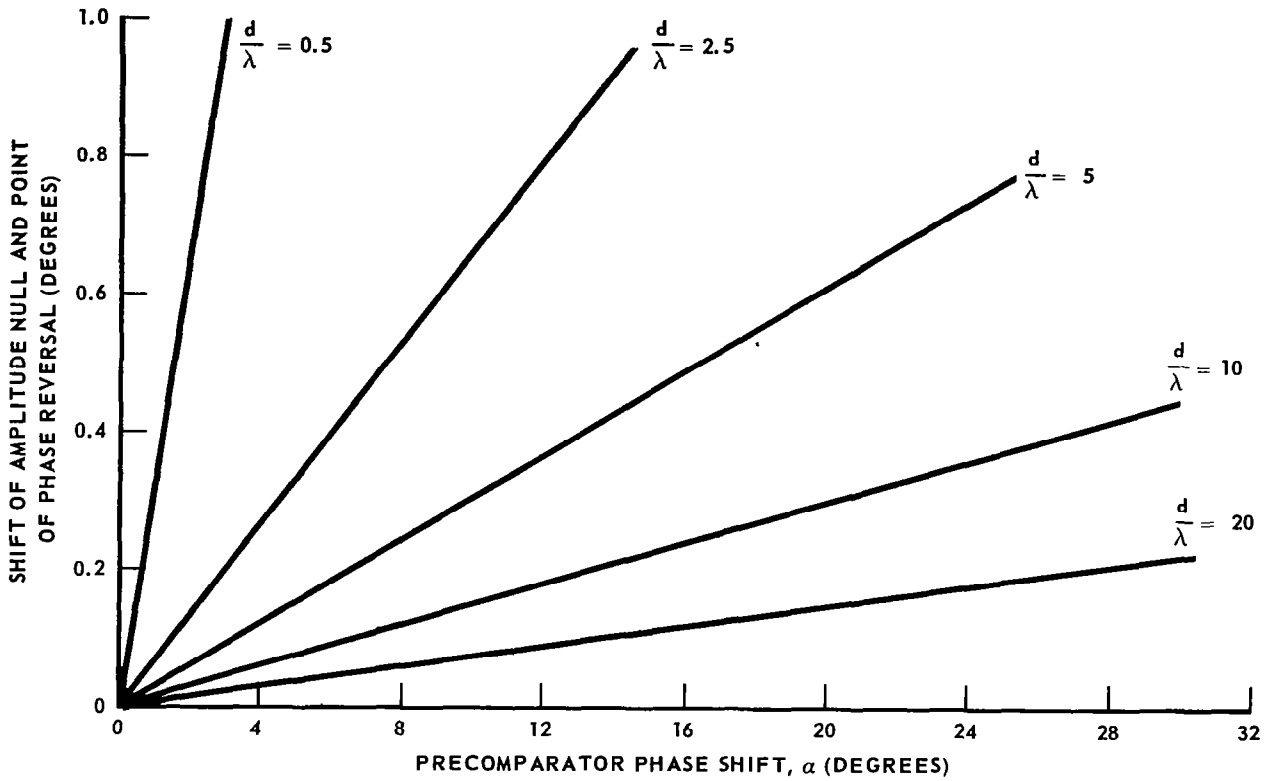


FIGURE 102 – BORESIGHT SHIFT RESULTING FROM PRECOMPARATOR PHASE SHIFT FOR VARIOUS ANTENNA SPACINGS

Voltage Unbalance Effects. - Consider now the case where channel A is attenuated k_z more than channel B, so that equations 367 and 368 are:

$$A = k_1 K_1 \sin(\omega_0 t + \phi) \quad (381)$$

$$B = K_1 \sin \omega_0 t \quad (382)$$

The sum and difference channel values become:

$$S = K_1 [(l \cos \phi + 1)^2 + (l \sin \phi)^2]^{1/2} \tan^{-1} \left(\frac{l \sin \phi}{l \cos \phi + 1} \right) \quad (383)$$

$$D = K_1 [(l \cos \phi - 1)^2 + (l \sin \phi)^2]^{1/2} \tan^{-1} \left(\frac{l \sin \phi}{l \cos \phi - 1} \right) \quad (384)$$

If k_1 is taken to be unity, the magnitude of the difference channel signal is:

$$|D| = [(l \cos \phi - 1)^2 + (l \sin \phi)^2]^{1/2} \quad (385)$$

Equation 385 is plotted in figure 103 for k_z having values of 1, .95, and .9. The sensitivity loss due to the null fill in around $\phi = 0$ is evident. The figure does not include antenna parameters so that the shape of the curve is not invariant for all phase monopulse systems.

Effects of Local Oscillator Phase Angle. - The phase angle of the local oscillator voltage at both the sum channel mixer and the difference channel mixer is:

$$V_{LOD} = K_{LOD} \sin(\omega_{LO} t + \alpha_{LOD}) \quad (386)$$

where α_{LOD} is the phase angle of the LO voltage at the mixer.

Then the total signal presented to the mixer is:

$$V_{MD} = 2K_1 \sin \frac{1}{2} \phi \sin(\omega_0 t + \alpha_D) + K_{LOD} \sin(\omega_{LO} t + \alpha_{LOD}) \quad (387)$$

The IF output of the difference channel mixer is:

$$V_{IFD} = v_{IFD} \sin[\omega_{IF} t + (\alpha_D - \alpha_{LOD})] \quad (388)$$

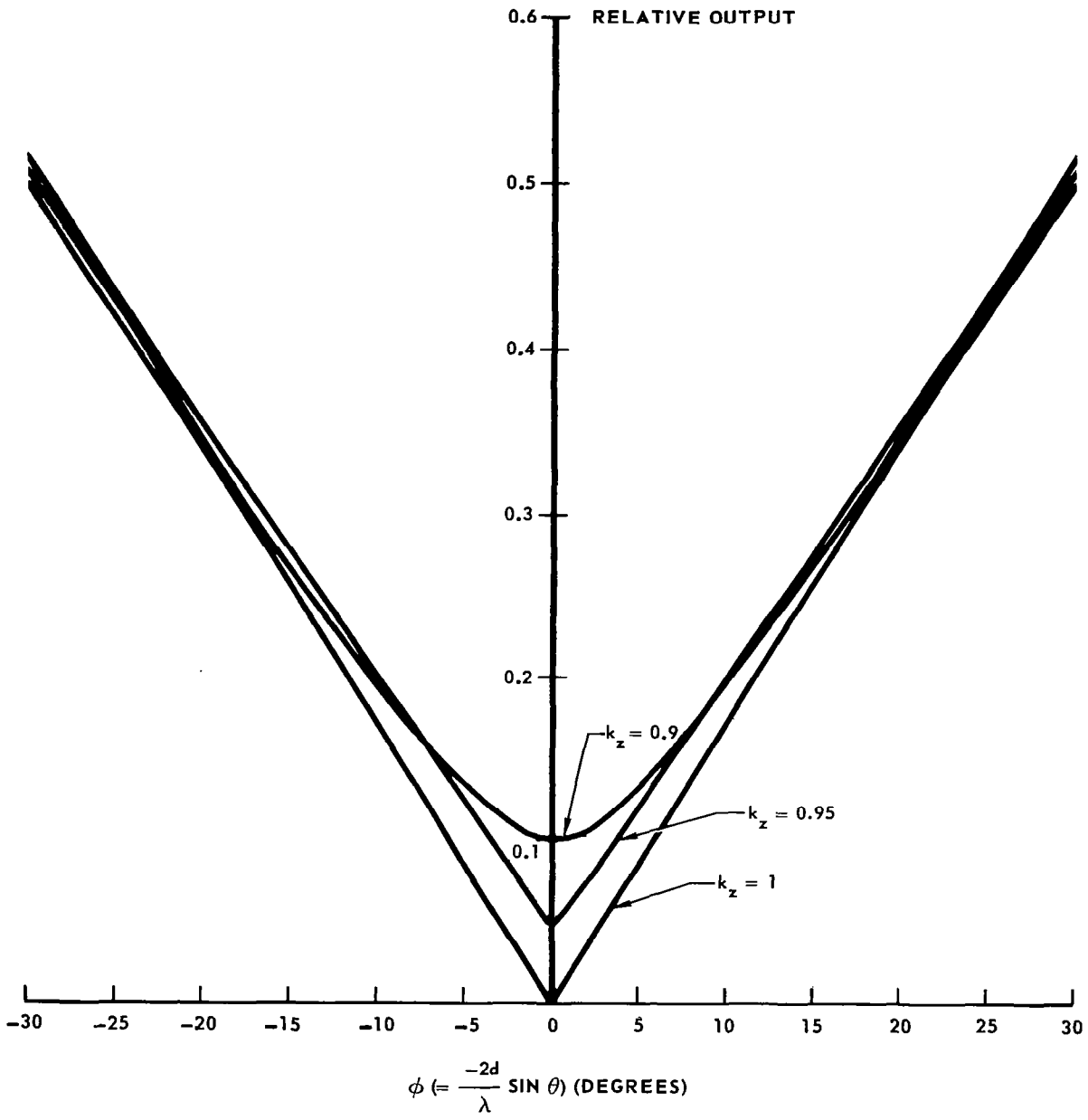


FIGURE 103 - LOSS OF SYSTEM SENSITIVITY DUE TO CHANNEL VOLTAGE UNBALANCE

Similarly, with a sum channel input phase angle from the LO of α_{OS} , the IF for the sum channel is:

$$V_{IFS} = v_{IFS} \sin [\omega_{IF}t + (\alpha_S - \alpha_{LOS})] \quad (389)$$

When the two signals represented by equations 388 and 389 are compared in the phase detector, the output is:

$$(\alpha_S - \alpha_{LOS}) - (\alpha_D - \alpha_{LOD}) = (\alpha_S - \alpha_D) - (\alpha_{LOS} - \alpha_{LOD}) \quad (390)$$

Equation 390 shows that a constant phase shift is introduced by the LO phase angles. The difference, $\alpha_S - \alpha_D$, is kept intact, however, and since the value of this difference is determined only by the incoming signals phase difference, ϕ , the point of phase reversal ($\phi = 0$) remains the same. The phase shift, $\alpha_{OS} - \alpha_{OD}$, does degrade the performance of the phase detector and, in essence, desensitizes it as is shown in figure 104. For instance, the output of the phase detector with an $(\alpha_{OS} - \alpha_{OD})$ of 60° would be 6 db down from that where $\alpha_{OS} - \alpha_{OD} = 0$. This then points out that precautions should be taken to make the electrical line lengths between the LO and the channel mixers equal to obtain best detector sensitivity.

Antenna Considerations. - The phase monopulse system measures phase difference and is not concerned with differences in amplitude. Contrary to the amplitude comparison system then, the phase monopulse antenna beams are not squinted off boresight, but are directed to illuminate a common volume in space. In general, separate antennas are used to produce independent beams covering the same special sector. Care must be taken, however, that in the design of the antenna system, the ambiguity angle, θ , of equation 375 is not included in the main beam.

Applicability of Phase Monopulse to Docking. - As a docking aid for non-cooperative missions, the phase monopulse system is no more promising than the amplitude monopulse system of the preceding section. As target size increases with range closure, target glint will increase until at some intermediate range (that is dependent on antenna beamwidth and target characteristics) the multiple and different valued signal returns will render the radar useless.

With a point source mounted on the target vehicle, the phase monopulse system can perform in to much closer ranges than in the noncooperative case. However, as distance closes to about 50 feet or less the system performance will be degraded seriously because of multipath and near field distortions.

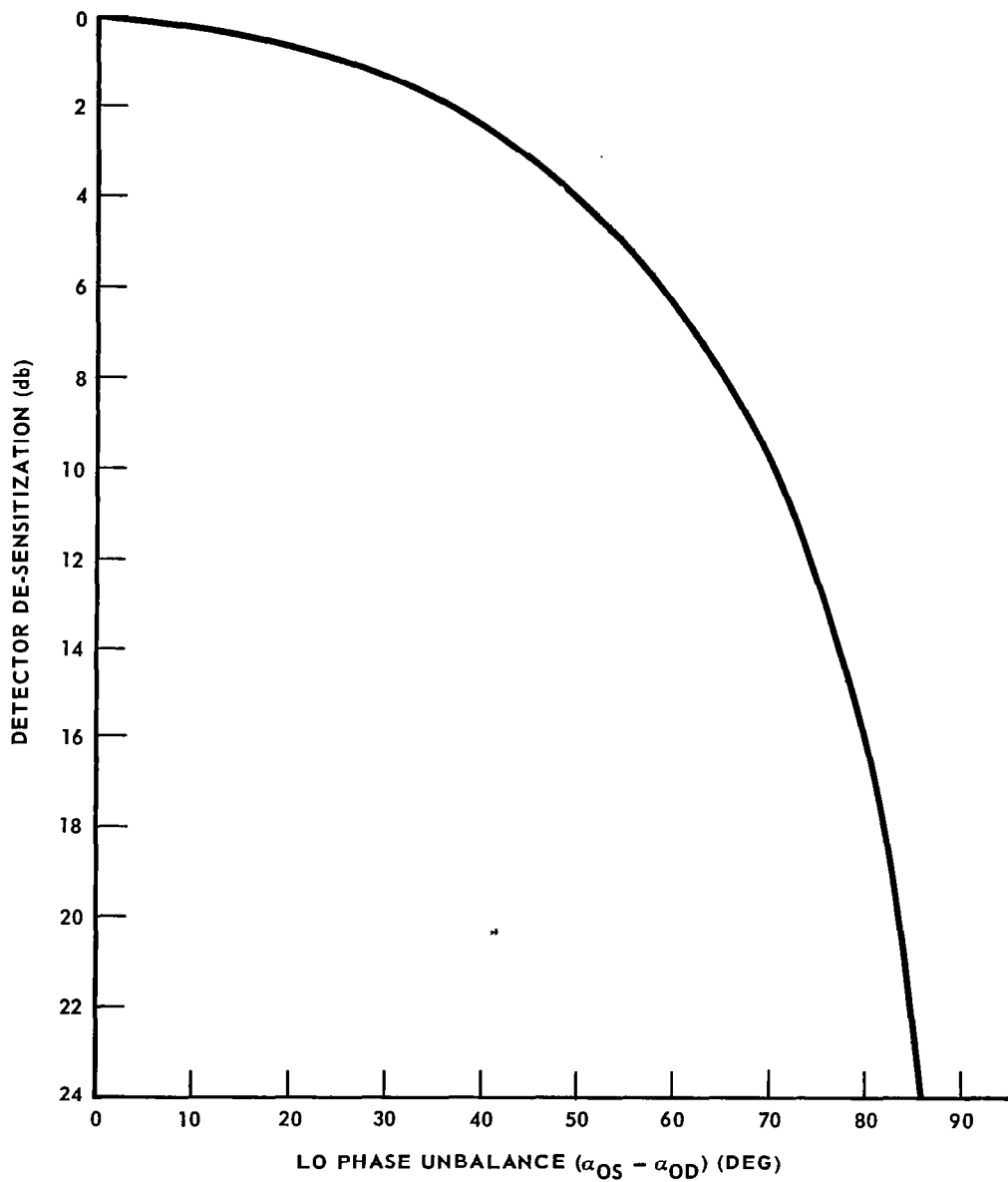


FIGURE 104 – LOSS IN DETECTOR SENSITIVITY DUE TO PHASE DIFFERENCES FROM LO TO CHANNEL MIXERS

Phase Angle Detection

The preceding analysis of the sum and difference system considers both pre-comparator and post-comparator errors. Pre-comparator phase errors introduce a boresight shift whereas post-comparator phase errors alone serve only to desensitize the phase detector performance. Similar consideration of the phase angle detection method (see figure 98) indicates that a relative phase shift, γ , between the parallel channels prior to the phase comparator introduces an effective boresight error equal to γ electrical degrees or approximately $\frac{\lambda}{2\pi d} \gamma$ mechanical degrees. Thus, the curves of figure 102 may be used to determine the boresight shift for the phase angle detection system where γ is the total parallel channel phase tracking error (including RF, IF, local oscillator phase, etc.) prior to the phase comparator. This is in contrast to the sum and difference system where phase errors at the IF do not alone result in boresight shifts.

Amplitude tracking is not a major factor in the phase angle detection system and, in fact, limiters may be used in place of AGC.

It should be noted that the sum-difference system makes more efficient use of the total antenna aperture. This is true since near boresight the sum channel signal may be up to 6 db greater (assuming a two-dimensional system employing four antennas) than that obtained in a single channel of the phase detection system. This consideration may be important with respect to probability of detection, AFC performance, and integration of command links.

TARGET ATTITUDE DETERMINATION TECHNIQUES

Target attitude can be determined by the use of any of the LOS angle determination techniques discussed earlier, using sensors on the target to track chascraft radiations. However, unless the target aligns itself with this LOS, the attitude data must then be relayed to the maneuvering chascraft via data link. Although these two approaches are competitive for some applications, a third approach is often indicated - that of generating a signal at the target which, when detected at the chascraft, is an unambiguous function of the aspect angle of the source. The signal can be generated by controlled passive reflectors or by specialized coded transponders.

Coded Reflectors and Retrodirectors

A considerable improvement on the passive reflector is possible by coding a reflected or retro-directed signal with information that contains the target craft's attitude. The solid angle for which lock-on is possible can be made very much greater if coding is placed on the reflected or retro-directed signal. The complexity of the target equipment required is still minimal, but the capability of the system is greatly improved and the complexity of the noncooperative radar system is reduced. Advantages of coding the reflected energy are:

- (a) Lock-on is generally not lost due to target tumble.
- (b) A continuous target attitude alignment error signal can be generated and used, if desired, for closed loop docking.

The primary limitations of this type system are:

- (a) No aid is provided beyond about 10,000 feet.
- (b) When both vehicles have their roll axis in alignment, roll orientation information is generally not available. Polarization sensing can be used to provide roll information, but linear polarization is required, which increases multipath error contributions to be sensed data. Also, polarization sensing systems are not known for high accuracy and tend to be ambiguous. A supplementary roll detection system is probably required.

An Example of a Fixed Coded Reflector.-A simple arrangement for coding the return signal is shown in figures 105 .

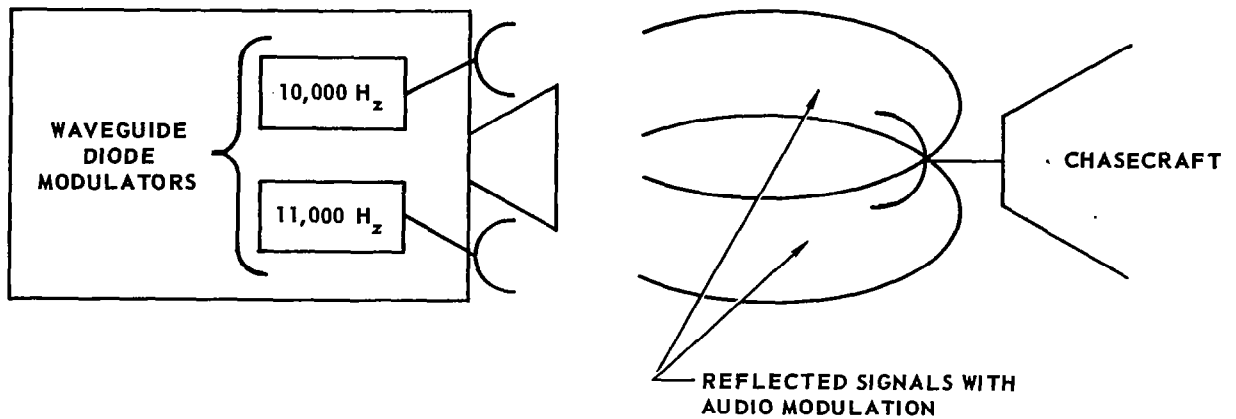


FIGURE 105 - FIXED CODED REFLECTORS

The radar system in the chascraft must be equipped with a section capable of detecting and amplitude-comparing the 10 kHz and 11 kHz azimuth alignment signals, and also the 12 kHz and 13 kHz elevation signals (not shown), to generate the off roll axis error signals.

An Example of a Mechanical Coded Reflector.-A simple mechanical coded reflector capable of providing the docking vehicle with all target attitude information except the relative roll angle is shown in figure 106. Other geometrical shapes could easily be used, but the square and triangle were chosen because of their simplicity. The basic noncooperative range, range rate, and LOS system aboard the chascraft can easily be modified to gather the attitude data from a mechanical aid of this type.

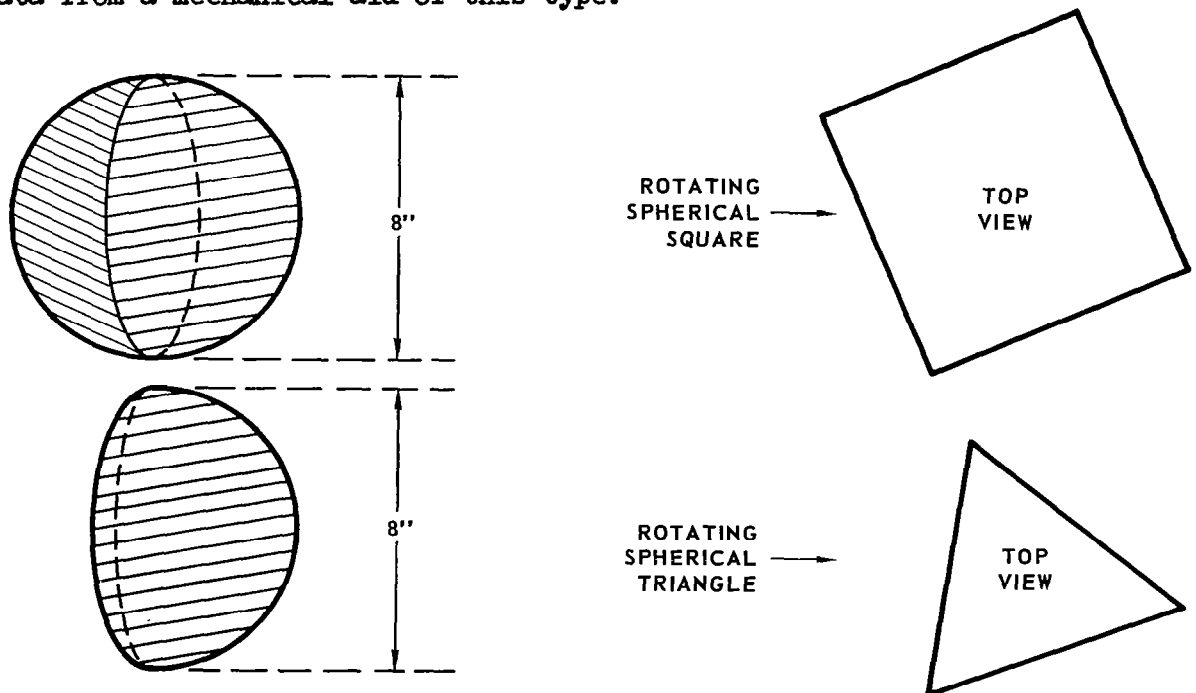


FIGURE 106 - MECHANICAL ATTITUDE AID

The spherical square and the spherical triangle rotate at different rates so that one face of the square and one face of the triangle appear simultaneously in a certain chosen direction. The chosen direction for this analysis is $\theta = 0^\circ$. The rotation rates to make this possible are chosen as 1 cps for the square, and $4/3$ cps for the triangle. It may be noted that only at $\theta = 0^\circ$ do the "flats" appear simultaneously.

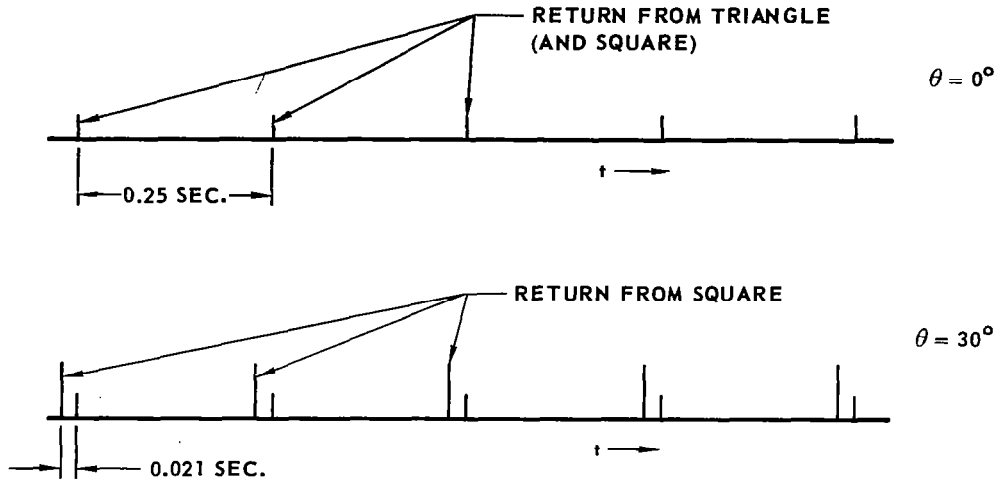


FIGURE 107 - TIMING OF SIGNAL RETURN

At look angles between $\theta = 0^\circ$ and $\theta = 180^\circ$, the triangle face appears before the square face. The amount of time lapsed between the appearance of a triangle face and the appearance of a square face is linearly, inversely proportional to the azimuth (or elevation) angle as shown in figure 108.

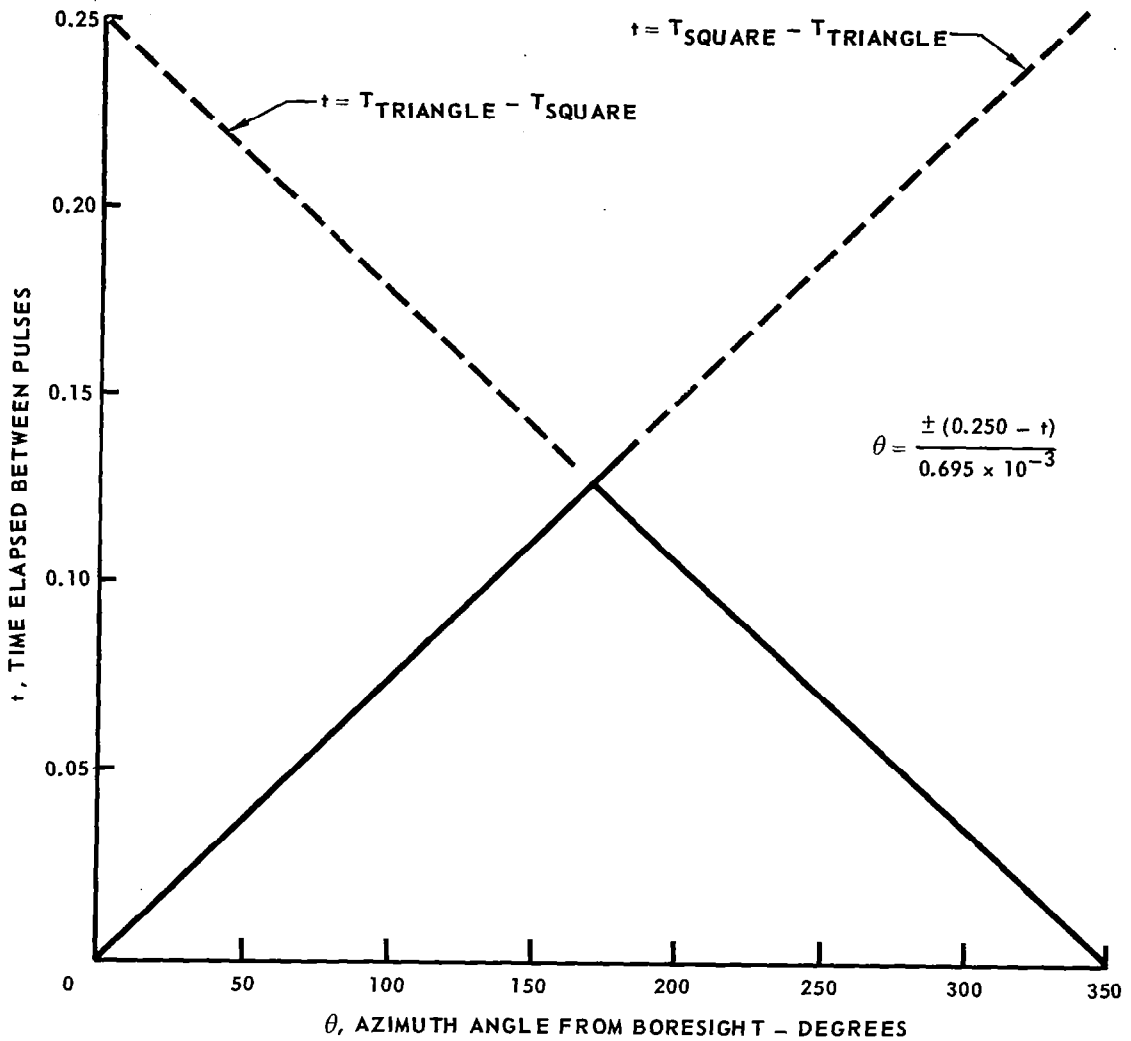
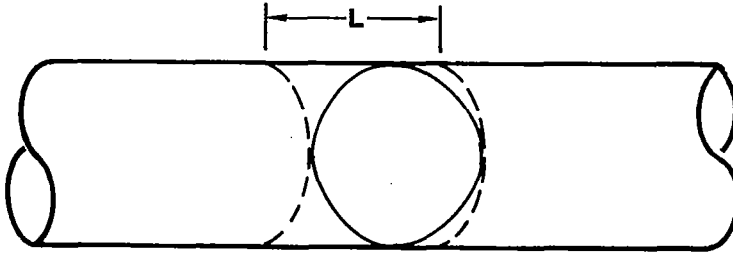


FIGURE 108 - TIME ELAPSED BETWEEN PULSES vs. AZIMUTH ANGLE OFF BORESIGHT

From 180° to 360° , the square face appears first and leads the triangle face by a time difference which is directly proportional to the increasing angles. These relationships provide the attitude determining capability.

With the use of a high microwave frequency radar system, (e.g., 70 GHz), the return from the rotating spheres will be very sharp (about 0.5° B.W.). Figure 109 shows the radar cross section calculation for the cylindrical section.



RADAR CROSS-SECTION OF CYLINDER

FOR SPHERICAL SQUARE $L = \sqrt{2R}$
 FOR SPHERICAL TRIANGLE $L = \sqrt{3R}$

RADAR CROSS-SECTION OF CYLINDER

$$\sigma = \frac{2\pi RL^2}{\lambda} \cos \theta \left[\frac{\sin(2\pi L/\lambda) \sin \theta}{2\pi L/\lambda \sin \theta} \right]^2$$

ASSUMING:

(1) THE RETURN OF THE OUTLINED SECTION IS 2/3 THE RETURN OF LENGTH L

(2) THE PATTERN FACTOR IN θ IS UNCHANGED

(3) THE PATTERN FACTOR IN ϕ IS $\cos \phi$

$$\sigma = \frac{4\pi R^3 \sqrt{2}}{3\lambda} \cos \theta \left[\frac{\sin(2\pi L/\lambda) (\sin \theta)}{2\pi L/\lambda \sin \theta} \right]^2 \cos \phi$$

FIGURE 109 – COMPUTATION OF REFLECTED ENERGY vs. ASPECT ANGLE

It can be seen that this system is not as attractive at X-Band and certainly not at L-Band. The normalized return from one face at 70 GHz is shown in figure 110. This directivity permits an aid of this type to become attractive. The mechanical aid would also provide a lock-on point for the gimballed antenna on the chascraft.

One face of a spherical square, at 70 GHz, with a 0.1 meter radius was calculated to have a radar cross section of 1.26 square meters, which could easily be seen at 100 feet by a 100 mw radar system with a moderate antenna gain.

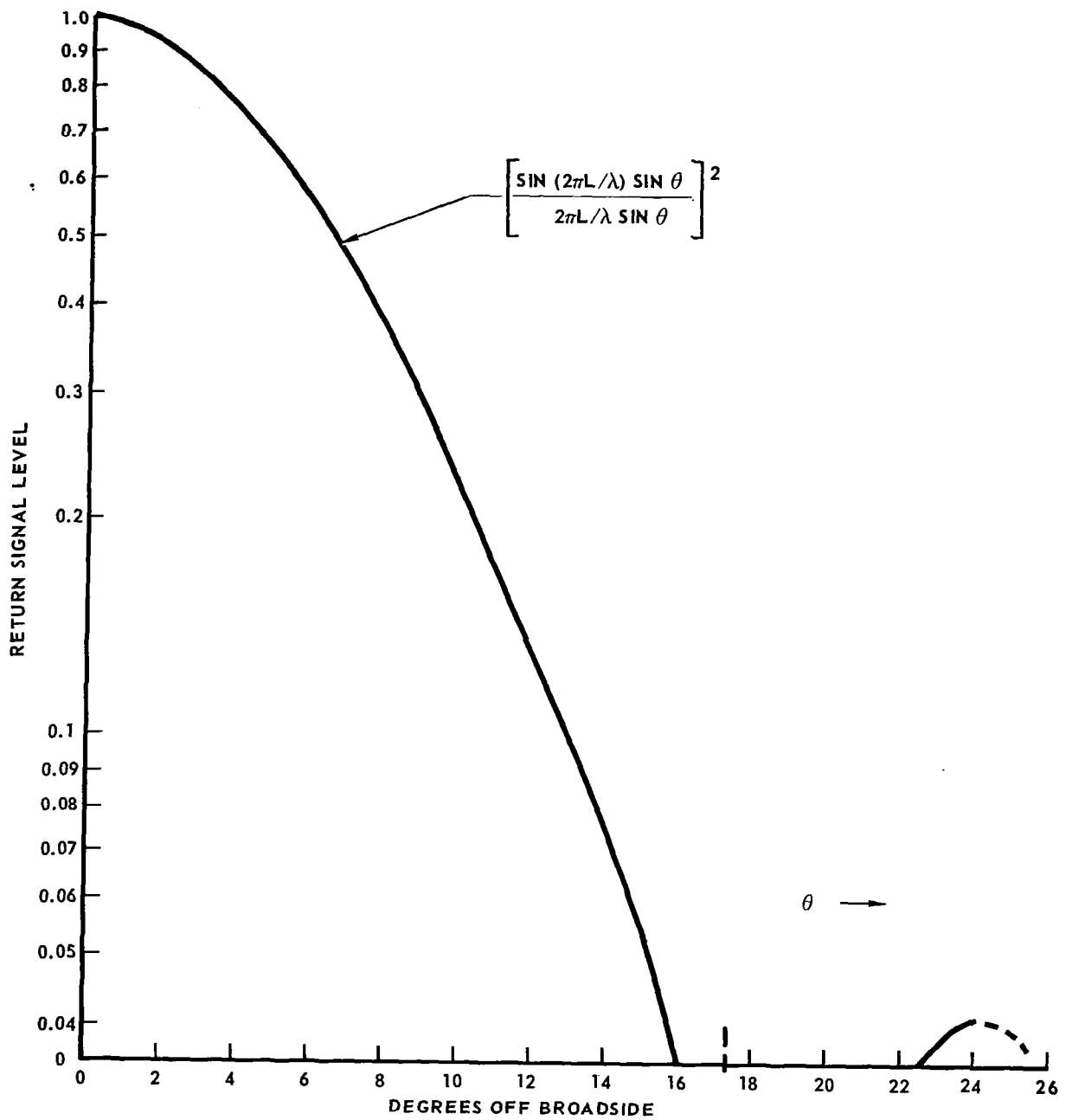


FIGURE 110 - AMPLITUDE PATTERN OF REFLECTED ENERGY

If the radar antenna is not highly directive, and illuminates much of the target vehicle including the mechanical aids, there is some limit as to how well the coded return can be separated from background clutter. (This factor would favor the use of high frequency, high antenna gain systems). If the background return appears fairly constant as compared to the coded information and exceeds it by about 20 db, the coded information should be easily separable. If, however, the clutter return is 40 db above the coded return level, the coded return represents a small percentage of amplitude modulation on the return signal and will be difficult to separate. Further investigation is required in this area. Also, when the clutter return has variations that appear at nearly the same frequency as the coded return, sophisticated processing circuitry is required in the "logic separator". A PRF gate offers a potential solution to this problem, however.

A block diagram of a proposed detection system is shown in figure 111.

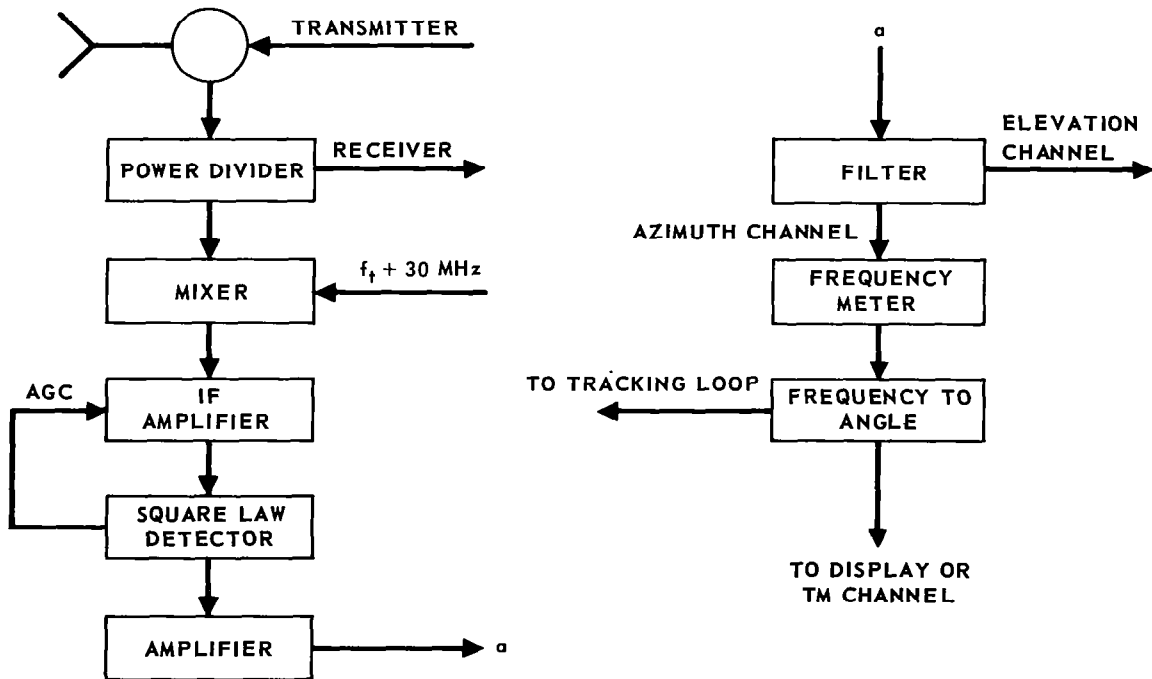


FIGURE 111 - MODULE FOR DECODING THE SIGNAL RETURN - ELECTROMECHANICAL AID

The coded information appears in the form of amplitude modulation of the return signal. The return signal is reduced to a coherent IF which is amplified. The AM code is then detected and amplified, and sent to the decoder. The decoder recognizes only signals which are followed by another signal in less than a prescribed time period. The time between the first and second signal is measured by gating on and off a high frequency counter. The count is then measured to give the angle from $\theta = 0^\circ$, in digital form. It is not known, at this point, whether the readout angle is clockwise or counterclockwise from $\theta = 0^\circ$. By moving one direction or the other, the ambiguity can be resolved. If the square return is made sufficiently larger than the triangle, it may be possible to resolve the ambiguity by an amplitude comparison of the pulses. Another similar mechanical aid can be placed at 90° from the first as shown in figure 112. This can be designed for rotation at different frequencies from the first for the purpose of separation before entry into the processing circuits. Alternately, the orthogonal mechanical aid can be made to reflect energy of the opposite polarization. This could be used to provide a means of separation for the azimuth pair from the elevation pair, rather than using different rotation rates; or it could offer some assistance in obtaining the relative roll angle between the two spacecraft. The polarized return method would suggest the use of a parabolic antenna on the chase-craft with three feeds, a circularly polarized transmitting feed, and horizontal and vertical receiving feeds.

This technique may have application with a radar system operating in the 70 GHz frequency region, such as one of the noncooperative radar systems.

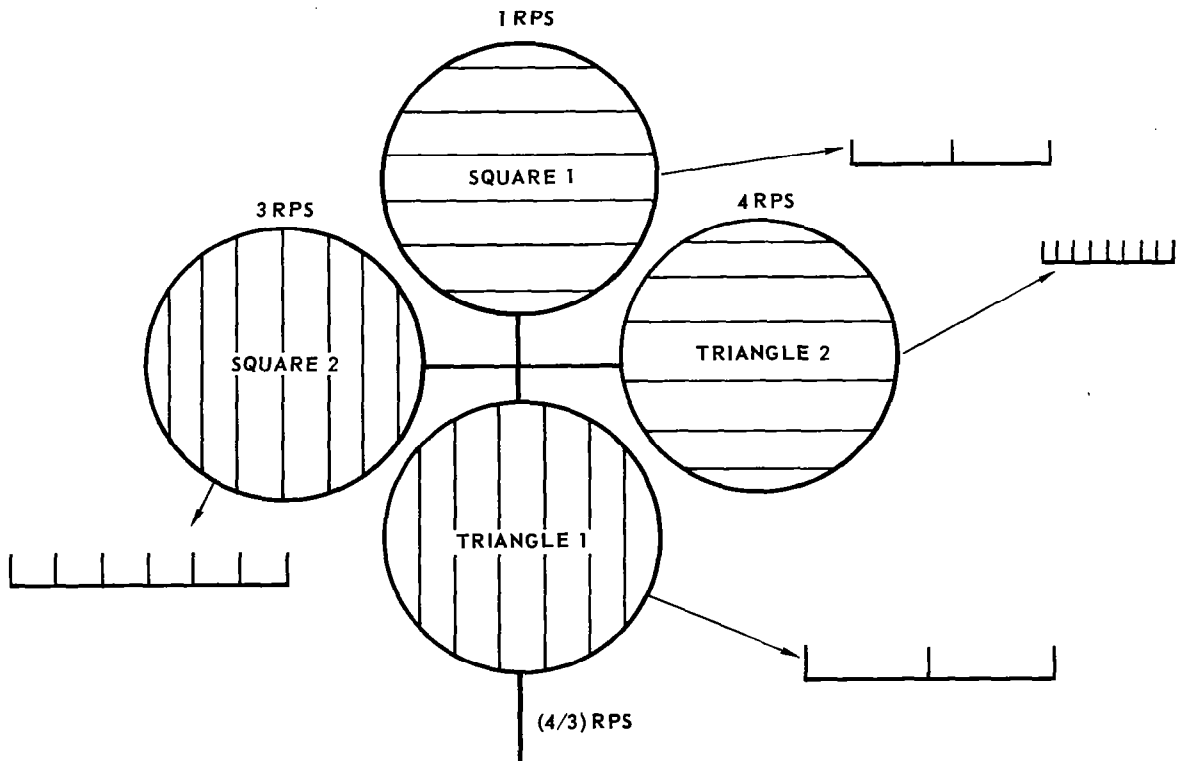


FIGURE 112 - ATTITUDE CODING BY ORTHOGONAL, POLARIZED, MOVING REFLECTORS

An Example of an Electro-Mechanical Coded Reflector. - The radiation pattern of a rotating cylindrical paraboloid reflector is made narrow in the plane of rotation (0.7°), and broad in the opposite plane (40°). A code, which contains the rotational position information relative to the roll axis of the target, is placed on the signal returned to the chasecraft.

A proposed system for accomplishing this is shown in figure 113.

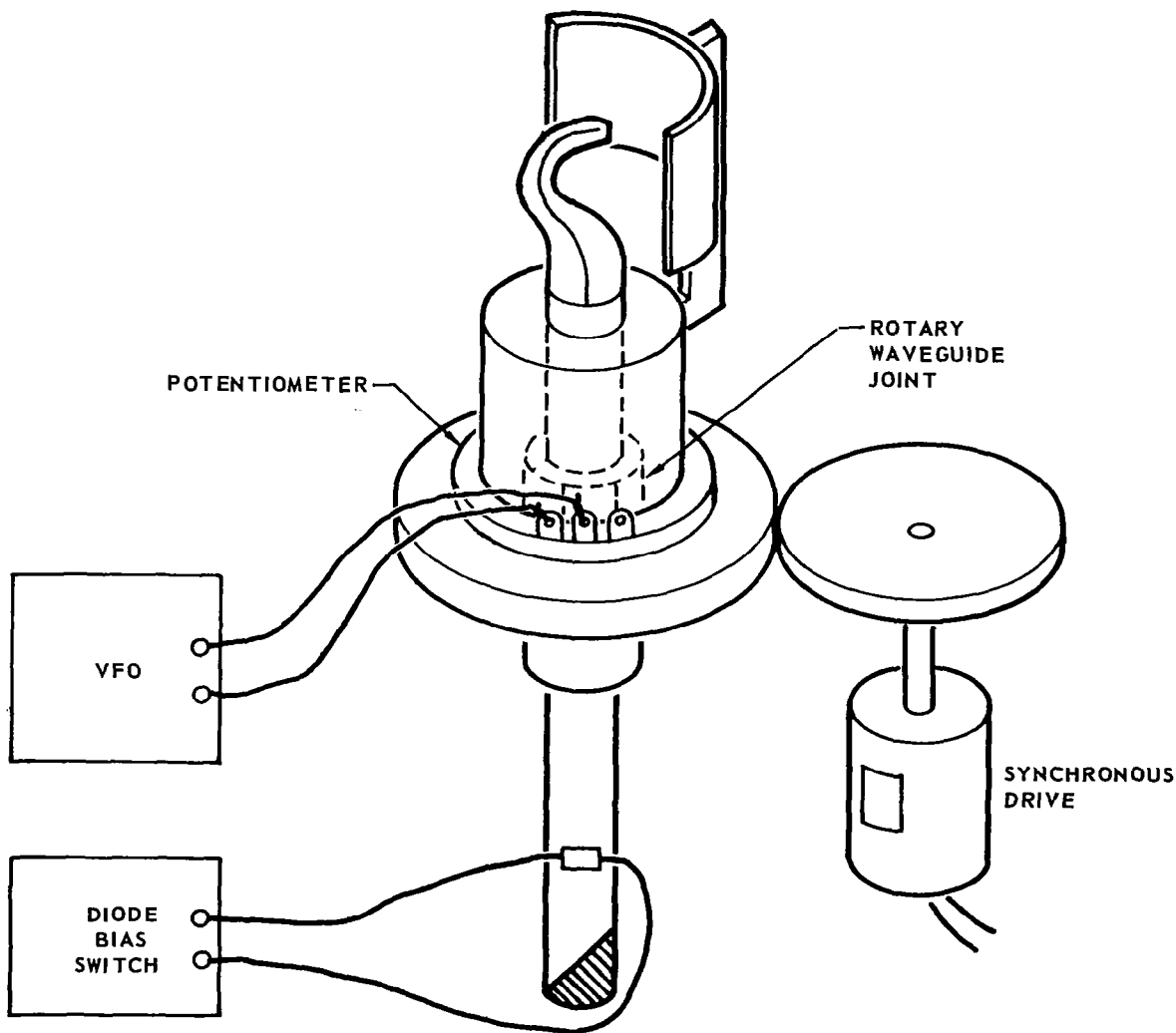


FIGURE 113 - AN ELECTROMECHANICAL ATTITUDE AID

As the antenna rotates at approximately 1 rad/s, the value of a potentiometer is varied as a function of shaft rotation. The potentiometer is an integral part of a variable frequency oscillator (V.F.O.), and controls its frequency. The V.F.O. operates within some convenient frequency (low RF) range, and controls the bias to a diode modulator which is placed in the waveguide line below the rotary joint. The waveguide is terminated in a perfect termination located below the diode modulator section. The waveguide is then alternately perfectly terminated and shorted, at a frequency controlled by the V.F.O. which is, in turn, controlled by the shaft position.

In comparing this system to the rotating spherical squares and triangles, it can be seen that a little more equipment complexity is involved at the target vehicle, but the docking vehicle system is even less complex than before. A simple modification to the basic range, range rate radar for separating and measuring the frequency of the AM coding on the return signal will provide one attitude angle.

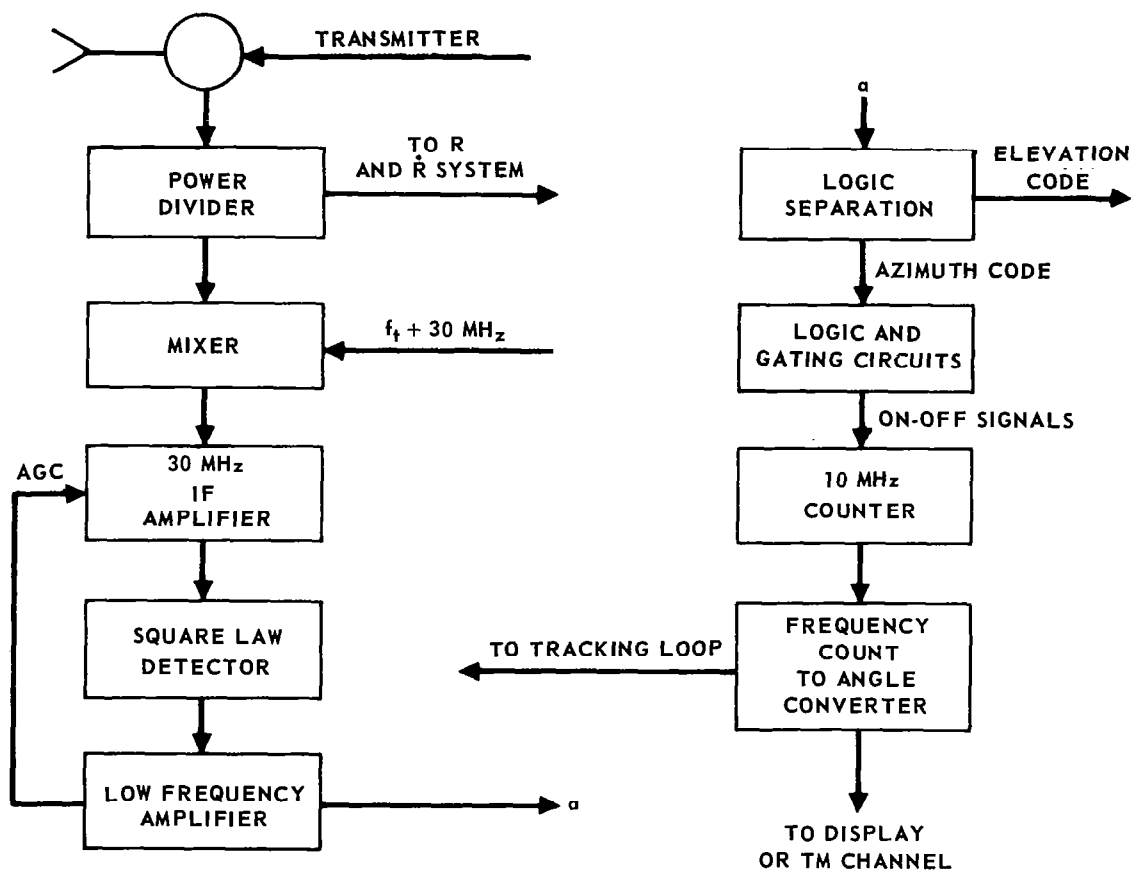


FIGURE 114 - MODULE FOR DECODING THE SIGNAL RETURN FROM MECHANICAL AID

Frequency Coded Beacon

The target can establish a frequency coded radiation pattern which can be detected by the chasecraft to determine target aspect.

Consider four circularly polarized antennas arranged as in Figure 115, each equipped with a separate electronic beacon operating in the region of 1 GHz. The antennas are arranged as a local azimuth pair and a local elevation pair. Each antenna is squinted 45° with boresight (roll axis) and each antenna is squinted 90° with the other pair member. The 3 db (or 6 db) cross-over of all antennas falls on boresight. The electronic beacon transmitters differ in frequency by an amount which (a) will be great enough to be easily separable by the chasecraft, (b) will be small enough to permit the use of one receiving antenna, and (c) will minimize EMI interaction. Simple 1 watt (or less) cw beacons with high amplitude stability are all that is required for operation to a range of a mile or more.

A fifth linearly polarized antenna with separate beacon which is aligned on boresight can be used for relative roll angle sensing. One or two more antennas and beacons may be desirable to fill in the solid space angle coverage to insure acquisition.

The radar cross section of the cylindrical paraboloid antenna can be calculated roughly as follows:

$$\begin{aligned} G \text{ in } \theta \text{ direction required for } 0.7^\circ, 3 \text{ db BW} &= 24 \text{ db} \\ G \text{ in } \phi \text{ direction required for } 40^\circ, 3 \text{ db BW} &= 6 \text{ db} \\ G = G_\theta + G_\phi &= 30 \text{ db} \end{aligned}$$

Using an operating frequency of 70 GHz:

$$\sigma = \frac{G^2 \lambda^2}{4\pi} = 10^6 (4.7 \times 10^{-3})^2 = 1.75 \text{ m}^2 \quad (391)$$

The required dimensions of the antenna are as follows. For 24 db gain in the " θ " direction a 15" parabola is required. The gain in the ϕ direction is controlled by the feed. An 8" reflecting surface should be sufficient as the antenna width. For practical design considerations, it is probably better to tilt the reflector back so that it will not illuminate the vehicle on which it is mounted, to minimize reflection problems. Two such docking aids mounted at right angles provide two of the three attitude angles. Relative roll is not provided by this method.

The chasecraft receives all of the beacon frequencies with an integrated receiver that has outputs corresponding to each beacon frequency. The outputs can be made DC, 1000 Hz, or whatever is convenient for processing. Amplitude comparisons are made as indicated in figure 116 to obtain the α and θ attitude angles. Other comparisons may be desirable in the final analysis, but the comparisons as shown were chosen because:

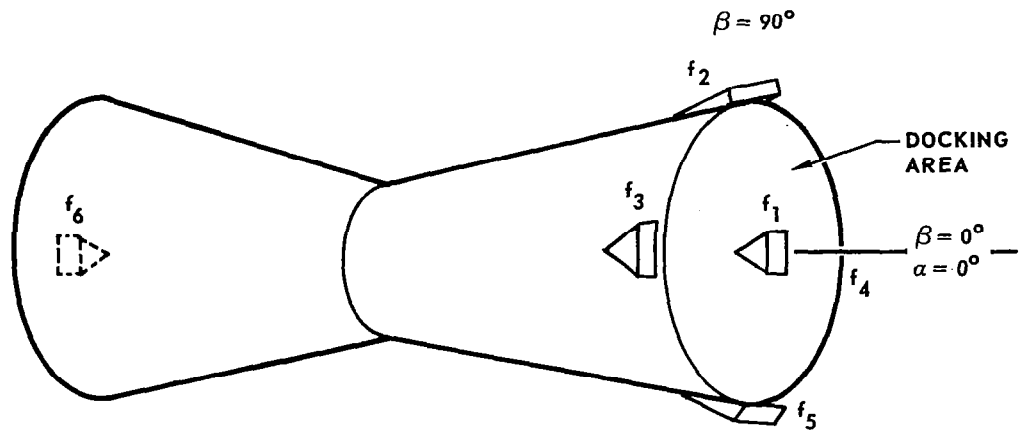


FIGURE 115 - TARGET ATTITUDE BY SQUINTED BROAD BEAM ANTENNAS

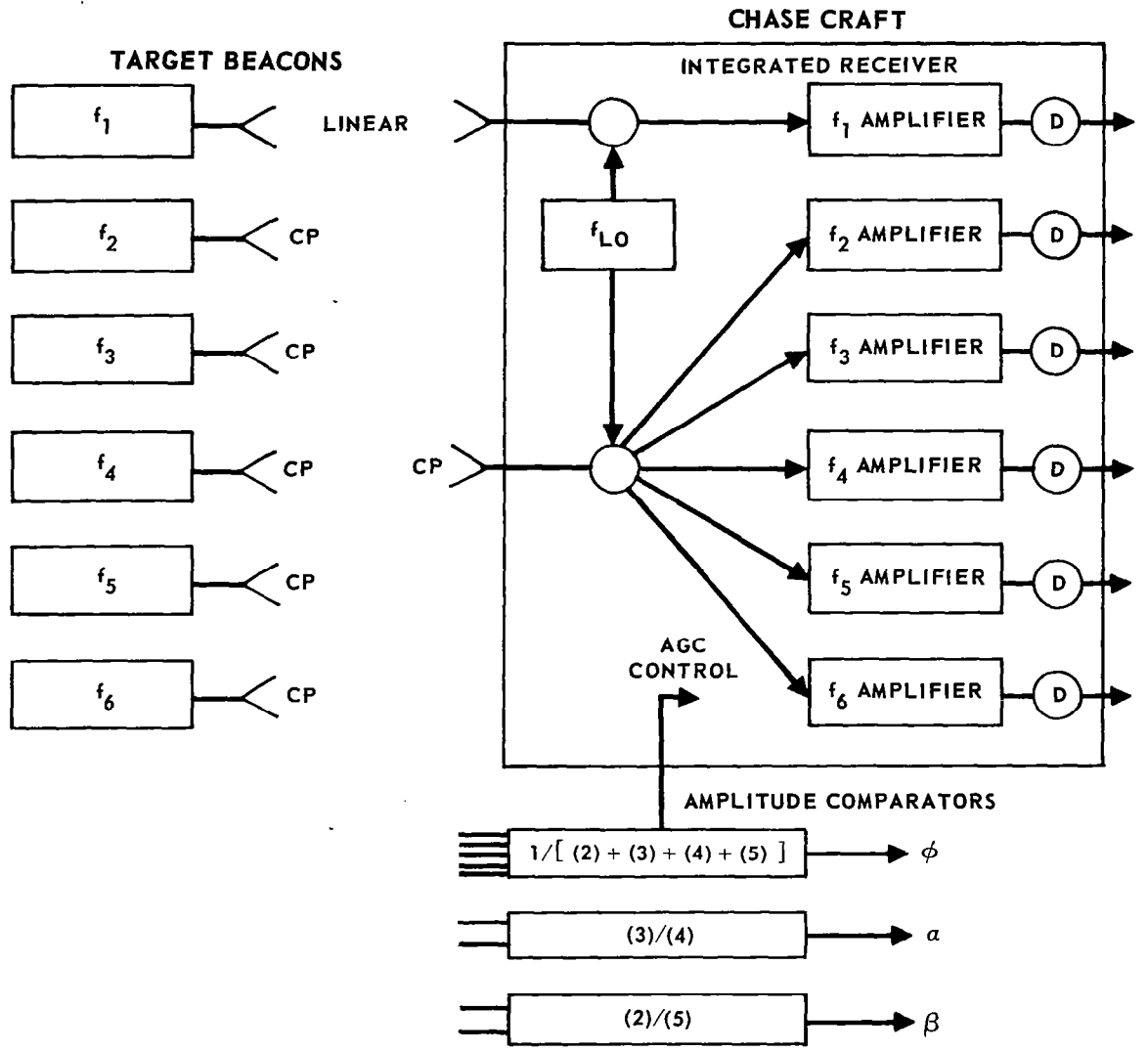


FIGURE 116 - AMPLITUDE COMPARISON

(a) The ratios formed by the α pair are reasonably independent of β angle as shown in figure 117, and vice versa.

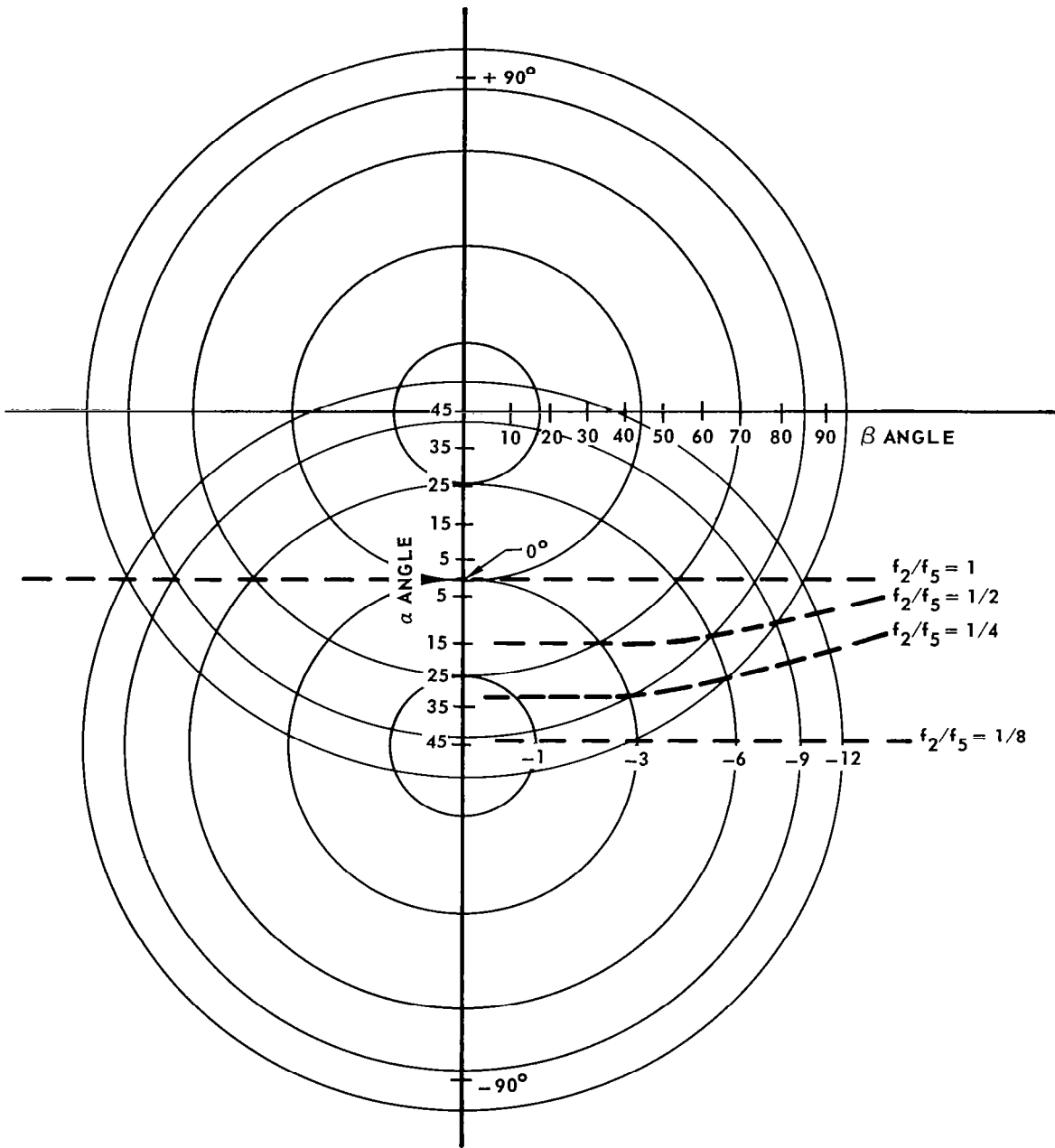


FIGURE 117 – VARIATION OF AMPLITUDE RATIOS AS FUNCTIONS OF THE TARGET ATTITUDE ANGLES

(b) The ratios are fairly linear measurements of the off-boresight angle, near boresight, as shown in figure 118.

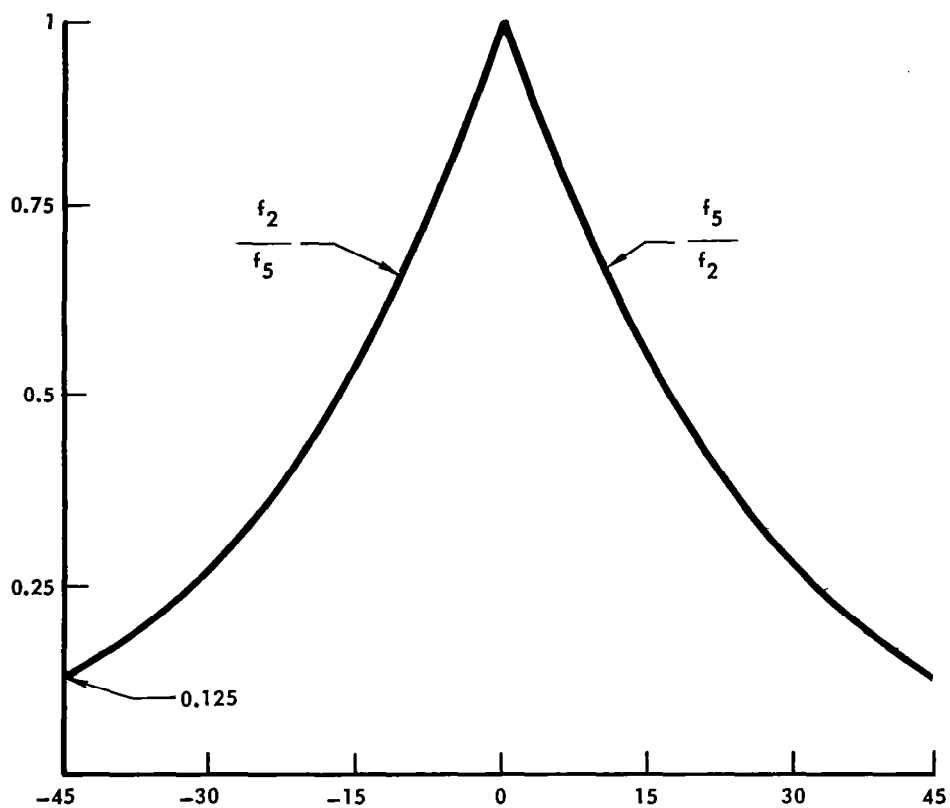


FIGURE 118 - AMPLITUDE RATIO AS A MEASURE OF TARGET ATTITUDE

(c) A roll angle error signal can be formed with a fairly consistent reference base, as shown in figure 119.

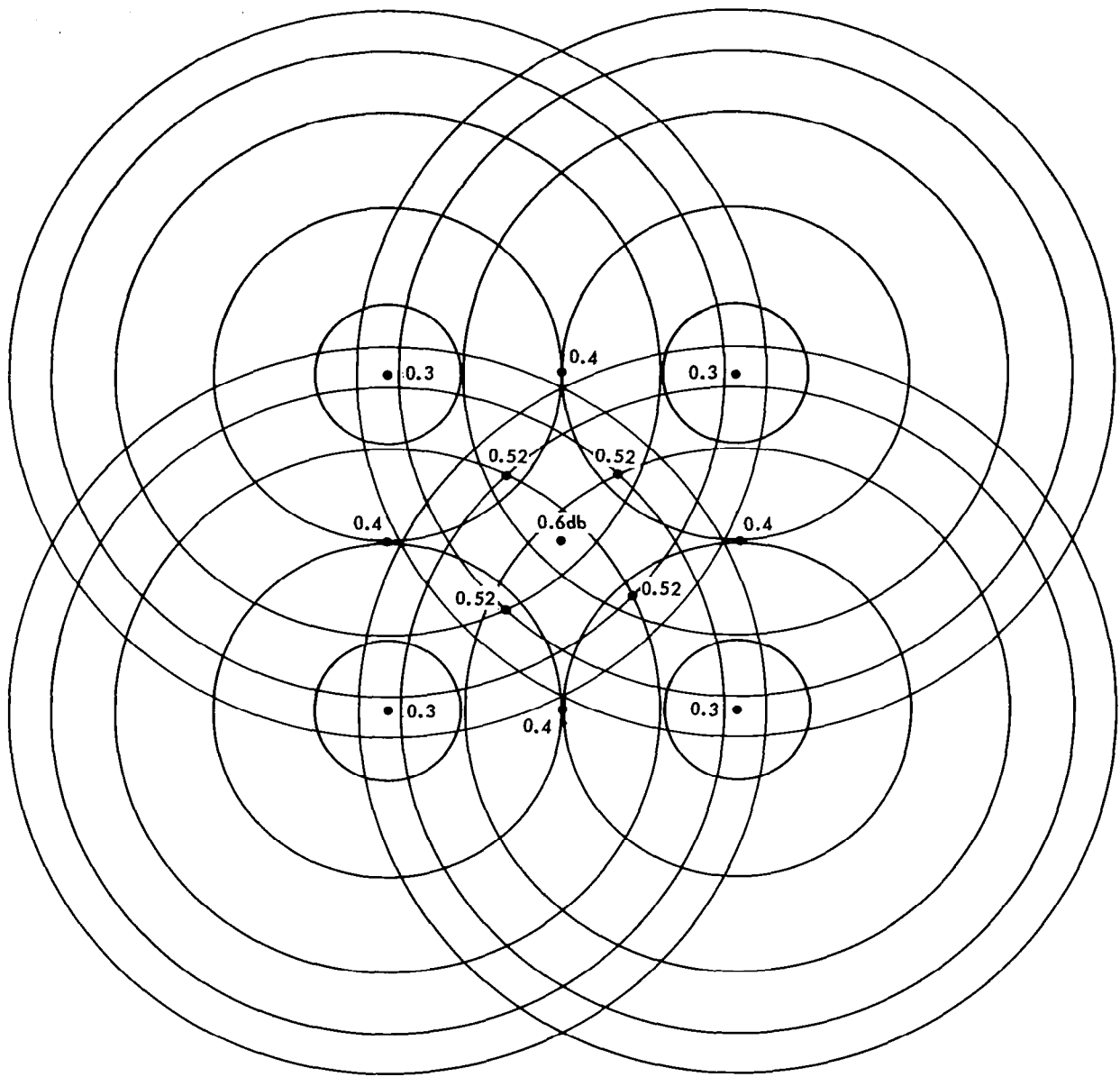


FIGURE 119 – SUPERIMPOSED CONTOUR PLOTS OF FOUR ANTENNAS
SQUINTED 45° WITH ROLL AXIS
(90° 6db – BEAMWIDTHS)

It must be pointed out that a 180° ambiguity in ϕ exists. The logic and control laws associated with this type system must therefore, be sufficiently sophisticated to make a test on ϕ by moving in one direction or the other and determining whether α and/or β increases or decreases. This will resolve the ambiguity. This type system would probably not be applicable for determining the precise magnitudes of α , β and ϕ when far from alignment, but would appear to be very useful if only the approximate magnitudes and directions are needed to implement a control system which becomes increasingly more accurate as alignment is approached.

Some errors which are common to amplitude comparison systems are:

- (a) unequal channel gain, (b) channel noise, and (c) pattern perturbations.

It is sometimes difficult to maintain two separate channels at exactly the same gain, especially high gain channels. Channel imbalance shows up directly as angle error. As can be seen from figure 120, the angle error is equal to the channel imbalance times the slope of the radiation pattern plot at the point of measurement.

For example, if the measurement is made at the cross over point of the broad lobes, and if the channel imbalance is 0.1 db (or in the case of the example, if the transmitted power varies by 0.1 db), the angle error will be as follows:

$$\Delta\theta = k_1 P \quad , \quad (392)$$

$$\Delta\theta = (5^\circ/\text{db})(0.1 \text{ db}) = 0.5^\circ \quad , \quad (393)$$

where :

$$\theta = (5^\circ/\text{db})(0.1 \text{ db}) = 0.5^\circ$$

θ = angle error

k_1 = slop of radiation pattern (in db)

P = is the imbalance in channel

$$k_1 = 5^\circ/\text{db}$$

On the narrow lobes squinted at 90° , where k_2 is $1.2^\circ/\text{db}$, the error is:

$$\Delta\theta = k_2 P \quad , \quad (394)$$

$$\Delta\theta = (1.2^\circ/\text{db})(0.1 \text{ db}) = 1.12^\circ \quad . \quad (395)$$

Consider the case of a single receiving antenna and a single point radiator. If the receiving antenna is oriented for its maximum gain in the direction of the reflection, the signal level in Channel A may be calculated as follows:

$$E_r = kE_m + RE_{me} j\phi = E_m (k + R_e j\phi) \quad , \quad (396)$$

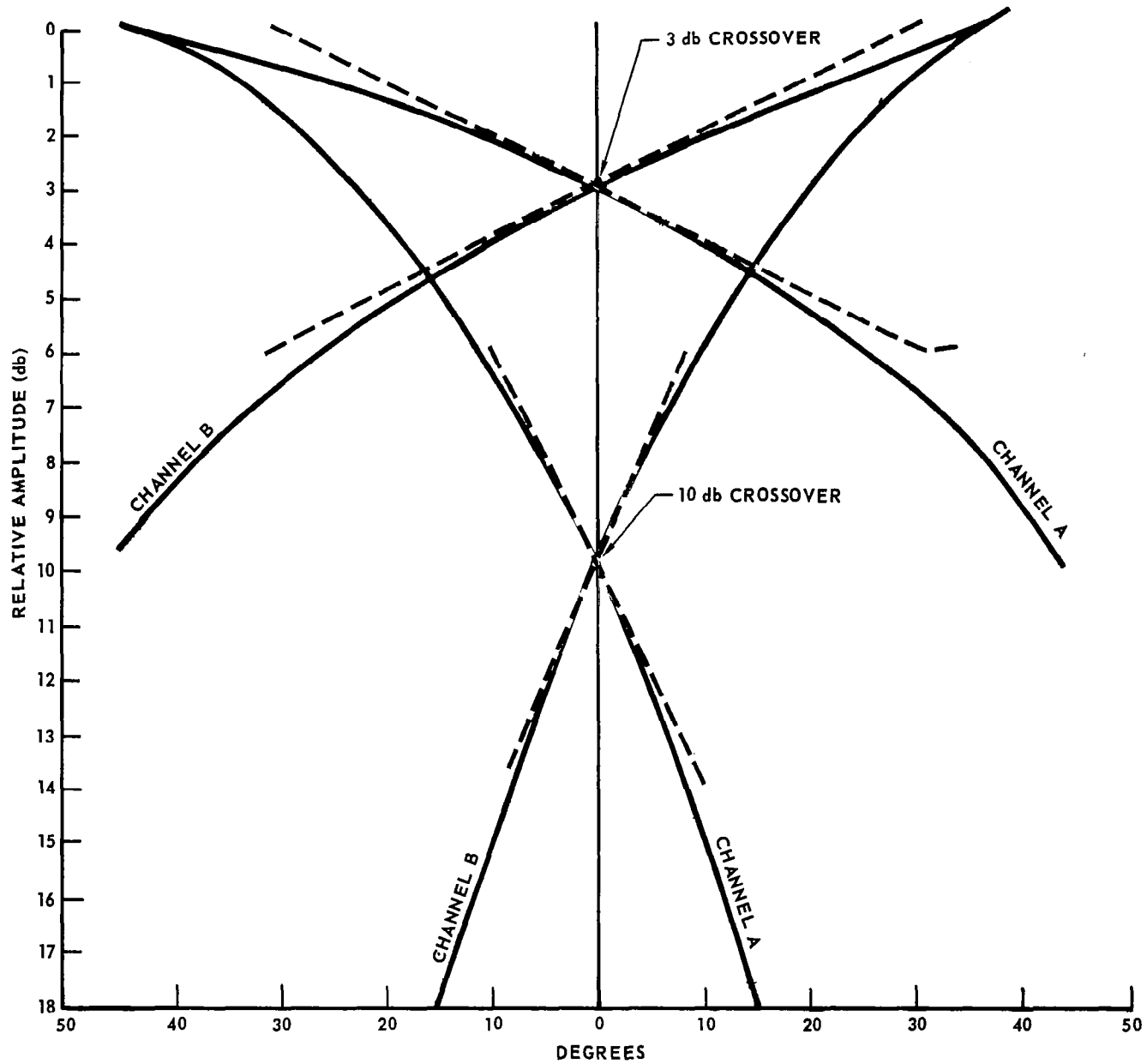


FIGURE 120 - SQUINTED BROAD BEAM ANTENNA CROSSOVER PATTERNS

where:

- E_m is the magnitude of the direct signal (at maximum orientation)
- E_r is the magnitude of the received signal
- k is the pattern taper factor
- R is the ratio of the indirect to direct signal level
- ϕ is the relative phase

Boresight shifts resulting from the reflected signal are plotted in figure 121.

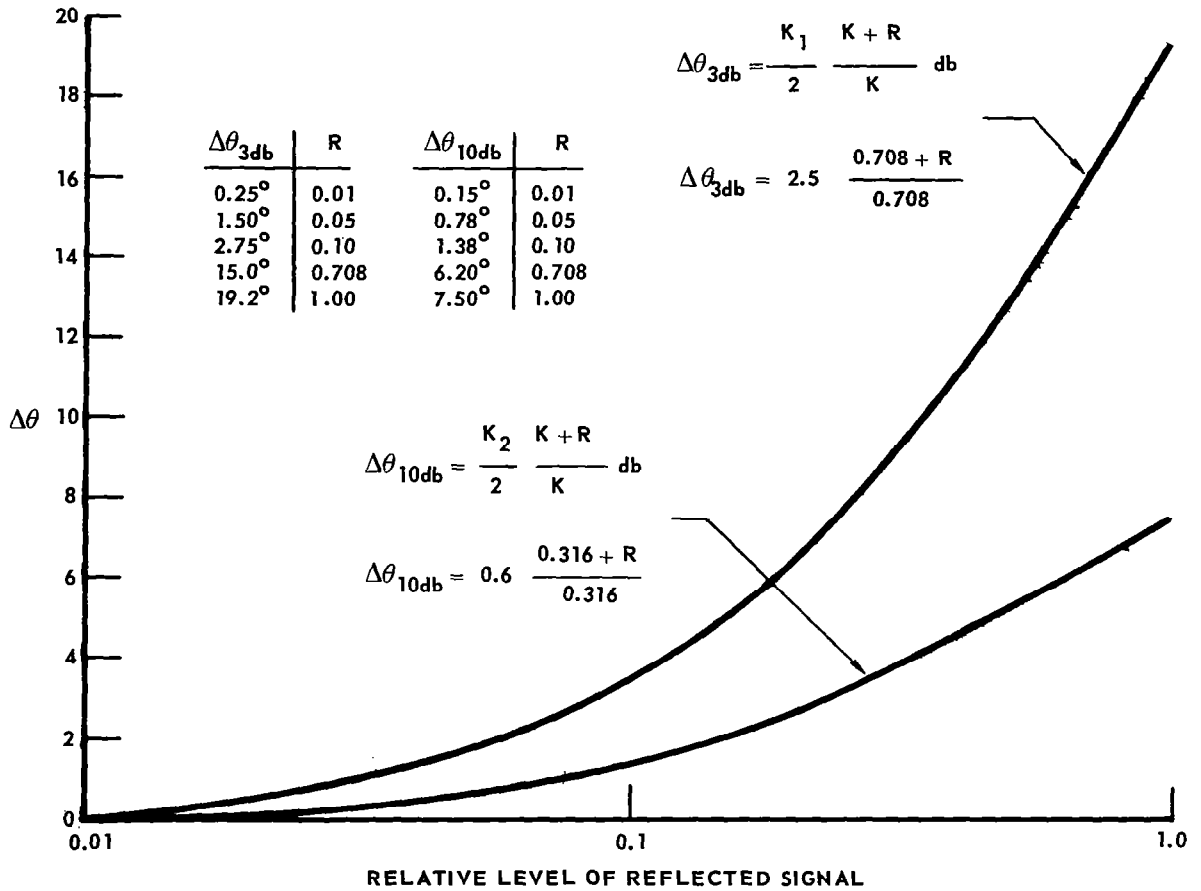


FIGURE 121 - MULTIPATH ERROR EFFECTS

The antenna patterns within the 3 db points can be closely approximated by:

$$e^{-[(\theta - \theta_s) a]^2} \text{ and } e^{-[(\theta + \theta_s) a]^2}, \quad (397)$$

where:

θ is the pointing angle measured from the boresight,

θ_s is the squint angle,

$$a = \frac{2}{\theta_{BW}} \sqrt{m^2},$$

$\theta_{BW} = 3$ db antenna beamwidth .

Thus, the ratio of the signal returned from the right channel (direction of positive angle) to the signal in the left channel is given by:

$$S_1/S_2 = e^{4\theta_s a \theta} \quad (398)$$

Taking the logarithm of both sides:

$$\ln S_1 - \ln S_2 = 4\theta_s a \theta \quad (399)$$

The standard deviation in θ due to noise in S_1 and S_2 can be obtained as follows:

$$d\theta = \frac{1}{4\theta_s a} \left(\frac{dS_1}{S_1} - \frac{dS_2}{S_2} \right), \quad (400)$$

$$\text{and } \sigma_\theta = \frac{1}{4\theta_s a} \sqrt{\frac{\sigma_{S_1}^2}{S_1^2} + \frac{\sigma_{S_2}^2}{S_2^2}}.$$

where $\sigma_{S_1}^2$ and $\sigma_{S_2}^2$ represent the total noise power in Channels 1 and 2 respectively.

Therefore:

$$\sigma_\theta = \frac{1}{4\theta_s a} \sqrt{\frac{1}{(S/N)_1} + \frac{1}{(S/N)_2}} \quad (401)$$

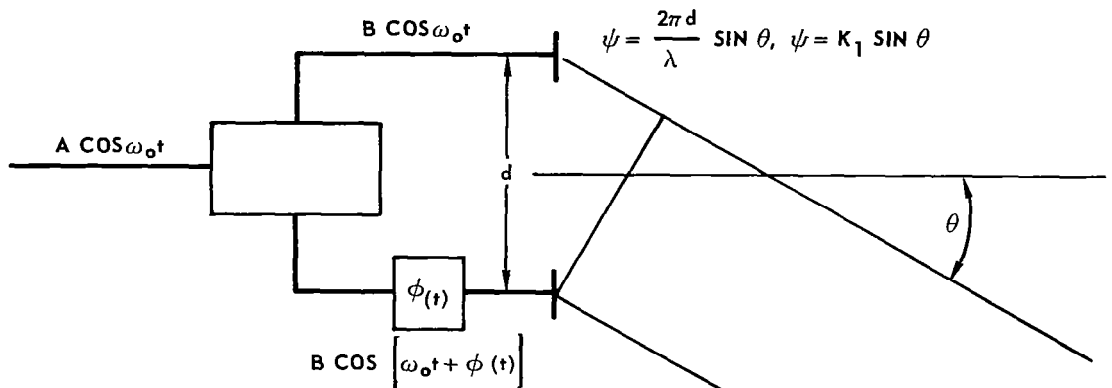
Where $(S/N)_1$ and $(S/N)_2$ represent the signal-to-noise ratios in Channels 1 and 2 respectively. It can be seen that the standard deviation in θ is relatively constant at all angles because the variations in $(S/N)_1$ and $(S/N)_2$ are inversely related.

Electronic Attitude Coding Using Beacons

Another promising system is, in some respects, comparable to the familiar "Omni" Airline Navigational System. This technique requires only simple, reliable, relatively inexpensive equipment on the target vehicle and only small additions to a cooperative range, range rate, LOS radar. In addition to retaining the capabilities of the previously mentioned techniques:

- (a) This technique lends itself well to integration with the favored cooperative PM-CW radar-transponder system, or it can be used as a supplement to a basically non-cooperative system.
- (b) It can function at long ranges (as well as short) for integration into the rendezvous mission phase, as well as the docking phase.
- (c) Relative roll angle is provided.

The technique utilizes two radiators, spaced about $1/4$ wavelengths apart. (see figure 122).



$$e(t) = B \cos \omega_0 t +$$

$$e(t) = B \cos \omega_0 t + B \cos [\omega_0 t + \phi(t)]$$

$$e(t) = \text{Re} [B (e^{j\omega_0 t} [1 + e^{j\phi(t)}])]$$

$$e(t) = B \cos \omega_0 t [1 + \cos (\phi(t) + \alpha)]$$

$$e(t) = B \cos \omega_0 t + B \cos \omega_0 t \cos (\phi(t) + \alpha)$$

THE SECOND TERM CAUSES THE RECEIVED SIGNAL TO BE OF BESSEL FUNCTION FORM WHEN $\phi(t)$ IS A SINUSOID.

FIGURE 122 – NULL SWEEPING USING A PHASE SHIFTER

The phase of one is made to lead (or lag) the other in a specified manner so as to provide the well known rotating null, radiation pattern. If the phase of one is varied cyclically from 90° to 180° to 270° to 180° to 90° with respect to the other, in one period, the null of the cardioid will move through 180° and back to its starting point. This relationship is shown in figure 123.

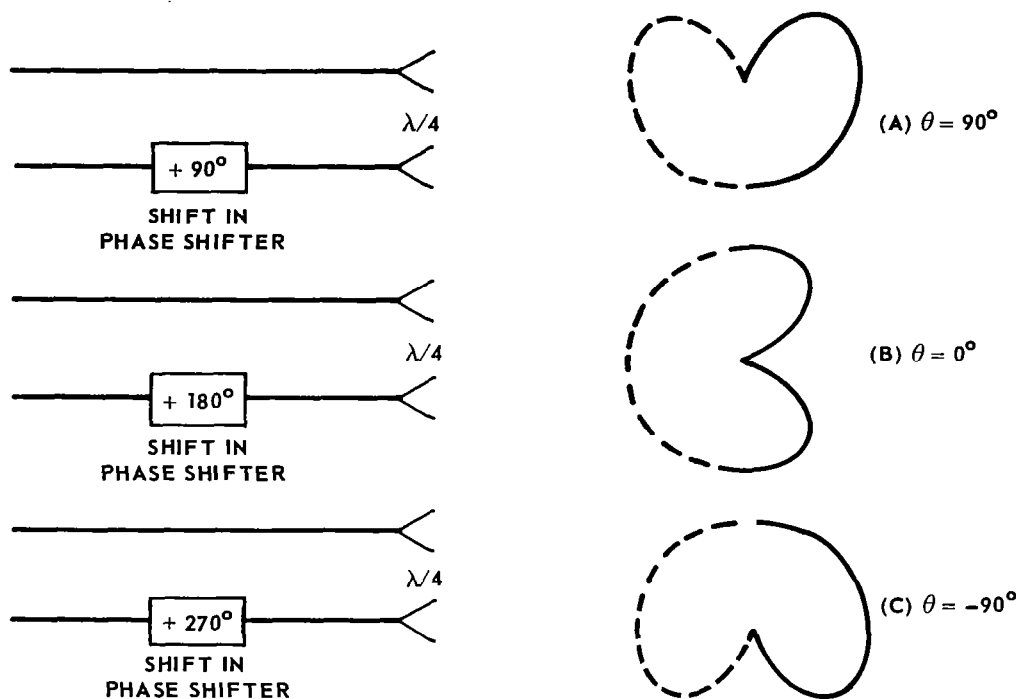
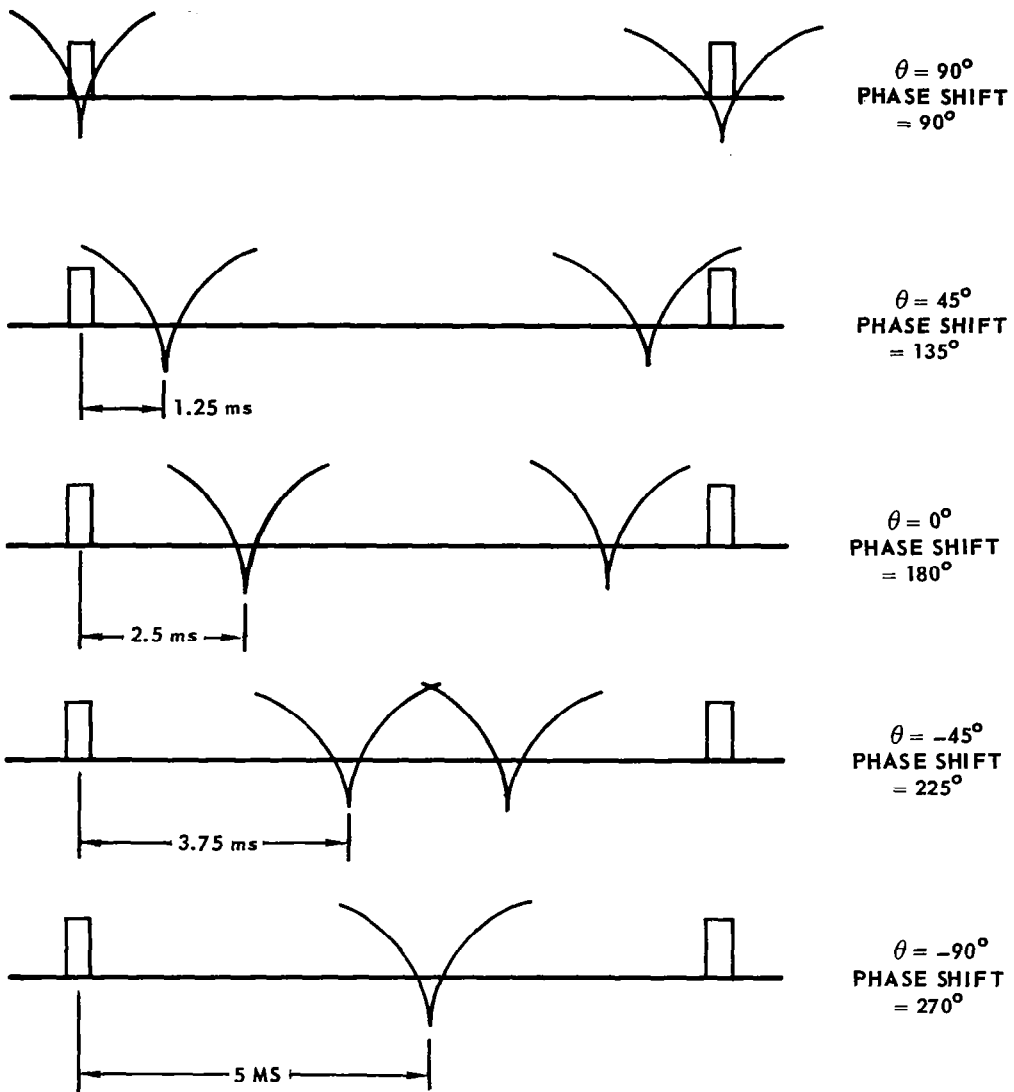


FIGURE 123 - PHASE SHIFT - PATTERN NULL RELATIONSHIP

The phase shifter is driven sinusoidally to provide linear movement of the null. This can be seen by inspection of the expression for received signal in figure 122.

One technique of coding the information is to send a reference burst of modulation on the carrier when the cardioid null appears at, for example, $\theta = 90^\circ$. The null in the cardioid will appear at some later time, which can be made a linear, unambiguous function of the " θ " angle. For example, let the burst reference signal be a 10 us pulse of 30 MHz modulation. Let the repetition rate be 100 Hz. Let each complete cycle of phase shift (90° to 180° to 270° to 180° to 90°) also occur at a 100 Hz rate. The time between the reference burst and the pattern null will be as shown in figure 124.



PLUS ANGLES ABOVE BORESIGHT (+ θ)

MINUS ANGLES BELOW BORESIGHT (- θ)

FIGURE 124 - TIME ELAPSED - REFERENCE BURST TO PATTERN NULL

If a 10 MHz counter is used in the docking vehicle, a one degree measurement will yield over 10 thousand counts. The primary factors that limit the accuracy of the system will be (a) the ability to obtain the center or leading edge of the reference burst pulse, (b) the depth of the pattern null, (c) the ability to find the center of the pattern null, and (d) false nulls, null broadening and null shifts, due to multipath interference, radiation pattern impurity, and inadequate S/N ratio.

In order to obtain relative roll angle, one additional antenna may be required, which is spaced as far as possible from the reference antenna. Roll information may be obtained by measuring the time from the null interception of the roll reference antenna to interception of the other antenna in the pair. The roll error signal can be made a function of this time measurement plus a logic determination of which antenna in the pair receives the null first. An ambiguity point is apparent in this type arrangement but the ambiguity point can be made unstable. This will be discussed further in a later section. It should be pointed out that a second channel can be added which is orthogonal to the first, if a complete unambiguous determination of the ϕ angle is desirable for the application of an improved control law, especially in the area of the "unstable" ambiguity point of the single roll channel technique.

Integrated Phase Techniques

An integrated phase system is capable of measuring target attitude and target attitude rates by phase measurements at the chasecraft. As previously discussed, one angle can be obtained by measuring the relative phase of the voltage induced in two antennas by a signal received from a distant source. Conversely, the same angle can be measured by coding a transmission from the two antennas and comparing the phase of the two received signals at the distant point. This coding can take the form of controlled modulation of the two signals, or a coherent signal can be switched alternately to each antenna and synchronously separated at the receiver. This latter technique is particularly attractive for determining target attitude. The target transponder output is switched to each of its three antennas in a programmed sequence. The chasecraft processes this time interlaced signal as received by each of its three antennas to determine the difference in the transmission path lengths. These differences are further processed to define target attitude with respect to the LOS and relative roll (as well as the LOS angles).

TARGET ATTITUDE RATE DETERMINATION TECHNIQUES

Target attitude rates can be determined from the attitude measurements discussed in the previous section. However, for cases in which target attitude cannot be obtained, other techniques will be required for obtaining rotation rates. Some of these techniques are: the sequential painting technique using a scanning narrow beam antenna, which obtains returns from different portions of the target sequentially; the quasi optical lens system using a field of sensors, which obtain returns from different portions of the target simultaneously; the short pulse radar technique using range resolution, which obtains returns from equirange elements of the target; and the signature analysis of radar returns using complicated processing, which receives returns from the entire target.

Target Scanning

By the use of a narrow beamwidth antenna with the radar system it is possible to scan the target in small systematic increments for the determination of its size and shape. Range, as determined by one of the methods outlined earlier, will be required to give significance to the scan data for an interpretation of size. The scanning process can theoretically be accomplished by (a) mechanical movement of the feed and/or the reflector of a parabolic reflector antenna, (b) systematic sampling with the multiple feeds of a parabolic reflector, (c) systematic sampling of the multiple feeds of a dielectric lens, (d) beam steering of a multielement array, (e) ferromagnetic beam steering, and so on. The mode of scan can be continuous or sequential. The target can be illuminated entirely over a one scan period (one frame) or one frame might only sample portions of the target, corresponding to restricted beam positions.

Useful data on target characteristics is needed at a range of about 100 feet, and will require a resolution of approximately one square foot. This requires a 50 db antenna, having a beamwidth of 0.5° . A 50 db antenna is of reasonable size at 70 GHz, but it can be seen that at 10 GHz, the size becomes impractical.

<u>Gain (db)</u>	<u>Frequency (GHz)</u>	<u>Size (inches)</u>
50	70	21.5
50	40	38.0
50	10	150.0

The distance required for the far field beam formation of an antenna is generally considered to be:

$$R = \frac{2D^2}{\lambda} , \quad (402)$$

where D is the diameter of the parabolic reflector (or the largest dimension of the horn) and λ is the wavelength in the same dimensional units. Since R increases with the square of the diameter and the first power of the operating frequency, an advantage is apparent in the use of higher operating frequencies.

A .5° beamwidth (50 db gain) antenna at 70 GHz would be suitable for "spot" scanning at 100 feet. However, as the range is decreased, beam defocusing effects cause the spot diameter to oscillate about a 1 foot average value. Figure 125 is a plot of the 3 db diameter spot size as a function of range for several different beamwidth antennas. As can be seen from this plot, a minimum spot size is reached for each beamwidth, at some specific range, and below this value a smaller spot size can be obtained only with a wider beamwidth antenna (appendix G).

For the investigation of a noncooperative tumbling object, it is desirable to remain at some distance, until information is gathered about the target. A distance of 100 feet represents a good compromise between safety and resolution. A separate antenna may be required for close approach if additional target scanning is required. A simple solution might be to turn the reflector feed around (180°) for use as the close approach antenna.

If the radar return is quantized into either a "return present" or "no return present," this will minimize the complexities associated with the magnitude of the return versus vehicle size, shape orientation, etc. If the quantized information is stored, along with the antenna pointing information, an outline of the object can be obtained at each scan frame, within the limits of the system resolution.

Table 8 shows scan speeds required as a function of tumble rates, based on restricting target rotation to not more than 10° in one frame to avoid significant image degradation.

TABLE 8 - SCAN RATE REQUIREMENTS

TARGET TUMBLE (°/SEC.)	SCAN SPEED
1	1 FRAME/10 SEC.
10	1 FRAME/SEC.
100	10 FRAMES/SEC.

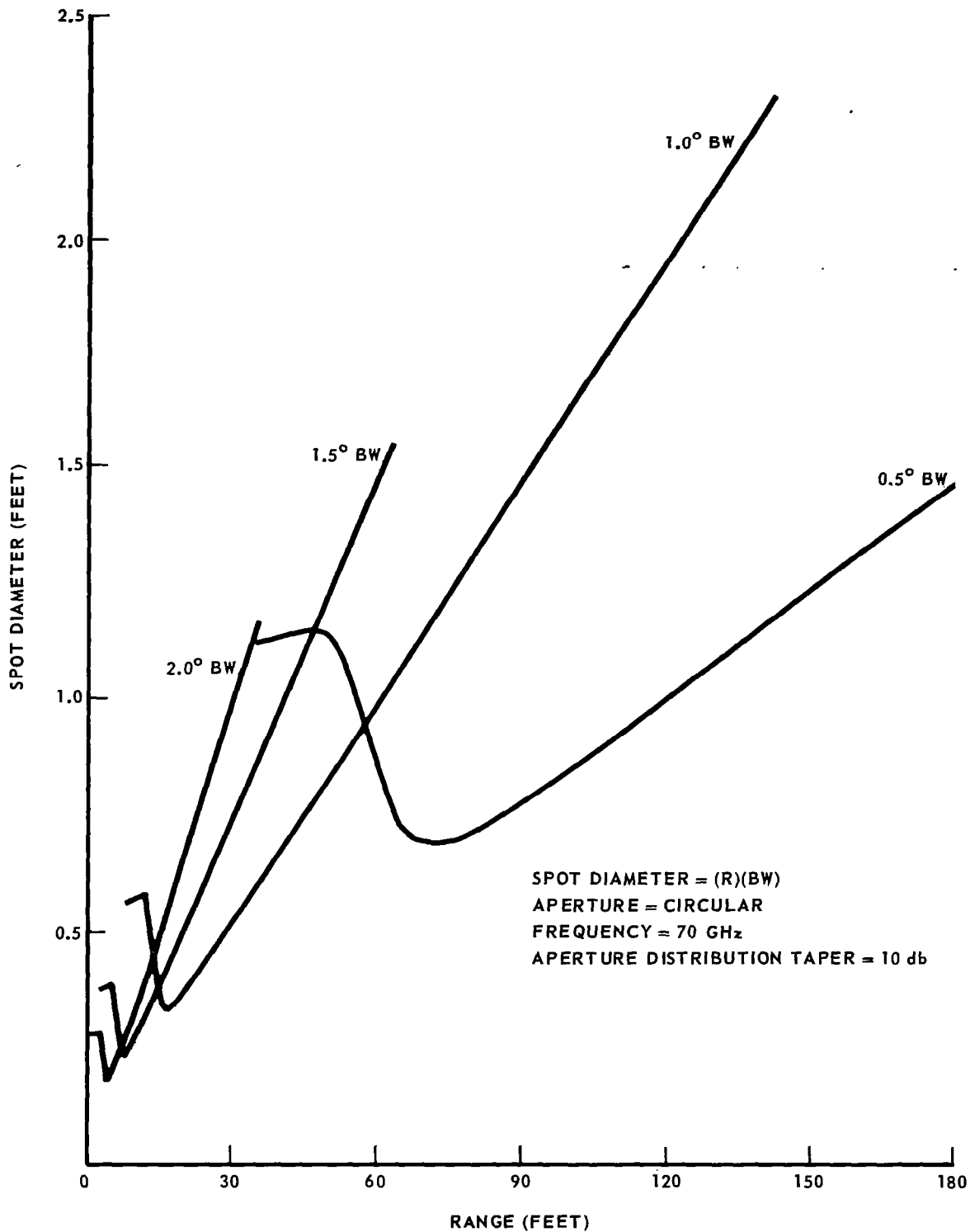


FIGURE 125 – SPOT DIAMETER vs. RANGE

Table 8 shows that a target tumbling at greater than 10° /second will probably require electronic rather than mechanical beam steering. Sequential lobing would be more easily instrumented electronically than continuous beam steering if a minimal number of beam positions is required. It is questionable whether or not the beamwidth can be made small enough using ferromagnetic steering, otherwise this technique would appear very desirable for rapid scan rates. Beamwidth considerations also greatly limit the use of steerable multielement arrays. Several hundred slots would be required in a linear slot array to provide a one degree beam width. A parabolic reflector with multiple feeds would not appear to be the perfect solution either, since only a few degrees of steering can be obtained without moving the reflector. Another possibility is the use of lenses with multiple feeds.

Data Storage and Processing

The radar return can be quantized as either "return present" or "return not present." For example, a "1" could be designated for "return present" and a "0" could be used for "no return present." If this information is stored on magnetic tape it could be stored as a given voltage "present" or "not present." It would probably be desirable to code the beam position information digitally in a similar manner for storage.

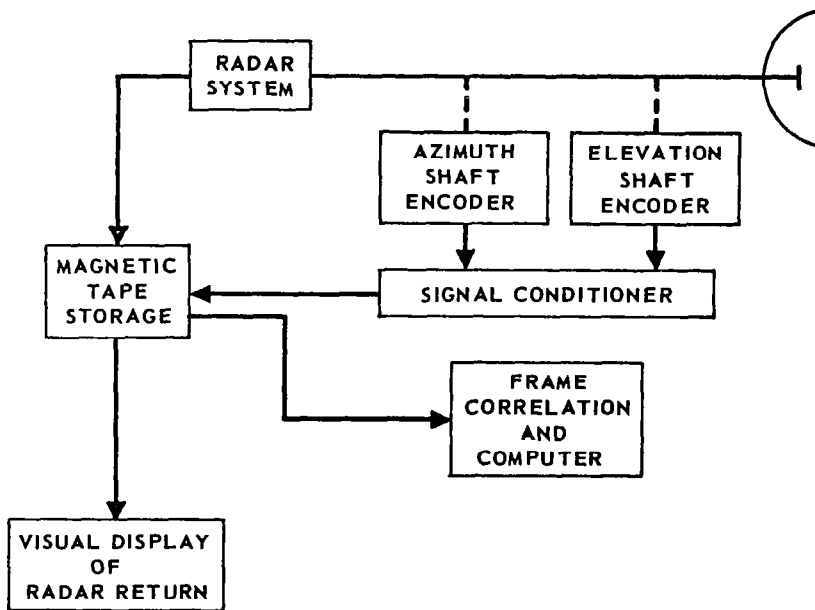


FIGURE 126 - SEQUENTIAL "PAINTING" RADAR

The mechanical scan system is shown in figure 126 as an illustration. An electronic scan system would be the same except that, rather than using mechanical shaft encoders, time synchronized driving voltages and currents would be available for signal conditioning. The magnetic tape can be arranged to store, in one frame, a description of the target size, shape and outline at one given period of time. Frame by frame storage contains the information necessary for determination of the target vehicle's movements, except spin on the axis of symmetry (this will probably require doppler techniques). It may also be possible to define the targets effective rotational axis in some cases.

The information stored on the tape may be telemetered to ground or, if a man is present on the rendezvous vehicle, the information may be supplied to a visual display. In order to determine relative altitude rates accurately, it would be necessary to supply the stored information to a computer, either on the ground or in the docking vehicle. The computer can determine tumble rate by storing one frame and making an attempted correlation with each subsequent frame. Until the same frame matrix reappears, no correlation is possible. When the duplicate frame reappears, the computer measures the time required. A procedure such as this will not work for a spherical target. It also will fail if the target is symmetrical in the plane of observation, because it will think the tumble rate is twice the actual tumble rate. The latter case is perhaps, not too unlikely. One way to avoid this error mode is to build symmetrical recognition into the system, which could be easily included in the computer. If the docking vehicle is unmanned and if docking is to take place by means of a closed-loop system, the computer must also have range and range rate inputs from the radar system. The computer must also be capable of making certain decisions based on information it obtains about the target. For example, docking may not be attempted for target vehicle tumble rates exceeding some limit. If the computer decides that docking is possible, it must send the appropriate commands to the thruster control system. The radar system then gathers a new set of data and so on. Features of a non-cooperative scan radar system can be integrated with a system also capable of cooperative operation, when desirable.

Doppler Techniques

Many radar systems use doppler techniques for the determination of range rate (or relative translational velocity). Doppler can also be used for the determination of certain relative attitude rates. Using the spotlight scanning technique previously discussed, if a portion of the target is spotlighted which is tumbling toward the docking ship, an "up" doppler shift is observed. A "down" shift would be observed when spotlighting the opposite side. Using the same frame and tumble rates assumed previously in this section, the maximum doppler due to target rotation can be calculated. This is shown in table 9 .

TABLE 9 - TARGET TUMBLE - DOPPLER RELATIONSHIPS

	REQUIRED FRAME RATES	TUMBLE RATE (°/SEC.)	EDGE TANGENT VELOCITY (FPS)	MAXIMUM DOPPLER AT 70 gc
A.	0.1./SEC.	1	0.175	24.50 Hz
B.	1.0/SEC.	10	1.750	245.00 Hz
C.	10.0/SEC.	100	17.500	2.45 kHz

If the antenna has 1 foot diameter resolution cell (at 100 feet) and the target is 10 feet in diameter, 100 resolution cells will be required, a 20 foot diameter target would require 400 cells.

A resolution field of 20 x 20 will handle most targets of interest that would be observed at 100 feet. Larger targets would be observed from distances greater than 100 feet. Observation (or dwell time) based on a conservative 500 cell field with a maximum of 10° rotation in any one frame will vary linearly from 20 ms for the 1°/second tumble rate to .2 ms for the 10°/second tumble rate.

S/N Requirements

With this observation time the required signal to noise ratio can be calculated from the following formula:

$$\delta_f = \frac{\sqrt{3}}{\pi T \left(\frac{2S}{N_0}\right)^{1/2}} \quad (403)$$

Since the doppler spread will be similar to 10% of the maximum doppler $\delta_f T$ will be a constant and the signal to noise ratio will be constant for the accuracies and tumble rate specified. A variable scan speed with appropriate processing will be required to maintain a constant percentage doppler error.

Transmitter Feedthrough

Transmitter feedthrough will appear as a zero velocity target. This has previously been analyzed in the section on FM-CW radar. The measured doppler, f'_d is given by:

$$f'_d = f_d \left[1 + \frac{\frac{e_f}{e_r} \cos 2\pi f_d t}{1 + \frac{e_f}{e_r} \cos 2\pi f_d t} \right], \quad (404)$$

where e_{ft} = feedthrough voltage
 e_r = reflected voltage

For :

$$f'_d = f_d \left[1 + \frac{e_f}{e_r} \cos 2\pi f_d t \right], \quad (405)$$

and the maximum fraction error is proportional to the ratio of the feedthrough to received signal ratio.

For a 10% error, the signal to feedthrough ratio would need to be 20 db. The isolation required to keep the feedthrough below this level can be calculated. This is calculated for the .5° beamwidth 70 GHz system at a range of 100 feet.

$$I = \frac{(4\pi)^3 R^4 L}{G^2 \lambda^2 \sigma \left(\frac{\text{Signal}}{\text{Feedthru}} \right)}, \quad (406)$$

$$= 63.4 \text{ db} \quad (407)$$

This isolation may be achieved with separate antennas or on-off switching using one antenna.

The accuracy with which the doppler frequency can be measured will be affected by the transmitter frequency stability. Errors in doppler measurements will be caused by frequency errors, long term drifts, and frequency modulation sidebands caused by noise modulation. For systems with the transmitter and local oscillator derived from a common source, frequency errors and long term drifts will result in an error in the doppler frequency measurement proportional to the percentage frequency error. If the transmitter and local oscillator are derived from separate sources, frequency errors and long term drifts can add directly. FM noise modulations on the transmitter and local oscillator will produce noise sidebands that will interfere with the doppler return. However, it can be seen by following an analysis similar to that of the FM-CW radar, that these noise sidebands will be greatly reduced when observed at the IF frequency. For example, the modulation index for a signal at $f_m = 10$ Hz with the target located 100 feet away will be reduced by the factor $2 \sin \frac{\omega_m \tau}{2} \approx \omega_m \tau$, round trip delay.

$$\tau = \frac{2(100)}{C} = 200 \text{ ns} \quad , \quad (408)$$

$$\omega_m \tau = 2\pi \times 10 \times 2 \times 10^{-7} \quad (409)$$

$$= 98 \text{ db} \quad (410)$$

Table 10 gives the noise reduction factor for other noise modulation frequencies.

TABLE 10 - FM NOISE REDUCTION FACTOR

Hz	db
10	98
100	78
1000	58
10,000	38

FM noise will have negligible effect on the system performance if coherence is maintained between the transmitter and the local oscillator.

The doppler frequencies produced by rotation rates between 1°/second and 100°/second can be measured if care is taken. The equipment required to process doppler information can be readily integrated with the radar spotlight scan technique.

Quasi-Optical Techniques

Another technique which is capable of obtaining target data is the quasi-optical technique. This technique obtains the same information as the painting technique, but does it simultaneously instead of sequentially. In this technique, an antenna with a beamwidth comparable to the lens field of view floodlights the target and the reflected energy is received by a field of sensors located behind a lens. Thus, a complete image of the target is obtained without the requirement of scanning. Figure 127 is a sketch of the optics of this system.

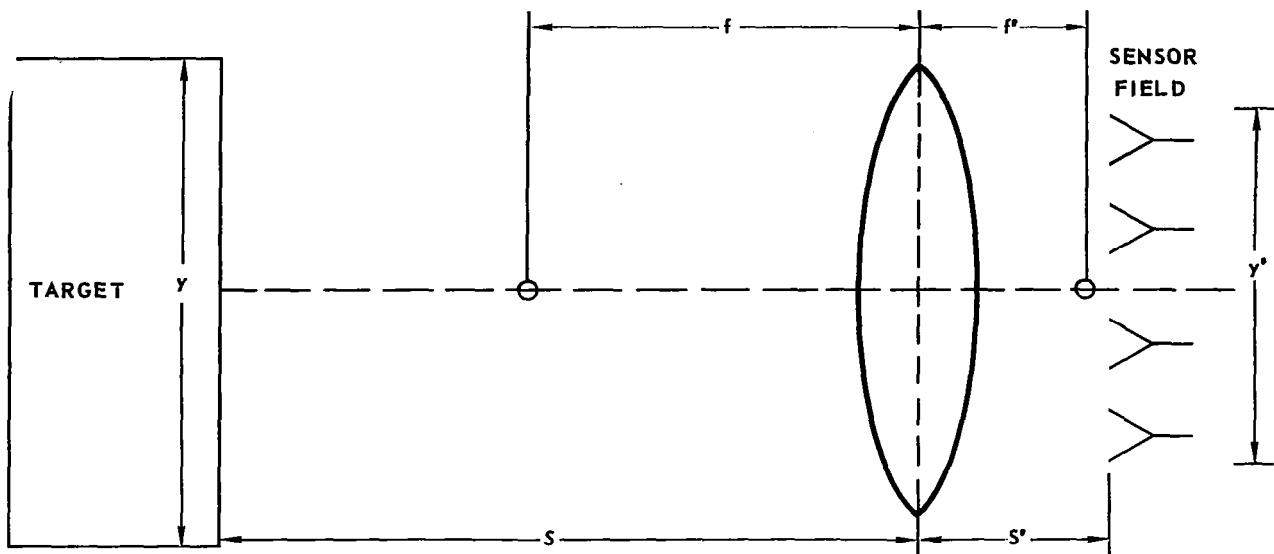


FIGURE 127 - IMAGING SYSTEM GEOMETRY

The lens diameter and operating frequency relationships are chosen to provide angular resolution adequate to resolve the scattering areas on the target vehicle. The same requirements exist as were discussed in the section on the sequential painting technique. This requires system operation at millimeter wave frequencies to keep the lens diameter from being excessive.

The rotation rate measurement is made at 100 feet. A power calculation shows that the received signal strength is not adequate for a video detection system, even at this range.

$$G_r = 10 \text{ db (30}^\circ \text{ beamwidth)}$$

$$G_t = 50 \text{ db}$$

$$\lambda = .0043$$

$$R = 100 \text{ feet}$$

$$\sigma = 1 \text{ square meter}$$

$$P_t = 100 \text{ mw}$$

$$L = 3 \text{ db}$$

$$P_r = -60 \text{ dbm}$$

(411)

A superheterodyne receiver is required for this sensitivity. Figure 128 is a block diagram of this system, which can measure rotation rates by doppler processing of the returned signal or by determining the periodicity of the image of the returned signal. The storage requirement is the same as that for the sequential painting system.

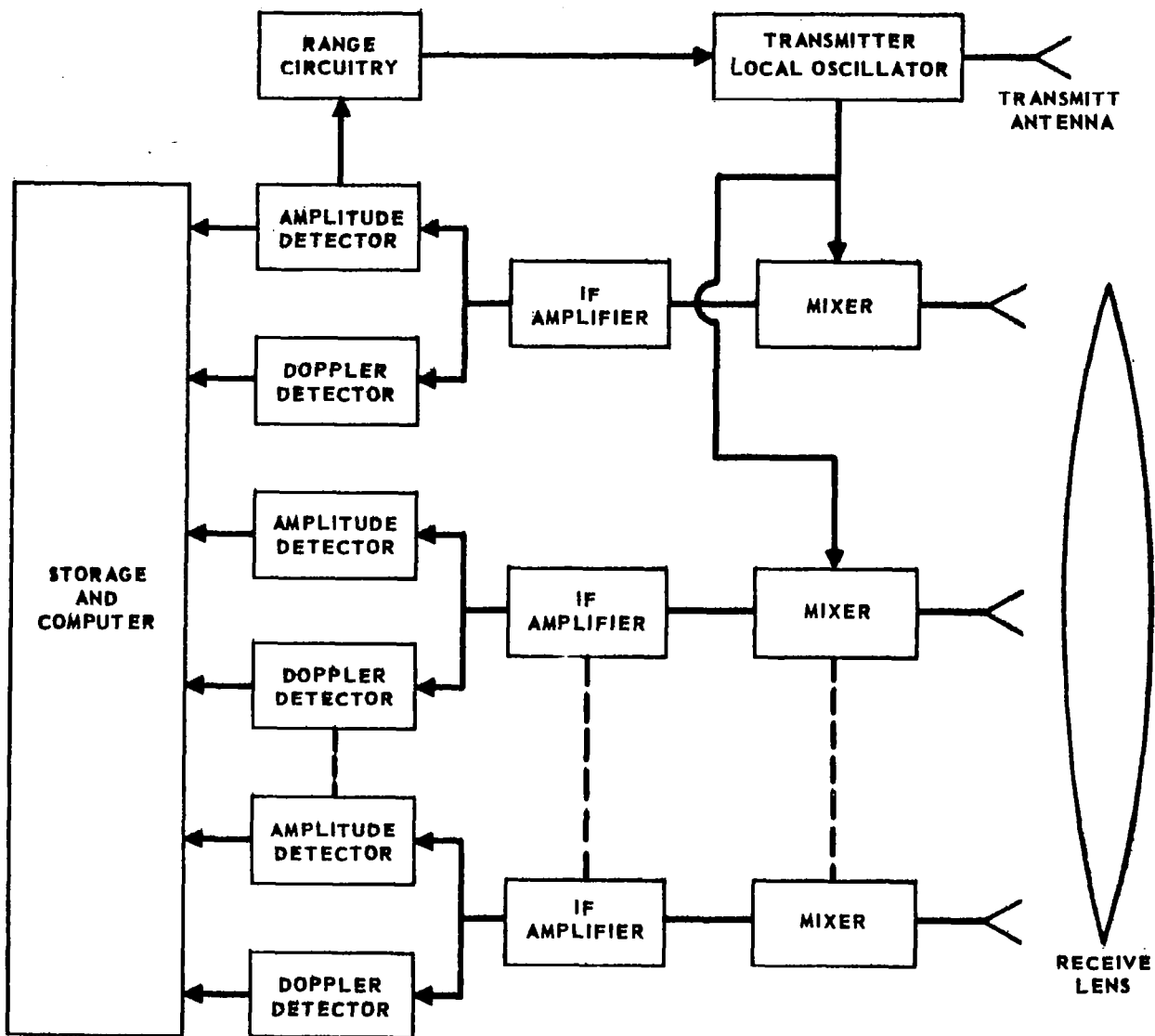


FIGURE 128 - IMAGING LENS SYSTEM

Short Pulse Radar Techniques

The range resolution capability of the short pulse radar has been used to determine the rotation rates of planets, but has very limited applicability to the docking situation. Since the planets are known to be spherical from visual observations, it is possible to determine their spin rate by observing the doppler speed in various range resolution cells (see figure 129).

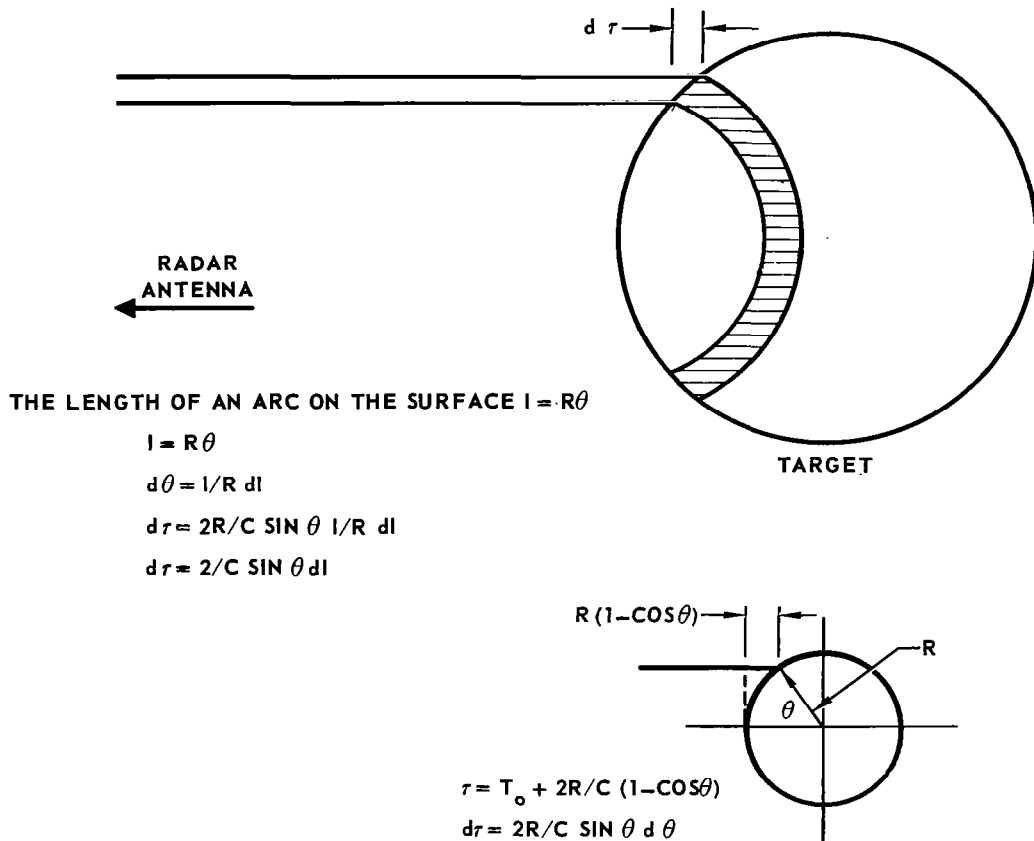


FIGURE 129 - RANGE RESOLUTION CELL

For a target having a diameter of ten feet, a one nanosecond pulse is required to obtain a one foot resolution cell at $\theta = 30^\circ$:

$$d\tau = \frac{2R}{C} \sin \theta dl, \quad d\tau = 1 \text{ ns} \quad (412)$$

Since this pulse width is not in agreement with the pulse widths required for the doppler accuracy measurement on a single pulse basis, it is necessary to measure the doppler on a pulse train basis.

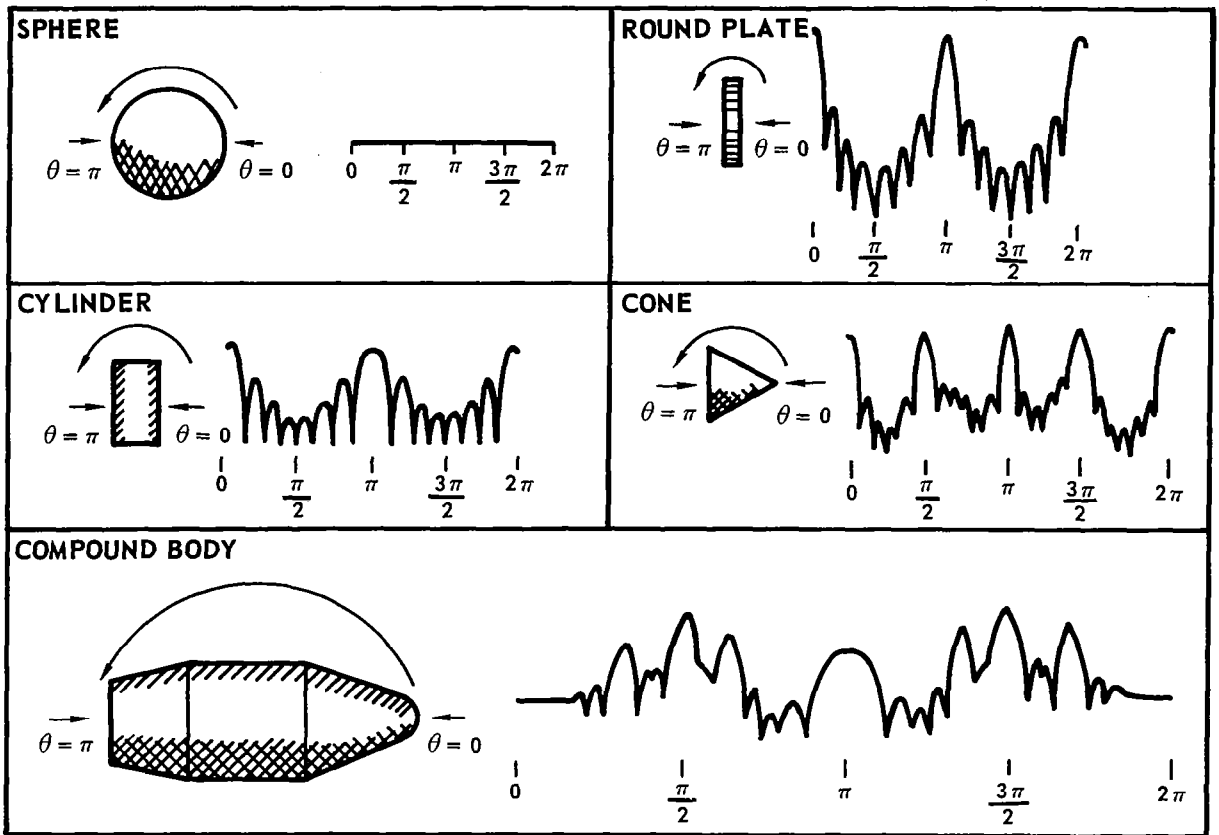
The doppler return gives a measure of the rotation rate of the target but, with resolution in range only, the axis cannot be measured from a fixed point. The docking vehicle must move off axis and observe the change in doppler spread. For the simple spherical shaped-body, this data could be processed to give an indication of proper direction to the spin axis. For complex target shapes, the problem becomes prohibitively difficult and tends to eliminate this system from consideration with targets of unknown shape.

Signature Analysis of Radar Returns

The study of objects by analysis of their radar return signatures has already been discussed in the section entitled, "Probes as Docking Aids." It was mentioned that a disadvantage in attempting to gather information by this method is the sophisticated data processing requirement. However, any non-cooperative scheme that forbids the use of visual observation, either directly or by television, requires a rather sophisticated system of analysis.

The returns from metallic objects of various shapes are characteristic. Some common shapes that might be encountered are shown in figure 130 with their characteristic signatures. The ability to recognize object shapes from radar data is based on the fact that the amplitude of the signal reflected from a target changes as the contour of the object which is pointed toward the radar changes. For a compound body, the signature is generally a combination of the signatures of simple bodies.

A computer, can be provided with correlation functions or programmed to analytically reproduce the shape of an object. A group of formulas are presently available for simple body shapes. L. Blasberg of RCA has derived a general mathematical expression for signature analysis which defines shape as a target aperture function (reference 27). A computer equipped with the Blasberg equations may be able to deduce much about symmetrical target objects.



THE ABILITY TO IDENTIFY SHAPES OF OBJECTS BY RADAR DATA IS BASED ON THE FACT THAT RADAR CROSS SECTION (OR AMPLITUDE OF THE SIGNAL REFLECTED FROM A TARGET) CHANGES AS THE CONTOUR OF THE OBJECT WHICH IS POINTED TOWARD THE RADAR (ASPECT ANGLE, θ) CHANGES. THE CHART ABOVE SHOWS ANALYTIC IDENTIFYING SIGNATURES (CROSS SECTION VERSUS ASPECT ANGLE) FOR FOUR SYMMETRICAL BODIES. FOR THE COMPOUND BODY, THE SIGNATURE IS A COMBINATION OF THE SIGNATURES OF THE FOUR SIMPLE BODIES.

FIGURE 130 – TARGET SIGNATURES

INTEGRATED SYSTEMS FOR NONCOOPERATIVE MISSIONS

Many missions requiring docking with a noncooperating target will be manned and will require, at most, sensors capable of deriving supplemental displays; others, as discussed earlier, will require quite sophisticated systems for sensing the rotation rate and rotation axis. To illustrate the application of the data presented in the previous sections, an unmanned satellite inspection mission is examined. This mission has very stringent requirements. The sensors are required to independently determine the entire set of target parameters (relative position, velocity, and rotation rate).

TRADE-OFF OF CONTENDING SYSTEMS

By combining the range measuring techniques with the angle and attitude measurement techniques described earlier, the following systems were synthesized.

- a. Sequential Painting - A block diagram of this system is shown in figure 131. This system uses the ICW radar technique for range and range rate measurement. A scanning narrow beam antenna is used for angle, rotation rate, and rotation axis determination.
- b. Imaging Lens System - A block diagram of this system is shown in figure 132. This system uses the ICW radar technique for range and range rate measurement. The imaging lens system is used for the angle, rotation rate, and rotation axis determination. This system provides the same information as the sequential painting system except that it is obtained simultaneously instead of sequentially.
- c. Multiple Beam - Doppler Sample - A block diagram of this system is shown in figure 133. Again use ICW radar technique for the range and range rate measurement. However, instead of obtaining a complete image of the target vehicle, the return from the target vehicle is only sampled. A four feed sequential lobing antenna tracking system is used to obtain the LOS angle. Rotation rates and axis are obtained by processing vertical and horizontal samples of doppler return from the target vehicle obtained by squinted narrow beams.
- d. Short Pulse Radar - A block diagram of this system is shown in figure 134. In this case, conventional pulse radar range measuring techniques are employed. A sequential lobing angle tracking system is used to keep the antenna centered on the target and to obtain the LOS angle measurements. The maximum doppler return is used to determine the rotation rate of the target.

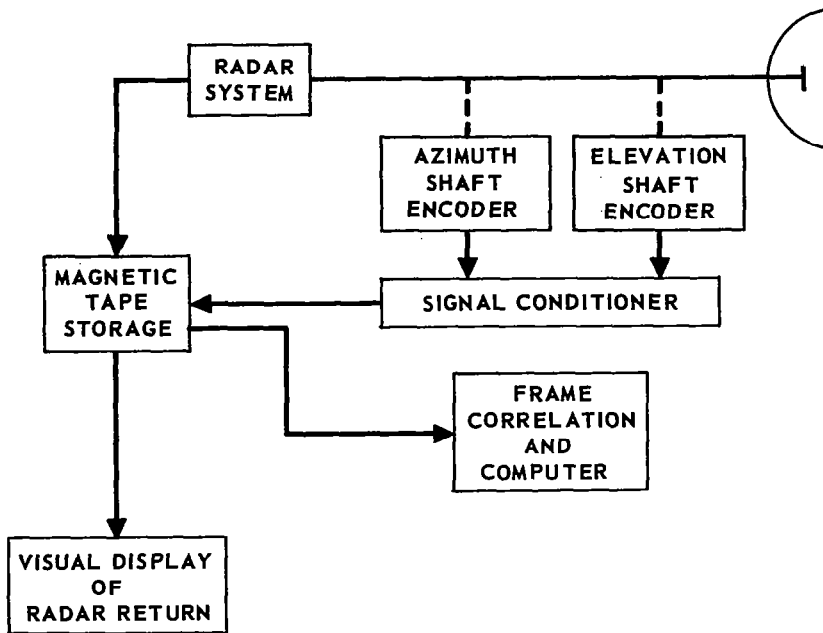


FIGURE 131 - SEQUENTIAL "PAINTING" RADAR

These systems will be compared on their ability to measure target size and shape, LOS angle, rotation rates, range, and on system complexity.

Target Size and Shape

Target size and shape will need to be determined to aid in making a decision to dock, not to dock, or how close an approach will be possible. If the target is quite large and has extended arms, it may not be possible to approach the target very close. The size will also determine the range at which the rotation axis alignment must be made. This section will compare the accuracy with which this parameter can be measured.

Sequential Painting. - The size of the target is measured by determining the number of angular resolution cells that the target covers. The lateral extent of the target can be measured within one beamwidth. Since this is an angular measurement, the linear error decreases with decreasing range.

For a $.5^{\circ}$ beamwidth antenna operating at 70 GHz, this error, which is equal to the beam spot diameter, is a function of range as shown in table 11.

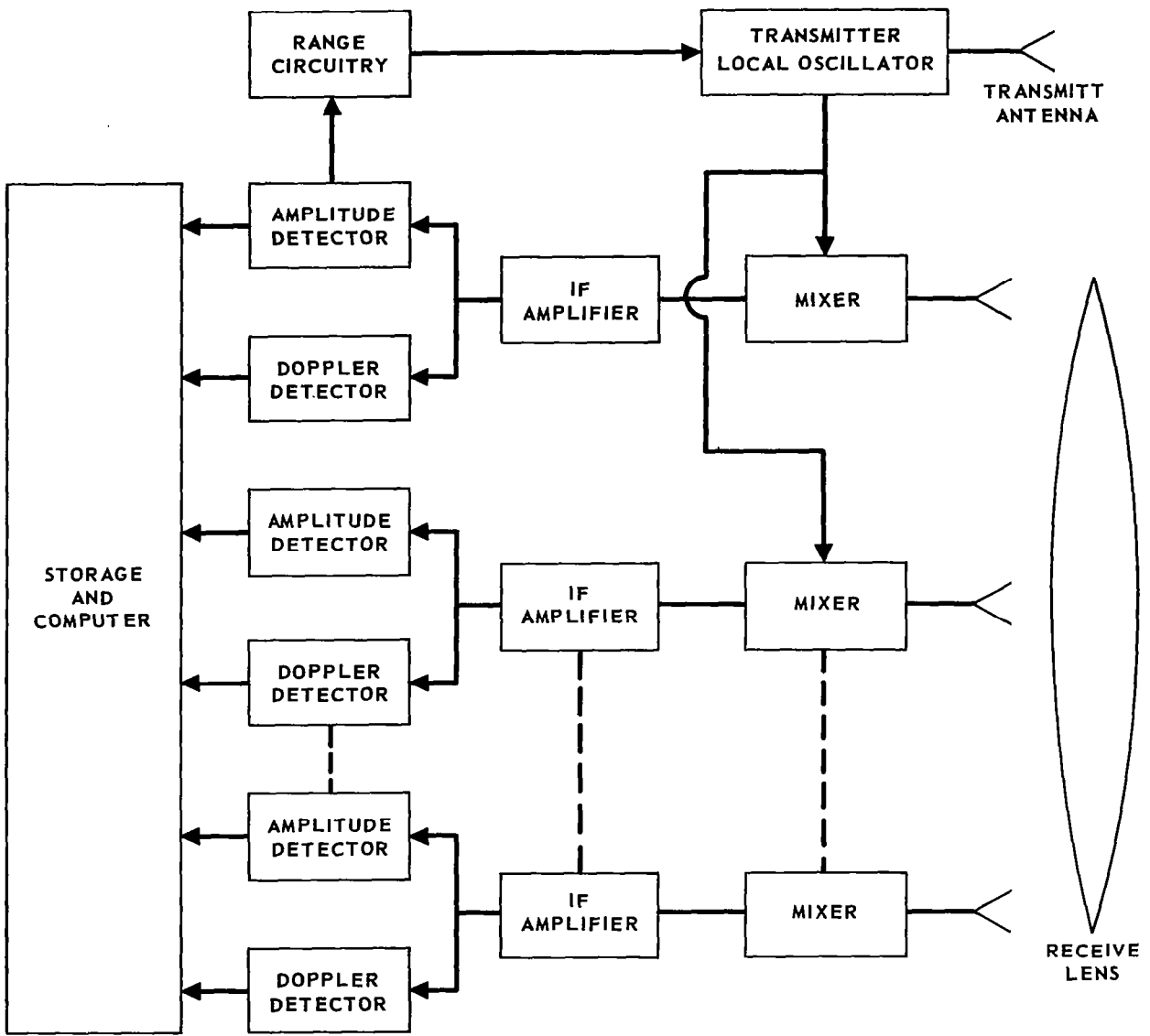


FIGURE 132 – IMAGING LENS SYSTEM

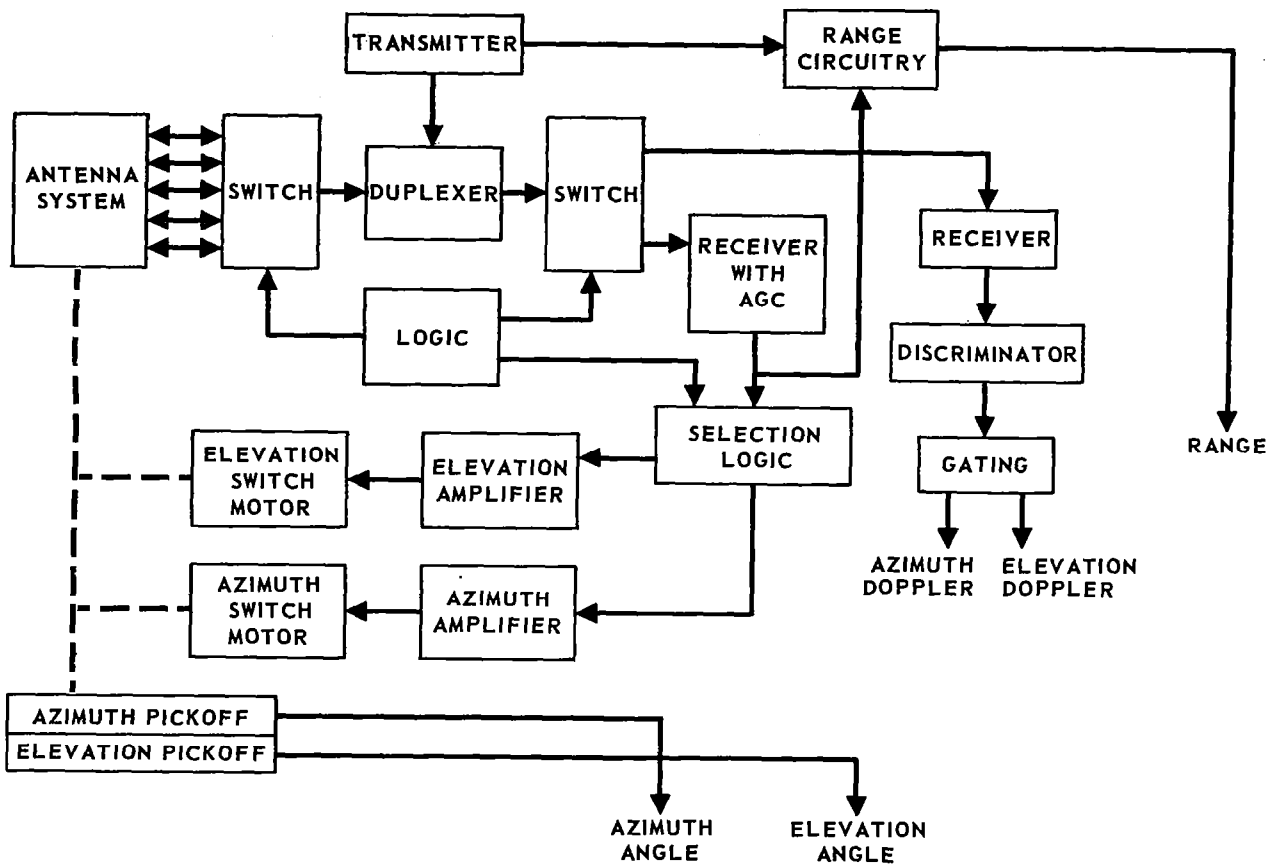


FIGURE 133 – MULTIPLE BEAM DOPPLER SAMPLE DOCKING RADAR SYSTEM

TABLE 11 – SPOT DIAMETER vs. RANGE

RANGE (FEET)	SPOT DIAMETER (FEET)
10,000	96
1,000	9.6
100	0.96

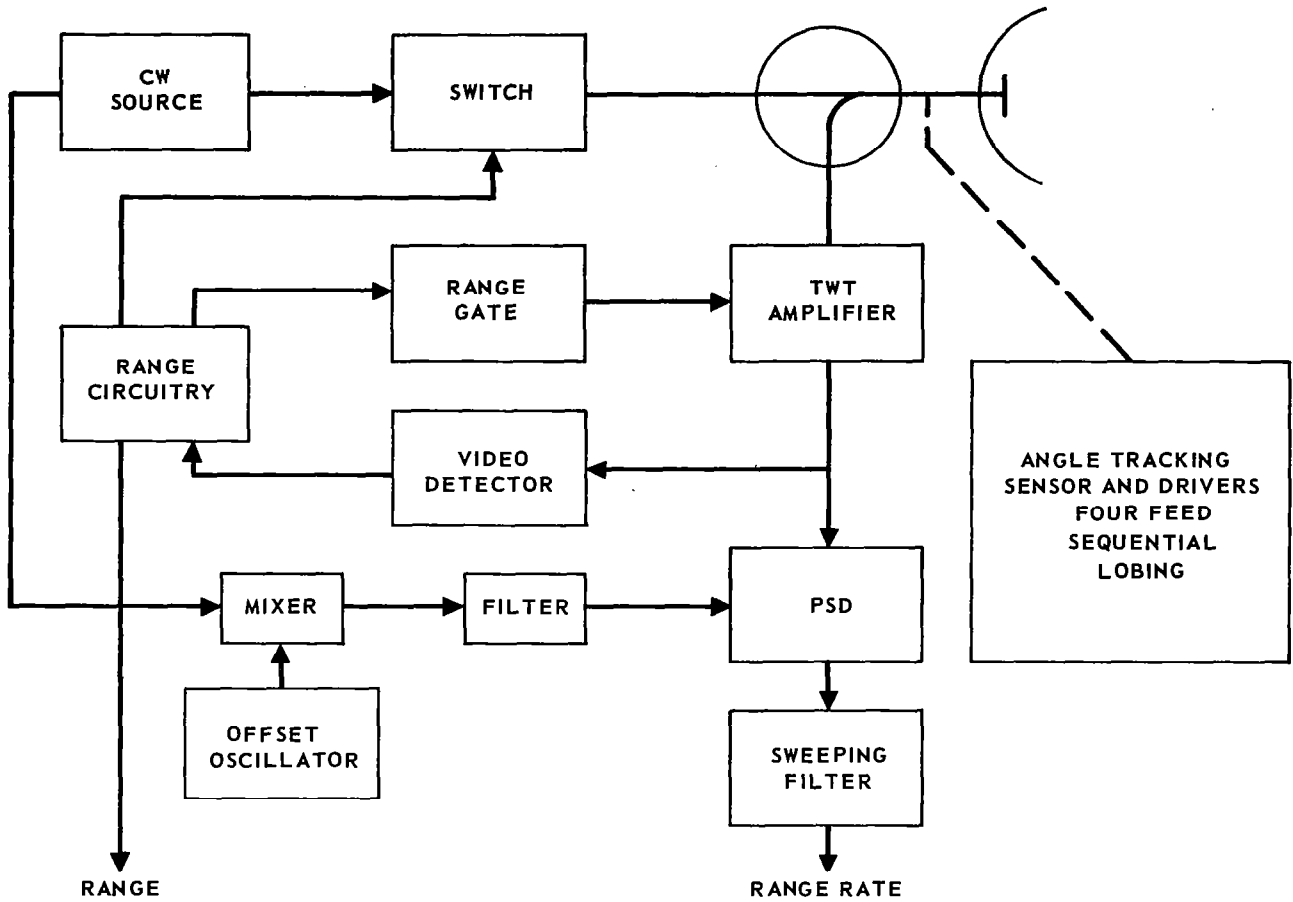


FIGURE 134 - SHORT PULSE - DOPPLER DOCKING RADAR SYSTEM

Imaging Lens System - The size and shape is determined by this system to the same degree of accuracy as the sequential painting system.

Multiple Beam-Doppler Sample - The size of the target vehicle is obtained in this system by measuring the range at which the target vehicle fills the pair of squinted narrow antenna beams. This measurement is very coarse and depends upon the target attitude. Only two orthogonal samples are obtained from this measurement. Additional docking vehicle maneuvers may be performed to obtain more measurements if the target vehicle is not rotating. However, if the target vehicle is rotating, it will not be necessary to maneuver the docking vehicle to obtain maximum size perpendicular to LOS. The accuracy of the estimation of the size of the target will then be essentially the same as that of the sequential painting system.

Short Pulse Radar - A short pulse radar with a 2 ns pulse width can measure range with a resolution of + 1 foot. This value is independent of range, and determines the size of the target in the direction of the range vector.

Size is determined in two dimensions by each of these systems, except the Short Pulse Radar which gives size in one dimension only. It is necessary to maneuver the docking vehicle around the target vehicle to determine its maximum size. A comparison of the accuracy of these systems is given in figure 135.

Line of Sight Angle

Sequential Painting - The centroid of the target (i.e., the geometric center of the target projection into a plane perpendicular to the vehicle-target line-of-sight, is determined and tracked in this system. If the target is stationary, this is a well defined point. If the target is rotating, it is necessary to maneuver the docking vehicle onto the spin axis. The angle to the centroid is defined as the LOS angle. The accuracy is within one beamwidth. This follows the geometrical beamwidth of the antenna.

Imaging Lens System - This system has the same measurement capabilities as the doppler paint system. The difference is that this system employs parallel processing while the doppler paint system employs sequential processing. A plot of the measurement capabilities of these systems is given in figure 136.

Multiple Beam-Doppler Sample - In this system, sequential lobing is used to derive an error signal to mechanically position a gimbaled antenna to point toward the target. The angular error in the LOS measurement in this system can be quite low at medium ranges and is limited by glint noise at short range. This can be limited to small values at ranges where the narrow squint angle beam just overlaps the edge of the target. At these ranges the angle accuracy is comparable to that obtained with painting techniques with antennas of comparable beamwidth.

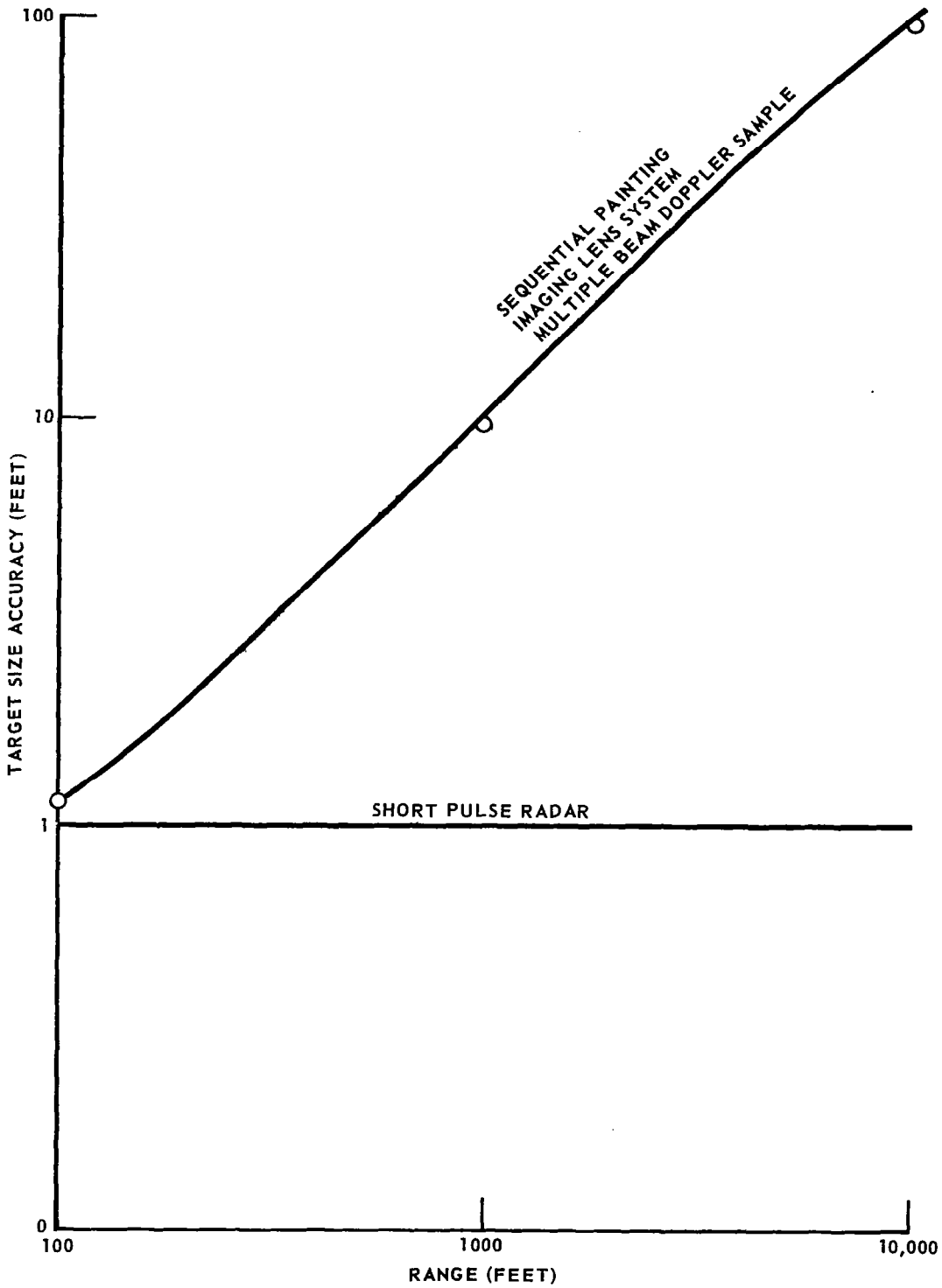


FIGURE 135 - TARGET SIZE ACCURACY

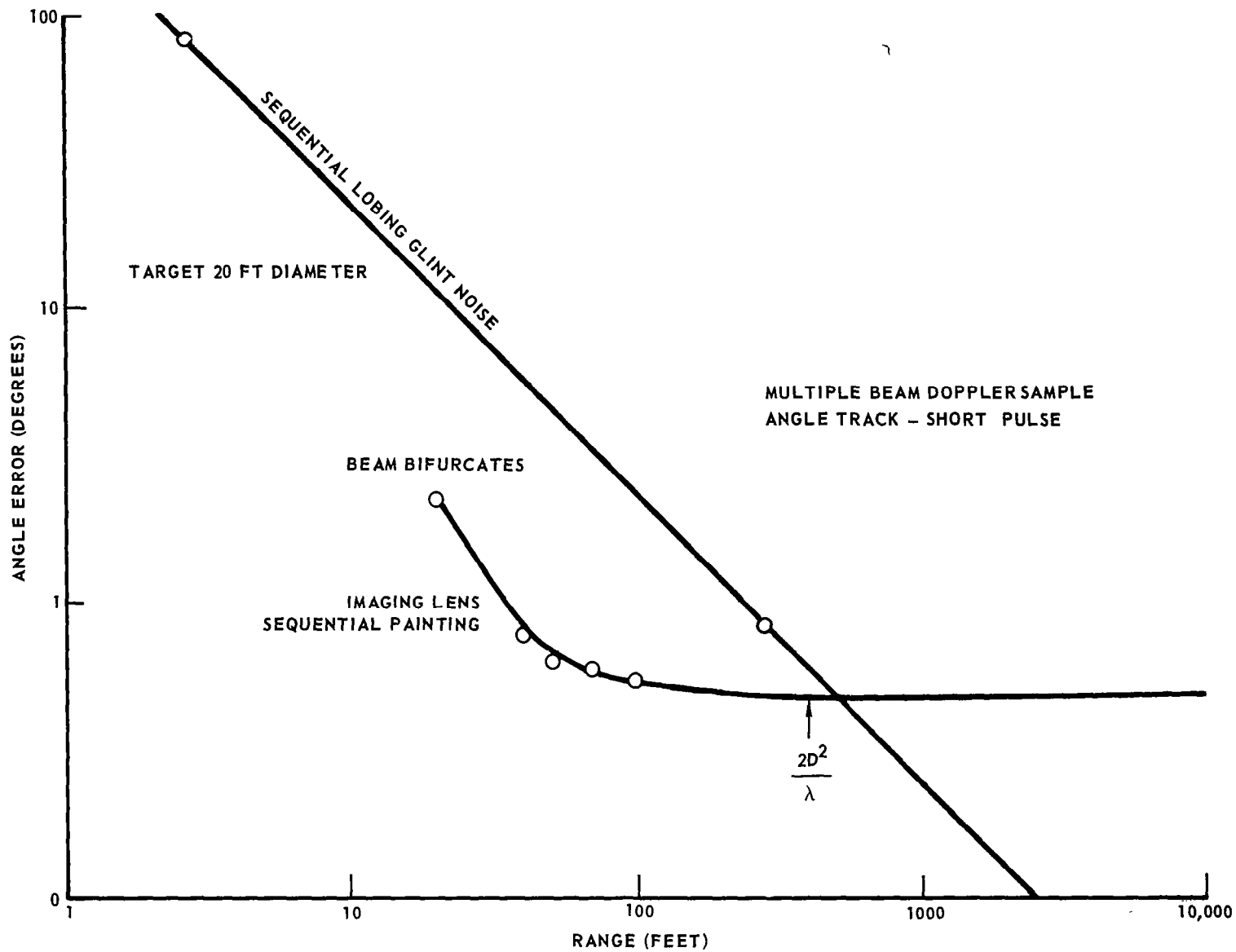


FIGURE 136 - LOS ANGLE ACCURACY

Short Pulse - Additional angle tracking circuitry is required for the short pulse system. A sequential lobing technique results in the usual glint errors.

Rotation Rate Measurement

The rotation rate of the target vehicle is measured by processing doppler returns from the target. The accuracy with which this measurement can be made by each technique will be discussed.

Sequential Painting. - The doppler return from each beam position is measured and stored, generating a complete doppler map of the target. Since this map is also used for obtaining the target size and shape, the target must be scanned rapidly to keep target motion from blurring the target image. In this case, bright spots on the target can cause the predominant doppler frequency to correspond to any point in the beam. This results in an error that is proportional to the ratio of spot size to diameter in any one beam measurement. However, many samples are available and by processing this information, the error can be greatly reduced. The error reduction approximately follows a $\frac{1}{\sqrt{n}}$ law.

Imaging Lens System. - A doppler map of the target is obtained with this system also, but in this case a field of sensors is used to receive the return from the target. All sensors receive energy from the target simultaneously and the rotation rate measurement is made by processing the doppler return from the target. Averaging (both time and spatial) can be used to improve the accuracy of the rotation rate measurement.

Multiple Beam Doppler Sample. - In this system the rotation rate is determined by measuring the doppler returns in two orthogonal pair of antenna beams. These beams essentially sample the doppler map that is obtained by the sequential painting and imaging system. Two samples are taken of each component of doppler to allow a measurement of the doppler difference instead of absolute doppler. This relaxes the requirement of antenna pointing. Since bright spots will result in erroneous indications, averaging techniques must be employed to increase the accuracy of this measurement. Since the limited number of samples eliminates the possibility of spatial averaging, time averaging is employed. Bright spot errors are reduced by integrating the target return over a period long enough for the bright spot to sweep through the antenna beam. At a range of 100 feet, the beam spot will cover an arc of 8.2° . The time required for a spot on the target to move through this distance for the different rotation rates is shown below.

<u>Rotation Rate</u>	<u>Time for Spot to Traverse Antenna Beam</u>
100°/sec.	.082 sec.
10°/sec.	.82 sec.
1°/sec.	8.2 sec.

The required averaging time for the 100°/second and 10°/second rotation rates are compatible with the averaging time of the other radar parameters. The magnitude of the error of the rotation rate of 1°/second measurement due to bright spot reflection will be within the tolerance on impact conditions.

Short Pulse Radar - The short pulse radar measures rotation rate by measuring the doppler spread of the target return and calculating the rotation rate using the previously determined target size.

Rotation Axis

Sequential Painting - The rotation axis is obtained by plotting lines of constant doppler. The accuracy of these plots will be limited by the angular resolution which determines the spot size of the doppler image. If the target is large and includes many resolution cells, the accuracy can be determined from geometry. The accuracy will depend upon the number of samples in the constant doppler line and the spot size.

$$\Delta\theta = \tan^{-1} \frac{2}{N} , \tag{413}$$

where

$\Delta\theta$ = max angular error ,

N = number of resolution cell .

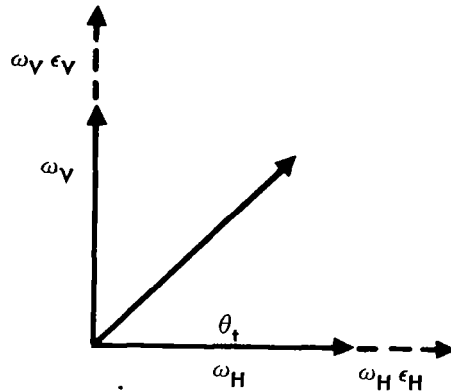
A 20 foot diameter vehicle has been chosen as a typical target size. The accuracy of the rotation axis then depends upon the spot size, as shown in table 12 .

TABLE 12 - ROTATION AXIS ACCURACY vs. SPOT SIZE

RANGE (FEET)	l (SPOT SIZE) (FEET)	$\Delta\theta$ (DEGREES)
20	0.8	4.5
50	0.55	3.0
100	1.0	5
1000	8.7	41

Imaging Lens System - The rotation axis will be measured in the same manner as for the doppler painting system and the same accuracies will result.

Multiple Beam Doppler Sample - In this system the rotation axis is determined from the direction of the resultant of the vector summation of the horizontal and vertical components of velocity. The accuracy with which the axis of rotation is measured is dependent upon the accuracy with which the rotation rate can be measured. This calculation is made with the aid of figure 137.



$$\theta_t = \text{TAN}^{-1} \frac{\omega_V (1 + \epsilon_V)}{\omega_H (1 + \epsilon_H)}$$

θ_ϵ - MEASURED ANGLE

θ_o - TRUE ANGLE

θ_ϵ - ERROR ANGLE

$$\theta_\epsilon = \theta_t - \theta_o = \text{TAN}^{-1} \frac{\omega_V (1 + \epsilon_V)}{\omega_H (1 + \epsilon_H)} - \text{TAN}^{-1} \frac{\omega_V}{\omega_H}$$

FIGURE 137 - VELOCITY COMPONENTS

For small ϵ the angle at which the error is a maximum is 45° . Then,

$$\theta_\epsilon = 45^\circ - \tan^{-1} \frac{1 \pm \epsilon_V}{1 \pm \epsilon_H} \quad (414)$$

Short Pulse Radar. - Short pulse radar will not be able to determine rotation axis directly. Docking vehicle maneuvering will be required to determine the rotation axis with this system.

Range

The ICW technique has been shown to be better than other CW techniques for noncooperative range measurements. Since range resolution is not required in three of the four systems being compared, the pulse width is limited only by the requirement that the transmitter be turned off before the reflected signal is received. This requirement also fits the ICW radar. If the prf and pulse width of the pulse radar is changed with range to keep a 50% duty cycle, the two systems become quite similar. The ICW radar requires a coherent integration and will result in greater sensitivity and better utilization of transmitted power. Also, all systems will measure doppler shift to determine range rate and rotation rates. Since this requires a coherent transmitter, the ICW radar will be the best choice. The short pulse radar is by definition a pulse radar technique. Again a coherent transmitter is required for doppler measurements.

Range Rate

The range rate on all systems is measured by doppler techniques. This can be accomplished readily with the narrowband circuitry, using a phase locked receiver, mixing the transmitted and received signal at I.F., and measuring the frequency of the difference signal. The instrumentation to measure range rate in the short pulse radar uses a PSD at microwave frequencies followed by box-car circuitry.

System Complexity

The systems being considered for noncooperative docking will be compared on the basis of system complexity. System complexity will be indicated by the quantity of parts or by the use of circuits with small tolerances.

As can be seen from table 13. the Imaging Lens system suffers from an excessive number of feeds. The antenna requirements for the other systems are roughly equivalent. The gimballed reflector assembly with multiple feeds is the most complex of the remaining three; however, the antenna for the sequential painting system is limited to obtaining data from slowly rotating targets.

TABLE 13 - SYSTEM COMPLEXITY

	IMAGING LENS SYSTEM	SEQUENTIAL PAINTING	MULTIPLE BEAM DOPPLER SAMPLE	SHORT PULSE
ANTENNA DIAMETER	24"			10"
TYPE	FIXED LENS	GIMBALLED PARABOLIC REFLECTOR		
FEEDS	500	1	16	5
TRANSMITTER	SOLID STATE MULTIPLIER CHAIN (MM WAVES)			SOLID STATE MULTIPLIER CHAIN (X BAND) & POWER AMPLIFIER
RECEIVER	NARROW BAND			BROADBAND
PROCESSING	COMPLEX		SIMPLE	VERY COMPLEX

Since all except the short pulse system use ICW radar for ranging, the transmitter will be the same for all three systems. A solid state multiplier chain with 100 mw power output at 70 GHz is required for the system. This is a state of the art requirement and requires development. However, once developed, this type transmitter offers solid state reliability and low voltage operation. The power requirements for a short pulse radar are much greater and cannot be obtained by solid state. An additional power amplifier is required - a vacuum tube (TWT) with an additional high voltage power supply and modulator.

All systems except the short pulse radar can use narrow band receivers. The short pulse radar requires a broadband receiver to achieve the full resolution capabilities of the transmitted pulse.

These complexity considerations are summarized in table 13 .

SELECTION OF MOST PROMISING SYSTEM

Four systems were compared for use as docking radar sensors. These systems were analyzed to determine their measurement capabilities, limitations, and accuracies. Table 14 summarizes the measurement technique employed by each system. As can be seen from this chart, a considerable overlap exists between the various systems. All systems use doppler measurements to determine range rate. The three systems using angular resolution, use similar target size determination techniques. The imaging lens system and the

TABLE 14 - MEASUREMENT TECHNIQUE

	IMAGING LENS SYSTEM	SEQUENTIAL PAINTING	MULTIPLE BEAM DOPPLER SAMPLE	SHORT PULSE
TARGET SIZE AND SHAPE DETERMINATION	TWO DIMENSIONAL DIRECTLY FROM IMAGE	TWO DIMENSIONAL BY SCANNING TARGET AND FORMING IMAGE	TWO DIMENSIONAL APPROXIMATED FROM ANGULAR EXTENT OF TARGET	ONE DIMENSIONAL (RANGE EXTENT OF TARGET)
LINE OF SIGHT ANGLE DETERMINATION	CENTROID COMPUTATION		SEQUENTIAL LOBING	
ROTATION RATE DETERMINATION	ROTATION RATE AND AXIS BY MEASURING HORIZONTAL AND VERTICAL DOPPLER			ROTATION RATE ONLY BY MEASURING DOPPLER SPREAD
RANGE DETERMINATION	ICW RADAR			NANOSECOND PULSE RADAR
RANGE RATE DETERMINATION	DOPPLER			

sequential painting system measure the target size and shape directly from the target image; the main difference is that the imaging lens systems obtains multiple samples from the target simultaneously, while the sequential painting system obtains the same information in time sequence. The multiple beam-doppler sample radar does not obtain complete image of the target but only approximates the size of the target from orthogonal samples obtained with squinted antennas. The short pulse radar is capable of measuring only one dimension of the target, its range extent. The docking vehicle must maneuver around the target to obtain a two dimensional measure of its size.

Rotation rate and axis measurement are made by doppler mapping of the target in the imaging lens systems and in the sequential painting system. The multiple beam-doppler sample system measures the rotation rate and axis by determining two orthogonal values of the rotation rate and performing the vector addition. The short pulse radar measures the magnitude of the rotation only. This is done by measuring the doppler spread and computing the rotation rate by using the previously determined target size.

The line of sight angle determination is obtained by a geometrical centroid computation in the imaging lens system and in the sequential painting system. The multiple beam doppler-sample system and the short pulse system

obtain this information as shaft angle output from a tracking antenna.

ICW radar is used to measure range on all systems except the short pulse radar system. The short pulse radar measures range as a time delay measurement.

The performance capability of these systems is summarized in table 15 .

TABLE 15 - PERFORMANCE COMPARISON

	IMAGING LENS SYSTEM	SEQUENTIAL PAINTING	MULTIPLE BEAM DOPPLER SAMPLE	SHORT PULSE
TARGET SIZE AND SHAPE	LIMITED ONLY BY SPOT SIZE		LIMITED BY SPOT SIZE AND NUMBER AND FEEDS	RESOLVES IN RANGE ONLY.
L.O.S. ANGLE	VERY ACCURATE AT LONG RANGE, ACCURATE TO ANTENNA BEAMWIDTH AT SHORT RANGE, .5° AT R > 100 FT 2.5° AT R = 20 FT		VERY ACCURATE AT LONG RANGE, DEGRADED AT SHORT RANGE BY LIMITED NUMBER OF SQUINT ANGLE	NOT DIRECTLY AVAILABLE. REQUIRE SEPARATE ANGLE TRACKING SYSTEM.
ROTATION RATE	ACCURACY IS DEPENDENT ON DOPPLER SMEAR IN BEAMWIDTH OF ANTENNA ≈ 10% AT R = 100 FT			DIFFICULT TO DETERMINE FOR OTHER THAN SPHERICAL TARGET
RANGE AND RANGE RATE	$\sigma = 1 \text{ FT } 0 < R < 100 \text{ FT}$ $\sigma = 0.1\% 100 \text{ FT} < R < 10,000 \text{ FT}$			$\sigma_r = 1' 0 < R < 100 \text{ FT}$ $\sigma_r \propto R^2 R > 100 \text{ FT}$

The target size and shape are measured equally well by the imaging lens system and the sequential painting system. The accuracy of the measurement is limited only by the spot size. The multiple beam-doppler sample system measurement is limited by the spot size and number of feeds. The measurement is along perpendicular lines. Some maneuvering of the spacecraft is necessary to improve this measurement. If a roll maneuver is performed, the maximum extent of the target can be determined to a much greater accuracy. This may need to be repeated at more than one range to improve the measurement. The short pulse radar resolves in range only. A volume search by maneuvering the docking spacecraft is required to obtain size information by this radar. The radar information requires considerable processing to be useful for docking.

The LOS angle is measured most accurately by the centroid computation used in the imaging lens system and sequential painting system. The amplitude comparison angle tracking systems are more accurate at long ranges but are degraded below the centroid seeking system during the final closure. However, as discussed in an earlier section, the angle measurement can be obtained at an intermediate range and held for the rest of the docking.

The rotation rate measurement accuracy is the same for the imaging lens system, the sequential painting system, and the multiple beam-doppler sample system. This is limited by the size of the antenna spot and size of the target. The short pulse radar measurement of the rotation rate is very difficult to determine for other than spherical targets.

The range and range rate measurement capability is the same for all systems except the short pulse radar. The short pulse radar is limited to operation at short range due to the excessive peak power requirements.

Table 16 summarizes the system complexity trade off considerations.

TABLE 16 - SYSTEM COMPLEXITY

	IMAGING LENS SYSTEM	SEQUENTIAL PAINTING	MULTIPLE BEAM DOPPLER SAMPLE	SHORT PULSE
ANTENNA DIAMETER	24"			10"
TYPE	FIXED LENS	GIMBALLED PARABOLIC REFLECTOR		GIMBALLED PARABOLIC REFLECTOR
FEEDS	500	1	16	5
TRANSMITTER	SOLID STATE MULTIPLIER CHAIN (MM WAVES)			SOLID STATE MULTIPLIER CHAIN (X BAND) AND POWER AMPLIFIER
RECEIVER	NARROW BAND			BROAD BAND
PROCESSING	COMPLEX		SIMPLE	VERY COMPLEX

The imaging lens system antenna is quite complex requiring a multiplicity of feeds (≈ 500) and associated processing circuitry. The sequential painting system using the gimbaled parabolic reflector with a single feed is much smaller and simpler; however, the scan rates that can be achieved with this antenna are limited to such a low value that only slowly rotating targets can be accommodated. The gimbaled parabolic reflector with multiple feeds is only slightly more complicated than the single feed sequential painting system. Rapid scanning of this system is not required. The short pulse radar uses the smallest and simplest antenna.

The transmitter requirement for all systems except the short pulse radar can be met with a solid state multiplier chain. This multiplier chain requires development but this development is within the state of the art. The short pulse radar requires a power amplifier to accomplish the required range performance.

A narrow band receiver is used on all systems other than the short pulse radar. The processing requirements vary from very complex for the short pulse radar, complex for the imaging lens system and sequential painting system, to relatively simple for the multiple beam-doppler sample system.

The multiple beam-doppler sample system has been chosen as the system to be investigated further. This system does not have all the measurement capabilities of the imaging lens system or sequential painting system for target size and shape determination. A completely unknown target vehicle with long extended arms may be beyond the capability of this system; however, targets of this nature comprise only a small part of the class of all possible noncooperative docking missions. The more probable missions require docking with a vehicle with which some prior size and shape information is available. In this case, the size information obtained by the radar is secondary, back up information. The size and complexity of the imaging lens system is prohibitive. The sequential painting system is attractive except for its limited scan rates. This limited scan rate would make this system useful for only those targets that are not rotating or are rotating very slowly. This restriction cannot generally be assumed. The short pulse radar system cannot directly make the measurements required. An excessive amount of docking vehicle maneuvering would be required to dock with this system.

PRELIMINARY DESIGN OF NONCOOPERATIVE DOCKING RADAR

A detailed block diagram of the multiple beam-doppler sample radar is shown in figure 138. This system measures range, range rate, measures and tracks the line of sight angles, and measures rotational doppler from which target rotation rate and target rotation axis are obtained.

Range is measured by the ICW radar technique, as described in the section on CW radar, using early-late gate tracking for ranges greater than 100 feet. For ranges below 100 feet, a video detection time delay measurement is used. The range rate is measured by phase lock techniques for all ranges. Angle

tracking and LOS angle measurement is accomplished using four beam sequential lobing, $.5^\circ$ beams for long range, 10° beams for closure. The target rotation doppler measurement is made using the squinted $.5^\circ$ beams. Figure 139 is a sketch of the antenna beams used in each phase of the docking mission. Not all measurements are needed at all ranges. Logic circuitry is provided to select the proper system function during each phase of the docking mission. Sequential processing is used in this system.

Operational Description

The satellite inspection mission, an example of a completely noncooperative docking mission, places stringent requirements on the measurement capability of the docking sensor. The approach described in this section includes maneuvering in to a range of approximately 100 feet, determining target motion from this range, and then maneuvering the remaining distance for docking. The maximum unassisted range of this system is 10,000 feet. However, if the information on which this mission was initiated is adequate to obtain an estimate of target range, range rate and line of sight angle, the range of this system may be extended to 100,000 feet.

The characteristics of the system will be better understood by examining the operational sequence, which has been divided into four modes: long range, medium range, observation range, and short range.

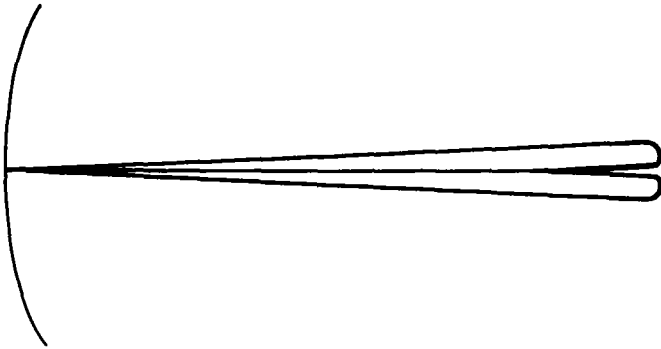
Long Range Operation. - At long ranges, 100,000 feet, the system measures R , \dot{R} and LOS angle. The four $1/2^\circ$ beamwidth, 3 db crossover antenna beams are used exclusively in this portion of the docking mission. A priori LOS, R and \dot{R} information are required to keep the signal acquisition time from being excessive. The acquisition is performed in the following sequence:

- a. Prior information is used to keep the antenna pointed at target.
- b. \dot{R} information from the rendezvous radar is used to coarse tune the VCO in the receiver phase lock circuitry. Then only a small frequency search is required to acquire the signal in doppler.
- c. After the signal has been acquired in doppler, the ICW modulation is swept to acquire the target in range.
- d. After the target has been acquired in range, the sequential lobing circuitry is placed in operation to track the target in angle.

Medium Range. - If the maximum range of the system is 10,000 feet, acquisition will be simplified. The phase-lock bandwidth can be increased to reduce the acquisition time.

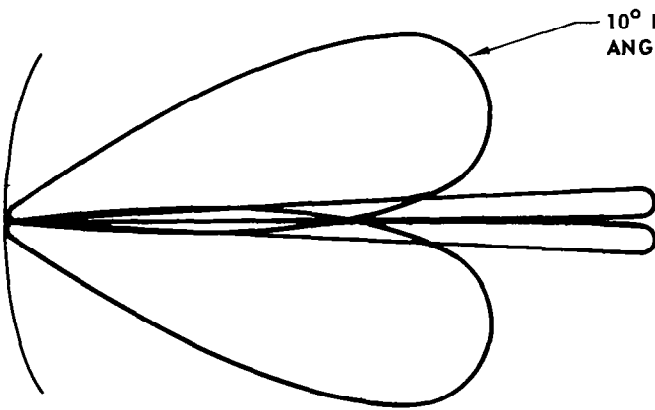
A completely unaided acquisition is performed by searching doppler and angle resolution cells. The number of antenna resolution cells, N , is approximately equal to the surface area of a sphere divided by the area of a spot, on the same sphere, illuminated by the antenna.

LONG RANGE



.5° BEAM .25° SQUINT
ANGLE TRACK
RANGE MEASUREMENT
RANGE RATE MEASUREMENT

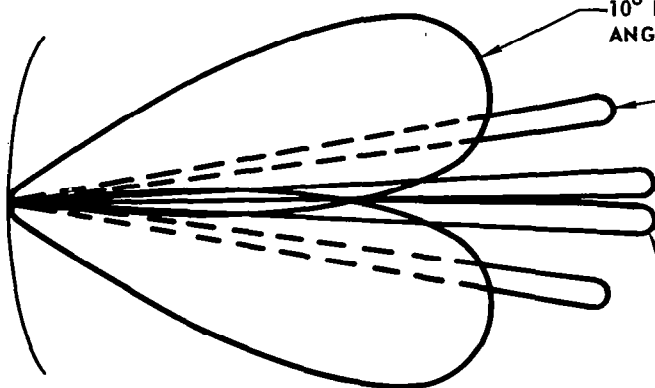
INTERMEDIATE RANGE



10° BEAM 5° SQUINT
ANGLE TRACK

.5° BEAM .25° SQUINT
RANGE MEASUREMENT
RANGE RATE MEASUREMENT

OBSERVATION AND CLOSURE



10° BEAM 5° SQUINT
ANGLE TRACK

.5° BEAM WIDTH 2.5° SQUINT
DOPPLER SAMPLE
(ROTATION RATE MEASUREMENT)
ROTATION AXIS

.5° BEAM WIDTH .25° SQUINT
RANGE MEASUREMENT
RANGE RATE MEASUREMENT

FIGURE 139 – ANTENNA OPERATION CHART

$$N = \frac{4/3 \pi r^2}{\pi \frac{(r\theta)^2}{4}} \quad (415)$$

$$N = \frac{16}{3\theta} \quad (416)$$

The above equation results in approximately 70,000 beam positions for the .5° beamwidth antenna. Approximately 15 db (S/N) is required for doppler acquisition; this allows a doppler channel bandwidth of 10,000 Hz. The maximum expected doppler is 150 kHz, therefore, 15 doppler cells are searched. The search time per doppler cell is 1×10^{-4} seconds. Since there are 7.0×10^{-4} angle cells, the acquisition time is $7.0 \times 10^{-4} \times 15 \times 1 \times 10^{-4} = 105$ seconds. After the target has been acquired in doppler and angle, the target is acquired in range. Filter bandwidths are then decreased to improve measurement accuracy.

When the range decreases to such a value that the target subtends an angle greater than the peak to peak separation on the .5° beamwidth .25° squint angle beams, the angle tracking function is switched to the broad beams.

Observation Range. - At R = 100 feet, the docking vehicle stops and observes the target vehicle. The following quantities are measured.

- a. Range, range rate
- b. Rotation rate
- c. Axis of rotation

The pointing direction is maintained by angle tracking with the broad beam antennas. Range and range rate are measured to the center of the target, using the narrow beam with .5° squint angle.

The 2.5 or 5° squint angle beams are used to measure the rotation rate and rotation axis. This measurement is inaccurate to the extent of the doppler spread in the beamwidth. This spread produces a larger fractional error as the squint angle is decreased. Therefore, for most accurate readings, the largest squint angle resulting in antenna beams intercepting the target is used. Since two sets of feeds are used for this measurement, target rotation rate and axis can be determined. The rotation rates and rotation axis obtained from these two samples of doppler are the projection of the values of these quantities into a plane perpendicular to the docking vehicles line of sight. The docking vehicle maneuvers until the line of sight axis perpendicular to the target rotation axis, as indicated by maximum measured rotation rate, is determined.

After the target rotation rate has been determined, a decision is made as to whether to continue the docking mission. This depends considerably on the purpose of the mission and the docking mechanism. If a docking maneuver is decided on and the target vehicle is spinning, the rotation axis information is

used to guide the docking vehicle to an on-axis approach. The docking vehicle then matches the measured spin rate of the target vehicle.

Short Range. - To complete the docking, the radar measures range, range rate, and LOS and samples the rotation doppler channels to maintain alignment with the axis of rotation of the rotating target vehicle.

The broadbeams are used for angle track during this portion of the mission.

The range measurement is made using the narrow beams with small squint angles. Since the ICW modulation rate would tend to infinity at zero range, the modulation frequency is held constant and range is measured by pulse techniques. Video detection circuitry is used for this measurement.

Functional Description

Antenna. - The antenna system chosen for this system consists of a parabolic reflector with three squint angles aided by auxiliary wide beam horns.

Parabolic Reflector Antenna Characteristics

Frequency - 70 GHz
Beamwidth - .5°
Gain - 50 db
Squint Angles - .25°, 2.5°, 5°.

This parabolic reflector is aided by four 10° beamwidth horns squinted 5° for use at very short range.

The .5° beamwidth, .25° squint angle beams are used for long range operation (range, range rate and angle track) and at short range (range and range rate).

The 2.5° and 5° squint angles are used to obtain doppler samples of the returned signal. Also, these beams are used to determine the approximate size of the target. These wide squint angle, narrow beams can be used to set limits on the angle tracking error.

The wide angle horns are used to develop amplitude comparison signals for angle tracking at short range. A sketch of the antenna beam positions is shown in figure 139.

Antenna Switching. - The 16 antenna beams require a microwave switching matrix to select the proper antenna beam and connect it to the transmitter receiver transmission line. The switching circuit is shown in figure 140 .

The antenna switching network requires 16 output states which meet the following specifications:

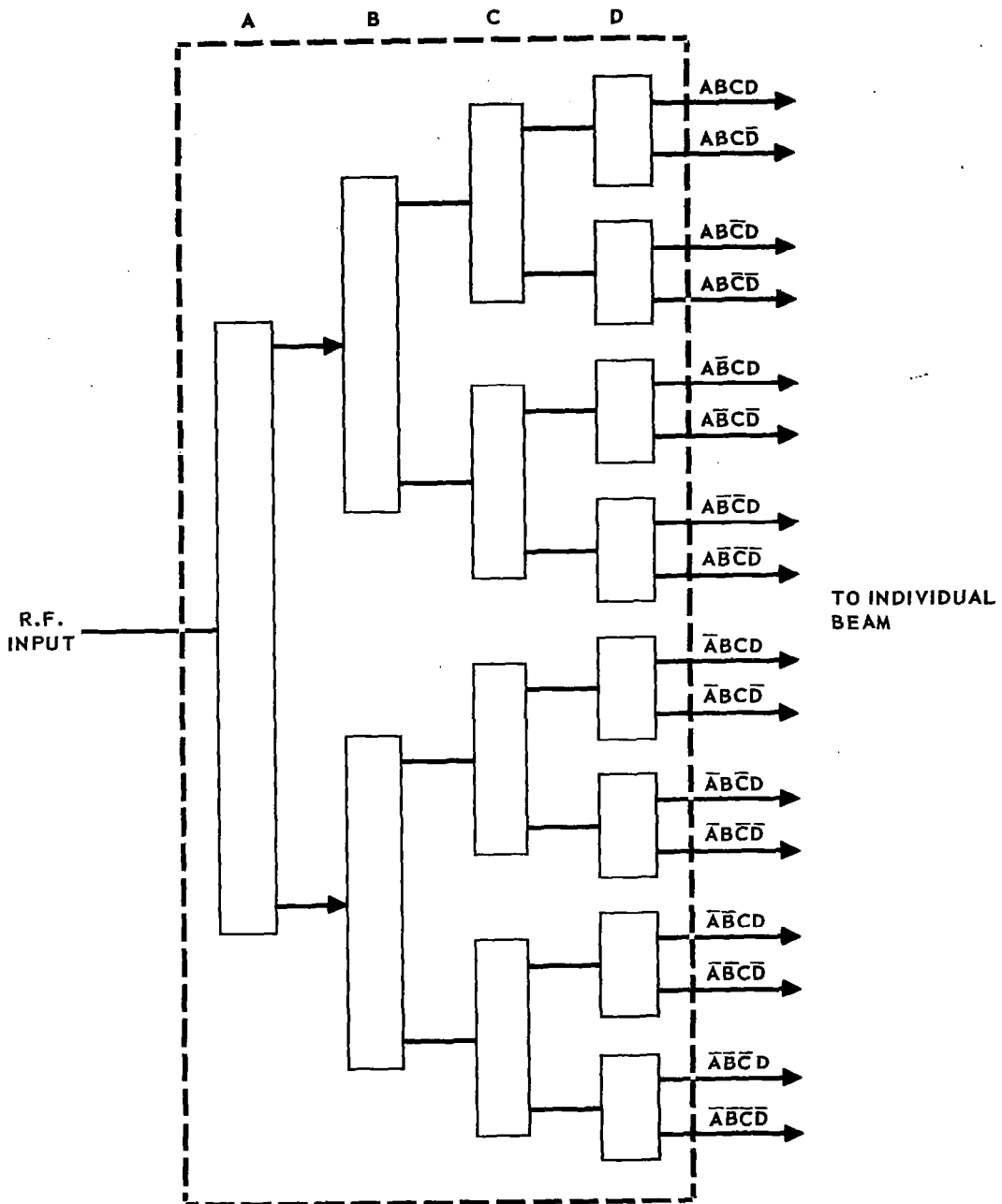


FIGURE 140 - BEAM SELECTION SWITCH

Frequency - 70 GHz
 Power - 100 mw
 Bandwidth - +500 MHz
 Insertion Loss - 1 db per switch (3 db total)
 ON-OFF ratio - 30 db

The switching elements considered are ferrite and diode phase shifters. A circuit to form the switch element is shown in figure 141.

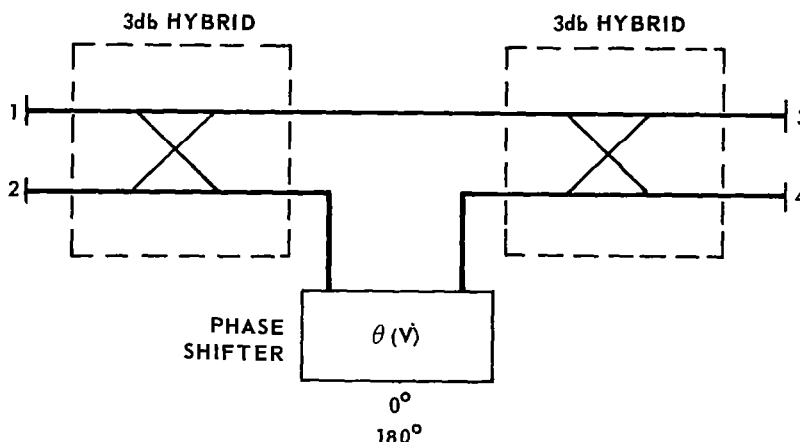


FIGURE 141 - A SWITCHING ELEMENT

The relationship in table 17 holds.

SWITCH PHASE	INSERTION LOSS	
	1-3	1-4
0°	HIGH	LOW
180°	LOW	HIGH

TABLE 17 - SWITCH TERMINAL RELATIONSHIPS

The device is bilateral, i.e., insertion loss 1-3 = insertion loss 3-1, etc. The required 16 output states require 15 switches (30 hybrids 15 phase shifters).

The 100 mw at 70 GHz power handling capability rules out diode switches, but is well within the capability of the ferrite switches.

Only 4 phase shifters need be energized at any one time. Then using the TRG E150, a typical phase shifter, the power required to operate this switch is .64 watts.

Transmitter. - The transmitter is a solid state multiplier chain with FSK switching for ICW ranging and ON-OFF switching for short range measurements.

Figure 142 is a block diagram of the multiplier chain. The transmitter includes a frequency synthesizer producing two CW frequency sources, which when multiplied to 70 GHz, differ in frequency by the IF frequency. A single pole double throw switch alternately connects the two frequencies to the multiplier chain. The microwave portion of this transmitter consists of six doublers with outputs at S, C, X, Ku, Ka, and V band. ON-OFF switching is accomplished by switching the input to the final multiplier stage.

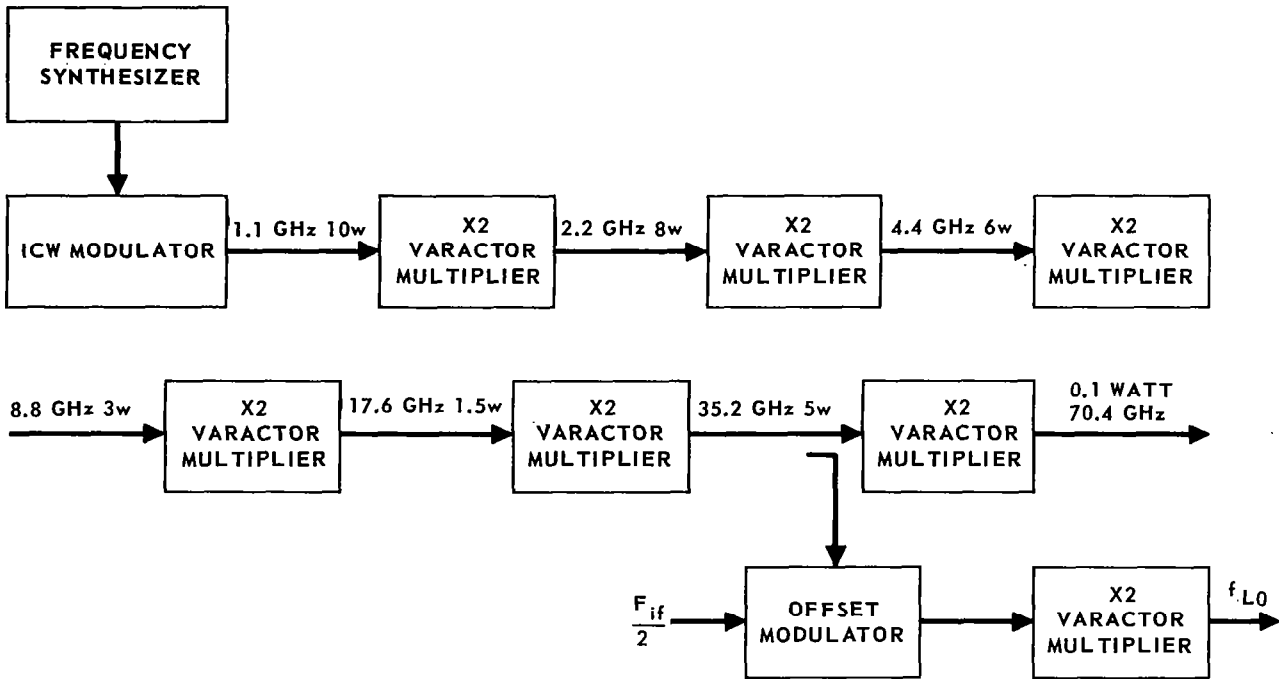


FIGURE 142 - A SOLID STATE 70 GHz TRANSMITTER

The local oscillator signal is generated directly in the multiplier chain for ICW ranging. For the short range measurement, it is necessary to generate the L.O. signal separately. This is done by coupling a signal from the Ka band multiplier to an offset modulator and doubling the output of this modulator.

A modulator to gate on the multiplier chain and to gate the receiver off is required at short range. ON-OFF ratios on the order of 60-70 db are required at 100 feet range. This is not presently possible with solid state switches at 100 mw power level. However, by switching an intermediate stage in the multiplier chain, this may be possible. To achieve minimum range performance of

1 ft, 2 ns rise and fall times are required.

At longer ranges, greater ON-OFF ratios are required to achieve adequate isolation; however, switching time measurements are relaxed. FSK (frequency shift keying) then appears promising, since much greater receiver isolation can be achieved with this gating technique.

Range Measuring Technique. - At long range, the ICW ranging technique, as described in an earlier section, is used. At ranges less than 100 feet, two techniques, a phase measuring technique and a time delay technique are considered for range measurement.

The phase measuring technique uses the phase of the ICW Modulation (a fixed 2.5 MHz, 50% duty cycle square wave for ranges < 100 feet) for the range measurement. A block diagram of this technique is shown in figure 143.

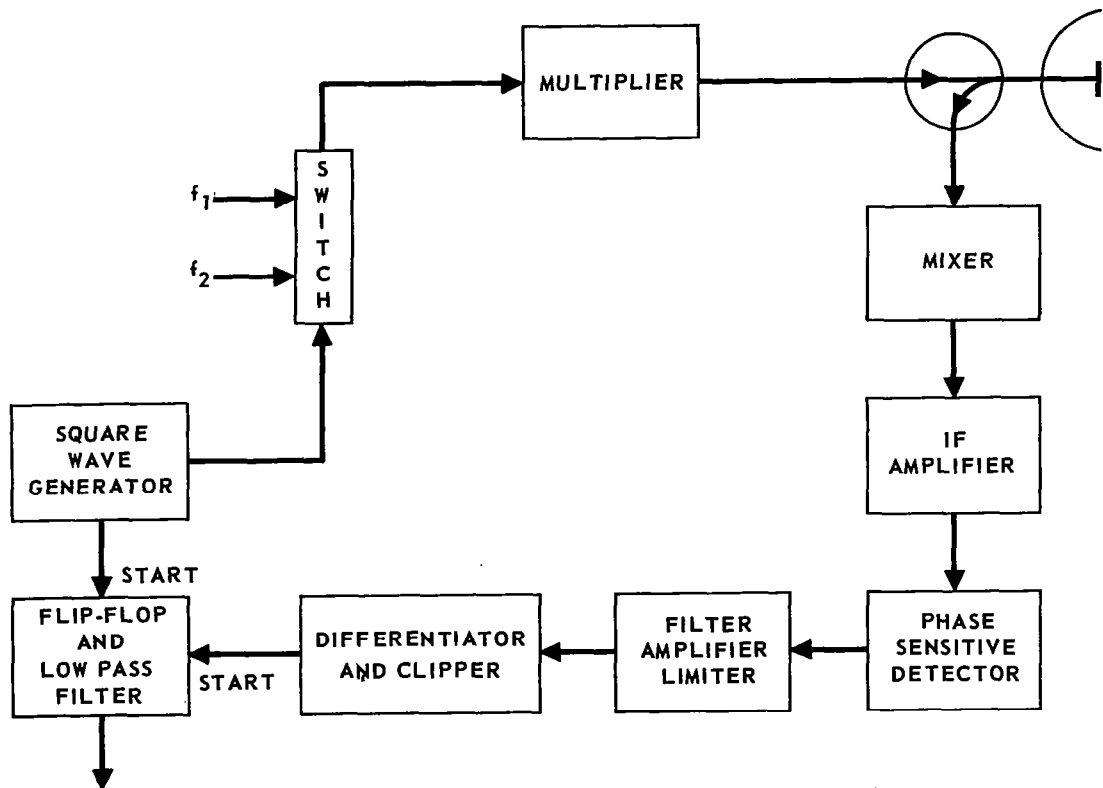


FIGURE 143 - NEAR RANGE MEASUREMENT BY MEASURING THE PHASE OF THE MODULATION FUNDAMENTAL FREQUENCY

The time relationship between the transmitted, received, and mixed frequencies is shown in figure 144.

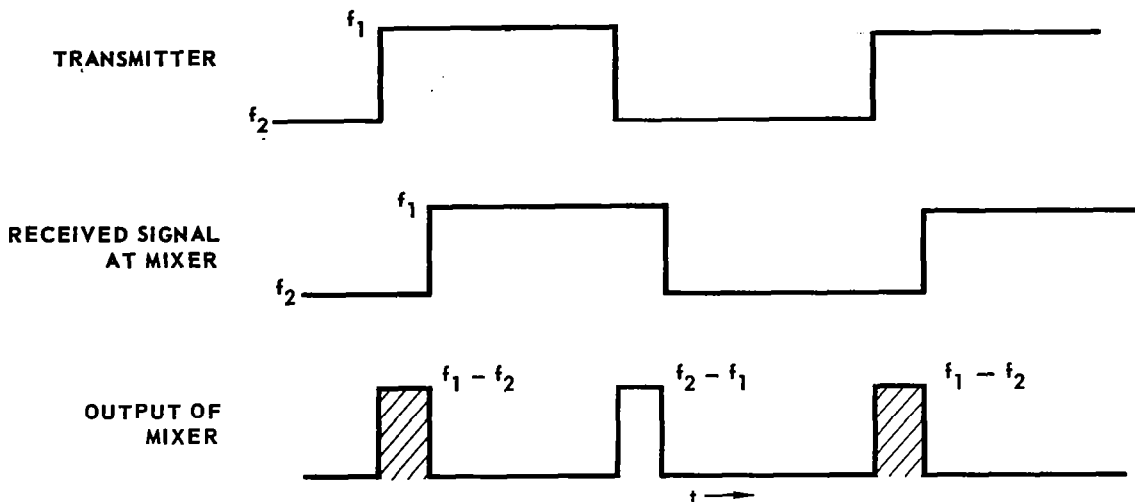


FIGURE 144 - PHASE MEASUREMENT TIME RELATIONSHIP

Let the receiver be represented by a band pass filter and the input represented by the pulsed function $x(t)$. Then :

$$y(t) = x(t) * h(t), \quad (417)$$

$$x(t) = \begin{cases} e^{-j\omega_0 t} & 0 < t < T, \\ 0 & \text{otherwise,} \end{cases} \quad (418)$$

$$h(t) = \text{Transform of } [H(\omega)], \quad (419)$$

$$h(t) = T \left[\frac{1}{1 + j 2Q \delta} \right], \quad (420)$$

$$h(t) = T \left[\frac{1}{1 + j \left(\frac{\omega_0}{\Delta\omega} \right) \left(\frac{\omega - \omega_0}{\omega_0} \right)} \right], \quad (421)$$

$$h(t) = e^{-j\omega_0 t} \frac{1}{\Delta\omega} e^{-\Delta\omega t}, \quad (422)$$

$$y(t) = \int_{-\infty}^{\infty} h(\tau) x(t - \tau) d\tau; \quad (423)$$

$$y(t) = \int_0^t \frac{e^{-j\omega_0\tau}}{\Delta\omega} e^{-\Delta\omega\tau} e^{j\omega_0 t} e^{-j\omega_0\tau} d\tau, t < T; \quad (424)$$

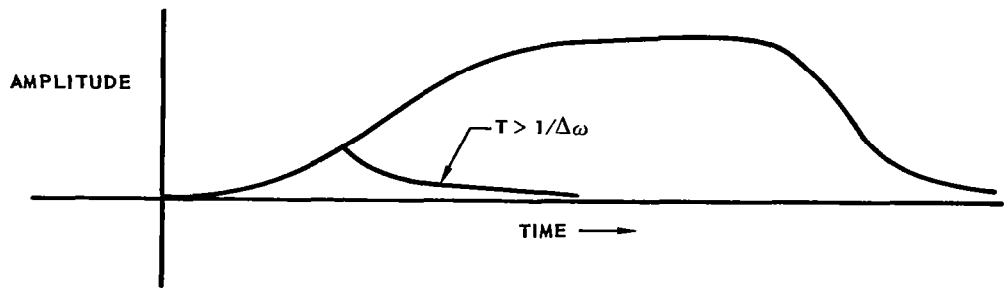
$$y(t) = \int_{t-T}^T \frac{e^{j\omega_0 t}}{\Delta\omega} e^{-j\Delta\omega\tau} d\tau, t > T; \quad (425)$$

$$y(t) = \begin{cases} \frac{e^{j\omega_0 t}}{j\Delta\omega 2} (1 - e^{-j\Delta\omega t}), & 0 < t < T; \\ \frac{e^{j\omega_0 t}}{j\Delta\omega 2} e^{-j\Delta\omega t} (e^{j\Delta\omega T} - 1), & t > T. \end{cases} \quad (426)$$

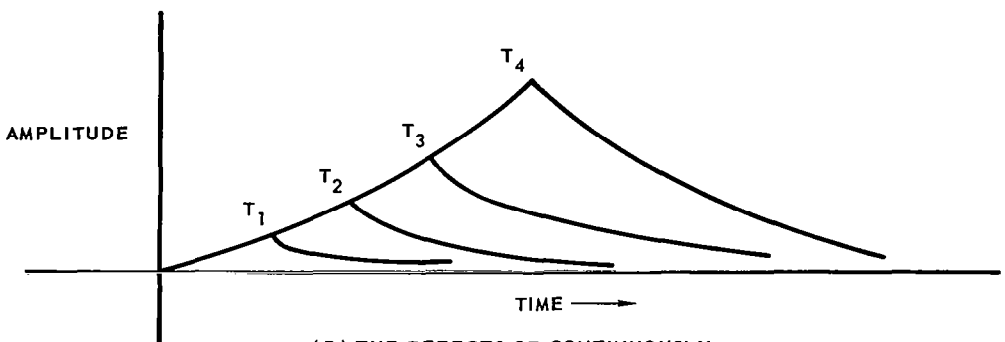
This envelope of this function is plotted in figure 145 A .

Of interest for minimum range performance is the response when T, the pulse width, is small compared with the rise time. Figure 145 B shows the filter response for different values of T.

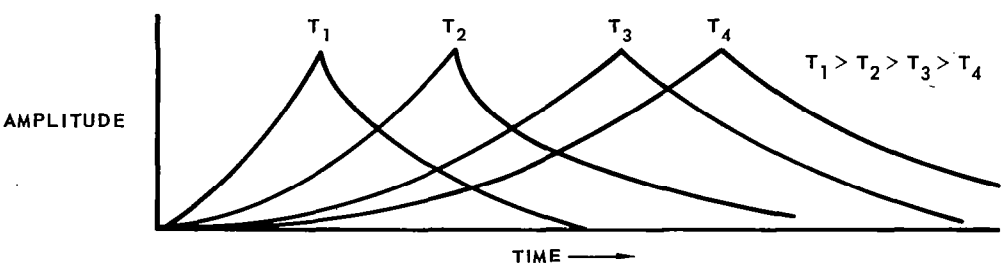
Since the amplifier has AGC, this response is normalized. The position of the peak output corresponds to the end of the IF pulse. (Figure 145C.) The width of the pulse however changes with delay. As the number of stages of filtering increases, the waveform is smoothed, and the peak is no longer well defined. (Figure 145 D.) The shift of the phase of the modulation becomes a very poor indication of the decreasing range. (Figure 146.)



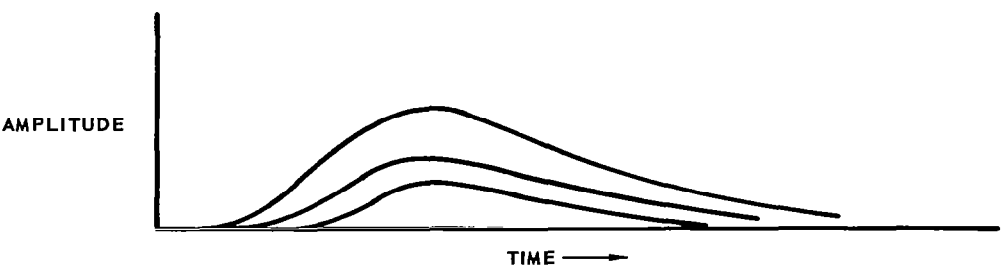
(A) COMPARING $T < 1/\Delta\omega$ AND $T \gg 1/\Delta\omega$



(B) THE EFFECTS OF CONTINUOUSLY DECREASING THE PULSE WIDTH.



(C) NORMALIZING EFFECTS OF THE AGC



(D) MULTISTAGE SMOOTHING

FIGURE 145 - IF OUTPUT ENVELOPE

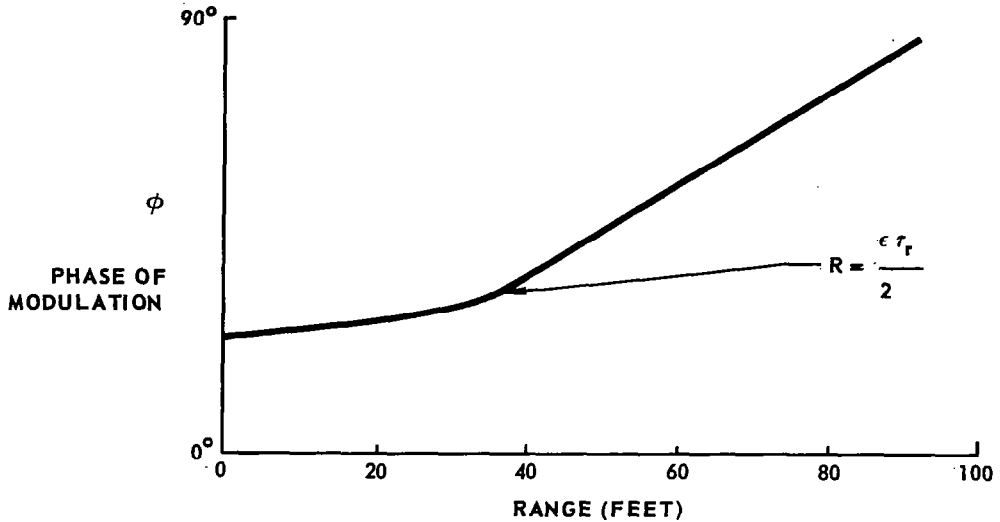


FIGURE 146 – DEGRADED PHASE RANGE RELATIONSHIP

Therefore, this technique does not appear to be suitable for accurately measuring short ranges.

The time delay technique can be implemented by measuring the time of arrival of the trailing edge of the returned radar signal or by measuring the time of arrival of the leading edge of the returned radar signal. Table 18 compares these techniques.

TABLE 18 – RANGE MEASUREMENT – LEADING EDGE TRAILING EDGE COMPARISON

	ADVANTAGES	DISADVANTAGES
LEADING EDGE (USING BROAD BEAM ANTENNA)	1. MEASURES CLOSEST RANGE 2. NOT DEPENDENT UPON TARGET SHAPE 3. NO MULTIPATH EFFECTS	1. REQUIRES ADDITIONAL MODU- LATION (SHORT PULSE) 2. LESS SENSITIVE, REQUIRES BROADBAND SUPERHETERO- DYNE RECEIVER
TRAILING EDGE (USING NARROW BEAM ANTENNA)	1. REQUIRES NO ADDITIONAL MODULATION 2. DOES NOT REQUIRE BROAD BAND RECEIVER	1. DEPENDENT UPON ANTENNA POINTING ACCURACY 2. SENSITIVE TO MULTIPATH

The trailing edge time delay measurement is chosen as the better technique for this application because of its simplicity, better sensitivity and equivalent measurement accuracy capability. Figure 147 is a block diagram for this system.

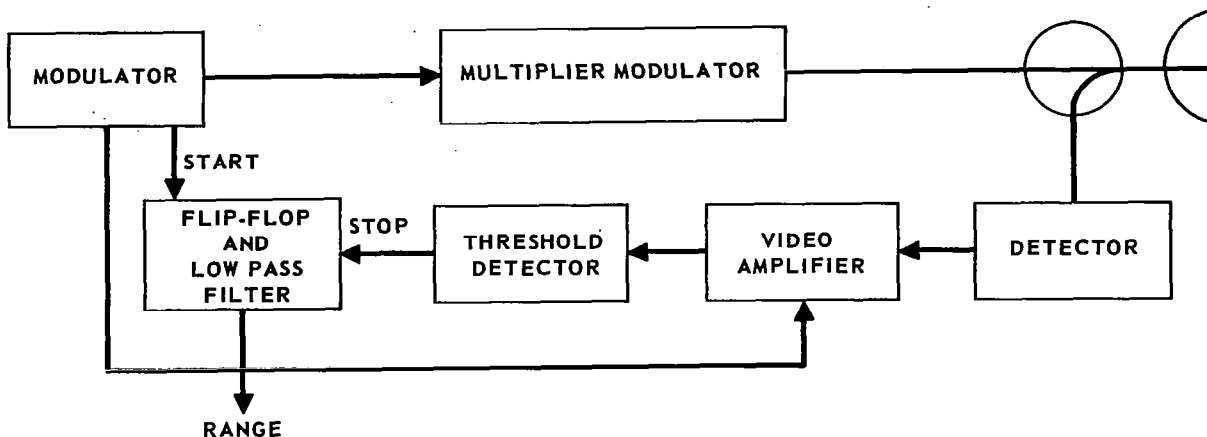


FIGURE 147 - VIDEO RANGE MEASUREMENT SYSTEM

It is necessary to gate the video amplifier until the received signal exceeds the feedthrough signal. A typical value for a feedthrough signal level is -30 db. A conservative value for the range for a unity received signal feedthrough signal ratio can be calculated if it is assumed that the transmitted signal is intercepted by the target and reflected with no directivity. Then the received power is

$$P_r = \frac{P_t G_t \lambda^2}{(4\pi R)^2} \quad (427)$$

The feedthrough signal $P_{FT} = \left(\frac{P_{FT}}{P_t}\right) P_t$

then equating P_r and P_{FT} and solving for R we obtain:

$$R = \left(\frac{G\lambda^2}{4\pi \frac{P_{FT}}{P_T}} \right)^{1/2} \quad (428)$$

Solving for R using the 50 db antenna at 70 GHz, a unity signal to feedthrough ratio is obtained at R = 11 feet. Figure 148 shows the relative signal and feedthrough at different ranges.

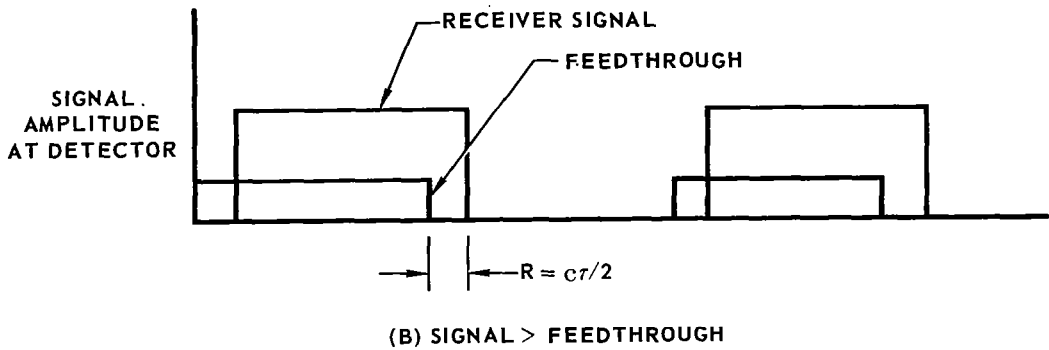
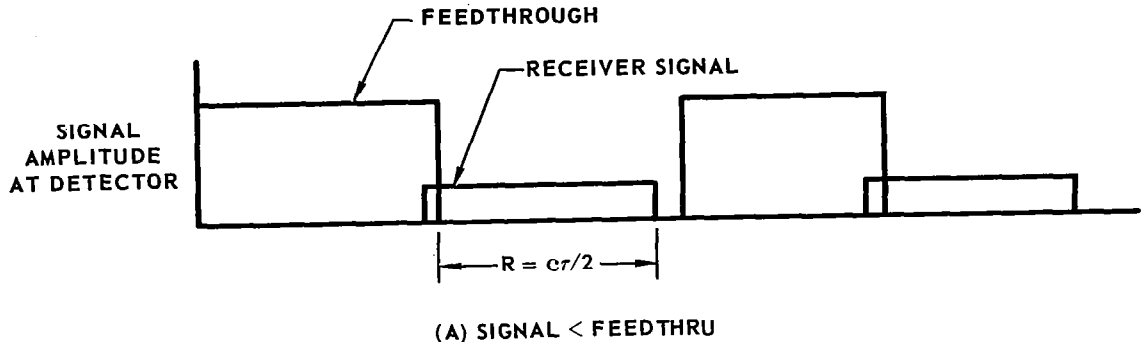


FIGURE 148 – SIGNAL – FEEDTHROUGH RELATIONSHIPS

The bandwidth requirement is primarily determined by the minimum range at which feedthrough gating is required. The occurrence of the threshold crossing of the trailing edge decreases linearly with decreasing range. At long ranges (ranges where the feedthrough is greater than the reflected signal) the input to the video amplifier is gated off to allow the video amplifier AGC signal to be derived from the reflected signal only. At short ranges, $\approx 10'$, the echo signal will be greater than the feedthrough signal and the gating can be removed. A video amplifier with a rise and fall time of $\tau = 20$ ns is required. This results in a 20 ns pulse at the input of the video amplifier. Using the usual rise time bandwidth relationship:

$$\tau = \frac{.45}{B}, \quad (429)$$

$$B = \frac{.45}{20} = 22.5 \text{ MHz}. \quad (430)$$

Time delay change due to changes in signal level and change in environmental conditions is the main source of error for this technique.

Range Accuracy. - The accuracy of the range measurement as a function of range is shown in figure 149. The errors are due to channel noise and instrumentation. The errors due to receiver noise for ranges greater than 100 feet are discussed in the section on ICW radar, and are given by:

$$\sigma_R^2 = \frac{C^2 B_s}{(8 \text{ fm})^2 (S/N_0)}. \quad (431)$$

This expression is a function of the smoothing bandwidth B_s , the highest modulation frequency f_m and the signal to noise power density ratio S/N_0 . In this calculation $B_s = 10 \text{ Hz}$, $f_m = 2.5 \text{ MHz}$ (the highest ICW modulation frequency used) and S/N_0 , which is range dependent is given by:

$$S/N_0 = \frac{P_t G_t^2 \sigma \lambda^2 L}{(4\pi)^3 R^4 kTB (NF)}, \quad (432)$$

where:

$$P = 100 \text{ mw} = -10 \text{ dbw},$$

$$\lambda = .42 \text{ cm} = 30 - 6.2 = -23.8 \text{ db/meter},$$

$$NF = 15 \text{ db},$$

$$G = 50 \text{ db},$$

$$\sigma = 1 \text{ sq. meter} = 0 \text{ db},$$

$$L = 3 \text{ db},$$

$$(4\pi)^3 = 33.6 \text{ db},$$

$$B = 1 \text{ Hz} = 0 \text{ db}.$$

The standard deviation σ_R is calculated from equation 431 and the results are plotted as curve A in figure 149. A .1% tracking bias error for the ICW tracking loop is a typical value for instrumentation error. This error is plotted as curve B in figure 149. It is seen that this is the larger error for the ranges at which the ICW technique is used.

At 100 feet, the range measurement technique is changed to a time delay measurement. The received signal strength of -35 dbm is sufficient to use video detection. Using a 1N2792 diode as a video detector with a tangential sensitivity of -45 dbm, a 20 db video signal to noise ratio will result, which yields:

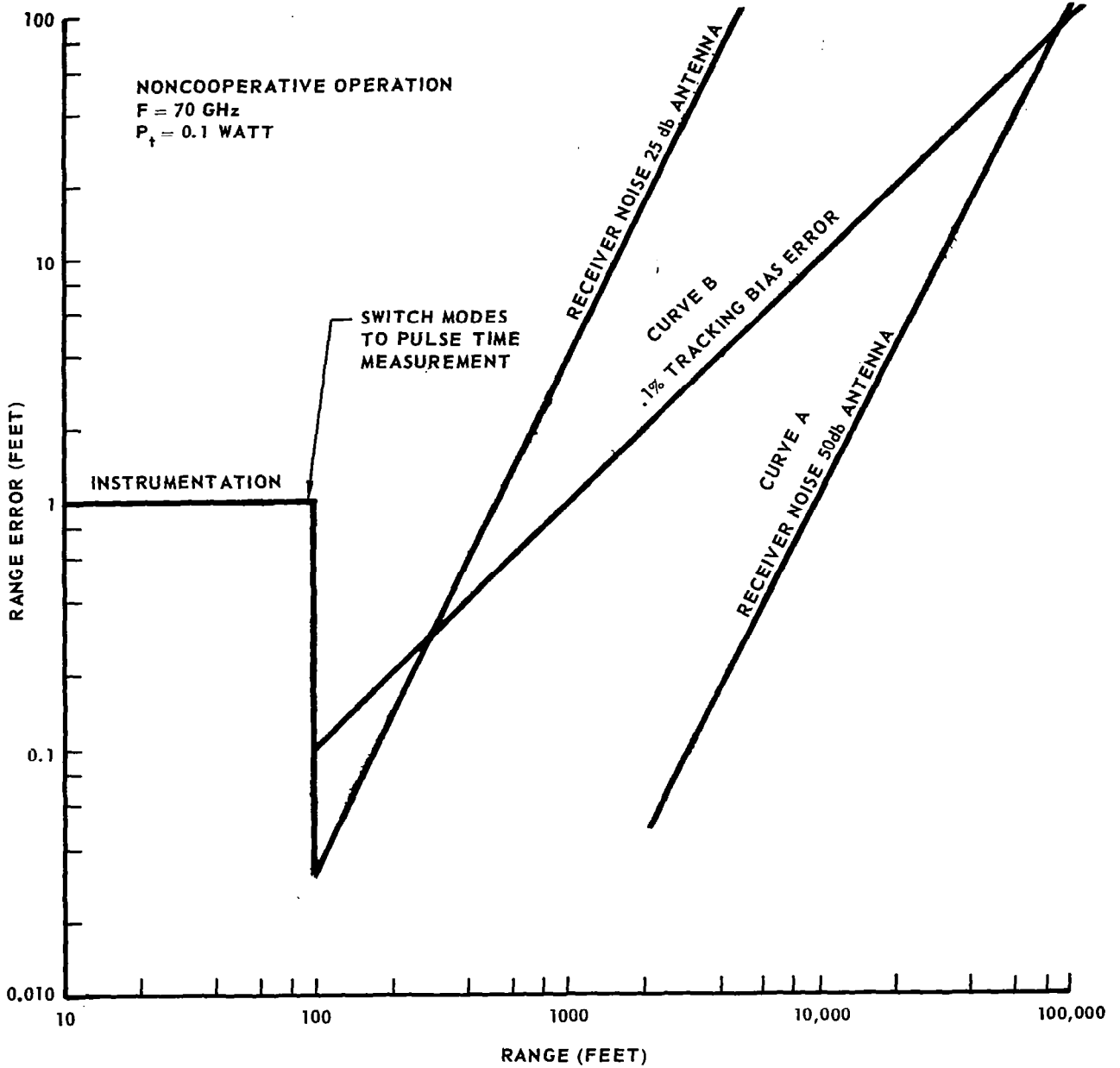


FIGURE 149 - RANGE ACCURACY

$$\delta_R = \frac{c \tau_r}{2 \sqrt{\frac{2S}{N}}} \quad (433)$$

$$\delta_R = \frac{c \cdot 20}{2 \sqrt{200}} = .035 \text{ feet.} \quad (434)$$

This value is considerably less than the lower limit on instrumentation errors which is estimated at 1 foot.

Range Rate Accuracy. - The range rate accuracy that can be achieved with ICW radar phase lock circuitry is given by:

$$\sigma_R^2 = \frac{\lambda^2 B_s^3}{G (S/N_0)} \quad (435)$$

At 10,000 feet, using $B_s = 10 \text{ Hz}$, $\lambda = 4.3 \text{ mm}$,

$$\sigma_R = 10^{-3} \text{ meter/sec,} \quad (436)$$

which is negligible.

Doppler Measurement. - At short range ($R = 100 \text{ ft.}$), the IF pulse is short, and spectrum fold over must be considered. However, by proper selection of the IF frequency and short range transmitter modulation frequency, the fold-over is interlaced with the transmitter modulation sidebands and interference is avoided. (figure 150.)

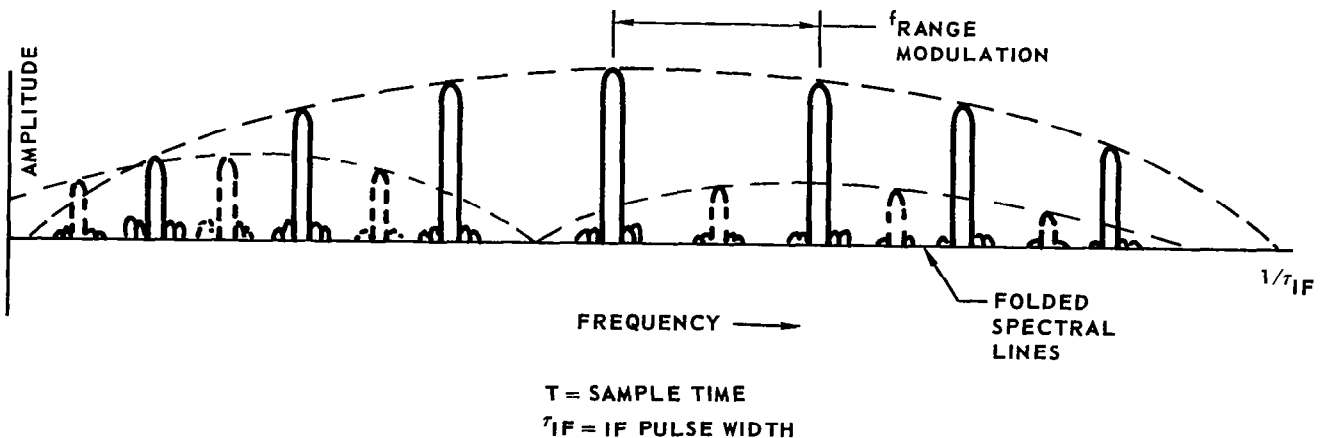


FIGURE 150 - IF SPECTRUM $R \ll 100$ FEET

The energy in the central spectral line decreases linearly as the pulse width decreases with range. However, the reflected power increases as $1/R^2$ and this more than makes up for the decrease in power with decreasing range.

As was indicated in the previous section on range rate accuracy, very high signal to noise ratios exist in the doppler channel. Therefore, narrow bandwidths and long smoothing times of the phase lock doppler measurement system are not needed, and the discriminator drawn in figure 151 is preferred for this measurement. (see table 19).

The radar measures range rate doppler ambiguously at long range. Previous considerations indicate that the maximum doppler to be measured will be 70,000 Hz (500 fps). To obtain unambiguous doppler information, the sampling frequency and ICW ranging frequency would need to be 140,000 Hz. The ICW frequencies at range of 100,000 to 10,000 ft. are 2.5 KHz - 2.5 MHz. A doppler ambiguity results. To eliminate this ambiguity problem, the radar will have to operate at a high ICW modulation frequency until the radar has locked up in doppler. Then the ICW ranging can start up and the radar will be locked to the central spectral line.

The rotation rate doppler measurement is made on a pulse basis and the accuracy is determined by the observation time and S/N ratio. Since this is a spot lighting operation, the $1/R^4$ radar equation does not hold. It will be conservatively assumed that all of the power transmitted illuminates a spot of finite dimension on the target and that this energy is reflected with isotropic scattering. The signal to noise ratio in the doppler channel is:

$$\frac{S}{N} = \frac{P_t LG \lambda^2}{(4\pi R)^2 KTB(NF)}, \quad (437)$$

$$= 86.6 \quad (438)$$

which results in a doppler accuracy of:

$$\delta_f = \frac{\sqrt{3}}{\pi T \sqrt{\frac{2S}{N}}}, \quad (439)$$

where $T = 11\text{ms}$,

$$\delta_f = 0.027 \text{ Hz.} \quad (440)$$

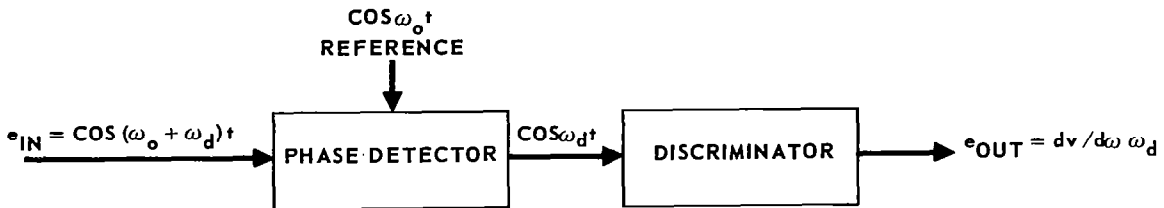
Angle Measurements. - The LOS angle is measured by tracking the LOS angle by sequential lobing amplitude comparison circuitry. This technique is described in the section on sequential lobing.

Since the sequential lobing frequency is fixed and the ICW modulation is a function of range unequal sample of energy in the comparison beams results. This results in channel unbalance as described in the section of amplitude comparison. However, since the $.5^\circ$ antenna is used at long range, this error is negligible. (A 2:1 unbalance results in only a $.063^\circ$ error).

The other source of error of importance at long range is the error caused by channel noise. From the section on sequential lobing, the expression for angular accuracy is:



(A) DISCRIMINATOR



(B) PHASE LOCK LOOP

FIGURE 151 – DOPPLER MEASUREMENT TECHNIQUES

TABLE 19 – DISCRIMINATOR vs. PHASE LOCK COMPARISON

	DISCRIMINATOR	PHASE LOCK
BANDWIDTH REQUIREMENTS	WIDE	NARROW
SAMPLING TIME REQUIREMENT	DEPENDS ON S/N RATIO	DEPENDS ON MIN DOPPLER TO BE MEASURED
PROCESSING REQUIREMENT	SEQUENTIAL	PARALLEL
INTEGRATION CAPABILITY	NONCOHERENT	COHERENT
ACCURACY CAPABILITY	LIMITED TO 0.1-1% MAXIMUM FREQUENCY	VERY ACCURATE. NOT DEPENDENT UPON MAXIMUM FREQUENCY.
AMBIGUITY CAPABILITY	NO AMBIGUITIES	AMBIGUOUS FOR $f \geq f_{\text{SAMPLING}}/2$.

$$\delta_{\theta} = \frac{\theta_{BW}}{\frac{2S^{1/2}}{N}} \quad (441)$$

This expression is plotted in figure 152 .

The limitation in angular accuracy at short ranges is glint noise. The RMS value of this error is approximately equal to 0.2 of the angle subtended by the target. This error is also shown in figure 152.

At a range of 100 feet, the docking radar must measure range, LOS, and the rotation rate of the target. This is done sequentially, using a frequency discriminator for the rotation rate doppler measurements. Since the doppler measurement ranges from 2.4 kHz (100^o sec rotation, 20 ft target) to 14 Hz (.1 fps velocity), it is necessary to read doppler to .1% of the maximum reading. This is difficult to achieve and may require two discriminators to cover this range.

Since a discriminator measures frequency on a single pulse basis, doppler ambiguities are not a problem. The sampling frequency is chosen to be compatible with the sequential lobing frequency and the bandwidth of the frequency discriminator.

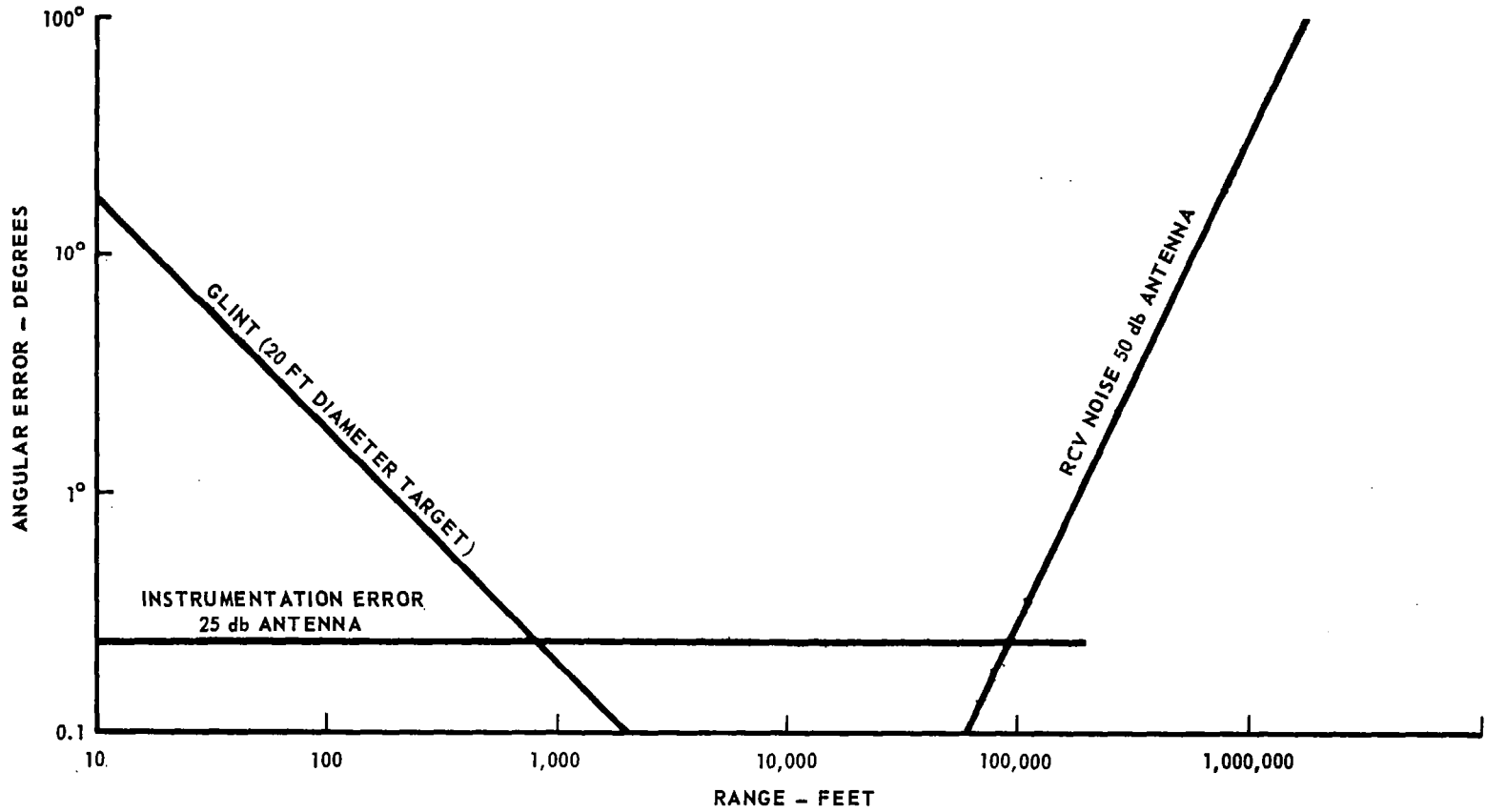


FIGURE 152 - ANGLE ACCURACY - MULTIPLE BEAM - ANGLE TRACK RADAR

COOPERATIVE INTEGRATED MEASUREMENT SYSTEMS

A "cooperative system" implies that some degree of cooperation is provided by equipment on the target vehicle as a part of a system which is required to measure the pertinent parameters associated with docking (and rendezvous). The degree of cooperation provided by the target vehicle can range in complexity from a simple passive reflector to an integrated "transponder - attitude transmitter". The target vehicle will, for some mission applications, be provided with self-attitude sensing and thrusters of its own so that it can align itself with the chasecraft for ease of docking. The target vehicle will, under some circumstances, have some degree of built-in stabilization. In general, the target vehicle can be physically identical to the chasecraft, it can be a structural mate, or it can be unrelated physically. The "best" cooperative measurement system, therefore will be a strong function of the mission application. Emphasis in this section is placed on systems which have "closed-loop" docking and rendezvous capabilities. It has already been demonstrated that rendezvous and docking can be performed by an astronaut who has available the necessary data and training to make the proper decisions and manually close the loop. It is felt, however, that in the future, closed loop docking will become commonplace and will provide the advantages of (a) higher reliability, (b) minimum fuel, (c) minimum time, and (d) minimum pilot involvement.

DESCRIPTION OF SYSTEMS WITH VARIOUS DEGREES OF TARGET COOPERATION

Typical cooperative system characteristics for various degrees of target cooperation are shown in Table 20. Typical LOS and target attitude angle measurement capabilities are shown in figures 153 and 154 respectively. For any specific mission application, it is desirable to maximize the system with respect to capability, reliability, and accuracy while minimizing the system for complexity, weight, size, and cost. An optimization of the above factors for one specific mission is, in general, not the correct optimization for a different mission. For example, the "best" system for docking a supply ship with a space station is probably not the optimum system for gathering sections for construction of a space station. The first case is expected to have a high degree of cooperation while the second has minimal cooperation.

Systems Using Passive Reflectors

A basic noncooperative chasecraft radar, when used with a passive reflector or an array of reflectors on the target vehicle, is the simplest form of cooperative system. The reflector can be simply a flat place on the surface of the target, a corner reflector, a retro-directing array, a scattering array,

TABLE 20 – COOPERATIVE SYSTEM CHARACTERISTICS FOR VARIOUS DEGREES OF TARGET COOPERATION

CASE	A	B	C	D	E	F	G
DEGREES OF TARGET COOPERATION	NONE	PASSIVE REFLECTORS ONLY	CODED REFLECTORS	ELECTRONIC ATTITUDE BEACONS	ELECTRONIC ATTITUDE BEACONS PLUS TRANSPONDER	TRANSPONDER WITH ANTENNA SEQUENCING	TRANSPONDER WITH DF AND SELF ALIGNING CONTROL SYSTEM
TARGET EQUIPMENT	NONE	STRUCTURAL	MECHANICAL	RF SOURCE AND SIMPLE ELECTRONICS	BASIC TRANSPONDER PLUS SIMPLE ELECTRONICS AND ANTENNA SWITCHING		BASIC TRANSPONDER PLUS PHASE COMPARISON DF EQUIPMENT
CHASE CRAFT EQUIPMENT	COMPLETE NONCOOPERATIVE RADAR				COOPERATIVE RADAR SYSTEM		
	COMPLEX TARGET ATTITUDE RATE SENSING		ADDITIONAL ATTITUDE DATA PROCESSING EQUIPMENT			MULTI-CHANNEL PHASE DETECTION AND PROCESSING	
MAXIMUM RANGE FOR ACCURATE TRACKING * (RANGE, RANGE RATE, LINE-OF-SIGHT ANGLES)	20 MILES				200 MILES		
MAXIMUM RANGE FOR ACCURATELY DETERMINING TARGET ATTITUDE	NO CAPABILITY		2 MILES	200 MILES			
MAXIMUM RANGE FOR ACCURATELY DETERMINING TARGET RATE	100 FEET		2 MILES	200 MILES			

* σ RANGE = 1 FT + 0.001R, σ RANGE RATE = 0.3 FPS + 0.001R

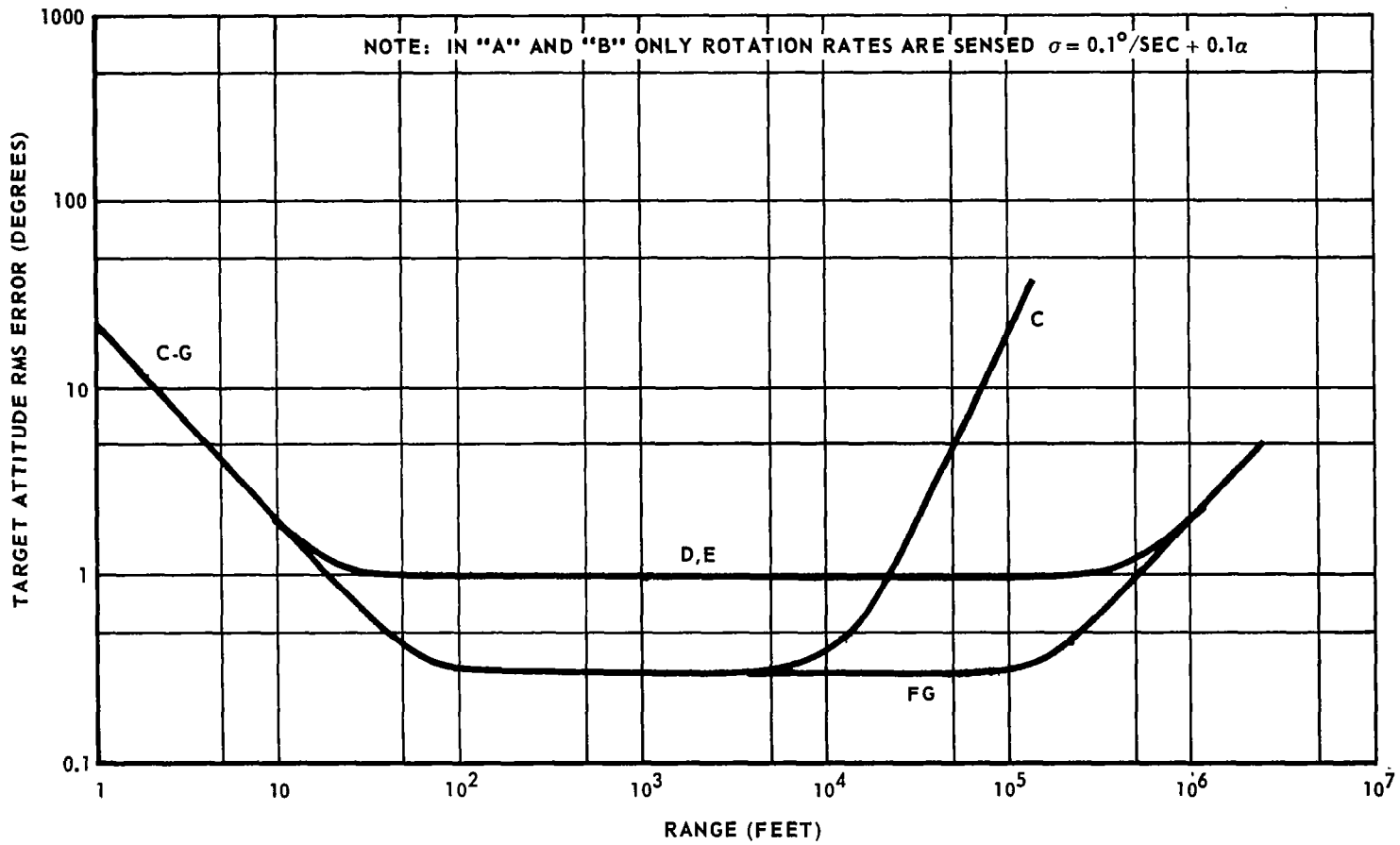


FIGURE 153 – TYPICAL TARGET ATTITUDE SENSING ACCURACIES

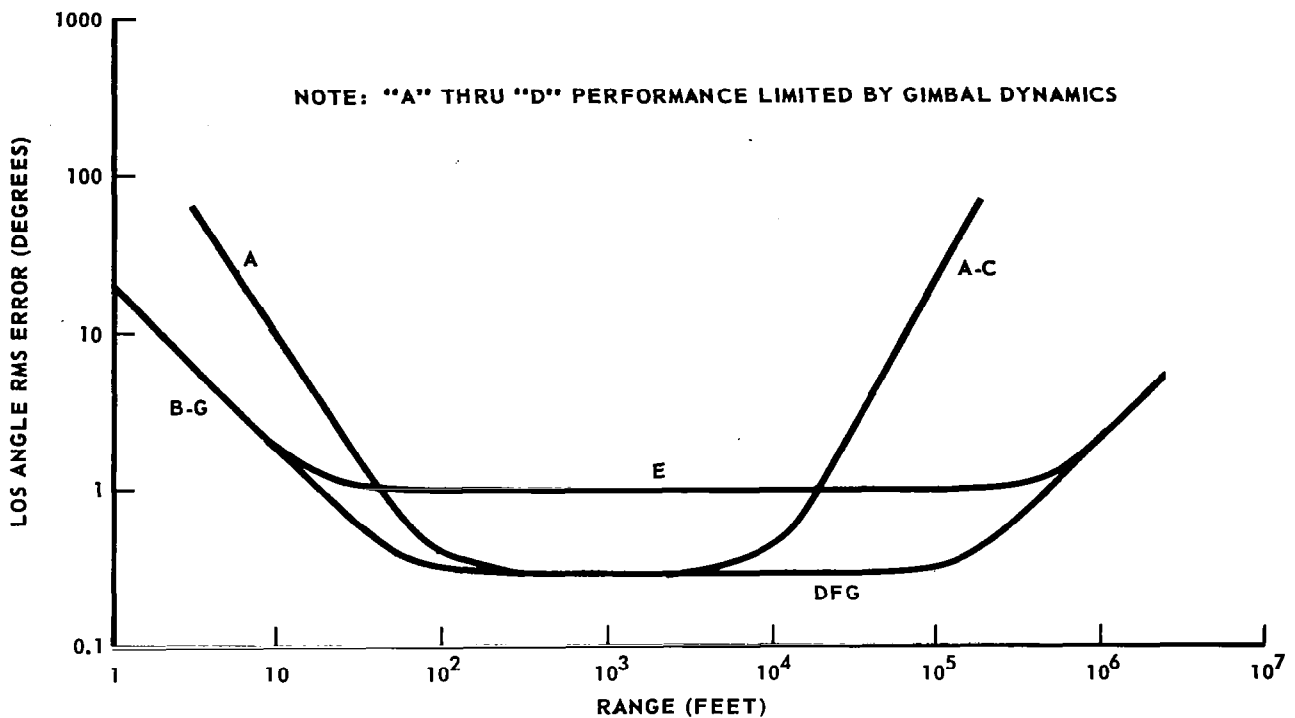


FIGURE 154 - TYPICAL LOS PERFORMANCE CHARACTERISTICS

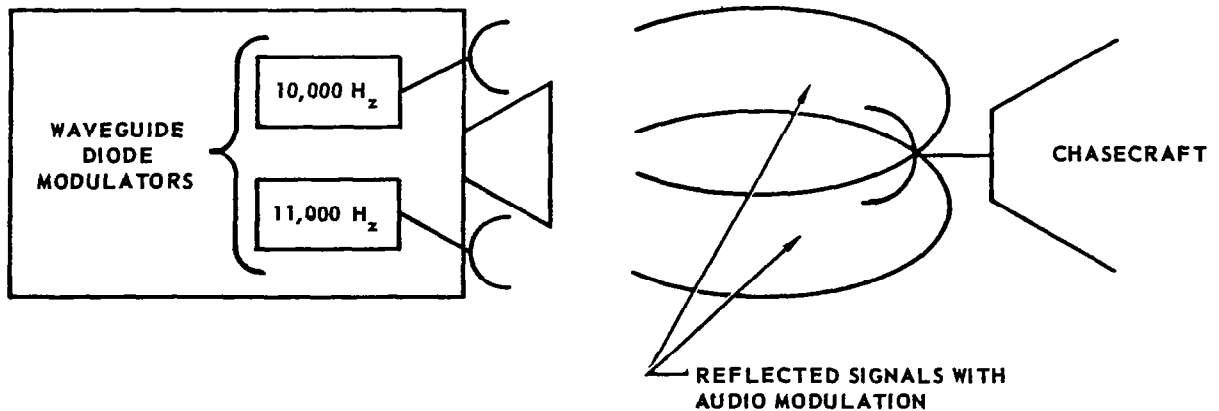
or a group of any of the above. A simple "flat" on the target has very limited usefulness if there is relative rotational motion between the two vehicles. If the target is stabilized, however, a simple reflecting surface or corner reflector provides a point for lock-on of the radar system to help eliminate "target extent" measurement errors. "Target extent" problems cause a completely noncooperative system to be considerably more complex than would otherwise be required. When relative rotation is present, a scattering array may have some application, if the returned signal is made to change by the rotational motion of the target in order to provide attitude and attitude rate data. However, the complicated processing requirements, slow data rates, and range restrictions inherent in this type of approach are serious disadvantages in many mission applications.

Systems Using Fixed Coded Reflectors

The complexity of a noncooperative docking radar system can be decreased at the chasecraft if attitude coded reflectors are provided on the target. At

the same time, the capability for closed-loop docking can be greatly enhanced. It is possible to code the signal returned from a fixed reflector or retro-director to (a) simplify lock-on, (b) provide a much greater solid angle in which lock-on is possible, (c) simplify processing, and (d) provide attitude alignment coding from which an alignment error signal can be generated. An example of placing coding on a set of fixed reflectors is shown in Figure 155 .

FIGURE 155 - FIXED CODED REFLECTORS



The transmitted energy impinging on each of four antennas is modulated with separate audio frequencies and reradiated in squinted patterns. The alignment error signal is generated by comparing the amplitude of the four modulation frequencies received in the chasecraft. This technique, however, suffers from the following disadvantages:

- a. The lock-on and tracking enhancement is dependent on target stability and will often be lost.
- b. Useful range is limited.

Systems Using Attitude Coding by Moving Reflectors

A basic noncooperative radar can be modified to decode the return from moving reflectors, shown in Figure 106 , by adding the module shown in Figure 114. This system, by using only two or three moving reflectors, provides target attitude information from almost any aspect.

Systems Using Multi-Frequency Beacons

Another promising system for determining target attitude combines a basic tracking radar with a set of multi-frequency beacons on the target. The use of

multi-frequency beacons as a target attitude coding technique was discussed in the section on target attitude determination techniques. This technique can be integrated with either a cooperative radar transponder or a noncooperative radar system by providing for amplitude comparisons to extract the target attitude information. The principal advantages of this method of obtaining target data are:

1. The transmitting and receiving equipment are of simple, highly reliable solid state design.
2. The generation of error signals is straightforward.
3. Continuous error signals and high data rates are available to accommodate closed-loop docking techniques.

Possible problem areas are:

1. Beacon frequencies must be chosen to minimize EMI with the range-range rate radar, communications, and LOS systems.
2. A high degree of amplitude stability is required on both ends of the link.

Integrated Phase System (IPS)

The IPS measures range, range rate, line of sight angles, and target attitude angles by phase measurement at the chasecraft. These parameters can be sensed throughout a wide variation in range, which makes the system suitable for rendezvous as well as docking. A simplified block diagram of the system is shown in Figure 156. Range and range rate are obtained by use of a four tone, sine wave modulated, PM-CW, radar-transponder system.

Multiple phase comparisons of signals received by a set of three antennas on the chasecraft from a similar set on the target provide LOS and target attitude data. The system will be described in more detail in the next section.

The Electronic "Omni" System (EOS)

A simplified block diagram of the Electronic Omni System is shown in Figure 157. The EOS employs the electronic attitude coding technique discussed in an earlier section, and makes use of a sine wave modulated, PM-CW, radar-transponder system using the same RF channel. Line of sight is obtained at the chasecraft by a null-seeking sum and difference phase comparator. This has been selected as one of the favored rendezvous and docking systems and will be discussed in more detail in a later section.

276

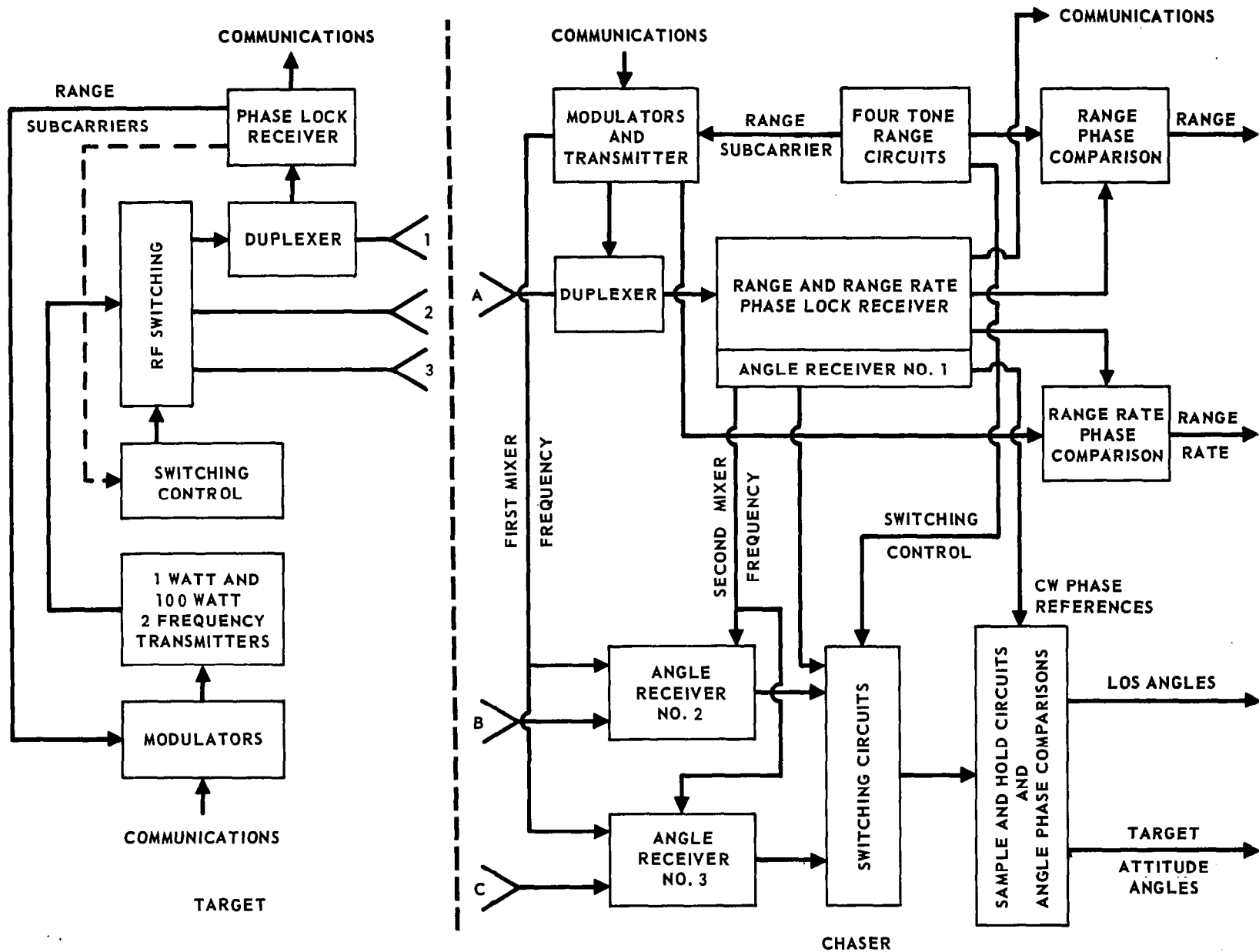


FIGURE 156 - IPS DOCKING (AND RENDEZVOUS) SYSTEM

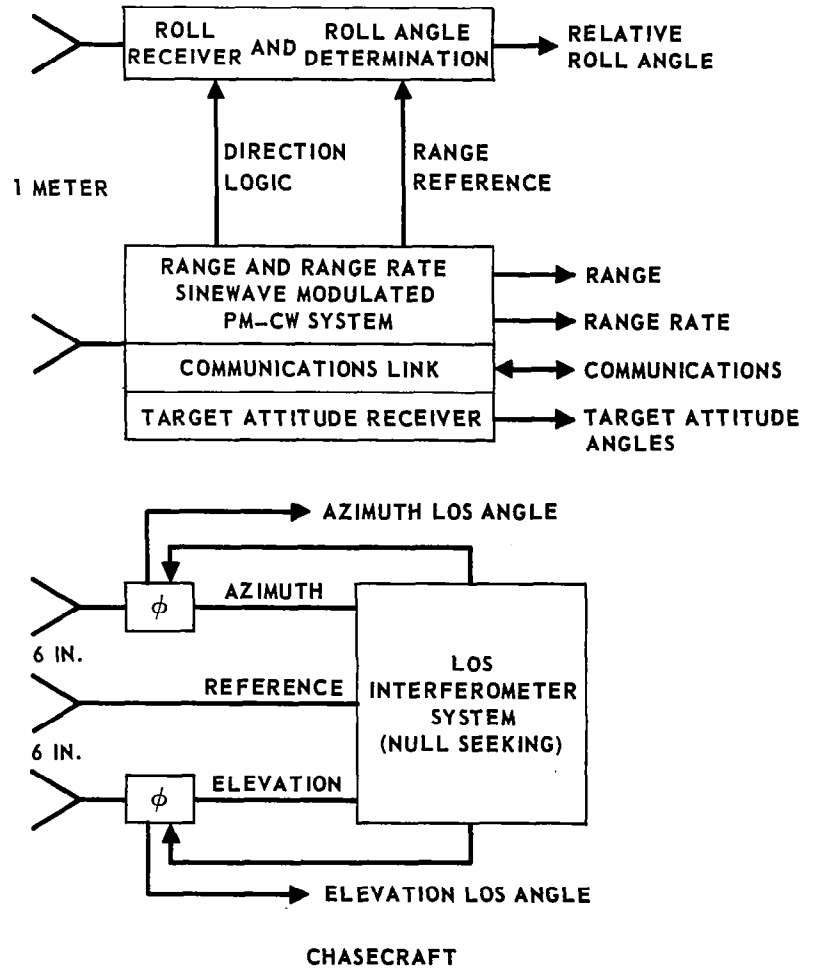
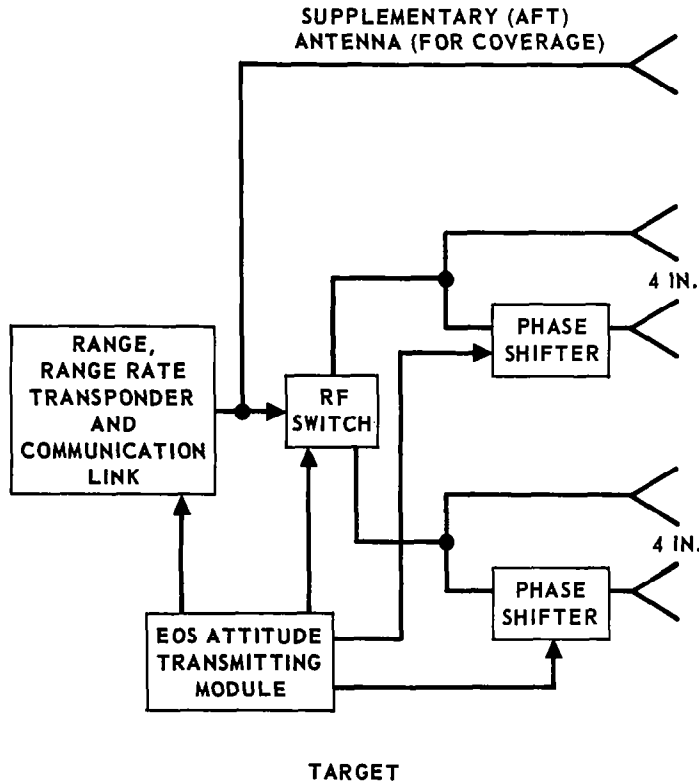
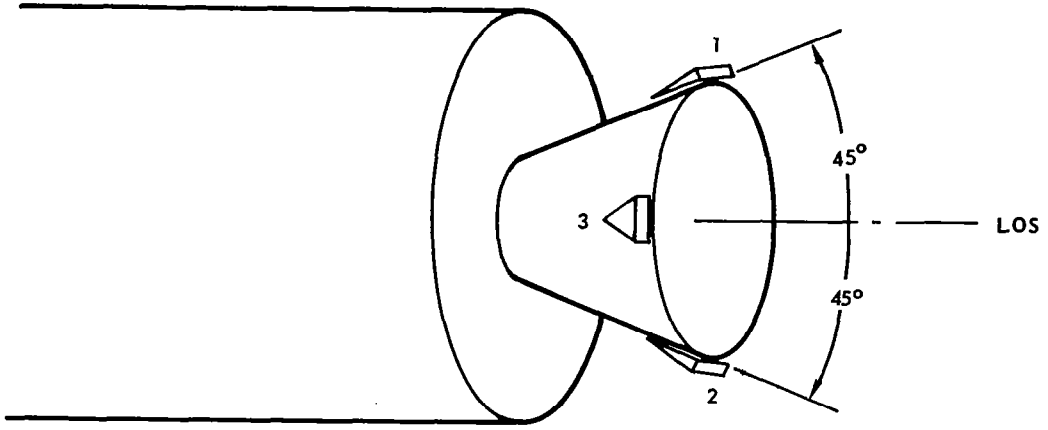


FIGURE 157 - EOS DOCKING AND RENDEZVOUS SYSTEM



**FIGURE 159 – ANTENNA CONFIGURATION FOR DOCKING
ALIGNMENT SYSTEM – TARGET SENSING**

angular rates. The alignment error signals are generated as follows. The signal being radiated from the chasecraft is received by two pair of elliptically polarized antennas. The relative amplitude in one pair is processed by the sum and difference or the ratio technique, as discussed earlier, to produce a measurement of one angle. The other angle is generated by the same method using an orthogonal antenna pair (not shown). For precise measurement of relative movements during close approach, doppler sensing (optional) is provided as shown. A frequency track loop tracks the carrier frequency of one of the antennas and provides the frequency to be mixed with the signal being received on the other antenna of the pair. The audio difference frequency is then a measure of rotational movements. The two antenna pair are of oppositely oriented elliptical polarizations, so that total amplitude differences in pairs can be used to detect relative roll movements.

Conclusions

Cooperative docking systems ranging from those which have minimum capability and cooperation to highly sophisticated ones capable of accurately sensing all dynamic parameters of the docking problem have application to one or more of the missions discussed in the requirements section. A system will usually be tailored to best fill the needs of a specific mission. For example, some docking missions will require only a simple range rate measuring device as an astronaut aid; others will require a complex system capable of rapid automatic docking. Although the selection of an optimum system for each of the many missions is beyond the scope of this study, an investigation of systems which meet the more stringent mission requirements illustrates the use of many of the techniques which are also applicable to missions having lesser requirements. Two systems were, therefore, selected which not only have the capability of accurately sensing all the parameters required for automatic docking, but also can be used during the rendezvous mode of the mission. These two systems, the Integrated Phase System and the Electric "Omni" System, are described in detail in the following two sections.

INTEGRATED PHASE SYSTEM (IPS)

The integrated phase system employs a combination of the sine wave modulated FM-CW radar; the phase comparison LOS tracker, and the integrated phase technique for target attitude measurement. A block diagram of the system is shown in Figure 156. Each of the spacecraft is provided with a set of three antennas, equally space about the centerline and oriented such that they are interlaced when in the docked position. Phase comparisons provide an indication of all transmission path differences, from which relative attitude is defined. The major subsystems, their capabilities, and their limitations are discussed in detail in this section.

Range and Range Rate Sensing.- The waveform transmitted by the chascraft is a CW, L-Band signal containing four phase modulated subcarriers. A coherent transponder on the target vehicle repeats the signal received at the target with a coherent carrier frequency translation and preserves the phase of the received range subcarrier modulation. In this manner, the signal received at the chascraft contains the desired modulation phase shift information and the carrier frequency doppler shift information. Since the frequency of the received signal at the chascraft is offset from the transmitted signal frequency the receiver feedthrough problem is minimized.

Several range subcarriers are required to provide both a large unambiguous range and the required accuracy. High subcarrier frequencies result in accurate information at the expense of range ambiguities. Thus, high frequency subcarriers are required to satisfy the accuracy requirements and lower frequency subcarriers are required to resolve the ambiguities. Four subcarrier frequencies provide a potential accuracy of ± 0.13 m with an unambiguous range of 4×10^5 m, allowing the system to double as a rendezvous radar. The results are shown in figure 160.

The signal transmitted by the chascraft uses the range subcarrier sinusoids to phase modulate the carrier signal. The carrier frequency is Kf_1 , where K is an integer determined by the frequency multiplication factor used in the target transponder discussed below. As shown in a later section, $K = 12$ and $f_1 = 81.2$ MHz, such that the transmitted frequency is 971 MHz. For illustrative purposes, consider only a single range subcarrier at a frequency, f_m . Then the form of the transmitted signal is:

$$\cos \{2\pi k f_1 t + \beta \cos (2\pi f_m t)\} , \quad (442)$$

where β is the modulation index. Then the form of the signal received by the target vehicles is:

$$\cos \left\{ 2\pi k f_1 \left(t - \frac{R}{c} \right) + \beta \cos \left[2\pi f_m \left(t - \frac{R}{c} \right) \right] \right\} , \quad (443)$$

where R is the target-to-chascraft range and c is the velocity of light.

Figure 161 shows the formation of the signal transmitted by the target transponder. The transponder employes a coherently offset phase locked loop to track the received carrier frequency. This loop outputs a signal at a frequency equal to $k/k-1$ times the received RF signal frequency. In addition to providing the coherently related offset frequency, the loop also serves to demodulate the phase modulated range subcarrier sinusoids. For the simple single tone case considered here, the signal resulting from the range subcarrier demodulation is:

$$\beta \cos \left[2\pi f_m \left(t - \frac{R}{c} \right) \right] , \quad (444)$$

and the form of the coherent offset signal is:

$$\cos \left[\frac{k^2}{k-1} 2\pi f_1 \left(t - \frac{R}{c} \right) \right] . \quad (445)$$

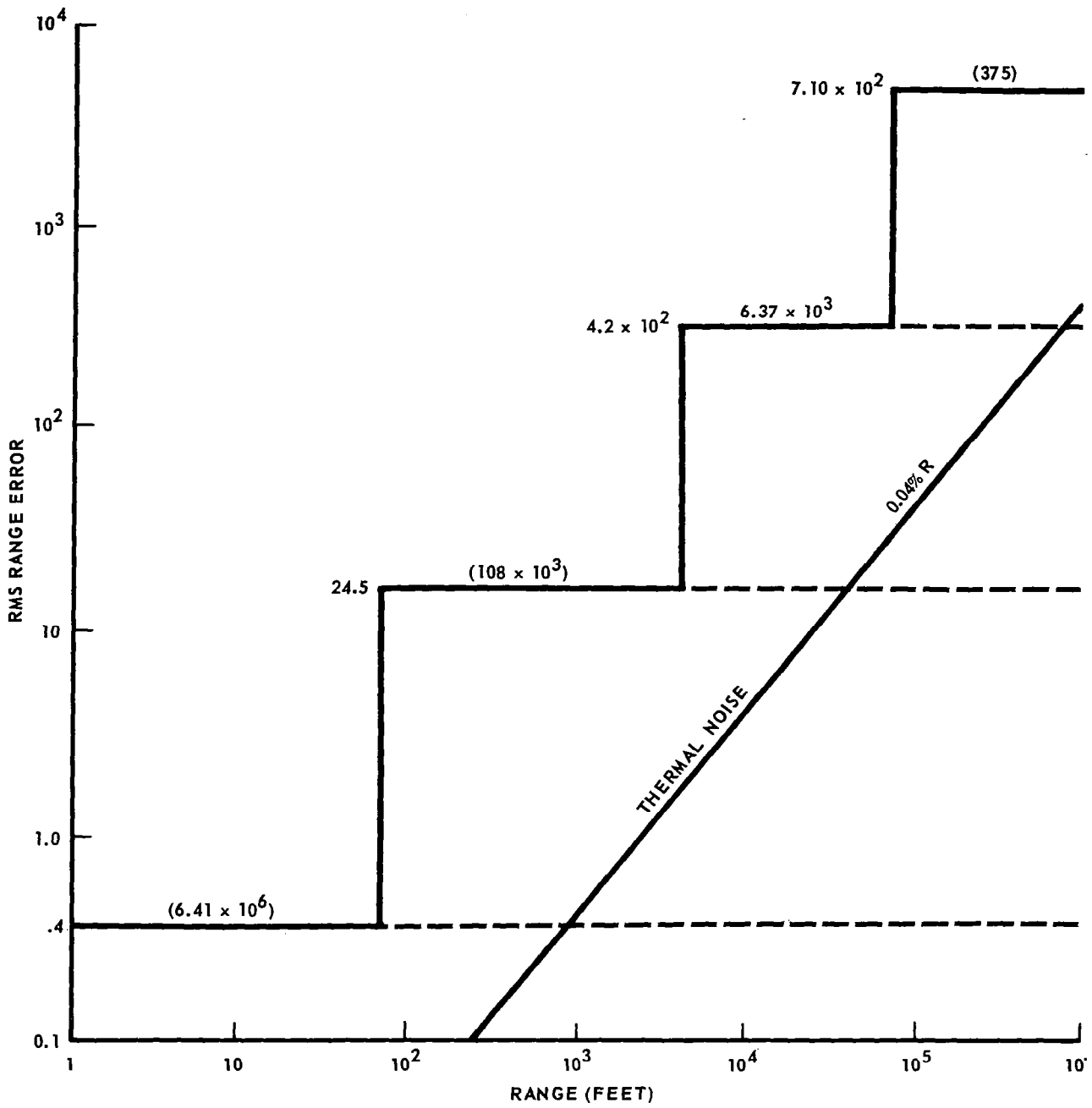


FIGURE 160 - RANGE ERRORS CW, 4 TONE, RADAR

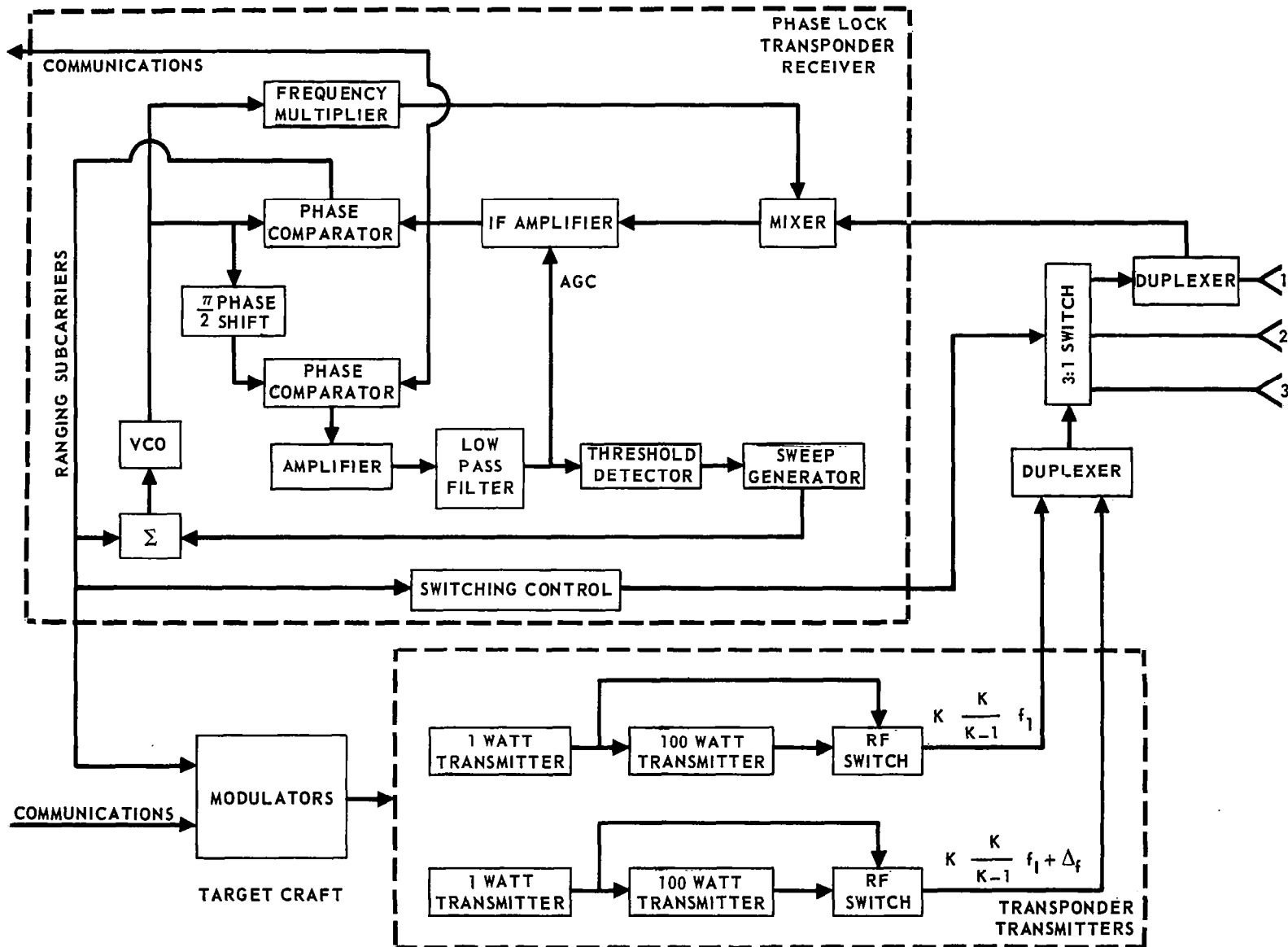


FIGURE 161 - IPS TRANSPONDER

At this point the demodulated range subcarrier signal is encoded on the coherent offset signal via phase modulation such that the form of the signal repeated by the transponder is:

$$\cos \left\{ \frac{k^2}{k-1} 2\pi f_1 \left(t - \frac{R}{c}\right) + \beta \cos \left[2\pi f_m \left(t - \frac{R}{c}\right) \right] \right\}. \quad (446)$$

The signal received at the chaser lags that at the transponder by the one way range delay, $\frac{R}{c}$ seconds. Then at the chaser:

$$\cos \left\{ \frac{k^2}{k-1} 2\pi f_1 \left(t - \frac{2R}{c}\right) + \beta \left[2\pi f_m \left(t - \frac{2R}{c}\right) \right] \right\}. \quad (447)$$

With no doppler shift the received carrier frequency is $\frac{k^2}{k-1} f_1$, or 1059 MHz.

It is noted that, in addition to the above signal, the transponder also provides a reply at 909 MHz. The purpose of this second reply frequency is to provide a frequency pair separated by 150 MHz for coarse angular measurements.

Figure 162 illustrates the method of deriving the range and range rate information. The received signal is first mixed with a local oscillator signal at $Kf_1 = 971$ mc to yield an intermediate frequency signal of the form:

$$\cos \left\{ \frac{k}{k-1} 2\pi f_1 t + \frac{k^2}{k-1} 4\pi f_1 \frac{R}{c} + \beta \cos \left[2\pi f_m \left(t - \frac{2R}{c}\right) \right] \right\}. \quad (448)$$

This signal serves as the input to a narrow band phase locked loop. The loop acts to track the carrier and demodulate the range subcarrier phase modulation. In this manner the output of the loop null detector is the desired range subcarrier signal, or:

$$\beta \cos \left[2\pi f_m \left(t - \frac{2R}{c}\right) \right], \quad (449)$$

and the loop VCO output is:

$$\cos \left\{ \frac{k}{k-1} 2\pi f_1 t + \frac{k^2}{k-1} 4\pi f_1 \frac{R}{c} \right\}. \quad (450)$$

Range information is obtained by comparing the phase of the demodulated range subcarrier signal with the appropriate range subcarrier oscillator signal, $\cos(2\pi f_m t)$. The resultant phase difference is:

$$\theta = 4\pi f_m \frac{R}{c}, \quad (451)$$

which is directly proportional to the target-to-chaser range. As discussed previously, four range subcarriers are used to resolve ambiguities. Range accuracy is shown in Figure 160.

The VCO output is mixed with a reference signal at frequency $\frac{k}{k-1} f_1$ to yield a signal with frequency:

$$\frac{k^2}{k-1} \frac{2f_1}{c} \frac{dR}{dt}. \quad (452)$$

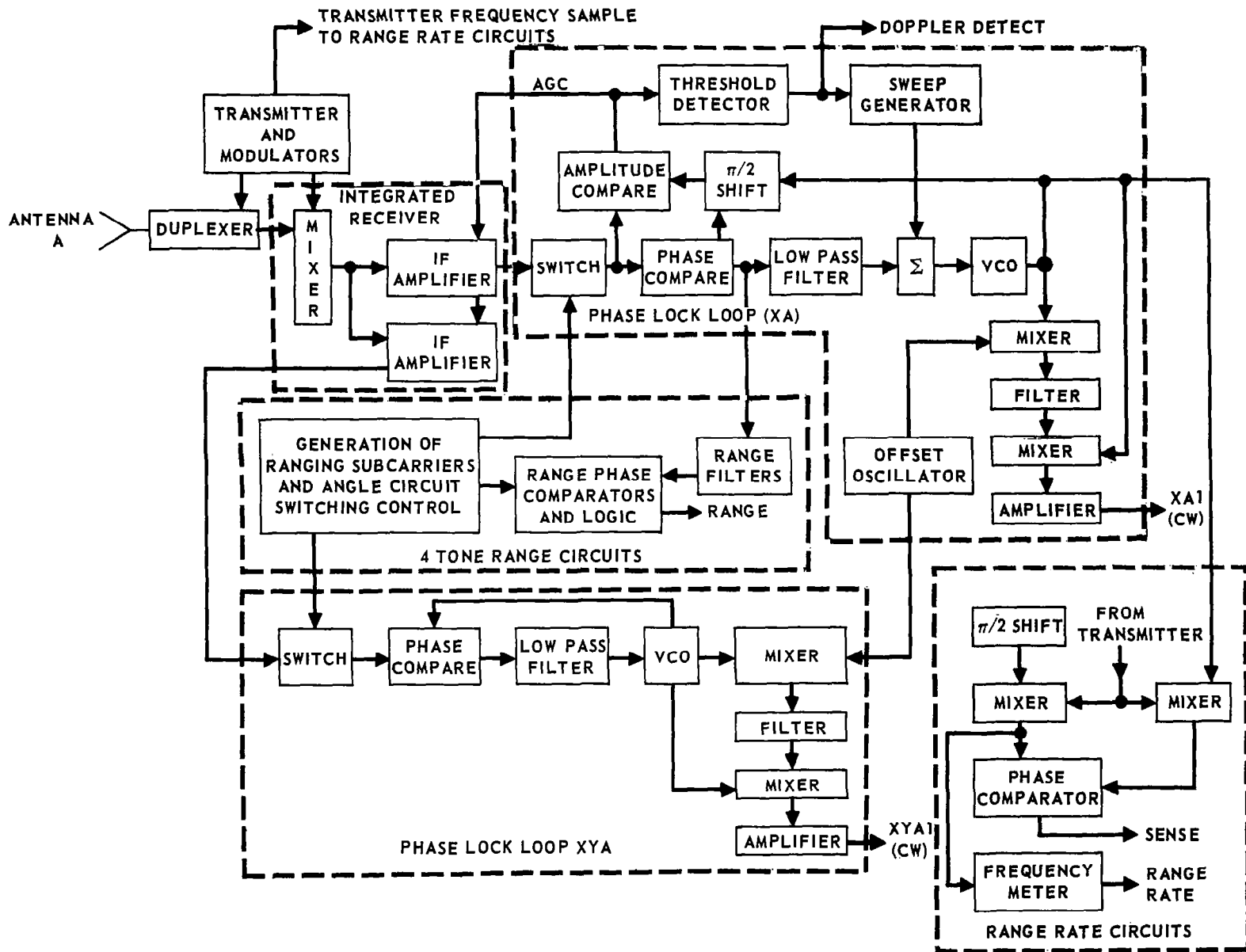


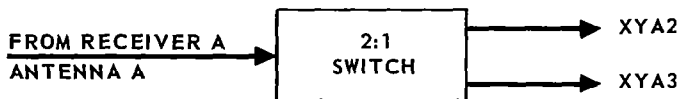
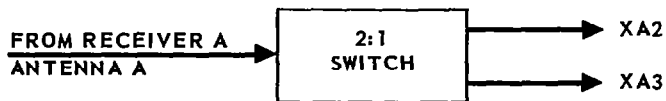
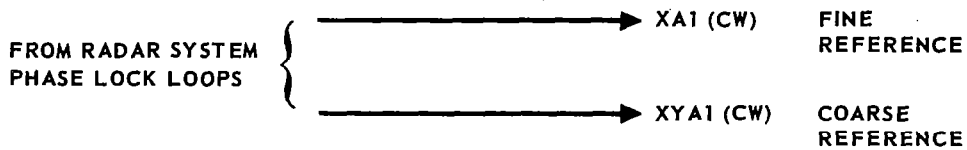
FIGURE 162 - IPS RANGE, RANGE RATE AND ANGLE REFERENCE CIRCUITS

which is the two way doppler shift at the frequency $\frac{k^2}{k-1} f_1$ or 1059 MHz and is directly proportional to the range rate. This is the quantity measured by the frequency meter. As shown in figure 162, the above indicated mixing process is performed with both in-phase and quadrature phase signals to allow determination of range rate sense. Errors associated with the range rate measurement are discussed later in this section.

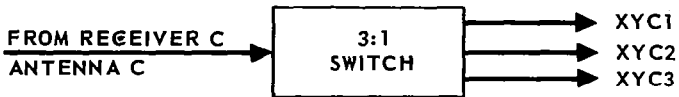
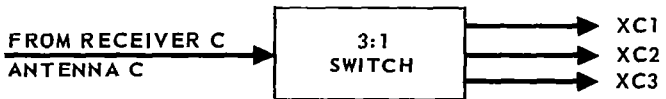
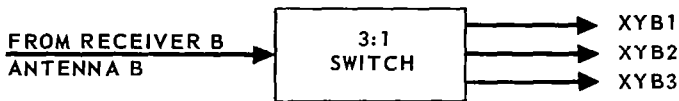
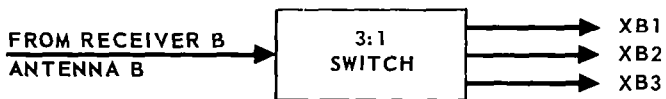
Angle Sensing.- Line-of-sight angles and target attitude angles are measured by phase comparison. The relationships between the phases of the induced voltage at two antennas and the difference in path length have been described previously in this report. In the IPS system, three antennas are used at each craft and several phase measurements are used to obtain all of the desired angle parameters. The geometry of the problem is not necessarily that described herein, but certain advantages will be pointed out for the equilateral triangle configuration on each craft. A spacing of one meter allows the antennas to be spaced around the perimeter of typical size spacecraft. A larger spacing when available, provides improved accuracy. The switching circuits for the synchronized time sharing measurement approach are shown in figure 163.

The phase references are continuous wave signals that are locked in the phase lock loop of the ranging system, figure 156. Phase comparisons are made sequentially at a 375 Hz rate with signals from the angle receivers, A, B and C. Three position switching is required at the outputs of receiver B and C while only two position switching is required on the signals from receiver A (since the CW reference signals are obtained from antenna A and receiver A). An example of one angle receiver is shown in figure 165. The received signals, as mentioned previously, are separated by 150 MHz. Both signals are first reduced to an IF frequency by a common LO from the transmitter. The signals are then amplified by precision phase-track IF amplifiers. The gain required at this point is expected to be about 60 db. A sample of the output of the "fine" measurement channel is mixed with the output of the IF amplifier in the coarse channel to produce an output at the difference frequency (150 mc). Second L.O. frequencies are obtained from the fine and coarse phase-lock-loops plus a 1 MHz offset. The 1 MHz "tone" is then filtered (in phase track filters) and amplified. The additional amplification is provided at this point rather than in the IF amplifiers to simplify the IF amplifier design and to provide higher overall stability.

The outputs from the receivers, as described above, are then switched at a 375 Hz rate, as described previously, into sample and hold circuits shown in figure 164. The phase integrity of each of the required coarse and fine 1 Mz "tones" is retained in individual narrow band phase holding circuits. All of the necessary phase comparison can then be made (also shown in figure 164) to produce the required LOS and target attitude angles. The phase differences, at the antennas, are a measure of the differences in propagation path lengths. The fine measurement gives the require accuracy and the coarse measurement is used to resolve the ambiguities in the fine measurements. The final docking configuration for the antennas is as shown in figure 166.



CROSS-CONNECTED TO SAMPLE-HOLD AND PHASE COMPARISON CIRCUITS



NOTE: SWITCHING RATE CONTROLLED BY 375 HZ RANGING TONE

FIGURE 163 – IPS SWITCHING CIRCUITS

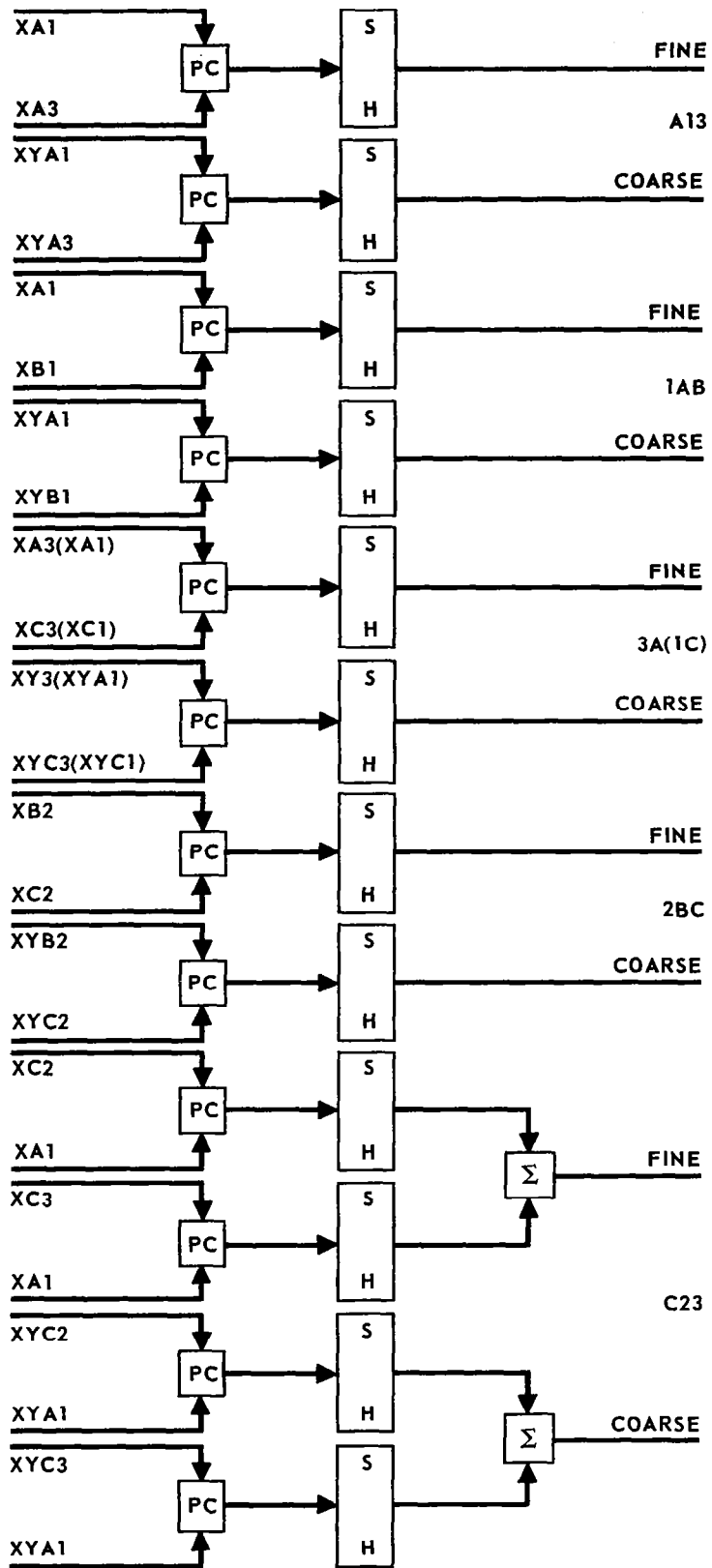
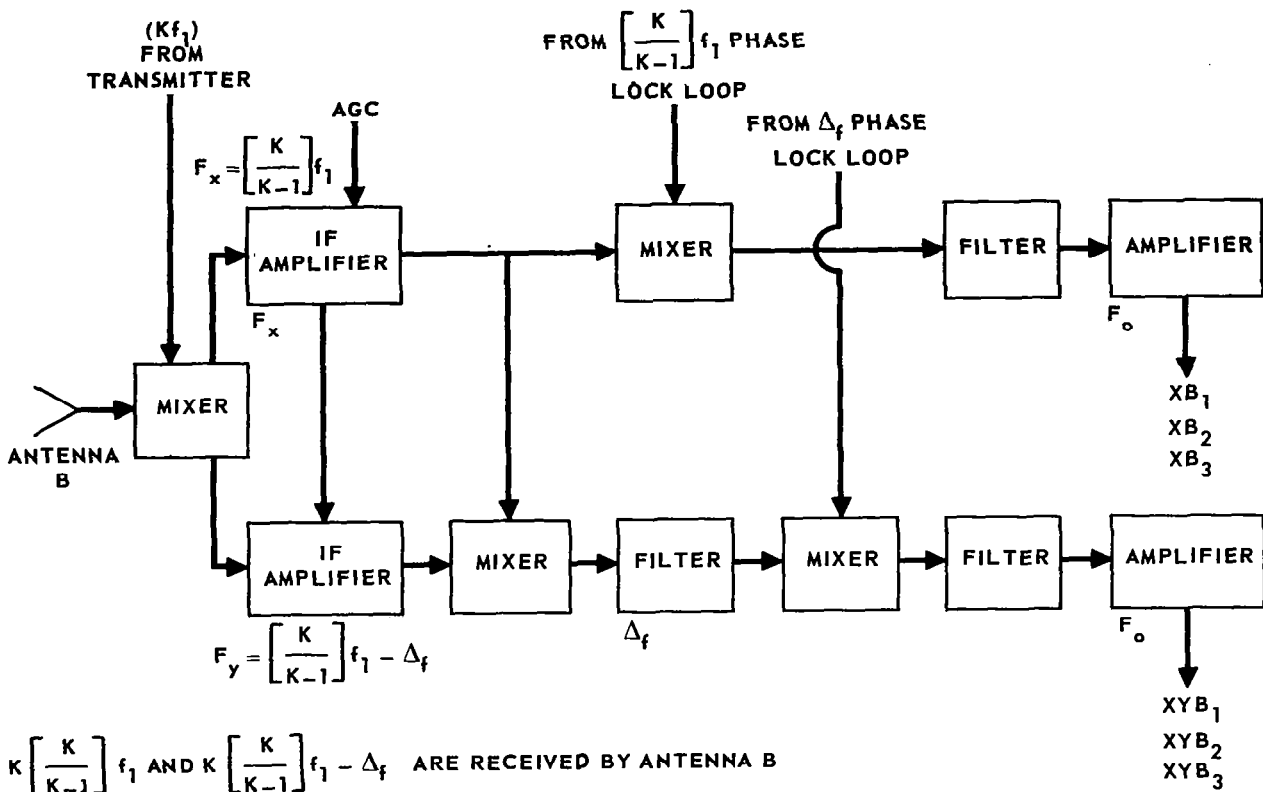


FIGURE 164 – IPS SAMPLE – HOLD AND PHASE COMPARISON CIRCUITS



$K \left[\frac{K}{K-1} \right] f_1$ AND $K \left[\frac{K}{K-1} \right] f_1 - \Delta_f$ ARE RECEIVED BY ANTENNA B

NOTE: IF AMPLIFIER AGC FROM RANGE CIRCUIT PHASE LOCK LOOP

FIGURE 165 – IPS ANGLE RECEIVER (B)

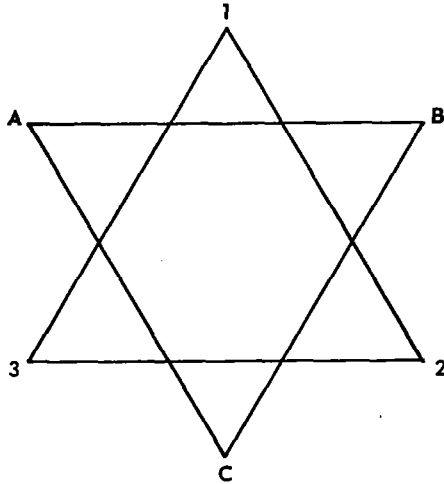


FIGURE 166 – DOCKED ANTENNA CONFIGURATION

where A, B and C are the chascraft antennas and 1, 2 and 3 are the target antennas. The processing of the phase difference outputs becomes somewhat different than the conventional technique when the range is not large with respect to the antenna spacing. The logic processing will not be investigated in this report, but it can be seen that the control error signals that are required for closed-loop docking can be generated. It should be noted that phase comparisons are made around the circumference of the vehicle body contours in order to eliminate close-range, direct propagation path blockage. Target attitude angle information is obtained by switching the transmitted frequencies from the target, sequentially from antennas 1, 2 and 3. This provides for determining the propagation path length differences from a given chascraft antenna to the antennas 1, 2 and 3 on the target. A synchronized time sharing method was chosen rather than using separate carriers, to tag antennas 1, 2 and 3 to avoid the RFI problem which tends to become insurmountable, using separate carriers, if reasonable accuracies are to be obtained. The sequential switching technique also involves less overall system complexity than the generation and processing of three times as many carrier frequencies.

Selection of Carrier Frequency

A carrier frequency in the 1 GHz region was chosen because this frequency is low enough to:

- a. Keep free space path loss low.
- b. Permit high solid state transmitter power.
- c. Keep RF system losses low.

But is high enough to:

- a. Permit the use of reasonably small antennas.
- b. Be nearly unaffected by ionospheric dispersion.
- c. Provide adequate spectrum for subcarriers, reference signals, commands, telemetry, and voice.

Communications

Provisions for telemetry, voice, and command data links are included as shown in figures 156 and 161. Although this system illustrates the ease with which communication channels can be added to integrated cooperative systems, several specific operational characteristics must be considered in selecting the modulation techniques:

1. The usual methods of coherent demodulation are precluded at close ranges at the chasecraft by the use of sequential switching among the target antennas, which results in discrete changes in carrier amplitude and phase at the switching rate.
2. Compensation for the doppler effect must be included when narrow band demodulation methods are used.
3. Care must be exercised in the selection of information subcarrier frequencies to minimize potential interference with the frequency pair technique and with the range subcarriers.
4. The range subcarrier frequencies available at both the target and the chasecraft may be used as the clock reference for data synchronization purposes.

One technique which shows promise of avoiding the sequential target antenna switching effect is the use of PCM/AM modulation of one of the frequency pair carriers. The "ones" and "zeros" of the PCM signal are indicated by the presence or absence of the amplitude modulation providing immunity to the carrier phase shift effects. Doppler shift compensation is available from the phase locked loops tracking the carrier in each spacecraft.

Another straightforward approach avoids the problem of sequentially switched target antennas by the use of a third low power carrier at close ranges. Since the target antenna switching is used only at short ranges, binary modulated subcarriers can easily provide the total capability needed throughout the mission. Doppler shift compensation is available as above.

It is obvious from the above discussion that the integration of communications capability must be tailored to the integrated measurement system. The sensors used are important in establishing the available capability, but of equal importance are the operational sequences associated with the sensors.

Frequency Selection and RFI Considerations

It has been shown that the chasecraft transmits at the frequency kf_1 . The transponder replies at frequencies $k\left(\frac{k}{k-1}\right)f_1$ and $k\left(\frac{k}{k-1}\right)f_1 - \Delta F$. The two reply frequencies separated by ΔF provide for a course angle measurement at an effective frequency of ΔF . The value of the frequency spread, ΔF , determines the unambiguous angle measurement range for a specified antenna separation. The phase difference between two RF signals is measured. The phase difference, θ , results from a path length difference, r . In the case of the coarse angle measurement, the output is:

$$\theta = \frac{2\pi r}{\lambda} = \frac{2\pi \Delta F r}{c} . \quad (453)$$

For the phase comparisons indicated on the previous block diagrams, the maximum path length differences is equal to the antenna spacing, d , which is 1 meter. Then, for a phase comparator characteristic repeating at intervals of 2π , unambiguous information is obtained for:

$$\theta = \frac{2\pi \Delta F d}{c} \leq \pi , \quad (454)$$

$$\Delta F \leq \frac{c}{2d} = 150 \text{ MHz} . \quad (455)$$

Unambiguous angle information with maximum accuracy will be obtained for

$$\Delta F = 150 \text{ MHz} \quad (456)$$

The IF frequencies are determined on the basis of RFI considerations. The input frequencies appearing at the first mixer of both the target and chasecraft are identical. However, the functions of these input frequencies differ in the target and the chasecraft. These considerations are summarized in the table following. For example, the frequency $kf_1\left(\frac{k}{k-1}\right) - \Delta F$ is a desired signal at the chasecraft receiver, but is undesired interference at the target receiver.

TABLE 21 – TARGET-CHASECRAFT FREQUENCY RELATIONSHIPS

FREQUENCY	CHASECRAFT	TARGET
kf_1	1. TRANSMITTED FREQUENCY 2. L.O.	1. RECEIVED FREQUENCY
$kf_1 \frac{k}{k-1}$	1. RECEIVED FREQUENCY	1. TRANSMITTED FREQUENCY 2. L.O.
$kf_1 \frac{k}{k-1} - \Delta F$	1. RECEIVED FREQUENCY	1. TRANSMITTED FREQUENCY

Then for either the target or the chascraft, the possible first mixer output frequencies resulting from the three input frequencies are given by the expression:

$$F_I = l [kf_1] + m [k (\frac{k}{k-1}) f_1] + n [k (\frac{k}{k-1}) f_1 - \Delta F], \quad (457)$$

$$F_I = (l + m + n) [kf_1] + m [(\frac{k}{k-1}) f_1] + n [(\frac{k}{k-1}) f_1 - \Delta F], \quad (458)$$

where l , m , and n are positive or negative integers. The order of the interference is given by $|l| + |m| + |n|$. It is convenient to let $F_x = (\frac{k}{k-1}) f_1$ and $F_y = (\frac{k}{k-1}) f_1 - \Delta F$ such that $|F_x|$ and $|F_y|$ represent the two chascraft receiver intermediate frequencies and $|F_x|$ represents the target receiver intermediate frequency. Note that the desired outputs F_x and F_y are second order.

Since kf_1 is much greater than either F_x or F_y , the only interference which must be considered is given by:

$$F_I = m F_x + n F_y \quad (459)$$

subject to the condition that $(l + m + n) = 0$. The form of equation 459 allows the use of the frequency interference chart of reference 64.

In order to avoid excessively high intermediate frequencies at the chascraft receiver, it is necessary to cause the desired received signal frequencies to straddle the local oscillator frequency at the chascraft receiver. Since F_x must be positive (the coherent transponder reply is above the received signal), this means that F_y will be negative. Then to obtain a frequency pair separated by ΔF we require:

$$F_x - F_y = \Delta F = 150 \text{ MHz} . \quad (460)$$

Using the frequency interference chart of reference 64 and considering values of $|m| + |n|$ up to 10, it is observed that $F_y = -0.7 F_x$ yields a large RFI window. Table 22 lists the interfering frequencies, F_I , near F_x and F_y for $F_y = -0.7 F_x$.

Then using $F_y = -0.7 F_x$ and $F_x - F_y = 150$ MHz, we obtain $F_x = 88.3$ MHz and $F_y = -61.7$ MHz.

It should be noted that the interference problem at the target transponder is more severe than at the chasecraft receiver. This is true because the target is transmitting two frequencies separated by ΔF , whose modulation products may compete with the relatively low power signal from the chasecraft. However, the chasecraft is transmitting only a single frequency and, thus, any interfering cross modulation terms will, in general, be of lower magnitude.

For example, consider the target and chasecraft employing transmitter powers of 100 watts at the maximum range of 4×10^5 meters. In this case, the received signal power is -97 dbm and the feedthrough at the chasecraft is +5 dbm, assuming 45 db duplexer rejection. Reference to table 22 indicates a possible relative 6th order interference term 8.9 MHz above the desired signal at 88.3 MHz. This interference term results from interaction among the local oscillator, feedthrough, and received signal, and consequently should be of a very low magnitude. If, however, we assume the 6th order terms are down only 36 db (6 db per order) relative to feedthrough, the resultant interference is at -31 dbm, as compared to the -97 dbm signal. If amplifier selectivity may be employed, if necessary, to provide an additional interference attenuation of 60 db resulting in an interfering signal at -91 dbm separated 8.9 MHz from the desired signal at -97 dbm. Since additional range subcarrier filtering will be provided after demodulation, this interference situation is tolerable.

As a second example, consider the target and chasecraft employing transmitter powers of 1 watt at a range of 30 meters. At this range, it is desired to use the high frequency ranging subcarrier and thus IF selectivity does not attenuate the interfering 8.9 MHz. The feedthrough level at the target transponder is -10 dbm, assuming -40 db antenna coupling. (At this range the target will be sequentially transmitting from each of its three antennas and the feedthrough level is determined by antenna coupling, as opposed to duplexer isolation.) The received signal power will be about -35 dbm. Again assuming the interference is down only 36 db (6 db per order) relative to the feedthrough, it is seen that the interfering signal power level is -46 dbm as compared to the -35 dbm signal. Additional subcarrier filtering may be employed if necessary.

In summary, the following parameters have been selected:

$$|F_x| = \text{Target and Chasecraft IF} = 88.3 \text{ MHz}, \quad (461)$$

$$|F_y| = \text{Second Chasecraft IF} = 61.7 \text{ MHz}, \quad (462)$$

$$\Delta F = \text{Frequency Pair Separation} = 150 \text{ MHz}. \quad (463)$$

Selecting the frequency multiplication factor, k , to be 12, and using the relationship $F_x = \left(\frac{k}{k-1}\right) f_1$ yields.

$$kf_1 = \text{Frequency Transmitted by Chasecraft} = 971 \text{ MHz}, \quad (464)$$

$$kf_1 \left(\frac{k}{k-1}\right) = \text{Coherent Transponder Reply Frequency} = 1059 \text{ MHz}, \quad (465)$$

$$kf_1 \left(\frac{k}{k-1}\right) - \Delta F = \text{Offset Transponder Reply Frequency} = 909 \text{ MHz}, \quad (466)$$

$$f_1 = \text{Base Frequency} = 81.2 \text{ MHz}. \quad (467)$$

TABLE 22 - RFI CONSIDERATIONS

NORMALIZED FREQUENCY F_1/F_x	n	m	l	ORDER $ l + m + n $	RELATIVE ORDER	$(F_1 \text{ MHz})$ @ $F_x = 88.3 \text{ MHz}$
0.3	1	1	-2	4	2	26.5
0.4	-2	-1	3	6	4	35.4
0.6	2	2	-4	8	6	53.0
0.7	-1	0	1	2	0	61.7
1.0	0	1	-1	2	0	88.3
1.1	-3	-1	4	8	6	97.2
1.2	3	3	-6	12	10	106.0
1.3	1	2	-3	6	4	114.9
1.4	-2	0	2	4	2	123.7

Range Subcarrier Selection and Error Analysis

Range information is obtained by introducing phase modulated range sub-carriers on the chasecraft transmission. For the case of a single range sub-carrier, the form of the transmitted signal is:

$$\cos [\omega_c t + \beta \cos \omega_m t], \quad (468)$$

where ω_m is the subcarrier radian frequency. For the target at range R , the subcarrier phase, as received by the chasecraft, is delayed by:

$$\theta = \frac{2R}{c} 2\pi f_m. \quad (469)$$

This parameter is measured to obtain an estimate of the target-to-chasecraft range. The maximum unambiguous range is:

$$R_u = \frac{c}{2f_m}. \quad (470)$$

In general, more than one subcarrier is transmitted to resolve range ambiguities.

Thermal Noise Errors.- System errors and thermal noise contribute to the total error in the range measurement. The fractional rms range error due to thermal noise at the target and chasecraft receivers is:

$$\frac{\Delta R}{R} = \frac{2f_c}{f_m \beta} \left(\frac{kT N F B_{LP}}{P_t G_t G_r L} \right)^{1/2}, \quad (471)$$

where f_c = carrier frequency (10^9 Hz),
 f_m = range subcarrier frequency (Hz),
 $kT N F$ = single sided thermal noise power spectral density (10^{-19} watts/Hz),
 B_{LP} = single sided range filter noise bandwidth (Hz),
 β = phase modulation index,
 P_t = transmitter power (1 or 100 watts),
 G_t = transmitter antenna gain (0 db),
 G_r = receiver antenna gain (0 db),
 L = loss factor (-3 db).

The numbers in brackets indicate the parameter values for the proposed system. Using these values with $P_t = 100$ watts:

$$\frac{\Delta R}{R} = (8.9 \times 10^{-2}) \frac{B_{LP}^{1/2}}{f_m \beta}. \quad (472)$$

For $P_t = 1$ watt the rms error increases by a factor of 10.

System Errors

From equation 469:

$$R = \frac{c \theta}{4\pi f_m}, \quad (473)$$

therefore, errors in the modulating frequency and phase measurement yield the following range errors:

$$\frac{dR}{R} = \frac{df_m}{f_m}, \quad dR = \frac{c}{4\pi f_m} d\theta. \quad (474)$$

For an oscillator stability of one part in 10^5 and a phase measurement accuracy of $\pm 2^\circ$, the above two error terms become:

$$\frac{dR}{R} = \frac{df_m}{f_m} = \pm 10^{-5}, \quad dR = \pm \frac{8.34 \times 10^5}{f_m} \text{ (m)}. \quad (475)$$

Then combining equations 472 and 475 the total range error equation is, for $P_t = 100$ watts:

$$\sigma_R = \left[\frac{6.96 \times 10^{11}}{f_m^2} + (1 \times 10^{-10} + \frac{B_{LP}}{(f_m B)^2} 7.91 \times 10^{-3}) R^2 \right]^{\frac{1}{2}} \text{ m}, \quad (476)$$

and for $P_t = 1$ watt:

$$\sigma_R = \left[\frac{6.96 \times 10^{11}}{f_m^2} + (1 \times 10^{-10} + \frac{B_{LP}}{(f_m B)^2} 7.91 \times 10^{-1}) R^2 \right]^{\frac{1}{2}} \text{ m}. \quad (477)$$

Parameter Selection.- It is desired to obtain unambiguous range information to a maximum range of 4×10^5 meters, with a maximum error of 0.1% (1σ). In addition, as the target-to-chasecraft range approaches 300 meters, it is desired to insure that the absolute error is less than 0.3 meters (1σ) with proportional error less than 0.1% (1σ). At long ranges the transmitters power will be 100 watts; at close approach the power will be reduced to 1 watt.

In this section the range subcarrier frequencies and phase modulation indices are selected. As an additional requirement, it is desired to avoid the use of large modulation indices to conserve the carrier power.

Since more than one range subcarrier is used, the probability of correctly resolving range ambiguities must be 0.998 (3σ) per decision.

In order to obtain unambiguous range information at $R = 4 \times 10^5$ m, equation 470 indicates the required subcarrier frequency is 375 Hz. Solution of equation 476 with $\beta = 0.1$ and $B_{LP} = \frac{\pi}{2}$ 40 Hz indicates that the range error equation for this subcarrier is:

$$\sigma_R = [4.94 \times 10^6 + (3.5 \times 10^{-4}) R^2]^{\frac{1}{2}} \text{ m}, \quad (478)$$

for the 100 watt transmission mode. The noise bandwidth of $\frac{\pi}{2}$ 40 Hz is conservative and corresponds to a single pole low pass filter with 3 db bandwidth equal to 40 Hz used in the docking simulation studies. This filter will be assumed throughout the remainder of this section. The modulation index value ($\beta = 0.1$) used is consistent with the desire to conserve carrier power. Larger values would reduce the percentage error proportionally.

Then in order to achieve the desired 0.1% (1σ) accuracy, additional subcarriers must be used. In selecting the next range subcarrier we require that its maximum unambiguous range correspond to the 3σ error associated with the preceding subcarrier. Then, the required unambiguous range (as determined by evaluation of equation 478 at $R = 4 \times 10^5$ m is 2.35×10^4 m. Then, from equation 470 the required subcarrier frequency is 6.37 kHz. Evaluation of equation 476 with $\beta = 0.1$ and $B_{LP} = \frac{\pi}{2}$ (40) Hz yields as the range error for this subcarrier:

$$\sigma_R = [1.72 \times 10^4 + (1.23 \times 10^{-6}) R^2]^{1/2} \text{ m ,} \quad (479)$$

for the 100 watt transmission mode.

The percentage error term in equation 479 is nearly equal to the desired 0.1%. However, the constant term in equation 479 will cause the net percentage to far exceed the desired 0.1% value with range closure. Thus, a third subcarrier is required. The required 3σ unambiguous range (as determined by evaluation of equation 479 at $R = 4 \times 10^5$ m is 1.39×10^3 m. From equation 470, the required carrier frequency is 108 kHz. Using equation 476 with $\beta = 0.05$ and $B_{LP} = \frac{\pi}{2}$ (40) Hz, the range error is:

$$\sigma_R = [5.96 \times 10^1 + (1.72 \times 10^{-8}) R^2]^{1/2} \text{ m ,} \quad (480)$$

and

$$\sigma_R = [5.96 \times 10^1 + (1.72 \times 10^{-6}) R^2]^{1/2} \text{ m .} \quad (481)$$

The constant error term of equation 480 is still much larger than the desired value of 0.3 m for the close approach situation. Thus, a fourth subcarrier is required.

The range at which the total error (rss of the two terms) given by equation 480 reaches 0.1% is 7.79×10^3 m. Thus, in order to maintain a total error of less than 0.1%, the fourth subcarrier must be used for ranges less than 7.79×10^3 m even in the 100 watt mode. In order to insure a 3σ resolution probability for the fourth subcarrier, we require that its unambiguous range be $3(7.79) = 23.37$ m. Using equation 470 the subcarrier frequency must be less than or equal to 6.41 MHz. Using $f_m = 6.41$ MHz with $\beta = 0.01$ and $B_{LP} = \frac{\pi}{2}$ 40 Hz, solution of equation 476 yields as the range error equation:

$$\sigma_R = [1.69 \times 10^{-2} + (2.22 \times 10^{-10}) R^2]^{1/2} \text{ m} , \quad (482)$$

and

$$\sigma_R = [1.69 \times 10^{-2} + (1.21 \times 10^{-8}) R^2]^{1/2} \text{ m} . \quad (483)$$

The constant error term of ± 0.13 m is somewhat less than the original requirement of ± 0.3 m.

It is desired to use the 1 watt mode up to the unambiguous range (1.39×10^3 m) of the subcarrier at 108 kHz . From equation 481, $R = 1.39 \times 10^3$ m, the 1σ range error is determined to be 7.92 m. This is approximately one third of the unambiguous range (23.37 m) associated with the 4.61 MHz subcarrier and, thus, the required 3σ resolution probability is achieved in the one watt mode. These parameters are summarized in table 23 .

TABLE 23 – SUMMARY OF RANGING PARAMETERS

MODULATION FREQUENCY f_m	MODULATION INDEX β	UNAMBIGUOUS RANGE R_u (METERS)	CONSTANT ERROR (1σ) METERS	PERCENTAGE ERROR (1σ)	3σ RESOLUTION RANGE (METERS)
375 Hz	0.1	4×10^5	$\pm 2.22 \times 10^3$	± 1.88	
6.37 kHz	0.1	2.35×10^4	$\pm 1.31 \times 10^2$	± 0.11	4×10^5
108 kHz	0.05	1.39×10^3	± 7.72	± 0.0131 $\pm 0.131^*$	4×10^5
6.41 MHz	0.01	23.37	± 0.13	± 0.0015 $\pm 0.011^*$	7.79×10^3 $1.39 \times 10^3^*$

* 1 WATT MODE

Range Rate Measurement Errors

An estimate of the target to chasecraft closing speed is obtained by measuring the two way doppler shift. Errors in this estimate may result from instrumentation errors, thermal noise and multipath effects. Multipath effects are discussed in appendix J. It is desired to provide a system with a maximum absolute error of 0.3 m/s and a maximum percentage error of 0.1%.

System Errors. - The parameter measured is the two way doppler shift:

$$f_d = \frac{2v}{\lambda} ; \quad (484)$$

where λ is the wavelength (0.3 m) and v is the target-to-chasecraft closing speed. Then the closing speed is given by:

$$v = \frac{\lambda f_d}{2} . \quad (485)$$

Errors in λ and measurement of f_d yield the following errors:

$$\frac{dv}{v} = \frac{d\lambda}{\lambda} , \quad dv = \frac{\lambda}{2} df_d . \quad (486)$$

For oscillator stabilities of one part in 10^5 (1σ) and a frequency measurement error of ± 2 Hz (1σ) the above errors become:

$$\frac{dv}{v} = \pm \frac{d\lambda}{\lambda} = \pm 10^{-5} , \quad dv = \pm \frac{\lambda}{2} d(f_d) = \pm 0.3 \frac{m}{s} . \quad (487)$$

The ± 2 Hz frequency measurement error requires a discriminator alignment to within ± 2 Hz or may be obtained by a frequency count over a period of 0.5 seconds.

Receiver Thermal Noise Errors.- In appendix I, it is shown that the mean squared closing velocity error due to receiver thermal noise is given by:

$$\Delta v^2 = \frac{\lambda^2 (kTNF) B_{LP}^3}{6S} , \quad (488)$$

where the units are those of λ^2 per (second)². In this equation λ is wavelength, kT is 4×10^{-21} watts/Hz, F is receiver noise figure, B_{LP} is the noise bandwidth (Hz) of the velocity smoothing filter, and S is the received signal power (watts). Using the radar range equation S is given by:

$$S = \frac{P_t G_t G_r \lambda^2 L}{(4\pi)^2 R^2} , \quad (489)$$

where, P_t = transmitted power (100 or 1 watt) ,
 G_t = transmitter antenna gain (0 db) ,
 G_r = receiver antenna gain (0 db) ,
 R = target-to-chasecraft range in meters ,
 λ = wavelength (0.3 meters) ,
 L = loss factor (-3 db).

The numbers in brackets indicate the proposed values for the target chasecraft system.

Combining equations 488 and 489 we obtain:

$$\Delta v^2 = \frac{(4\pi)^2 R^2 (kTNF) B_{LP}^3}{6 P_t G_t G_r L} . \quad (490)$$

Then using the above indicated parameter values with $P_t = 100$ watts, $F = 14$ db, and $B_{LP} = \frac{\pi}{2}$ (40) cps, we obtain as the root mean squared closing velocity error:

$$\Delta v_{rms} = R (1.15 \times 10^{-6}) \frac{m}{s} . \quad (491)$$

For $P_t = 1$ watt the above error is increased by a factor of 10. The value used for B_{LP} corresponds to a single pole low pass filter with 3 db bandwidth equal to 40 cps. This 40 Hz value was used in the docking simulation studies.

Using a general docking control law, $v = kR$, in equation 491, the fractional error due to thermal noise becomes:

$$\frac{\Delta v_{rms}}{v} = \frac{(1.15 \times 10^{-6})}{k} , \quad (492)$$

for the 100 watt mode. Since the control law will only apply for velocities less than the maximum value (assumed to be 3×10^3 m/s), the above equation is only valid for $V < 3 \times 10^3$ m/s. The minimum value of k being considered is 0.01, which yields a percentage error equal to 0.012% in the 100 watt mode and 0.12% in the 1 watt mode. For larger values of k , the errors will be proportionally lower. At ranges where the control law ceases to be valid, and the closing velocity reaches its maximum value of 3×10^3 m/s, the error due to thermal noise given by equation 491 corresponds to 0.015% at a range of 4×10^5 meters.

Summary.- Combining root sum of the squares equations 487 and 491 the total range rate measurement error (1σ) is given by:

$$\sqrt{9 \times 10^{-2} + R^2 (1.32 \times 10^{-12}) + v^2 (10^{-10})} , \quad (493)$$

for the 100 watt mode, and:

$$\sqrt{9 \times 10^{-2} + R^2 (1.32 \times 10^{-10}) + v^2 (10^{-10})} , \quad (494)$$

for the 1 watt mode. The units are in meters per second where R is in meters and V in meters per second.

From the previous results, it is seen that the maximum percentage error occurs in the 1 watt mode with a control law of the form, $V = 0.01R$, and is equal to 0.12%. For control laws allowing greater closing velocities this percentage error will be less. The constant error is 0.3 m/s.

Angle Error Analysis for the Integrated Phase System

The target and chasecraft are each provided with three antennas. On a given spacecraft these antennas form an equilateral triangle with length of sides equal to one meter. Phase comparison techniques are employed to determine both the target line-of-sight (LOS) angular error relative to the chasecraft and target attitude. In addition, a frequency pair technique is used to provide both coarse and fine angle information.

The target may transmit from any of its three antennas, and the chasecraft may receive via any of its three antennas. Then for any combination of three antennas involving at least one antenna at each spacecraft, the quantity measured is the electrical phase difference resulting from the particular path length differences. In general this quantity is given by:

$$\theta = \frac{2\pi d}{\lambda} \sin \epsilon \quad (495)$$

where $d \sin \epsilon$ is the path length difference, and d is the antenna spacing, which in this case is one meter. λ is the wavelength.

In the combinations involving two target antennas and a single chasecraft antenna, some form of multiplexing must be provided. In this case time division multiplexing is used whereby the transmissions from the target antennas (when more than one is used) occur sequentially.

For purposes of discussion, designate the three chasecraft antennas as A, B and C, and the three target antennas as 1, 2 and 3. Eighteen possible combinations of three antennas involving at least one at each spacecraft result. Of these, only two are used at long range to determine the target line-of-sight (LOS) angular error relative to the chasecraft. These two are LAB and LAC. Thus, at long ranges only a single target antenna (1) will be transmitting and no multiplexing will be required. At short ranges, a second set of measurements will be provided to allow proper alignment of the two spacecraft. The second set of measurements consists of LAB, 2BC, 3AC, A13, and C23. This allows alignment as shown in figure 166.

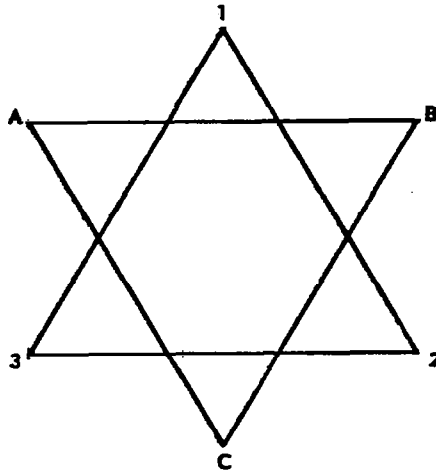


FIGURE 166 – DOCKED ANTENNA CONFIGURATION

Thus, for the short range set of measurements, the time division multiplexing is required. The particular multiplexing technique employs the 375 Hz range subcarrier (available at both the target and chasecraft) as a switching reference signal, such that transmission from each of the three target antennas occurs at a 375 Hz rate with a duty factor of about 1/3. The 375 Hz signal is used to provide appropriate channel gating and two phase lock loops (PLL) serve as storage devices to facilitate the phase comparison of non-coincident transmissions (e.g., A13 and C23).

As noted previously, the frequency pair technique for derivation of both coarse and fine angle information is provided for by simultaneous transmission of carriers at 1059 MHz and 909 MHz. Thus, the fine angle measurement is accomplished at a frequency of 1059 MHz and the coarse at the difference frequency or 150 MHz.

In addition to the two angle measurement modes, two transmitted power modes are provided. Transmitter power of 100 watts is provided at long ranges and is decreased to 1 watt at the shorter ranges. The power mode switchover is accomplished prior to the angle mode switchover so that the target antenna switching is required only in the one watt mode.

System Errors.— The quantity measured at the chasecraft receiver is:

$$\theta = \frac{2\pi d}{\lambda} \sin \epsilon , \quad (496)$$

where d is 1 meter, λ_1 is 0.284 m or 2 m, and ϵ is the boresight error. Then for $\epsilon < \frac{\pi}{4}$, the available estimate of the boresight error is:

$$\epsilon = \frac{\lambda}{2\pi d} \theta, \quad (497)$$

where the units for ϵ are mechanical degrees for θ in electrical degrees.

Then:

$$\Delta\epsilon = \epsilon \left[\frac{\Delta\lambda}{\lambda} - \frac{\Delta d}{d} \right] + \frac{\lambda}{2\pi d} \Delta\theta. \quad (498)$$

With a spacing accuracy of +1 part in 10^3 and a oscillator stability of +1 part in 10^5 , the first two terms in the above equation combine to give a fractional error of about 10^{-3} . The last term which is proportional to the phase measurement error, $\Delta\theta$, yields a constant error. The primary contributor to $\Delta\theta$ will be the parallel channel phase tracking error. Allowing 6° for IF tracking and 2° for RF tracking in the fine angle measurement mode (1059 MHz), the rms value of $\Delta\theta$ is $+6.32^\circ$ which corresponds to a constant rms mechanical error of $+0.29^\circ$ for the fine mode. In the coarse mode, the RF phase error is not significant. Thus, the rms value of $\Delta\theta$ is 6° which results in a constant rms mechanical error of $+1.91^\circ$ in the coarse angular measurement mode.

Thermal Noise Effects on the Angle Estimate.— The effects of chasecraft receiver thermal noise on the angle measurements is considered for a simple two channel interferometer system. The signal plus noise received in channels 1 and 2 are:

$$\text{Channel 1: } = A_c \cos \left(\omega_c t + \frac{2\pi d}{\lambda_1} \right) + x_1 \cos \omega_c t - y_1 \sin \omega_c t, \quad (499)$$

$$\text{Channel 2: } = (A_x + x_2) \cos \omega_c t - y_2 \sin \omega_c t. \quad (500)$$

In the above equations, receiver thermal noise is represented by narrow band gaussian random processes. The effective interferometer wavelength λ_1 , in the case of the coarse frequency pair measurement, is not equal to the carrier wavelength, $\lambda_c = \frac{2\pi c}{\omega_c}$. The noise in channel 1 is independent of that in channel 2. The single sided power spectral density of each of the low

frequency noise terms (x , x_2 , y_1 , and y_2) is $2\eta = KTF$ where $KF = 4 \times 10^{-21}$ watts/Hz and F is the receiver noise figure. The amplitude of the signal term in each channel is given by the radar range equation:

$$\frac{A_c^2}{2} = S = \frac{P_t G_t G_r \lambda_c^2 L}{(4\pi)^2 R^2}, \quad (501)$$

where: P_t = transmitter power,
 G_t = transmitter antenna gain,
 G_r = receiver antenna gain,
 R = target-to-chaser range,
 L = loss factor,
 λ_c = carrier wavelength.

For high signal-to-noise ratios, equations 499 and 500 may be written as:

$$\text{Channel 1: } A_c \cos \left(\omega_c t + \frac{2\pi d}{\lambda} \sin \epsilon + \frac{y_1}{A_c} \right), \quad (502)$$

$$\text{Channel 2: } A_c \cos \left(\omega_c t + \frac{y_2}{A_c} \right). \quad (503)$$

A phase comparison between channels 1 and 2 yields:

$$\theta = \frac{2\pi d}{\lambda} \sin \epsilon + \frac{y_1 + y_2}{A_c}. \quad (504)$$

For $\epsilon < \frac{\pi}{4}$ and letting $z = y_1 + y_2$, where the power spectral density of z is now 4η , the above may be written as:

$$\theta = \frac{2\pi d}{\lambda} \epsilon + \frac{z}{A_c}. \quad (505)$$

For a low pass filter with a single sided noise bandwidth equal to B_{LP} Hz following the phase comparator, the resultant output noise power is:

$$P_n = \frac{E[(z^1)^2]}{A_c^2} = \frac{4n B_{LP}}{A_c^2} = \frac{2kTNF B_{LP}}{S} \left(\frac{\text{Electrical}}{\text{radians}} \right)^2, \quad (506)$$

where the prime denotes the variable z after filtering. Thus, the rms mechanical angular error is:

$$\epsilon_N(\text{rms}) = \frac{\lambda_I}{2\pi d} \left[\frac{2kTNF B_{LP}}{S} \right]^{1/2}. \quad (507)$$

Reference to the block diagram of the chascraft receiver of figure 156 indicates that the final angle measurements involve only two channels. Thus, equation 507 applies to all fine measurements. Similar consideration of the coarse angle measurements indicates that each of these involve four channels. Then, for coarse measurements, the rms angle noise will be a factor of $\sqrt{2}$ greater than that given by equation 507.

Using $P_t = +20$ dbw, $G_t = G_m = 0$ db, $L = -3$ db, $F = 14$ db, $c = 0.284$ m, $\lambda_I = 2$ m, and $B_{LP} = 40 \frac{\pi}{2}$ Hz in equation 507, the rms mechanical angle error becomes:

$$\epsilon_N(\text{rms}) = 4 \times 10^{-8} R, \quad (508)$$

and:

$$\epsilon_N(\text{rms}) = 5.1 \times 10^{-7} R, \quad (509)$$

for the fine and coarse measurements, respectively, with R in meters. Included is the $\sqrt{2}$ factor in the coarse measurement as discussed above. These equations apply in the 100 watt mode with no antenna switching. The

low pass filter bandwidth of $40 \frac{\pi}{2}$ Hz corresponds to the value used in the docking simulator studies. Evaluation of the above two equations at the maximum range of 4×10^5 meters yields $\pm 2 \times 10^{-2}$ and ± 0.20 degrees for the fine and coarse modes, respectively.

At short ranges ($R \leq 300$ m), the transmitter power is 1 watt and the target transmits sequentially from its three antennas at a 375 Hz rate with a per antenna duty factor of about 1/3. Then for integration of a single sample (pulse), the effective noise bandwidth of the low pass filter following the phase detector is 562 Hz. Evaluation of equation 507 with $P_t = 1$ watt and $B_{LP} = 562$ Hz (all other parameters remaining the same) yields:

$$\epsilon_N(\text{rms}) = 1.51 \times 10^{-6} R, \quad (510)$$

and:

$$\epsilon_N(\text{rms}) = 1.5 \times 10^{-5} R, \quad (511)$$

for the fine and coarse modes. At a range of 3×10^2 meters, the above two equations yield 4.53×10^{-4} and 4.5×10^{-3} mechanical degrees for the fine and coarse modes, respectively.

Multipath Effects on Angle Measurement.- A simple two channel phase comparison system is considered. The desired signal received in each channel is of unity amplitude, and the interfering signal is of amplitude r where $r < 1$. The total received signals is then:

$$\text{Channel 1: } \cos(\omega_c t) - r \sin(\omega_c t + \alpha_1), \quad (512)$$

$$\text{Channel 2: } \cos(\omega_c t + \theta) - r \sin(\omega_c t + \theta + \alpha_2), \quad (513)$$

where $\theta = 2\pi d/\lambda \sin(\epsilon)$ is the desired output of the phase comparator. The effect of the interfering signal depends on its relative phase. Worst case phasing results when $\alpha_1 = 0$ and $\theta + \alpha_2 = \pi$ in which case the above equations become:

$$\text{Channel 1: } \cos[\omega_c t + r], \quad (514)$$

$$\text{Channel 2: } \cos[\omega_c t + \theta - r], \quad (515)$$

with $r \ll 1$. A phase comparison between channels 1 and 2 yields:

$$\theta_A = \theta - 2r = \frac{2\pi d}{\lambda} \sin \epsilon - 2r. \quad (516)$$

Thus, the magnitude of the electrical phase error is $2r$ radians which corresponds to a mechanical phase error of:

$$\Delta = \frac{\lambda r}{\pi d}, \quad (517)$$

for

$$\epsilon \leq \frac{\pi}{4},$$

Then, in order to insure that the bias in the angle measurement is less than 0.3 mechanical degrees, the multipath interference is required to be down 25 db relative to the desired signal.

The various possible multipath modes are discussed in appendix J. For the case of bounces between the two spacecraft, equation J4 is used to determine the relative interference level. The two bounce case results in the maximum value of r. From equation J4 for the two bounce case:

$$r(\text{db}) = -22 - 40 \log R, \quad (518)$$

where R is the target-to-chasecraft range in meters. The solution of this equation shows that the interference is down 25 db at R = 1.2 meters.

For the case of intra-spacecraft bounces, the magnitude of the undesired multipath interference is difficult to predict analytically. However, with proper antenna design and mounting these effects can be minimized.

Summary.- The combined results of the analysis, exclusive of multipath effects, are summarized in table 24. It is observed that the error due to receiver thermal noise is small compared to the other errors. Also, the total coarse error is always much smaller than the unambiguous range (180°) of the fine measurements, thus insuring proper resolution of ambiguities.

ELECTRONIC OMNI SYSTEM (EOS)

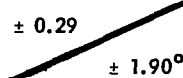
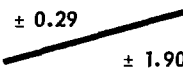
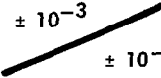
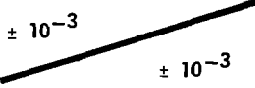
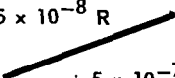
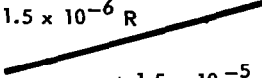
An overall block diagram of the Electronic Omni System is provided in Figure 157. Range and range rate is again obtained by a sine wave modulated, PM-CW radar transponder system. Target attitude data is obtained by the "Omni" system technique, and LOS angles by a conventional "L" interferometer.

The EOS equipment description, the principles of operation, and a discussion of system capabilities and limitations are included in this section.

Description of Operation

Range and Range Rate Measurement.- The range and range rate PM-CW, four tone, radar-transponder system is identical to that previously described in the discussion of the IPS system.

**TABLE 24 – IPS–RMS ANGULAR ERRORS NEAR BORESIGHT ($\epsilon < 45^\circ$)
(MECHANICAL DEGREES)**

TYPE OF ERROR (SOURCE)	LONG RANGE ($R > 3 \times 10^2$ METER)	SHORT RANGE ($R < 3 \times 10^2$ METER)
CONSTANT (PHASE TRACKING)	± 0.29  $\pm 1.90^\circ$	± 0.29  ± 1.90
PROPORTIONAL ($\Delta d/d$)	$\pm 10^{-3}$  $\pm 10^{-3}$	$\pm 10^{-3}$  $\pm 10^{-3}$
RANGE DEPENDENT (THERMAL NOISE)	$\pm 5 \times 10^{-8} R$  $\pm 5 \times 10^{-7} R$	$\pm 1.5 \times 10^{-6} R$  $\pm 1.5 \times 10^{-5} R$

*THE THERMAL NOISE ERRORS ARE BASED ON A 100 WATT CW TRANSMITTER WITH A LOW PASS FILTER NOISE BANDWIDTH OF 40 Hz IN THE LONG RANGE MODES. IN THE SHORT RANGE MODE A 1 WATT TRANSMITTER AND A LOW PASS FILTER NOISE BANDWIDTH OF 562 Hz HAS BEEN ASSUMED.



Angle Measurements.— In the Electronic Omni System, three separate angle measurement techniques are employed. Line-of-sight angles are obtained in the EOS by a null-seeking sum and difference "L" type interferometer as shown in Figure 167. Three closely spaced (one-half wavelength or less) antennas are used at the chasecraft which receive the target vehicle carrier. One antenna is used as a reference for two orthogonal pairs on a time sharing basis and the phase induced in the antennas is processed in a conventional manner to obtain the line-of-sight angles. A precision phase shifter with a calibrated shaft readout is servo-positioned to produce a null at the difference hybrid. The sum hybrid is used as an AGC control and as a reference for angle sense.

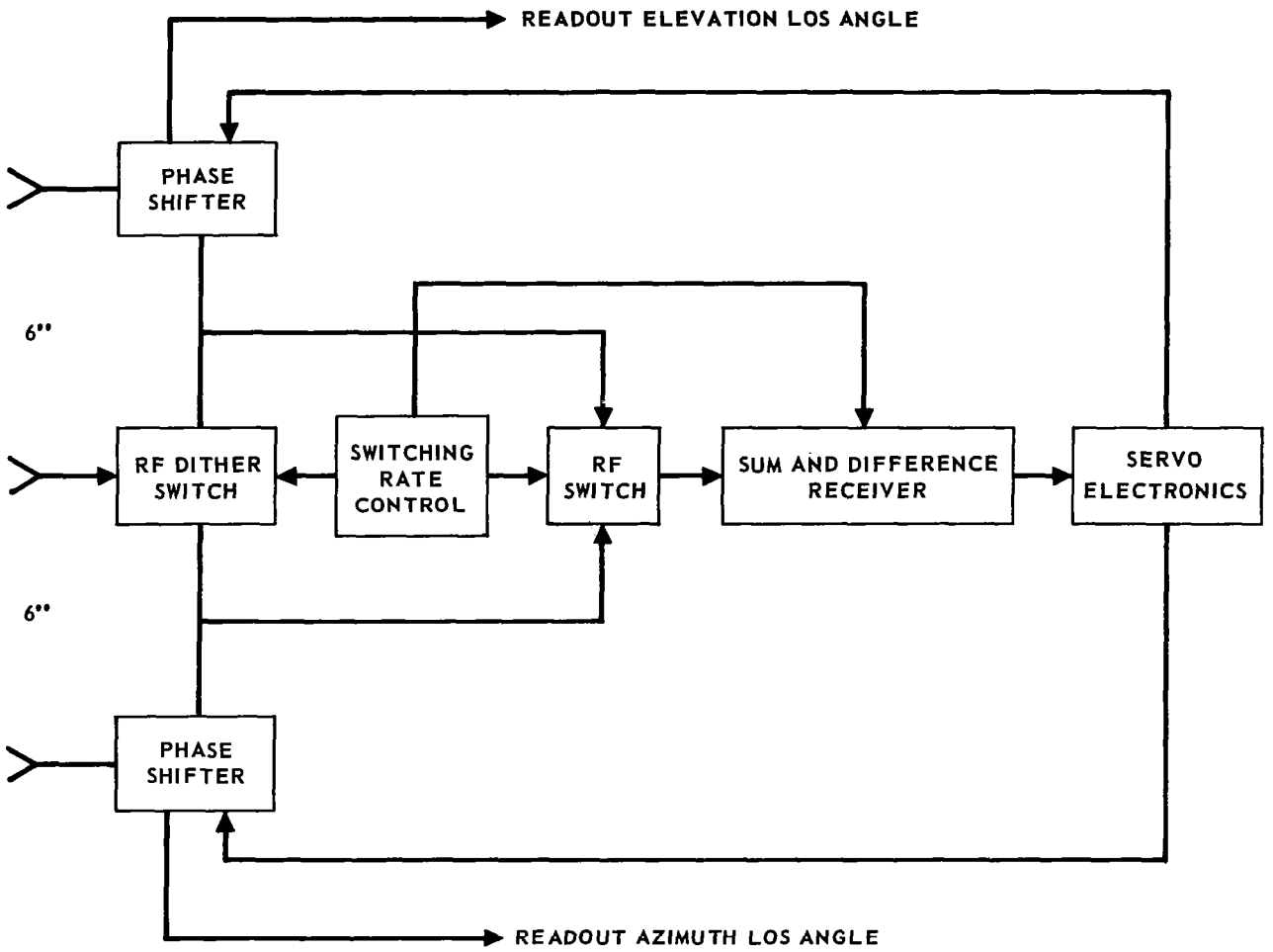


FIGURE 167 - EOS-LOS INTERFEROMETER SYSTEM

Target attitude angles are obtained by the "Omni" null sweep technique as outlined earlier in this report. A block diagram of the attitude transmitter is shown in Figure 168. The attitude receiver block diagram is shown in Figure 169. Relative roll angle is obtained by measuring the time elapsed from reception of the null by a widely spaced roll antenna (one meter or so if possible) and a common target attitude receiving antenna. This time measurement along with the range measurement is processed to provide the relative roll error signal indication. The angle accuracies of the EOS and IPS are compared in Figure 170.

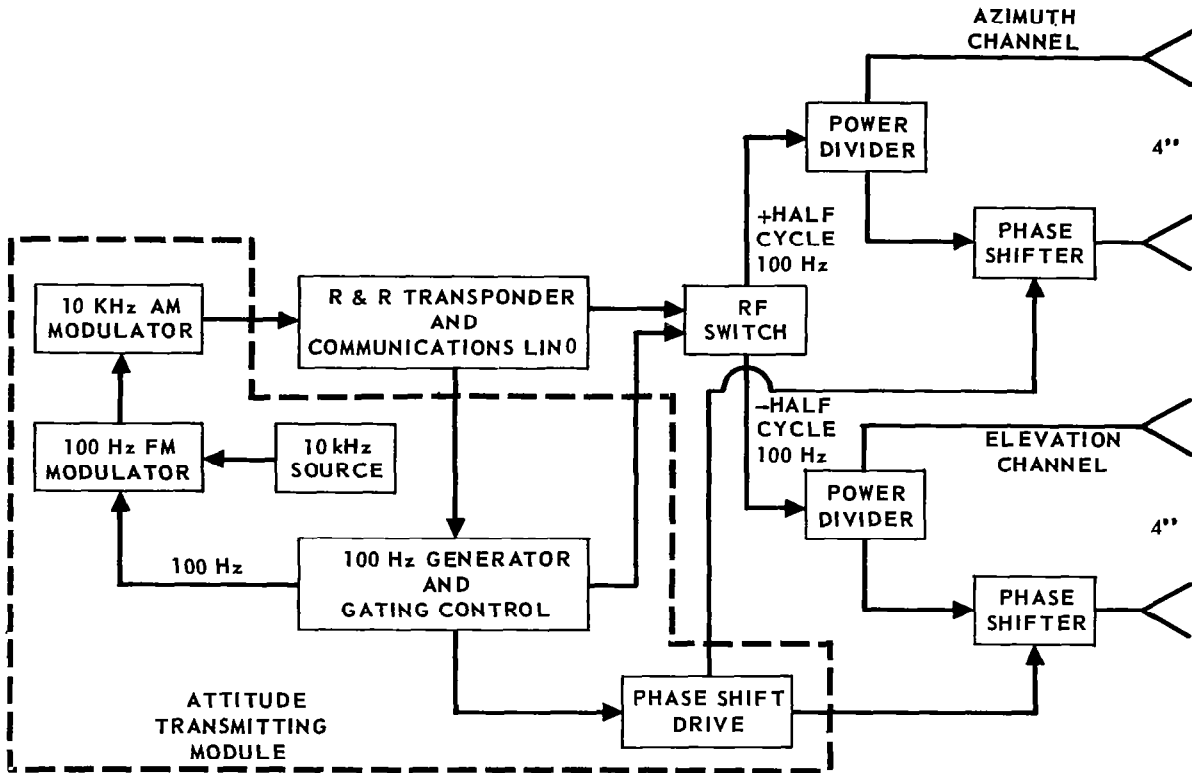


FIGURE 168 - TARGET CRAFT

Frequency Selection and RFI Considerations

In the Electronic Omni System, the target and chasecraft frequency relationships are similar to those of the Integrated Phase System as discussed earlier.

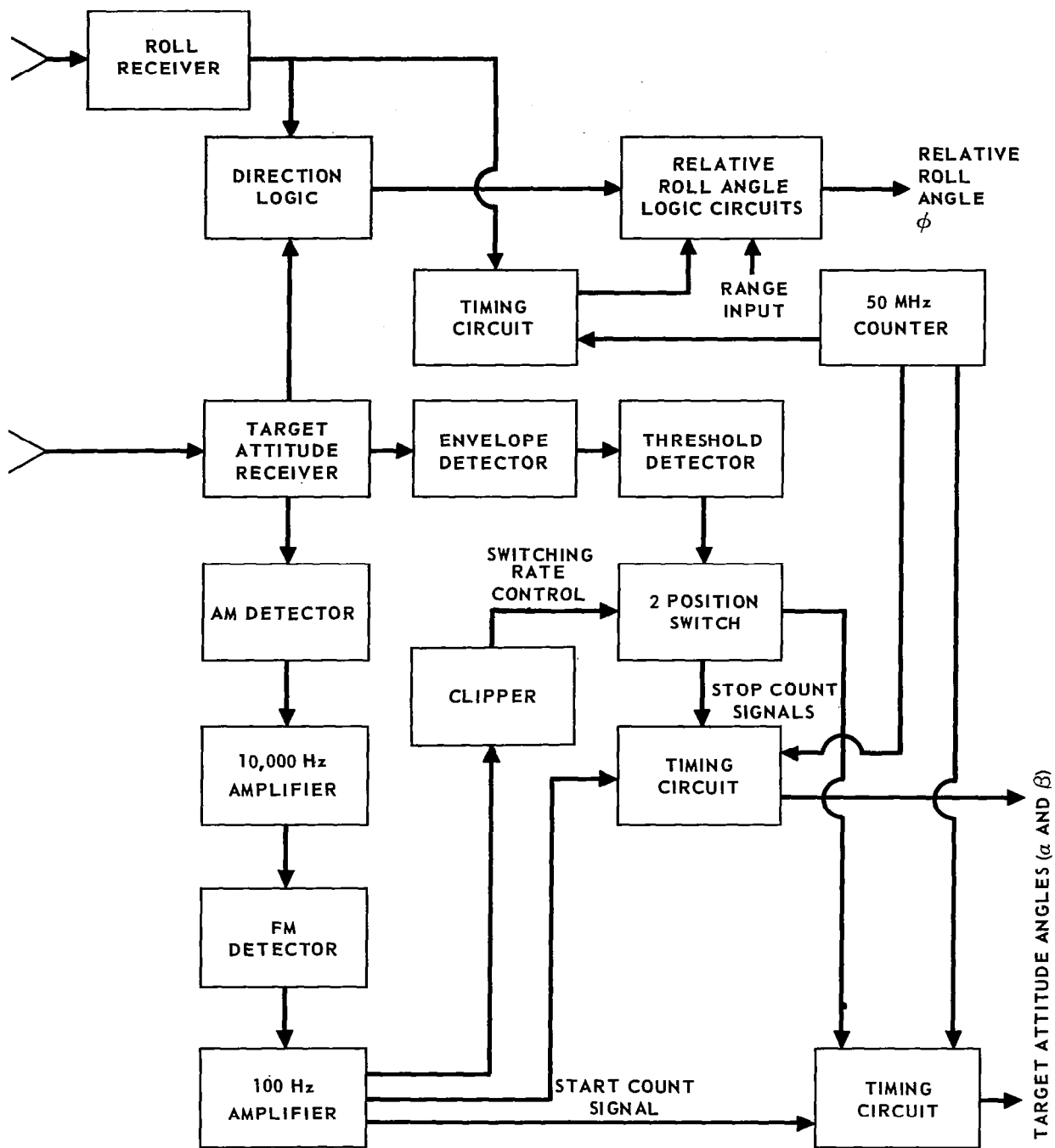


FIGURE 169 - ATTITUDE ANGLE RECEIVER

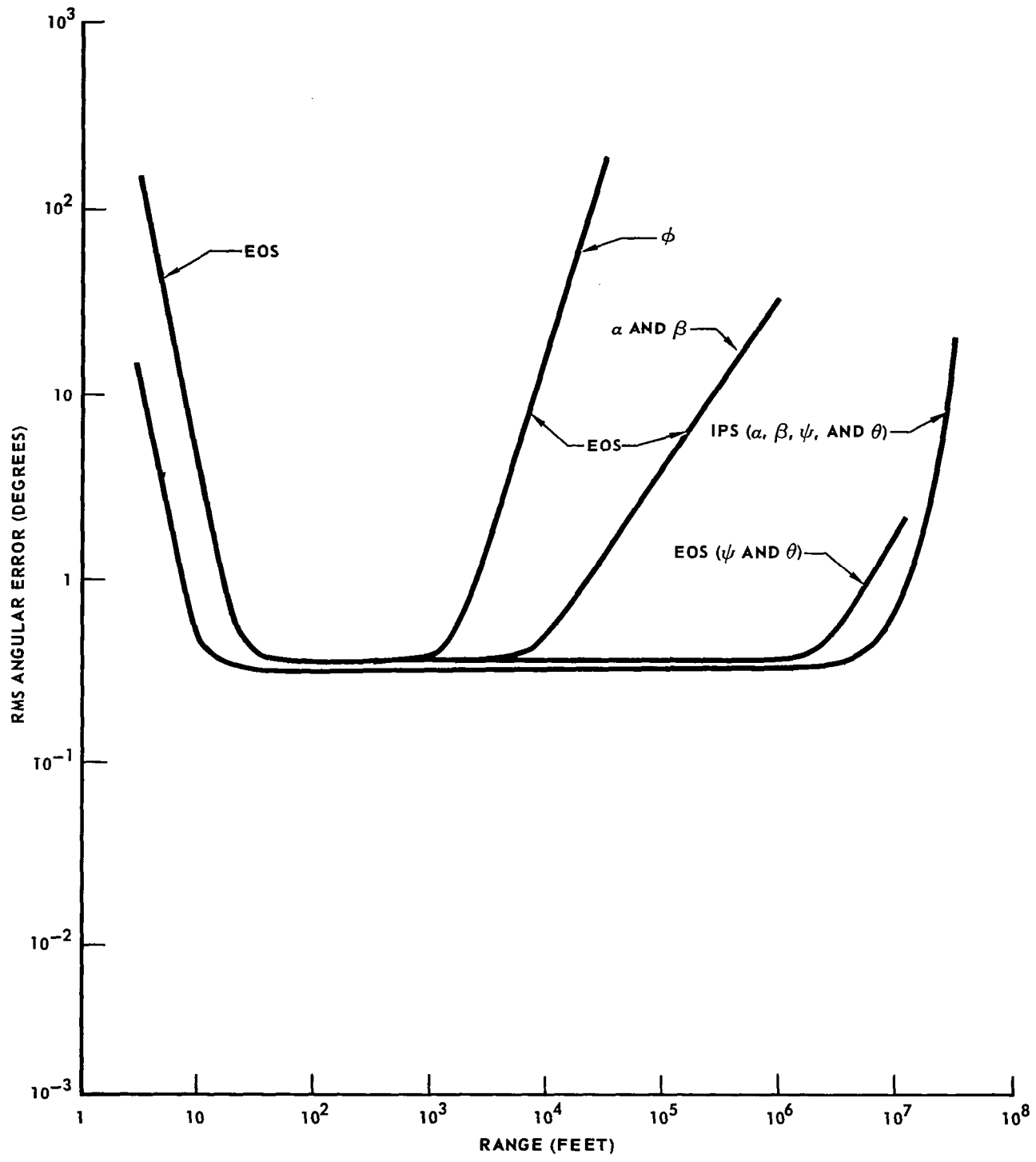


FIGURE 170 – IPS-EOS MEASUREMENT ERROR COMPARISONS

The major difference is that the Electronic Omni System does not employ the frequency pair technique and thus only two frequencies are present at the first mixer of either the target or chasecraft receiver.

The chasecraft transmits at the frequency kf , and the target transponder replies at the frequency $\frac{k}{k-1} kf_p$. The transponder reply is coherently related to the chaser transmitter frequency but is offset by $\frac{k}{k-1} f_1$ Hz.

At both the target and chaser the respective transmitter frequencies also serve as the reference signal at the first mixer. Then at either spacecraft, only the two RF signals appear at the first mixer. This is in contrast to the case of the Integrated Phase System where three RF signals are present (the third resulting from the frequency pair requirement). The problem of selecting the intermediate frequency to minimize RFI is therefore much less complicated than for the Integrated Phase System. The primary considerations are minimum RFI, reasonable intermediate frequency values, and a reasonable frequency multiplication factor k .

For example, letting the transponder reply frequency, $\frac{k}{k-1} kf_1$, be 1 GHz and the frequency multiplication factor, k , be 12, the chaser transmitter frequency, kf_1 , becomes 917 MHz. Thus, the intermediate frequency at both the target and chaser receivers is 83 MHz and the nearest significant interfering signal is 83 MHz away from the desired signal.

Ranging in the Electronic Omni System

Range information is obtained by introducing phase modulated range subcarriers on the chasecraft transmission in the same manner as previously described for Integrated Phase System (IPS). The target transponder reply is caused to repeat this phase modulation such that a phase comparison at the chasecraft yields the desired phase information.

In order to provide a completely integrated system, it is desired to let the RF waveform used in the formation of the swept null pattern (See appendix K) contain the range subcarrier modulation. That is, if the signal transmitted by the chasecraft is of the form:

$$\cos [\omega_0 t + \beta \cos \omega_m t], \quad (519)$$

the reply signal received by the chasecraft would be of the form (neglecting the transponder frequency offset):

$$E(t) \cos \left[\omega_0 \left(t - \frac{2R}{c} \right) + \beta \cos \omega_m \left(t - \frac{2R}{c} \right) \right], \quad (520)$$

where ω_0 is the carrier radian frequency,
 ω_m is the subcarrier radian frequency,
 β is the modulation index,
 c is the velocity of light,
 R is the target-to-chasecraft range,
is the modulation on the received signal resulting from the swept null technique (See appendix K).

As shown in appendix K, the modulating function, $E(t)$, may be represented as:

$$E(t) = \sum_{m=0}^{\infty} b_m \cos(m \omega_s t + a_m), \quad (521)$$

where b_m and a_m are functions of the target yaw and pitch angular errors. ω_s is the null sweep radian frequency.

In the special case where the target roll axis is directed toward the chasecraft, we have:

$$E(t) = 2 \sum_{\substack{m=1 \\ m \text{ odd}}}^{\infty} J_m\left(\frac{\pi}{2}\right) \sin(n \omega_s t), \quad (522)$$

where J_m represents the m th order Bessel function.

Demodulation to obtain the range subcarriers at the chasecraft receiver would normally be accomplished via a phase locked loop (PLL) tracking the carrier as in the case of the Integrated Phase System. However, in attempting to deal with the waveform described by equations 520 and 522 at least two problems become apparent. First, when tracking the carrier the output of the PLL null detector will be:

$$E(t) \beta \cos\left[\omega_m\left(t - \frac{2R}{c}\right)\right]. \quad (523)$$

That is, the demodulation process translates the spectrum of $E(t)$ to the range subcarrier frequency, $\frac{\omega_m}{2\pi}$. Then in order to make the desired phase comparison

with the range subcarrier reference signal, the sidebands due to $E(t)$ must be eliminated. This represents a major filtering problem since the subcarrier frequency may be as high as several megahertz and the sidebands may be only a few hundred hertz from the desired subcarrier.

Secondly, for the case where the target pitch and yaw errors approach zero, the carrier amplitude also goes to zero as illustrated by equation 522. Thus, demodulation via a PLL tracking the carrier is not possible. However, the PLL could be caused to track one of the two adjacent sidebands (the amplitude of which is proportional to $[J_1 \frac{\pi}{2} = 0.28]$ in this exact alignment case.

A complete analysis of the above noted problems is beyond the scope of the report. However if further consideration so dictates, an additional carrier frequency may be provided at the target transmitter so that the range subcarrier modulation need not be provided on the swept null waveform. In addition,

increasing the null sweep frequency, $\frac{\omega_s}{2\pi}$, would ease the filtering problem at the expense of decreasing the accuracy of the timing reference signal used for target attitude determination. Then in either event the ranging performance of the Electronic Omni System would be made similar to that of the Integrated Phase System.

Range Rate Measurement in the Electronic Omni System

Range rate information is obtained by measuring the two way doppler frequency shift. This basic technique is identical to that employed in the Integrated Phase System (IPS).

In this manner the target receives the signal transmitted by the chasecraft and replies with a coherent frequency offset such that the two way doppler shift is measured at the chasecraft. In order to provide a completely integrated system, it is desired to let the target reply frequency be used in the formation of the swept null pattern (see appendix K). As discussed above, this means that the reply waveform received at the chasecraft will contain the swept null pattern modulation, $E(t)$, as well as the desired doppler shift information. That is, if the chasecraft transmits a signal of the form:

$$\cos(\omega_0 t), \quad (524)$$

the signal received by the chasecraft will be of the form (neglecting the frequency offset):

$$E(t) \cos[\omega_0 t + 2\omega_d t], \quad (525)$$

where: ω_0 is the carrier radian frequency,

ω_d is the one way doppler radian frequency shift,

$E(t)$ is the modulation function resulting from the swept null pattern technique.

From appendix K, $E(t)$ may be represented as:

$$E(t) = \sum_{m=0}^{\infty} b_m \cos(\omega_s t + a_m), \quad (526)$$

where ω_s is the null sweep radian frequency, and b_m and a_m are functions of the target yaw and pitch angular errors.

The modulation function, $E(t)$, may complicate the recovery of the desired doppler shift information. This is similar to the problems associated with the range measurement in the Electronic Omni System. First, the presence of sidebands at the multiples of $\frac{\omega_m}{2\pi}$ from the carrier frequency may create ambiguities in the doppler measurement. Secondly, as noted in appendix K, when the target roll axis is directed toward the chasecraft the carrier amplitude approaches zero.

With proper processing and logic, the above two problems may be overcome. For example, when the carrier null condition occurs, the doppler shift information may be derived from the adjacent sideband. However, further analysis is required to determine the best approach. If further consideration so dictates, an additional carrier frequency may be provided at the target transmitter so that the doppler shift information need not be derived from the swept null waveform. In any event, the range rate measurement capability of the Electronic Omni System would be similar to that of the Integrated Phase System as described in

Angle Error Analysis for the Electronic Omni System

System error leading to errors in the measurement of target pitch, yaw, roll, and line-of-sight are considered in the following three sections. The results are presented at the end of each section.

Yaw and Pitch Angular Errors.- As described in appendix K, the null of the radiation patterns transmitted by the target is caused to sweep alternately in azimuth and elevation. The null is swept in a linear manner at ω_s mechanical radians per second. For the case of the azimuth sweep (elevation sweep considerations are identical), the chasecraft azimuth coordinate relative to the target antenna boresight is determined by comparing the time of the null occurrence at the chasecraft with a timing reference signal.

From equation K5 of appendix K, the angular position of the desired null is defined by:

$$\beta \sin(\omega_s t) + \frac{2\pi d}{\lambda} \sin \epsilon = 0, \quad (527)$$

where β is the peak value of the time varying phase shift,
 λ is the wavelength,
 d is the distance between phase centers of the target interferometer antenna pair,

In appendix K, it is shown that in order to achieve a linear null sweep with no ambiguities for $-90^\circ < \epsilon < 90^\circ$, we require $\beta = \frac{2\pi d}{\lambda} \leq \pi$. Then for this condition with $\beta = \frac{2\pi d}{\lambda}$, the null position as a function of time is:

$$-\epsilon = \omega_s t_1, \quad (528)$$

and under these conditions the parameter measured, or the time of the null occurrence is:

$$T = -\frac{\epsilon A}{\omega_s}. \quad (529)$$

However, the radiation pattern generated by the target interferometer antenna pair may deviate from the ideal case considered in appendix K. First, variations in β and/or $\frac{2\pi d}{\lambda}$ will invalidate equation 528. Secondly, an RF phase shift in one of the feeds to the target antenna pair will invalidate equation 527.

First, consider deviations in β (or equivalently $\frac{2\pi d}{\lambda}$) from the desired value of π . In equation 527 we replace $\bar{\beta}$ by $\beta + \Delta\beta$ to obtain as the null condition:

$$(\beta + \Delta\beta) \sin \omega_S t + \frac{2\pi d}{\lambda} \sin \epsilon = 0, \quad (530)$$

$$\left(1 + \frac{\Delta\beta}{\pi}\right) \sin \omega_S t + \frac{2\pi d}{\lambda} \sin \epsilon = 0, \quad (531)$$

$$\left(1 - \frac{\Delta\beta}{\pi}\right) \sin \epsilon = -\sin \omega_S t. \quad (532)$$

But for small values of $\frac{\Delta\beta}{\pi} \tan \epsilon$, we use the following approximation:

$$\sin \left[\epsilon - \frac{\Delta\beta}{\pi} \tan \epsilon \right] \approx \left[1 - \frac{\Delta\beta}{\pi} \right] \sin \epsilon. \quad (533)$$

Then the null condition of equation 532 becomes:

$$\sin \left[\epsilon - \frac{\Delta\beta}{\pi} \tan \epsilon \right] = -\sin \omega_S t, \quad (534)$$

or for small values of ϵ (i.e., near boresight):

$$\epsilon(t) \approx \left[1 + \frac{\Delta\beta}{\pi} \right] \omega_S t. \quad (535)$$

Then for the chasecraft at ϵ_T , the time of occurrence of the null is:

$$T = \frac{\epsilon_T}{\left(1 + \frac{\Delta\beta}{\pi}\right) \omega_S}, \quad (536)$$

and using equation 529 the apparent azimuth coordinate is:

$$A = \epsilon_S t \approx \epsilon_T \left[1 - \frac{\Delta\beta}{\pi} \right], \quad (537)$$

and the error due to $\Delta\beta$ is:

$$\epsilon_A - \epsilon_T = -\epsilon_T \frac{\Delta\beta}{\pi}. \quad (538)$$

The units are mechanical degrees for ϵ_T in degrees and $\Delta\beta$ in radians. $\Delta\beta$ may be considered an error in either the modulation index, β , or the parameter

$\frac{2\pi d}{\lambda}$. Note that equation 538 is valid only near boresight.

Variations in d and β will be the primary contributors to $\Delta\beta$. For example we require that $d = \frac{\lambda}{2}$ or $d = 0.15$ m at an operating frequency of 1 GHz. Then

± 1 mm variations in d will cause fractional variations of $\pm 6.7 \times 10^{-3}$ in $\frac{\Delta\beta}{\pi}$.

Considering variations in the modulation index, β , as well as in d , the total (rss) equivalent fractional variation in $\frac{\Delta\beta}{\pi}$ is 0.01, such that equation becomes:

$$\epsilon_A - \epsilon_T = \pm 10^{-2} \epsilon_T.$$

This equation represents angular measurement error due to variations in the parameters β and $\frac{2\pi d}{\lambda}$ from the desired value of π . The equation is valid near boresight.

An RF phase shift in one of the feeds to the target interferometer antenna pair introduces an undesired phase shift, $\Delta\theta$. Then, instead of equation 527, the null condition is defined by:

$$\Delta\theta + \beta \sin \omega_S t + \frac{2\pi d}{\lambda} \sin \epsilon = 0, \quad (539)$$

or letting $\beta = \frac{2\pi d}{\lambda} = \pi$ the null condition is:

$$\frac{\Delta\theta}{\pi} + \sin \epsilon = -\sin \omega_S t. \quad (540)$$

But for small values of $\frac{\Delta\theta}{\pi \cos \epsilon}$, we may use the following approximation:

$$\sin \left[\epsilon + \frac{\Delta\theta}{\pi \cos \epsilon} \right] \approx \frac{\Delta\theta}{\pi} + \sin \epsilon, \quad (541)$$

such that the null condition defined by equation 540 becomes:

$$\sin \left[\epsilon + \frac{\Delta\theta}{\pi \cos \epsilon} \right] = -\sin \omega_S t, \quad (542)$$

or

$$\epsilon = -\frac{\Delta\theta}{\pi \cos \epsilon} - \omega_S t. \quad (543)$$

Comparing this equation with equation 528, it is seen that the angular measurement error due to an RF phase shift of $\pm \Delta\theta$ electrical degrees is:

$$\pm \frac{\Delta\theta}{\pi \cos \epsilon}. \quad (544)$$

Then for an RF tracking tolerance of $\pm 1^\circ$, the mechanical angular error is $\pm 0.32^\circ$ at boresight.

In addition to the previously considered errors due to parameter variations at the target transmitter array, error will be introduced in the measurements made at the chasecraft receiver. The parameter measured at the chasecraft is the time of occurrence, T , of the null relative to the timing reference signal. Then from equation 529, the estimate of the angular coordinate is given by:

$$\epsilon_A = -\omega_S t. \quad (545)$$

Errors in ω_s and T contribute to the errors in the estimate as follows:

$$\Delta \epsilon_A = -[\Delta \omega_s t + \Delta T \omega_s], \quad (546)$$

$$\Delta \epsilon_A = -\left[\frac{\Delta f_s}{f_s} \epsilon_A + \Delta T \omega_s\right]. \quad (547)$$

As indicated above, fractional errors in the scan frequency, f_s , result in a measurement error proportional to the azimuth error, ϵ_A . For a scan frequency stability of one part on 10^7 the proportional error will be $10^{-5} \epsilon_A$. Timing measurement errors result from receiver thermal noise, absolute timing accuracy limitations (e.g., counter accuracy), and errors in the timing reference signal. Thermal noise errors will be discussed later. For a 1 MHz counter, the maximum error is one count of $\pm 1 \mu s$. This $\pm 1 \mu s$ error corresponds to 0.014 mechanical degrees for $f_s = 375$ Hz.

Errors in the timing reference signal depend on the method of providing the signal. In general, target yaw and pitch measurements will only be required at relatively close ranges. Then the timing reference signal may be provided by using the 375 Hz range subcarrier available at both the target and chasecraft. In this manner, the sweep frequency, f_s , is equal to 375 Hz, and the 375 Hz reference signal at the chasecraft leads the 375 Hz modulation by a time interval corresponding to the two way range delay. That is, the timing reference signal will cause an error in ΔT equal to:

$$\sigma_\theta \Delta T = \frac{2R}{c}. \quad (548)$$

In appendix L, it is shown that the mean squared angular error or angle jitter variance (AJV) due to chasecraft receiver thermal noise is:

$$\sigma_\theta^2 = \left(\frac{2}{\pi}\right)^2 \frac{4kTNF f_s}{S \cos^2 \epsilon_A} \left(\frac{\text{Mechanical}}{\text{Radians}}\right)^2, \quad (549)$$

where $kT = 4 \times 10^{-21}$ watts/Hz,

$F =$ receiver noise figure,

$f_s =$ sweep frequency,

$\lambda =$ the chasecraft azimuth coordinate relative to the target antenna borewight,

$S =$ received signal power as determined by the radar range equation.

The above mean squared error is that for a single sweep. If a low pass filter with noise bandwidth equal to B_{LP} is used to integrate over several sweeps the above angle jitter variance will be reduced by the factor, $\frac{1}{2 B_{LP}}$.

The received signal power is given by the radar range equation:

$$S = \frac{P_t G_t G_r \lambda^2 L}{(4\pi)^2 R^2}, \quad (550)$$

where P_t = transmitted power (+ 20 dbw),
 G_t = transmitter antenna gain (0 db),
 G_r = receiver antenna gain (0 db),
 R = target-to-chasecraft range (m),
 λ = wavelength (0.3 m),
 L = loss factor (-3 db).

The quantities in brackets indicate the parameter values for the proposed system. Then, substituting the range equation into the angle jitter variance expression, we obtain:

$$\sigma_\theta^2 = \left(\frac{2}{\pi}\right)^2 \frac{4f_s k T N F (4\pi)^2 R^2}{\cos^2 \epsilon_A P_t G_t G_r \lambda^2 L}, \quad (551)$$

$$\sigma_\theta^2 = \frac{(16)^2}{\cos^2 \epsilon_A} \frac{f_s k T N F R^2}{P_t G_t G_r \lambda^2 L}. \quad (552)$$

Using the above indicated parameter values with $F = 14$ db and $f_s = 375$ Hz, we obtain as the rms mechanical angular error due to thermal noise:

$$\sigma_\theta = 2.52 \times 10^{-6} \frac{R}{\cos \epsilon_A}, \quad (553)$$

for R in meters. Note that this is the angle noise based on a single sweep.

For a low pass filter with noise bandwidth equal to $40 \frac{\pi}{2}$ Hz, the single sweep rms angular error due to thermal noise is reduced by the factor:

$$\left(\frac{f_s}{2 B_{LP}}\right)^{\frac{1}{2}} = \left(\frac{375(2)}{2(40)\pi}\right)^{\frac{1}{2}} = \frac{1}{1.73}, \quad (554)$$

such that the rms mechanical error becomes:

$$\sigma_\theta = 1.46 \times 10^{-6} \frac{R}{\cos \epsilon_A}, \quad (555)$$

for R in meters. The noise bandwidth of $\frac{40\pi}{2}$ Hz is consistent with that used in the docking simulation study.

The results are summarized in table 25 where each term contributing to the angle measurement error is listed separately. In general, the yaw and pitch data are not required for ranges greater than about 300 m. At this range, the bias error is 0.027 mechanical degrees and the remaining terms result in an rms error equal to about 0.33 mechanical degrees, assuming the on boresight ($\epsilon = 0$) case.

TABLE 25 – SUMMARY OF YAW AND PITCH ANGULAR ERRORS

TYPE OF ERROR	SOURCE	ERROR (MECHANICAL DEGREES)
CONSTANT TERM (1σ)	COUNTER ERROR	$\pm 0.014^\circ$
	RF PHASING	$\pm 0.32^*$
PROPORTIONAL TERM (1σ)	$\frac{\Delta f_s}{f_s}$	$\pm 10^{-5} \epsilon$
	$\Delta B/B$	$\pm 10^{-2} \epsilon^*$
RANGE AND ANGLE DEPENDENT (1σ)	RECEIVER THERMAL NOISE	$\pm 1.46 \times 10^{-6} \frac{R}{\cos \epsilon}$
BIAS	TIMING REFERENCE ERROR	$(9 \times 10^{-5})R$

* denotes near boresight approximation
 ϵ = yaw (pitch) error in mechanical degrees
 R = target-to-chasecraft range in meters

Roll Angular Error in the Electronic Omni System.— The relative roll orientation of the target and chasecraft are determined by measuring the time interval required for the swept null pattern to move between two widely spaced antennas on the chasecraft. The method of generating the swept null pattern is presented in appendix K.

Let the antenna spacing on the chasecraft be d . Let the null pattern be swept at an angle $((90-\theta)^\circ)^\circ$, relative to a line between the two widely spaced antennas as shown in figure 171.

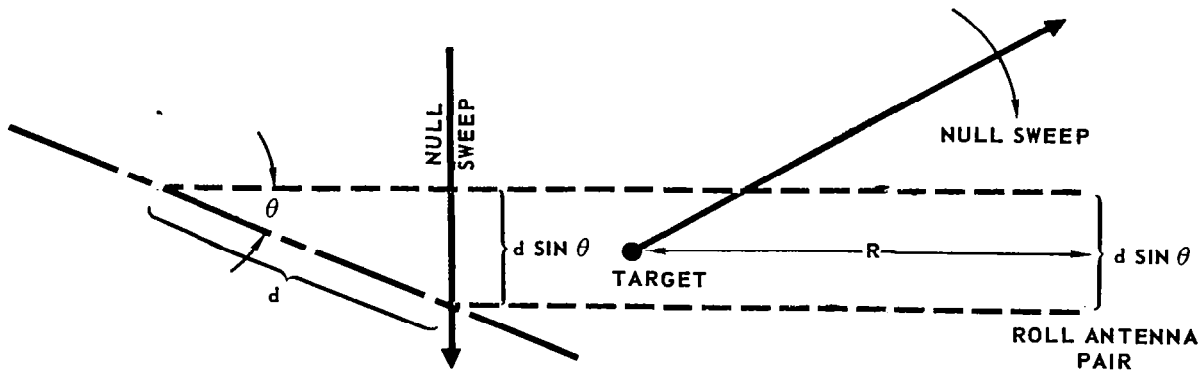


FIGURE 171 - ROLL PAIR NULL SWEEP RELATIONSHIP

Then for a sweep rate of ω_s mechanical radians per second, the time, T , required for the null to sweep from one antenna to the other is given by:

$$T = \frac{d \sin \theta}{R \omega_s}, \quad (556)$$

where R is the chasecraft-to-target range. The roll angle, θ , is given by:

$$\theta = \sin^{-1} \left\{ \frac{R \omega_s T}{d} \right\}, \quad (557)$$

which for $\theta \leq \pi/4$ may be approximated by:

$$\theta = \frac{R \omega_s T}{d}. \quad (558)$$

Note that in order to determine θ a knowledge of the target-to-chasecraft range, R , is required. An estimate of the range, R , is available from the range/range rate radar.

From equation 558 errors in R , T , and d yield the following errors in the roll angle measurement:

$$\Delta \theta = \theta \left[\frac{\Delta R}{R} + \frac{\Delta \omega_s}{\omega_s} + \frac{\Delta T}{T} - \frac{\Delta d}{d} \right] \quad (559)$$

$$\Delta \theta = \theta \frac{\Delta f_s}{f_s} - \theta \frac{\Delta d}{d} + 360 \frac{R}{d} f_s \Delta T + \theta \frac{\Delta R}{R}. \quad (560)$$

In the latter equation, the units of $\Delta \theta$ are in mechanical degrees for θ in degrees.

The first two terms result in proportional errors. For an oscillator stability of one part in 10^5 , we have $\frac{\Delta f_s}{f_s} = \pm 10^{-5}$ and for a spacing accuracy of one part in 10^3 we have $\frac{\Delta d}{d} = \pm 10^{-3}$. Then the first two terms combine to give a total fractional error equal to about $\pm 10^{-3}$.

The third term yields an error proportional to the target-to-chasecraft range, R, for a constant timing error, ΔT . For a 1 MHz counter we have $\Delta T = \pm 1 \mu s$. Then using $f_s = 375 \text{ MHz}$ (as determined in the discussion of yaw and pitch errors) and $d = 1 \text{ m}$ the third term becomes $(1.35 \times 10^{-3})R$ for R in meters. Timing errors due to thermal noise will be considered later.

The fourth term results from range measurement errors, ΔR . Since the range measurement capability of the Electronic Omni System is similar to that of the Integrated Phase System, we may use the earlier results to determine ΔR . From that paragraph, using the 100 watt mode results, it is seen that for $R \leq 870 \text{ m}$, the range error R is approximately (within 10%) constant and equal to $\pm 0.13 \text{ m}$. Then at the relatively short ranges, where the roll measurements would be used the fourth term becomes $\pm 0.13 \frac{\theta}{R}$ mechanical degrees for R in meters and θ in degrees.

To this point, only measurement errors at the chasecraft receiver have been considered; errors in the formation of the swept null waveform at the target have not. In the discussion of target yaw and pitch angular measurement errors, it was noted that errors, $\Delta\beta$, in the modulation index (or equivalent in $\frac{2\pi d}{\lambda}$) could cause the time of occurrence of the null at the chasecraft antenna with angular coordinate ϵ_T , (relative to the target antenna boresight) to be in error by $\frac{\Delta\beta}{\pi\omega_s} \epsilon_T$ seconds. This result is valid for small $\Delta\beta$ and ϵ_T . Then in the case of the roll measurement the timing error will be:

$$\Delta T = \frac{\Delta\beta}{\pi\omega_s} (\epsilon_{T_1} - \epsilon_{T_2}), \quad (561)$$

where ϵ_{T_1} and ϵ_{T_2} are the angular coordinates in radians of the two antennas used in the roll measurement. But:

$$\epsilon_{T_1} - \epsilon_{T_2} = \frac{d \sin \theta}{R}, \quad (562)$$

where d is the roll antenna pair spacing and θ is the relative roll angle. The roll error, $\Delta\theta$, resulting from a timing error, ΔT , is given by $\Delta\theta = \frac{R\omega_s}{d} \Delta T$, such that the error in roll measurement due to $\Delta\beta$ becomes:

$$\Delta\theta = \frac{R\omega_s}{d} \frac{\Delta\beta}{\pi\omega_s} \frac{d \sin \theta}{R} \approx \frac{\Delta\beta}{\pi}.$$

The units on $\Delta\theta$ above are in mechanical degrees for $\Delta\beta$ in radians and θ in mechanical degrees. Then for $\frac{\Delta\beta}{\pi} = \pm 10^{-2}$, we have $\theta = 10^{-2} \theta$. Note that the expression is valid for roll angles, $\theta, < \frac{\pi}{4}$; yaw (or pitch) angles,

$$\epsilon_1 < \frac{\pi}{4}; \text{ and } \Delta\beta \ll \pi.$$

In the discussion of yaw and pitch angular measurement errors, it was noted that an RF phase shift is one of the legs of the target pair used to generate the swept null pattern would cause a constant error as given by equation 544. No similar effect will occur in the roll measurement because the constant error will cancel when the time difference is taken.

In a manner similar to that discussed in the section on pitch and yaw measurement errors, receiver thermal noise will result in errors in determining the time of the null occurrence at each of the antennas in the chasecraft roll antenna pair. Using equation M11, of appendix M, the mean squared timing error or timing jitter variance in measuring the time required for the null to sweep from one antenna to the other will be:

$$\sigma_T^2 = \frac{4\eta}{\pi^4 S f_s} \left[\frac{1}{\cos^2 \epsilon_1} + \frac{1}{\cos^2 \epsilon_2} \right], \quad (563)$$

where ϵ_1 and ϵ_2 are the angular coordinates, relative to the target antenna boresight, respectively of the two chasecraft antennas used for the roll measurement. The angles, ϵ_1 and ϵ_2 , are functions of the roll angle, θ as shown in figure 172.

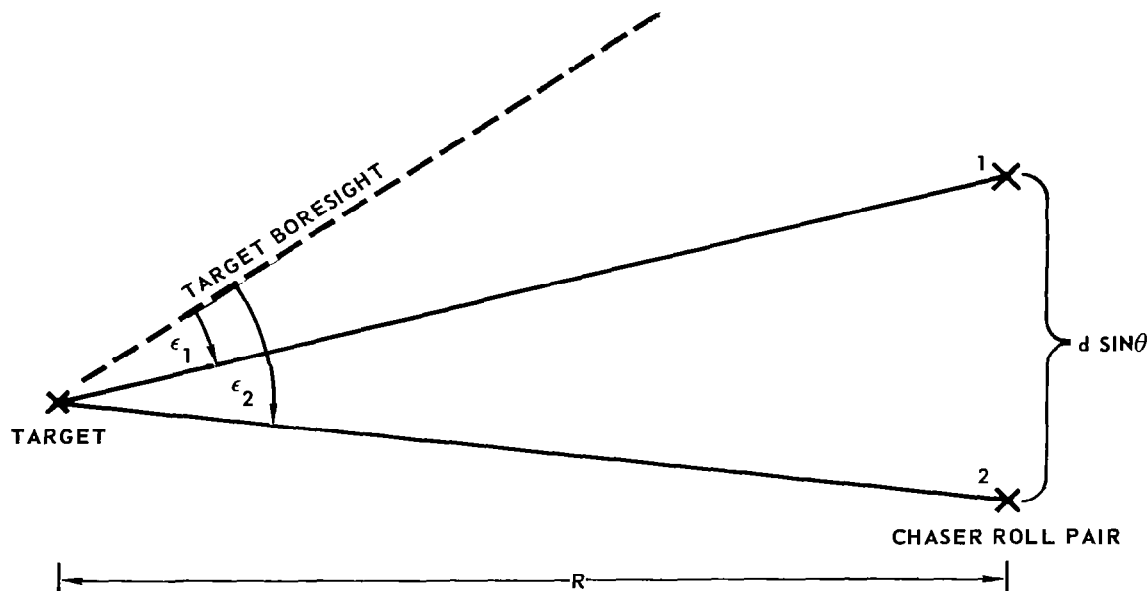


FIGURE 172 - TARGET ATTITUDE EFFECT ON RELATIVE ROLL MEASUREMENTS

When the target yaw and pitch errors have been corrected, the target roll axis will be directed somewhere (depending on the relative antenna positions at the chasecraft) between the two chasecraft roll antennas. Then the minimum value of $\cos \epsilon_1$, or $\cos \epsilon_2$ is:

$$\frac{R}{\sqrt{R^2 + (d \sin \theta)^2}}, \quad (564)$$

where θ is the relative roll angle. Then for $R \gg d \sin \theta$, we have $\epsilon_1 \approx \epsilon_2 \approx 0$ and at smaller values of R , the roll angle, θ , should approach zero such that we still have $\epsilon_1 \approx \epsilon_2 \approx 0$. Then the rms timing error equation becomes:

$$\sigma_T = \left(\frac{8n}{\pi^4 S f_s} \right)^{1/2}. \quad (565)$$

But from previous results a timing error, T, yields a roll measurement error, θ , equal to:

$$\theta = 360 \frac{R}{d} f_s \Delta T . \quad (\text{Mechanical Degrees}) \quad (566)$$

Then combining the previous two equations, the per sweep rms roll measurement error is:

$$\Delta\theta = \frac{(360) R f_s}{d} \left(\frac{8\eta}{\pi^4 S f_s} \right)^{1/2} . \quad (\text{Mechanical Degrees}) \quad (567)$$

If a low pass filter with bandwidth equal to B_{LP} is used to average over several sweeps the resultant rms angle noise is reduced by the factor $\left(\frac{2 B_{LP}}{f_s} \right)^{1/2}$ such that the resulting rms angular error is:

$$\Delta\theta = \frac{(1440) R}{d \pi^2} \left(\frac{\eta B_{LP}}{S} \right)^{1/2} . \quad (\text{Mechanical Degrees}) \quad (568)$$

Substituting for S from Equation (22) we have:

$$\Delta\theta = \frac{(5760)^2 R^2}{d \pi \lambda} \left(\frac{k T N F B_{LP}}{P_t G_t G_r L} \right)^{1/2} , \quad (569)$$

where we have used $\eta = K T F$. F is the receiver noise figure and $k T = 4 \times 10^{-21}$ watts/Hz .

Then, using $d = 1m$, $\lambda = 0.3m$, $F = 14db$, $B_{LP} = 40 \frac{\pi}{2}$ Hz , $L = -3db$, $P_t = +20dbw$, and $G_t = G_m$ odb, we have:

$$\Delta\theta = (2.16 \times 10^{-6}) R^2 , \quad (\text{Mechanical Degrees}) \quad (570)$$

for R in meters.

The above derived results for roll measurement errors in the electronic Omni system are summarized in Table 26 .

**TABLE 26 –
SUMMARY OF ROLL MEASUREMENT ERRORS IN THE ELECTRONICS OMNI SYSTEM**

TYPE OF ERROR	SOURCE	MEASUREMENT ERROR (MECHANICAL DEGREES) (FOR $\theta < 45^\circ$)
PROPORTIONAL (1σ)	ROLL ANTENNA SEPARATION $\Delta d/d$	$10^{-3} \theta$
	$\Delta B/B$	10^{-2} (1), (2)
RANGE DEPENDENT (1σ)	COUNTER TIMING ERROR	$(1.35 \times 10^{-3}) R$
	RECEIVER NOISE	$(2.16 \times 10^{-6}) R^2$ (1)
RANGE AND ROLL ANGLE DEPENDENT (1σ)	ΔR	$0.13 \frac{\theta}{R}$

θ RELATIVE ROLL ANGLE IN MECHANICAL DEGREES

R = TARGET-TO-CHASER RANGE IN METERS

d = ROLL ANTENNA PAIR SEPARATION (1m)

(1) $d \sin \theta \ll R$

(2) $\Delta B \ll \pi$

LOS Measurement Errors in the Electronic Omni System.- A phase sensing sum and difference monopulse technique is employed to measure the target angular coordinates relative to the chasecraft antenna boresight. A simplified (heterodyning omitted) single plane receiver is shown in figure 173.

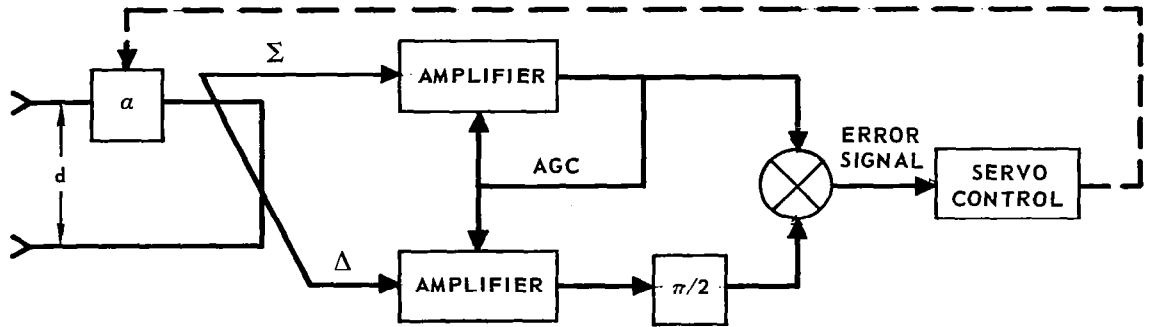


FIGURE 173 - EOS-LOS MEASUREMENT SYSTEM

As shown, the angular error signal is developed in the normal manner for a sum and difference system. A more complete discussion of the angle sensing technique is given in appendix L. The error signal is used to control the variable phase shift, α , such that a null is maintained. Thus, the value of α yielding a null is a means of the electronic boresight, which is an estimate of the target angular coordinate.

For a target angular coordinate, ϵ , the electrical phase difference between the signals induced at the two interferometer antennas is:

$$\phi = \frac{2\pi d}{\lambda} \sin \epsilon, \quad (571)$$

where d is the interferometer separation, and λ is the wavelength. The phase shifter, α , causes the apparent phase difference to be $\phi' = \phi - \alpha$. But from appendix L, the angular error output is proportional to $\sin\left(\frac{\phi'}{2}\right)$. Then in order to achieve a null, the phase shifter must be adjusted such that $\phi' = 0$ or:

$$\alpha = \frac{2\pi d}{\lambda} \sin \epsilon. \quad (572)$$

For small ϵ we may replace $\sin \epsilon$ by ϵ such that the estimate of the target position becomes:

$$\epsilon = \frac{\lambda}{2\pi d} \alpha . \quad (573)$$

Then errors in λ , d , and α yield the following measurement errors:

$$\Delta\epsilon = \epsilon \frac{\Delta\lambda}{\lambda} - \epsilon \frac{\Delta d}{d} + \left(\frac{\lambda}{2\pi d}\right) \Delta\alpha . \quad (574)$$

For an oscillator stability of one part in 10^5 and a spacing accuracy of one part in 10^2 , the first two terms combine to yield a proportional error term approximately equal to $10^{-2}\epsilon$.

The last term results from errors in the knowledge of the phase shifter values. Primary contributors to this error source are precomparator (RF) phase shifts and phase shifter readout errors. Assuming ± 1 electrical degree, due to RF phase tracking, and ± 0.5 electrical degrees, due to readout errors, the last term in equation 574 becomes 0.36 mechanical degrees. Here we have used $\lambda = 2d$, which corresponds to the maximum allowable value of d without ambiguities, as discussed in appendix L.

Thermal noise errors are discussed in Appendix L. Equation L-21 gives the mean squared angular error or angle jitter variance near chasecraft antenna borewidth for high IF signal-to-noise ratios. Using this equation, the rms mechanical angular error in units of mechanical degrees is:

$$\sigma_{\theta} = \frac{\lambda}{d} \frac{180}{\pi} \left(\frac{B_{LP} \eta}{0.65 S}\right)^{1/2} . \quad (575)$$

where d is the interferometer spacing,
 λ is the wavelength,
 η is KTF,
 $KT = 4 \times 10^{-21}$ watts/MHz,
 F = receiver noise figure,
 B_{LP} = noise bandwidth of the zero loop,
 S = received signal power.

Note that a factor of two in the mean squared error has been included to account for time sharing the receiver between azimuth and elevation measurements. The received signal power, S , is given by equation 550. Then substituting for S , the rms mechanical error in units of mechanical degrees becomes:

$$\sigma_{\theta} = \frac{284 R}{d} \left(\frac{B_{LP} kT \eta F}{P_t G_t G_r L}\right)^{1/2} . \quad (576)$$

Evaluation of this equation using $d = 0.15$ m, $B_{LP} = 40 \frac{\pi}{2}$ Hz, $F = 14$ db, $L = -3$ db, $\epsilon_t = \epsilon_m = 0$ db and $P_t = +20$ dbw yields $(6.67 \times 10^{-7}) R$ for R in meters. The assumed low pass filter bandwidth corresponds that used in the docking simulation studies. The value of d used corresponds to the unambiguous requirement for $\lambda = 0.3$ m.

The LOS angle measurement errors are summarized in the following table.

**TABLE 27 – SUMMARY LOS ANGULAR ERRORS IN THE ELECTRONIC OMNI SYSTEM
(NEAR BORESIGHT)**

TYPE OF ERROR	SOURCE	ERROR (MECHANICAL DEGREES)
CONSTANT (1σ)	RF PHASE AND READOUT ERRORS	0.36
PROPORTIONAL (1σ)	$\Delta d/d$	$10^{-2}\epsilon$
RANGE DEPENDENT (1σ)	RECEIVER NOISE	$6.67 \times 10^{-7} R$

R = TARGET-TO-CHASER RANGE IN METERS

ϵ = LOS BORESIGHT ERROR IN MECHANICAL DEGREES

VENDOR SURVEY

McDonnell distributed the questionnaire shown in the next page to 91 electronic industries. Responsive replies were received from 9 companies, which are being supplied to the Contracting Officer. The meager response is believed to be primarily because most of the work in this area is proprietary in nature. Also, many firms indicated that they were not doing work that directly related to the problem. The companies responding were:

Airborne Instruments Laboratory
Autonetics of North American
Cubic Corporation
General Dynamics/Electronics
Honeywell, Inc.
Motorola
Norden Division of United Aircraft
Polarad
Raytheon

The response from Airborne Instruments Laboratory was in the form of recommended systems for the measurement of range, range rate, tilt, and rotation. A basic block diagram of each separate system was provided along with an operational description. The recommended ranging system is cooperative PM-CW operating at L Band. The range-rate system is a noncooperative CW sine wave modulated system operating at X-Band. The recommended tilt and rotation system is a path-length-difference multiple antenna measurement system similar in principle to the Cubic system and to the recommended IPS of this report.

Autonetics of North American replied by letter in which they briefly pointed out their developments in the field of long range "chirp" altimeters which can operate to 2,000 kilometers; and their tri-mode radar which can operate as a rendezvous radar altimeter for ranges to 250 miles.

Cubic Corporation responded with information concerning their "Integrated Position Altitude - Data System". In this system range is measured by a cooperative phase modulated CW technique. The position-attitude angle measurements are made by the path-length-difference phase comparison technique. The suggested use of L-band frequency pairing for fine and coarse angle measurement is common in principle to the IPS system of this report, but uses many carrier frequencies rather than the sequential antenna switching used by the IPS system.

The General Dynamics reply included a brief description of their "Aircraft Station Keeper System". It was pointed out that range and range rate can be accomplished by using either pulse or CW techniques and that angle measurements are accomplished by multiple interferometers. The operating frequency mentioned is in the X-band region. The ASK techniques appear to be applicable to the docking and rendezvous problem.

**FIGURE 174 –
ELECTROMAGNETIC MEASUREMENT SYSTEM DESIGN PARAMETERS**

- Measurement System _____
- System Function _____
- Applicable Documents and Contracts _____
- Abstract of system operation and operational procedures
- Target Characteristics
- Physical Parameters
 - Size
 - Weight
 - Power
 - Gimballed or fixed
- Electromagnetic Parameters
 - Type of antenna(s) or sensor(s)
 - Size of antenna(s) or sensor(s)
 - Band width
 - Directivity
 - Positioning with respect to spacecraft axes
- Electronic Parameters
 - Type of signal generation and detection
 - Output signal format (analog, digital, scale factor, bits, data rate, etc.)
- System Parameters
 - Range limits and accuracy
 - Range rate limits and accuracy
 - Angular coverage and determination
 - Angular accuracy
 - Accuracy of determination of relative attitude and rate of change
 - Target size and shape
 - Dynamic response
 - Computational requirements
 - Reliability
 - Mounting requirements and location
- Environmental control requirements (temperature limits, vibration, radiation, shock, etc.)
- Cost
- Design status
- Incremental cost for design improvements
- Susceptibility to anomalies
- Operational limits (day, night, vehicle attitude maneuver range, etc.)
- Applicability to simultaneous communication and/or command link
- Developmental flight tests required

Honeywell, Inc. supplied a description of their "Trilign" three-axis passive optical alignment system. The system is based on the principles of transmitting collimated light from an optical unit to a remotely located transponder. The system begins operating at about 100 feet provided that a supplementing system is used up to this point for coarse alignment. The "Trilign" becomes more accurate with closure. Another system such as a radar altimeter or laser range finder is required for docking. A communication link is not presently provided.

Motorola, Inc. enclosed a paper entitled, "Unified S-Band Rendezvous Sensor" which was presented at the National Space Navigation and Communication Meeting on April 29 and 30, 1965, in Houston, Texas. The unified system provides range, range rate, and line-of-sight angle measurement for rendezvous and also a voice channel, telemetry, and tracking by way of a unified S-band transmitter, transponder, and receiver. The paper considers how the system can be applied to satisfy the Apollo LEM - Command Module requirements.

Norden enclosed with their response, Report No. C930080-12, "Ultrasonic Light Scanning and Active Optical Imaging System" and Proposal No. PRO815A, "Laser Imaging, Detecting, and Ranging Radar (LIDRR)". The LIDRR system is capable of target identification location. This appears to be a promising approach to the noncooperative docking problem although it does not have provision for the measurement of target attitude orientation angles, angle rates, or target rotational axes and rates in its present form.

Radiometric Division of Polarad Corporation responded with a description of their "Radiometrics Electromagnetic Measurement System Design Parameters". The pulse radar range system and azimuth-elevation type line-of-sight angle measurement system use an X-band, broadband, biconical antenna.

Raytheon responded with four documents describing (a) a two-tone PM-CW cooperative X-band system, using a gimbaled parabolic antenna, (b) tests and evaluations of the system, (c) a cooperative range, range-rate, and LOS angle measurement system, and (d) a short range noncooperative triangularly modulated FM/CW range and range rate system.

The above inputs were quite useful to the study. They were very late and do not fully meet the requirements, but do tend to support the tentative conclusions regarding feasibility of some of the subsystems.

CONCLUSIONS

The results of this study have indicated that, although mission requirements vary over a wide spectrum, sensors capable of meeting these requirements can be developed. The wide variety of mission requirements was recognized from the beginning and defined early in the study. It is evident that no one system is optimum for all requirements; the complex systems required for the more demanding missions are larger, heavier, and more costly than required for a system having lesser requirements. However, the development program for a system capable of measuring all the parameters of interest will, by its very nature, include development of technology which will also have application to the lesser requirements.

Manned spacecraft, such as Gemini, which have been specifically designed to dock with a mating section and to provide a clear view of the docking mechanisms, do not necessarily need a docking sensor, once rendezvous has been completed. However, even for this type of spacecraft, an accurate short range distance indicator would provide useful supplementary data. When direct visual monitoring is precluded by other higher priority mission requirements, a closed circuit television system is an attractive approach; but in this case, the distance measuring equipment becomes more important as a complementary portion of the system. The two devices which show most promise for this short range distance measuring requirement are the nuclear system, for cooperative applications, and antenna probes for the non-cooperative ones. The nuclear system, with Mossbauer range rate sensing, is still in the conceptual stage, but offers short range performance beyond any known requirements. Antenna probes have many shortcomings (limited range, sensitivity to target material and shape, etc.), but are quite promising as a short range assist system against a known target.

As the requirements on the sensor system increase to include LOS tracking and ranging to greater distances, radars come into their own. As discussed in detail in an earlier section, CW radar techniques have a general advantage over pulsed radars for this application. However, some of the more attractive systems require considerable switching of the CW signal; antenna sequencing and ICW ranging techniques. Light weight non-coherent optical systems are potentially applicable, but are in an earlier stage of development. Additional detailed analyses will be required before concluding the tradeoff between RF and optical radars as docking systems.

Target attitude determination becomes a particularly significant problem when the mission requirements indicate the need of an automatic closed loop docking system. Certain missions avoid the problem by including provisions for the target to control its attitude to some known inertial reference, requiring only that the chasecraft control its attitude in a similar manner, approach the target from the proper direction, and control relative velocity. Another promising technique, when the target has enough equipment allowance,

is to provide a closed loop LOS tracker and alignment system within the target, requiring only that the chasecraft control its alignment to the LOS, maintain a constant direction of approach, and program range rate as a function of range. Since techniques for performing these functions are straightforward and would be included as an incidental part of programs pointed toward the more difficult missions, little emphasis was placed on their investigation.

The Integrated Phase System (IPS) represents a particularly attractive system for development at this time since (a) it is versatile enough to satisfy the docking requirements of many missions, (b) it includes many of the more promising measurement techniques as subsystems, and (c) it yields very good extended range performance, thereby doubling as a rendezvous radar. However, several of the new features of the Integrated Phase System require experimental evaluation to establish the magnitude of the instrumentation errors.

The Electronic Omnirange System (EOS) also measures the full set of docking parameters within the chasecraft. The accuracy of the system is somewhat less than that provided by the Integrated Phase System. However, the Electronic Omnirange System is approximately 30% less complex and has fewer potential developmental problems than the Intergrated Phase System. No clear-cut choice between the two systems is apparent, the choice being a function of a tradeoff between development time, accuracy, and complexity.

The noncooperative system selected as being worthy of further analysis and development is the multi-beam doppler sample (MBDS) system. This system represents a slight compromise in capability to avoid some of the extreme data processing requirements of the other approaches. Several experiments associated with its development have broad application to the general docking problem.

RECOMMENDATIONS

A broad spectrum of systems are applicable to some phase of one or more of the missions involving docking. However, much of the technology required by these systems is being developed on other programs, some of which are for applications other than rendezvous and docking. It is therefore recommended that:

- a. Other development programs continue to be monitored and their outputs analyzed for applicability to docking systems.
- b. A nuclear system using the Mossbauer effect be developed for short range application and carried through the feasibility demonstration stage.
- c. An antenna probe system be further evaluated in a design study and feasibility demonstration.
- d. An extensive trade-off study be performed to better evaluate the relative advantages and disadvantages of applying noncoherent optical carrier techniques to the recommended rf docking systems.
- e. The multi-beam doppler sample (MBDS) system be developed for non-cooperative application and carried through the feasibility demonstration stage.
- f. A cooperative system be developed for application to the class of missions which require precise automatic control.

Recommended program plans for implementing the above recommendations are given in the following paragraphs. Each of these programs has been organized to provide for convenient phasing of major tasks.

ANALYSES OF RELATED PROGRAMS

Several current developmental programs should be closely monitored to determine the applicability of the systems or subsystems to docking requirements. The LEM docking radar, being developed by RCA, and the Laser radar, being developed by ITT, San Fernando for the NASA Marshall Space Flight Center, are of particular interest. It is recommended that data from these and other related programs be compiled and analyzed to establish which portions of the total spectrum of requirements are being fulfilled by the systems or subsystems under development.

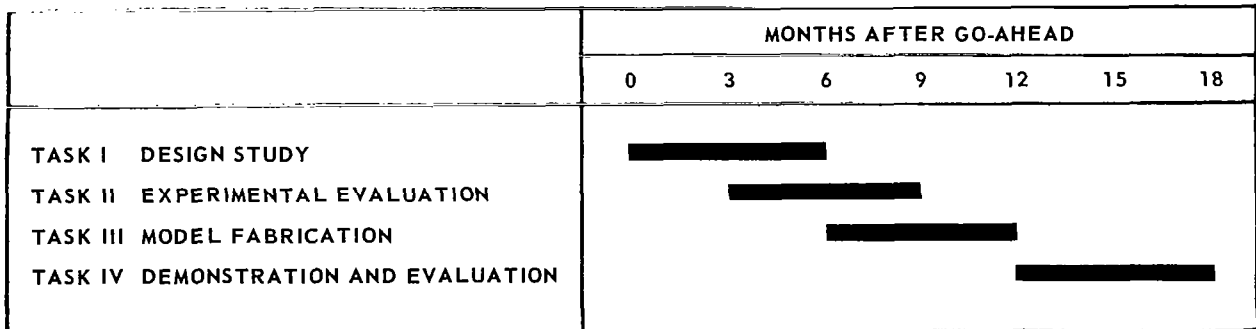
NUCLEAR (MOSSBAUER) SYSTEM PROGRAM PLAN

Evaluation of the nuclear range and range rate sensing technique as a short range assist system includes four tasks:

- a. Task I - Conduct a design study to establish source materials to be evaluated, technique for moving the absorber, and scope of experimental program.
- b. Task II. - Evaluate, by laboratory experiments, significant parameters, such as absorber characteristics, source configuration, temperature effects, and detector placement.
- c. Task III. - Fabricate a feasibility demonstration model of the system.
- d. Task IV. - Demonstrate feasibility and evaluate the applicability of the system.

The schedule for accomplishing the above tasks is shown in figure 175 .

FIGURE 175 - SCHEDULE - NUCLEAR SYSTEM PROGRAM



ANTENNA PROBE SYSTEM PROGRAM PLAN

Evaluation of the antenna probe sensing technique as a short range assist system includes four tasks:

- a. Task I. - Conduct a design study to establish the best operating frequency (above the plasma frequency associated with the ionosphere), the desired directivity, and the type of measurement (e.g., VSWR).
- b. Task II. - Evaluate, by laboratory experiments, the significant parameters to establish feasibility.
- c. Task III. - Fabricate a feasibility demonstration model of the system.
- d. Task IV. - Demonstrate feasibility and evaluate the applicability of the system.

The schedule for accomplishing the above tasks is shown in figure 176 .

FIGURE 176 - SCHEDULE - ANTENNA PROBE SYSTEM PROGRAM

	MONTHS AFTER GO-AHEAD						
	0	3	6	9	12	15	18
TASK I DESIGN STUDY	██████████						
TASK II EXPERIMENTAL EVALUATION		██████████					
TASK III MODEL FABRICATION			██████████				
TASK IV DEMONSTRATION AND EVALUATION				██████████			

ANALYSIS OF APPLICABILITY OF NONCOHERENT OPTICAL TECHNIQUES

As discussed in the section on optical radar systems, many of the rf docking systems lend themselves to modification for the use of an optical carrier, in which the usual rf carrier is amplitude modulated on a noncoherent optical carrier, is demodulated when it returns, and is then processed in the usual manner. Since the state-of-the-art is changing rapidly in this area of technology, it is recommended that a comprehensive trade-off study be conducted to evaluate the relationships of size, weight, cost, reliability, availability, etc. for a given operational capability using the two approaches; i.e., with and without the added optical carrier.

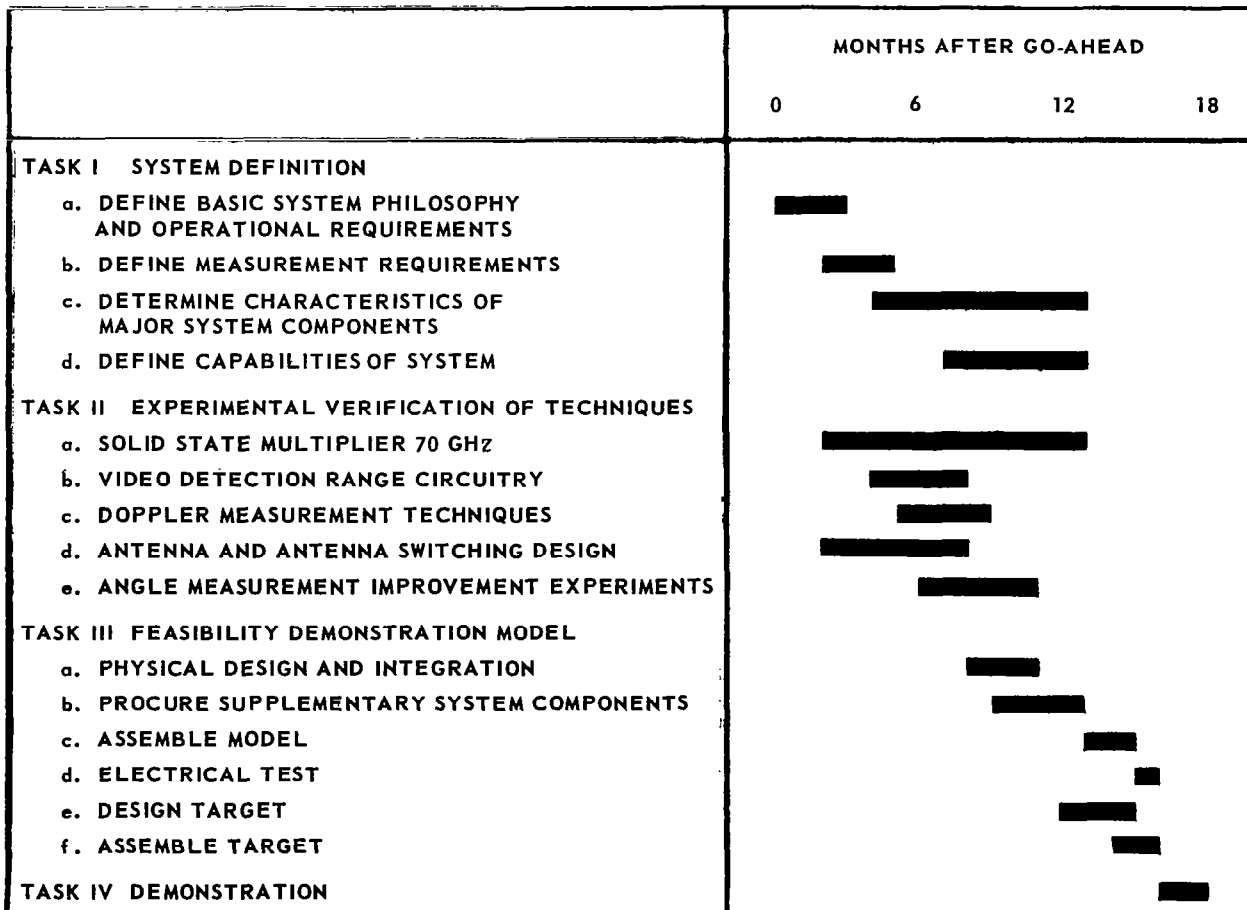
NONCOOPERATIVE DOCKING RADAR PROGRAM PLAN

Evaluation of the multi-beam doppler sample (MBDS) system as a non-cooperative docking radar includes four tasks:

- a. Task I. - System Definition
- b. Task II. - Experimental Verification of Techniques
- c. Task III. - Feasibility Demonstration Model Fabrication
- d. Task IV. - Demonstration and Evaluation

The schedule for accomplishing the above tasks is shown in figure 177 .

FIGURE 177 – SCHEDULE – NONCOOPERATIVE DOCKING RADAR PROGRAM



System Definition

The system definition task includes an extension of the Electromagnetic Guidance Study analyses to:

- a. Define Basic System Philosophy and Operational Requirements
- b. Define Measurement Requirements
- c. Determine Characteristics of Major System Components
- d. Define Capabilities of System

Experimental Verification of the Techniques

It is recommended that early evaluation of the following techniques be initiated:

- a. Solid State Multiplier, 70 GHz - The purpose of this task is to develop a varactor multiplier developing 100 mW at 70 GHz; to develop a switching technique with adequate switching speeds and on-off ratios; and to provide a source with frequency stability adequate for the required doppler measurement.
- b. Video Detection Range Circuitry - The purpose of this task is to demonstrate in the laboratory the capabilities of short range (<10 ft.) measurement techniques.
- c. Doppler Measurement Technique - The purpose of this task is to develop and demonstrate the pulsed frequency measuring technique required for the rotation rate measurement.
- d. Antenna and Antenna Switching Design - The purpose of the task is to design the antenna with the multiple beams and the waveguide switching circuitry. It includes investigation to determine if the waveguide switching circuitry can be reduced in size.
- e. Angle Measurement Improvement Experiments - The purpose of this task is to determine the magnitude of the glint error and its dependence upon beamwidth and squint angle and to investigate such techniques as frequency agility to reduce the effect of this error.

Feasibility Demonstration Model

This phase of the program includes the design and construction of a feasibility demonstration model with the measurement capabilities required for the noncooperative docking radar. This model uses specialized system components developed in the techniques experiments, standard system components procured from specialty subcontractors, and standard laboratory components, where applicable. A docking target having translational and rotational motion capabilities is needed for this demonstration.

- a. Physical Design and Integration - The purpose of this task is to design the physical layout of the system, to perform electrical system integration, and to solve interface problems between subsystems.
- b. Procure Supplementary System Components - The purpose of this task is to specify and purchase standard system components for the feasibility demonstration model.
- c. Assemble Feasibility Demonstration Model
- d. Electrical Test Feasibility Demonstration Model - The purpose of this task is to electrically test the feasibility demonstration model to insure that it meets specified performance.
- e. Design Target - The purpose of this task is to design a target representative of anticipated targets. This target should be designed so that translational and rotation motion can be produced by the target and can be monitored.
- f. Assemble Target - The purpose of this task is to provide the target to be used for the demonstration.

Demonstration

The feasibility demonstration requires an echo-free environment such as an anechoic chamber. The feasibility demonstration model is used to demonstrate its capability of measuring range, range rate, LOS angle, target rotation rate and rotation axis. Adequate instrumentation is required to produce a permanent record of this test.

COOPERATIVE DOCKING RADAR PROGRAM PLAN

Evaluation of a cooperative docking radar includes the following tasks:

Task I. - Complete the definition of the Integrated Phase System and the Electronic "Omni" System, their logic circuits, and error analyses, and select the system to be developed.

Task II. - Experimental Verification of Techniques - Specific tasks are functions of which system is selected. The IPS requires investigation of:

- a. Antenna switching and its effect on the phase lock loops.
- b. The sample and hold circuits.
- c. The phase lock receiver.

The EOS requires investigation of:

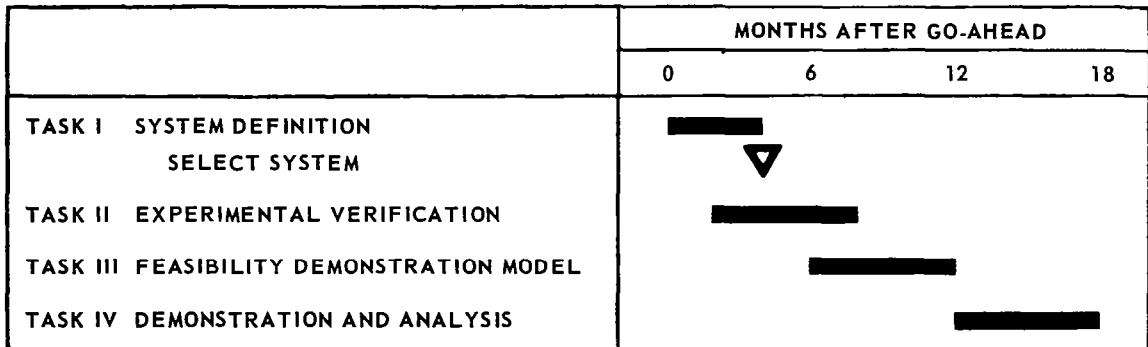
- a. The swept null attitude transmitter and receiver.
- b. The phase lock loops.
- c. The relative roll attitude receiver.

Task III.- Fabricate Feasibility Demonstration Model

Task IV. - Demonstration and analysis of applicability.

The schedule for accomplishing these tasks is shown in figure 178 .

FIGURE 178 - SCHEDULE - COOPERATIVE DOCKING RADAR PROGRAM



APPENDICES

APPENDICES

APPENDIX A - SURVEY OF CW RADAR SYSTEMS

In the past, CW radars have been used extensively on aircraft for measuring altitude. More recently, they have been proposed for use on spacecraft as rendezvous and landing sensors. The characteristics of some of these systems are summarized in this appendix.

Aircraft Radio Altimeter (AL-101) Developed by Collins Radio (reference 19)

Modulation: Wideband (100 MHz), triangular modulated, FM-CW; 100 Hz modulation frequency; measure difference frequency between transmitted and received signal to determine range; no range-rate.

Transmitter: 0.5 watt; 4.2 - 4.4 GHz (C-Band); solid-state frequency multiplier chain.

Receiver: Direct mixing with crystal mixer; 0 frequency IF; automatic tracking filters; filter roll-off above the frequency expected at any altitude is varied with altitude to reduce receiver bandwidth.

Altitude (Earth Surface): 0 to 2,500 feet; accuracy of ± 2 feet or $\pm 2\%$ to 500 feet, and $\pm 5\%$ from 500 to 2,500 feet.

Antenna: Separate transmit and receive antennas; two small horns separated by 36 inches.

Physical Characteristics: Weight including antennas and indicator of 23 pounds; packaged in a 1/2-ATR-short case; primary power of 70 watts; all solid-state; has built in time delay for calibration check at 100 feet altitude plus several continuous malfunction detectors.

Space Rendezvous and Landing Radar
Proposed for LEM by Emerson Electric
Laboratory Feasibility Demonstrated
(reference 16)

Modulation: Wideband, sine wave modulated, FM-CW; several tones for resolving ambiguities and providing range accuracy; phase of received tones measured to determine range; carrier doppler measured to determine range rate.

Transmitter: 0.1 watt; 16 GHz (Ku-Band); klystron oscillator.

Receiver: Balanced crystal mixer; 20 MHz IF; phase lock frequency demodulator; active feedthrough cancellation for noncooperative operation.

Cooperative Range: 10 feet to 250 nautical miles; accuracy of 1% or \pm 5 feet.

Noncooperative Range: 10 feet to 3 nautical miles on 10 square meter target; accuracy same as above

Altitude (Lunar Surface): 10 feet to 20 nautical miles; accuracy same as above.

Range Rate: 0 to \pm 6,000 feet/second; accuracy 1% or \pm 1 foot/second.

Horizontal Velocity (Landing): 0 to \pm 6,000 feet/second; accuracy 1% or \pm 1 foot/second.

Antenna: Two foot parabola; conical scan for angle tracking during rendezvous and horizontal velocity determination during landing; angle tracking accuracy of \pm 1 milliradian; angle rate accuracy of \pm 1 milliradian per second.

Physical Characteristics: Radar weight - 28 pounds; radar volume - 2,000 cubic inches excluding antenna; radar prime power - 75 watts; transponder weight - 5 pounds; transponder volume - 640 cubic inches; all solid state except for transmitter klystron.

Space Rendezvous and Landing Radar
Proposed for LEM by Raytheon
(reference 20)

Modulation: For rendezvous - sine wave modulated PM-CW; multiple tones phase modulate carrier $\pm 1/2$ radian; phase of received tones measured to determine range; carrier doppler measured to determine range rate. For landing - 50 MHz sawtooth sweep, linear FM-CW at 70 Hz modulation frequency.

Transmitter: 0.5 watt (rendezvous), 5.0 watt (landing), 13.5 GHz, klystron oscillator; ferrite phase shifter for phase modulation.

Receiver: Crystal mixer; 24 MHz IF (multiplied up from 2 MHz ranging sub-carrier in transponder); phase lock demodulators.

Cooperative Range: 5 feet to 200 nautical miles; accuracy ± 2 feet.

Altitude (Lunar Surface): 10 feet to 20 nautical miles; accuracy $\pm 4\%$ or ± 2 feet.

Range Rate: Accuracy of $1/2$ foot per second with $1/10$ second smoothing.

Horizontal Velocity: Three beams (based on APN-113) accuracy of ± 1 foot/second or 0.1% .

Antenna: Combined antenna is 21 inches in diameter by 13 inches thick; uses elliptical folded metal lens for velocity tracking and 4.5 inches parabola for close in rendezvous; angle tracking accuracy of 0.015 degrees.

Physical Characteristics: Total radar weight of 34 pounds including 15 pounds for antenna gimbals; primary power of 150 watts; transponder weight of 8.5 pounds; transponder primary power of 20 watts.

Space Rendezvous Radar (STELATRAC)
Proposed by Space Technology Labs
Laboratory Model Developed
(references 21 and 22)

Modulation: Sine wave modulated PM-CW for cooperative operation with 4MHz modulation signal; range ambiguities resolved by linearly sweeping the 4 MHz ranging subcarrier in frequency; phase of ranging subcarrier measured to determine range; interrupted CW for noncooperative ranging; carrier doppler measured to determine range rate.

Transmitter: 0.5 watt, 10.4 GHz (X-Band) solid state multiplier.

Receiver: Crystal mixer; phase lock demodulation.

Cooperative Range: 0 to 120 nautical miles; accuracy of ± 1 foot.

Range Rate: Accuracy of ± 0.05 foot/second.

Antenna: Uses 22 db horns and measures angle by phase interferometer technique; uses injected reference technique to compensate for phase shifts through IF amplifiers; angle accuracy of ± 1 milliradian with 2 foot baseline.

Physical Characteristics: Total weight of radar and transponder is 40 pounds plus 10 pounds for antenna; all solid state.

Unified S-Band Rendezvous Radar
Proposed by Motorola (Reference 23)

Modulation: Sine-wave modulated FM-CW (450kHz); range ambiguities resolved by 60K bit/sec. biphasic PN modulation of range modulation. Range signal frequency multiplexed with 2 way voice and data transmission. Cooperative rendezvous only.

Transmitter: 0.250 watt S-Band (Part of DSIF transponder)

Receiver: Crystal mixer; phase lock demodulation

Range: 740 miles unambiguous; accuracy \pm 10 meters at 400 miles

Range Rate: Accuracy of \pm .1 meter/sec at 400 miles

Antenna: Parabolic reflector, 2 ft. dia. for transmitt, 4 helix interferometer for receive. Omnidirectional antenna on target vehicle.

Physical Characteristics: Radar weighs 23 pounds plus 20 pounds for antenna. When used with existing DSIF-S-band transponder and antenna, rendezvous function requires only 14 pounds. Target vehicle transponder weighs 14 pounds.

NOMAD (Noise Modulation and Detection) Radar
Proposed by Westinghouse
(reference 24)

Modulation: Interrupted CW with 20% duty cycle; 2.5 millisecond pulses at a PRF of 80 Hz; during 2.5 millisecond pulse transmits binary ranging codes that phase modulate carrier zero degree for 1's and 180° for 0's; have a coarse, medium, and fine code for resolving ambiguities and accurate range determination; carrier doppler used to determine range rate.

Transmitter: 0.1 watt, 9.8 GHz (X-Band), solid-state multiplier.

Receiver: Crystal mixer; 38 MHz IF with offset accomplished in transponder; phase lock demodulator.

Cooperative Range: 0 to 500 nautical miles, accuracy of .0008% or 1.4 foot (fine range clock frequency is 781.25 kHz).

Range Rate: 0 to + 5,000 feet/second; accuracy of 1% or 1 foot/second.

Antenna: Antenna not specified other than a "lobing technique" with lobing frequency synchronous with PRF.

Physical Characteristics: Radar weight (excluding antenna) is 22.85 pounds; radar volume is 524.15 cubic inches; radar primary power is 69 watts; transponder (excluding antenna) weight is 17.66 pounds; transponder volume is 427.7 cubic inches; transponder primary power is 32 watts; assume modular circuits will be used to a great extent.

Space Rendezvous and Landing Radar
Proposed for LEM by Laboratory for Electronics (LFE)
(Reference 25)

Modulation: Interrupted CW; alternately pulse transmitter and local oscillator; 50% duty cycle; range determined by having PRF track down to 1,000 feet, and measuring PRF; phase of received modulation measured to determine range to zero feet; carrier doppler used to determine range rate.

Transmitter: 0.3 watt, 9.8 GHz (X-Band), solid state multiplier.

Receiver: Crystal mixing with phase lock frequency trackers.

Cooperative Range: 0 to 250 nautical miles, accuracy 1/2% or \pm 2 feet.

Noncooperative Range: 0 to 12 nautical miles, accuracy 1/2% or \pm 2 feet.

Altitude (Lunar Surface): 0 to 20 nautical miles, accuracy 1% or \pm 2 feet.

Range Rate and Horizontal Velocity: 0 to 6,000 feet/second; accuracy of \pm 1/2 foot/second.

Antenna: Uses 10 inch dielectric lens antenna containing three beams for horizontal velocity determination, and four lobe monopulse for angle tracking; angle tracking accuracy is \pm 2 milliradians.

Physical Characteristics: Radar weight (including antenna) is 34 pounds; radar volume (including antenna) is 1,900 cubic inches; radar primary power is 84 watts; transponder weight is 5 pounds; transponder volume is 130 cubic inches; all solid state.

PRADOR (PRF Ranging Doppler Radar)
Developed by Westinghouse
(References 26 and 27)

Modulation: Interrupted CW; diode switch switches RF to dummy load; use PRF tracking and measure PRF to determine range; carrier doppler measured to determine range rate; 37.5% duty cycle.

Transmitter: 0.125 watt, 8.7 GHz (X-Band), solid state multiplier.

Receiver: Crystal mixer, 34 MHz IF, phase lock demodulator.

Cooperative Range: 0 to 500 nautical miles; accuracy of 0.5% or 3 feet.

Noncooperative Range: 25 to 25,000 feet (with added 4 pounds, 50 cubic inches and 2.5 watts).

Range Rate: 0 to \pm 5,000 feet/second; accuracy of 1% or 1 foot/second.

Antenna: Flat plate array with 5 degrees beamwidth and sequential lobing; angle accuracy of 3 milliradians; antenna 16 inches by 16 inches and weighs 24.5 pounds.

Physical Characteristics: Radar weight (excluding antenna) is 24.0 pounds; transponder weight (excluding antenna) is 22.0 pounds; radar volume (excluding antenna) is 1.75 cubic feet; transponder volume (excluding antenna) 1.5 cubic feet; all solid state.

APPENDIX B - PHASE AND FREQUENCY NOISE

Phase and frequency noise has been analyzed by Mische Schwartz, (reference 4).

Assume the received signal is a sine wave at frequency ω_0 and amplitude A_0 which is added to a noise signal $n(t)$ at frequency $(\omega_0 + \omega)$ with amplitude A_n , i.e.:

$$e_r(t) + n(t) = A_0 \cos \omega_0 t + A_n \cos (\omega_0 + \omega)t . \quad (B1)$$

The power in the noise signal at frequency $(\omega_0 + \omega)$ is equal to the power spectral density of the noise (assumed flat) times the differential bandwidth, i.e.:

$$\frac{A_n^2}{2} = N_0 df . \quad (B2)$$

The received signal plus noise can be written as:

$$e_r(t) + n(t) = A(t) \cos [\omega_0 t + \theta(t)] . \quad (B3)$$

That is, the received signal is amplitude and phase modulated. Assume the amplitude modulated term is removed by hard limiting prior to demodulation. The phase modulation term is:

$$\theta(t) = \tan^{-1} \frac{A_n \sin \omega t}{A_0 + A_n \cos \omega t} \approx \tan^{-1} \frac{A_n}{A_0} \sin \omega t \approx \frac{A_n}{A_0} \sin \omega t , \quad (B4)$$

for $A_0 \gg A_n$ (large signal-to-noise ratio).

Thus, the received carrier is phase modulated by the noise term given by (B4). The power in this phase noise component is:

$$dN_\theta = \frac{1}{2} \left(\frac{A_n}{A_0} \right)^2 = \frac{1}{2} \left(\frac{A_n^2}{2} \right) \left(\frac{2}{A_0^2} \right) = \frac{N_0}{2S} df , \quad (B5)$$

from (B2) and letting $\frac{A_0^2}{2} = S$ be the power in the received carrier. If the

phase of the carrier is detected in a phase detector with output noise bandwidth B_0 , the total phase noise power at the output is:

$$N_\theta = \int_{-B_0}^{+B_0} \frac{N_0}{2S} df , \quad (B6)$$

or assuming flat noise again with zero mean:

$$N_{\theta} = \sigma_{\theta}^2 = \frac{N_0 B_0}{S}. \quad (\text{B7})$$

Going back to Equation (B2), and considering the frequency of the carrier:

$$\omega(t) = \frac{d\theta(t)}{dt} = \omega \frac{A_n}{A_0} \cos \omega t, \quad (\text{B8})$$

the power in this frequency noise component is:

$$dN_{\omega} = \frac{1}{2} \left(\frac{\omega A_n}{A_0} \right)^2 = \frac{\omega^2 N_0}{2S} df, \quad (\text{B9})$$

The total frequency noise at the output of a frequency discriminator with output noise bandwidth B_0 is:

$$N_{\omega} = \int_{-B_0}^{+B_0} \frac{(2\pi)^2 N_0}{2S} f^2 df, \quad (\text{B10})$$

Assuming flat power spectral density and noise with zero mean, the total frequency noise power at the output is:

$$N_{\omega} = \sigma_{\omega}^2 = \frac{(2\pi)^2}{3} \left(\frac{N_0}{S} \right) B_0^3. \quad (\text{B11})$$

APPENDIX C - AMBIGUITY FUNCTION FOR SINE-WAVE MODULATED FM-CW RADAR SYSTEMS

Using Siebert's notation (Reference 6), the general expression for the ambiguity function is:

$$\psi(\tau, \omega) = \frac{1}{2} \left| \int_{-\infty}^{+\infty} S_0(t) S_0^*(t + \tau) e^{j\omega t} dt \right|, \quad (C1)$$

where the transmitted signal is:

$$s_0(t) = \text{Re} [S_0(t) e^{j\omega_0 t}]. \quad (C2)$$

For the frequency modulated system using a sine-wave modulation signal, the transmitted signal can be represented as:

$$s_0(t) = \text{Re} \left[A e^{j(\omega_0 t + \frac{\Delta F}{f_m} \sin \omega_m t)} \right], \quad (C3)$$

$$= \text{Re} \left[\left(A e^{j \frac{\Delta F}{f_m} \sin \omega_m t} \right) e^{j\omega_0 t} \right]. \quad (C4)$$

Therefore, from the above notation:

$$S_0(t) = A e^{j \frac{\Delta F}{f_m} \sin \omega_m t}, \quad (C5)$$

and the ambiguity function is:

$$\psi(\tau, \omega) = \frac{1}{2} \left| \int_{-\infty}^{+\infty} A e^{j \frac{\Delta F}{f_m} \sin \omega_m t} A e^{-j \frac{\Delta F}{f_m} \sin \omega_m (t + \tau)} e^{j\omega t} dt \right|, \quad (C6)$$

Combining terms, (C6) can be written as:

$$\psi(\tau, \omega) = \frac{A^2}{2} \left| \int_{-\infty}^{+\infty} e^{j\{\omega t + f(\tau) \sin [\omega_m t - \phi(\tau)]\}} dt \right|, \quad (C7)$$

where:

$$f(\tau) = \frac{2\Delta f}{f_m} \sin(\omega_m \tau/2) \quad (C8)$$

$$\phi(\tau) = \tan^{-1} \frac{\sin \omega_m \tau}{1 - \cos \omega_m \tau}, \quad (C9)$$

(C6) could also be written as:

$$\psi(\tau, \omega) = \frac{A^2}{2} \left| \int_{-\omega}^{+\omega} e^{j\{\omega t - f(\tau) \cos[\omega_m(t + \tau/2)]\}} dt \right| \quad (C10)$$

To start with, however, (C7) will be used to derive the ambiguity function along the $\omega = 0$ and $\tau = 0$ axis.

Let $\omega = 0$ in (C5). Then it can be written as:

$$\begin{aligned} \psi(\tau, 0) &= \frac{A^2}{2} \left| \int_{-\infty}^{+\infty} \cos\{f(\tau) \sin[\omega_m t - \phi(\tau)]\} dt + j \int_{-\infty}^{+\infty} \sin\{f(\tau) \sin[\omega_m t - \phi(\tau)]\} dt \right|, \\ &= \frac{A^2}{2} \left| \int_{-\infty}^{+\infty} J_0[f(\tau)] dt + \int_{-\infty}^{+\infty} 2 \sum_{n=1}^{\infty} J_{2n}[f(\tau) \cos 2n[\omega_m t - \phi(\tau)]] dt + \right. \\ &\quad \left. j \int_{-\infty}^{+\infty} 2 \sum_{n=1}^{\infty} J_{2n-1}[f(\tau) \sin(2n-1)[\omega_m t - \phi(\tau)]] dt \right|. \end{aligned} \quad (C11)$$

Since the Bessel Function terms are all constant with respect to t , and assuming that the signal is on for a finite time between $t = 0$ and $t = T$:

$$\begin{aligned} \psi(\tau, 0) &= \frac{A^2}{2} \left| J_0[f(\tau)] \int_0^T dt + 2 \sum_{n=1}^{\infty} J_{2n}[f(\tau)] \int_0^T \cos 2n[\omega_m t - \phi(\tau)] dt \right. \\ &\quad \left. + 2j \sum_{n=1}^{\infty} J_{2n-1}[f(\tau)] \int_0^T \sin(2n-1)[\omega_m t - \phi(\tau)] dt \right|, \\ &= \frac{A^2}{2} \left| J_0[f(\tau)] T \right. \end{aligned} \quad (C12)$$

$$\begin{aligned} &\quad \left. + 2 \sum_{n=1}^{\infty} \frac{J_{2n}[f(\tau)]}{2n \omega_m} \{ \sin 2n[\omega_m T - \phi(\tau)] + \sin 2n[\phi(\tau)] \} \right. \\ &\quad \left. + 2j \sum_{n=1}^{\infty} \frac{J_{2n-1}[f(\tau)]}{(2n-1) \omega_m} \{ \cos(2n-1)[\phi(\tau)] - \cos(2n-1)[\omega_m T - \phi(\tau)] \} \right|. \end{aligned} \quad (C13)$$

Now assume the signal is on for an integer number of modulation cycles, i.e., $T = m/f_m$. Then:

$$\sin 2n [\omega_m T - \phi(\tau)] + \sin 2n [\phi(\tau)] \quad (C14)$$

$$= [\sin 4nm\pi \cos 2n\phi(\tau) - \cos 4nm\pi \sin 2n\phi(\tau) + \sin 2n[\phi(\tau)]], \quad (C15)$$

$$= -\sin 2n\phi(\tau) + \sin 2n\phi(\tau) = 0 \quad (C16)$$

and:

$$\cos (2n-1)\phi(\tau) - \cos (2n-1)[\omega_m T - \phi(\tau)] \quad (C17)$$

$$= \cos (2n-1)\phi(\tau) - [\cos (2n-1)2m\pi \cos (2n-1)\phi(\tau) + \sin (2n-1)2m\pi \sin (2n-1)\phi(\tau)], \quad (C18)$$

$$= \cos (2n-1)\phi(\tau) - \cos (2n-1)\phi(\tau) = 0. \quad (C19)$$

for all integer values of n and m . Thus (C13) simplifies to:

$$\psi(\tau, 0) = \frac{A^2}{2} | J_0 [f(\tau) | T |], \quad (C20)$$

which on substituting (C8) for $f(\tau)$, and since $J_0(f(\tau))$ is real:

$$\psi(\tau, 0) = \frac{A^2 T}{2} \left\{ J_0 \left[\frac{2\Delta F}{f_m} \sin(\omega_m \tau/2) \right] \right\}. \quad (C21)$$

Now let $\tau = 0$ in (C7). When $\tau = 0$, $f(\tau) = 0$, and (C7) can be written as:

$$\psi(0, \omega) = \frac{A^2}{2} \left| \int_{-\infty}^{+\infty} e^{j\omega t} dt \right|, \quad (C22)$$

again the signal is on for $t = 0$ to $t = T$, so that:

$$\psi(0, \omega) = \frac{A^2}{2} \left| \int_0^T e^{j\omega t} dt \right|, \quad (C23)$$

$$= \frac{A^2}{2} \left| \frac{e^{j\omega t} - 1}{j\omega} \right|, \quad (C24)$$

$$= \frac{A^2}{2} \left| \frac{\cos \omega T + j \sin \omega T - 1}{j\omega} \right|, \quad (C25)$$

$$= \frac{A^2}{2} \left[\frac{(\cos \omega T - 1)^2 + (\sin \omega T)^2}{\omega^2} \right]^{1/2}, \quad (C26)$$

$$= \frac{A^2}{2} \left[\frac{2(1 - \cos \omega T)}{\omega^2} \right]^{1/2}, \quad (C27)$$

which becomes:

$$\psi(0, \omega) = \frac{A^2}{2} \left[\frac{4 \sin^2 \omega T/2}{\omega^2} \right]^{1/2}, \quad (C28)$$

$$= \frac{A^2 T}{2} \left[\frac{\sin \left(\frac{\omega}{2} T \right)}{\left(\frac{\omega}{2} T \right)} \right]. \quad (C29)$$

Normally the ambiguity function is normalized with respect to the total energy in the signal. The total energy in the signal is the power in the sine wave

$\frac{A^2}{2}$ times the duration of the sine wave T , which is $\frac{A^2 T}{2}$. Dividing both (C21)

and (C29) by the total energy results in :

$$\psi(\tau, 0) = \left\{ J_0 \left[\frac{2\Delta F}{f_m} \sin \left(\omega_m \frac{\tau}{2} \right) \right] \right\}, \quad (C30)$$

$$\psi(0, \omega) = \frac{\sin \left(\frac{\omega}{2} T \right)}{\left(\frac{\omega}{2} T \right)}. \quad (C31)$$

APPENDIX D - IONOSPHERIC PROPERTIES PERTINENT TO THE PROPAGATION
CHARACTERISTICS OF ELECTROMAGNETIC ENERGY

Free electrons and ions in the ionosphere cause severe changes in the conductivity and dielectric constant at frequencies up to and below the natural resonant frequency of the medium. This frequency is primarily a function of the number of ionized particles per cubic volume. For electrons:

$$\omega_p^2 = \frac{Ne^2}{\epsilon_0 m} = 9 \sqrt{N}, \quad (D1)$$

where: N = number of free electrons per cubic meter,
e = charge per electron,
 ϵ_0 = permittivity of free space,
m = electron mass,

At about 300 Km, a typical figure for electron density is 10^{12} per cubic meter for which the plasma frequency is 9 MHz. The ion natural resonant frequency is several orders of magnitude lower than this because of its greater mass.

Below the critical frequency of the medium, it has high conductivity, going to its highest value when $\omega = 0$ (or the DC case). This limit is:

$$\sigma_0 = N \frac{e^2}{m} \tau. \quad (D2)$$

τ is the time between ion-electron collisions. At 300 Km this is $\sigma_0 = 20$ mho/m. At 5000 Hz which is the normal frequency used with the capacity bridge in the direct capacitance altimeter, the capacity probe will be "shorted out" by this type medium. At 300 Km, $\sigma(\omega)$ is:

$$\sigma_\omega = \frac{\sigma_0}{1 + j\omega\tau} \approx -j 1.0 \frac{\text{mho}}{\text{meter}}, \quad (D3)$$

also the dielectric constant is:

$$\epsilon_\omega = \epsilon_0 \left[1 - \frac{\omega_p^2}{\nu^2 + \omega^2} \right] = 56 \times 10^{-6}, \quad (D4)$$

where ν is $\frac{1}{\tau}$.

and the characteristic impedance of the medium is:

$$\eta_\omega = \sqrt{\frac{\mu_0}{\epsilon_0}} \left(1 - \frac{\omega_p^2}{\omega^2} \right)^{-1/2} \approx -j 0.15. \quad (D5)$$

The characteristic impedance at audio frequencies is, therefore, very low and reactive acting similar to a waveguide below cutoff.

Interestingly enough, however, using the same set of formulae, if the frequency used in the measurement system is significantly above the natural frequency of the medium, say 30 MHz, the characteristic impedance returns to that which is very near free space. It is concluded that "ionospheric effects" can, therefore, be greatly minimized by operating frequencies considerably above the natural resonant frequency of the "worst case" ionosphere.

APPENDIX E - CAPACITY CALCULATIONS FOR CAPACITY PROBE
EXTERNAL CIRCUITS

The external capacitances of Figure E1 may be combined as:

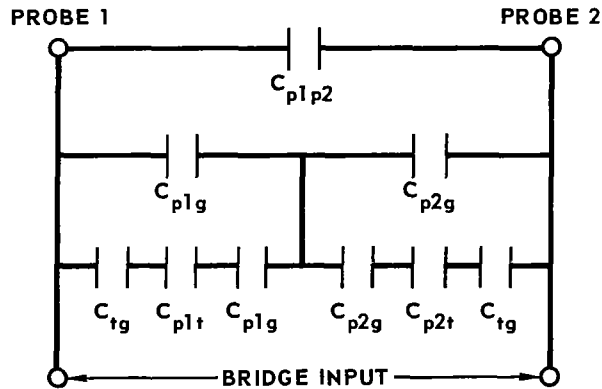


FIGURE E1

but C_{pt} and C_{pg} are very large compared to C_{pt} , except when the docking vehicle is very close, therefore, the circuit can be drawn:

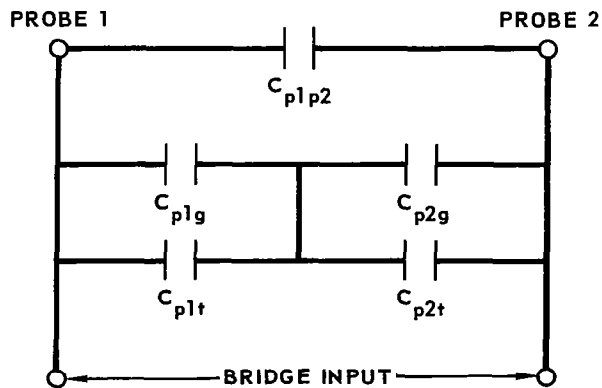


FIGURE E2

C_p, C_{pr}, C_{plg} and C_{p2g} can be obtained as C_o and C_{plt}, C_{p2t} which vary with target distance (size, shape, etc.) can be considered as ΔC_o .

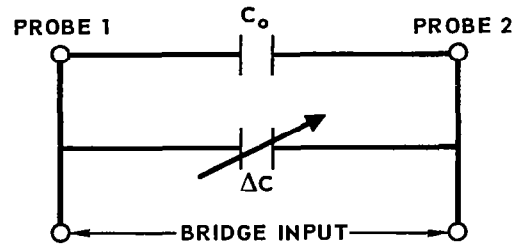


FIGURE E3

Calculation of each of the capacities associated with the external circuit is by method of images and/or by calculation of the capacity of two spheres, i.e.:

$$C = 2\pi\epsilon_0 a \sum_{n=0}^{\infty} m^n, \quad (E1)$$

where: $m = \frac{a}{d}$,
 a = radius of probe,
 d = separation of sphere centers.

As an example consider the following geometry for the problem:

Probe radius = 0.01 meter,
 Distance from probe to ground = 0.1 meter,
 Vehicle separation = 1 meter,
 Vehicle radius = 1 meter.

Then C_o becomes about 1 uuf and the ΔC_o about 300 uuuf.

APPENDIX F - TARGET GENERATED NOISE

In addition to the always present thermal noise, angle tracking systems must contend with noise generated by the target. This target generated noise is caused by phase interference of the various scatterers making up a complex target, and has two effects: the amplitude of the target return varies randomly; and the point indicated by the angle servo as the center of reflectivity wanders randomly. These two phenomena are generally lumped together under the heading of scintillation noise, with the term "glint" reserved as the title for the center of reflectivity wander.

The study of scintillation is difficult to handle analytically unless some simplifying assumptions are made concerning the target. The target model to be discussed is used in most analyses of the scintillation problem and is quite simplified. However, it has been found in practice that this simplified model yields results closely related to experimental evidence. Many people have investigated this problem. (Reference 58 to 63) The references which will be primarily relied upon here are Delano (Reference 58) and Muchmore (Reference 59).

Fading Noise

Briefly, the target model can be described as follows (References 58 and 59). The scatterers are spread over the target in an irregular manner. There are a large number of individual scatterers whose phases are independent, and whose scattering lobe patterns are large compared to the lobe pattern of the whole array. Thus, only phase changes cause the total back scatter pattern to change. If the target is assumed to be reasonably symmetrical, the two tracking axes can be considered separately.

The simplest target motion to consider is uniform turning. Muchmore (Reference 59) has shown that for a target turning at a uniform rate Ω_0 (rad/sec) the normalized fading spectrum out of a square law envelope detector is given by:

$$W_E(f) = 1/f_m (1 - f/2f_m), \quad (F1)$$

where:

$$f_m = \frac{L\Omega_0}{\lambda_0},$$

L = target length along the tracking axis,
 λ_0 = operating wavelength.

For the model assumed, the RF signal is asymptotically normal and the envelope has a Rayleigh distribution. It can be shown that the variance of the amplitude fluctuations is given by:

$$\sigma_E^2 = \left(\frac{4}{\pi} - 1\right) \bar{E}^2 = 0.271 \bar{E}^2. \quad (F2)$$

Thus the total fading noise spectrum is given by:

$$W_E(f) = \frac{0.271 \bar{E}^2}{f_m} \left(1 - \frac{f}{2f_m}\right). \quad (F3)$$

For a system with angular sensitivity b_o per unit volt per unit radian, the equivalent angle noise spectrum is given by:

$$\begin{aligned} W_\theta(f) &= \frac{0.271 \bar{E}^2}{b_o^2 \bar{R}^2 f_m} \left(1 - \frac{f}{2f_m}\right) \frac{(\text{rad})^2}{\text{Hz}}, \\ &= \frac{0.271}{b_o^2 f_m} \left(1 - \frac{f}{2f_m}\right) \frac{(\text{rad})^2}{\text{Hz}}. \end{aligned} \quad (F4)$$

For a system with a 3 db beam crossover point, b_o can be closely approximated by:

$$b_o = \frac{2}{\theta_{BW}^2}, \quad (F5)$$

where θ_{BW} is the 3 db antenna beamwidth. Thus,

$$W_\theta(f) = \frac{0.068 \theta_{BW}^2}{f_m} \left(1 - \frac{f}{2f_m}\right) \frac{(\text{rad})^2}{\text{Hz}}. \quad (F6)$$

With a lobing system the angular error is due to fading noise within the servo noise bandwidth of the lobing frequency. Assuming the servo bandwidth is narrow, the angle variance can be obtained by multiplying equation F6, evaluated at the lobing frequency, by $2B_s$, where B_s is the servo noise bandwidth, and the factor of 2 is introduced to account for noise both above and below the lobing frequency f_s . Thus,

$$\sigma_\theta^2 = \frac{0.136 B_s \theta_{BW}^2}{f_m} \left(1 - \frac{f_s}{2f_m}\right). \quad (F7)$$

The worst case is the fast turning target. Consider the following example:

$$\begin{aligned} L &= 20 \text{ ft;} \\ B_s &= 5 \text{ Hz;} \\ \Omega_o &= 1.75 \text{ rad/sec (100}^\circ\text{/sec)} \\ f_s &= 80 \text{ Hz} \\ \lambda_o &= .0143 \text{ ft. (70 GHz operating frequency);} \\ \theta_{BW} &= 10^\circ \end{aligned}$$

Thus,

$$f_m = \frac{L\Omega_0}{\lambda_0} = 2450 \text{ Hz},$$

and

$$\sigma_\theta^2 = \frac{0.136 (0.031) (.98)^5}{2450} = 8.45 \times 10^{-6} (\text{rad})^2,$$

$$\sigma_\theta = 2.9 \text{ milliradians.}$$

When the target is turning slowly, fading noise will contribute essentially nothing to the tracking errors.

Glint

There are two quantities to consider when discussing glint: the effective radar center; and the apparent radar center. The apparent radar center is the point which a zero time constant antenna servo or a system with a very fast AGC would track. Neither of these conditions apply to the case under study, so the statistics of the apparent radar center will not be considered further.

The effective radar signal is the point which a long time constant antenna servo tends to seek. Delano (Reference 58) has shown that the perturbing glint signal for this case has zero mean (since this is the average point the servo is tracking) and a variance given by:

$$\bar{U}^2 = \frac{b_0^2}{2} \bar{E}^2 \frac{\bar{X}_n^2}{R^2}, \quad (\text{F8})$$

where b_0 and E are defined as before, X_n is the distance of the n th reflecting element from the center of the target, and R is the range to the target. The equivalent angular variance is given by:

$$\sigma_\theta^2 = \frac{\bar{X}_n^2}{2 R^2}. \quad (\text{F9})$$

For the target model under discussion, it can be shown that:

$$\sigma_\theta^2 = \frac{L^2}{24R^2} (\text{rad})^2. \quad (\text{F10})$$

Equation (F10) represents the angular error due to glint, if the glint spectrum is so narrow that the servo does no smoothing. For a 20 ft. target at 100 ft. range, $\sigma_\theta = 40$ milliradians.

The other extreme is when the glint noise is very wide compared to the servo bandwidth. This results when the target is rotating at a high rate. In this case the angular variance due to glint can be obtained by multiplying the glint spectrum at zero frequency by $2B_s$.

Muchmore (Reference 59) has shown that the normalized glint spectrum at zero frequency $W_g(0)$ is given by $1/f_m$. Thus, the variance due to glint is given by:

$$\sigma_\theta^2 = \frac{L^2 2B_s}{24R^2 f_m} \quad (F11)$$

For the $100^\circ/\text{sec}$ target rotation considered previously:

$$\begin{aligned} L &= 20 \text{ ft;} \\ R &= 100 \text{ ft;} \\ f_m &= 2450 \text{ Hz;} \\ B_s &= 5 \text{ Hz;} \end{aligned}$$

and:

$$\sigma_\theta = \frac{40}{\sqrt{\frac{2450}{10}}} = 2.56 \text{ milliradians.} \quad (F12)$$

Further Study

The target model used in the preceding analysis, and the resultant noise predictions are the best available. However, these are two problems that should be mentioned:

- a. When the target is so close that it subtends an angle larger than the difference beam (about 60 ft. in the example considered) the model breaks down. This is because all of the scatterers that make up the target are not added and subtracted to determine the error signal at any one time.
- b. If the target shape is very irregular, gross aspect changes will cause the fading and glint spectra to be different from that predicted above.

These two problems require further study, and probably can best be handled by simulation.

APPENDIX G - THE SCALAR NEAR FIELD FOR CIRCULAR APERTURE ANTENNAS

Approximations are made to reduce the vector solution for the fields radiated by an antenna to a scalar solution. This scalar solution appears as an integral for the diffraction field, and for a planar aperture is of the form:

$$U_p = \frac{1}{4\pi} \int_{\text{Aperture}} F(\xi, \eta) \frac{e^{-jk r}}{r} \left[\left(jk + \frac{1}{r} \right) \vec{i}_z \cdot \vec{r}_1 + jk \right] d\xi d\eta, \quad (G1)$$

where $F(\xi, \eta)$ is the aperture distribution function with the coordinate system defined as in Figure G1. Further approximations are applied to equation G1 to yield solutions for the far field region and the Fresnel region. The near region, or that region immediate to the aperture, has no simplifying approximations.

The approximations used for the far field are known to produce valid results both in predicting the far fields from a known aperture function and in synthesizing an aperture function to produce a desired far field pattern. The fields that exist between the far field and the near region are more complex, however, and approximate solutions for them are of necessity less accurate. The Fresnel region is a definition of the fields in this region and arises from the following approximations for the integral of equation G1

$$\left[\left(jk + \frac{1}{r} \right) \vec{i}_z \cdot \vec{r}_1 + jk \right] = jk (1 + \cos \theta), \quad (G2)$$

$r = R$ is the amplitude term,

$$r = R - \xi \sin \theta \cos \phi - \eta \sin \theta \sin \phi + \frac{1}{2R} [\xi^2 + \eta^2 - (\xi \sin \theta \cos \phi + \eta \sin \theta \sin \phi)^2], \quad (G3)$$

in the phase term.

The integral of Equation G1 then becomes:

$$U_p = (1 + \cos \theta) \frac{j e^{-jkR}}{2\lambda R} \int_{\text{Aperture}} F(\xi, \eta) e^{jks \sin \theta (\xi \cos \phi + \eta \sin \phi)} \quad (G4)$$

$$e^{-\frac{jk}{2R} [\xi^2 + \eta^2 - \sin^2 \theta (\xi \cos \phi + \eta \sin \phi)^2]} d\xi d\eta. \quad (G5)$$

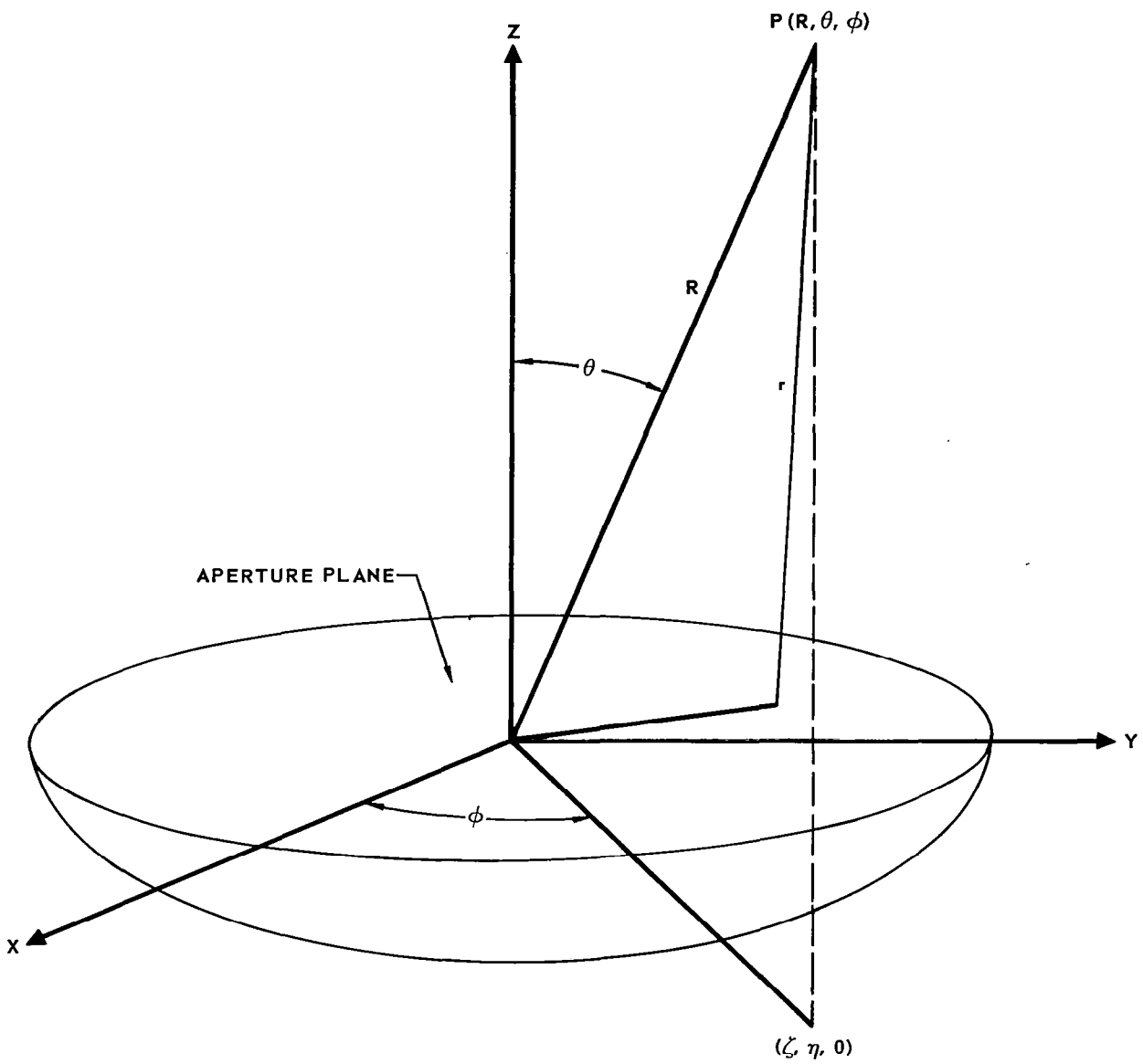


FIGURE G1 - COORDINATE FRAME

Recently, however, it has been established that Equation G1 can be evaluated in the Fresnel region with the aid of computers by making only the

approximation that $\left[\left(jk + \frac{1}{r} \right) \vec{i}_z \cdot \vec{r}_1 + jk \right] = jk (1 + \cos \theta)$,

and Equation G1 becomes:

$$UP = (1 + \cos \theta) \frac{j}{2\lambda} \int_{\text{Aperture}} F(\xi, \eta) \frac{e^{-jkr}}{r} d\xi d\eta. \quad (G6)$$

Since no approximations for r are made, this prediction of the fields between the near region and the far field region is more exact. In order to emphasize this more accurate solution, the fields are called the scalar near fields (SNF) and not the Fresnel fields. The SNF is valid from a point close to the aperture (generally thought to be one antenna diameter from the aperture) where the radial component of field is negligible, out to infinity.

Mathematical Formulation of SNF for Circular Apertures (Reference 50)

The scalar near field for a planar circular aperture, radius a , illuminated by a circularly-symmetric distribution function is:

$$F(R, \theta) = (1 + \cos \theta) \frac{ja^2}{2\lambda} \int_0^{2\pi} \int_0^1 f(\rho) \frac{e^{-jkr}}{r} \rho d\rho d\beta, \quad (G7)$$

where:

$$r = [R^2 + a^2 \rho^2 - 2a\rho R \sin \theta \cos(\phi - \beta)]^{\frac{1}{2}}. \quad (G8)$$

By the addition theorem for spherical Bessel functions:

$$\frac{e^{-jkr}}{r} = jkh_0^{(2)}(kr) = jk \sum_{n=0}^{\infty} (2n+1) P_n[\sin \theta \cos(\theta - \beta)] j_n(ka\rho) h_n^{(2)}(kR), \quad (G9)$$

$R > a$

where $h_n^{(2)}(kR)$ is the spherical Hankel function of the second kind, $j_n(ka\rho)$ is the spherical Bessel function and $P_n[\sin \theta \cos(\phi - \beta)]$ is the Legendre polynomial.

The β integral can be performed with the aid of the addition theorem for Legendre polynomials:

$$P_n[\sin \theta \cos(\phi - \beta)] = P_n(0) P_n(\cos \theta) + 2 \sum_{m=1}^n \frac{(n-m)!}{(n+m)!} P_n^m(0) P_n^m(\cos \theta) \cos m(\phi - \beta). \quad (G10)$$

where $P_n^m(\cos \theta)$ is the associated Legendre polynomial. Because of the factor $\cos m(\phi - \beta)$, every term in Equation (G10) except the first vanishes when integrated over β through the range 2π . Thus:

$$\int_0^{2\pi} P_n(\sin \theta) \cos(\phi - \beta) = 2\pi P_n(0) P_n(\cos \theta). \quad (G11)$$

The SNF of Equation (G7) thus becomes:

$$F(R, \theta) = \frac{1 + \cos \theta}{2} jka^2 \sum_{n=0}^{\infty} (2n+1) P_n(0) P_n(\cos \theta) h_n^{(2)}(kR) \int_0^1 f(\rho) j_n(ka\rho) \rho d\rho. \quad (G12)$$

Equation (G12) is useful in the fact that the integral is independent of the space coordinates R and θ . Hence, for any antenna, the integral need be evaluated only once, and the series summed for various choices of (R, θ) to determine the spatial distribution of energy.

In most cases for parabolic reflectors, the primary feed patterns are quadratic in nature and can be suitably matched by choosing appropriate coefficients in the function:

$$f(\rho) = 1 + a_1 \rho^2 + a_2 \rho^4 + a_3 \rho^6. \quad (G13)$$

Universal curves have been developed that relate the coefficients to the taper on the aperture. The dependence of the curves on the F/D ratio is slight and can be ignored in most practical cases. By using Equation (G13) the integral in Equation (G12) becomes:

$$\begin{aligned} \int_0^1 f(\rho) j_n(ka\rho) \rho d\rho &= \int_0^1 j_n(ka\rho) \rho d\rho + a_1 \int_0^1 \rho^2 j_n(ka\rho) \rho d\rho \\ &+ a_2 \int_0^1 \rho^4 j_n(ka\rho) \rho d\rho + a_3 \int_0^1 \rho^6 j_n(ka\rho) \rho d\rho. \end{aligned} \quad (G14)$$

Let:

$$G(n) = \frac{1 + \cos \theta}{2} jka^2 \sum_{n=0}^{\infty} (2n+1) P_n(0) P_n(\cos \theta) h_n^{(2)}(kR), \quad (G15)$$

Then using equations (G14) and (G15), equation (G7) becomes:

$$\begin{aligned}
 F(R, \theta) = G(n) \int_0^1 j_n(ka\rho) \rho d\rho + a_1 G(n) \int_0^1 \rho^2 j_n(ka\rho) \rho d\rho \\
 + a_2 G(n) \int_0^1 \rho^4 j_n(ka\rho) \rho d\rho + a_3 G(n) \int_0^1 \rho^6 j_n(ka\rho) \rho d\rho.
 \end{aligned}
 \tag{G16}$$

Each of the integrals of equation (G16) is purely real, but the function $G(n)$ is complex due to the spherical Hankel function $h_n^{(2)}(kR)$. Thus the SNF is complex. Let I_1, I_2, I_3 and I_4 denote the first, second, third and fourth terms, respectively, of equation (G16). The SNF can thus be written as:

$$\begin{aligned}
 F(R, \theta) = \text{Re} [I_1] + \text{Im} [I_1] + a_1 \text{Re} [I_2] + a_1 \text{Im} [I_2] + a_2 \text{Re} [I_3] + a_2 \text{Im} [I_3] \\
 + a_3 \text{Re} [I_4] + a_3 \text{Im} [I_4].
 \end{aligned}
 \tag{G17}$$

Equation (G17) shows that, once the real and imaginary terms have been evaluated, the SNF for any aperture distribution of the form of equation (G13) may be found by merely changing a_1, a_2 and a_3 and performing the indicated multiplication and addition.

Data for I_1, I_2, I_3 and I_4 is available (reference 50) for forty values of range in the interval $\frac{2D^2}{\lambda}$ to $0.0125 \frac{D^2}{\lambda}$ for an 80λ circular aperture.

Analysis reveals that this same data is highly accurate in predicting the SNF for apertures ranging from 40λ to 120λ . Figure G2 shows a plot of the magnitude of equation (G17).

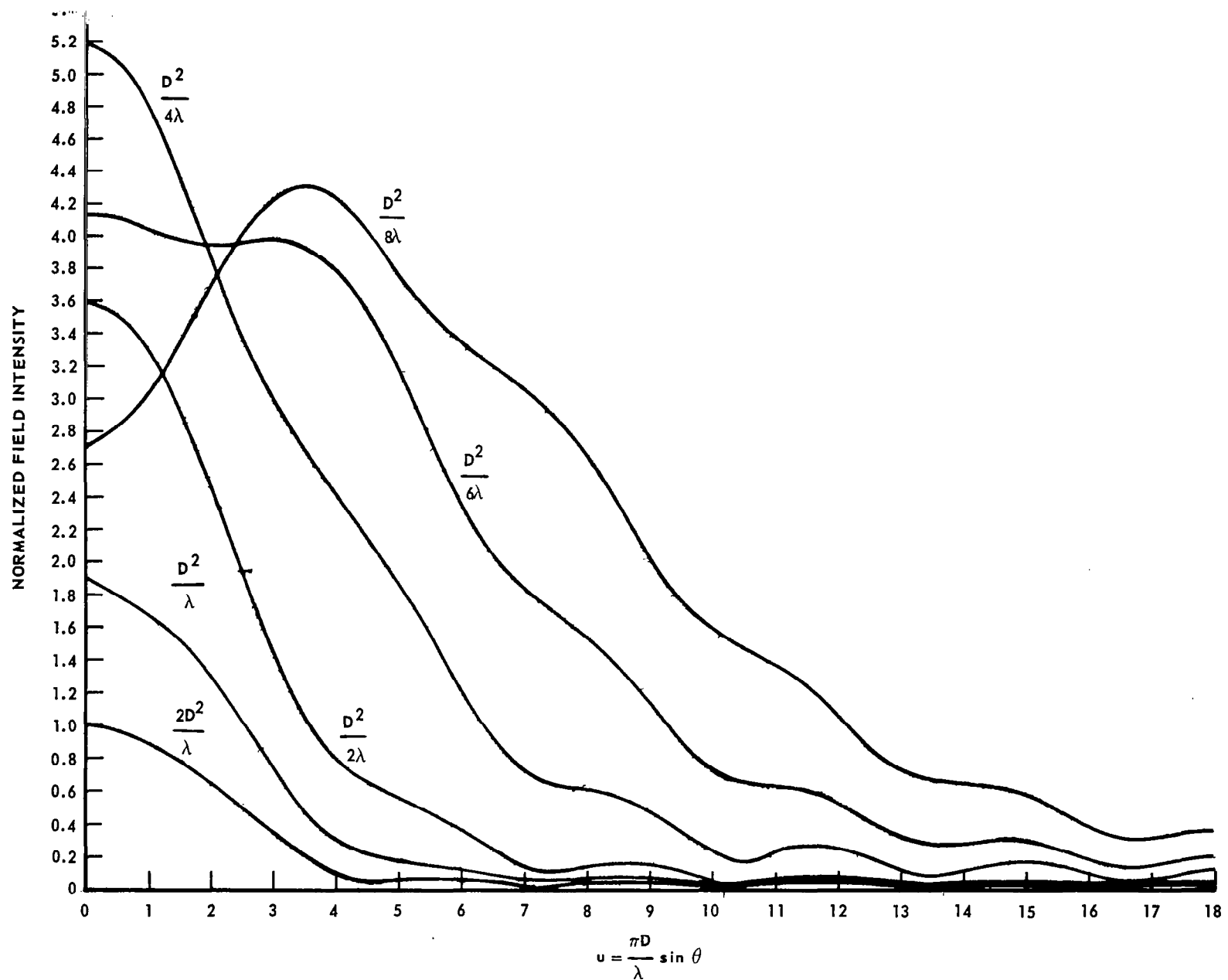


FIGURE G2 – THE SCALAR NEAR FIELD PATTERN FOR CIRCULAR APERTURE ANTENNAS

APPENDIX H - THERMAL NOISE EFFECTS ON RANGE MEASUREMENT

In the PM-CW system using a single ranging subcarrier, the phase modulated signal transmitted by the chasecraft is:

$$A \cos [\omega_c t + \beta \cos \omega_m t], \quad (\text{H1})$$

where ω_m is the subcarrier radian frequency. The received signal plus thermal noise at the target is:

$$A_T \cos [\omega_c (t - \tau) + \beta \cos \omega_m (t - \tau)] + n_T(t), \quad (\text{H2})$$

$$A_T \cos [\omega_c (t - \tau) + \beta \cos \omega_m (t - \tau)] + x_T(t) \cos \omega_c t + y_T(t) \sin \omega_c t, \quad (\text{H3})$$

where A_T represents the amplitude of the received signal at the target and the thermal noise, $n(t)$, is a gaussian random process. τ is the time delay due to the finite range between target and chasecraft. The random variables x and y have zero mean with identical single sided power spectral densities given by:

$$S_{x_T}(f) = S_{y_T}(f) = 2n = 2kTNF, \quad (\text{H4})$$

over the bandwidth of interest. $kT = 4 \text{ a } 10^{-21} \text{ watts/Hz}$ and F is the target receiver noise figure.

The phase locked loop (PLL) in the target vehicle receiver demodulates the range subcarrier. The output of the PLL voltage controlled oscillator (VCO) is proportional to $\sin \omega_c t$, therefore the output of the PLL null detector is:

$$A_T \beta \cos [\omega_m (t - \tau)] - y_T(t), \quad (\text{H5})$$

where we have assumed small β . This signal is filtered and reinserted on the target transponder reply with the same modulation index. Thus, the transponder reply is (neglecting the frequency offset):

$$\cos \left[\omega_c (t - \tau) + \beta \cos \omega_m (t - \tau) - \frac{y'_T}{A_T} \right], \quad (\text{H6})$$

where the prime indicates the filtered noise term. The single sided power spectral density of y'_T is:

$$S_{y'_T}(f) = 2n = 2kTNF, \quad |f-f_m| \leq \frac{B}{2},$$

$$= 0, \text{ in all other cases,} \quad (H7)$$

where B is bandwidth of the range subcarrier filter.

Then from equation y'_T the received reply signal plus thermal noise at the chasecraft receiver is:

$$A_C \cos \left[\omega_C (t-2\tau) + \beta \cos \omega_m (t-2\tau) - \frac{y'_T (t-\tau)}{A_T} \right] + n_C (t), \quad (H8)$$

where $n_C(t)$ represents the chasecraft receiver thermal noise. Then, the output of the chasecraft PLL null detector becomes:

$$A_T \left[\beta \cos \omega_m (t-2\tau) - \frac{y'_T (t-\tau)}{A_T} - \frac{y_C (t)}{A_C} \right], \quad (H9)$$

where the derivation is similar to that of equation H4. Assuming $A_T = A_C = A$, identical target and chasecraft subcarrier rectangular filters, and identical target and chasecraft noise figures, the output of the chasecraft subcarrier filter is:

$$\beta \cos \omega_m (t-2\tau) - \frac{y'_T (t-\tau) + y'_C (t)}{A}, \quad (H10)$$

where the single sided power spectral densities of the independent random variables y'_T and y'_C are identical and given by:

$$S_{y'_T}(f) = S_{y'_C}(f) = \begin{cases} 2n = kTNF & |f-f_m| < B. \\ 0 & \end{cases} \quad (H11)$$

Here B is the subcarrier filter bandwidth. Again the prime denotes filtering.

The filtered noise terms in equation H9 represent a narrow band process. That is:

$$y'_T (t-\tau) + y'_C (t) = u(t) \cos \omega_m t - v(t) \sin \omega_m t, \quad (H12)$$

where the single sided power spectral densities for the new process are:

$$S_u(f) = S_v(f) = 8n = 8kTNF. \quad (H13)$$

Then, for high signal-to-noise ratios, the output of the chasecraft subcarrier filter, given by equation(H10)is:

$$\beta \cos \left[\omega_m (t-2\tau) + \frac{u(t)}{\beta A} \right]. \quad (H14)$$

A phase comparison with the range subcarrier oscillator signal, $\cos \omega_m t$ yields the desired output:

$$2 \omega_m t - \frac{u(t)}{\beta A}, \quad (H15)$$

or, after low pass filtering:

$$2\pi f_m \frac{2R}{c} - \frac{u'(t)}{\beta A}, \quad (H16)$$

$\tau = \frac{R}{C}$, where R is the range. The prime denotes the noise term after low pass filtering.

Then the mean squared range error is:

$$\sigma_R^2 = \left(\frac{c}{4\pi f_m A \beta} \right)^2 (8n B_{LP}), \quad (H17)$$

where B_{LP} is the single sided low pass filter noise bandwidth in Hz. The units are (meter)² for c in meters per second. This may be rewritten in terms of the received signal power, $S = A^2/2$ and receiver noise figure, F, as:

$$\sigma_R^2 = \left(\frac{c^2}{(2\pi f_m \beta)^2} \right) \left(\frac{kTNF}{S} \right) B_{LP}, \quad (18)$$

From the radar range equation:

$$S = \frac{P_t G_t G_r \lambda^2 L}{(4\pi)^2 R^2}, \quad (H19)$$

where P_t = transmitted power,
 G_r = receiver antenna gain,
 λ = wavelength,
 R = range,
 L = loss,

Thus, equation(H19)becomes:

$$\sigma_R^2 = R^2 \left(\frac{2f_c}{f_m \beta} \right)^2 \left(\frac{kTNF B_{LP}}{P_t G_t G_r L} \right), \quad (H20)$$

or, the fractional rms error is:

$$\frac{\Delta R}{R} = \frac{2f_c}{f_m \beta} \left(\frac{kTNF B_{LP}}{P_t G_t G_r L} \right)^{1/2}. \quad (H21)$$

APPENDIX I - THERMAL NOISE EFFECTS ON RANGE RATE MEASUREMENT

The chasecraft transmits a signal of the form:

$$\cos \omega_0 t, \quad (I1)$$

where ω_0 is the carrier radian frequency. The signal plus thermal noise as received at the target transponder is:

$$A_T \cos(\omega_0 t + \omega_d) t + x_T(t) \cos(\omega_0 + \omega_d) t - y_T(t) \sin(\omega_0 + \omega_d) t \quad (I2)$$

where A_T is the amplitude of the received signal and $\omega_d = \frac{2\pi v}{\lambda}$ is the one way

doppler shift. Here v represents the closing velocity and λ , the wavelength. In the narrow band random process used to represent the transponder thermal noise x_T and y_T are independent gaussian random variables. x_T and y_T have identical single sided power spectral densities equal to $2n_T = 2kTF$ where F is the target receiver noise figure and $kT = 4 \times 10^{-21}$ watts/Hz.

The subscript T is used to designate target parameters, whereas the subscript c is used for chasecraft parameters.

At high signal-to-noise ratios, equation I2 may be written as:

$$A_T \cos[(\omega_0 + \omega_d)t + \frac{y_T(t)}{A_T}]. \quad (I3)$$

The phase locked loop (PLL) in the target transponder serves to filter the input phase noise such that the reply signal is of the form:

$$\cos[(\omega_0 + \omega_d)t + \frac{y'_T(t)}{A_T}], \quad (I4)$$

where the prime denotes the filtered noise term. The single sided power spectral density of the filtered noise term, y'_T is $2n_T$ for frequencies less than the PLL bandwidth and is zero otherwise.

Then the reply signal received by the chasecraft plus thermal noise may be written as (neglecting the transponder frequency offset):

$$A_c \cos[(\omega_0 + 2\omega_d)t + \frac{y'_T(t)}{A_T}] + x_c(t) \cos(\omega_0 + 2\omega_d)t - y_c(t) \sin(\omega_0 + 2\omega_d)t. \quad (I5)$$

where A_c represents chasecraft received amplitude. The representation of the chasecraft receiver thermal noise is similar to that used for the target receiver.

In a similar manner to that employed in the derivation of equation I4, it is seen that the signal out of the chascraft PLL is of the form:

$$\cos \left[(\omega_c + 2\omega_d)t + \frac{y'_T}{A_T} + \frac{y'_C}{A_C} \right], \quad (I6)$$

where again the primes denote the effects of PLL filtering. The single aided power spectral densities of y'_T and y'_C are $2n_T = 2kTNF_T$ and $2n_C = 2kTNF_C$ respectively for frequencies less than the respective PLL bandwidths. Here F denotes noise figure and $kT = 4 \times 10^{-21}$ watts/Hz. Note that y'_T and y'_C are independent random variables with zero means.

The output of a discriminator tuned to ω_0 is:

$$2\omega_d + \frac{d}{dt} \left[\frac{y'_T(t)}{A_T} + \frac{y'_C(t)}{A_C} \right]. \quad (I7)$$

Assume that the target and chascraft have identical noise figures and received powers. Then equation (I7) may be written as:

$$\frac{2\pi 2V}{\lambda} + \frac{1}{A} \frac{d}{dt} [y'_T(t) + y'_C(t)], \quad (I8)$$

where $A = A_T = A_C$. Since the power spectral density of $(y'_T + y'_C)$ is the sum of the individual power spectral densities or $4n$, the power spectral density of the term on the right of equation I8 is:

$$\frac{\omega^2}{A^2} 4n,$$

where $n = n_C = n_T = kTNF$. Then, for a low pass filter with noise bandwidth equal to B_{LP} Hz the mean square error associated with this estimate of V is seen to be:

$$\left(\frac{\lambda}{4\pi} \right)^2 \frac{1}{A^2} \int_0^{B_{LP}} (2\pi)^2 f^2 4n df = \frac{\lambda^2 n (B_{LP})^3}{6S}. \quad (I9)$$

Where S , the signal power is equal to $A^2/2$. The units are in those of λ^2 per (second)².

APPENDIX J - MULTIPATH EFFECTS ON RANGE RATE MEASUREMENT

In the desired mode of operation, the signal frequency as seen at the receiving spacecraft differs from that at the transmitting spacecraft by the one way doppler shift. This doppler shift is used as an indication of range rate. However, multipath conditions can result in the existence of signals with erroneous doppler information.

In considering the possible multipath situations that can result in erroneous doppler signals, it must be realized that multipath interference at the chasecraft (target) is a result of the target (chasecraft) transmission because a frequency offset is provided at the target transponder. Furthermore, only an even number of bounces is allowed since circular polarization is employed.

With these considerations in mind, it is seen that erroneous doppler signals can result from any even numbered bounce situation similar to those shown in figure J-1. The solid line indicates the direct path and the dashed line the multipath.

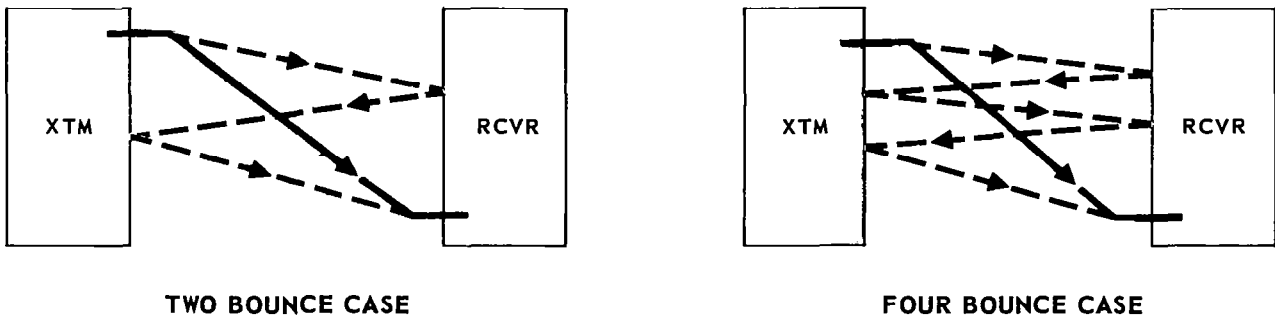


FIGURE J1 CHASE CRAFT-TARGET MULTIPATH

Let the n th multipath mode be that mode associated with $2n$ bounces. Then the doppler shift for the n th mode is seen to be:

$$f'_d = f_d (1 + 2n), \quad (J1)$$

where f_d is the one way doppler shift associated the direct mode ($n = 0$).

The received signal power in the nth mode is given by application of the radar range equation:

$$P_n = \frac{P_t G_t G_r \lambda^2}{(4\pi)^2 R^2} \left[\frac{\sigma_C \sigma_T}{(4\pi)^2 R^4} \right]^n, \quad (J2)$$

where P_t = transmitter power,
 G_t = transmitter antenna gain,
 G_m = receiver antenna gain,
 λ = wavelength,
 R = target-to-chase range,
 σ_C = radar cross section of chasecraft,
 σ_t = radar cross section of target.

Then the ratio of the power received in the nth multipath mode to that received via the direct path is from equation (J2):

$$\frac{P_n}{P_o} = \left[\frac{\sigma_C \sigma_T}{(4\pi)^2 R^4} \right]^n. \quad (J3)$$

Assuming $A_C = A_t = 1$ square meter and expressing the ratio in db, we have:

$$\frac{P_n}{P_o} \text{ (db)} = -22n - 40n \log R, \quad (J4)$$

for R in meters.

The range of validity of equations J3 and J4 may be determined by reference to equation (J2). For $n = 0$ equation J2 is valid in the Fraunhofer region of the transmitting and receiving antennas. For the anticipated aperture dimensions at an operating frequency of 1GHz the Fraunhofer region will exist for ranges greater than 0.1 meters.

For $n > 0$ equation (J2) will only be valid in the effective Fraunhofer region of the spacecraft (considered to be a radiating aperture). For a spacecraft diameter of 3 meters this effective region is defined at ranges greater than 60 meters for $\lambda = 0.3$ meters. Using equation (J2) at ranges less than 60 meters with $n > 0$ will yield power levels above the true value. With these considerations in mind, it is seen that equations (J3) and (J4) are valid at ranges beyond 60 meters and yield an upper limit on the relative interference level for $0.1 < R < 60$ meters.

Some insight into the doppler interference problem may be had by considering the range at which the signal received in the first multipath mode ($n = 1$) is down 10db relative to that received via the direct path ($n = 0$). From equation (J4) this occurs when the target-to-chasecraft ranges is 0.5 meters. If docking control-law is $R = 0.2R$, then at $R = 0.5$ m the one way doppler shift is 0.33 Hz and the one way doppler shift associated with the first ($n = 1$) multipath mode is $3f_d$ or 1 Hz. If we assume the phase locked loops (PLL) in both the target and chasecraft lock onto the signal with doppler shift $3f_d$ (which is a worst case assumption since a favorable power ratio of 10db is assumed) then, the chasecraft doppler discriminator output will be in error by a factor of 3. That is, the apparent range rate would be 0.3 m/s as

opposed to the correct value of 0.1 m/s. This error represents an upper limit because of the assumptions involved with respect to Fraunhofer regions and the PLL performance. Note that the worst case error, 0.2 m/s, is less than the desired accuracy of 0.3 m/s. It is then concluded that this multipath mechanism is not a significant error contributor.

It is noted that, while the above example represents a worst case, upper limit on doppler interference for the mechanism considered, other effects due to the finite spacecraft dimensions are observed at short range. In particular, reflections from the skin of the transmitting spacecraft will cause a finite width doppler spectrum even in the direct mode. The mechanism is illustrated in the figure J-2.

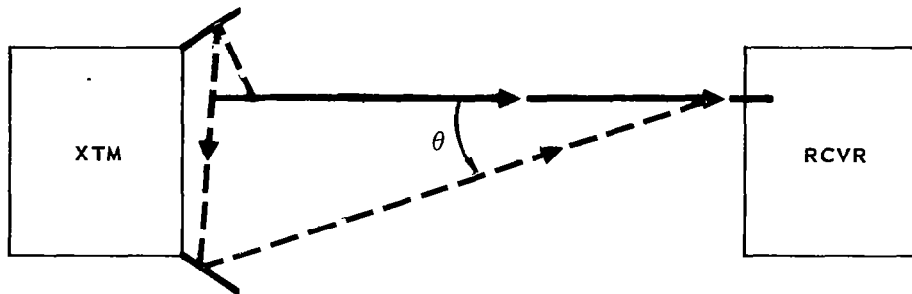


FIGURE J2

Reference to the figure indicates that the doppler shift on the signal received via the bounce path is:

$$f_d \cos \theta = f_d \frac{R}{\sqrt{R^2 + D^2}} \quad (J5)$$

where f_d is the direct path doppler shift, R is the target-to-chase range, and D is the spacecraft diameter. Considering bounces from the entire spacecraft skin, it is seen that the finite size results in a continuous spectrum with minimum shift equal to $f_d \cos \theta$ and maximum shift equal to f_d . This situation is illustrated in figure J-3.

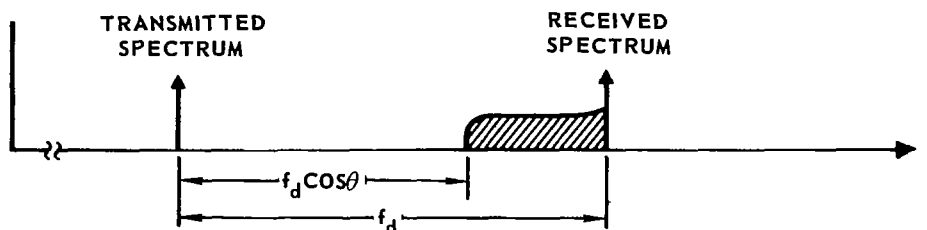


FIGURE J3

Then for the simple case considered here, the net effect of the finite space-craft size is to shift the power centroid of the received doppler spectrum down (for a positive closing velocity) in frequency. This error is difficult to predict analytically. However, at the short ranges where the spectrum spreading becomes significant, the skin reflections compete with the main beam and with proper design this effect may be minimized.

APPENDIX K

FORMATION OF SWEEP NULL PATTERN (EOS)

The target transmitting antenna array generates a pattern whose null position varies linearly with time. By comparing the time of the null occurrence with a timing reference signal, the chaser receiver is able to determine the target attitude.

The method of generating the sweep null pattern is shown in figure K1

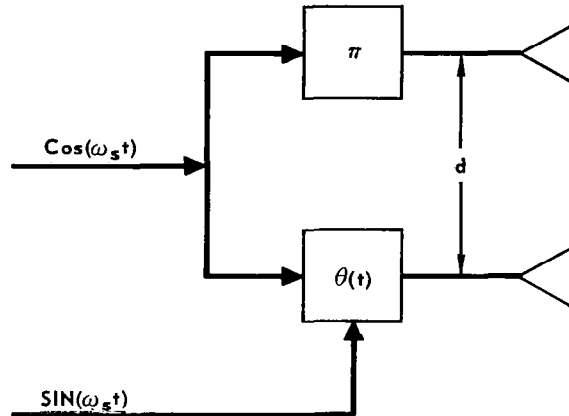


FIGURE K-1 - TARGET TRANSMITTING ARRAY

Defining ϵ to be the mechanical angular error relative to the above single plane array boresight, the signal received by the chaser at ϵ is of the form:

$$\cos \left[\omega_0 t + \frac{\theta(t)}{2} + \frac{\phi}{2} - \frac{\pi}{2} \right] + \cos \left[\omega_0 t - \frac{\theta(t)}{2} + \frac{\pi}{2} \right], \quad (K-1)$$

$$= 2 \sin \left[\frac{\theta(t)}{2} + \frac{\phi}{2} \right] \cos [\omega_0 t]. \quad (K-2)$$

where $\phi = \frac{2\pi d}{\lambda} \sin \epsilon$ and ω_0 is the carrier frequency. The null of this pattern is caused to vary according to the time varying phase shift, $\theta(t)$. For a sinusoidal drive:

$$\theta(t) = \beta \sin \omega_s t, \quad (K-3)$$

where β is the modulation index and $\frac{\omega_s}{2\pi}$ is the modulation frequency. Then the form of the signal received at the chaser may be written as:

$$2 \sin \left\{ \frac{\beta}{2} \sin \omega_s t + \frac{1}{2} \frac{2\pi d}{\lambda} \sin \epsilon \right\} \cos \omega_0 t. \quad (K-4)$$

Then the pattern null condition is defined by:

$$\beta \sin \omega_s t + \frac{2\pi d}{\lambda} = \pm 2n\pi, \quad (K-5)$$

where n is zero or an integer. Defining the principal null to be that which exists at boresight when $\omega_s t = 0$, in order to linearly sweep this null from $\epsilon = +90^\circ$ to -90° we require:

$$\beta = \frac{2\pi d}{\lambda}. \quad (K-6)$$

Furthermore, in order to avoid ambiguities (sweeping more than one null past the target) we require:

$$\beta = \frac{2\pi d}{\lambda} \leq \pi. \quad (K-7)$$

Then using $\beta = \frac{2\pi d}{\lambda} = \pi$ the form of the signal received at the chaser becomes:

$$2 \sin \left[\frac{\pi}{2} \sin \omega_s t + \frac{\pi}{2} \sin \epsilon \right] \cos \omega_0 t. \quad (K-8)$$

The above equation applies to the simple single plane case. In order to derive target attitude errors in two dimensions a swept null technique is required in both the target azimuth and elevation planes. In the proposed system both azimuth and elevation sweeps are provided by the addition of a third antenna to form a "L" shaped array. The antenna driven by the sinusoidal phase shift is used as the common antenna in the "L" configuration. The remaining two antennas are time shared such that an azimuth sweep is accomplished during one half cycle of the sinusoid controlling the phase shifter in the common antenna feed, and an elevation sweep is accomplished during the other half cycle. This results in a uni-directional sweep in

both azimuth and elevation. Then using equation K-8 the form of the received signal at the chaser with target azimuth and elevation coordinates given by ϵ_A and ϵ_E respectively is:

$$2 [S_A(t) \sin \left\{ \frac{\pi}{2} [\sin \omega_S t + \sin \epsilon_A] \right\} + [1 - S_A(t)] \sin \left\{ \frac{\pi}{2} [\sin \omega_S t + \sin \epsilon_E] \right\}] \cos \omega_0 t, \quad (K-9)$$

where $S_A(t)$ represents a square wave sampler synchronized with the phase shifter drive:

$$S_A(t) = \frac{1}{2} \sum_{n=-\infty}^{\infty} \frac{\sin(n \frac{\pi}{2})}{n(\frac{\pi}{2})} e^{jn \omega_S t}. \quad (K-10)$$

The time sharing function is illustrated in figure K2

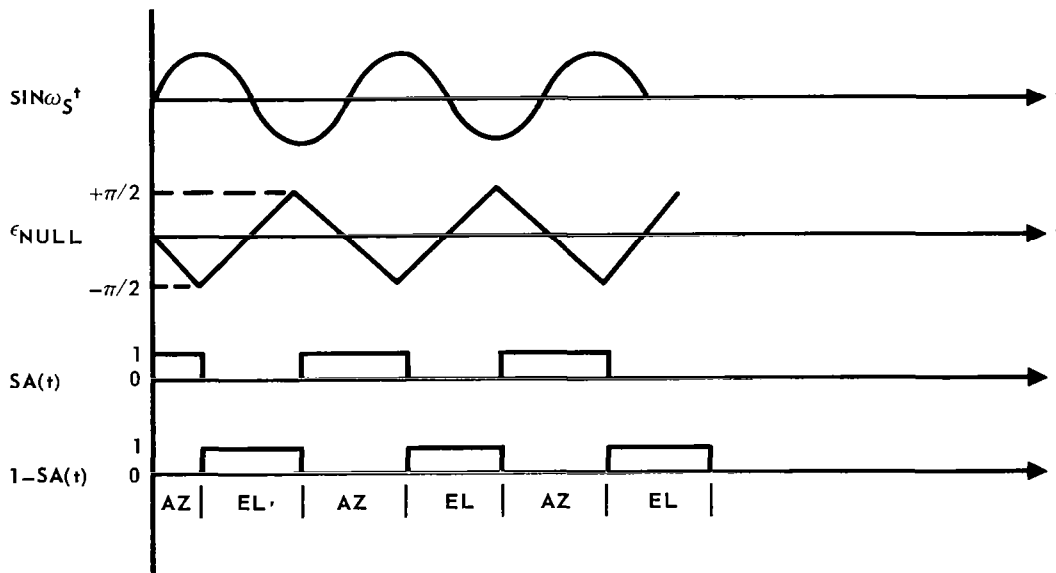


FIGURE K-2 - AZIMUTH AND ELEVATION TIME SHARING

The envelope of the received signal given by equation K-9 is defined to be:

$$E(t) = S_A(t) \sin \left\{ \frac{\pi}{2} [\sin \omega_s t + \sin \epsilon_A] \right\} \quad (K-11)$$

$$+ (1 - S_A(t)) \sin \left\{ \frac{\pi}{2} [\sin \omega_s t + \sin \epsilon_E] \right\}.$$

Considering the Bessel function expansions of the sinusoids with time varying sinusoidal arguments and the form of $S_A(t)$ given by equation K-10, it is seen that a general Fourier series for $E(t)$ will contain only frequencies at multiples of $\frac{\omega_s}{2\pi}$. Then the envelope may be written as:

$$E(t) = \sum_{m=0}^{\infty} b_m \cos(m \omega_s t + a_m). \quad (K-12)$$

The received signal at the chaser may be represented as:

$$A E(t) \cos(\omega_0 t), \quad (K-13)$$

where A is the amplitude of the received signal as determined by the radar range equation. $E(t)$ is given by either equation K-11 or K-12.

In equation K-12 generally b_m and a_m will be a function of ϵ_A and ϵ_E . In fact as ϵ_A and ϵ_E approach zero the dc component of $E(t)$ approaches zero. This can be demonstrated as follows. In equation K-11 let $\epsilon_A = \epsilon_E = 0$. Then equation K-11 becomes:

$$E(t) = \sin \left[\frac{\pi}{2} \sin \omega_s t \right], \quad (K-14)$$

$$= 2 \sum_{n \text{ odd}}^{\infty} J_n \left(\frac{\pi}{2} \right) \sin(n \omega_s t). \quad (K-15)$$

This result indicates that the received carrier amplitude at the chaser reaches zero when the target roll axis is directed toward the chaser. In this case the amplitude of each adjacent sideboard is $A J_1 \left(\frac{\pi}{2} \right)$ or $0.28A$.

APPENDIX L

THERMAL NOISE EFFECTS ON TARGET LOS DETERMINATION (EOS)

A phase sensing monopulse technique will be employed at the chaser to determine the target line-of-sight angular error. A simplified (heterodyning omitted) single plane receiver diagram is shown in figure L-1

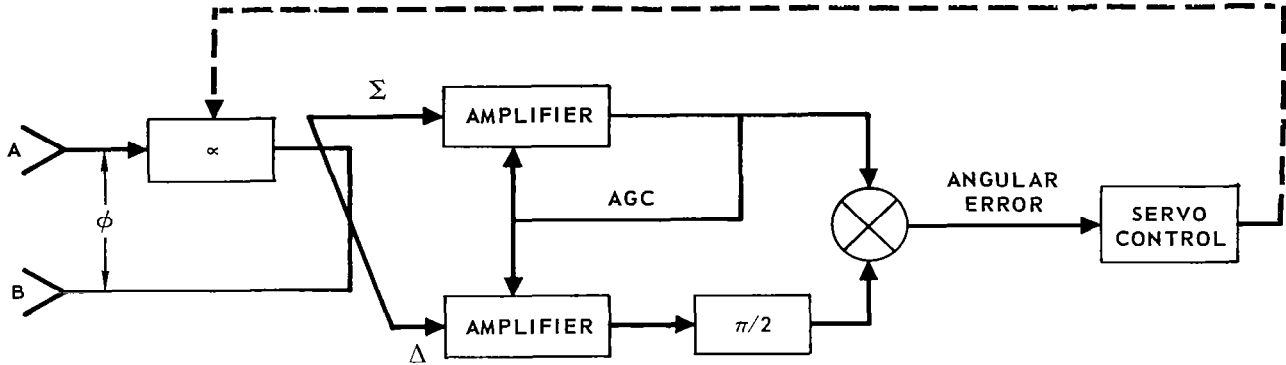


FIGURE L-1 - SINGLE PLANE PHASE SENSING MONOPULSE

As shown in the figure, a sum and difference system is used so that parallel channel IF tracking errors are effectively post-comparator errors as opposed to the more serious precomparator errors. The angle error indication is developed in the normal sum and difference manner. This error signal controls the variable RF phase shifter, α , such that a null is maintained. In this manner the angular position of the phase shifter yields the electronics boresight which, in turn, gives the target direction.

From equation K-13 of Appendix K, the signals received at antennas A and B respectively are:

$$AE(t) \cos \left(\omega_0 t + \frac{\phi}{2} \right). \tag{L-1}$$

and:

$$AE(t) \cos \left(\omega_0 t - \frac{\phi}{2} \right), \quad (L-2)$$

where A is the amplitude of the received signal as determined by the radar range equation. And in the above two equations:

$$\phi = \frac{2\pi d}{\lambda} \sin \epsilon, \quad (L-3)$$

where d is the chaser interferometer separation, τ is the carrier wavelength, and ϵ is the target angular error relative to the chaser boresight.

With no loss in generality we assume the value of the phase shifter α is zero. Then accounting for receiver thermal noise the sum channel hybrid output is:

$$\frac{2}{\sqrt{2}} AE(t) \cos \frac{\phi}{2} \cos \omega_0 t + n_{\Sigma}(t), \quad (L-4)$$

and the difference channel hybrid output is:

$$\frac{2}{\sqrt{2}} AE(t) \sin \frac{\phi}{2} \sin \omega_0 t + n_{\Delta}(t). \quad (L-5)$$

In the above two equations the receiver thermal noise is represented by n_{Σ} and n_{Δ} for the sum and difference channels respectively. The sum and difference noise processes are independent with single sided power spectral densities equal to $n_{\Delta} = n_{\Sigma} = n = kTF$ watts/Hz where $kT = 4 \times 10^{-21}$ watts/Hz and F is the receiver noise figure. In the above two equations the $\sqrt{2}$ factor accounts for conservation of power through the hybrid.

Let the sum and difference channel amplifier gains be K. Then accounting for the $\pi/2$ phase shift in the difference channel the inputs to the phase sensitive detector (considered to be an ideal multiplier) are:

$$K \left[\sqrt{2} AE(t) \cos \frac{\phi}{2} \cos \omega_0 t + n_{\Sigma}(t) \right], \quad (L-6)$$

and:

$$K[\sqrt{2} AE(t) \sin \frac{\phi}{2} \cos \omega_0 t + n_{\Delta}(t)], \quad (\text{L-7})$$

for the sum and difference channels respectively. Note we have neglected the $\pi/2$ phase shift on the noise term, n_{Δ} , since it is of no consequence.

Then the multiplier output is given by the product of the above two equations:

$$K^2 \{ 2A^2 E^2(t) \sin \frac{\phi}{2} \cos \frac{\phi}{2} \cos^2 \omega_0 t + n_{\Delta}(t) \sqrt{2} AE(t) \cos \frac{\phi}{2} \cos \omega_0 t + n_{\Sigma}(t) \sqrt{2} AE(t) \sin \frac{\phi}{2} \cos \omega_0 t + n_{\Sigma}(t) n_{\Delta}(t) \}. \quad (\text{L-8})$$

Since the servo loop serves as a low pass filter we are interested only in the low frequency components in the above equation. The low frequency component of the first-term in the above equation will yield the desired angular error signal. The low frequency components of the second two terms result in noise that will compete with the desired error signal. For high signal-to-noise ratios the noise power resulting from the fourth term will be small compared to that from the second and third terms and will be neglected.

Let us proceed to determine the low frequency signal component from the first term and low frequency noise power spectral density resulting from the second and third terms. From equation K-12 of Appendix K we may express $E(t)$ as:

$$E(t) = \sum_{m=0}^{\infty} b_m \cos(m\omega_s t + a_m). \quad (\text{L-9})$$

Then the effective error signal input to the low pass filter is:

$$K^2 A^2 \sin \frac{\phi}{2} \cos \frac{\phi}{2} \left[b_0^2 + \frac{1}{2} \sum_{m=1}^{\infty} b_m^2 \right]. \quad (\text{L-10})$$

Now consider the low frequency single sided power spectral density resulting from the second term of equation L-8. This term may be written as:

$$D \left\{ \sum_{m=0}^{\infty} b_m \cos(m \omega_s t + a_m) \right\} n_{\Delta}(t) \cos \omega_o t, \quad (\text{L-11})$$

where $D = K^2 \sqrt{2} A \cos \frac{\phi}{2}$. From this formulation it is seen that each signal sideband of amplitude $\frac{Db_m}{2}$ (there are two of these) can mix with the noise,

$n_{\Delta}(t)$, at the same frequency to yield a low frequency noise term of amplitude $\frac{n_{\Delta} Db_m}{4}$. Accounting for both sidebands and the zero frequency

foldover, the resulting single sided power spectral density is $4 \left(\frac{Db_m}{4} \right)^2 n_{\Delta}$.

Now considering noise translated to zero frequency by the carrier term (which corresponds to b_o) the resultant single sided power spectral density is

$2 \left(\frac{Db_o}{2} \right)^2 n_{\Delta}$. Then the total low frequency power spectral density

resulting from the second term in equation L-8 is:

$$\frac{1}{2} (Db_o)^2 + \frac{D^2}{4} \sum_{m=1}^{\infty} (b_m)^2 = \frac{(K^2 \sqrt{2} A \cos \frac{\phi}{2})^2 n_{\Delta}}{2} \left[b_o^2 + \frac{1}{2} \sum_{m=1}^{\infty} (b_m)^2 \right], \quad (\text{L-12})$$

$$= \frac{(K^2 \sqrt{2} A \cos \frac{\phi}{2})^2 n_{\Delta}}{2} \left[b_o^2 + \frac{1}{2} \sum_{m=1}^{\infty} (b_m)^2 \right]. \quad (\text{L-13})$$

A similar analysis of the low frequency power spectral density resulting from the third term in equation L-8 yields:

$$\frac{(K^2 \sqrt{2} A \sin \frac{\phi}{2})^2 n_{\Sigma}}{2} \left[b_o^2 + \frac{1}{2} \sum_{m=1}^{\infty} (b_m)^2 \right]. \quad (\text{L-14})$$

Since the sum and difference channel noise processes are independent and $n_{\Sigma} = n_{\Delta} = n$, the total single sided power spectral density at the multiplier output is given by the sum of the above two equations:

$$K^4 A^2 n [b_0^2 + \frac{1}{2} \sum_{m=1}^{\infty} (b_m)^2]. \quad (L-15)$$

Let the effective noise bandwidth of the servo power transfer function be B_{LP} Hz. Then from equation L-15 the resultant noise power is:

$$B_{LP} K^4 A^3 n [b_0^2 + \frac{1}{2} \sum_{m=1}^{\infty} (b_m)^2]. \quad (L-16)$$

This noise competes with the error signal given by equation L-10. For small boresight errors equation L-10 becomes:

$$\frac{K^2 A^2}{2} \left(\frac{2\pi d}{\lambda}\right) \epsilon [b_0^2 + \frac{1}{2} \sum_{m=1}^{\infty} (b_m)^2]. \quad (L-17)$$

Then combining the above two equations the mean squared angular error or angle jitter variance is:

$$\sigma_{\theta}^2 = \left(\frac{\lambda}{2\rho d}\right)^2 \frac{2^2 B_{LP} n}{S [b_0^2 + \frac{1}{2} \sum_{m=1}^{\infty} (b_m)^2]}, \quad (L-18)$$

where $S = \frac{A^2}{2}$ is the per horn received signal power in the absence of the modulation, $E(t)$, (i.e., $E(t) = 1$). Note that this equation agrees with that obtained for a normal continuous wave interferometer system when we let $E(t) = 1$ (i.e., $b_0 = 1, b_1 = b_2 = b_3 \dots = 0$). Note that the factor,

$b_0^2 + 1/2 \sum_{n=1}^{\infty} b_n^2$, is merely the average power of the modulation function

$E(t)$. Thus, the angle jitter variance expression becomes:

$$\sigma_{\theta}^2 = \left(\frac{\lambda}{2\pi d}\right)^2 \frac{2^2 B_{LP} n}{S P_E}, \quad (L-19)$$

where P_E denotes the average power of $E(t)$. We may compute the value of P_E for small target attitude errors by letting $\alpha_A = \epsilon_E = 0$ in equation K-11 of Appendix K:

$$\begin{aligned}
P_E &= \frac{1}{T} \int_0^T E^2(t) dt \quad , \\
&= \frac{1}{T} \int_0^T \sin^2 \left\{ \frac{\pi}{2} \sin \frac{2\pi}{T} t \right\} dt \quad , \\
&= \frac{1}{2T} \int_0^T [1 - \cos(\pi \sin \frac{2\pi}{T} t)] dt \quad , \\
&= \frac{1}{2} - \frac{1}{2} J_0(\pi) \quad , \\
&\approx 0.65 \quad .
\end{aligned}
\tag{L-20}$$

Then for the case of small target attitude errors the angle jitter variance near chaser boresight is:

$$\sigma_\theta^2 = \left(\frac{\lambda}{2\pi d} \right)^2 \frac{2^2 B_{LP} n}{S(0.65)} \quad .
\tag{L-21}$$

The above equation does not account for any time sharing of receiver channels at the chaser. The proposed implementation calls for time sharing a common sum and difference receiver to provide both azimuth and elevation data. In this case the duty factor on the error signal will be 0.5 and the angle jitter variance given by equation L-21 must be increased by a factor of two.

As shown in the previous diagram the AGC control voltage is developed from the sum channel amplifier output. Assuming a square law envelope detector is employed followed by a low pass filter resultant output is the average value of:

$$K^2 2A^2 E^2(t) \cos^2 \frac{\phi}{2} \quad ,
\tag{L-22}$$

where we have used equation L-4 and neglected the noise terms. Note that the average of $E^2(t)$ is P_E . Assume the AGC serves to hold the average value of the above quantity equal to a constant, $2C$, such that the required gain K is given by:

$$K^2 = \frac{C}{A^2 P_E \cos^2 \frac{\phi}{2}} \quad \cdot \quad (L-23)$$

Using the value of K^2 in equation L-10 the normalized error signal becomes $C \tan \frac{\phi}{2}$. Had we considered the noise terms in equation L-4, it can be shown that the error signal is:

$$C \tan \left(\frac{\phi}{2} \right) \left[1 + \frac{\frac{1}{n} B_{IF}}{2SP_E \cos^2 \frac{\phi}{2}} \right] \quad \cdot \quad (L-24)$$

where B_{IF} is the IF amplifier bandwidth in Hz. Note that this indicates the error signal gain is a function of the sum channel signal-to-noise ratio. Thus, the error signal and servo bandwidth will decrease with decreasing signal-to-noise ratio. This effect has been neglected in the previous angle jitter variance equation which is valid at high signal-to-noise ratios.

The unambiguous single sided angular range is defined by:

$$\frac{\phi}{2} = \frac{1}{2} \frac{2\pi d}{\lambda} \sin \epsilon \leq \frac{\pi}{2} \quad \cdot \quad (L-25)$$

Then in order to obtain unambiguous information for ϵ up to $\pi/2$ we require:

$$d \leq \frac{\tau}{2} \quad \cdot \quad (L-26)$$

APPENDIX M

THERMAL NOISE EFFECTS ON TARGET YAW AND PITCH DETERMINATION

IN THE ELECTRONIC OMNI SYSTEM

The null of the radiation pattern transmitted by the target is caused to sweep alternately in azimuth and elevation. This technique is described in Appendix K. Consider the azimuth sweep. From equations K-11 and K-13 of Appendix K the signal received at the chascraft during one azimuth sweep is:

$$e(t) = A \sin \left\{ \frac{\pi}{2} [\sin \omega_s t + \sin \epsilon_A] \right\} \cos \omega_o t \quad . \quad (M-1)$$

where A is the peak amplitude of the received signal referred to the chascraft receiver input, ω_o is the carrier radian frequency, ω_s is the null sweep radian frequency, and ϵ_A is the chascraft azimuth coordinate relative to the target antenna boresight. An estimate of ϵ_A is obtained by comparing the time at which the null sweeps past the chascraft with a timing reference signal.

The above received signal must compete with receiver noise which may be represented by the following narrow band gaussian random process:

$$n(t) = x(t) \cos \omega_o t - y(t) \sin \omega_o t \quad . \quad (M-2)$$

In this representation $x(t)$ and $y(t)$ are slowly varying independent processes with single sided power spectral densities equal to $2n$ where $n = kTF$. Here $kT = 4 \times 10^{-21}$ watt/Hz and F is the receiver noise figure. $X(t)$ and $y(t)$ have zero means.

Let the signal plus noise be supplied to a linear envelope detector. Then for high signal-to-noise ratios the envelope detector output is:

$$e_d(t) = |A \sin \left\{ \frac{\pi}{2} [\sin \omega_s t + \sin \epsilon_A] \right\} + x(t)| \quad . \quad (M-3)$$

Now assume a zero crossing detector is used to determine the time of occurrence of the null. (In reality the crossing detector must have a slightly positive threshold since the envelope detector output cannot be negative.) The slope of the envelope detector output near the null (i.e., $\omega_S t \approx -\epsilon_A$) in the absence of noise is:

$$D = \left. \frac{d(e_d)}{dt} \right|_{\substack{\omega_S t = -\epsilon_A \\ x(t) = 0}} = A \frac{\pi}{2} \omega_S \cos \epsilon_A \quad . \quad (M-4)$$

Thus the noise term, $x(t)$, will cause an error in the time of the occurrence of the null equal to:

$$\Delta t = \frac{x(t)}{D} \quad . \quad (M-5)$$

But since the null is swept in a linear manner at ω_S mechanical radians per second, this timing error results in a mechanical angular error equal to:

$$\epsilon_N = \omega_S \Delta t \quad , \quad (M-6)$$

$$\epsilon_N = \frac{2 x(t)}{\pi A \cos \epsilon_A} \quad . \quad (M-7)$$

The mean squared value of ϵ_N is the angle jitter variance (σ_θ^2):

$$\sigma_\theta^2 = \left(\frac{2}{\pi}\right)^2 \frac{E[x^2(t)]}{A^2 \cos^2 \epsilon_A} \quad . \quad (M-8)$$

But the second moment of $x(t)$ is determined by the IF noise bandwidth preceding the envelope detector. The second moment becomes:

$$E[x^2(t)] = n B_{IF} \quad . \quad (M-9)$$

where B_{IF} is the noise bandwidth in Hz. In order to reproduce the envelope generated by the swept null, a bandwidth of about $8 \frac{\omega_s}{2\pi}$ Hz would be required. Using the value of B_{IF} the angle jitter variance becomes:

$$\sigma_{\theta}^2 = \left(\frac{2}{\pi}\right)^2 \frac{n^4 f_s}{S \cos^2 \epsilon_A} \quad , \quad (M-10)$$

where we have used $A^2 = 2S$ and $\omega_s = 2\pi f_s$. This expression represents the mean squared error per sweep and does not include any errors in the timing reference signal. If a low pass filter with single sided noise bandwidth equal to B_{LP} Hz is used to average over many sweeps the angle jitter variance

will be reduced by the factor $\frac{2 B_{LP}}{f_s}$.

Note that mean squared timing error or time jitter variance is given by:

$$\sigma_T^2 = \frac{4n}{\pi^4 S f_s \cos^2 \epsilon_A} \quad . \quad (M-11)$$

This result will be used in the derivation of roll measurement errors.

APPENDIX N

INTERFEROMETER ANGLE NOISE

Consider the simple interferometer system shown in figure N1 which is representative of the angle measurement technique employed in the Integrated Phase System (IPS).

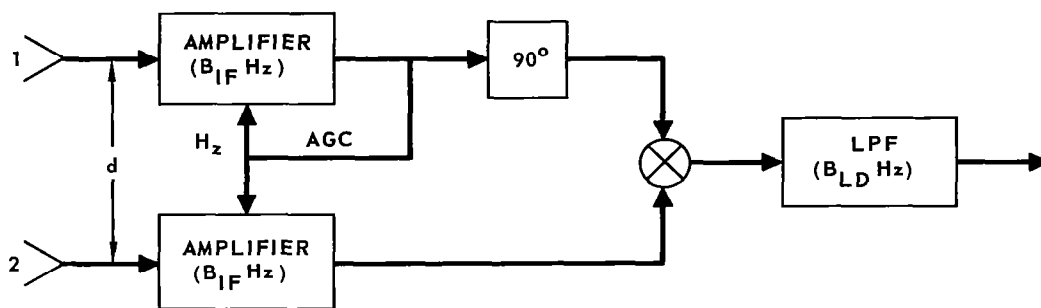


FIGURE N-1 - INTERFEROMETER SYSTEM

Let the signal plus noise at the phase comparator input in channels 1 and 2 respectively be:

$$A \sin (\omega_0 t + \theta) + n_1(t) \quad , \quad (N-1)$$

$$A \cos (\omega_0 t) + n_2(t) \quad . \quad (N-2)$$

A is the received signal voltage, and ω_0 is the carrier radian frequency. The electrical phase difference is:

$$\phi = \frac{2\pi d}{\lambda} \sin(\epsilon) \quad , \quad (N-3)$$

where d is the interferometer separation, λ is the wavelength, and ϵ is the boresight error.

The noise in each channel is considered to be narrow band gaussian noise with single sided power spectral density equal to $N = kTF$ where $kT = 4 \times 10^{-21}$ watt/Hz and F is the receiver noise figure. The noise in channels 1 and 2 respectively is:

$$n_1(t) = x_1(t) \cos \omega_0 t - y_1(t) \sin \omega_0 t = v_1(t) \cos(\omega_c t + \theta_1(t)) \quad , \quad (N-4)$$

and :

$$n_2(t) = x_2(t) \cos \omega_0 t - y_2(t) \sin \omega_0 t = v_2(t) \cos(\omega_c t + \theta_2(t)) \quad . \quad (N-5)$$

Then considering the phase detector to be an ideal multiplier the effective input to the low pass filter is:

$$\frac{1}{2} [A^2 \sin \phi + Ax_1 + Ax_2 \sin \phi - Ay_2 \cos \phi + x_1 x_2 + y_1 y_2] \quad , \quad (N-6)$$

where we have yet to account for AGC normalization. Assuming ideal AGC the signal component at the low pass filter input is:

$$\frac{1}{2} \sin \phi \quad . \quad (N-7)$$

And the noise term is:

$$\frac{1}{2A^2} [Ax_1 + Ax_2 \sin \phi - Ay_2 \cos \phi + x_1 x_2 + y_1 y_2] \quad . \quad (N-8)$$

The power spectral density of the low pass filter input noise is easily determined since x_1 , x_2 , y_1 , and y_2 are independent random variables. From previous assumptions the single sided power spectral density of each of these random variables is identical and is as shown in figure N-2 for a rectangular IF filter.

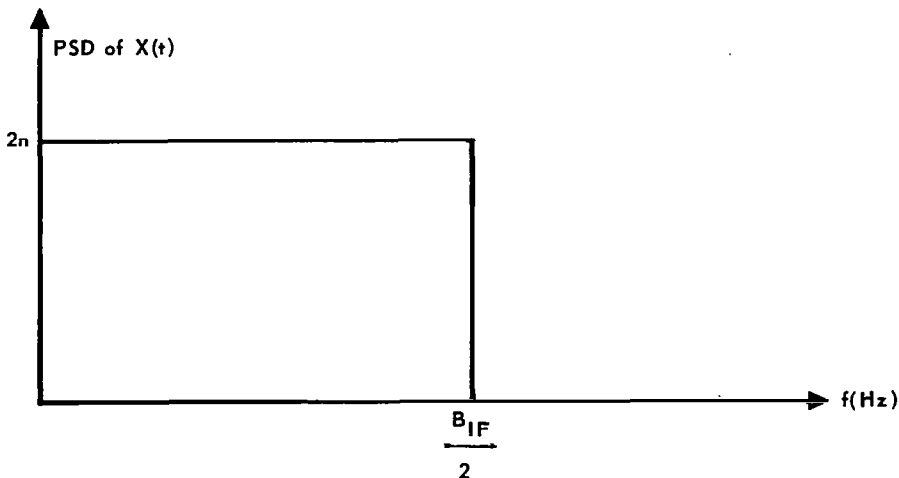


FIGURE N-2 - POWER SPECTRAL DENSITY OF X(t)

The power spectral density of each of the terms x_1 , x_2 and y_1 , y_2 is identical and is given by convolution of the individual rectangular densities as shown in figure N-2. The result is shown in figure N-3.

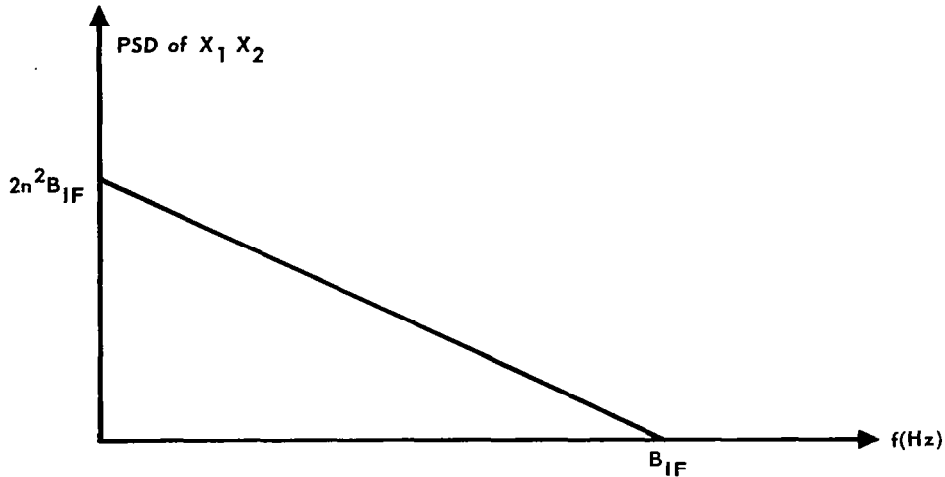


FIGURE N-3 - POWER SPECTRAL DENSITY OF $X_1(t) \cdot X_2(t)$

Then the low pass filter output noise power is determined by passing each of the noise terms in equation N-8 through the filter. Assuming a low pass filter rectangular bandwidth equal to B_{LP} Hz that is small compared to B_{IF} the output noise power is determined to be:

$$\frac{n B_{LP}}{A^2} \left[1 + \frac{n B_{IF}}{A^2} \right] \cdot \quad (N-9)$$

But from equations N-7 and N-3 the output signal at small angular errors may be approximated by:

$$\frac{1}{2} \epsilon \left(\frac{2\pi d}{\lambda} \right) \cdot \quad (N-10)$$

Thus, the mean squared angular error or angle jitter variance is:

$$\sigma_{\theta}^2 = \left(\frac{\lambda}{2\pi d} \right)^2 \frac{4n B_{LP}}{A^2} \left[1 + \frac{n B_{IF}}{A^2} \right] \cdot (\text{Mechanical Radians})^2 \quad (N-11)$$

Using the fact that the signal power S is $\frac{A^2}{2}$ and $n = KTF$ the rms angular error becomes:

$$\sigma_{\theta} = \left(\frac{\lambda}{2\pi d}\right) \left[\frac{2kTNF B_{LP}}{S} \left(1 + \frac{n B_{IF}}{2S}\right) \right]^{1/2} \quad (\text{Mechanical Radians}), \quad (\text{N-12})$$

where $kT = 4 \times 10^{-21}$ watts/Hz and F is the receiver noise figure.

REFERENCES

1. Page, C. H., et al "IEEE Recommended Practice for Units in Published and Technical Work", IEEE Spectrum, March 1966.
2. Hatch Riley, Cobb, "Simulating Gemini-Agena Docking", Astronautics and Aeronautics, November 1964.
3. Lindorff, D. P., "Theory of Sampled Data Control Systems", John Wiley and Sons, Inc., 1965.
4. Rice, S. O., "Mathematical Analysis of Random Noise", Selected Papers on Noise and Stochastic Processes, Dover Publications, Inc., 1954.
5. Schwartz, Mische, "Information Transmission, Modulation, and Noise", McGraw-Hill, 1959 (Page 300).
6. Woodward, P. M., "Probability and Information Theory, With Applications to Radar", Pergamon Press, Second Edition 1964.
7. Siebert, William McC., "A Radar Detection Philosophy", IRE Transactions on Information Theory, September 1956.
8. "Independent Research and Development Program for Fiscal Year 1964", Emerson Electric Report No. 1643, dated 23 December 1963.
9. Saunders, W. K., "Postwar Developments in Continuous-Wave and Frequency Modulated Radar", IRE Transactions on Aerospace and Navigational Electronics, March 1961.
10. Luck, D. G. C., "Frequency Modulated Radar", McGraw-Hill, 1949.
11. Cook, C. E., "Matched Filtering, Pulse Compression and Waveform Design - Part 2", Microwave Journal, November 1964.
12. Craig, S. E., et al, "Continuous-Wave Radar With High Resolution and Unambiguous Velocity Determination", IRE Transactions on Military Electronics, April 1962.
13. "How Coded-Pulse Techniques Extend Radar Range", Electronics, November 1963.
14. Peterson, W. D., et al, "Signal-Power Comparison of Coded and Tone Ranging Systems for Spacecraft Vehicles", IEEE Transactions on Aerospace and Navigational Electronics, June 1965.
15. Cook, C. E., et al, "Matched Filtering, Pulse Compression and Waveform Design - Part IV", the Microwave Journal, January 1965.

16. Hooper, J., et al, "An FM-CW Radar Sensor For Space Vehicle Rendezvous and Landing", Space Electronics Symposium, Miami Beach, Florida, October 1963.
17. O'Hara, F. I., et al, "A High Performance CW Receiver Using Feedthrough Nulling", The Microwave Journal, September 1963.
18. Harmer, J. D., et al, "Some Advances in CW Radar Techniques", Military Electronics Conference, 1961.
19. Klass, Philip, "Altimeter Monitors Its Own Performance", Aviation Week, 12 July 1965.
20. Bonelle, G. J., "Radar Design for Manned Space Vehicles", Military Electronics Winter Convention, Los Angeles, California, 7, 8, 9 February 1962
21. Heidbreder, G. R., "Stelatrac, a Modular Spaceborne Terminal Guidance Radar", Space Electronics Symposium, Miami Beach, Florida, 1962.
22. Aviation Week, 16 July 1962.
23. Knudsen, J. T., "Unified S-Band Rendezvous Sensor", presented at National Space Navigation and Communications Meeting, Houston, Texas, April 1965.
24. Westinghouse, Air Arm Division, "A Phase Coded Radar and Communication System", Baltimore, Maryland, 27 January 1964
25. Goldberg, H. B., et al, "A Coherent Solid-State Radar for Space Rendezvous and Planetary Landings", Space Electronics Symposium, Miami Beach, Florida October 1963.
26. Westinghouse Electric Corporation Report (Air Arm Division), Baltimore, Maryland, "PRADOR, An Advanced Rendezvous Radar for Space Flight Operations", 15 October 1963.
27. Space/Aeronautics, April 1964, Page 116.
28. Wright, R. D., et al, "Alluminum Alloy Junction Backward Diodes in Microwave Detection Systems", 1965 International Solid-State Circuits Conference, University of Pennsylvania, 17, 18, 19 February 1965.
29. Hael, R., "Design of the Hot Carrier Mixer and Detector", 1965 International Solid-State Circuits Conference, University of Pennsylvania, 17, 18 and 19 February 1965.
30. "Micronotes", Microwave Associates, Incorporated, July/August 1964.
31. Kazel, S., et al, "Improvement in Tracking Accuracy of Pulse Radar by Coherent Techniques", IRE-PGMIL, October 1961

32. Roczynski, A. T., "Some Factors Affecting Size and Weight of Traveling Wave Tubes", Sperry Technical Paper.
33. Schwarzkopf, "The Traveling Wave Resonator As a Short Pulse Generator", Microwave Journal, October 1962.
34. Jordan, E. C., "Electromagnetic Waves and Radiating Systems", Prentice Hall, Incorporated, 1960.
35. Watton, W. L., et al, "A Direct-Capacitance Aircraft Altimeter", Paper Presented at a Joint Meeting of the Measurements and Radio Sections, January 1949.
36. Ross, M., et al, "Microwave Bandwidth Optical Communications Systems", IRE Proceedings National Space Electronics and Telemetry Symposium, October 1962. Also see M. Ross's "Laser Receivers", John Wiley and Sons, Incorporated, 1966, Pages 118 through 122.
37. Ashby, D., et al, "Performance of the He-Ne Laser as an Interferometer for Measuring Plasma Density", Journal of Applied Physics, 29 January 1965, Page 36.
38. Ross, M., et al, "High Sensitivity Fast Response Laser Detection Systems", IEEE Transactions Aerospace - Electronic Systems, January 1966.
39. Gaddy, O., et al, "A Microwave Frequency Crossed-Field Photomultiplier", Proceedings IEEE 31, January 1963, Page 153. Also see M. Ross's, "Laser Receivers", John Wiley and Sons, Incorporated, 1966, Chapter 2.
40. Oliver, D. "Thermal and Quantum Noise", IEEE Proceedings 53, May 1965, Page 436.
41. M. Ross "Laser Receivers" John Wiley and Sons, Incorporated, Chapter 2, 1966.
42. Rowe, H., "Amplitude Modulation With a Noise Carrier", IEEE Proceedings 53, April 1964, Page 389.
43. Hallicrafters Progress Report Number 2, NASA Contract Number NAS 5-3777, September 1964.
44. Goldstein, B., et al, "X-Band Modulation of Gallium Arsenide Lasers", IEEE Proceedings 53, February 1965, Page 195.
45. Rome Air Development Center, "Study and Investigation of Missile Liftoff Measurement System", RADC-TDR-63-540, December 1964.
46. Cohen, W., et al, "Amplitude and Phase Sensing Monopulse System Parameters", Microwave Journal, Volume 2, October and November 1959.

47. Sharenson, S., "Angle Estimation Accuracy with a Monopulse Radar in the Search Mode", IRE PGANE, September 1962.
48. Dunn, J. H. and Howard, D. D., "Precision Tracking with Monopulse Radars", Electronics, 22 April 1960.
49. Barton, D. K., "Instrumentation Radar AN/FPS-16(XN-1), Evaluation and Analysis of Radar Performance", RCA, Moorestown, New Jersey, 1959.
50. Gerlock, R. A., "Study of Interference Aspects of Fresnel Region Phenomena", Volumes I and II, USAF (RADC) TDR-62-495, August 1962.
51. Skolnik, M. I., "Introduction to Radar Systems", McGraw-Hill, 1962.
52. Honey, R. C. and Jones, E. M. T., "A Versatile Multiport Biconical Antenna", IRE, October 1957.
53. Locke, A. S., "Guidance", D. Van Nostrand Company, Incorporated, Princeton, New Jersey, 1955.
54. Povejsil, Raven, and Waterman, "Airborne Radar", D. Van Nostrand Company, 1961.
55. Rhodes, D. R., "Introduction to Monopulse", McGraw-Hill, 1959.
56. Manassie, R. "Maximum Angular Accuracy of Tracking a Radio Star by Lobe Comparison", IRE PGAP, Volume AP-8, January 1960.
57. Scharfman, Rothman, Guthart, and Morita, "Doploc System Studies", Part B, Final Report, Stanford Research Institute, Contract Number DA-04-200-ORD-674, July 1960.
58. Delano, R. H., "A Theory of Target Glint or Angular Scintillation in Radar Tracking", IRE Proceedings, Volume 41, Pages 1778 through 1784, December 1953.
59. Muchmore, R. B., "Aircraft Scintillation Spectra", IRE Transactions on Antennas and Propagation, Pages 201 through 212, March 1959.
60. Freeman, J. J., "Principles of Noise", J. Wiley and Sons, Inc. New York, New York, 1958.
61. Dunn, J. H., Howard, D. D., and King, A. M., "Phenomena of Scintillation Noise in Radar Tracking Systems", IRE Proceedings, Volume 47, Pages 855 through 864, May 1959.
62. Delano, R. H. and Pfeffer, I., "The Effect of AGC on Radar Tracking Noise", IRE Proceedings, Volume 44, Page 801 through 810, June 1956

63. Brockner, C. E., "Angular Jitter in Conventional Conical - Scanning, Automatic Tracking Radar Systems", IRE Proceedings, Volume 39, Pages 855 through 864, May 1959.
64. Brown, T. T., Mixer Harmonic Chart, "Electronics", Page 293 through 294, April 1951.

"The aeronautical and space activities of the United States shall be conducted so as to contribute . . . to the expansion of human knowledge of phenomena in the atmosphere and space. The Administration shall provide for the widest practicable and appropriate dissemination of information concerning its activities and the results thereof."

—NATIONAL AERONAUTICS AND SPACE ACT OF 1958

NASA SCIENTIFIC AND TECHNICAL PUBLICATIONS

TECHNICAL REPORTS: Scientific and technical information considered important, complete, and a lasting contribution to existing knowledge.

TECHNICAL NOTES: Information less broad in scope but nevertheless of importance as a contribution to existing knowledge.

TECHNICAL MEMORANDUMS: Information receiving limited distribution because of preliminary data, security classification, or other reasons.

CONTRACTOR REPORTS: Scientific and technical information generated under a NASA contract or grant and considered an important contribution to existing knowledge.

TECHNICAL TRANSLATIONS: Information published in a foreign language considered to merit NASA distribution in English.

SPECIAL PUBLICATIONS: Information derived from or of value to NASA activities. Publications include conference proceedings, monographs, data compilations, handbooks, sourcebooks, and special bibliographies.

TECHNOLOGY UTILIZATION PUBLICATIONS: Information on technology used by NASA that may be of particular interest in commercial and other non-aerospace applications. Publications include Tech Briefs, Technology Utilization Reports and Notes, and Technology Surveys.

Details on the availability of these publications may be obtained from:

SCIENTIFIC AND TECHNICAL INFORMATION DIVISION
NATIONAL AERONAUTICS AND SPACE ADMINISTRATION
Washington, D.C. 20546